6-23-2022

Shear Friction Capacity of Corrugated Pipe Connection in Precast Footings

Fatima C. Vieira
Florida International University, fviei003@fiu.edu

FLORIDA INTERNATIONAL UNIVERSITY

Miami, Florida

SHEAR FRICTION CAPACITY OF CORRUGATED PIPE CONNECTION IN PRECAST FOOTINGS

A dissertation submitted in partial fulfillment of

the requirements for the degree of

DOCTOR OF PHILOSOPHY

in

CIVIL ENGINEERING

by

Fatima Vieira Sousa

2022

To: Dean John L. Volakis
College of Engineering and Computing

This dissertation, written by Fatima Vieira, and entitled Shear Friction Capacity of Corrugated Pipe Connection in Precast Footings, having been approved in respect to style and intellectual content, is referred to you for judgment.

We have read this dissertation and recommend that it be approved.

_____
Atorod Azizinamini

_____
Kingsley Lau

_____
Armin Mehrabi

_____
Wallied Orabi

_____
David Garber, Major Professor

Date of Defense: June 23, 2022.

The dissertation of Fatima Vieira is approved.

_____
Dean John L. Volakis
College of Engineering and Computing

_____
Andrés G. Gil
Vice President for Research and Economic Development
and Dean of the University Graduate School

Florida International University, 2022

DEDICATION

To my parents, without their support, dedication, and encouragement this journey would have not been the same. I am profoundly thankful for their presence in my life and for giving me the opportunity to do things that they could not do. I am proud to be their daughter.

ACKNOWLEDGMENTS

The authors would like to thank the Florida Department of Transportation (FDOT) for providing the funding that made this project possible. Also, the authors would like to recognize the team of engineers and staff at the Marcus H. Ansley Structures Research Center for their efforts on instrumentation and testing of all the small and large specimens throughout the research period – in particular, Steven Eudy, William Potter, Paul Tighe, Justin Robertson, Ben Allen, and Miguel Ramirez.

Special thanks are also due to the project manager, Mr. Bruno Vasconcelos, for his support and technical contributions to the project.

Finally, the authors would like to acknowledge Coreslab Structures Inc. for the construction of the second and third series of small-scale specimens, CDS Manufacturing Inc. for the construction of the large-scale specimens, and the staff at FDOT's Structural Materials Laboratory for testing the shear friction capacity of the specimens.

ABSTRACT OF THE DISSERTATION

SHEAR FRICTION CAPACITY OF CORRUGATED PIPE CONNECTION IN PRECAST FOOTINGS

by

Fatima Vieira

Florida International University, 2022

Miami, Florida

Professor David Garber, Major Professor

Prefabricated Bridge Elements and Systems (PBES) are being more widely used, as they can significantly reduce on-site construction time impacting traffic. The main concerns when using PBES are the final assembly of the elements to achieve the monolithic behavior of the structure. The currently recommend connection detail between the precast pile cap and precast pile is a pocket connection, which relies on the bearing strength between the end of the pile and pile cap and the shear friction capacity between the cast in place (CIP) plug and the precast cap. Current code expressions for shear friction include components for cohesion or aggregate interlock and a contribution from steel crossing the interface or a clamping force, but were developed primarily on the basis of shear friction tests with steel crossing the interface. In pocket connections there is no steel crossing the shear friction interface meaning that the shear friction failure is controlled by the cohesion and interlock of the CIP concrete to precast concrete or surrounding material. An experimental investigation was conducted on thirty-seven small-scale specimens and eight large-scale specimens to explore experimentally the behavior of this interface and the effect of different variables like reinforcement configuration around the pocket, type of pipe used to make the pocket, and surface preparation of the interface. Three principal conclusions were made (1) all specimens simulating pocket connections had a shear friction failure at the

interface, (2) having a corrugated interface and 1/4-inch roughness in the interface led to higher capacity and (3) equation found on AASHTO LRFD Guide Specifications for ABC led to conservative results and it is recommended to estimate the shear friction capacity in pocket connections. Findings, current code performance, and design recommendations from the numerical and experimental work are presented in this dissertation.

TABLE OF CONTENTS

CHAPTER PAGE

LIST OF TABLES

TABLE PAGE

LIST OF FIGURES

FIGURE PAGE

Chapter 1: **Introduction**

1.1. Overview

Prefabricated Bridge Element and Systems (PBES) are being more widely used, as they can dramatically reduce on-site construction time impacting traffic. The main concerns when using PBES are the on-site final assembly of the elements and the type of connection used between elements. One type of connection used between precast piles and precast pile caps is a pocket connection, which relies largely on the shear friction capacity along the interface between a cast-in-place plug and the precast pile cap. Current code expressions for shear friction include components for cohesion or aggregate interlock as well as a contribution from steel crossing the interface or clamping force. These expressions were developed primarily based on shear friction tests with steel crossing the interface. The main objective of this project is to evaluate the shear friction capacity of the precast pile cap to precast pile connection where there is no steel crossing the interface. This connection relies on the shear friction capacity of the interface, which is a behavior that has not been appropriately studied.

1.2. Project Objective

The objective of this research was to evaluate the failure mechanism and shear friction capacity of the plane between the precast pile cap and CIP plug. The hypothesis was that, although there is no reinforcement crossing this interface, the confinement provided by the surrounding concrete and reinforcement will provide the clamping force needed to engage the cohesion and aggregate interlock components of the shear friction capacity.

The use of PBES in the implementation of the Accelerated Bridge Construction (ABC) technique is a key factor for reducing the time of construction impacting traffic. Many connections have been developed to implement this new technique however more details on the design and construction are required to well understand the behavior of the connection. The final goal of this study was to provide more details on the construction of the pile cap-to-pile connection and develop an appropriate design equation to estimate the capacity of the interface to avoid unexpected shear friction failure.

1.3. Project Scope

The research objective was accomplished through three interdependent research efforts: (1) review of previous research and current design specifications, (2) numerical investigation, and (3) experimental investigation of the interface behavior. The first part of the research involved an extensive literature review to develop the appropriate knowledge in shear friction and the parameters involved in the capacity on an interface between two concrete cast at different times. The next step was to develop the appropriate testing protocol and test matrix to test the cap-to-pile connection in small-scale. This step involved the develop of construction drawings, fabrication, and testing of the specimens. Based on the results in the small-scale testing, the large-scale testing was developed. As well as the previous step, in this step the testing protocol, test matrix, construction documents, fabrication, and testing of the specimens needed to be done. Then, with the obtained results, design equations and details were developed as new recommendations for implementation in the AASHTO LRFD Bridge Design Specification.

1.4. Thesis Organization

This thesis is divided into seven chapters and a series of appendices. Chapter 2 presents a complete literature review on shear friction, current codes expressions and estimation procedures, prefabricated substructure connections and the currently recommended connection between precast pile cap and pile. Chapter 3 introduces finite element details and modeling of the cap-to-plug connection. The experimental procedure and results to evaluate the shear friction capacity between precast cap and CIP plug without reinforcement crossing the interface is presented in Chapter 4. Chapter 5 presents the estimation performance of the small- and large-scale testing with the evaluation of the current cohesion and friction components. Chapters 6 includes the design and construction recommendations based on the findings of this research and Chapter 7 presents a summary and conclusions of this research.

Chapter 2: **Background of Shear Friction and Prefabricated Bridge Elements and Systems**

2.1. Overview of Bridge Components

Bridges are mainly divided in two parts: superstructure components and substructure components. The elements on each component vary based on the type of bridge and its materials (concrete, steel, or composite bridge) as shown in Figure 2-1. Some examples of superstructure elements are deck slab, girders, truss, etc. The bridge superstructure can transfer axial loads, lateral loads, and moments to the bridge substructure which helps to distribute the loads to the bridge footings and foundations (piles and pile caps). The substructure consists of piers, abutments, footings, piles, etc. The connection experimentally tested and evaluated in this research is part of the substructure of a bridge, specifically, the connection between a prefabricated pile to pile cap. In most cases, these elements would resist axial compression loads coming from the superstructure and sub-structure elements such as self-weight of all elements and the standard HL-93 applied live load. Pure compression load was experimentally considered to evaluate the precast pile-to-pile cap connection.

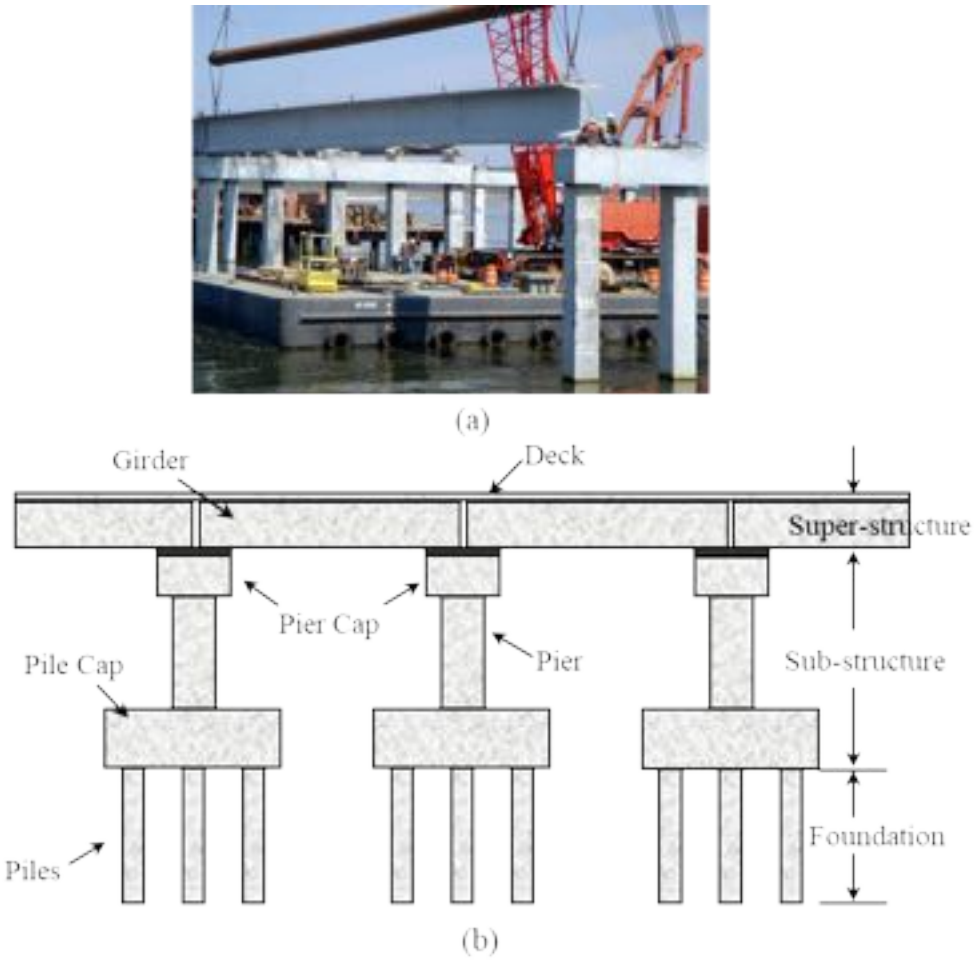

Figure 2-1: (a) Construction of a bridge (courtesy of Corven Engineering), (b) super-structure and sub-structure components on a bridge

2.2. Prefabricated Substructure Connection Details

Prefabricated Bridge Elements and System (PBES) are one of the primary techniques used to accelerate bridge construction. The prefabrication of these elements or systems improves the quality of the members themselves, as they are generally cast at precast plants with better quality control than on-site construction. These prefabricated bridge elements include both superstructure (e.g. beams and decks) and substructure components (e.g. piles, pile caps, columns, abutments, and bents).

Prefabricated bridge elements require on-site connections between elements, which often become the critical component of the overall bridge design. Over the years, many types of connections in precast elements have been evaluated to ensure the monolithic behavior of

the entire structure. The details of these connections vary depending on which elements are being connected. As mention before, the main objective of this project is to evaluate the connection between precast pile caps and piles. An overview of the primary connection details between these elements is presented in this section.

2.2.1. Pile to Pile-Cap Connection

There are two primary types of connections between these elements defined by AASHTO T-4 (A. Hawash, personal communication, April 19, 2018) and the "Recommended AASHTO Guide Specification for ABC Design and Construction" (Culmo et al., 2018).

- ***Pocket Connections***: A connection between two prefabricated elements thru the projection of multiple bars or connectors of one element into a single void that is cast internal to the receiving element. The void is then filled with either concrete, grout, or other suitable material.
- ***Socket Connections***: A connection between two prefabricated elements thru the projection of a single portion of one element into a single void of the receiving element. The gap between the two elements is then filled with either concrete, grout, or other suitable material.

These definitions are also similar to those proposed by Marsh et al. . Details for pocket and socket connections are shown in Figure 2-2 and Figure 2-3, respectively. The defining characteristics of the pocket connection are highlighted in Figure 2-2 (a). For this connection, the precast pile does not extend into the pocket in the precast pile cap. The precast pile cap is erected onto the precast pile using temporary flexible shims (shown in Figure 2-2 (a)). Then, reinforcement is extended from the precast pile into the pile cap and cast-in-place (CIP) concrete or grout is placed to fill the pocket, develop the reinforcement, and connect the two members. Once the pocket material is placed and cured there should be no load transfer considered through bearing between the precast pile cap and the precast piles. A corrugated metal pipe or duct is often used to form the void to enhance the bond between the CIP concrete or grout and the precast pile cap. Two examples of details used in actual bridges are shown in Figure 2-2 (b) and (c).

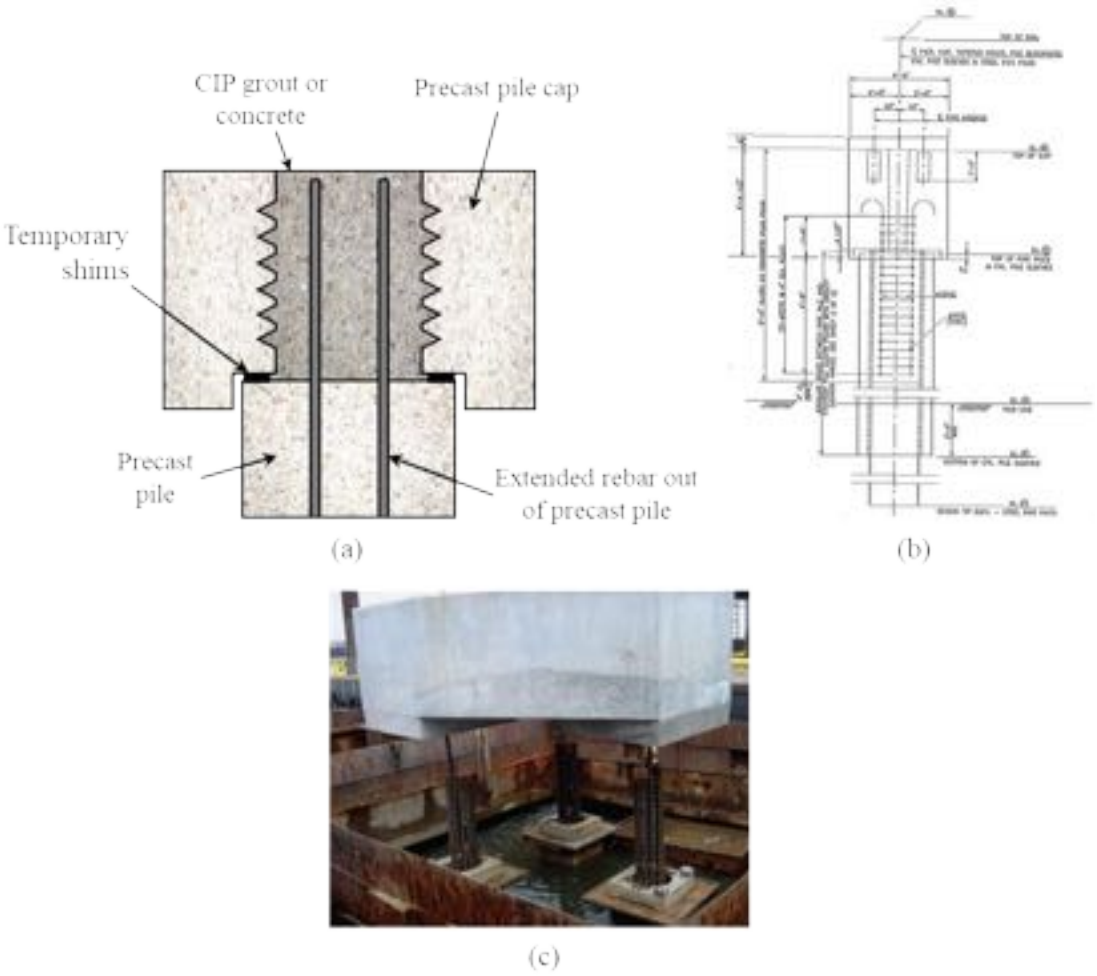

Figure 2-2: Examples of Pocket Connection between pile cap and pile: (a) connection between two precast elements; (b) connection use in Beaufort and Morehead Railroad Trestle Bridge(North Carolina Department of Transportation, 1999); (c) connection use in I-10 Bridge over Escambia Bay(Rudie et al., 2008).

The defining characteristics of a socket connection are shown in Figure 2-3 (a). For this connection, the precast pile is extended into a void in the pile cap and CIP grout or concrete is placed to connect the elements. Reinforcement can be present between the elements, as shown in the example of a socket connection detail shown in Figure 2-3 (b).

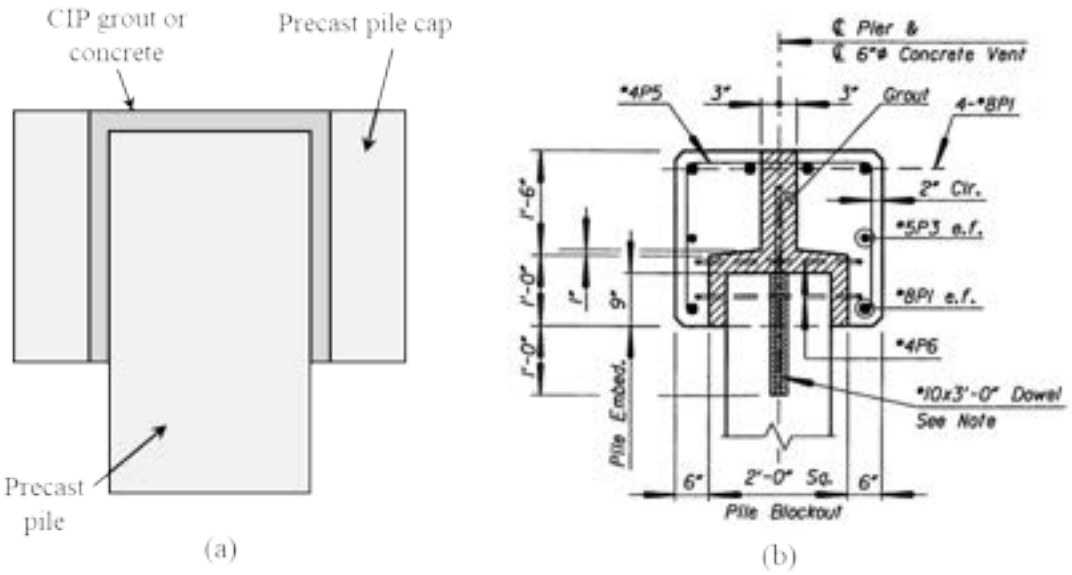

Figure 2-3: Examples of Socket Connections between Pile cap and pile: (a) connection between two precast elements; (b) connection used in Parker River Bridge (2007)(Department of Transportation Federal Highway Administration, 2004).

A list of past projects that have utilized both precast piles and precast pile caps is provided in Table 2-1. This list was obtained from the ABC Project Database developed by Garber(Garber, 2016). These projects include the use of both pocket and socket connections with steel H piles and precast concrete piles.

Table 2-1: ABC Projects Database

Bridge Number	Bridge Name	Year	State	Type of Connection	Description
1	Pelican Creek	1992	Alaska	Socket Connection	▪ H Steel Piles ▪ Pre-cast Pile Cap ▪ Pockets filled with concrete
2	Beaufort and Morehead Railroad Trestle Bridge	1999	North Carolina	Pocket Connection	▪ Pre-cast Pile Cap

Bridge Number	Bridge Name	Year	State	Type of Connection	Description
3	Kouwegok Slough Bridge	2000	Alaska	Socket Connection	▪ Pre-cast Pile Cap ▪ Prefabricated Piles
4	Mackey Bridge	2006	Iowa	Pocket Connection	▪ Pre-cast Pile Cap ▪ Full Depth Pockets ▪ Corrugated metal pipe ▪ High-early-strength concrete mix
5	Parker River Bridge	2007	Massachusetts	Socket Connection	▪ Pre-cast Pile Cap ▪ Prefabricated Piles ▪ 2 ft Depth Voids
6	I-10 Bridge over Escambia Bay	2007	Florida	Pocket Connection	▪ Pre-cast Pile Cap ▪ Prefabricated Piles ▪ Pockets filled with concrete
7	NC 12 Bridge over Molasses Creek	2009	North Carolina	Socket Connection	▪ Pre-cast Pile Cap ▪ Prefabricated Piles ▪ Partial Depth Voids
8	US 17 Bridge over Tar River	2010	North Carolina	Socket Connection	▪ Pre-cast Pile Cap ▪ Prefabricated Piles ▪ Pockets filled with concrete
9	Kickapoo Bridge	2010	Mississippi	Socket Connection	▪ Pre-cast Pile Cap ▪ Partial depth pockets ▪ Concrete Piles

Bridge Number	Bridge Name	Year	State	Type of Connection	Description
10	TH 61 Bridge over Gilbert Creek	2011	Minnesota	Pocket Connection	▪ Pre-cast Pile Cap ▪ Prefabricated Piles ▪ High-strength flowable grout ▪ Intentionally roughened pocket.
11	UPRR Bridge	2011	Kansas	Socket Connection	▪ H Steel Piles ▪ Pre-cast Pile Cap ▪ Partial Depth Pockets
12	TH 36 over Keller Lake Bridge	2013	Minnesota	Pocket Connection	▪ Pre-cast Pile Cap ▪ Prefabricated Piles ▪ High-strength flowable grout ▪ Intentionally roughened pocket

Pocket and socket connections are mainly used in the connection between precast pile to pile cap and pier to pier cap or bent cap as shown in Figure 2-4 and Figure 2-5.

2.2.2. Currently Recommended FDOT Connection

FDOT is continually trying to improve construction methods to reduce the onsite construction as well as to minimize traffic impact, leading to their use of PBES in construction. FDOT developed a section in their Structures Detailing Manual (Florida Department of Transportation, 2017) specific to PBES (Chapter 25) and also a set of PBES Conceptual Drawings (Florida Department of Transportation, 2015).The primary focus of research is the connection between precast pile to pile cap. The Florida Department of Transportation (FDOT) currently recommends a pocket connection between precast piles and precast pile caps. The precast pile cap is constructed with a void at the location of the pile that is slightly smaller than the piles and then placed on the driven piles. Reinforcement is then placed between the elements and the connection is filled with concrete to finish the

connection. This connection detail relies on the shear friction capacity between the CIP plug and the precast cap. In this recommended connection there is no steel crossing the interface. This means that the shear friction component in this connection is made up of only the cohesion and interlock component of the CIP concrete (poured to finish the connection) to the surrounding material or precast element. The current connection details are shown in Figure 2-4 and Figure 2-5.

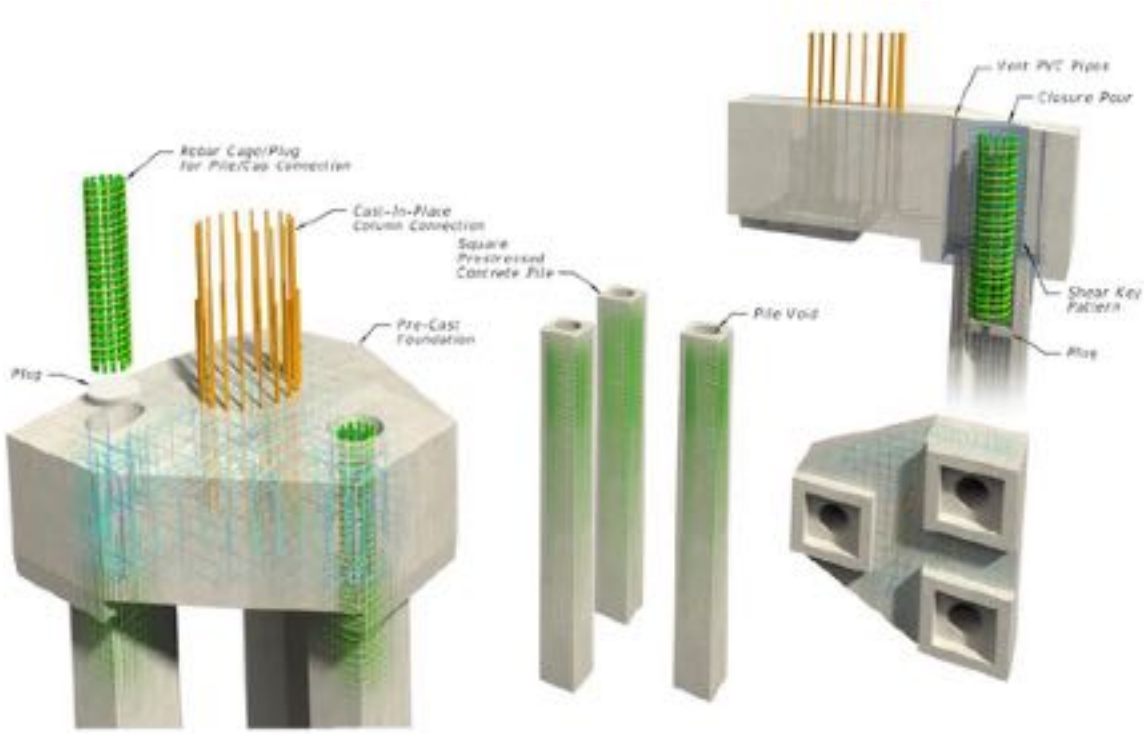

Figure 2-4: Precast Footing Connection use for FDOT (Florida Department of Transportation, 2017).

Some of the main details for this type of connection presented in the FDOT *Structures Detailing Manual* (Florida Department of Transportation, 2017) are shown in Figure 2-6 and listed below:

- Use of corrugated pipe to simulate a shear key system to transfer the shear (in the absent of reinforcement crossing the interface)
- Use a square pile into a circular void to provide a larger bearing area
- Use of a shrinkage reduce add mixture and seven-day moist cure of plug concrete
- Sand or water blast the interface surface

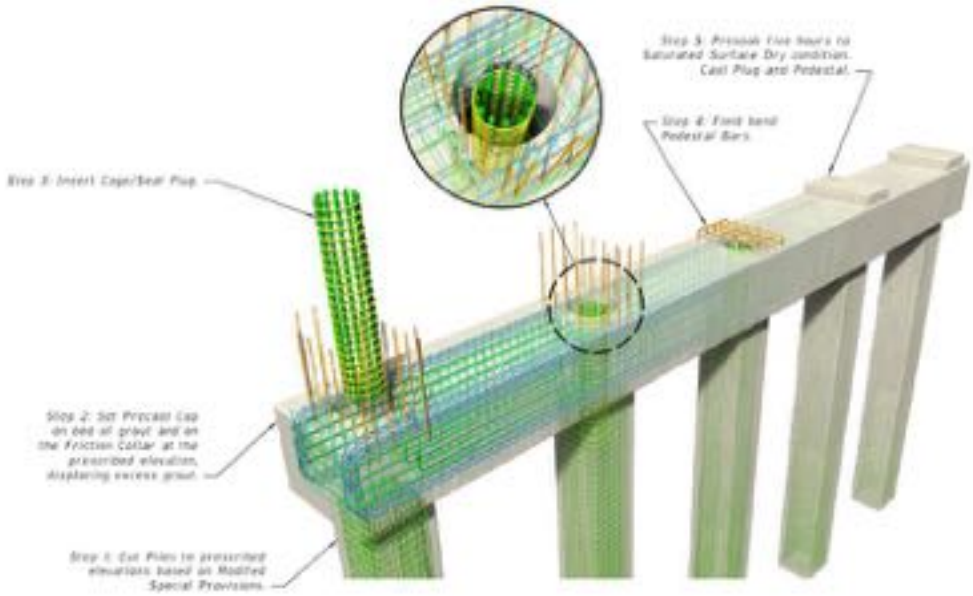

Figure 2-5: Pile Cap Erection Process (Florida Department of Transportation, 2017)

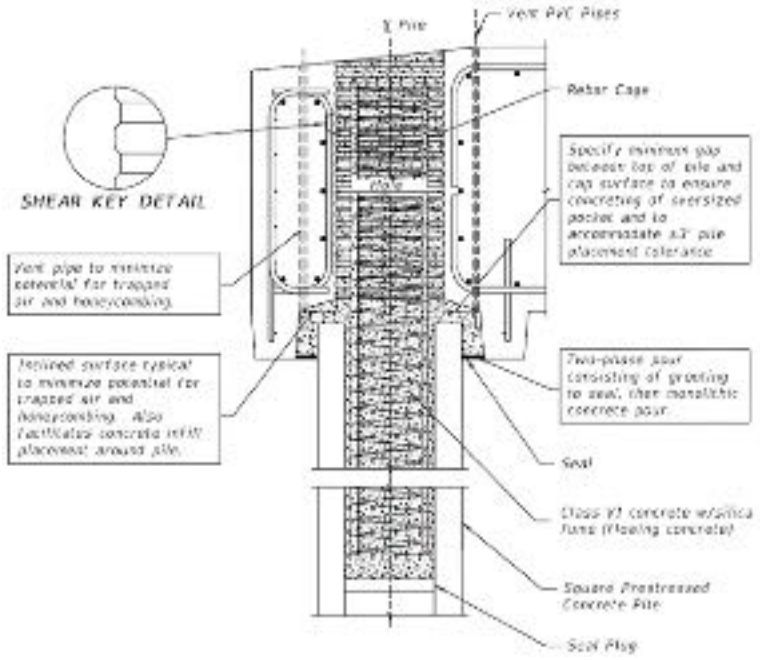

Figure 2-6: Precast Footing Details (Florida Department of Transportation, 2017)

2.3. Shear Friction Overview

This chapter includes an overview of theoretical background of the shear friction mechanism and prefabricated bridge elements and systems.

Shear friction is a term used to describe the shear transfer mechanism along the interface between two concrete members or two adjacent sections of one member that can slip relative to each other (Rahal, 2010). Shear friction is also known as concrete-to-concrete friction, interface shear transfer, and aggregate interlock (Ali & White, 1999). Shear friction is typically critical either at cold joints or geometric discontinuities, where a small piece of concrete enters a large concrete region. Some examples of shear friction in practice include (International Federation for Structural Concrete (fib), 2010):

- Repairing or strengthening an existing reinforced concrete member through adding new concrete layers;
- Supplementing precast elements with concrete cast on the site;
- Casting a new concrete against a concrete that has been completely hardened because the erection process was interrupted;
- Post-installations of concrete elements attached to existing members for introduction of loads; and
- Field connection of precast elements using cast-in-place concrete connections.

Some of these examples found in practice are shown in Figure 2-7.

The shear friction capacity of an interface is dependent on many different factors and has been studied by numerous researchers (Ali & White, 1999; Bass et al., 1989; Hofbeck et al., 1969b; Julio et al., 2004; Mattock & Hawkins, 1972; Mohamad et al., 2015; Randl, 2013; Santos et al., 2007; Santos & Julio, 2011). As will be discussed later, the primary parameters affecting the shear transfer in a concrete interface include (Mattock & Hawkins, 1972):

- Surface roughness and preparation,
- Reinforcement crossing the interface,
- Applied normal force,
- Concrete strength, and
- Concrete curing conditions.

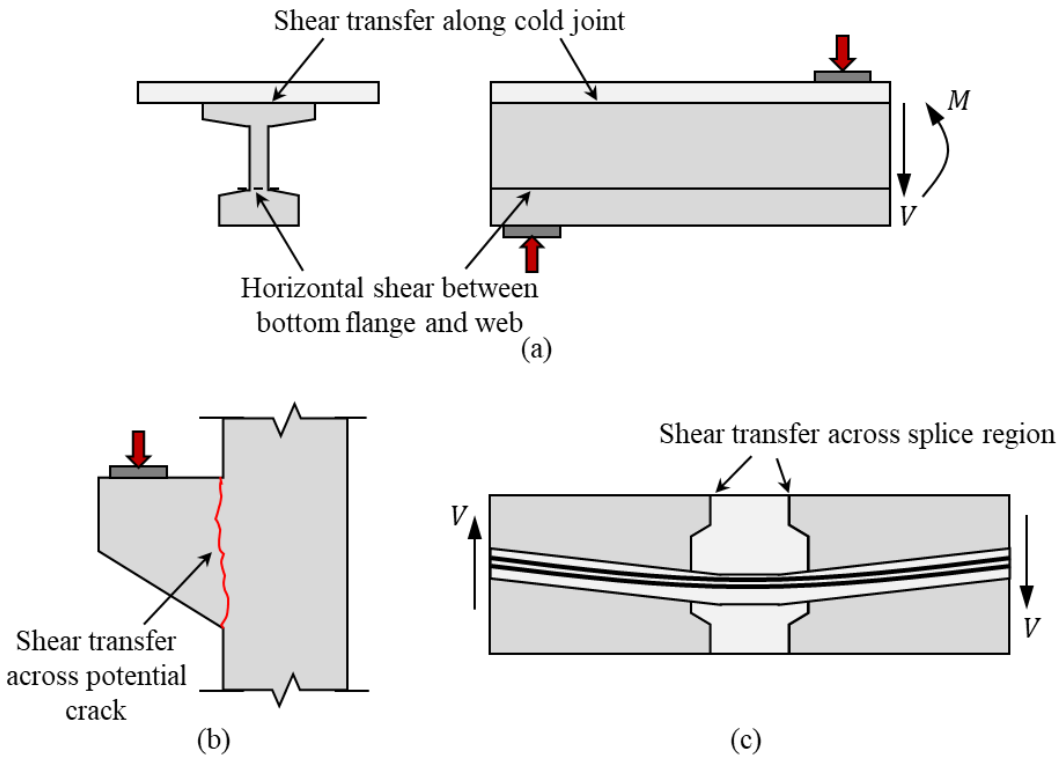

Figure 2-7: Examples of shear friction in (a) composite girder, (b) corbel, and (c) splice region (or other joint between precast members)

The most common test to evaluate the shear capacity in an interface is known as "push-off" test, as shown in Figure 2-8, where typically two L-shaped sections are cast against each other letting one harden before the other one is connected at the interface. Over the years, more tests have been developed to evaluate the bond strength and the tension strength in the interface connection, but the push-off test is still the standard.

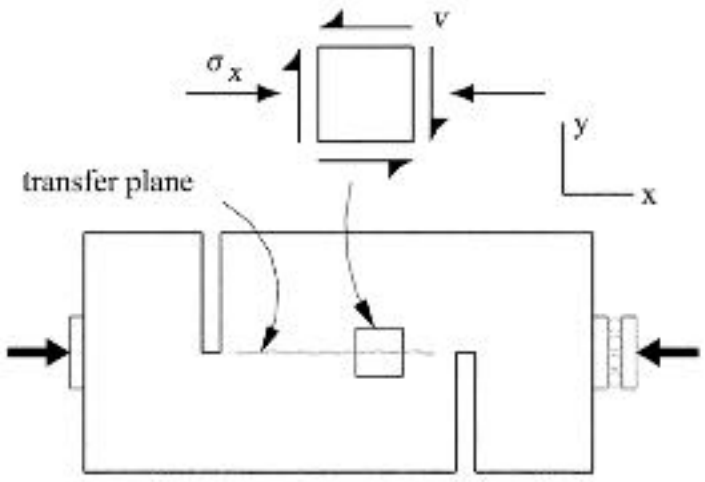

Figure 2-8: Typical push-off specimen and state of stress along shear transfer plane (Rahal, 2010)

2.4. History of Shear Friction

Throughout the years many changes and improvements have been made in the way engineers account for the shear transfer capacity of interfaces between two different materials: either concrete to steel or concrete to concrete. A selection of the studies summarized in this paper are described in more detail in this section to give a brief overview of the history of shear friction research efforts and development of predictive equations.

2.4.1. Original Shear Friction Theory

Birkeland and Birkeland (Birkeland & Birkeland, 1966) was one of the earliest efforts to propose a shear friction theory. During their larger project investigating the connection between precast elements, Birkeland and Birkeland highlighted that many of these connections show distress around the shear interfaces. For this reason, they attempted to develop a shear friction hypothesis to represent the observed behavior of this interface. Their theory revolves around the difference in friction behavior between smoother and rougher interfaces, as shown in Figure 2-9.

Typically, friction capacity is dependent on the normal force that is present perpendicular to the friction plane, shown in Figure 2-9 (a). Birkeland and Birkeland (Birkeland & Birkeland, 1966) proposed that along the rougher shear friction planes present in reinforced

concrete structures sliding along the friction plane can cause separation of the planes. This separation is then resisted by steel crossing the plane, which introduces the "normal force" required in the typical friction model, as shown in Figure 2-9 (b). This model is referred to as a "saw tooth model" and has been used to explain the shear friction mechanism ever since.

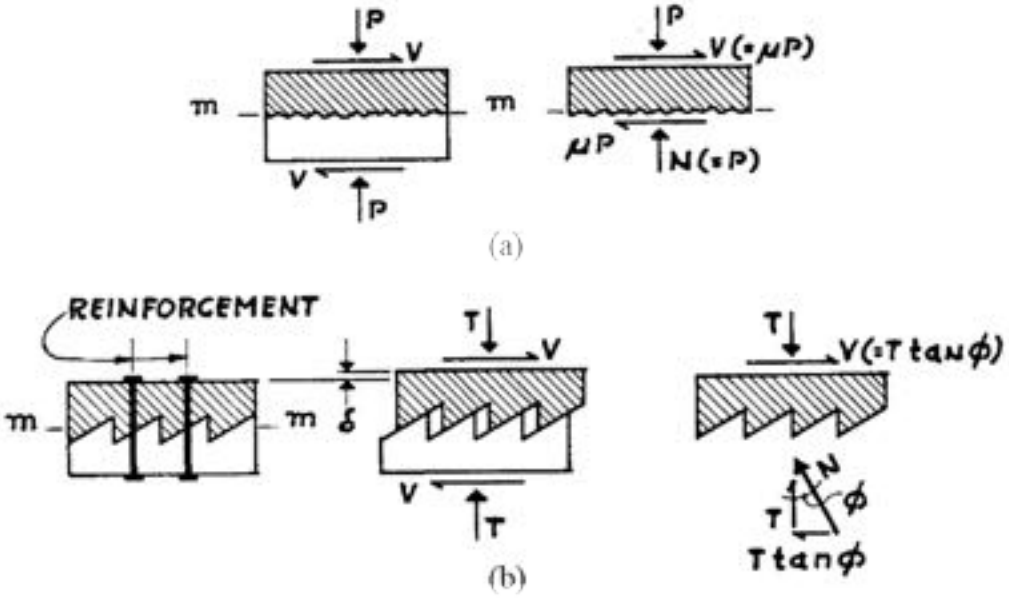

Figure 2-9: Shear friction models for (a) smoother and (b) rougher surfaces (Birkeland & Birkeland, 1966)

Birkeland and Birkeland (Birkeland & Birkeland, 1966) developed a linear expression to estimate the shear transfer capacity between two concrete interfaces based on their above saw-tooth model, shown in Equation 2-1.

$$v_u = \rho f_y \mu \qquad \text{Equation 2-1}$$

Where:

- ρ = reinforcement ratio
- f_y = reinforcement yield strength
- μ = friction coefficient, represented by $\tan\phi$ in Figure 2-9 (b)

Birkeland and Birkeland (Birkeland & Birkeland, 1966) determined their friction coefficients and validated their proposed equation based on previous data from push-off tests (Anderson, 1960) (Mast, 1962), and girder tests (Mattock & Kaar, 1961). Birkeland and Birkeland (Birkeland & Birkeland, 1966) decided to provide limits on Equation 2-1 based on results from unpublished work by Mast (Mast, 1962).

- $\rho < 1.5\%$
- $v_u < 800$ psi

2.4.2. Dowel Action and Cohesion Components

Mattock and Hawkins (Mattock & Hawkins, 1972) undertook a large experimental investigation on shear friction behavior looking primarily at the following variables:

1. Characteristics of the shear plane,
2. Characteristics of the reinforcement,
3. Concrete strength, and
4. Direct stresses acting parallel and transverse to the shear plane.

The specimens were tested using push-off, pull-off, and modified push-off test configurations, described later in Section 2.4.5.

From their experimental results and further development of the shear friction theory, Mattock and Hawkins (Mattock & Hawkins, 1972) suggested that in addition to the saw-tooth effect observed in already cracked concrete, there will also be capacity gained from the dowel action of the reinforcement and some stress carried through a compression strut crossing uncracked concrete. They observed that by not considering the dowel action and other contributions, the model developed by Birkeland and Birkeland (Birkeland & Birkeland, 1966) yields overly conservative results.

Mattock and Hawkins (Mattock & Hawkins, 1972) proposed an alternative equation for estimating the shear friction capacity of a joint, as shown in Equation 2-2. The first term of the equation is related to cohesion and reinforcement dowel action, and the second one is due to clamping forces.

$$v_u = 200 + 0.8(\rho f_y + \sigma_n) \text{ (psi)} \qquad \text{Equation 2-2}$$

Where:

v_u = ultimate shear stress at the interface (should not be more than 0.3f'c)

ρ = reinforcement ratio

f_y = reinforcement yield strength (50.0-66.0 ksi)

σ_n = normal stress at the interface (positive for compressive stress and negative for tensile)

Mattock further developed his shear friction theories in later works (Mattock, 1994) (Mattock et al., 1976). Equation 2-2 is beginning to take the shape of the current AASHTO LRFD expression for shear friction capacity.

2.4.3. Consideration of Concrete Strength

While many earlier research efforts considered concrete strength as an experimental variable, it was not until work by Loov (Loov, 1978) that the concrete strength was explicitly included into a shear friction capacity equation. He developed the expression shown in Equation 2-3.

$$v_u = k\sqrt{f_c(\rho f_y + \sigma_n)} \qquad \text{Equation 2-3}$$

Where:

f_c = concrete compressive strength

f_y = reinforcement yield strength

σ_n = normal stress at the interface

ρ = reinforcement ratio

k = constant (0.5 for initially uncracked interfaces)

Several researchers after Loov (Loov & Patnaik, 1994) continued including the influence of the concrete compressive strength in their estimation procedures.

Walraven, et al. (Walraven et al., 1987) proposed a non-linear expression to obtain the shear transfer capacity in the interface including the concrete strength (f_c), reinforcement

ratio (ρ), and the reinforcement yield strength (f_y) between a range of 50.0-79.0 ksi, shown in Equation 2-4 to Equation 2-6.

$$v_u = C_1(0.007\rho f_y)^{C_2} \text{ (psi)} \quad \text{Equation 2-4}$$

$$C_1 = 15.686 f_c^{0.406} \text{ (psi)} \quad \text{Equation 2-5}$$

$$C_2 = 0.0353 f_c^{0.303} \text{ (psi)} \quad \text{Equation 2-6}$$

Later, Randl (Randl, 1997) developed an alternate expression to calculate the shear transfer strength in a concrete to concrete interface taking in consideration the influence of cohesion, friction, and dowel action, as shown in Equation 2-7.

$$v_u = \tau_{coh} + \mu\sigma_n + \alpha\rho\sqrt{f_c f_y} \quad \text{Equation 2-7}$$

Where:

τ_{coh} = concrete cohesion due to aggregate interlock

μ = friction coefficient

σ_n = normal stress at the interface due to external load and tension in the shear reinforcement

α = coefficient of flexural resistance of reinforcement (dowel action)

ρ = reinforcement ratio

f_c = concrete compressive strength

f_y = reinforcement yield strength

2.4.4. Maximum Valley Depth (R_v)

Recent research conducted by Santos and Julio (Santos & Julio, 2010) looked more closely at the impact of surface preparation and roughness on the shear friction capacity. The

researchers constructed specimens with several different surface preparations, as shown in Figure 2-10. The surface preparations included:

- As-cast against steel formwork,
- Roughened with wire brush,
- Roughened by sand-blasting,
- Roughened by shot-blasting, and
- Hand scrubbing or raking.

The roughness was quantified using the 2D-LRA method (ASTM International, 2015) and the roughness parameter Maximum Valley Depth (R_v). While previous researchers have considered surface roughness, Santos and Julio (Santos & Julio, 2010) were one of the first to quantify it in this way.

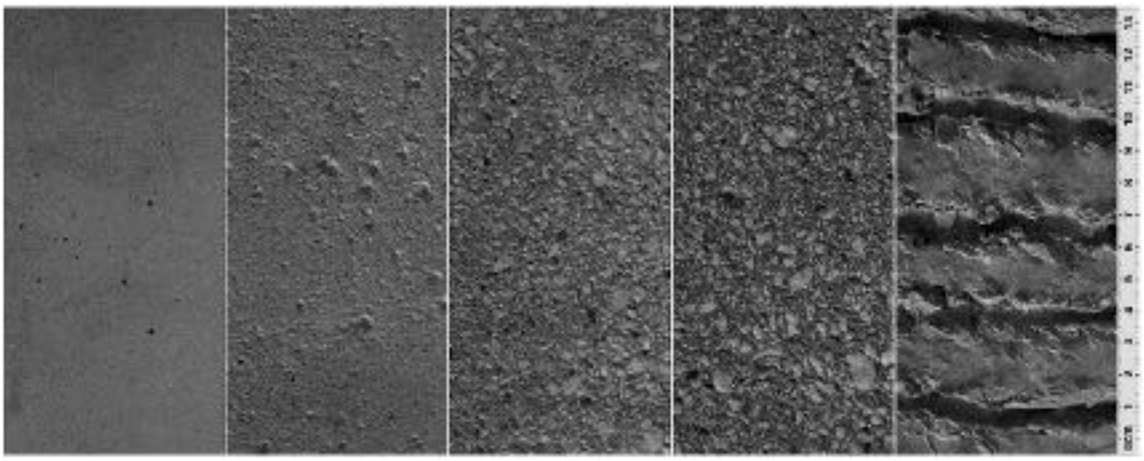

Figure 2-10: Surface preparations for specimens from Santos and Julio (Santos & Julio, 2010)

Santos and Julio (Santos & Julio, 2010) found in their experimental results that the differential shrinkage, the differential stiffness, and the surface preparation are very important factors that could significantly change the behavior of concrete to concrete interfaces.

When no reinforcement is crossing the shear interface, the ultimate shear is shown in Equation 2-8:

$$v_u = c_d f_{ctd} \leq 0.25 f_{cd} \qquad \text{Equation 2-8}$$

When there are reinforcement crossing the shear interface, the proposed expression is shown in Equation 2-9.

$$v_u = \mu_d(\sigma_n + \rho f_y) \leq 0.25 f_{cd}$$ Equation 2-9

In addition to these expressions, they concluded that cohesion and friction coefficients should be calculated in relation to a texture parameter.

$$c_d = \frac{1.062 R_{vm}^{0.145}}{\gamma_{coh}}$$ Equation 2-10

$$\mu_d = \frac{1.366 R_{vm}^{0.041}}{\gamma_{fr}}$$ Equation 2-11

Where:

f_{ctd} = tensile strength of the weakest concrete

f_{cd} = design value of the concrete compressive strength

σ_n = normal stress at the interface due to external load

ρ = reinforcement ratio

f_y = reinforcement yield strength

c_d = design cohesion coefficient

μ_d = design friction coefficient

R_{vm} = Mean Valley Depth of the primary profile of the surface in millimeter

γ_{coh} = partial safety factor for the cohesion coefficient

γ_{fr} = partial safety factor for the friction coefficient

The Mean Valley Depth is taken from Figure 2-11 for five different surface situations: left as cast (LAC), wire brushing (WB), sand blasting (SAB), shot blasting (SHB), and hand scrubbing (HS) or raking.

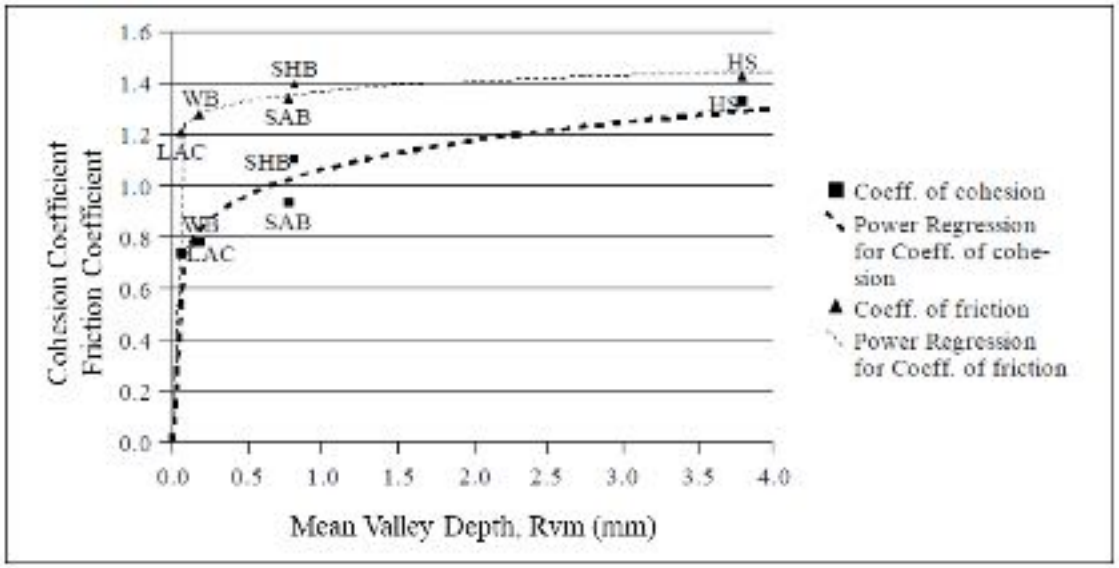

Figure 2-11: Correlation between the Mean Valley Depth (R_{vm}) and the cohesion and friction coefficient (Santos & Julio, 2010)

2.4.5. Conventional Test Methods

Many studies have been carried out to test the shear friction capacity of a variety of different interface planes. The primary four test methods that have been used are: (1) push-off, (2) pull-off, (3) modified push-off, and (4) push-through tests. Typical specimens for these tests are shown in Figure 2-12 and a sample of the previous studies using these tests are summarized in Table 2-2.

Table 2-2: Primary test types for shear friction and list of studies using each type

Test Type	List of Studies	
Push-Off	▪ Bass et al. (Bass et al., 1989) ▪ Figueira et al. (Figueira et al., 2016) ▪ Frenay (Frenay, 1985) ▪ Hanson (Hanson, 1960) ▪ Hofbeck et al. (Hofbeck et al., 1969b) ▪ Kahn (L. Kahn & Mitchell, 2002) ▪ Mattock and Hawkins (Mattock & Hawkins, 1972)	▪ Mattock et al. (Mattock et al., 1976) ▪ Mayers et al. (Myers et al., 2013) ▪ Mohamad et al. (Mohamad et al., 2015) ▪ Pruijssers and Lung (Pruijssers & Lung, 1985) ▪ Walraven and Reinhardt (Walraven & ReinHardt, 1981) ▪ Walraven and Stroband (Walraven & Stroband, 1994)

Test Type	List of Studies	
		▪ Xu et al. (Xu et al., 2015)
Pull-Off	▪ Julio et al. (Julio et al., 2004) ▪ Mattock and Hawkins (Mattock & Hawkins, 1972) ▪ Momayez et al. (Momayez et al., 2005) ▪ Long and Murray (Long & Murray, 1984)	▪ Santos at al. (Santos et al., 2007)
Modified Push-Off	▪ Mattock and Hawkins (Mattock & Hawkins, 1972)	
Push Through	▪ Williams et al. (Williams et al., n.d.)	

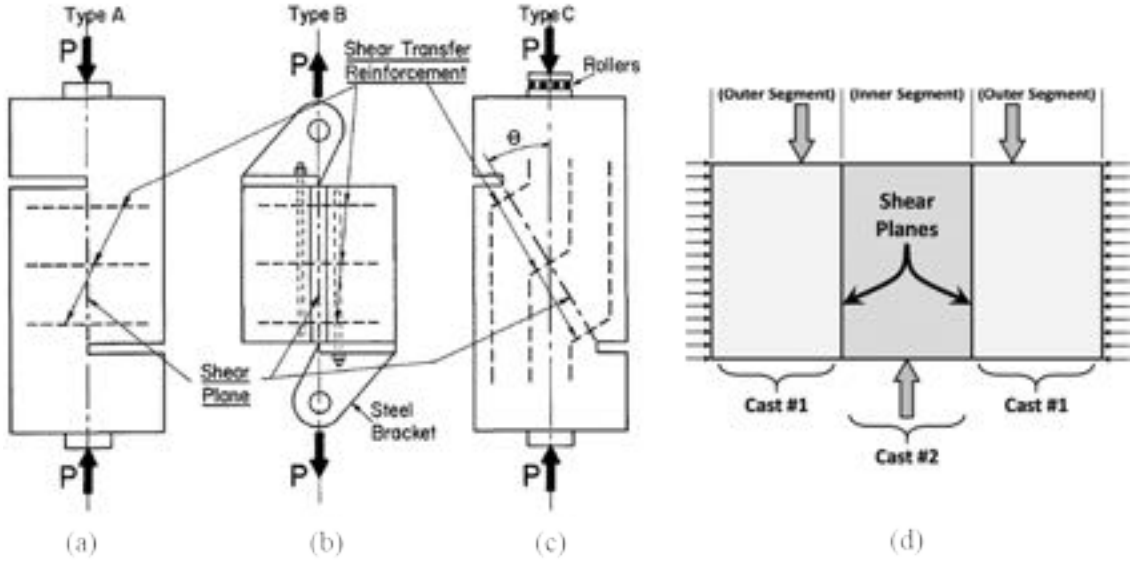

Figure 2-12: Typical test specimens used for (a) push-off tests, (b) pull-off tests, and (c) modified push-off tests (Mattock & Hawkins, 1972) and (d) push-through tests (Williams et al., n.d.)

2.4.5.1. Push-Off Test

The most common test to evaluate the shear friction capacity in an interface between dissimilar materials is called a "push-off" test. Even though the push-off test is not a standard test (i.e. it is not standardized by ASTM), it is a well-known test which has been used by many researchers, as shown in Table 2-2. Examples of push-off tests are illustrated in Figure 2-9 and Figure 2-12.

There have been several different varieties of the push-off test, but most of them have the same key steps, components and characteristics, as shown in Figure 2-13. Normally, the push-off test involves first casting an L-shaped specimen and allowing it to harden, as shown in Figure 2-13 (a). This L-shaped specimen will have reinforcement to strengthen the L-shaped component itself and reinforcement that will cross the interface plane. After the first L-shaped component sufficiently hardens, the second L-shaped component is formed and cast, shown in Figure 2-13 (b). This second L-shaped component typically has the same geometry and reinforcement as the first L-shaped component. After the second L-shaped component is allowed to harden, the specimen is tested, as shown in Figure 2-13 (c). A normal force can be applied perpendicular to the shear plane to provide a clamping force if desired.

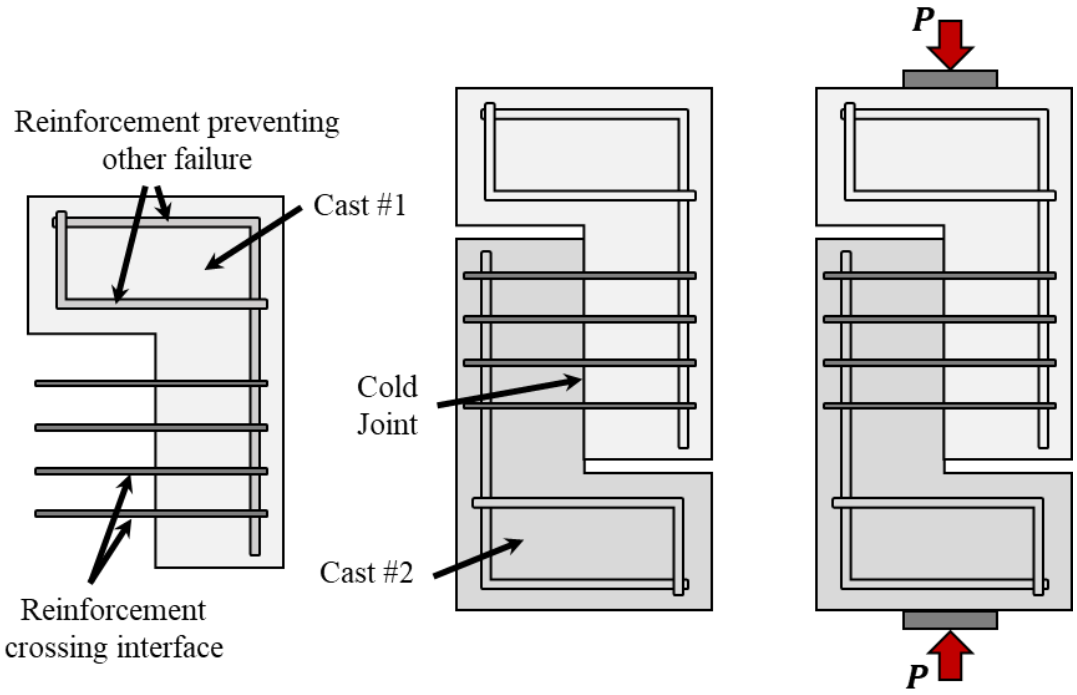

Figure 2-13: Typical casting and testing procedure for push-off tests: (a) casting of first L-shaped component, (b) casting of second L-shaped component, and (c) testing and loading (designated by P) of push-off specimen

While this is the standard construction and testing procedure, there have been several researchers who have modified the procedure to look at specific applications. Hanson (Hanson, 1960) tested the shear strength of the interface between a precast rectangular girder and cast-in-place top deck, shown in Figure 2-14.

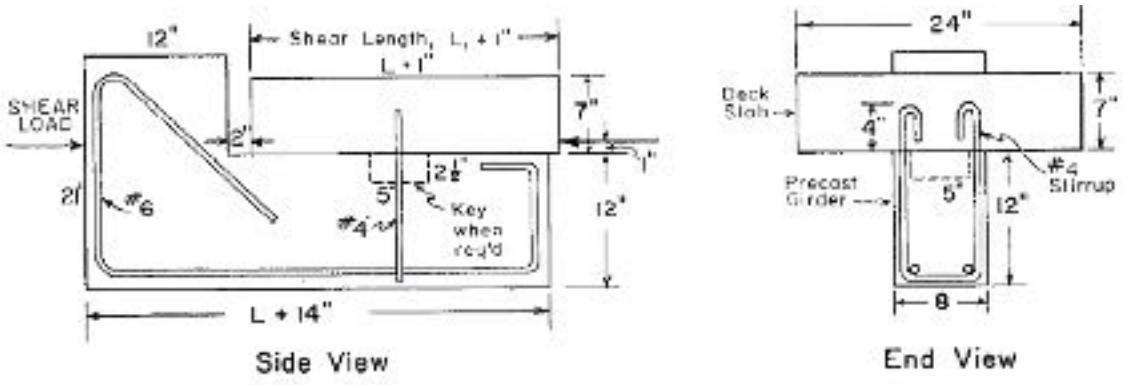

Figure 2-14: Push-off specimen in casting position for looking at interface between beam and composite deck (Hanson, 1960).

Mohamad et al. (Mohamad et al., 2015) constructed specimens with two rectangular concrete layers casted at different times with different compressive concrete strengths and surfaces preparations without steel crossing the interface, as shown in Figure 2-15.

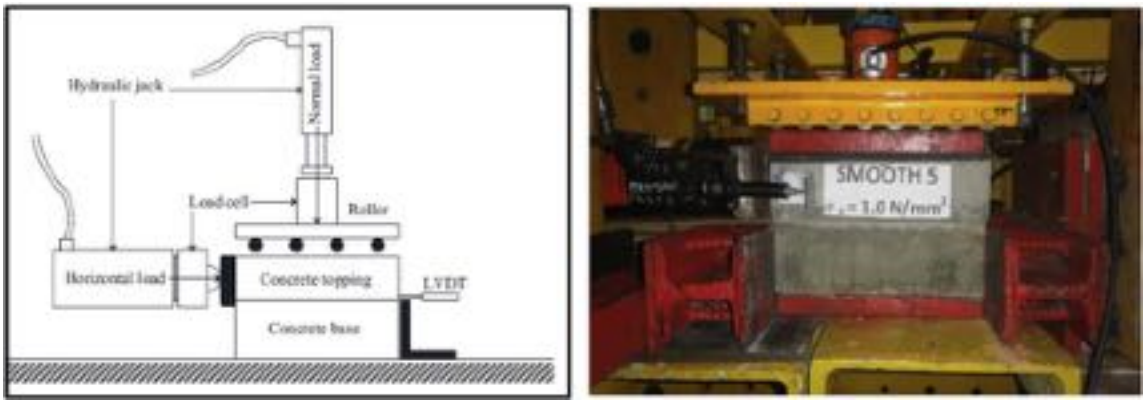

Figure 2-15: Push-off Test Setup (Mohamad et al., 2015)

Hovel et al. (Hovell et al., 2013) also modified the push-off specimen geometry slightly to mimic the bottom flange in a U-beam, where the section is not symmetric outside of the shear plane, shown in Figure 2-16.

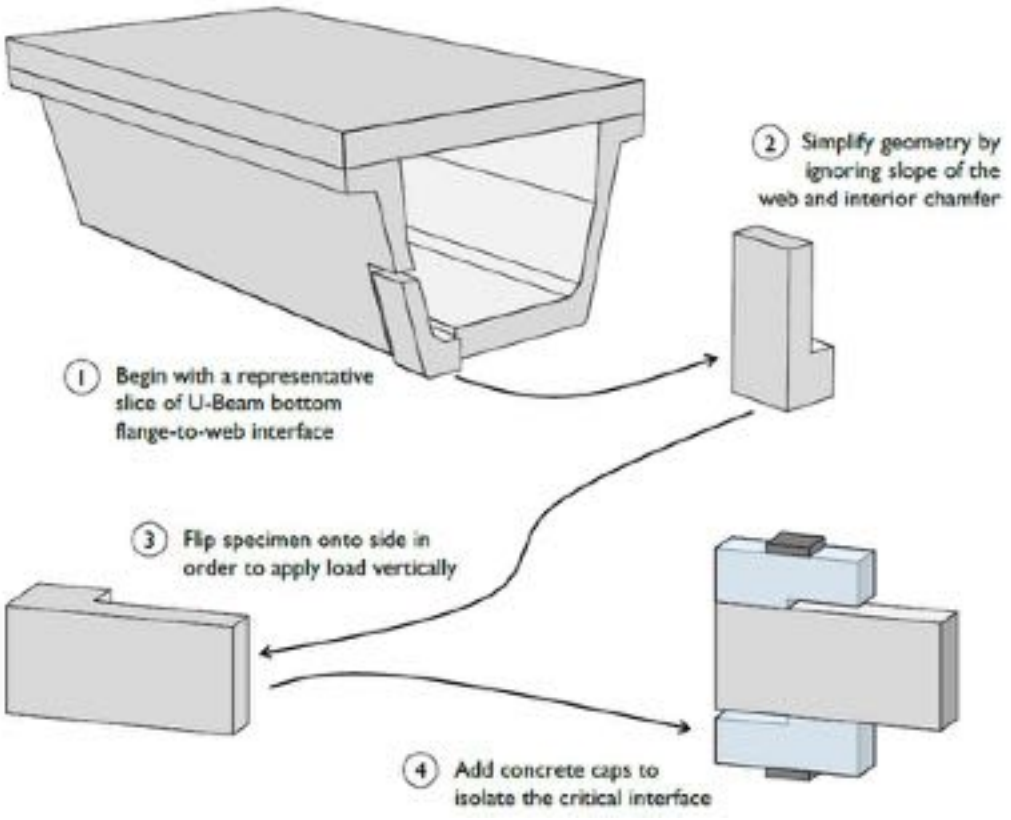

Figure 2-16: Location of shear friction specimen in actual U-beam (Hovell et al., 2013)

The specimen geometry for these tests is shown in Figure 2-17. The reinforcement in these specimens did not cross at the center of the shear plane, as the web reinforcement in the actual U-beam extends into the bottom flange toward the outside face.

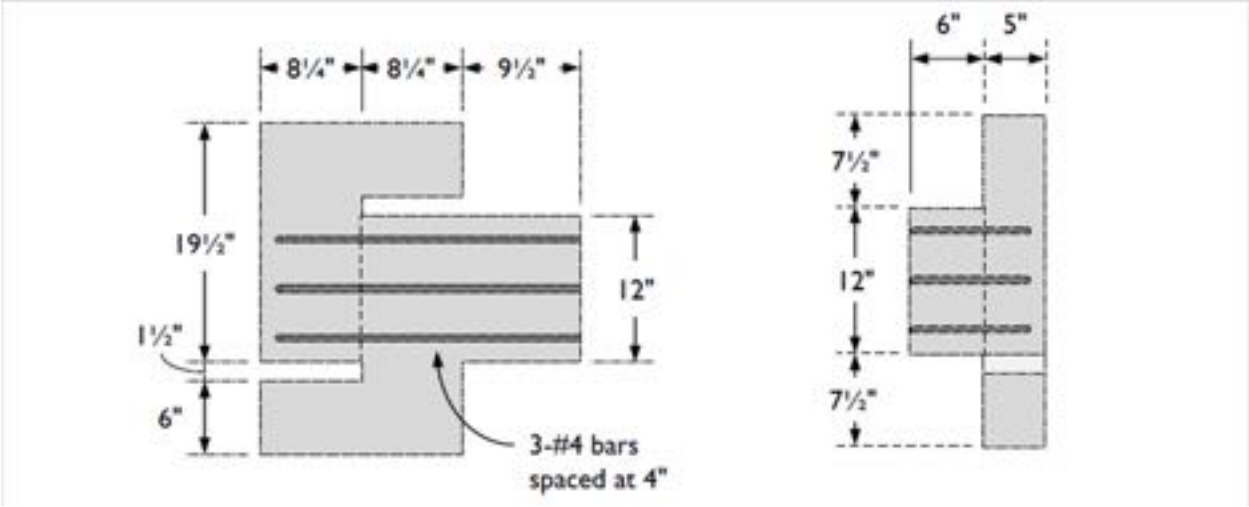

Figure 2-17: Geometry of final specimens with asymmetric reinforcement crossing the shear plane: (a) front view and (b) side view

2.4.5.2. Pull-Off Test

There are two different types of "pull-off" tests that have been used to evaluate the strength of interface planes. The first type was introduced by Mattock and Hawkins (Mattock & Hawkins, 1972) and is similar to the push-off test, shown in Figure 2-12 (b) and Figure 2-18. For this test, a rectangular component is first cast with reinforcement extending out to attach to the load apparatus and to cross the interface plane, shown in Figure 2-18 (a). After the first component hardens, a second rectangular component is formed and cast with reinforcement extending to attach to the load apparatus, shown in Figure 2-18 (b). After the second component hardens, the load apparatus is attached to the specimen and a tension force applied until failure of the shear plane, shown in Figure 2-18 (c).

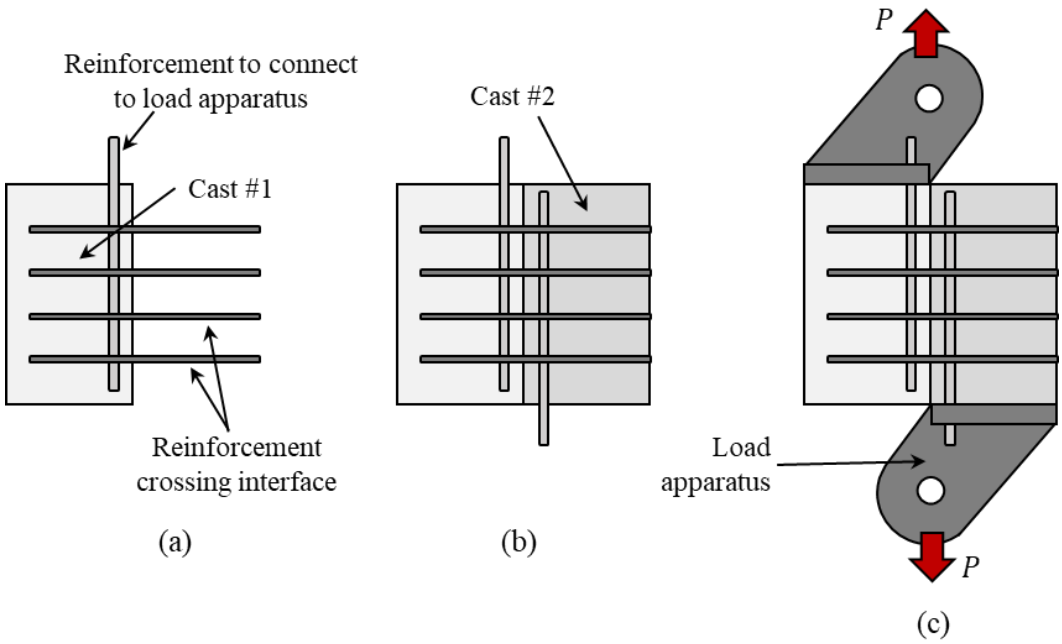

Figure 2-18: Typical casting and testing procedure for pull-off tests: (a) casting of first component, (b) casting of section component, and (c) attaching load apparatus and testing of pull-off specimen.

The second type of "pull-off" test is used to measure the bond strength in tension of concrete-to-concrete interfaces, shown in Figure 2-19. The cast procedure is similar to above, requiring two casts. Unlike above, no reinforcement is typically provided across the interface plane.

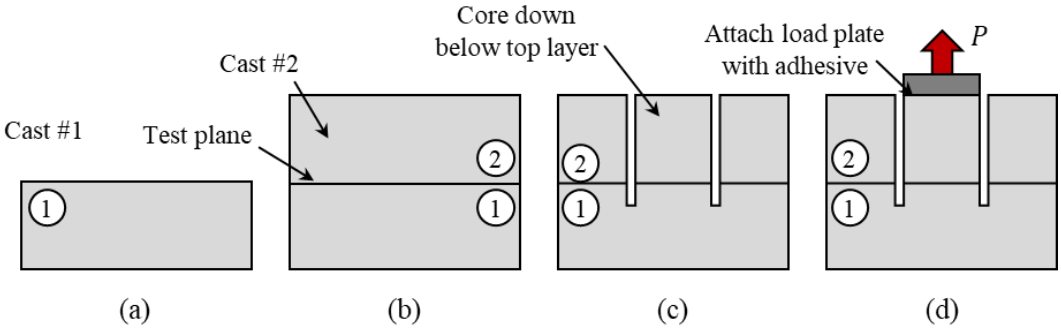

Figure 2-19: Casting and testing procedure for alternate pull-off test: (a) casting of first layer, (b) casting of second layer, (c) core through top layer into bottom layer, and (d) attach load plate and apply tensile force to failure (designated by P)

Although this test does not directly measure the interface shear capacity, bond is closely related to interface shear, so it has been used in the past with other tests to evaluate the performance of interfaces (Julio et al., 2004) (Santos et al., 2007) (Long & Murray, 1984).

2.4.5.3. Modified Push-Off Test

A modified push-off test was also conducted by Mattock and Hawkins (Mattock & Hawkins, 1972) to study the effect of compressive forces acting perpendicular to the interface. The difference between the regular push-off test and the modified push-off test is the angle of inclination (θ) of the interface plane and the reinforcement crossing the interface. The casting and testing procedure for the modified push-off test is similar to push-off tests and is shown in Figure 2-20.

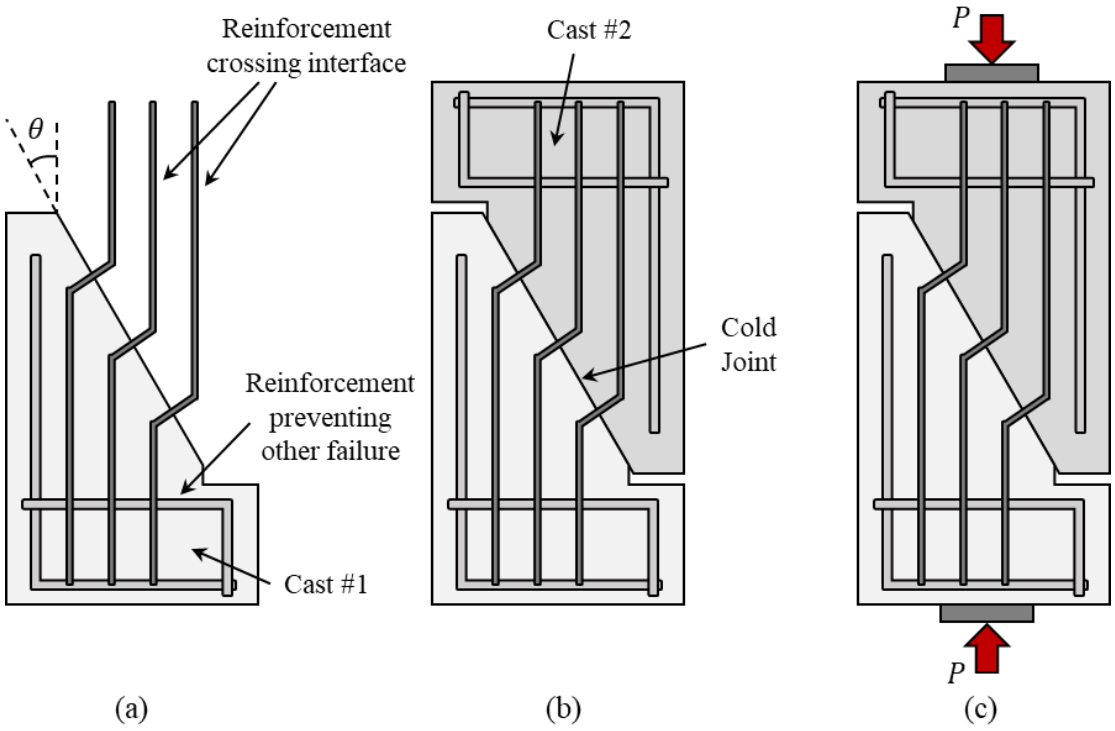

Figure 2-20: Typical casting and testing procedure for modified push-off tests: (a) casting of first component, (b) casting of second component, and (c) testing of modified push-off specimen

Mattock and Hawkins (Mattock & Hawkins, 1972) tested specimens with different angles of inclination and observed two different types of failure: shear failure along the shear plane when the angle was 45 degrees or less and crushing failure for an angles of 60 or 75 degrees.

The modified push-off test is similar to ASTM C882 – Standard Test Method for Bond Strength of Epoxy-Resin Systems Used with Concrete by Slant Shear (ASTM

International, 2013) The difference being that the slant shear test does not typically have reinforcement crossing the shear plane.

2.4.5.4. Push-Through Test

A "push-through" test was proposed and used by Williams et al. (Williams et al., n.d.) to evaluate both the shear friction capacity and the bond strength in the interface between two concrete cast at different times. Williams et al. (Williams et al., n.d.) were specifically investigating the splice region in spliced, post-tensioned girders. Construction and testing of the specimens for the push-through tests is similar to push-off tests, requiring the casting of two outer segments that are cast at the same time and an inner segment cast at later date directly between the outer segments, as shown in Figure 2-21. The effect of shear keys was also investigated by Williams et al. (Williams et al., n.d.).

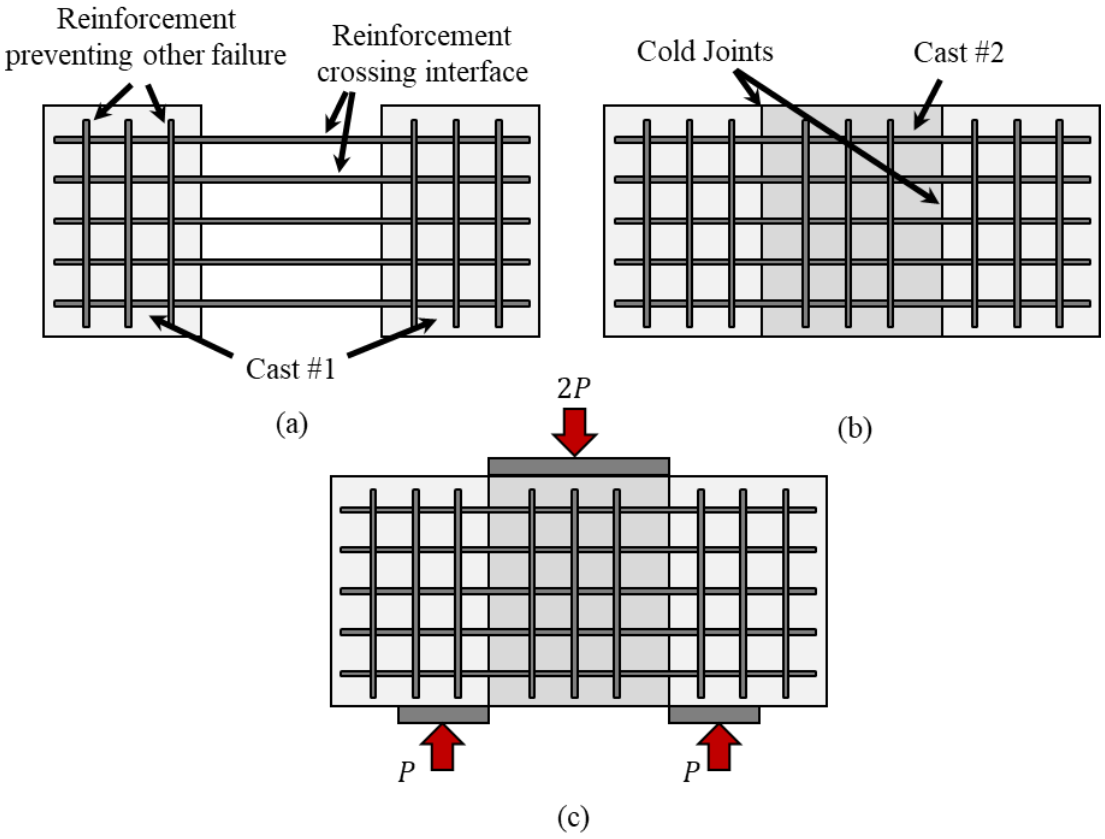

Figure 2-21: Typical casting and testing procedure for push-through tests: (a) casting of first component, (b) casting of second component, and (c) loading (designated by P) and testing of push-through specimen

A mockup of the specimen and test setup for the research is shown in Figure 2-22 Hydraulic cylinders were used to apply a normal force to the friction plane; this was to simulate post-tensioning forces present at the splice region.

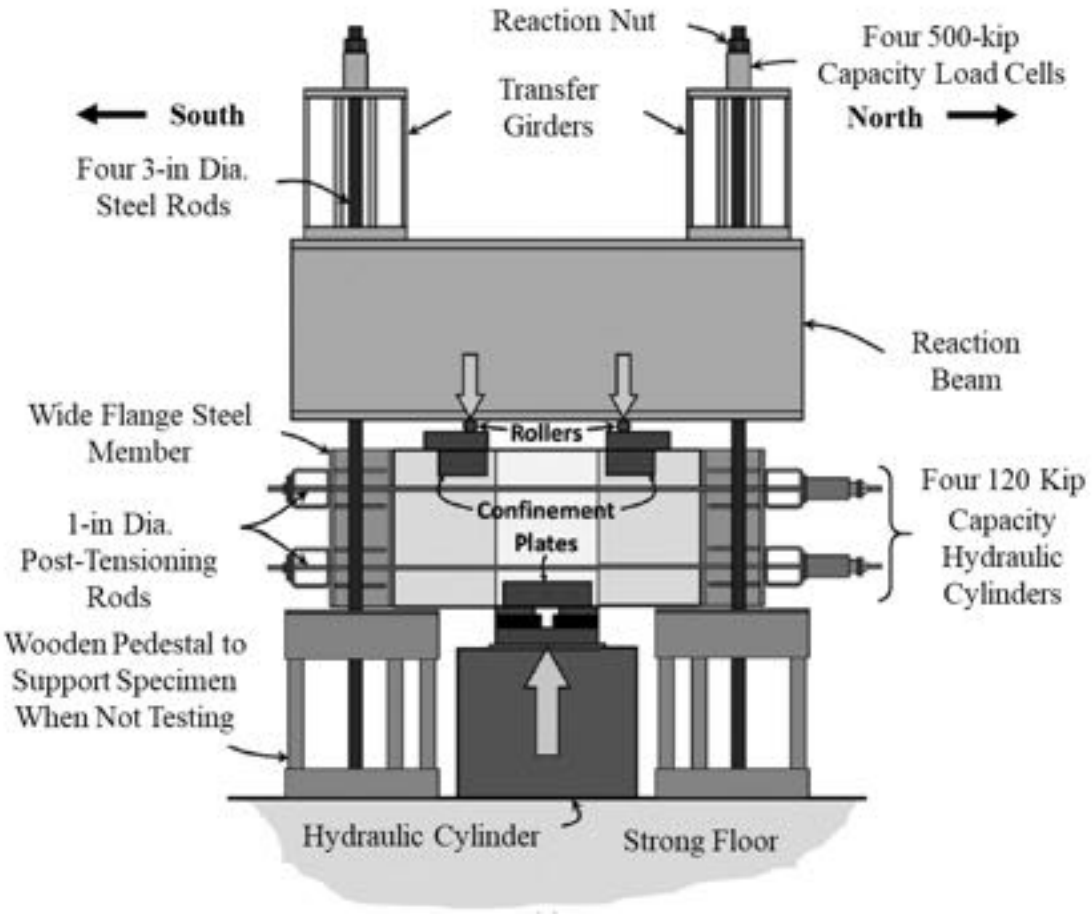

Figure 2-22: Test Setup – Elevation View (Williams et al., n.d.)

2.4.6. Primary Factors Affecting Shear Transfer

The primary parameters affecting the shear transfer in a concrete interface include (Mattock & Hawkins, 1972):

- Surface roughness and preparation,
- Reinforcement crossing the interface,
- Applied normal force,
- Concrete strength, and
- Concrete curing conditions.

The surface roughness, surface preparation and concrete strength will all impact the adhesive bonding between materials at the joint. Better adhesive bonding (or cohesion) can be achieved by having a rougher surface, pre-wetted or pre-treated with an adhesive, and a higher strength concrete closure pour. Cleaning the first-cast surface will also improve the adhesion between layers.

The correlation between the surface texture and preparation and the bond strength in a concrete to concrete surface has been studied for many years by many researchers (Santos et al., 2007), (Kono et al., 2003), (Julio & Santos, 2008). The higher the degree of roughness of a surface, the higher the friction and adhesion bonding (Mohamad et al., 2015). There are several different available techniques to obtain rough surfaces such as high-pressure water-jetting (HPW), milling, shot-blasting or sand-blasting (Randl, 2013). A paste retarder can also be painted on formwork to create an exposed aggregate finish with satisfactory surface roughness.

The curing condition of the joint material has also been suggested to influence the transfer of stresses between concrete surfaces (Santos & Julio, 2011). Improper curing of the joint material can lead to excessive shrinkage, which will introduce a tensile stress between layers and can cause loss of adhesion and cracking at the interface prior to any load being applied. Cracking at the joint can also be caused by temperature deformations or stresses induced during construction (e.g. accidental dropping, twisting during placement, etc.) (Mattock & Hawkins, 1972). Other researchers (Hofbeck et al., 1969b) (Mast, 1962) have also found that this cracking will significantly decrease the shear capacity.

Achieving good adhesive bonding between interfaces will lead to a good development of the mechanical interlocking, which is the second mechanism involved in transferring shear stresses along the friction plane. Mechanical interlocking is illustrated in Figure 2-23. Adhesive bonding at other locations along the friction plane will allow for mechanical interlocking to engage at cracked sections. The friction and mechanical interlocking both depend on the surface roughness and concrete strength.

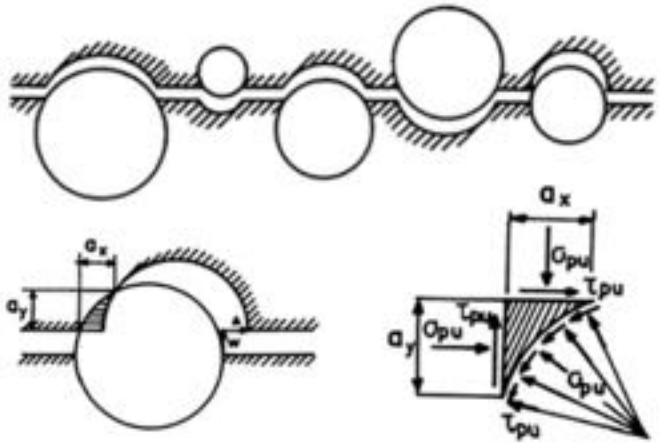

Figure 2-23: Transmission of forces between crack faces (mechanical interlocking) (Randl, 2013)

Mechanical interlocking will decrease as the adhesive bonding fails. This is when the reinforcement crossing the interface will be engaged if present. When there is no reinforcement crossing the interface the shear friction capacity is thought to only be achieved when normal forces are applied and the surface texture of the two layers of concrete are in contact (Randl, 2013). This behavior can be represented in Equation 2-12.

$$\tau = C + \mu\sigma \qquad \text{Equation 2-12}$$

Where:

τ = interface shear strength

C = cohesion strength

μ = friction coefficient

σ = normal stress

The presence of reinforcement crossing the interface will play two roles when transmitting stresses. First, as they slide relative to each other and try to separate, the reinforcement will be placed in tension and will cause a compression (clamping) force to develop at the concrete interface. This clamping force will act like an applied normal force and will cause a friction component to the resistance. Additionally, shifting in the interfaces causes a bending stress in the reinforcement (dowel action), which will lead to crushing of the

concrete in the bending angle (Ali & White, 1999). These mechanisms are illustrated in Figure 2-24.

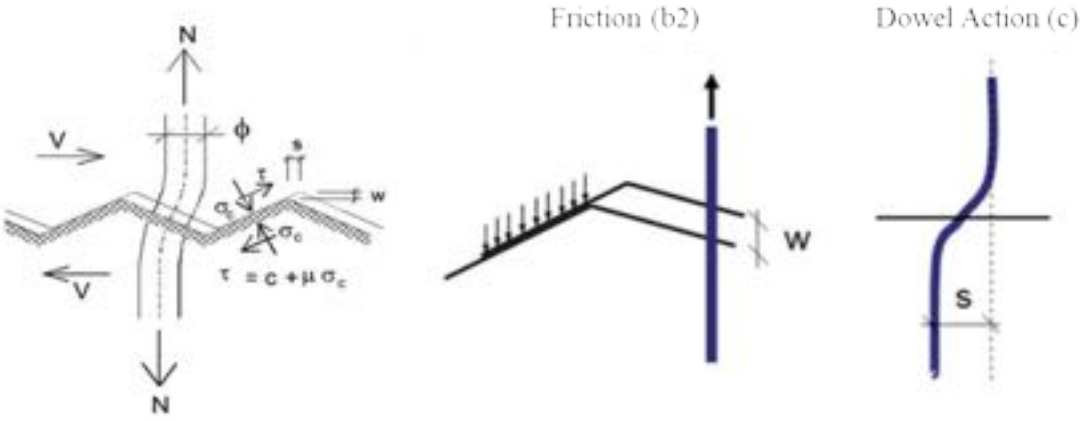

Figure 2-24: Shear resistance mechanisms when reinforcement is crossing interface (Randl, 2013)

According to Randl (Randl, 2013) the presence of the reinforcement as a connector between interfaces will also determine whether a ductile or brittle shear friction failure occurs. When there is no reinforcement the behavior of the section will be brittle. The section loses capacity when adhesion is overcome, and a rigid bond-slip failure occurs. In contrast, when the interface is reinforced the behavior is more ductile, due to the clamping force and dowel action provided by the reinforcement.

2.5. Shear Friction Estimation Procedures

There are numerous procedures for estimating the shear friction capacity of a concrete structure or interface. An overview of several of the prominent procedures is introduced in this section. The procedures discussed include:

- ACI 318-19
- AASHTO LRFD Bridge Design Specification (2017)
- AASHTO LRFD Guide Specification for Accelerated Bridge Construction (2018)
- Federal Internationale de la Precontrainte (fip) 1999
- federation international du beton (fib) Model Code (2010)
- Canadian Standard Association (CSA)

A summary of these codes gives a reasonable overview of how shear friction capacity is currently estimated for buildings and bridges in the US and around the world.

As discussed in the previous section, there are several different components to the shear friction capacity that are common in the design codes, including:

- Cohesion of the concrete-to-concrete interface (cA_{cv}),
- Friction of the interface plane where the normal force is provided by the steel crossing the plane (μA_{vf}) or an applied clamping force (μP_c),
- Limit on capacity based on concrete strength and interface area ($< Kf'_cA_{cv}$)

The components that included in each design code are shown in Table 2-3. Note that each component has a different form in each of the different design codes.

Table 2-3: Summary of components included in shear friction estimation.

Design Code	**Components**			
	$\boldsymbol{cA_{cv}}$	$\boldsymbol{\mu A_{vf}}$	$\boldsymbol{\mu P_c}$	$\boldsymbol{< Kf'_cA_{cv}}$
ACI 318-14		X		
AASHTO LRFD	X	X	X	X
AASHTO ABC	X*			
FIP (1999)	X		X	
Fib Model Code	X	X	X	X
CSA	X	X	X	X

*c on the AASHTO ABC Guide Specification is determine based on square root of concrete strength.

2.5.1. ACI 318-19

The shear transfer strength in any specific plane should be calculated in the presence of:

- An existing or potential crack,
- Interface between dissimilar materials, or
- Interface between two concretes cast at different times.

For each applicable load combination, the design shear strength shall satisfy the relationship shown in Equation 2-13.

$$\phi V_n \geq V_u$$

Equation 2-13

ACI 318-19 (22.9.3.1)

The shear friction capacity depends on the inclination angle of the shear friction reinforcement crossing the interface: Equation 2-14 applies for cases where reinforcement is perpendicular to the shear plane and Equation 2-15 applied for cases where reinforcement is inclined to the shear plane.

$$V_n = \mu A_{vf} f_y$$

Equation 2-14

ACI 318-19 (22.9.4.2)

Where:

A_{vf} = area of reinforcement crossing the shear plane

μ = friction coefficient (Table 2-4: Friction Coefficients (Table - 22.9.4.2 in ACI 318-19)(American Concrete Institute (ACI) Committee 318, 2019).)

Table 2-4: Friction Coefficients (Table - 22.9.4.2 in ACI 318-19)(American Concrete Institute (ACI) Committee 318, 2019).

Contact Surface Condition	**μ**
Concrete placed monolithically.	1.4λ
Concrete placed against hardened concrete that is clean, free of laitance and intentionally roughened to a full amplitude of approximately 1/4in.	1.0λ
Concrete placed against hardened concrete that is clean, free of laitance, and not intentionally roughened.	0.6λ
Concrete placed against as-rolled structural steel that is clean, free of paint, and with shear transferred across the contact surface by headed studs or by welded deformed bars or wires.	0.7λ

Where:

λ = 1.0 for normal weight concrete

= 0.75 for lightweight concrete

If not, λ is calculated based on volumetric proportions of lightweight and normal weight concrete according to part 19.2.4 in ACI 318-19 (American Concrete Institute (ACI) Committee 318, 2019), but λ shall not exceed 0.85.

For cases where reinforcement is inclined to the shear plane, Equation 2-15 applies.

$$V_n = A_{vf} f_y (\mu \sin\alpha + \cos\alpha)$$

Equation 2-15

ACI 318-19 (22.9.4.3)

Where:

α = angle between shear friction reinforcement and the shear plane

μ = friction coefficient (Table 2-4: Friction Coefficients (Table - 22.9.4.2 in ACI 318-19)(American Concrete Institute (ACI) Committee 318, 2019).

The value of the nominal shear strength (V_n) across the interface shall not exceed the limits in Table 2-5. In the case of different strength concretes cast against each other, the lesser of f'$_c$ should be used in Table 2-5.

Table 2-5: Maximum nominal shear strength across the interface (V_n) (Table-22.9.4.4 in ACI 318-19) (American Concrete Institute (ACI) Committee 318, 2019).

Condition	**Maximum V_n**		
Normal weight concrete placed monolithically or placed against hardened concrete intentionally roughened to a full amplitude of approximately 1/4in.	Least of (a), (b), and (c).	$0.2f'_cA_c$	(a)
		$(480 + 0.08f'_c)A_c$	(b)
		$1600A_C$	(c)
Other cases	Lesser of (d) and (e).	$0.2f'_cA_c$	(d)
		$800A_C$	(e)

2.5.2. AASHTO LRFD (2017)

The interface shear transfer in a given interface shall be considered in four cases:

- In the presence of an existing or potential crack,
- In the interface between different materials,
- In the interface between two concrete cast at different ages, or
- In the interface between different elements of the cross-section.

The factored interface shear capacity, V_{ri}, shall be taken as shown in Equation 2-16:

$$V_{ri} = \phi V_{ni}$$

Equation 2-16

AASHTO (5.7.4.3-1)

And the design shall satisfy:

$$V_{ri} \geq V_{ui}$$

Equation 2-17

AASHTO (5.7.4.3-2)

Where:

V_{ni} = nominal interface shear resistance (kip)

V_{ui} = factored interface shear force due to total load based on the applicable strength and extreme event load combinations (kip) based on Table 3.4.1-1 in AASHTO (American Association of State Highway and Transportation Officials (AASHTO), 2017b).

ϕ = resistance factor for shear specified in Table 2-6. For the extreme limit state event ϕ may be taken as 1.0

Table 2-6: Shear Resistance Factor ϕ (American Association of State Highway and Transportation Officials (AASHTO), 2017b).

Condition	**ϕ**	
For shear and torsion in reinforced concrete sections	Normal weight concrete	0.90
	Lightweight concrete	0.90

Condition	ϕ	
For shear and torsion in monolithic prestressed concrete sections and prestressed concrete sections with cast-in-place closures or with match cast and epoxied joints having bonded strands or tendons.	Normal weight concrete	0.90
	Lightweight concrete	0.90
For shear and torsion in monolithic prestressed concrete sections and prestressed concrete sections with cast-in-place closures or with match cast and epoxied joints having unbonded or debonded strands or tendons.	Normal weight concrete	0.85
	Lightweight concrete	0.85

The nominal shear capacity in the interface can be found using Equation 2-18. The capacity differs from the expression found in ACI 318 as it includes a concrete cohesion component (cA_{cv}) and applied clamping force (P_c).

$$V_{ni} = cA_{cv} + \mu(A_{vf}f_y + P_c)$$

Equation 2-18

AASHTO (5.7.4.3-3)

There are two limits placed on the nominal shear friction capacity based on the concrete compression strength (f'_c) and the area of the concrete interface plane (A_{cv}), as shown in Equation 2-19 and Equation 2-20.

$$V_{ni} = K_1 f'_c A_{cv}$$

Equation 2-19

AASHTO (5.7.4.3-4)

$$V_{ni} = K_2 A_{cv}$$

Equation 2-20

AASHTO (5.7.4.3-5)

$$A_{cv} = b_{vi} L_{vi}$$

Equation 2-21

AASHTO (5.7.4.3-6)

Where:

b_{vi} = width of the interface considered to be involved in the shear transfer (in)

L_{vi} = length of the interface considered to be involved in the shear transfer (in)

c = cohesion factor (ksi) (Table 2-7)

μ = friction coefficient (Table 2-7)

Pc = compressive force perpendicular to the shear plane; if force is tensile, Pc = 0.0 (kip)

f'_c = compressive concrete strength of the weaker concrete (ksi)

K_1 = fraction of concrete strength available to resist the interface shear (Table 2-7)

K_2 = limiting interface shear resistance (ksi) (Table 2-7)

All the factors related to the above expressions are shown in Table 2-7:

Table 2-7: Factors to determine the interface shear capacity (American Association of State Highway and Transportation Officials, 2016)

Interface condition	**c (ksi)**	**μ**	**K_1**	**K_2 (ksi)**	
Cast-in-place concrete slab on clean concrete girder surfaces, free of laitance with surface roughened to an amplitude of 0.25in.	0.28	1.0	0.3	Normal weight concrete	1.8
				Lightweight concrete	1.3
Normal weight concrete placed monolithically.	0.40	1.4	0.25	1.5	
Lightweight concrete placed monolithically, or placed against a clean concrete surface, free of laitance with surface intentionally roughened to an amplitude of 0.25 in.	0.24	1.0	0.25	1.0	

Interface condition	c (ksi)	μ	K_1	K_2 (ksi)
Normal weight concrete placed against a clean concrete surface, free of laitance, with surface intentionally roughened to an amplitude of 0.25in.	0.24	1.0	0.25	1.5
Concrete placed against a clean concrete surface, free of laitance, but not intentionally roughened.	0.075	0.6	0.2	0.8
Concrete anchored to as-rolled structural steel by headed studs or by reinforcing bars where all steel in contact with concrete is clean and free of paint.	0.025	0.7	0.2	0.8

2.5.3. AASHTO LRFD Guide Specification for Accelerated Bridge Construction (2018)

The nominal shear transfer resistance at the pocket to precast interface, V_n, shall be calculated as shown in Equation 2-22.

$$V_n = 0.13\sqrt{f'_{cp}}A_{cv}$$

Equation 2-22

ABC Guide (3.6.6.6-1)

Where:

V_n = nominal shear transfer resistance between aa corrugated metal pipe void concrete and precast element (kip).

f'_{cp} = nominal compressive stress of the pocket concrete (ksi).

A_{cv} = cylindrical shaft area of the pocket (in^2).

The area of the pocket, A_{cv}, shall be taken as:

$$A_{cv} = \pi d_v h_v$$

Equation 2-23

ABC Guide (3.6.6.6-2)

Where:

d_v = inside diameter of the CMP pocket (in.).

h_v = effective height of the CMP pocket (in.).

The effective height of the pocket should account the pile embedment length and the distance from the top of the pile to the top of the cap.

2.5.4. FIP (1999)

The recommendations of the International Federation for Prestressing (FIP) points out that the capacity between two concrete interfaces to transfer stresses across them depends on the material characteristics of both faces and the interface conditions. The weaker of the interface materials will control the design.

The FIP equation for shear friction stress capacity is shown in Equation 2-24. There is a cohesion component (βf_{ctd}) and a friction component ($\mu\sigma_{fd}$). The friction component only considers the normal stress applied on the interface (σ_{fd}), not steel crossing the interface plane.

$$\tau_{fd} = \beta f_{ctd} + \mu\sigma_{fd}$$

Equation 2-24

FIP 1999 (5.15)

Where:

β = coefficient depending of the interface condition (Table 2-8)

σ = normal stress on interface (positive is compression)

μ = friction coefficient (Table 2-8)

f_{ctd} = design value of concrete tensile strength

The coefficients β and μ depends on the interface condition, as shown in Table 2-8.

Table 2-8: Coefficients for the friction resistance joints (Table – 5.1 in FIP 1999) (Federation Internationale de la Precontrainte, 1999)

Interface Condition	**β**	**μ**
Very smooth (e.g. cast against steel or plywood formwork)	0.1	0.6
Smooth (e.g. slip formed or extruded, or left without further treatment after compacting)	0.2	0.6
Rough or toothed (indented) (e.g. with expose aggregate, roughened by raking or brushing, or provided with shear keys [indentations])	0.4	0.9

2.5.5. fib Model Code (2010)

In the International Federation for Structural Concrete there are two ways to calculate the shear stress in the interface between two concrete cast at different ages: (1) interfaces intersected by reinforced steel and (2) interfaces connected by dowels. Equation 2-25 should be used for interfaces intersected by reinforced steel. The demand shear (v_{Edi}) must be kept less than the design shear (v_{Rdi}).

$$v_{Edi} \leq v_{Rdi}$$

Equation 2-25

fib (Model Code 2010) (7.3-31)

Where:

v_{Edi} = design value of the shear stress in the interface.

v_{Rdi} = design limit value for the shear in the interface.

$$v_{Edi} = \frac{\beta V_{Ed}}{(z b_i)}$$

Equation 2-26

fib (Model Code 2010) (7.3-32)

$$v_{Rdi} = c f_{ctd} + \mu \sigma_n + \rho f_{yd}(\mu \sin\alpha + \cos\alpha) \leq 0.5 v f_{cd}$$

Equation 2-27

fib (Model Code 2010) (7.3-33)

Where:

β = ratio of the longitudinal force in the new concrete and the total longitudinal force either in the compression or tension zone, both calculated for the section considered

z = inner lever arm of the composed section

b_i = width of the interface

v_{Ed} = shear force on the composed section

c = cohesion factor (Table 2-9)

μ = friction coefficient (Table 2-9)

ρ = reinforcement ratio of the reinforcing steel crossing the interface

σ_n = force normal to the interface

α = inclination of the reinforcement crossing the interface

Table 2-9: Coefficients for the determination of the interface shear strength (Table – 7.3-1 in fib Model Code 2010) (International Federation for Structural Concrete (fib), 2010)

Surface characteristics of the interface	**c**	**μ**
Very smooth (steel, plastic, specially treated timber formwork)	0.025	0.5

Surface characteristics of the interface	c	μ
Smooth (concrete surface without curing)	0.35	0.6
Rough (strongly roughened surface)	0.45	0.7
Very rough	0.5	0.9

The values of *c* found in Table 2-9 must be reduced by 50-percent under fatigue or dynamic loads.

To achieve appropriate interface properties sometimes structures are retrofitted by roughening the interface surface and providing dowels. Equation 2-28 should be used for these cases, interfaces connected by dowels.

$$v_{Rd} = 0.09 k_c f_{ck}^{1/3} + \mu\left(\kappa\rho f_{yd} + \frac{\sigma_n}{\gamma}\right) + \alpha_F\sqrt{f_{yd} f_{cd}} \leq \beta_c f_{cd} b$$

Equation 2-28

fib (Model Code 2010)

(7.3-34)

Where:

k_c = roughness coefficient (Table 2-10)

κ = coefficient for tensile force activated in the reinforcement or the dowels (Table 2-10)

α_F = flexural resistance coefficient (Table 2-10)

β_c = compressive struts coefficient (Table 2-10)

μ = friction coefficient (Table 2-10)

Table 2-10: Coefficients for surface roughness in interfaces reinforced with dowels (Table – 7.3-2 in fib Model Code 2010) (International Federation for Structural Concrete (fib), 2010)

Surface	k_c	κ			μ

Roughness			α_F	β_c	$f_{ck} \geq 20$	$f_{ck} \geq 35$
High pressure water jetting R ≥ 0.5mm	2.3	0.5	0.9	0.5	0.8	1.1
Sand blasting R ≥ 0.5mm	0	0.5	1.0	0.4	0.7	
Smooth	0	0	1.4	0.4	0.5	

2.5.6. CSA (2010)

The Canadian Standards Association has similar design equations for calculating the shear resistance to transfer forces between concrete cast monolithically or concrete placed against hardened concrete with a clean or rough surface. The shear resistance of the plane is found using Equation 2-29.

$$V_r = \lambda \phi_c k \sqrt{\sigma f'_c} + \phi_s \rho_v f_y cos\alpha_f \qquad \text{Equation 2-29}$$

CSA (11-25)

$$\lambda \phi_c k \sqrt{\sigma f'_c} \leq 0.25 \phi_c f'_c$$

Where:

k = 0.5 for concrete placed against hardened concrete

= 0.6 for concrete placed monolithically

α_f = angle between the shear friction reinforcement and the shear plane

$$\sigma = \rho_v f_y sin\alpha_f + \frac{N}{A_g} \qquad \text{Equation 2-30}$$

CSA (11-26)

$$\rho_v = \frac{A_{vf}}{A_{cv}}$$ Equation 2-31

CSA (11-27)

N = unfactored permanent load perpendicular to the shear plane, positive for compression and negative for tension.

Chapter 3: **Experimental Procedure and Testing**

3.1. Introduction

This chapters summarize the test matrix, specimen details, construction of specimens, test setup, loading protocol, instrumentation schedule, experimental and analysis of results of the small and large scale specimens tested to evaluate the shear friction capacity of the interface on pocket connections.

3.2. Small -Scale Testing

The overall objective of the second task was to experimentally evaluate the behavior of the interface between pile cap and plug in the pocket connection used between precast piles and precast pile caps. The primary variables evaluated in this testing were: (1) interface surface condition, (2) corrugation spacing and depth, (3) reinforcement detail around the pocket, and (4) edge distance between the edge of the plug and edge of the pile.

Three different series of tests were used to develop an appropriate test setup and protocol for investigating the behavior of the interface and to evaluate these four variables:

- Series I (4 specimens): used to develop appropriate test setup and protocol
- Series II (20 specimens): evaluate (1) interface surface condition and (2) corrugation spacing and depth
- Series III (13 specimens): primarily evaluate (3) reinforcement detail around pocket and (4) edge distance between plug and edge of pile

This report will summarize the test matrix, specimen details, construction of specimens, test setup and load protocol, instrumentation schedule, estimated strengths, and experimental results.

3.2.1. Test Matrix and Experimental Variables

The experimental variables that were evaluated in this task are presented in Table 3-1 and explained in this section.

Table 3-1: Experimental variables for small-scale testing

Experimental Variable	**Possible Values for Test Matrix**
Interface surface condition	Sandblasted; corrugated pipe left in place; exposed aggregate finish
Corrugation spacing and depth	Smooth, corrugated plastic duct (h_{rib} = 0.875", L_{rib} = 1", s_{rib} = 2"), corrugated metal duct (h_{rib} = 0.5", L_{rib} = 0.75") with different spacing (2.67" and 5.33")
Reinforcement around pocket	Different amounts of reinforcement around the pocket and in the longitudinal direction crossing the splitting plane
Edge distance	$1d_{plug}$, $0.75d_{plug}$, $0.5d_{plug}$

Definitions for the rib length (L_{rib}), height (h_{rib}), and spacing (s_{rib}) are provided in Figure 3-1.

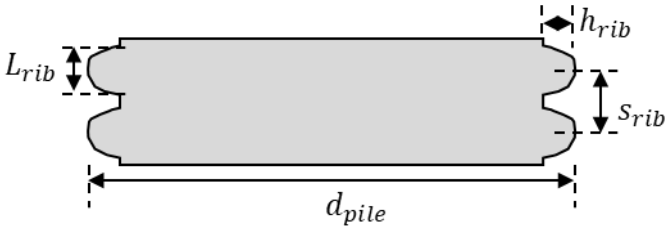

Figure 3-1: Corrugations spacing and depth definitions

The combinations of these variables that were tested are summarized in the test matrices shown in Table 3-2 to Table 3-4.

Table 3-2: Experimental matrix for Series I specimens

#	h_{cap} (in)	Corrugation Spacing and Depth				Interface Surface Condition
		Description	h_{rib} *(in)*	L_{rib} *(in)*	s_{rib} *(in)*	
S1-1	36	Corrugated plastic	0.875	1	2	Sandblasted (1/16" roughness)

#	h_{cap} (in)	Corrugation Spacing and Depth				Interface Surface Condition
		Description	h_{rib} *(in)*	L_{rib} *(in)*	s_{rib} *(in)*	
S1-2	18	Corrugated plastic	0.875	1	2	Sandblasted (1/16" roughness)
S1-3	18	Corrugated plastic	0.875	1	2	Sandblasted (1/16" roughness)
S1-4	36	Smooth	0	0	0	Sandblasted (1/16" roughness)

Table 3-3: Experimental matrix for Series II specimens

#	h_{cap} (in)	Corrugation Spacing and Depth				Interface Surface Condition
		Description	h_{rib} *(in)*	L_{rib} *(in)*	s_{rib} *(in)*	
S2-1	18	Smooth	0	0	0	Sandblasted (1/16" roughness)
S2-2	18	Smooth	0	0	0	Paste retarder (1/4" roughness)
S2-3	18	Single rib (corrugated plastic)	0.875	1	15	Sandblasted (1/16" roughness)
S2-4	14	Smooth	0	0	0	Paste retarder (1/4" roughness)
S2-5	14	Single Rib (corrugated plastic)	0.875	1	11	Sandblasted (1/16" roughness)
S2-6	14	Double Rib (corrugated plastic)	0.875	1	5.5	Sandblasted (1/16" roughness)

S2-7	18	Corrugated metal	0.5	0.75	2.67	Sandblasted (1/16” roughness)
S2-8	18	Corrugated metal (1/2 spacing)	0.5	0.75	5.33	Sandblasted (1/16” roughness)
S2-9	18	Corrugated metal	0.5	0.75	2.67	Corrugated pipe
S2-10	14	Corrugated metal	0.5	0.75	2.67	Sandblasted (1/16” roughness)
S2-11	14	Corrugated metal (1/2 spacing)	0.5	0.75	5.33	Sandblasted (1/16” roughness)
S2-12	14	Corrugated metal	0.5	0.75	2.67	Corrugated pipe
S2-13	18	Smooth	0	0	0	Sandblasted (1/16” roughness)
S2-14	14	Smooth	0	0	0	Sandblasted (1/16” roughness)
S2-15	14	Smooth	0	0	0	Paste retarder (1/4” roughness)
S2-16	18	Corrugated metal	0.5	0.75	2.67	Sandblasted (1/16” roughness)
S2-17	18	Corrugated metal	0.5	0.75	2.67	Corrugated pipe
S2-18	14	Corrugated metal	0.5	0.75	2.67	Sandblasted (1/16” roughness)
S2-19	14	Corrugated metal	0.5	0.75	2.67	Corrugated pipe
S2-20	18	Corrugated metal	0.5	0.75	2.67	Sandblasted (1/16” roughness)

Table 3-4: Experimental matrix for Series III specimens (h_{cap} = 14-inch)

#	Reinforcement		Interface Type	Interface Surface Condition	Edge Distance	
	Around Pocket	*Longitudinal*			*x*	*y*
S3-1	Typical	None	Corrugated pipe	Sandblasted (1/16" roughness)	$1d_{plug}$	$1d_{plug}$
S3-2	None	Typical	Corrugated pipe	Sandblasted (1/16" roughness)	$1d_{plug}$	$1d_{plug}$
S3-3	Typical	2 #4 in all faces	Corrugated pipe	Sandblasted (1/16" roughness)	$1d_{plug}$	$1d_{plug}$
S3-4	2 stirrups 8 vertical bars	Typical	Corrugated pipe	Sandblasted (1/16" roughness)	$1d_{plug}$	$1d_{plug}$
S3-5	None	Typical	Corrugated pipe	Corrugated pipe	$1d_{plug}$	$1d_{plug}$
S3-6	2 stirrups 8 vertical bars	Typical	Corrugated pipe	Corrugated pipe	$1d_{plug}$	$1d_{plug}$
S3-7	Typical	3 #4 in two faces 1 #7 in two faces	Corrugated pipe	Sandblasted (1/16" roughness)	$1d_{plug}$	$1d_{plug}$
S3-8	Typical	3 #4 in three faces 1 #7 in one face	Corrugated pipe	Sandblasted (1/16" roughness)	$1d_{plug}$	$1d_{plug}$
S3-9	Typical	3 #4 in three faces 1 #7 in one face	Corrugated pipe	Sandblasted (1/16" roughness)	$0.5d_{plug}$	$1d_{plug}$
S3-10	Typical	3 #4 in two faces 1 #7 in two faces	Corrugated pipe	Sandblasted (1/16" roughness)	$0.5d_{plug}$	$0.5d_{plug}$
S3-11	Typical	3 #4 in three faces 1 #7 in one face	Corrugated pipe	Sandblasted (1/16" roughness)	$0.75d_{plug}$	$1d_{plug}$
S3-12	Typical	3 #4 in two faces 1 #7 in two faces	Corrugated pipe	Sandblasted (1/16" roughness)	$0.75d_{plug}$	$0.75d_{plug}$
S3-13	Typical	Typical	Monolithic Cast	Monolithic Cast	$1d_{plug}$	$1d_{plug}$

3.2.2. Specimen Geometry and Construction

Details for construction of the cap and plug and the surface preparation used in this task are explained in this section. Some specimens were constructed at FDOT's Structures Research Center (SRC) and some at a precast plant in Miami, FL. The same construction procedure was followed at both locations.

3.2.2.1. Cap and Plug Construction

The procedure for constructing the modified push-through test was as follows:

1. A cube was cast with a cylindrical void in the center (referred to as the "cap"). The size of the cap and the diameter of the void varied. The cylindrical void was constructed using corrugated metal pipes, corrugated plastic pipes, and Sonotubes (smooth cylindrical tubes) to vary the corrugation spacing and depth, as shown in Figure 3-2.

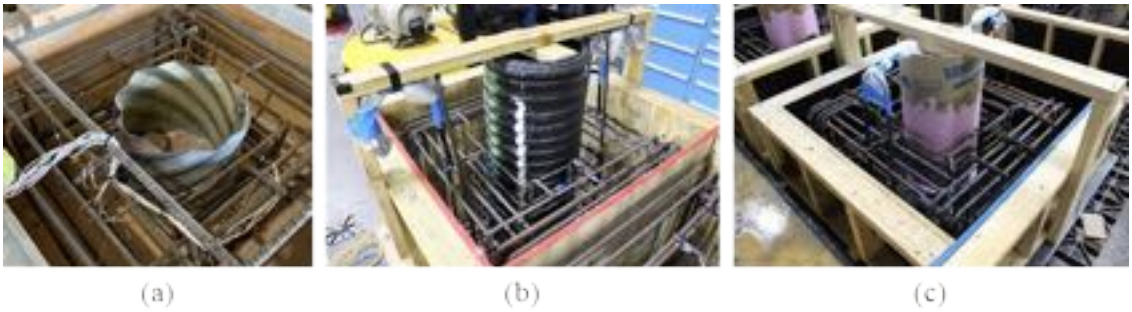

Figure 3-2: Construction of cap and installation of blockout for void with (a) corrugated metal pipe, (b) corrugated plastic pipe, and (c) Sonotube

2. The pipe was removed after the concrete in the cap hardened (typically 1 to 3 days after casting of the cap), as shown in Figure 3-3. The surface preparation after removal of the pipe varied based on the desired interface condition.

Figure 3-3: (a) Removal of corrugated pipe and (b) surface finish after removal of pipe and sandblasting

3. After the pipe was removed and the interface surface properly prepared, a 3-inch cylindrical form with the same diameter as the plug was placed on top of the cap and a 3-inch blockout was installed at the bottom of the plug, as shown in Figure 3-4. The plug was cast between 5 and 163 days after the cap (see §3.2.2.4).

Figure 3-4: Plug construction: (a) typical plug reinforcement, (b) 3-inch cylindrical form on top of cap, (c) casting of plug concrete, and (d) 3-inch blockout on bottom of plug (after testing)

4. After the concrete had hardened, the formwork and foam blockout were removed. The precast specimens were then shipped to FDOT's Structures Research Center and prepared for testing. The finished specimens were tested between 16 and 178 days after initial casting.

Figure 3-5: Finished specimens for (a) part of Series II and (b) Series III

3.2.2.2. Surface Finishes

Three different surface preparations were used for the specimens: Sandblasted (1/16'' of roughness), exposed aggregate (1/4'' of roughness), and keeping the metal duct in place, as shown in Figure 3-6. The sandblasted surface condition was obtained by:

1. Removing the corrugated pipe used to form the pocket in the pile cap,
2. Sand or water blasting the interfacing surface,
3. Prewetting of the surface using wet burlap on the surface for 4 to 5 hours, and
4. Removing the wet burlap prior to pouring concrete.

The prewetting of the surface was done with a yard type sprayer used periodically throughout the day rather that sealing and filling the void with potable water due to the logistical challenges of filling the void with water in the laboratory where the about half of the specimens were constructed. The sandblasted surface condition is shown in Figure 3-6 (a).

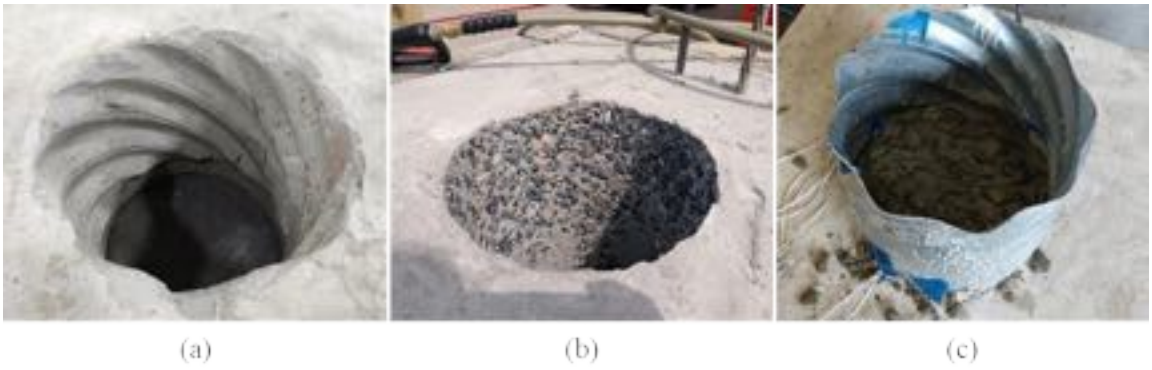

Figure 3-6: Surface preparation for second series of specimens: (a) sandblasted, (b) paste retarder, and (c) corrugated metal duct

A ¼-inch exposed aggregate finish, shown in Figure 3-6 (b), was achieved using the following procedure:

1. A polyurethane clear coat was applied to the cylindrical void to prevent the set retarding agent from primarily being absorbed by the form, as shown in Figure 3-7 (a).
2. The set retarding agent was applied to the formwork where the exposed aggregate finish was desired (i.e. the plug) within 24 hours of the casting time, shown in Figure 3-7 (b). The specimens were cast either inside the SRC or under cover at the precast facility, so the specimens were not exposed to any moisture. It is important

to protect the specimens from moisture as the set retarding agent is moisture activated.

3. The plug void was then placed in the cap, Figure 3-7 (c), and the cap concrete cast.
4. The plug form was removed within 24 hours of casting and a pressure washer was used to wash away the unhydrated paste on the surface of the plug. Care was taken to ensure the paste was washed away without fracturing the aggregate.
5. The surface of the plug interface was prewetted similar to the specimens with sandblasted finish.

Figure 3-7: Procedure for achieving exposed aggregate finish: (a) application of polyurethane clear coat, (b) application of set retarding agent, (c) placement of void in cap, and (d) finish after pressure washing surface

Finally, several of the specimens had the corrugated metal duct left in place, creating a smooth concrete on steel connection, as shown in Figure 3-6 (c).

3.2.2.3. Observations from Construction

One adjustment was made in the construction of some of the Series II and all the Series III specimens when the corrugated pipe was left in place. Rotation of the plug was observed in the first two specimens in Series II with the corrugated metal duct left in place (S2-9 and S2-12), as shown in Figure 3-8 (a). For later specimens, the corrugated metal duct was cut at mid-height and rotated so that the corrugations did not align at the cut, as shown in Figure 3-8 (b). This was done to try and resist the rotation of the plug during testing. The two pieces were welded, and tape was used inside the pipe to avoid intrusion of the concrete when pouring the cap, as shown in Figure 3-8 (c).

Figure 3-8: (a) Rotation observed in S2-12, (b) detail of the corrugated metal pipe when the pipe was left in place in later specimens, and (c) installed metal pipe with tape inside blocking voids

3.2.2.4. Casting Dates for Caps and Plugs

The casting dates for the caps and plugs, the age of the cap at time of plug casting, and the age of the plug at the time of testing are summarized in Table 3-1. Specimen S2-20 was cast specifically to investigate the effect of additional time between casting of the cap and plug.

Table 3-5: Casting dates for caps and plugs and age of cap at time of plug casting

Specimens	**Casting Date**		**Age of Cap at Plug Cast (days)**	**Avg. Plug Age at Testing (days)**
	Cap	*Plug*		
S1-1 to S1-4	12/13/18	1/11/19	29	38
S2-1 to S2-6	6/26/19	7/29/19	33	18
S2-7 to S2-12	7/24/19	7/29/19	5	23
S2-13 to S2-19	3/2/20	3/9/20	7	150
S2-20	3/2/20	8/12/20	163	16
S3-1 to S3-13	8/11/20	8/18/20	7	35

3.2.3. Test Setup and Loading Protocol

A schematic and photograph of the test setup are shown Figure 3-9. The load was applied to the specimens using a 750-kip hydraulic jack and a 600-kip load cell attached to a load frame with a 1,000-kip capacity. The load cell was calibrated to 150% overload, so 750 kips was still within the calibrated range of the load cell.

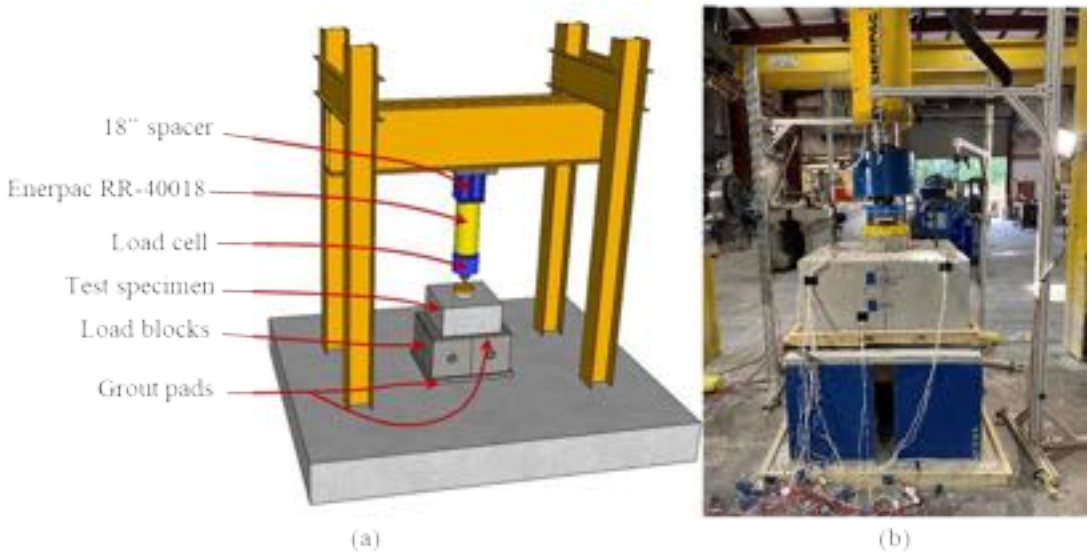

Figure 3-9: (a) Schematic and (b) photograph of test setup for small-scale specimens

The specimens were placed on top of four load blocks for testing. The load blocks were separated 2 to 3-inch apart, as shown in Figure 3-10, to leave room for a laser displacement transducer to measure the deflection of the bottom of the plug.

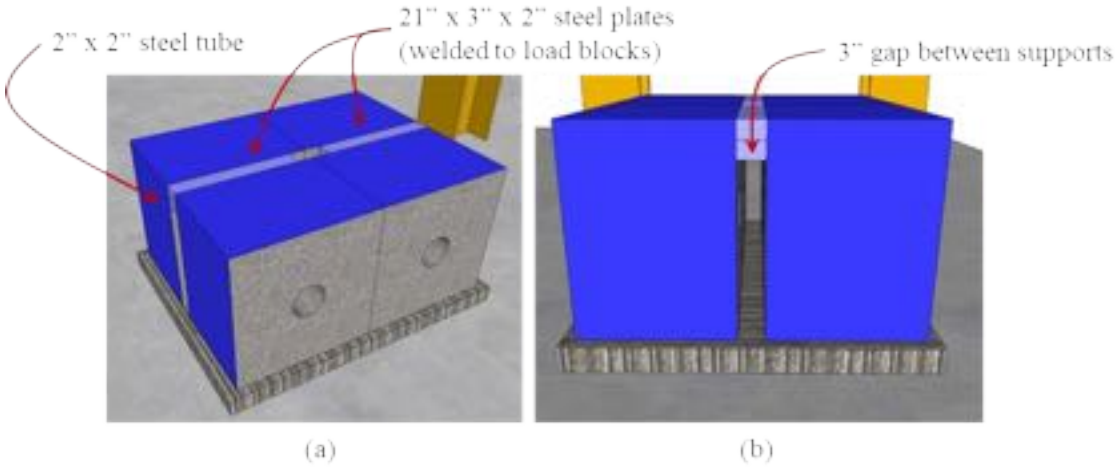

Figure 3-10: Load blocks used in the test setup with 3-inch of separation (a) overview and (b) lateral view of gap.

All specimens were tested using the same loading procedure. The load was applied at a rate of 0.2 kips per second until a load of 200 kips for all specimens. A sample load versus deflection plot for S3-1 with the load of 200 kips highlighted is shown in Figure 3-11 (a). The 200-kip load was held on the specimens at this point while the specimens were inspected for cracks; cracks were marked, labeled, and documented, as shown in Figure

3-11 (b). Load was then applied at the same load rate (0.2 kips per second) until failure of the interface or test capacity was reached. Cracks were marked on all sides (including the bottom) of the specimens after they were removed from the test frame. A sample crack pattern on the bottom of Specimen S3-1 after failure is shown in Figure 3-11 (c).

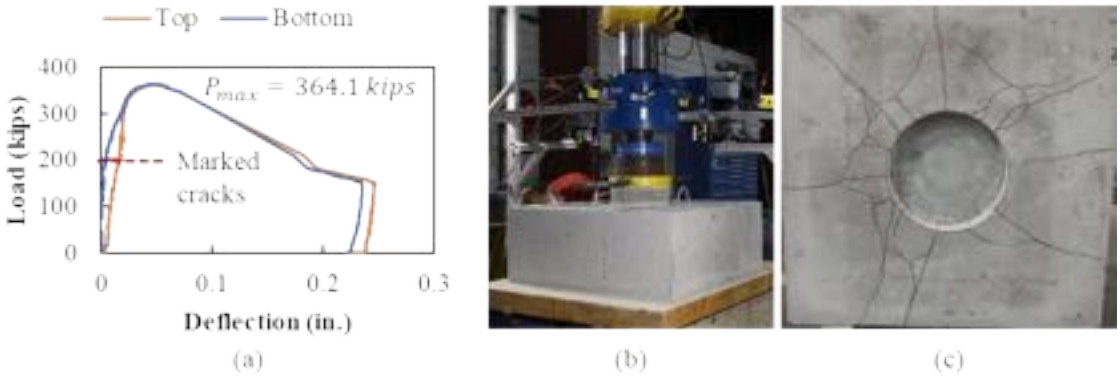

Figure 3-11: (a) Sample load versus deflection plot, (b) crack pattern at 200 kips, and (c) crack pattern on bottom after failure for Specimen S3-1

3.2.4. Instrumentation Schedule

In most of the specimens three different types of measurements were used: concrete strain gage (CSG), rebar strain gages (RSG), and laser transducer displacement (LTD). Concrete strain gages (CSG) were used to monitor crack development on the surface of the specimens during testing. Rebar strain gages (RSG) were used to measure the engagement of the reinforcement while loading. Finally, at least three to five laser displacement transducers (LDT) were used to monitor the displacement of the top and bottom of the plug relative to the cap.

The instrumentation scheme used for Series I specimens is shown in Figure 3-12. Instrumentation was provided on all faces for these specimens to determine the behavior and failure mechanism for the specimens. Only one LDT was provided on the top of the plug for these specimens.

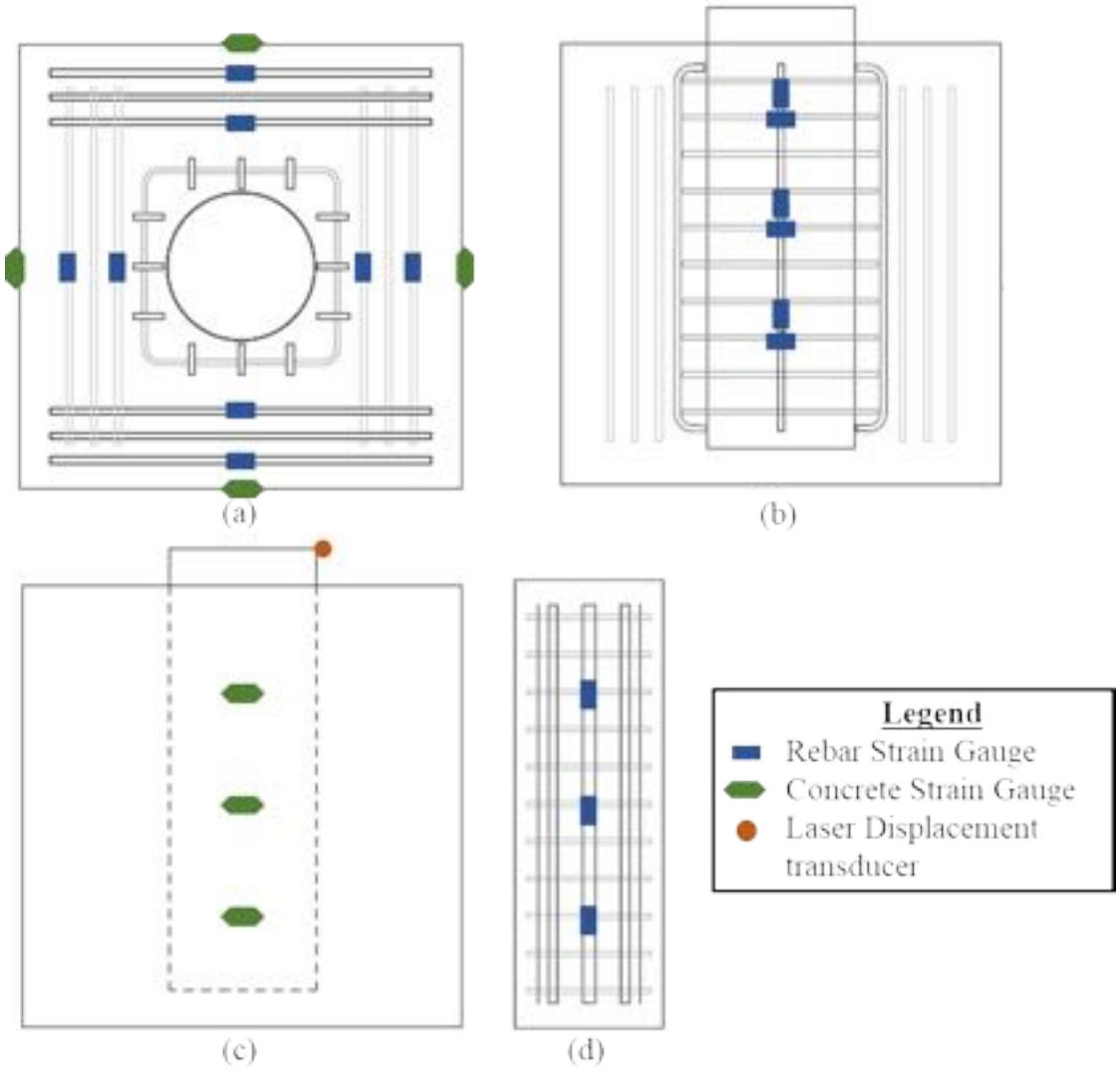

Figure 3-12: Instrumentation plan for Series I specimens: (a) pile cap bottom view (b) cap-elevation (c) pile cap, and (d) plug elevation.

A symmetrical response to the load was observed in Series I tests. A splitting crack was observed in either the east-west or north-south direction with similar rebar engagement and cracking patterns on opposite faces. For this reason, a reduced RSG and CSG schedule was used for Series II and III tests, as shown in Figure 3-13, with gages only on two adjacent faces of the specimens. Five LDTs were used in these specimens to measure displacement on the (1) opposite sides of the top of the plug, (2) opposite sides of the top of the cap, and (3) bottom of the plug.

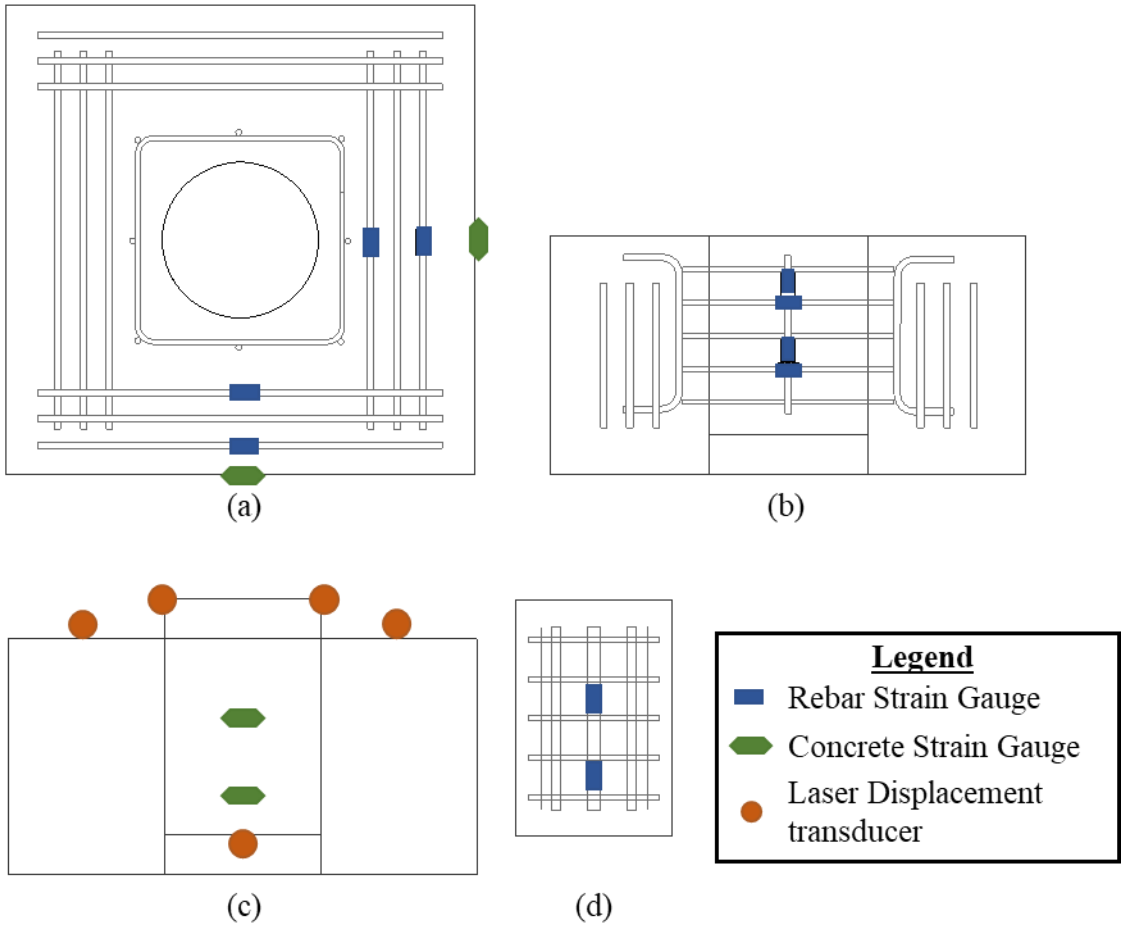

Figure 3-13: Instrumentation plan for Series II and III specimens: (a) pile-cap bottom view (b) cap-elevation, (c) plan cap, and (d) plug elevation.

There were eight specimens in Series II that were prefabricated without internal instrumentation. These were specimens with similar characteristics to other specimens in Series II with internal instrumentation. These eight specimens had the instrumentation schedule shown in Figure 3-14.

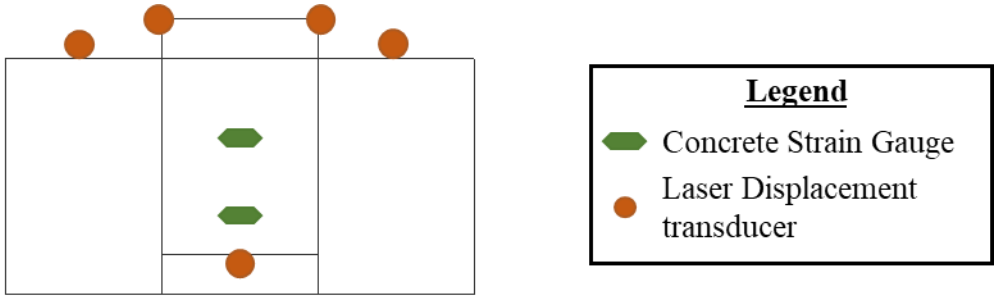

Figure 3-14: Instrumentation plan for Series IIb specimens.

3.2.5. Experimental Results of Small-scale Testing

3.2.5.1. Normalization of Failure Loads

Two different normalizations were used to analyze the data (based on available specifications):

1. Based on AASHTO LRFD Bridge Design Specification 8th Edition (American Association of State Highway and Transportation Officials (AASHTO), 2017b):

$$V_{ni} = cA_{cv} + \mu(A_{vf}f_y + P_c) \qquad \text{Equation 3-1 AASHTO (5.7.4.3-3)}$$

$$c = \frac{V_{ni,ex}}{A_{cv}} \qquad \text{Normalization based on cohesion (when } A_{vf} = P_c = 0\text{)}$$

2. Based on AASHTO LRFD Guide Specification for ABC 1st Edition (American Association of State Highway and Transportation Officials (AASHTO), 2018):

$$V_n = 0.13\sqrt{f'_{cp}}\,A_{cv} \qquad \text{Equation 3-2 (3.6.6.6-1)}$$

$$k = \frac{V_{ni,ex}}{\sqrt{f'_{cp}}A_{cv}} \qquad k \text{ normalization}$$

The interface area in both equations is:

$$A_{cv} = \pi d_v h_v \qquad \text{Equation 3-3}$$

Both normalizations were used to analyze, explain, and present the experimental results.

3.2.5.2. Summary of Results

The measured compressive strengths, cracking loads, ultimate loads, and normalized ultimate loads are summarized in Table 3-6 for all the specimens tested under Task 2. The specimen names describe the series and number in the series (e.g., S2-5 is the 5th specimen tested in Series 2). An analysis of these results is provided in the following subsections.

Table 3-6: Measured concrete strength and estimated versus measured ultimate strength and displacement for small-scale specimens

Specimen	Compressive Strength on Test Day (ksi)		Cracking Load (kips)	Ultimate Load (kips)	$c = \frac{V_{ni,ex}}{A_{cv}}$	$k = \frac{V_{ni,ex}}{\sqrt{f'_{cp}} A_{cv}}$
	Cap	*Plug*				
S1-1	7.57	8.45	690	> 750.0	-	-
S1-2	7.96	8.79	340	> 750.0	-	-
S1-3	7.69	8.20	--	243.8*	0.862	0.301
S1-4	8.05	7.98	300	429.7	0.345	0.122
S2-1	6.26	6.95	180	339.0	0.599	0.227
S2-2	6.33	6.98	250	> 750	-	-
S2-3	6.20	6.95	180	320.2	0.566	0.215
S2-4	6.33	6.98	170	615.4	1.484	0.562
S2-5	6.02	6.91	120	356.0	0.858	0.327
S2-6	6.41	6.91	110	418.6	1.009	0.384
S2-7	6.30	6.91	142	719.5	1.272	0.484
S2-8	6.85	7.29	124	553.5	0.979	0.362
S2-9	6.39	7.29	125	662.2	1.171	0.434
S2-10	6.72	7.11	163	575.4	1.388	0.520
S2-11	6.59	7.11	95	399.8	0.964	0.362
S2-12	6.59	7.11	110	521.6	1.258	0.472
S2-13	5.25	7.42	360	605.6	1.071	0.393
S2-14	5.52	7.40	130	441.3	1.064	0.391
S2-15	5.52	7.40	100	631.2	1.522	0.560
S2-16	5.54	7.76	400	> 750.0	-	-
S2-17	5.52	7.40	160	533.3	0.943	0.347
S2-18	5.55	7.97	200	569.2	1.373	0.486
S2-19	5.55	7.97	150	482.6	1.164	0.412
S2-20	5.77	7.11	200	666.0	1.178	0.442
S3-1	4.58	4.59	140	364.1	0.878	0.410
S3-2	4.58	4.59	150	444.6	1.072	0.500
S3-3	4.58	4.59	110	440.9	1.063	0.496
S3-4	4.66	4.68	200	493.8	1.191	0.550
S3-5	4.66	4.68	100	340.7	0.822	0.380

Specimen	Compressive Strength on Test Day (ksi)		Cracking Load (kips)	Ultimate Load (kips)	$c = \frac{V_{ni,ex}}{A_{cv}}$	$k = \frac{V_{ni,ex}}{\sqrt{f'_{cp}} A_{cv}}$
	Cap	*Plug*				
S3-6	4.66	4.68	80	283.8	0.684	0.316
S3-7	4.69	4.65	100	413.6	0.997	0.463
S3-8	4.66	4.68	100	379.3	0.915	0.423
S3-9	4.69	4.65	100	364.6	0.879	0.408
S3-10	4.69	4.65	90	330.7	0.797	0.370
S3-11	4.67	4.68	100	352.4	0.850	0.393
S3-12	4.69	4.68	130	363.2	0.876	0.406
S3-13	4.67	4.68	125	387.5	0.934	0.432
				Average =	1.010	0.407
				St. Dev. =	0.257	0.096
				Coefficient of Variation =	0.255	0.235

The normalized experimental results for specimen in Series II and III based on both codes (c and k normalization) are shown in Figure 3-15 and Figure 3-16. The highest cohesion value found in AASHTO LRFD Bridge Design Specification is 0.4 used for monolithic placed concrete as indicated with the red line in Figure 3-15. The currently recommended value for k in the AASHTO LRFD Guide Specification for ABC is 0.13 as shown in Figure 3-16. Both figures show how current specifications are conservative regardless of interface surface condition, corrugated type, or reinforcement layout.

The *k* normalization will be used in the comparisons of the analysis of the results as it also includes concrete strength in its normalization. The comparisons are divided per variable in the test matrix: interface surface condition, corrugation spacing and depth, edge distance, and confinement reinforcement around pocket

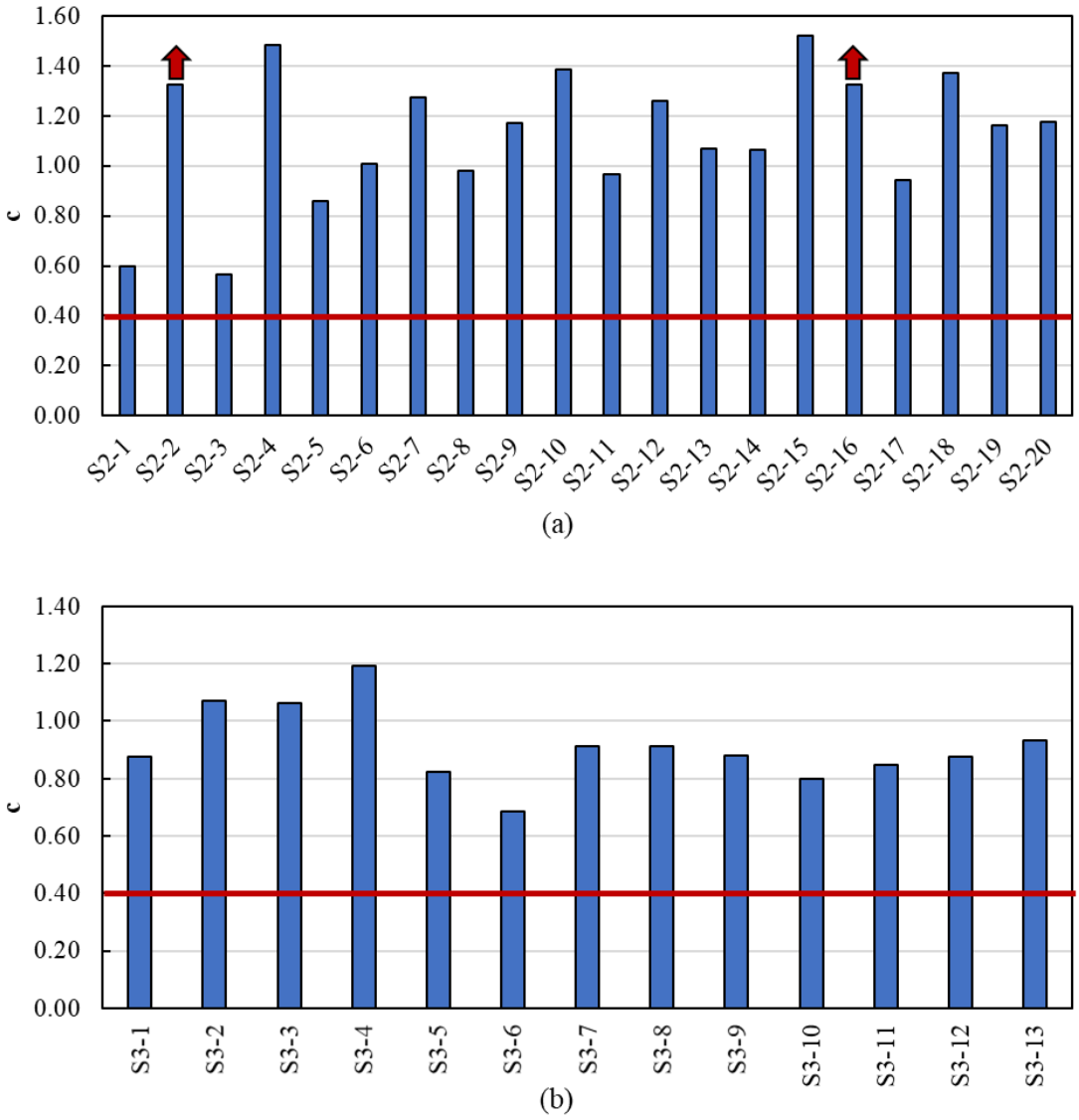

Figure 3-15: c normalization for (a) Series II and (b) Series III specimens

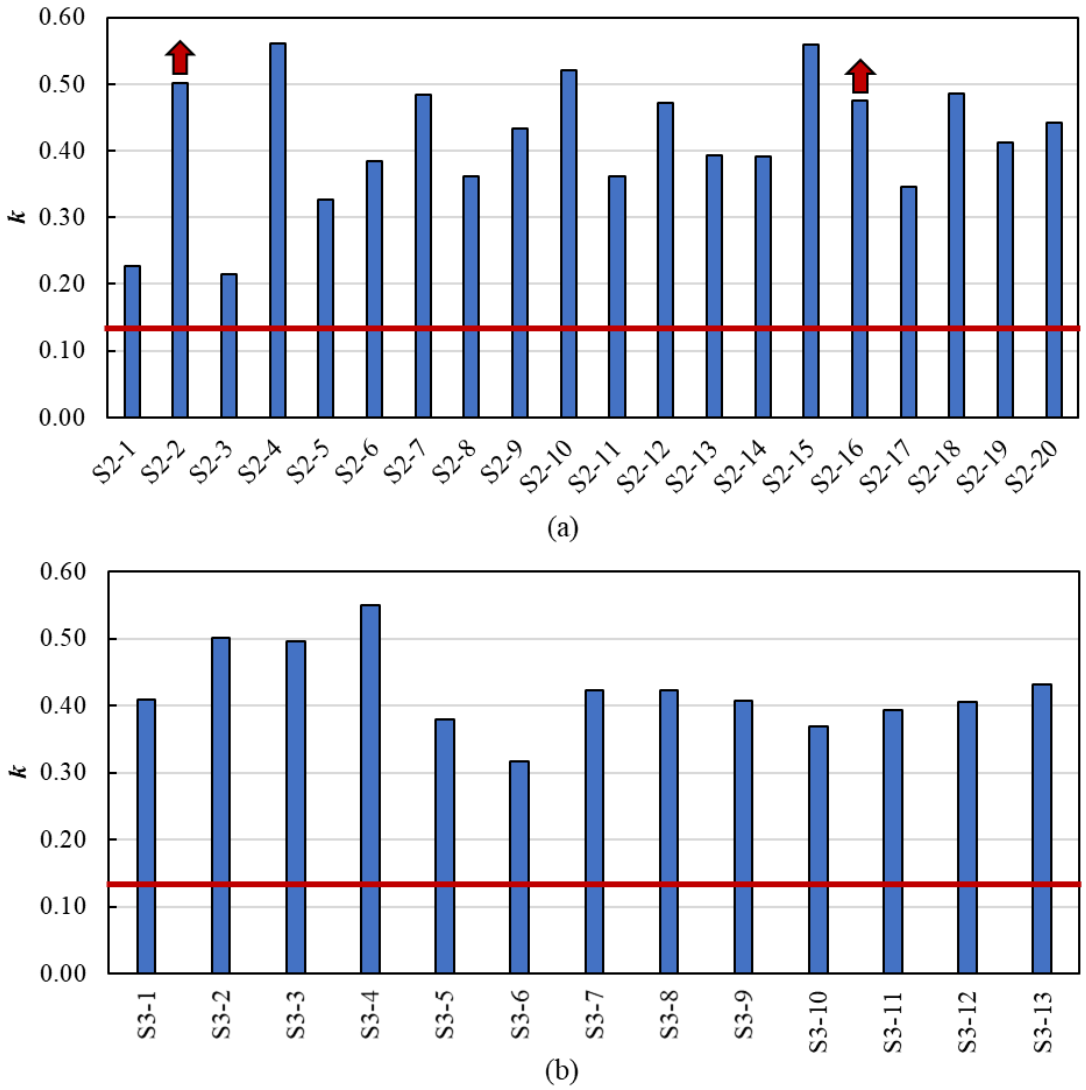

Figure 3-16: k normalization for (a) Series II and (b) Series III specimens

3.2.5.3. Analysis of Results

Failure Mechanism

After evaluating the responses of the specimens, a similar failure mechanism and progression to failure was seen in most of them. First cracking occurs on one face or parallel faces between 16% and 70% of the ultimate capacity with an average of 32% of ultimate capacity. The first cracking load can be clearly determined from rebar strain gage (RSG) and concrete strain gage (CSG) readings as indicated in Figure 3-17. RSG and CSG readings would remain linear until first cracking. At first cracking, strain in RSGs would

greatly increase (as the reinforcement engaged after cracking), as shown in Figure 3-17. The CSG would abruptly change from tensile strains to compression strains (if the crack occurred next to the gage) or have a dramatic increase in tensile strain (if the crack extended through the CSG). The cracking loads obtained from CSG and RSG readings for all the specimens are summarized in Table 3-6. The same cracking load was typically obtained from both types of gages; an average between the two gages was used if there was a difference.

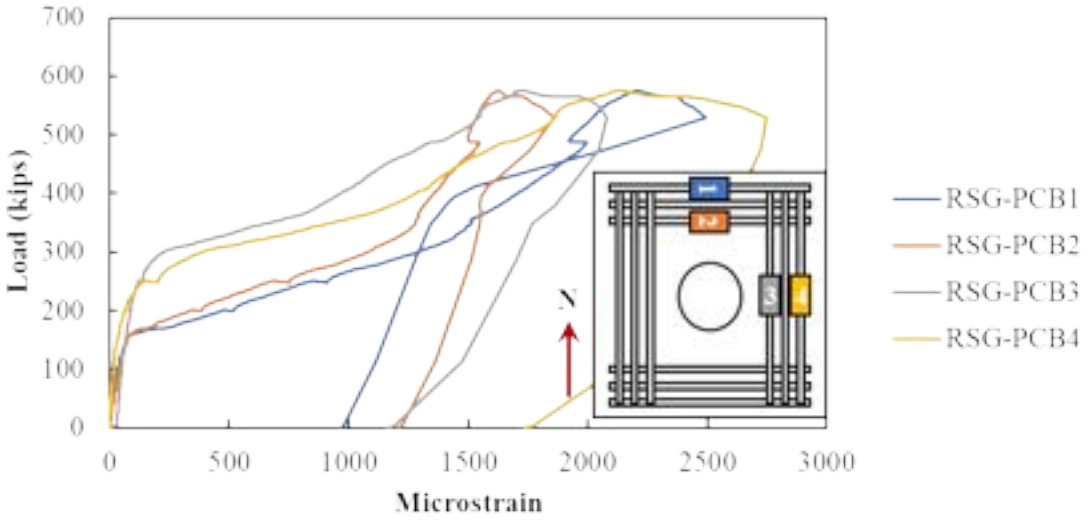

Figure 3-17: Rebar strain gages in the longitudinal reinforcement on bottom of specimen S2-10

First cracking in the side of the cap did not have a significant impact on the load versus plug displacement response. The load-deflection curve would typically remain linear elastic until extensive cracking would develop in the cap (typically accompanied by several large cracks), which was then typically followed by sliding of the plug, as shown in Figure 3-18. Deflection occurred at both the top and bottom of the plug when the plug began to slide, as shown in Figure 3-18 (b). The maximum applied failure loads are summarized in Table 3-6.

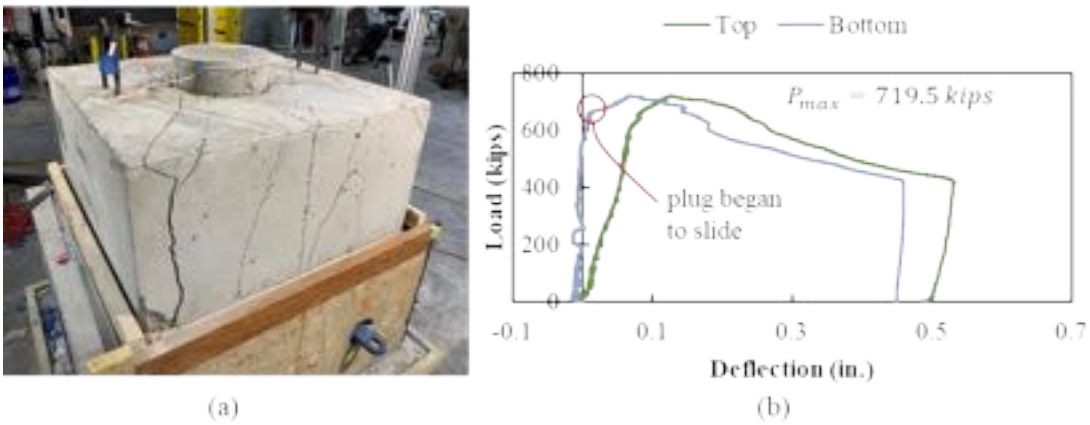

Figure 3-18: Failure mechanism of specimen S2-7: (a) crack pattern and (b) load-deflection curve

The cracking extended the full depth of the caps, as observed by similar cracks on top and bottom of the caps. Some sample crack patterns marked on the bottom of three specimens are shown in Figure 3-19. A large diagonal crack extending from the plug was a common characteristic of many of the plug specimens at failure.

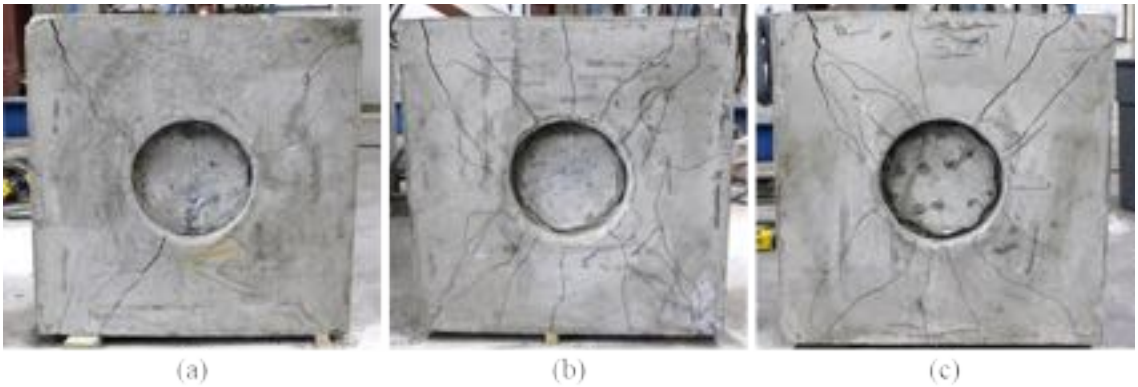

Figure 3-19: Sample crack patterns on the bottom of specimens (a) S2-7, (b) S2-8, and (c) S2-9

Effect of Interface Surface Condition

The interface surface condition directly influences the cohesion component of the shear friction capacity. The conditions that were evaluated for this variable were: sandblasted (1/16'' of roughness), corrugated pipe left in place (metal finish), and exposed aggregate finish (1/4'' of roughness). The exposed aggregate finish created a 1/4-inch roughened surface and thus affected the interface condition and may act as a type of corrugation creating mechanical interlock along the length of the interface. For this reason, it is

included in both sections. A monolithic specimen (S3-13) was also cast to compare a specimen with no cold joint to those with the cold joints at the interface. A comparison of the normalized failure loads between the specimen with different interface surface conditions is shown in Figure 3-20. Specimens S2-2 and S2-16 did not fail within the maximum capacity of the test setup (750 kips), so an arrow is shown in Figure 3-20 indicating that their failure loads were greater than the value shown. Specimen S2-20 was like S2-7 and S2-16 except that there was a longer time provided between the time of casting for the cap and the plug (163 days compared to 7 days).

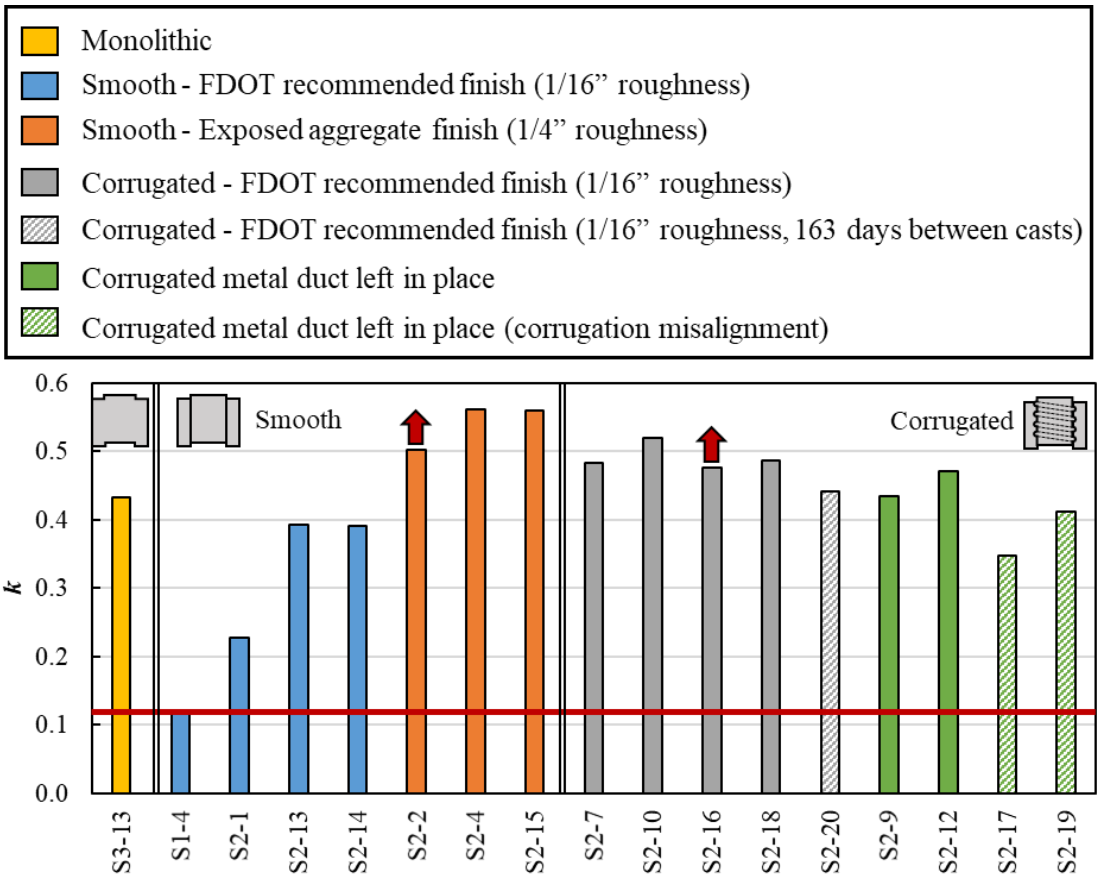

Figure 3-20: Comparisons for second series of specimens based on interface surface condition

The following subsections discuss some of the main conclusions on the effect of interface surface condition on the behavior of these specimens.

Monolithic Concrete Specimen (S3-13)

Although there was no cold joint, the monolithic cast specimen (S3-13) also experienced a sliding failure along the interface between the plug and cap. The concrete strength was

lower (4.7 ksi for cap and plug) than the specimens in Series I and II, so the normalized loads *k* are used for comparisons. Cracking began in the specimen at a normalized load *k* of 0.139 (125 kips), which was close to the average normalized cracking load k_{avg} of 0.133 for all the specimens tested. The observed crack pattern was like the typical crack pattern seen in the other specimens, as shown in Figure 3-21 (a) and (b). One difference was that concrete on the sides of the extended plug progressively spalled off during testing, as shown in Figure 3-21 (c) and (d).

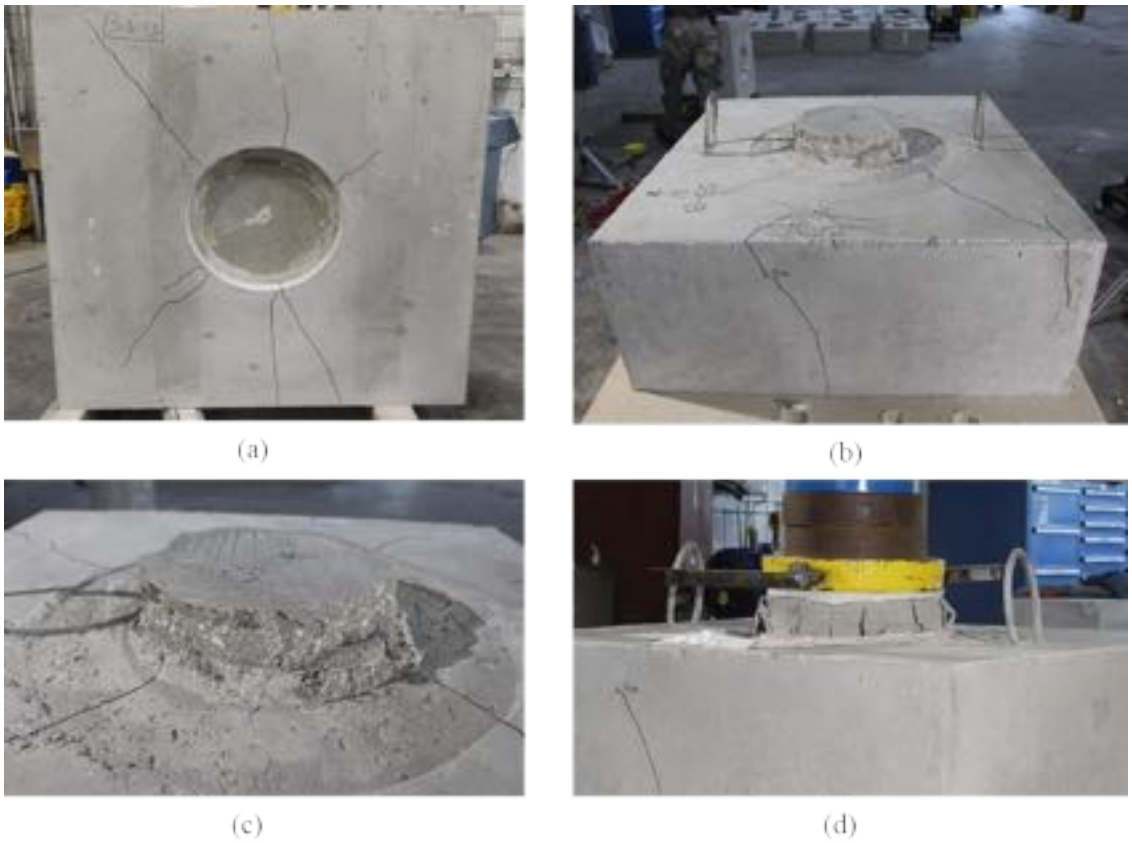

Figure 3-21: Failure details on (a) bottom, (b) cap, (c) top of plug and (d) plug detail during testing of the Specimen S3-13

Sliding was determined based on the LDT readings on the top and bottom of the plug, shown in Figure 3-22 (a). Displacement in the bottom of the plug began at approximately the same time first cracking occurred in the sides of the specimen (125 kips). After this there was similar displacement measured on the top and bottom of the plug until sliding began at the failure load of 387.5 kips. The reinforcement around the pocket began to

engage when first cracking occurred and approached the yield strain at time of failure; strains in the longitudinal reinforcement are shown in Figure 3-22 (b).

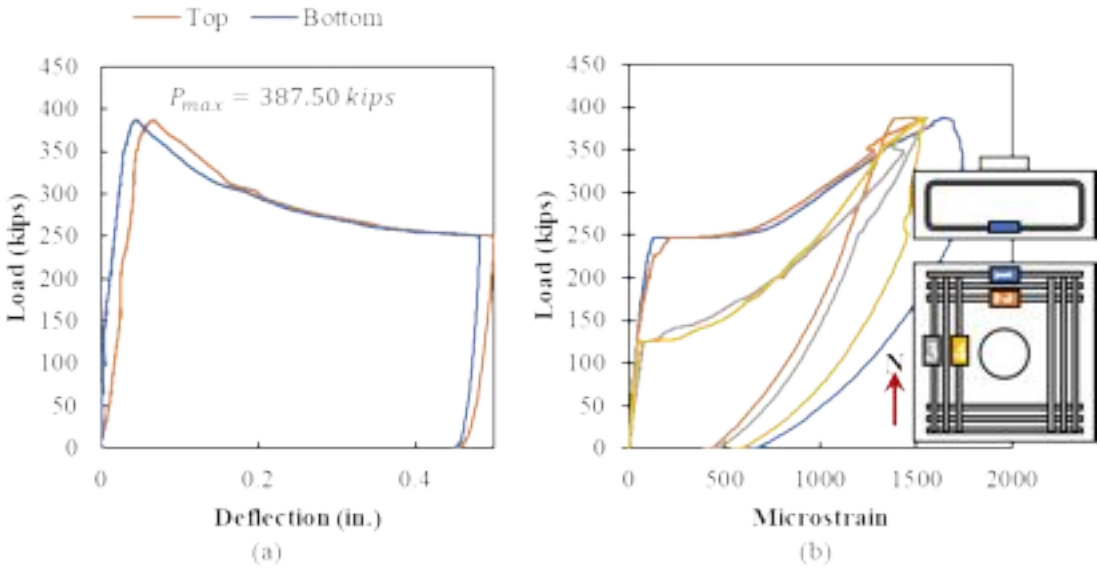

Figure 3-22: (a) Load versus deflection curve and (b) load versus strain in the longitudinal reinforcement for S3-13

The monolithic specimen will be used as a baseline comparison in the following sections.

1/16-inch versus 1/4-inch Surface Roughness (Smooth)

The normalized load (*k*) versus deflection plots for the specimens with no corrugation and 1/16-inch and 1/4-inch surface roughness are shown in Figure 3-23. The response of the specimen with a monolithically cast plug (S3-13) is also shown in Figure 3-23 (a) and (b) as a comparison. S2-2 did not fail before reaching the 750-kip test capacity; this plot is shown as a dotted line in Figure 3-23 (b). The cohesion is related to the negative slope following the maximum load. After cohesion is overcome, it is assumed the load will have a sharp decrease and then level out at a load related to the kinetic coefficient of friction between the plug and cap.

The exposed aggregate finish (1/4-inch roughness) increased the strength compared to the sandblasted finish (1/16-inch roughness) when using a smooth pipe. The increased roughness likely improved both the cohesion and friction (due to surface roughness) components of the interface capacity leading to the higher strength and steeper decline following the maximum failure load.

The specimens with 1/4-inch surface roughness reached higher normalized failure loads than the monolithic specimen, but the specimens with a 1/16-inch surface roughness failed at lower loads. The normalized load versus displacement plot for the monolithic specimen had a similar shape to the other specimens where there was strong cohesion (S2-13, S2-14, S2-4, and S2-15).

The variation in the behavior of the smooth interface with 1/16-inch surface roughness is likely due to the sensitivity of these specimens to the casting procedure. Specimens S1-4 and S2-1 were both cast at the FDOT Structures Research Center, while Specimens S2-13 and S2-14 were both precast at Coreslab Structures (Miami), Inc. The casting procedure did not have as significant an effect on the specimens with the 1/4-inch exposed aggregate finish, as the S2-4 (cast at SRC) and S2-15 (cast at Coreslab) both had very similar behavior.

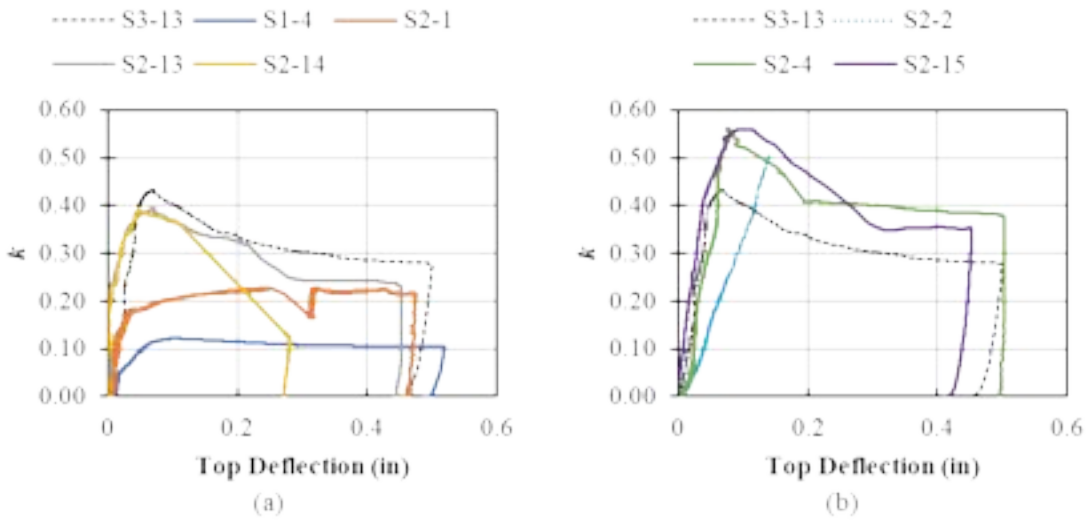

Figure 3-23: Normalized load (k) versus top deflection plots for specimens with no corrugations with (a) 1/16-inch and (b) 1/4-inch interface surface roughness

The strain readings in the rebar strain gages (RSGs) on the longitudinal steel in S2-1 and S2-2 are shown in

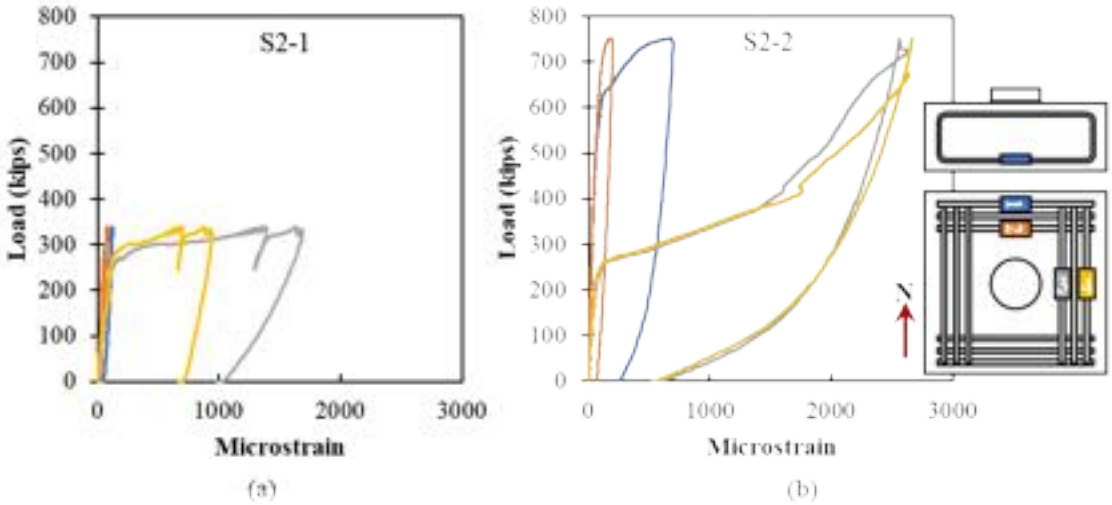

Figure 3-24. The only difference between specimens S2-1 and S2-2 was the interface surface condition: S2-1 had a 1/16-inch roughness and S2-2 had a 1/4-inch roughness. The reinforcement in S2-1 did not begin to engage until a slightly higher load than S2-2, and the amount that the reinforcement engaged was less in S2-1 than in S2-2. The cracking in S2-1 also was later (with respect to the failure load) than S2-2. These observations are like those seen in the other rebar gages and in other similar specimens. The 1/4-inch surface roughness led to more rebar engagement and more significant cracking than the 1/16-inch roughness. The rebar engagement in the specimens with 1/4-inch surface roughness was similar to that observed in the monolithically cast specimen, see Figure 3-22 (b).

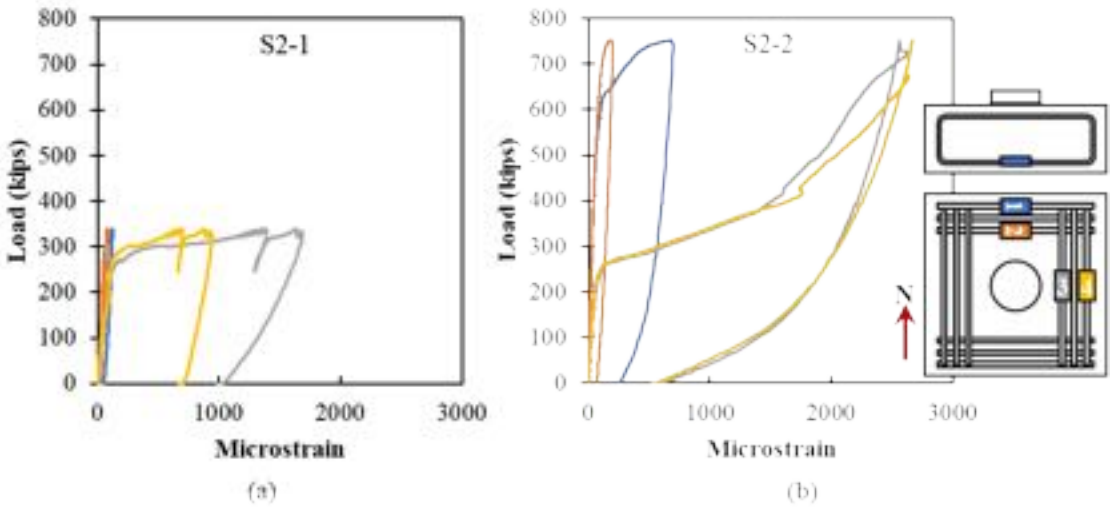

Figure 3-24: Rebar strain in longitudinal bars on bottom of specimen (a) S2-1 and (b) S2-2

1/16-inch Concrete versus Steel (Corrugated)

All the specimens with corrugation and the 1/16-inch surface roughness reached their peak load and then decreased in load as the plug pushed through, as shown in Figure 3-25 (a). S2-7, S2-10, and S2-18 all gradually decreased in load as the plug pushed through, while S2-16 had a sudden failure when the cohesion was overcome. S2-20 had less cohesion (i.e., non-linear response prior to reaching the maximum load and a less dramatic drop in strength following the maximum load) than the other specimens with the 1/16-inch finish; this was likely due to the longer time between casting of the cap and plug (163 days compared to 5 to 7 days for the other specimens). The specimens with corrugation and the 1/16-inch surface roughness all reached a higher capacity than the monolithically cast specimen (S3-13).

The metal finish had a lower cohesion and strength than 1/16-inch roughness, as shown in Figure 3-25 (b). The normalized load versus displacement in the top of the plug began non-linear behavior between a *k* of 0.25 and 0.3. After this, the load continued to increase while the plug was pushing through.

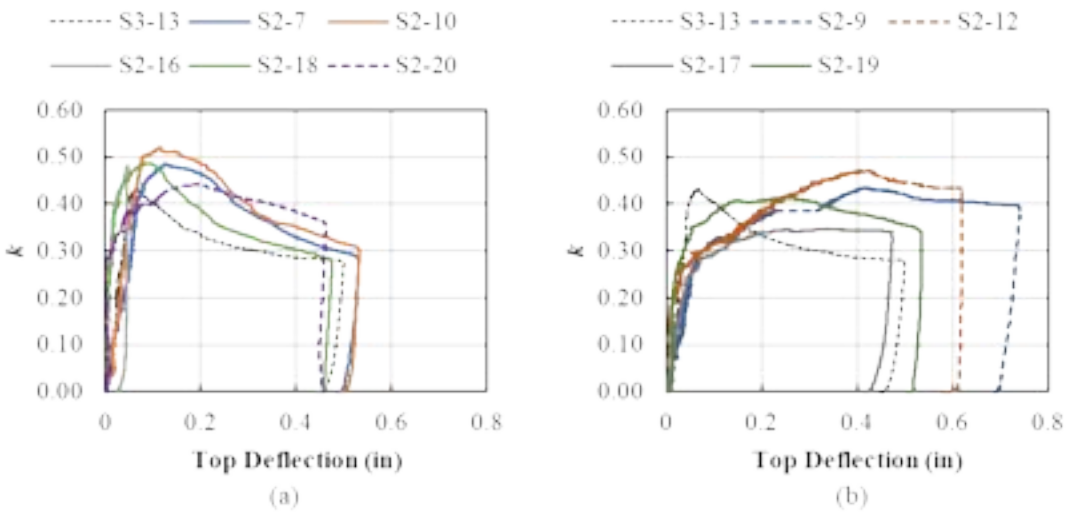

Figure 3-25: Normalized load (k) versus top deflection plots for specimens with corrugations with (a) 1/16-inch concrete finish and (b) concrete to metal interface

In general, more symmetrical early engagement of the reinforcement surrounding the pocket was observed in the specimens with the corrugated metal pipe left in place. The load versus rebar strain for specimens S2-7 (1/16-inch surface roughness) and S2-9 (corrugated metal) is shown in Figure 3-26. All the rebar in the specimen with the corrugated metal pipe left in place (S2-9) began to engage at around 150 kips. The rebar in the specimen with the metal pipe removed and surface roughened to 1/16-inch magnitude (S2-7) was engaged between 175 and 425 kips.

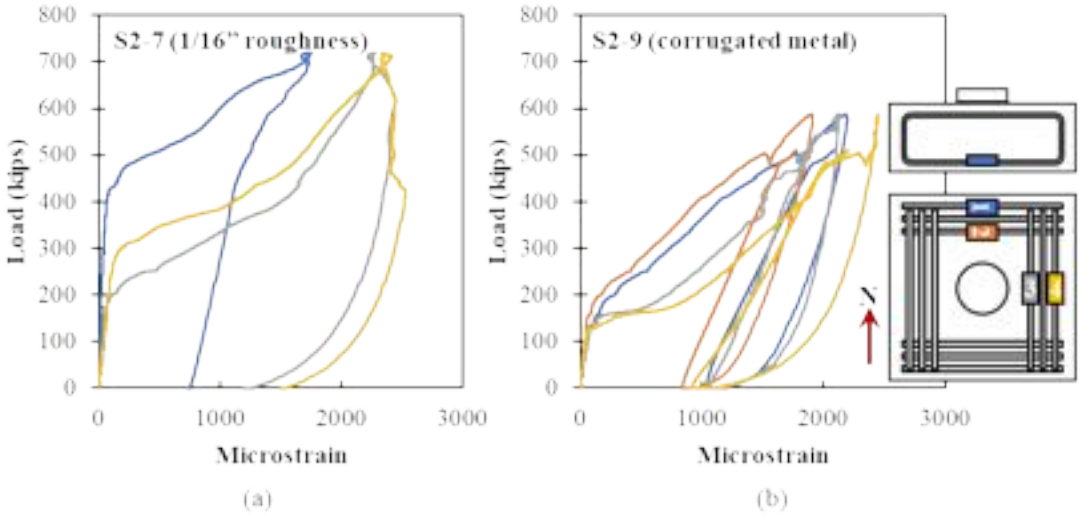

Figure 3-26: Rebar strain in longitudinal bars on bottom of specimen (a) S2-7 and (b) S2-9

Rotation of Plug

Two of the specimens with the corrugated metal duct left in place (S2-9 and S2-12) experienced clear rotation of the plug as the plug was pushed through (following the angle of rotation), as shown in Figure 3-27.

Figure 3-27: Observed rotation in S2-12 (a) before and (b) after testing

The metal duct was cut at mid-depth and rotated to make the corrugations discontinuous at the cut in S2-17 and S2-19 to try and prevent the rotation of the plug during testing (see §3.2.2.3). Only slight rotation was observed in these specimens, as shown in Figure 3-28, but they did end up failing at lower normalized loads than the specimens where clear rotation was observed.

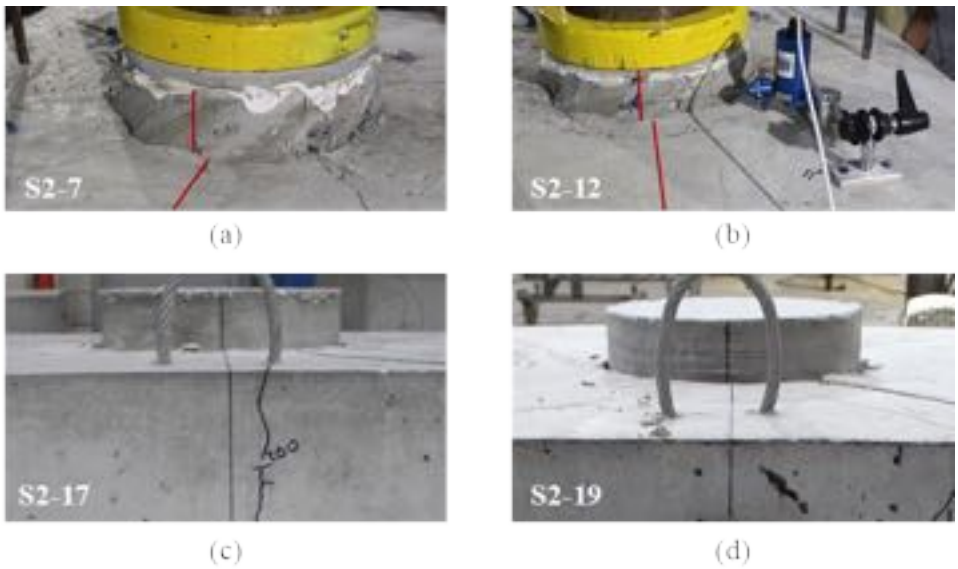

Figure 3-28: Observed rotation in specimens with the corrugated metal pipe left in place with continuous corrugations (a) S2-7 and (b) S2-9 and discontinuous corrugations (c) S2-17 and (d) S2-19

Corrugation Spacing and Depth

The corrugation spacing and depth influence the interlock and friction components between the plug and cap after cohesion has been overcome. Several different corrugation configurations were investigated in Series II: smooth, single rib at the bottom of the plug, double rib at the bottom of the plug, half-spacing of the ribs along the plug length, and full corrugations. All these specimens had the corrugated metal pipe removed and a 1/16-inch roughness finish on the concrete surface. The normalized failure loads for all specimens in this comparison are shown in Figure 3-29. All specimens with the interface were cast at FDOT SRC other than S2-13 and S2-14; these are differentiated in Figure 3-29.

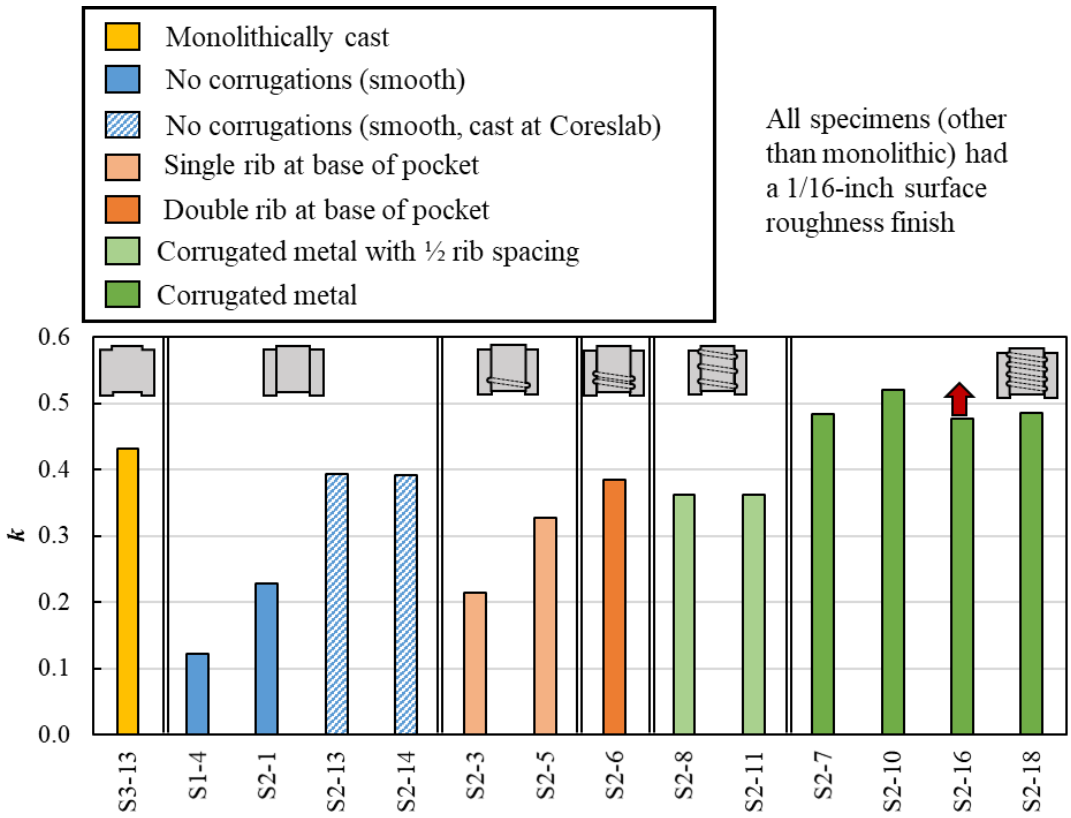

Figure 3-29: Comparison for Series II specimens based on corrugation spacing and depth

The specimens with the full corrugation (created using the corrugated metal pipe) had the highest normalized strength, which was also comparable with the strength of the monolithically cast specimen. Comparing only the specimens cast at FDOT's SRC, the specimens with the other variations of less corrugation (one rib, two ribs, and half-spacing of the ribs) had normalized strengths greater than the smooth interface but less than the full corrugations. As mentioned above, the smooth specimens cast at Coreslab Structures (Miami), Inc. had a higher strength than those cast at FDOT's SRC due to the sensitivity of the behavior of these specimens to casting procedure.

More cracking and larger cracks were observed in specimens with corrugation compared to those with smooth interfaces. The crack pattern at failure for S2-1 (with a smooth interface) and S2-10 (with full corrugations) are shown in Figure 3-30.

Figure 3-30: Crack patterns at failure for (a) S2-1 (smooth) and (b) S2-10 (full corrugation)

A comparison of the strain in the longitudinal reinforcement and confinement reinforcement around the pocked between the different types of corrugation provided is provided in Figure 3-31 and Figure 3-32. The specimens without corrugation (S1-4 and S2-1) did not have significant engagement of the longitudinal or confinement reinforcement until the plug began to slide. All specimens with any type of corrugation saw engagement of the longitudinal and confinement reinforcement start at the time of first cracking. Significant cracking and reinforcement engagement only occurred on two faces for the specimens with a single rib (S2-5). Specimens with two ribs, half-rib spacing, and full corrugation all had cracking and engagement of reinforcement on all faces.

In all specimens with corrugation, the engagement of the confinement reinforcement started at the bottom and then to the top. The bottom layers of confinement reinforcement experienced larger strains than the top layers, which would suggest that failure of the plug initiated toward the bottom of the plug.

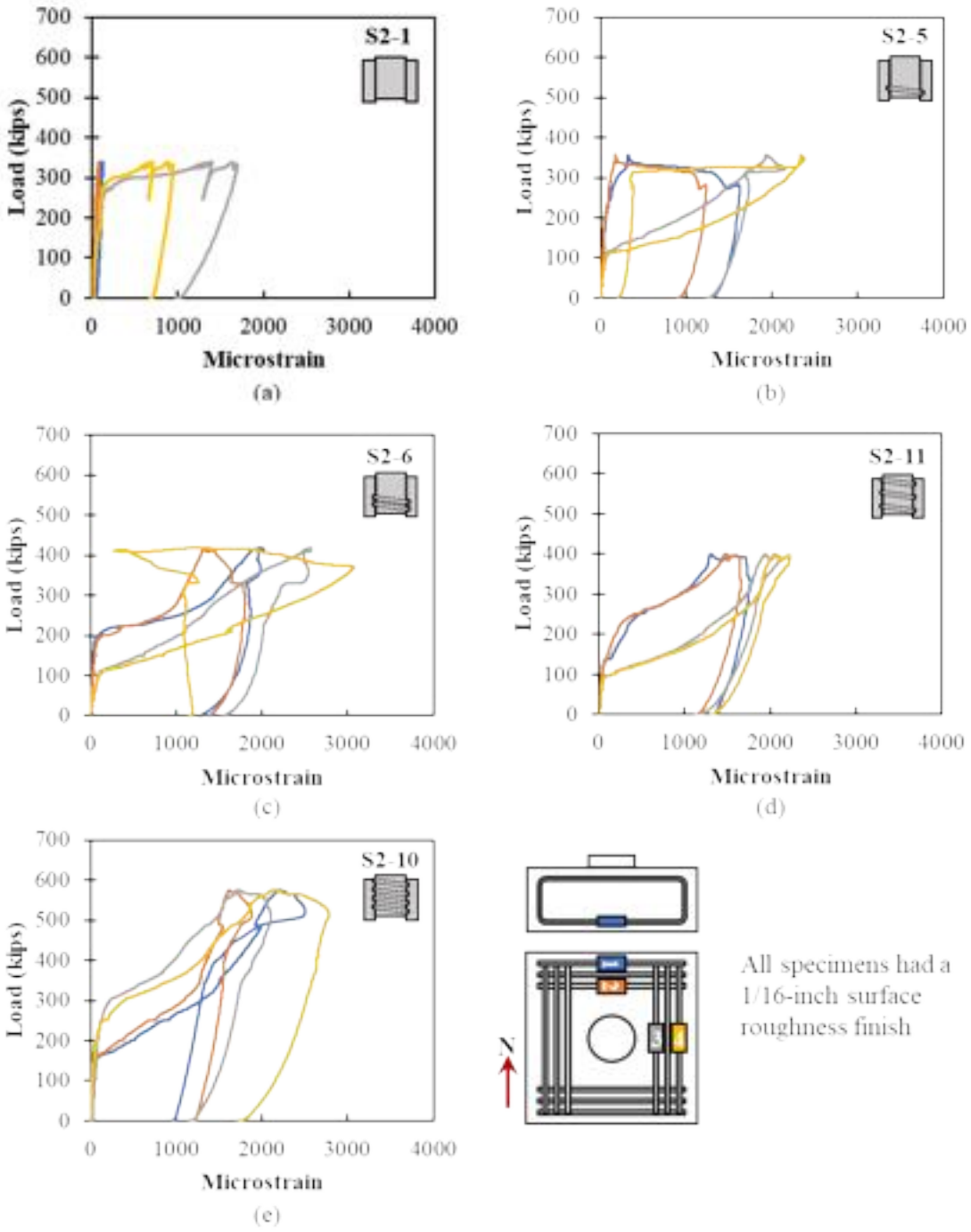

Figure 3-31: Load versus strain in longitudinal reinforcement for (a) S2-1, (b) S2-5, (c) S2-6, (d) S2-11, and (e) S2-10

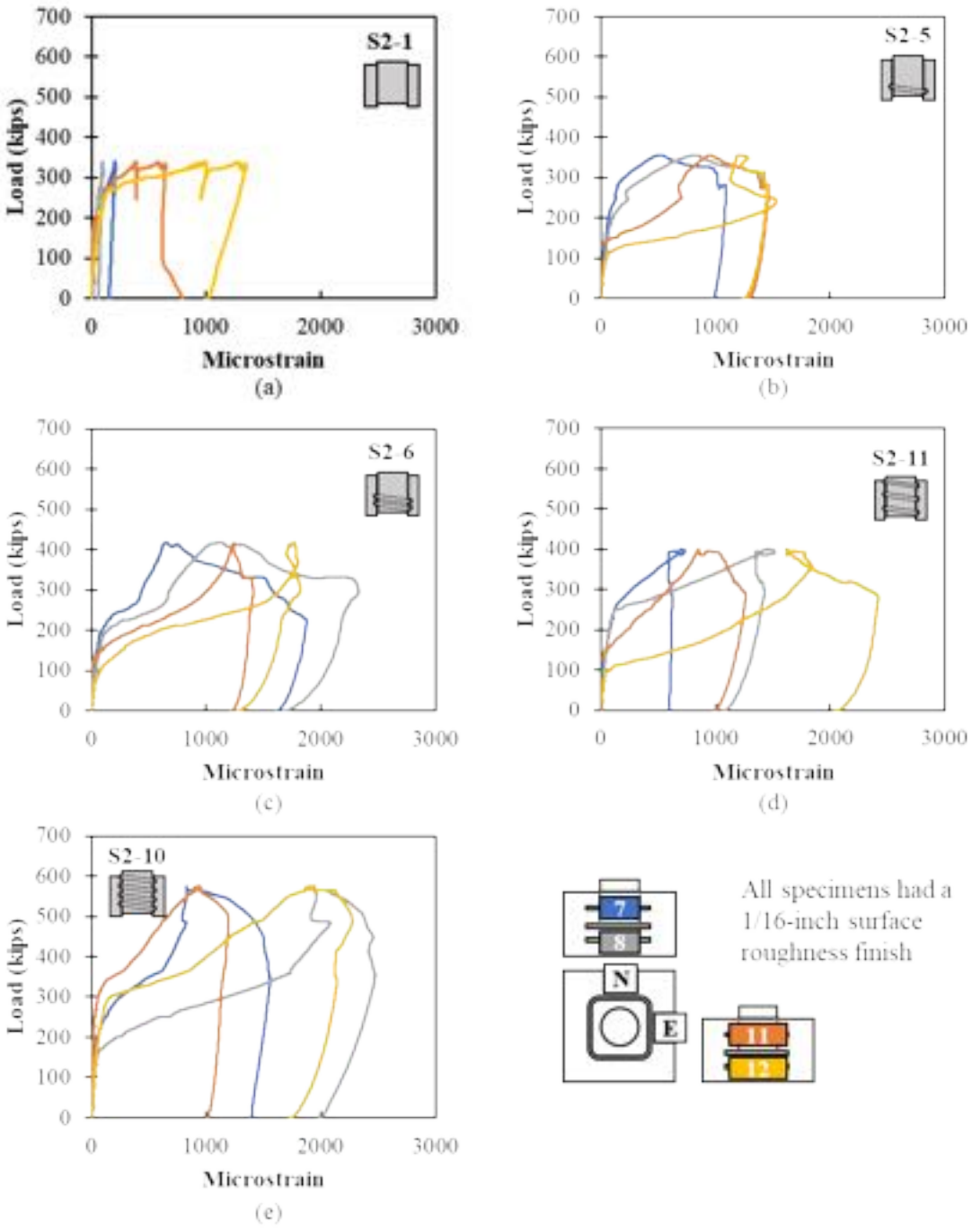

Figure 3-32: Load versus strain in confinement reinforcement for (a) S2-1, (b) S2-5, (c) S2-6, (d) S2-11, and (e) S2-10

The load versus strain curves for the vertical reinforcement in the plug and cap for S2-1 and S2-7 are shown in Figure 3-33. The rebar strain gages at the top of the vertical plug reinforcement (RSG-13 and RSG-15) saw larger strains than those at the bottom of the

plug, showing how stress was transferring from the plug to the cap in all specimens. Only the gages at the bottom of the cap (6 and 10) were initially engage in the specimen with smooth interface (S2-1), while the gages at both the top and bottom of the cap reinforcement were initially engaged in the specimen with full corrugation (S2-7), which shows the quicker force transfer from plug to cap for the corrugated interface. The vertical reinforcement in the cap began to go into tension in some of specimens, suggesting that vertical tension begins to develop in the cap around the pocket as the interface stress increases. This is like the stresses observed in the numerical modeling. These results were similar for other specimens with smooth and various corrugated finishes.

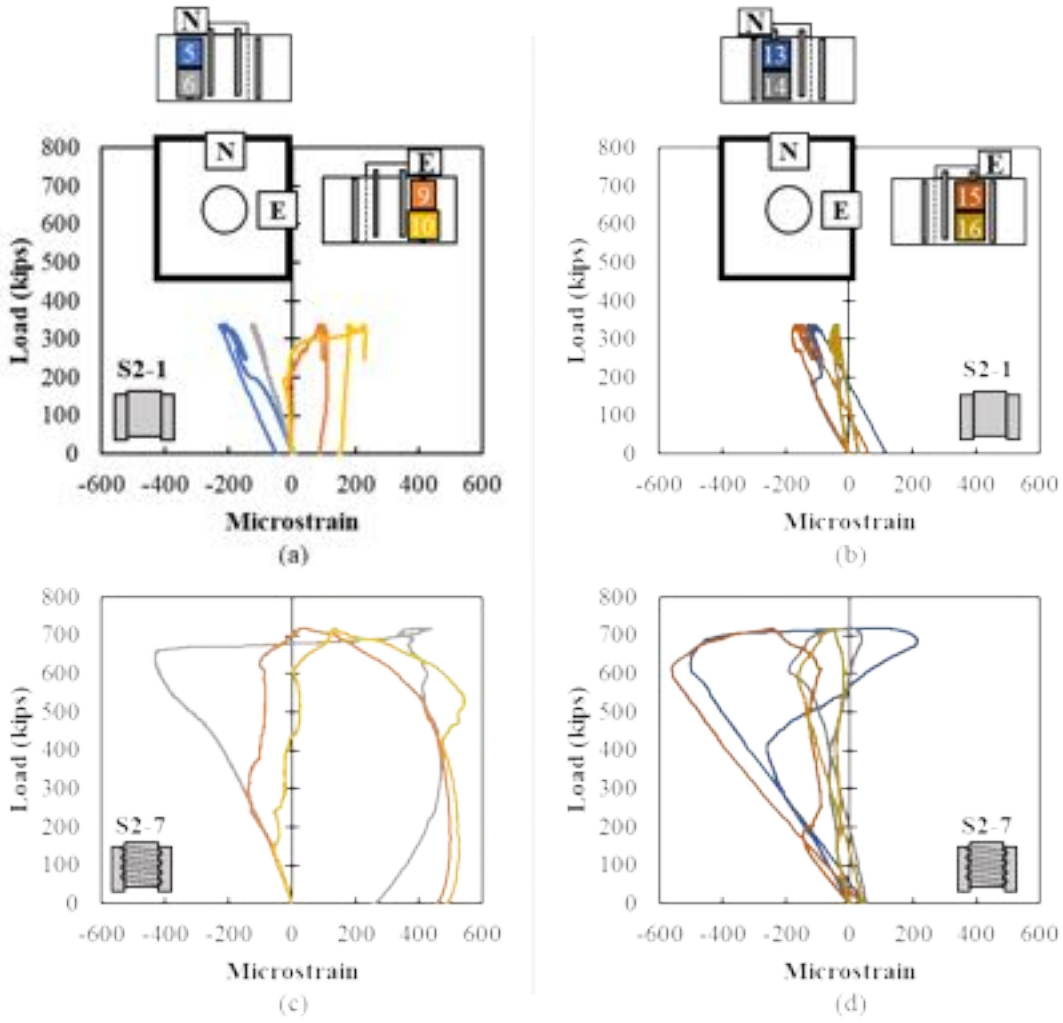

Figure 3-33: Load versus strain in (a) vertical reinforcement in pile cap for S2-1, (b) vertical reinforcement in plug for S2-1, (c) vertical reinforcement in plug for S2-7, and (d) vertical reinforcement in plug for S2-7

Edge Distance

Three different edge distances (d_{edge}) were tested with decreasing edge distances in one and two directions of $1d_{plug}$, $0.75d_{plug}$, and $0.5d_{plug}$, as shown in Figure 3-34. All specimens tested in this comparison had a corrugated interface with 1/16-inch surface roughness. The reinforcement was also kept consistent in specimens in this comparison, with 1 #7 longitudinal bar on the face with the decreasing dimension, 3 #4 longitudinal bars on the other faces, and the typical #4 confining bars around the pocket. Results from a similar specimen tested in Series II with 3 #4 longitudinal bars in all faces (S2-10) are also provided in this section.

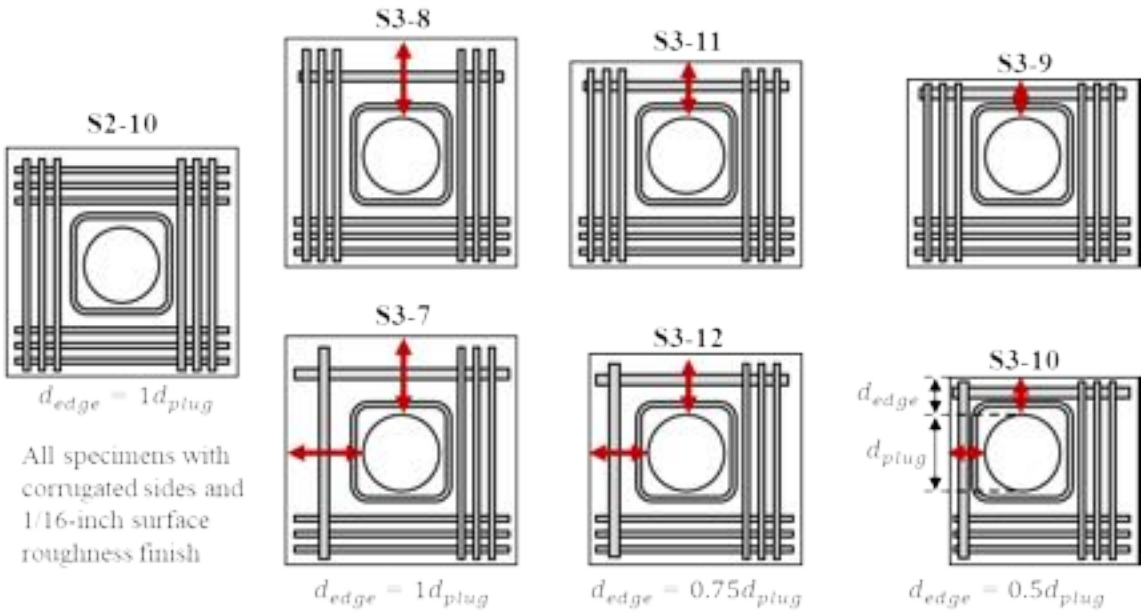

Figure 3-34: Specimens details for edge distance comparisons

The normalized strength of all specimens in the edge distance comparison are shown in Figure 3-35 grouped by specimens with decreasing edge distance on one side and two sides. There was a drop in normalized strength when 1 #7 bar was used in place of the 3 #4 bars in one or two faces. There was approximately a 7 percent drop in strength when the edge distance was decreased in one direction (from $1d_{plug}$ to $0.75d_{plug}$ or $0.5d_{plug}$). There was a 12.3 percent drop in strength when the edge distance was reduced in two directions from $1d_{plug}$ to $0.75d_{plug}$ and an additional 8.9 percent drop when reduced from $0.75d_{plug}$ to $0.5d_{plug}$.

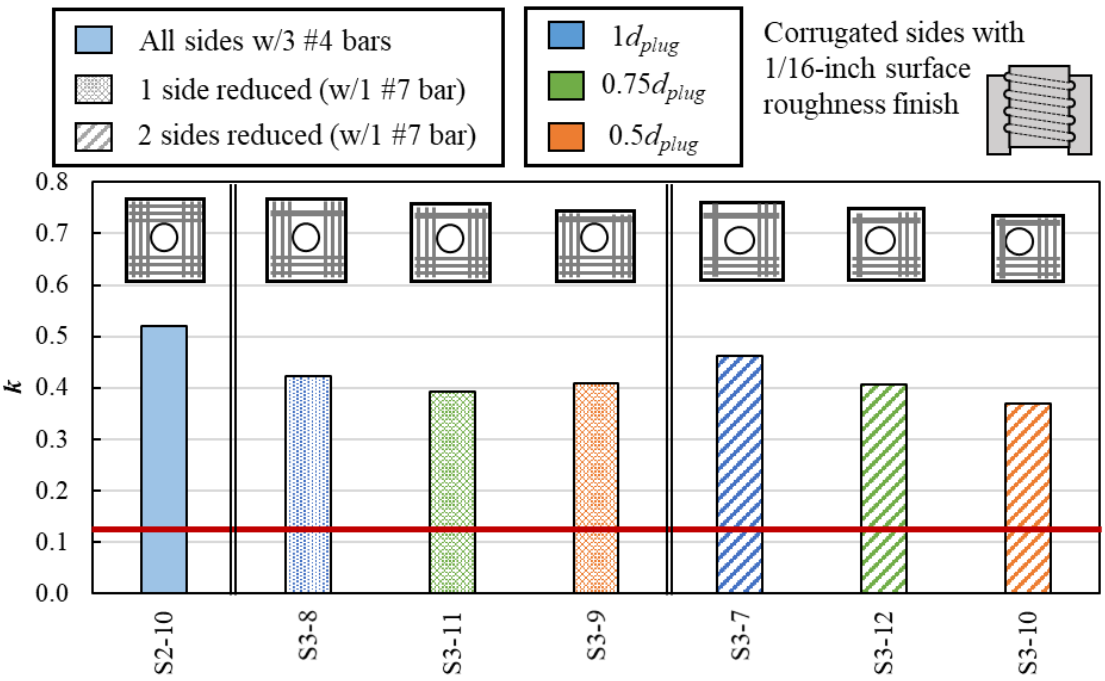

Figure 3-35: Comparison graph for specimen varying the edge distance

Specimen S2-10, with 3 #4 longitudinal bars in all faces had a higher strength than the other specimens with $1d_{plug}$ edge distance on all sides and 1 #7 bar on one (S3-8) or two faces (S3-7). The load versus strain in the longitudinal reinforcement curves for these specimens are shown in Figure 3-36. The strains in the longitudinal bars increased in all specimens. The concrete strength was lower in the Series III specimens compared to Series II (7.1 ksi versus 4.7 ksi for plug concrete strength). Because of the lower concrete strength, shearing along the interface in S3-7 and S3-8 occurred at a lower load and with less plug expansion, which is why there was less engagement of the longitudinal reinforcement. Larger cracks were observed in specimen S2-10, which corresponds to the larger observed strains in the reinforcement, as shown in Figure 3-37. There was not a noticeable difference in cracking between the faces with 1 #7 bar and 3 #4 bars in S3-7 and S3-8.

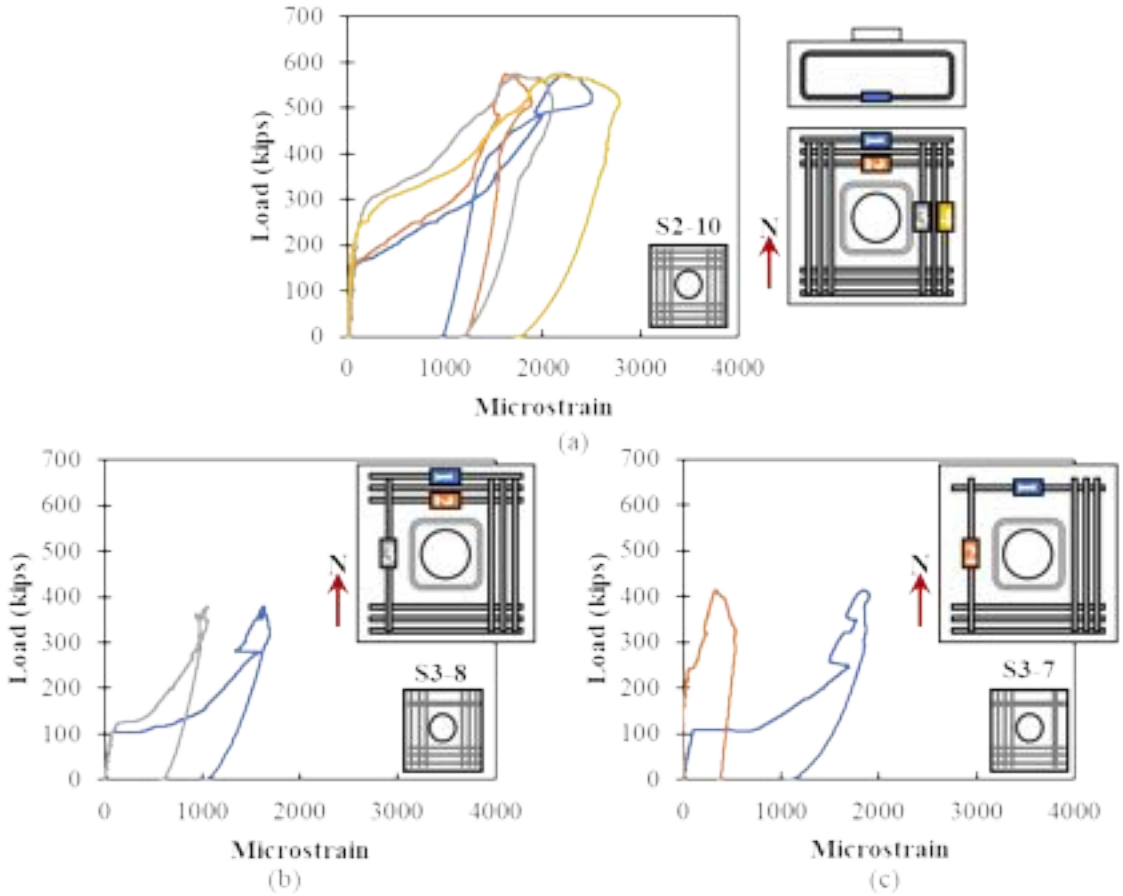

Figure 3-36: Load versus strain in longitudinal reinforcement for specimens with $1d_{plug}$ edge distance and different types of longitudinal reinforcement (a) S2-10, (b) S3-8, and (c) S3-7

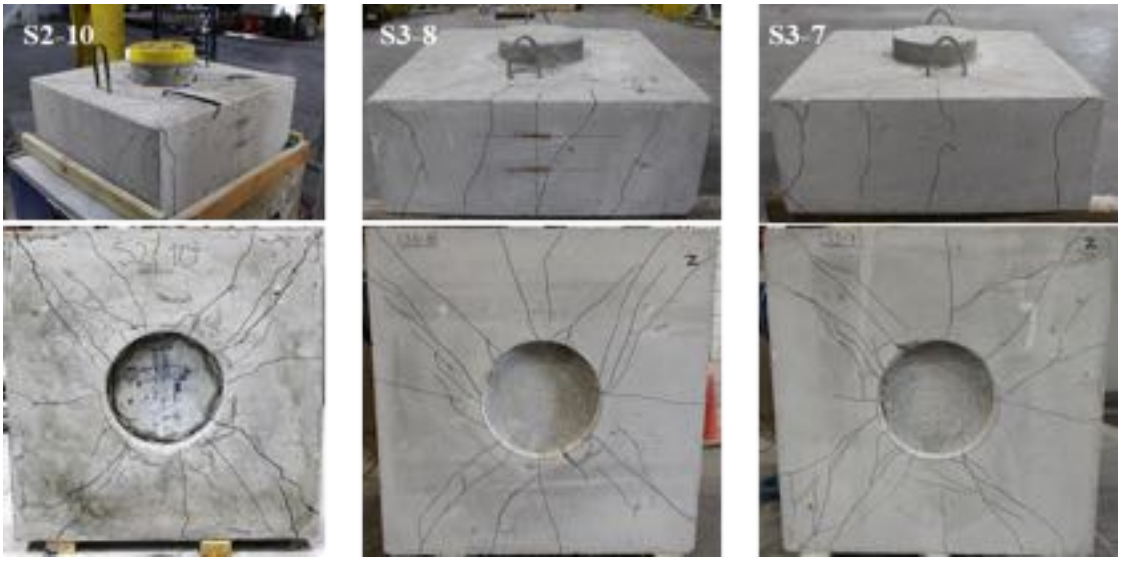

Figure 3-37: Cracking at failure for (a) S2-10, (b) S3-8, and (c) S3-7

The normalized load versus top of plug deflection curves for all the edge distance specimens are shown in Figure 3-38. All specimens saw a relatively linear-elastic response until cohesion was overcome along the interface and sliding of the plug began.

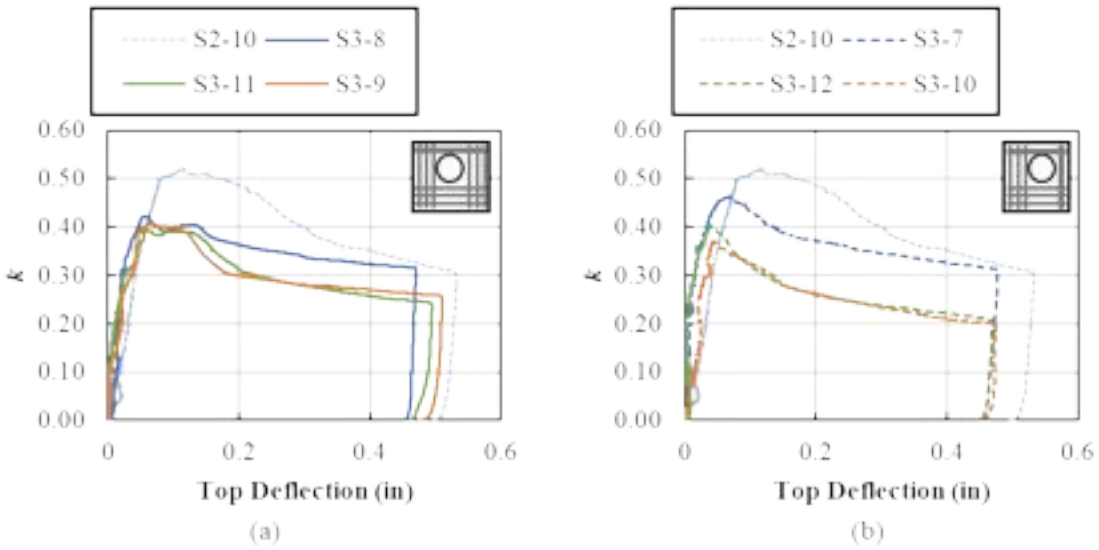

Figure 3-38: Normalized load (k) versus top deflection plots for specimens with corrugations, 1/16-inch concrete finish, and varying edge distance in (a) one direction and (b) two directions

The crack patterns for three of the specimens (S3-7, S3-12, and S3-10) with decreasing edge distances in two directions are shown in Figure 3-39. The cracking became more extensive and more concentrated toward the corner between the two shorter edges as the edge distance was decreased. The specimen with only $0.5d_{plug}$ edge distance in two directions had most cracking concentrated at the corner between the short edges.

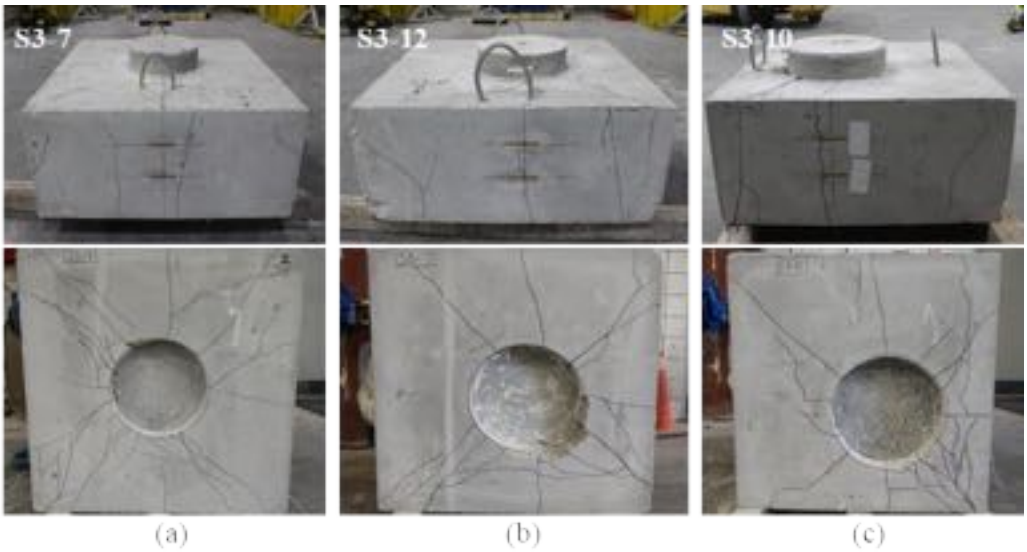

Figure 3-39: Crack pattern after failure for specimens with decreasing edge distances in two directions (a) S3-7, (b) S3-12, and (c) S3-10

The load versus strain in the longitudinal reinforcement for the specimens with decreasing edge distances in two directions are shown in Figure 3-40. Specimens with the decreased edge distance saw progressively less engagement of the longitudinal reinforcement.

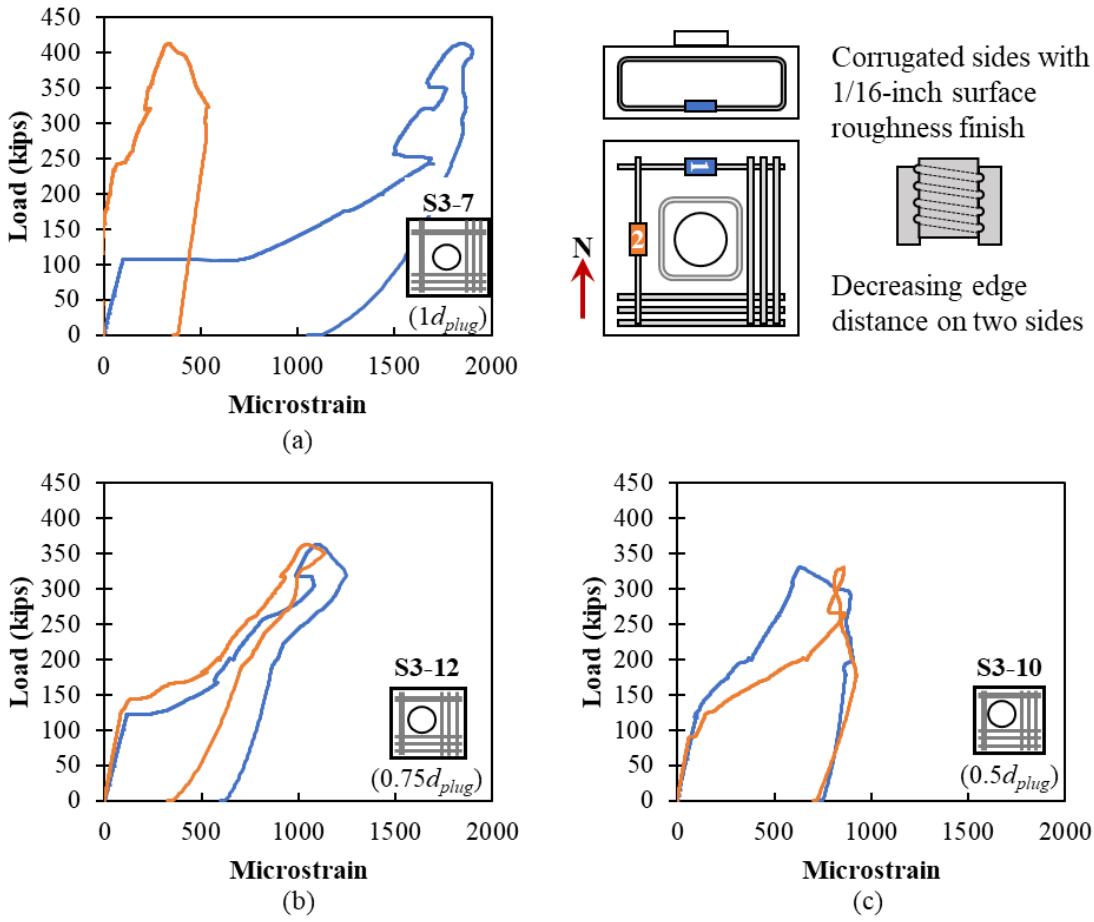

Figure 3-40: Load versus strain in longitudinal reinforcement for specimens with decreasing edge distance in two directions (a) S3-7 (1d_{plug}), (b) S3-12 (0.75d_{plug}), and (c) S3-10 (0.5d_{plug})

The load versus strain in the confinement reinforcement for the specimens with decreasing edge distances in two directions are shown in Figure 3-41. The confinement reinforcement became more engaged as the edge distance was decreased. These observations suggest that the confinement reinforcement (reinforcement around the pocket) is more important than the longitudinal reinforcement for the specimens with smaller edge distances.

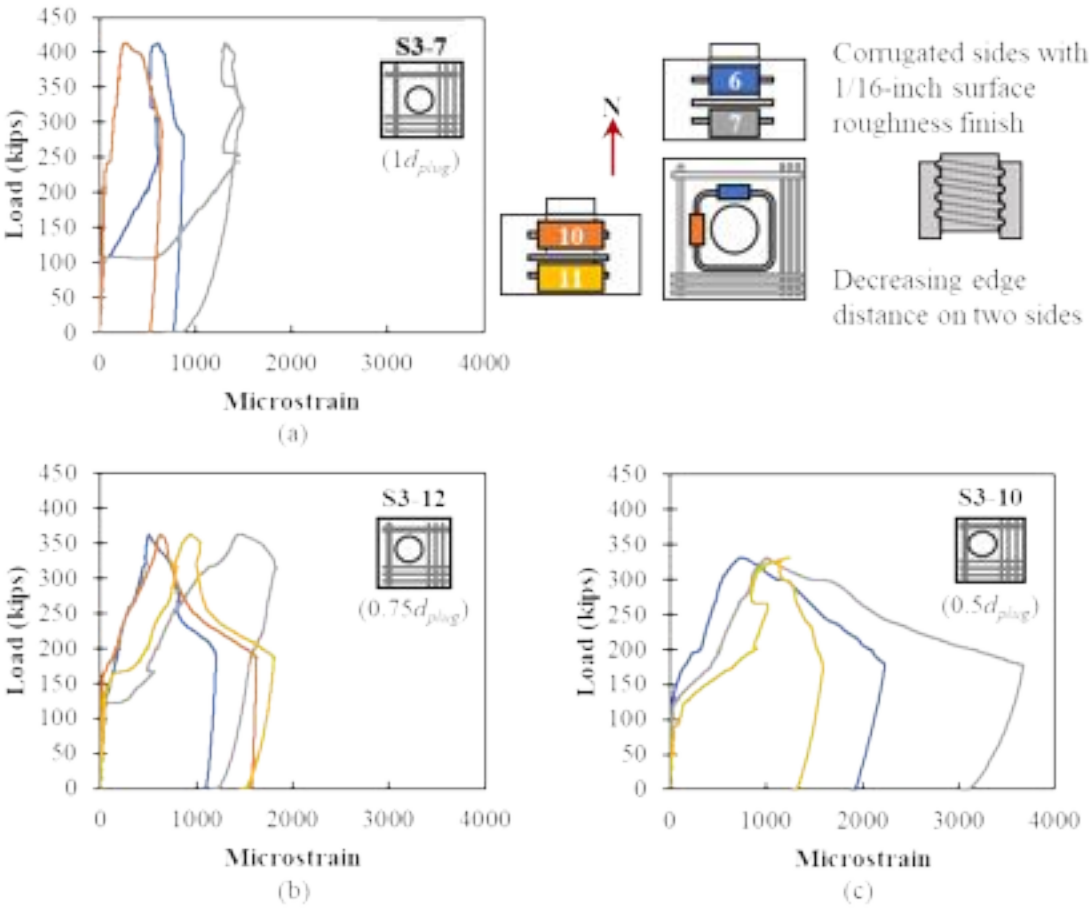

Figure 3-41: Load versus strain in confinement reinforcement for specimens with decreasing edge distance in two directions (a) S3-7 (1d_{plug}), (b) S3-12 (0.75d_{plug}), and (c) S3-10 (0.5d_{plug})

Longitudinal Reinforcement

Three specimens were tested specifically to determine the effect of the longitudinal reinforcement, three with and three without the corrugated metal pipe left in place, as shown in Figure 3-42. Typical confinement reinforcement around the pocket was used in all these specimens. These specimens were all 14 inches deep, had 1d_{plug} edge distance on all sides, and had a corrugated interface with 1/16-inch concrete surface finish.

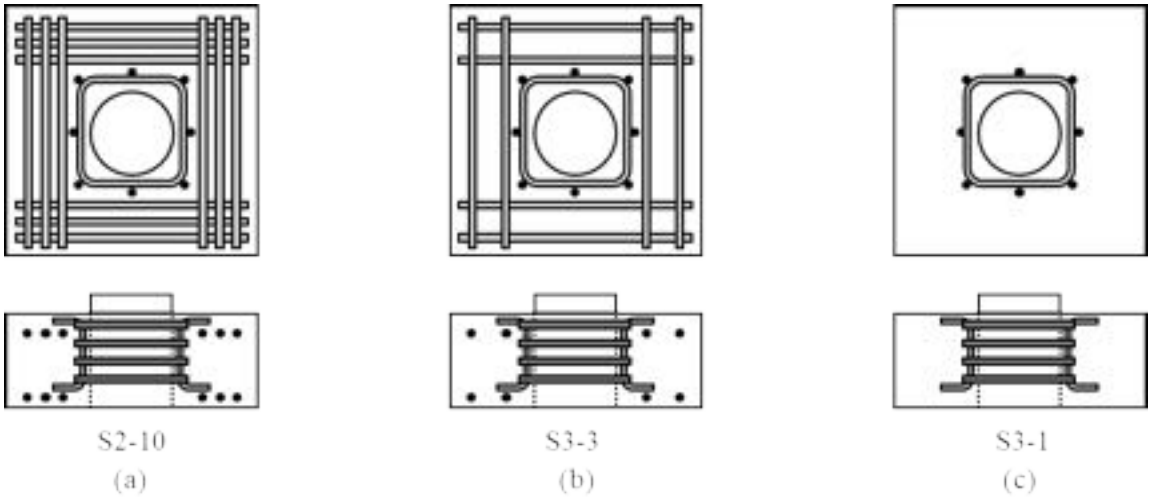

Figure 3-42: Reinforcement details for longitudinal reinforcement specimens, (a) full longitudinal reinforcement, (b) 2/3 longitudinal reinforcement, and (c) no longitudinal reinforcement

The normalized failure load and normalized load versus deflection of the top of the plug for specimens with various amounts of longitudinal reinforcement are shown in Figure 3-43. The normalized strength decreased in specimens with less longitudinal reinforcement. All specimens had a linear response until reaching the maximum load and then had a drop in strength as the cohesion was overcome. The drop in strength immediately following the maximum failure load was steeper in specimens with less longitudinal reinforcement. The specimen with no longitudinal reinforcement around the pocket (S3-1) experienced a more sudden failure after reaching the ultimate load. The other specimens (S2-10 and S3-3) held load as the pocket slid along the interface.

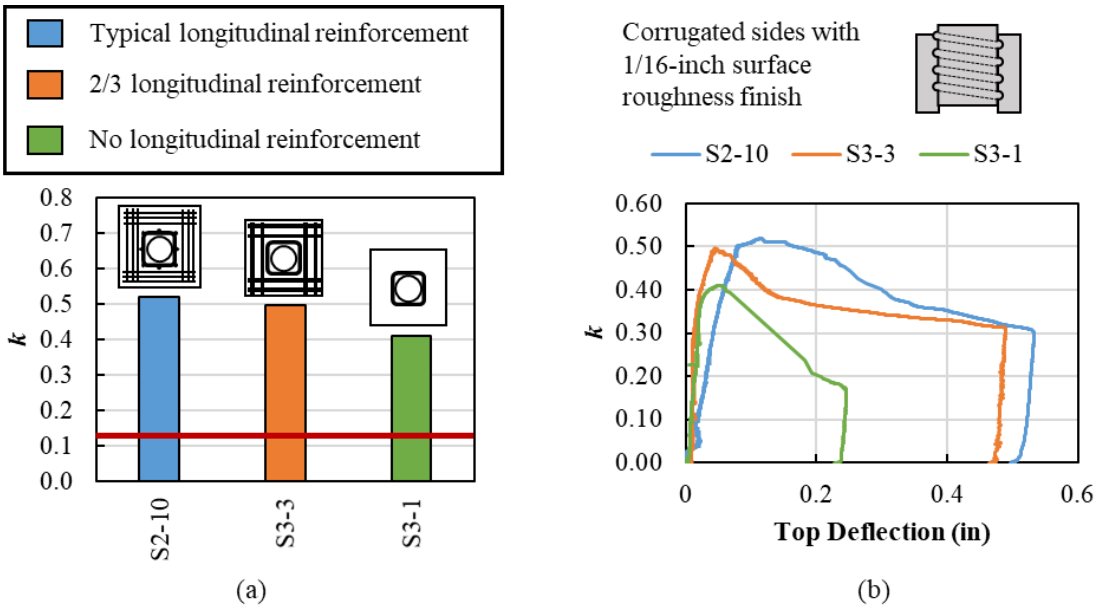

Figure 3-43: (a) Normalized failure loads and (b) normalized load versus top of plug displacement curves for specimens with varying longitudinal reinforcement

The load versus strain curves for the confinement reinforcement around the pocket for the specimens with varying amounts of longitudinal reinforcement are shown in Figure 3-44. The confinement reinforcement in the specimen with full longitudinal reinforcement (S2-10) had a more gradual engagement after cracking; this is because the longitudinal reinforcement was also crossing the splitting crack. The confinement reinforcement in the specimens with less or no longitudinal reinforcement saw a jump in strain without any increase in load at cracking when the stresses were transferred from the uncracked concrete to the confinement reinforcement.

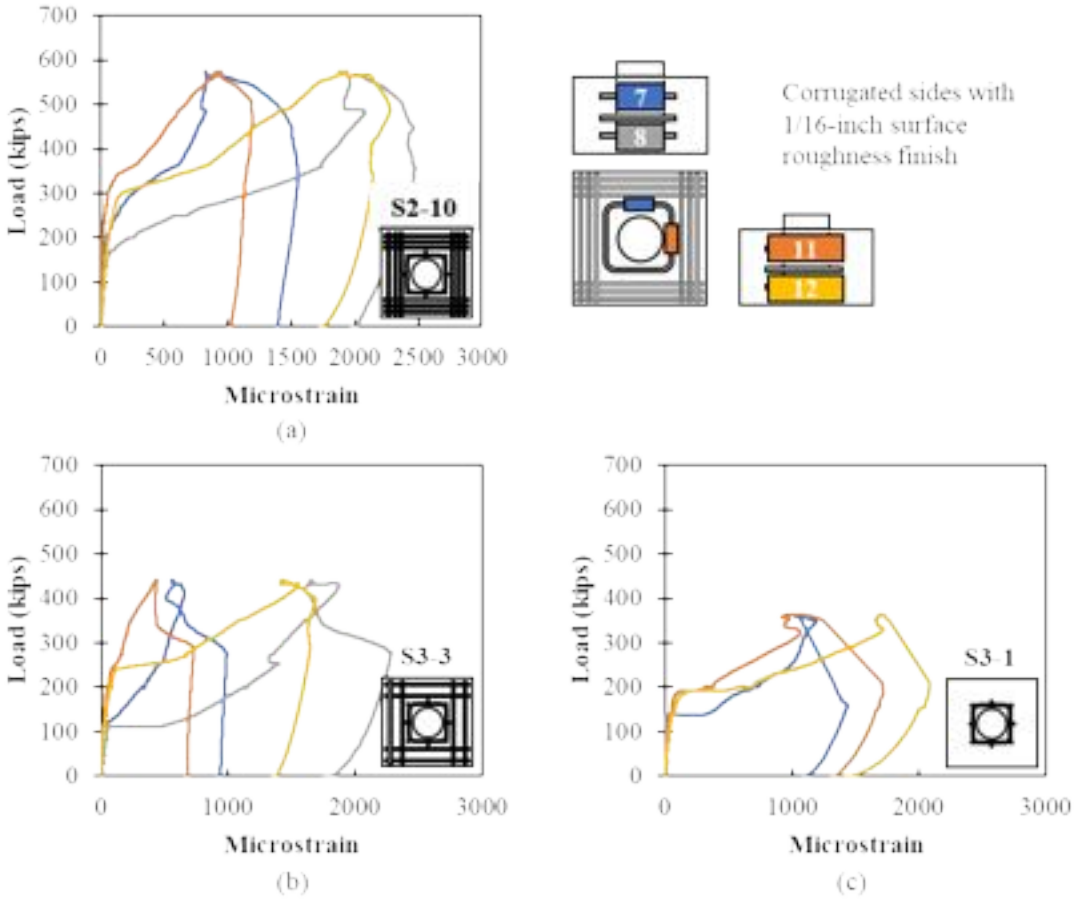

Figure 3-44: Load versus strain in the confinement reinforcement for specimens with varying amounts of longitudinal reinforcement (a) typical, (b) 2/3, and (c) no longitudinal reinforcement

The observed cracking patterns at failure of the specimens with different amounts of longitudinal reinforcement are shown in Figure 3-45. Radial cracks extending from the plug were observed in all specimens with the largest cracks observed in the specimen with full longitudinal reinforcement and the higher concrete strength (S2-10). Cracking surrounding the pocket (transverse to the radial direction) was observed in the specimen without longitudinal reinforcement (S3-1). While some of the other specimens did have some radial cracking, S3-1 was the only specimen where the radial cracking was so pronounced and the primary cracking in the specimen.

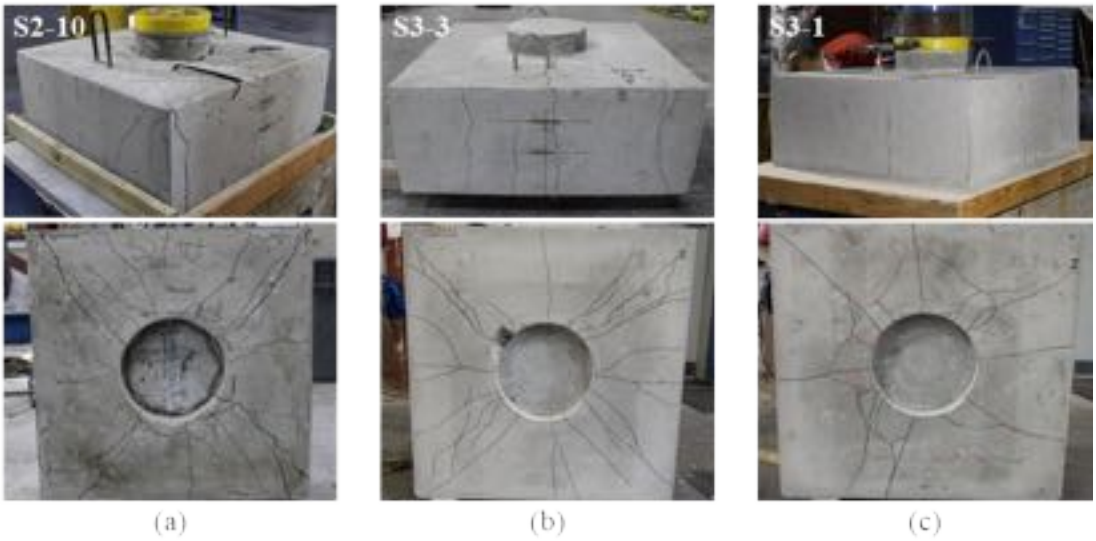

Figure 3-45: Crack pattern at failure for specimens with varying amounts of longitudinal reinforcement (a) typical, (b) 2/3, and (c) no longitudinal reinforcement

Confinement Reinforcement

Six specimens were tested specifically to determine the effect of the confinement reinforcement around the pockets, three with and three without the corrugated metal pipe left in place, as shown in Figure 3-46. Typical longitudinal reinforcement around the pocket was used in all these specimens. These specimens were all 14 inches deep and had $1d_{plug}$ edge distance on all sides. Half of these specimens had a corrugated interface with 1/16-inch concrete surface finish and half had the corrugated metal pipe left in place to see if the corrugated metal pipe provided similar restraint as the confinement reinforcement, as was previously observed by Restrepo et al. (Restrepo et al., 2011).

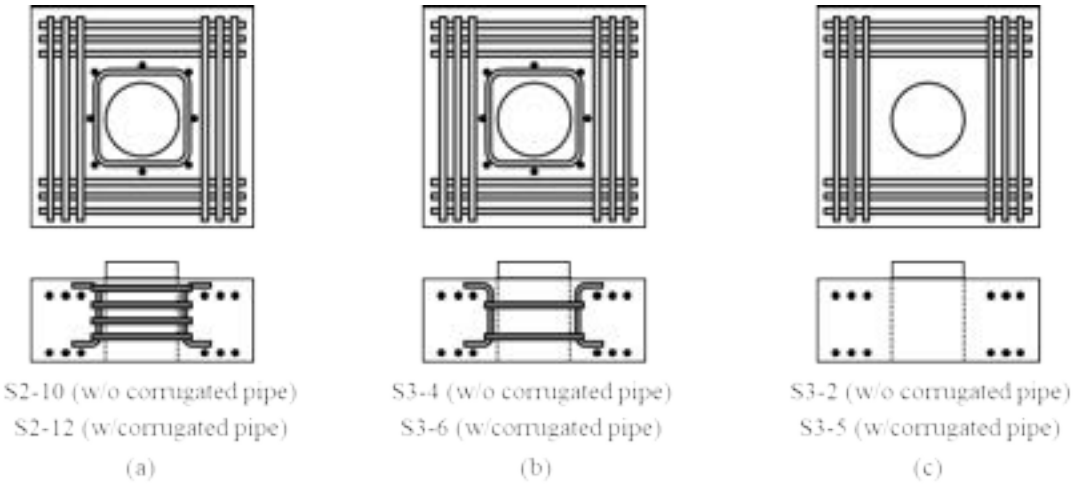

Figure 3-46: Reinforcement details for confinement reinforcement specimens, (a) full longitudinal reinforcement, (b) 2/3 longitudinal reinforcement, and (c) no longitudinal reinforcement

The normalized failure loads for all specimens with different amounts of confinement reinforcement for specimens with a 1/16-inch concrete finish and a corrugated metal pipe finish are shown in Figure 3-47. For the specimens with 1/16-inch concrete finish on the interface, the specimen with no confinement reinforcement had a 4 percent lower strength than the full confinement reinforcement and 9 percent lower strength than the half confinement reinforcement specimen.

The specimens with the corrugated metal pipe finish and less confinement reinforcement had between 19 percent (no confinement reinforcement) and 33 percent (half confinement reinforcement) lower strength than the specimens with corrugated metal pipe finish and full confinement reinforcement. As mentioned above, specimen S2-12 experienced rotation of the plug as the plug pushed through; compared with S3-6 and S3-7 which only experienced minor rotation of the plug.

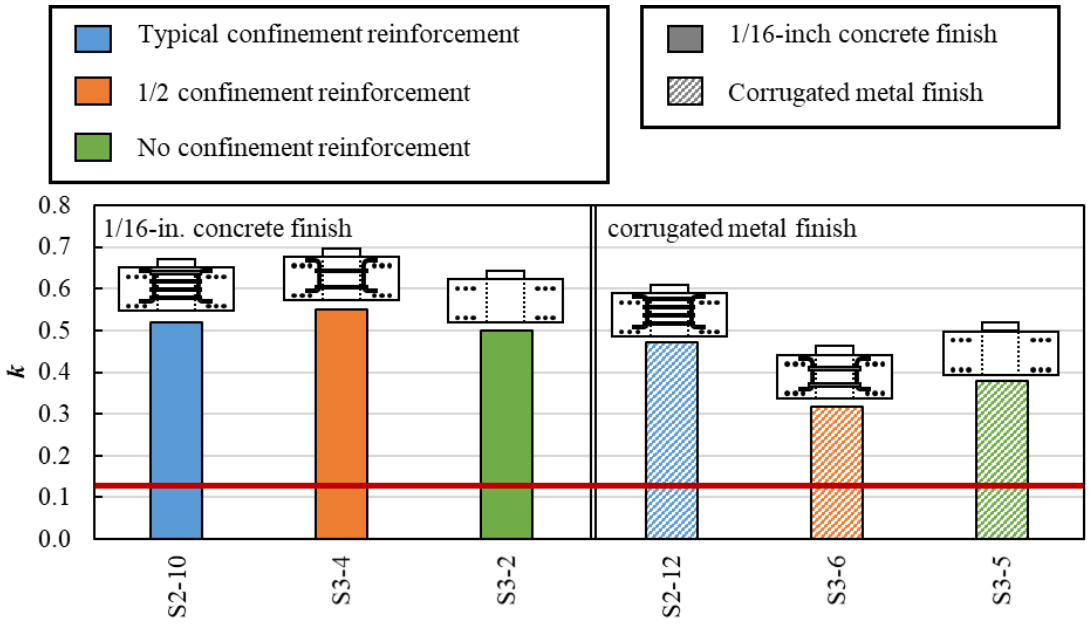

Figure 3-47: Comparison graph for specimens with varying confinement reinforcement around the pocket

The normalized load versus top plug deflection curves for specimens with varying amounts of confinement reinforcement with a 1/16-inch concrete finish and corrugated metal pipe finish are shown in Figure 3-48. The specimens with a 1/16-inch concrete finish, Figure 3-48 (a), all had a relatively linear response until overcoming the cohesion and reaching the failure load. The specimens with less confinement reinforcement seemed to have a more dramatic decrease in strength after reaching the ultimate capacity. Specimens with the corrugated metal pipe finish also had similar responses with a nonlinear response before reaching the ultimate capacity and then maintaining of load as the plug was pushed through, Figure 3-48 (b).

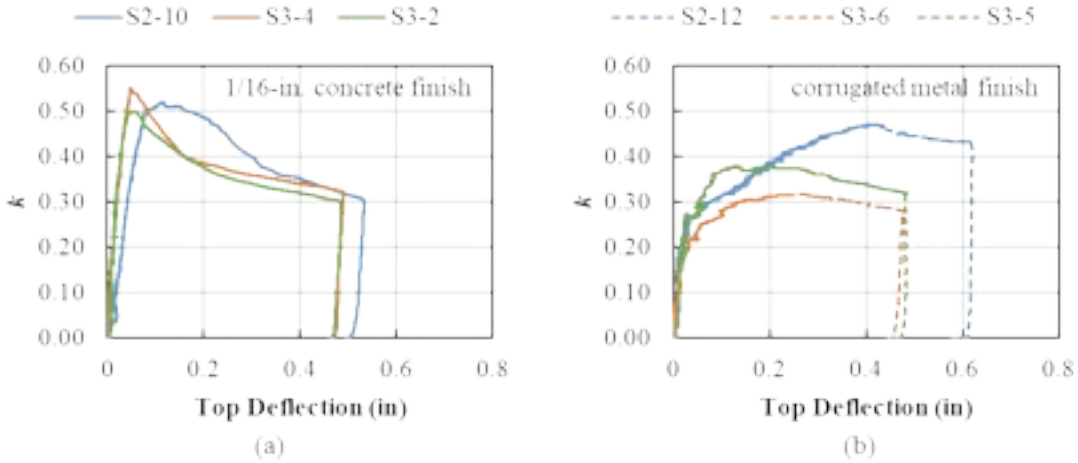

Figure 3-48: Normalized load versus top of plug displacement for specimens with varying confinement reinforcement around the pocket and (a) 1/16-inch concrete finish and (b) corrugated metal finish

The load versus strain curves for the confinement reinforcement in specimens with full reinforcement with 1/16-inch concrete finish and corrugated metal pipe finish are shown in Figure 3-49. The strain in the confinement reinforcement was higher in the top of the specimens with the corrugated pipe left in place and higher in the bottom of the specimens without the corrugated pipe left in place. This would suggest that there is larger expansion of the plug toward the bottom of specimens with the 1/16-inch finish and toward the top of the specimens with the pipe left in place.

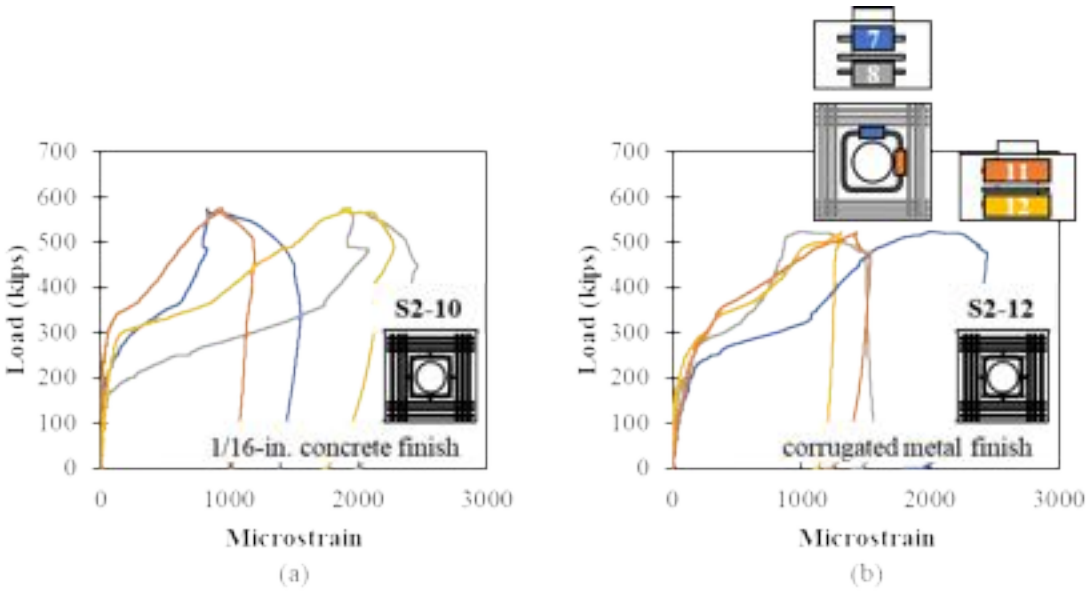

Figure 3-49: Load versus strain for confinement reinforcement for specimens with full reinforcement with (a) 1/16-inch concrete finish and (b) corrugated metal pipe finish

The load versus strain in the longitudinal reinforcement curves for specimens with and without confinement steel and with 1/16-inch concrete finish and corrugated metal pipe finish are shown in Figure 3-50. The longitudinal reinforcement had similar engagement for the fully reinforced specimens with 1/16-inch concrete finish and corrugated metal pipe finish, comparing Figure 3-50 (a) and (b). The specimen without confinement reinforcement and with the corrugated metal pipe left in place (S3-5) saw a larger increase in strain in the longitudinal reinforcement immediately following cracking.

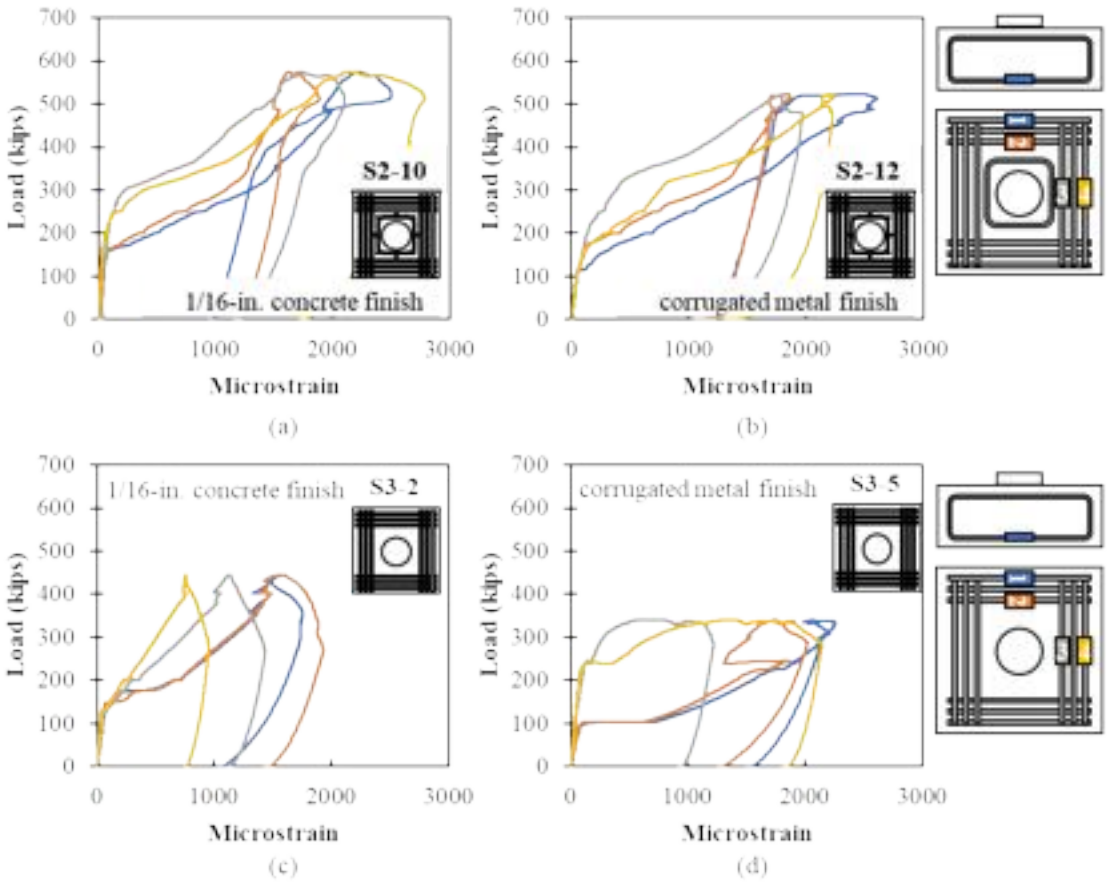

Figure 3-50: Load versus strain in longitudinal reinforcement for (a) full reinforcement with 1/16-inch concrete finish, (b) full reinforcement with corrugated metal pipe, (c) no confinement reinforcement with 1/16-inch concrete finish and (d) no confinement reinforcement with corrugated metal pipe

Two main observations can be stated here:

1. Varying the reinforcement around the pocket does not affect the capacity of the specimen (S2-10, S3-2, S3-4). This means that adding or not confinement to the pocket does not affect the expansion of the plug that occurs during loading.
2. Leaving the corrugated pipe left in place decreases the strength of the specimens.

3.3. Large – Scale Testing

The overall objective of this task was to experimentally evaluate the behavior of the interface between pile cap and plug using pocket and socket connections. Three different series of tests were developed based on the results of the small-scale testing to investigate and evaluate the shear friction capacity and behavior of the connection. Each series has

different experimental variables, specimen geometry, and specimen dimensions. The series were divided as follows:

1. **Larger Diameter Plugs**: The main objective of the first type of testing was to evaluate the interface capacity of the cap-to-plug connection with a larger plug diameter than that tested in Task 2. Four specimens were built in which the primary variables to evaluate were (1) interface surface condition and (2) corrugation spacing and depth.
2. **Multi-Plug Systems**: The objective of this testing was to investigate if there was a negative effect if there are multiple plugs located on the splitting plane of the cap. These specimens had two plugs that were loaded simultaneously using two actuators. Two specimens were built for this series in we evaluated (1) interface surface condition, (2) corrugation spacing and depth, and (3) interface height.
3. **Socket Connection**: The objective of this testing was to evaluate the shear friction failure mechanism for socket type connections where a pile is embedded in the connection region. Two specimens were built in which the primary variables to evaluate were (1) interface surface condition and (2) corrugation spacing and depth.

This report will summarize the test matrix, specimen details, construction of specimens, test setup and load protocol, instrumentation schedule, estimated strengths, and experimental results of each series.

This report provides a summary of each test and test series. A more in depth comparison with the test specimens from Task 2 will be provided in the final report for this project.

3.3.1. Series I: Larger Diameter Plug Testing

This section describes the details of the geometry, construction, test setup/protocol, experimental matrix, and the experimental results for the larger diameter plug specimens.

3.3.1.1. Experimental Variables and Test Matrix

The primary variables to evaluate in this testing were the corrugation spacing and depth and interface surface condition as shown in Table 3-7.

Table 3-7: Experimental variables for Large Diameter Plug Specimens

Experimental Variable	Values for Test Matrix
Interface surface condition	Sandblasted (1/16-inch roughness); corrugated pipe left in place
Corrugation spacing and depth	Smooth, exposed aggregate finish, and metal corrugated pipe

A summary of the combination of these experimental variables that were tested is provided in Table 3-8. The specimen naming included in the table is used to identify these specimens throughout this document.

Table 3-8: Experimental Matrix for Larger Plug Diameter Specimens

#	h_{cap} (in)	d_{plug} (in)	Corrugation Spacing and Depth				Interface Surface Condition
			Description	h_{rib} *(in)*	L_{rib} *(in)*	s_{rib} *(in)*	
LP-1	14	18	Smooth	0	0	0	Sandblasted (1/16" roughness)
LP-2	14	18	Smooth	0	0	0	Paste retarder (1/4" roughness)
LP-3	14	18	Corrugated metal	0.5	0.75	2.67	Sandblasted (1/16" roughness)
LP-4	14	18	Corrugated metal	0.5	0.75	2.67	Corrugated pipe

3.3.1.2. Specimen Geometry and Construction Procedure

Details for construction of the cap and plug and the surface preparation used in the first series of large-scale specimens are explained in this section. The specimens were constructed at CDS Manufacturing Inc in Gretna.

Cap and Plug Construction

The procedure for constructing the larger plug diameter specimens was as follows:

1. A cube was cast with a cylindrical void in the center (referred to as the "cap"). The caps were 14 inches tall and 54 inches wide and deep with an 18-inch diameter cylindrical void. The cylindrical void was constructed using corrugated metal pipes and Sonotubes (smooth cylindrical tubes) to vary the corrugation spacing and depth, as shown in Figure 3-51.

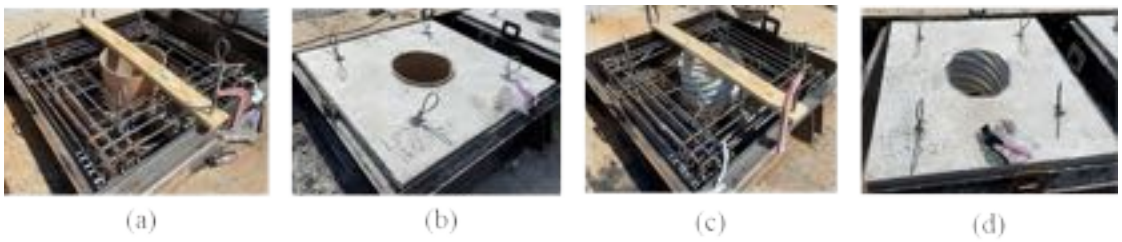

Figure 3-51: Construction and casting of cap: (a) placement of reinforcement and (b) casting of cap concrete for specimen with Sonotube and (c) placement of reinforcement and (d) casting of cap concrete for specimen with corrugated metal pipe.

2. The pipe was removed after the concrete in the cap hardened (4 days after casting of the cap), as shown in Figure 3-52. The surface preparation after removal of the pipe varied based on the desired interface condition.

Figure 3-52: Surface finish after removal of pipe with (a) sonotube and (b) corrugated pipe.

3. After the pipe was removed and the interface surface prepared, a 3-inch-tall cylindrical form with the same diameter as the plug was placed on top of the cap and a 3-inch blockout was installed at the bottom of the plug, as shown in Figure 3-53.

Figure 3-53: Plug construction: (a) 3-inch cylindrical form on top of cap before casting, (b) after casting the plug and (c) close up of the 3-inch cylindrical form.

4. After the concrete had hardened, the formwork and foam blockout were removed. The specimens were then shipped to FDOT's Structures Research Center and prepared for testing.

(a) (b)

Figure 3-54: Delivered specimens at FDOT's Structures Research Center

Surface Finishes

Three different surface preparations were used for these specimens: sand-blasted (1/16-inch surface roughness), exposed aggregate (1/4-inch surface roughness), and corrugated metal duct (pipe left in place).

The sand-blasted surface condition (currently recommended by FDOT) which creates a 1/16-inch roughness is obtained by:

1. Removing the Sonotube or corrugated pipe used to form the pocket in the pile cap.
2. Sand or water blasting interfacing surface.
3. Sealing and filling void with potable water for 4 to 5 hours.
4. Removing water to achieve SSD condition prior to cast concrete. Water should be removed within a few hours of casting the concrete.

This surface finish was achieved in a different manner by the precaster since they did not have a sandblaster available on site. The sandblasted (1/16-inch roughness) surface condition was achieved at CDS using a demolition hammer with a chisel attachment. They chipped away parts of the concrete as shown in Figure 3-55 (a). Additionally, the interface surfaces were not prewetted before casting of the plugs (as specified in Step 3).

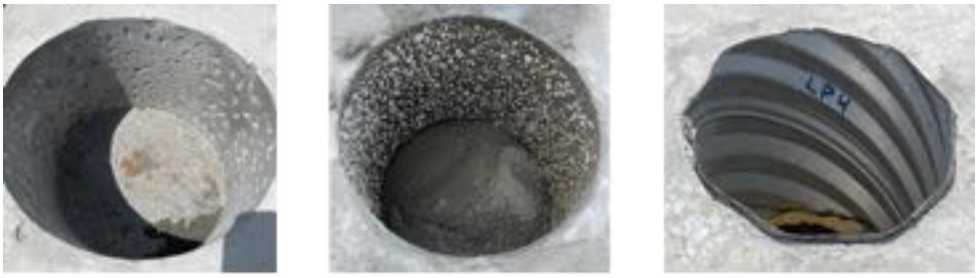

Figure 3-55: Surface finishes for larger-plug specimens: (a) electrical hammer with chisel attachment, (b) exposed aggregate finish, and (c) metal pipe left in place.

A 1/4-inch exposed aggregate finish, shown in Figure 3-56 (c) was achieved using the following procedure:

1. A polyurethane clear coat was applied to the cylindrical void to prevent the set retarding agent from primarily being absorbed by the form.
2. The set retarding agent was applied to the formwork where the exposed aggregate finish was desired (i.e., the plug) within 24 hours of the casting time.
3. The plug void was then placed in the cap, Figure 3-56 (a), and the cap concrete cast.
4. The plug form was removed, and a pressure washer was used to wash away the unhydrated paste on the surface of the plug, as shown in Figure 3-56 (b). Care was taken to ensure the paste was washed away without fracturing the aggregate.

Figure 3-56: Exposed aggregate finish: (a) pipe with the set retarding agent, (b) pressure washing the surface, and (c) surface finish.

3.3.1.3. Test Setup and Loading Protocol

A photograph of the test setup is shown Figure 3-57. The load was applied to the specimens using a 1000-kip hydraulic jack.

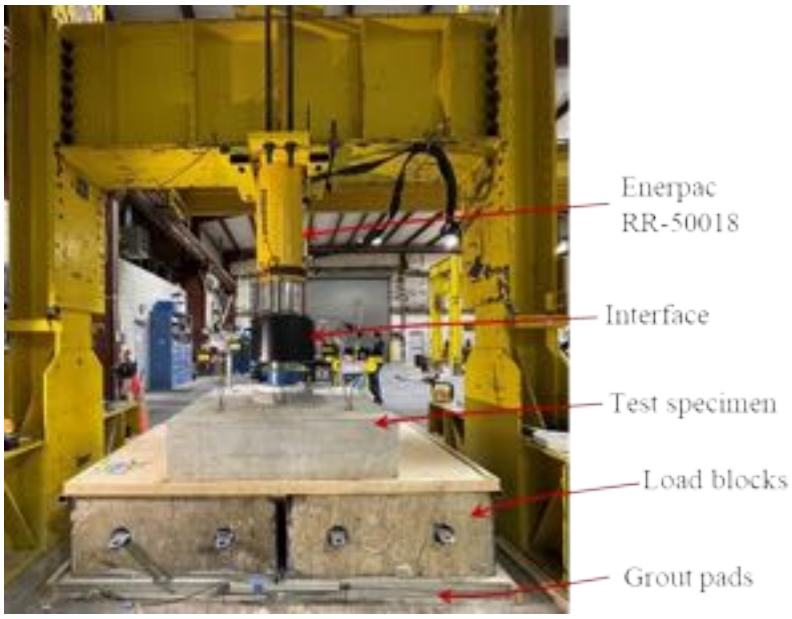

Figure 3-57: Photograph of test setup for larger plug specimens.

The specimens were placed on top of 12 load blocks for testing. The load blocks were slightly separated in the east-west direction to allow for the displacement of the bottom of the plug to be measured. This detail is shown in Figure 3-58.

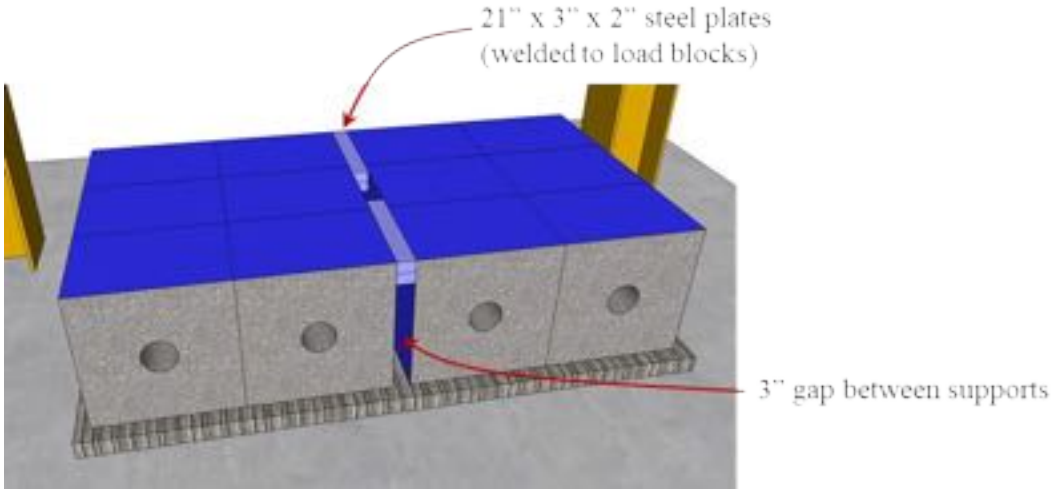

Figure 3-58: Schematic of supports with 3-inch space between load blocks

All specimens were tested using the same loading procedure. The load was applied at a rate of 0.2 kips per second until a load of 200, 300, and 400 kips was reach for all specimens. In each stop, the respective load was held on the specimens while the specimens were inspected for cracks; cracks were marked, labeled, and documented, as shown in Figure 3-59. A sample load versus deflection plot for LP-1 with the stops made during testing are highlighted in Figure 3-59 (b). Load was then applied at the same load rate (0.2 kips per second) until failure of the interface or test capacity was reached. Cracks were marked on all sides (including the bottom) of the specimens after they were removed from the test frame. A sample crack pattern on the bottom of Specimen LP-1 after failure is shown in Figure 3-59 (c).

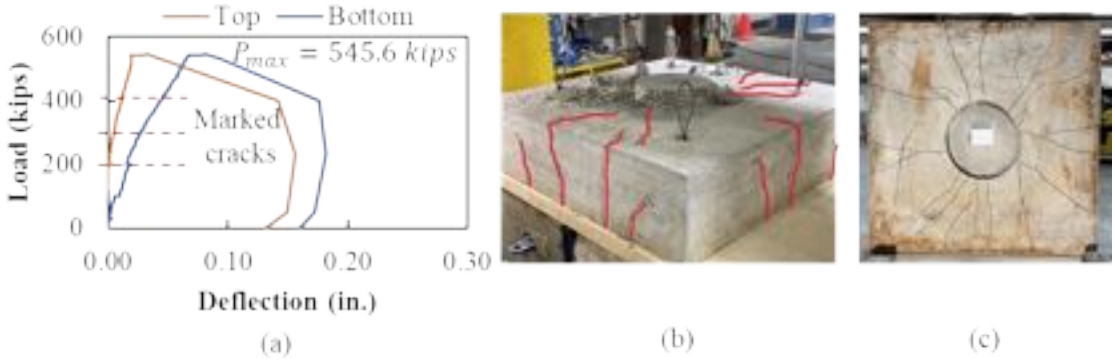

Figure 3-59: (a) Sample load versus deflection plot with stops, (b) crack pattern after failure, and (c) crack pattern on bottom specimen after failure for Specimen LP-1

3.3.1.4. Instrumentation Schedule

The instrumentation scheme used for larger plug specimens is shown in Figure 3-60. Three different types of instrumentation were used: concrete strain gauge (CSG), rebar strain gauges (RSG), and laser displacement transducers (LDT). CSGs were used to monitor crack development on the surface of the specimens during testing. RSGs were used to measure the engagement of the reinforcement while loading. Finally, five LDTs were used to monitor the displacement of the top and bottom of the plug relative to the cap.

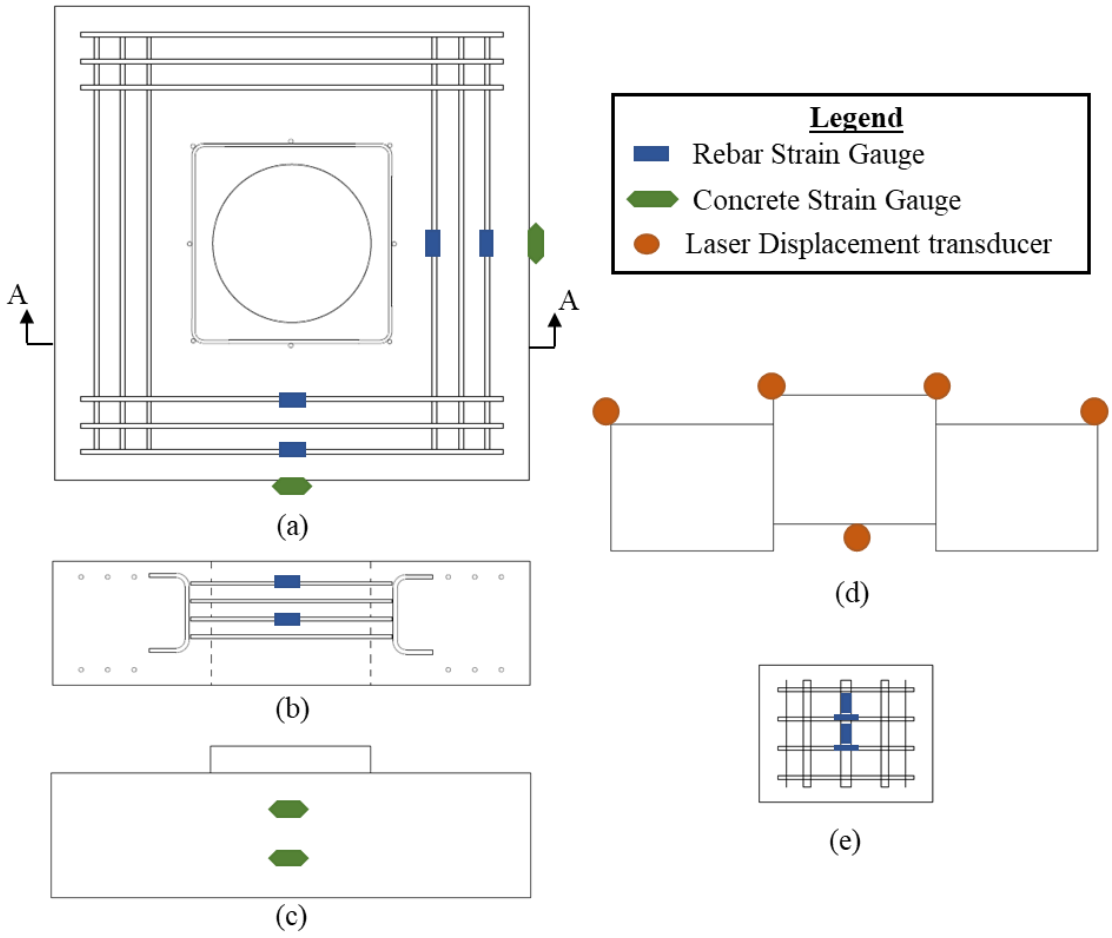

Figure 3-60: Instrumentation scheme for larger plug specimens: (a) pile cap bottom view, (b) section A-A, (c) cap elevation, (d) specimen elevation through centerline, and (e) plug reinforcement detail.

3.3.2. Series II: Multi-Plug Testing

This section describes the details of the geometry, construction, test setup/protocol, the experimental matrix, and experimental results for the multi-plug testing.

3.3.2.1. Experimental Variables and Test Matrix

The principal variable evaluated in the multi-plug system was the interface surface condition, as shown in Table 3-9. The same corrugation spacing and depth (created using the metal corrugated pipe) and same interface height (9 inches) were used for both specimens.

Table 3-9: Experimental Variables to Evaluate in the Multi-plug System Testing.

Experimental Variable	Possible Values for Test Matrix
Interface surface condition	Sandblasted (1/16-inch roughness), metal corrugated pipe
Corrugation spacing and depth	Metal corrugated pipe
Interface height	9-inch

The experimental matrix based on these variables is shown in Table 3-10.

Table 3-10: Experimental Matrix to test Multi-plug System.

#	h_{cap} (in)	d_{plug} (in)	Corrugation Spacing and Depth				Interface Surface Condition
			Description	h_{rib} *(in)*	L_{rib} *(in)*	s_{rib} *(in)*	
MP-1	14	12	Corrugated metal	0.50	0.75	2.67	Corrugated metal
MP-2	14	12	Corrugated metal	0.50	0.75	2.67	Sandblasted (1/16" roughness)

3.3.2.2. Specimen Geometry and Construction Procedure

Details for construction of the cap and plugs and the surface preparation used in the second series of large-scale specimens are explained in this section. The specimens were also constructed at CDS Manufacturing Inc in Gretna.

Cap and Plugs Construction

The construction procedure for this testing was similar to the larger plug diameter testing described above. The procedure was as follows:

1. A reinforced concrete prism was cast (referred to as the "cap") with two 12-inch diameter cylindrical voids spaced 24 inches apart (edge to edge). The cylindrical voids were constructed using 12-inch diameter corrugated metal pipe.

Figure 3-61: Construction and casting of multi-plug specimens: (a) reinforcement layout, (b) corrugated pipes placed, and (c) after concrete had hardened.

2. After the concrete had hardened, one of the plug forms was removed (4 days after casting of the cap) and the surface of the plugs were prepared as indicated in the test matrix. In the other cap, the pipes were left in place.
3. After the pipes were removed and the interface properly prepared, a 3-inch-tall cylindrical form with the same diameter as the plug was placed on top of the cap and 5-inch blockout was installed at the bottom of each plug to create the correct dimensions for the plug. The plug reinforcement was then placed, and concrete cast as show in Figure 3-62.

Figure 3-62: Casting of the plug: (a) 3-inch form and reinforcement was placed and (b) concrete was cast.

4. After the concrete had hardened, the formwork and foam blockout were removed. The precast specimens were then shipped to FDOT's Structures Research Center and prepared for testing.

Surface Finish

Only the sandblasted (1/16-inch roughness), surface preparation was used for this testing. This surface condition creates a 1/16-inch roughness and was obtained by:

1. Removing the corrugated pipe used to form the pocket in the pile cap.

2. Sand or water blasting interfacing surface.
3. Sealing and filling void with potable water for 4 to 5 hours.
4. Removing water to achieve SSD condition prior to pouring concrete. Water should be removed within a few hours of casting the concrete.

Like the larger plug specimens, an alternate procedure was used to create this surface finish, and the plugs were not prewetted for the same reasons explained above. See §0 for more details.

3.3.2.3. Test Setup and Loading Protocol

A schematic and photograph of the test setup for the multi-plug testing is shown in Figure 3-63. The load was applied to the specimens using two 500-kip hydraulic jacks.

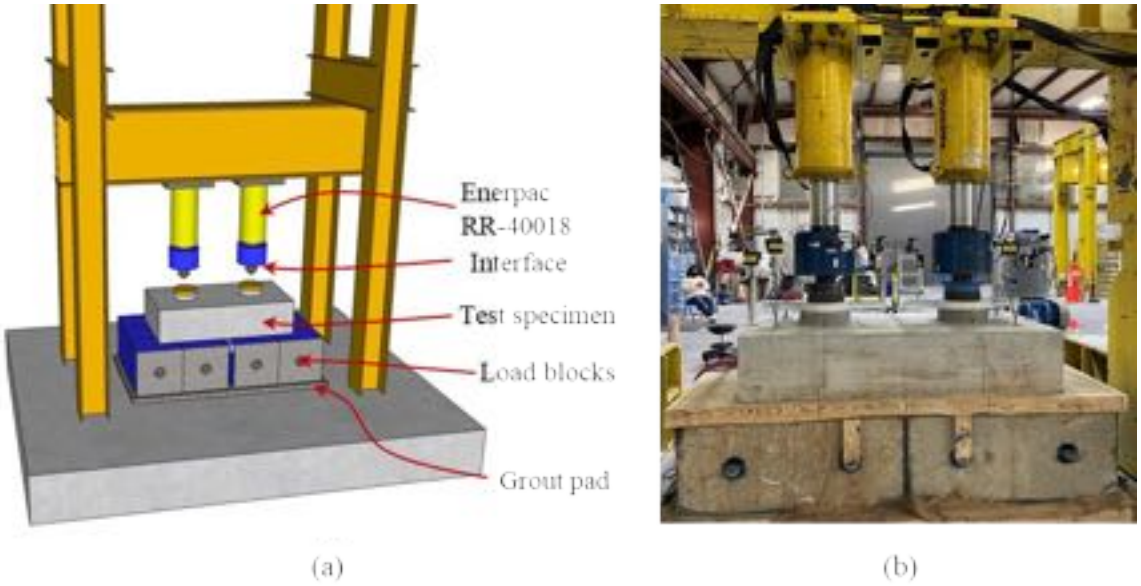

Figure 3-63: (a) Schematic and (b) photograph of test setup for multi-plug specimens.

The specimens were placed on top of 12 load blocks for testing. The blocks were slightly separated (3-inch) to allow for measurement of the displacement of the bottom of the plugs as shown in Figure 3-64.

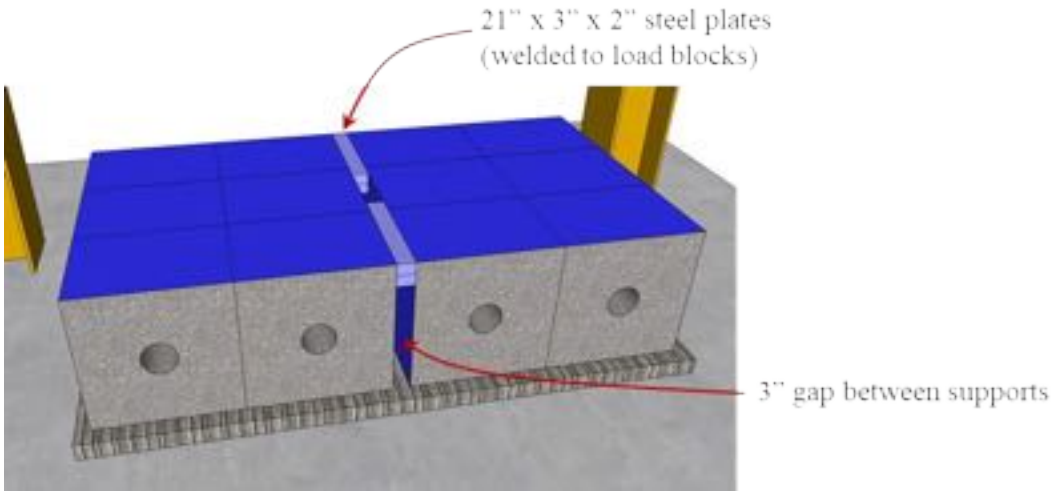

Figure 3-64: Schematic of supports with 3-inch space between load blocks

Both specimens were tested using the same loading procedure explained in this section. This testing was limited to 1000 kips of total load, which is the capacity of the load frame. The load was applied at a rate of 0.2 kips per second until a load of 150, 250, and 350 kips per plug was reached for all specimens. The respective load was held on the specimens during each stop while the specimens were inspected for cracks; cracks were marked, labeled, and documented, as shown in Figure 3-65. Load was then applied at the same load rate (0.2 kips per second) until the maximum capacity of test frame (500 kips per plug).

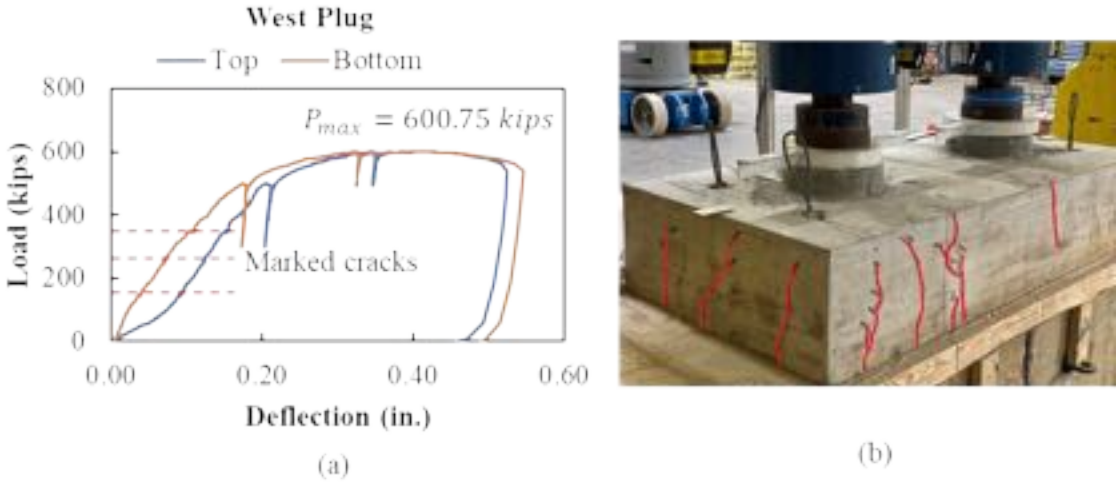

Figure 3-65: (a) Sample load versus deflection plot with stops for west plug and (b) crack pattern after failure of MP-2

Neither of the multi-plug specimens failed when there was 500-kips per plug on the system. The capacity of the load frame was 1000 kips, so no additional load could be applied to both plugs at the same time. At this point, the load was decreased on both plugs. The load on the east plug was held constant at a lesser load while the load on the west plug was increased until the reaction reached 500 kips on one side of the load frame. For simplicity, the load frame system was assumed to be simply supported to determine the maximum load that could be applied on the west plug with different loads being held on the east plug, as shown in Figure 3-66.

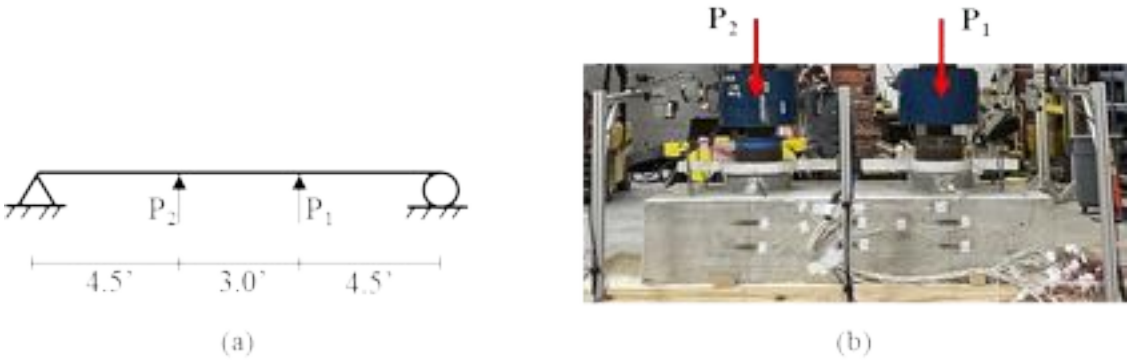

Figure 3-66: (a) Assumed loading and boundary conditions for load frame and (b) side view of specimen during testing for the multi-plug test specimens

These three different stages of loading are summarized in Table 3-11. After maximum capacity in MP Load Stage 1, both plugs were unloaded to 300 kips and the west plug was loaded to 600 kips while keeping the east load constant at approximately 300 kips. If no failure was seen, the load on the east plug was unloaded to 160 kips and kept constant while the loading in the west plug was increased to 700 kips or failure of the specimen.

Table 3-11: Maximum loading per plug for MP Load Stages

MP Load Stage	Max Load on West Plug (P_2)	Max Load on East Plug (P_1)
Stage 1	500 kips	500 kips
Stage 2	600 kips	333 kips
Stage 3	700 kips	167 kips

After failure, cracks were marked on all sides (including the bottom) of the specimens after they were removed from the test frame.

3.3.2.4. Instrumentation Schedule

The instrumentation scheme for multi plug specimens is shown in Figure 3-67. Like the larger plug specimens, three different types of instrumentation were used: concrete strain gages (CSG), rebar strain gages (RSG), and laser displacement transducers (LDT).

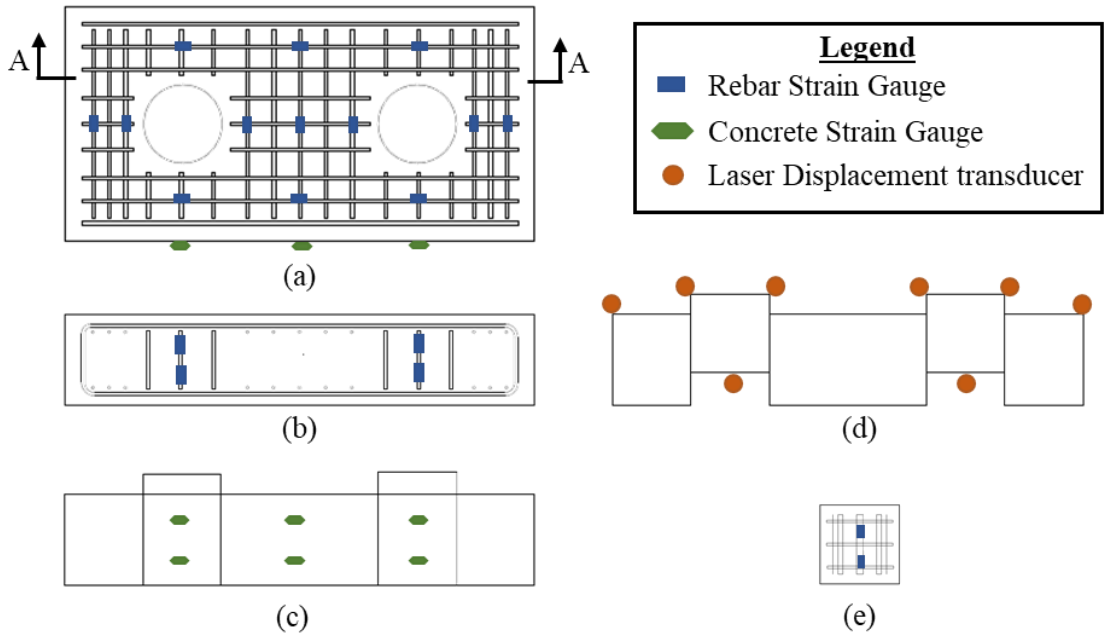

Figure 3-67: Instrumentation scheme for multi plug specimens: (a) pile cap bottom view, (b) section A-A, (c) cap elevation, (d) specimen elevation through centerline, and (e) plug reinforcement detail.

3.3.3. Series III: Socket Connection

This section describes the details of the geometry, construction, test setup/protocol, the experimental matrix, and experimental results for the socket connection specimens.

3.3.3.1. Experimental Variables and Test Matrix

The primary variable evaluated in this testing was the interface surface condition, as shown in Table 3-12. Metal corrugated pipe was used to create the void in both specimens in this series.

Table 3-12: Experimental variables to Socket Connection Testing

Experimental Variable	Values for Test Matrix
Interface surface condition	Sandblasted (1/16-inch roughness); corrugated pipe left in place
Corrugation spacing and depth	Metal corrugated pipe

The experimental test matrix is shown in Table 3-13.

Table 3-13: Experimental test matrix for socket connection specimens

#	h_{cap} (in)	d_{plug} (in)	Corrugation Spacing and Depth				Interface Surface Condition
			Description	h_{rib} *(in)*	L_{rib} *(in)*	s_{rib} *(in)*	
SC-1	14	30	Corrugated metal	0.50	0.75	2.67	Sandblasted (1/16" roughness)
SC-2	14	30	Corrugated metal	0.50	0.75	2.67	Corrugated metal

3.3.3.2. Specimen Geometry and Construction Procedure

Details for construction of the socket connection and the surface preparation used for this series are explained in this section. The specimens were also constructed at CDS Manufacturing Inc in Gretna.

Socket Connection Construction

The construction procedure for this testing is similar to the larger-plug specimens. The procedure is as follows:

1. An 18-inch pile with a 20-inch length was cast beforehand. The 20-inch length was cut from a longer standard 18-inch pile cast for a different job.
2. A reinforced concrete cube (referred as the "cap") was cast with a 30-inch cylindrical void in the center. The cylindrical void was constructed using corrugated metal pipe as shown in Figure 3-68.

(a) (b)

Figure 3-68: (a) construction of the socket connection specimen and (b) casting of the cap.

3. After the concrete had hardened, one of the plug forms was removed (4 days after casting of the cap) and the surface was prepared as indicated in the test matrix. In the other cap, the pipe was left at place.
4. After the pipe was removed and the interface surface properly prepared, a 3-inch foam blockout was placed at bottom to create void.
5. After placing the reinforcement in plug (Figure 3-69 (c)), the 18-inch pile was suspended above the plug with a 4-inch embedment into the void. The plug concrete was cast around the sides of the plug.

(a) (b) (c)

Figure 3-69: Construction of Socket Connection: (a) and (b) details of 18-inch pile and (c) reinforcement in the plug.

6. After the concrete had hardened, the formwork and foam blockout were removed. The precast specimens were then shipped to FDOT's Structures Research Center and prepared for testing.

Observation from Construction

The precaster experienced some difficulties when trying to place and hold the embedded pile in the void while casting the concrete. As a result, the actual pile embedment length and squareness varied slightly from the construction plans for both specimens (SC-1 and

SC-2). The specified length of the pile was 20-inch, and the specified embedment length was 4-inch. The measured length of the four corners of the pile after casting are shown in Figure 3-70 (a) for SC-1 and Figure 3-71 (a) for SC-2. These measurements were taken at CDS the same day when the void was cast. The resulting embedment lengths (based on the specified 20-inch pile length) are shown in Figure 3-70 (b) and (c) for SC-1 and Figure 3-71 (b) and (c) for SC-2. The average embedment length for Specimen SC-1 is 5.38-inch and for Specimen SC-2 is 4.31-inch. These values were used as the interface length for the estimation procedures for these specimens.

The pile in Specimen SC-1 was leaning about three degrees to the south-west corner as shown in Figure 3-70. The pile in this corner was embedded about 6 inches into the socket, while the pile embedment in the opposite corner was about 5 inches.

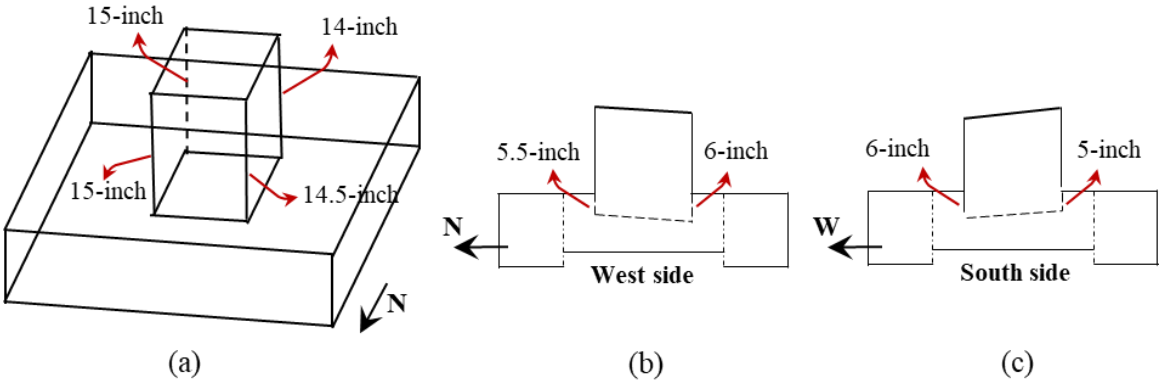

Figure 3-70: Pile embedment details in specimen SC-1: (a) measurements taken at site, (b) west side view and embedment of the pile, and (c) south view and embedment of the pile.

The pile in Specimen SC-2 was leaning two to three degrees to the south-west corner as shown in Figure 3-71. The pile in this corner was embedded about 5 inches into the socket, while the pile embedment in the opposite corner was about 4 inches.

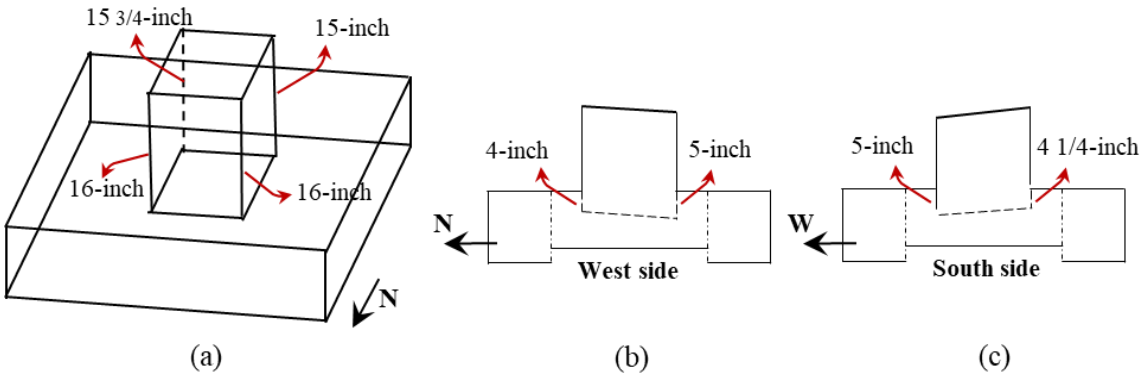

Figure 3-71: Pile embedment details in specimen SC-2: (a) measurements taken at site, (b) west side view and embedment of the pile, and (c) south view and embedment of the pile.

A level grout pad was poured on top of the pile before testing to make the top of the pile parallel with the top of the cap. The specimens seemed to fail on the side with the larger embedment of the pile.

Surface Finish

Only the sandblasted (1/16-inch roughness) surface preparation was used for this testing. This surface condition was obtained by:

1. Removing the corrugated pipe used to form the pocket in the pile cap.
2. Sand or water blasting interfacing surface.
3. Sealing and filling void with potable water for 4 to 5 hours.
4. Removing water to achieve SSD condition prior to pouring concrete.

Like the larger plug specimens, an alternate procedure was used this surface finish, and the plugs were not prewetted for the same reasons explained above. See §0 for more details.

3.3.3.3. Test Setup and Loading Protocol

A photograph of the test setup is shown Figure 3-72. The load was applied to the specimens using a 1000-kip hydraulic jack.

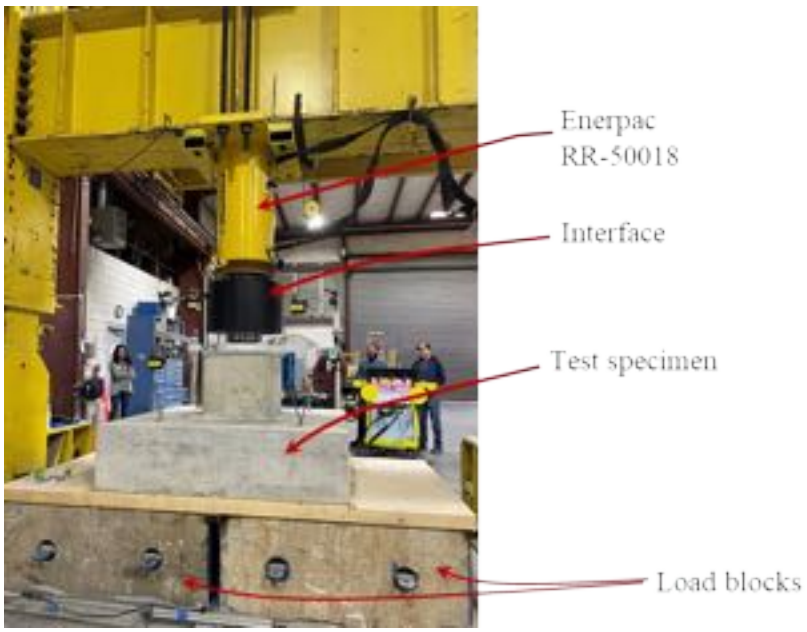

Figure 3-72:Photograph of test setup for socket connection specimens

As in the larger plug specimens, socket connection specimens were placed on top of six load blocks for testing. The load blocks were slightly separated in the north-south direction to allow for the displacement of the bottom of the plug to be measured.

Both specimens were tested using the same loading procedure. The load was applied at a rate of 0.2 kips per second until a load of 175 and 350 kips was reached. For specimen SC-1 only one stop at 350 kips was made, and for SC-2 both stops at 175 and 350 kips were made. In each stop, the respective load was held on the specimens while the specimens were inspected for cracks; cracks were marked, labeled, and documented, as shown in Figure 3-73. The load versus deflection plot for SC-1 with the stops made during testing are highlighted in Figure 3-73 (a). Load was then applied at the same load rate (0.2 kips per second) until failure of the specimen. Cracks were marked on all sides of the specimens after they were removed from the test frame.

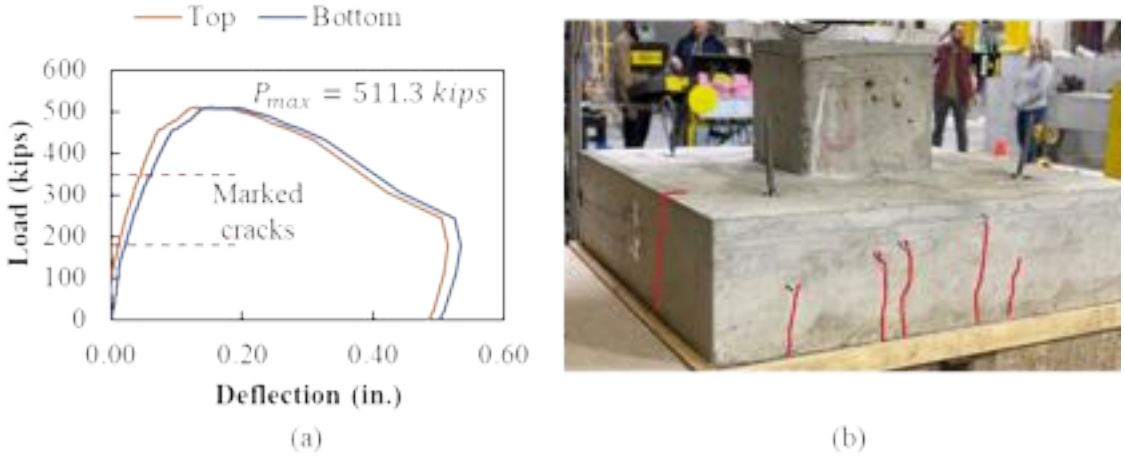

Figure 3-73: (a) Sample load versus deflection plot with stops and (b) crack pattern at 350 kips for specimen SC-1

3.3.3.4. Instrumentation Schedule

The same types of instrumentation as the previous specimens were used for these specimens: concrete strain gage (CSG), rebar strain gages (RSG), and laser displacement transducers (LDT). The instrumentation scheme for socket connection specimens is shown in Figure 3-74.

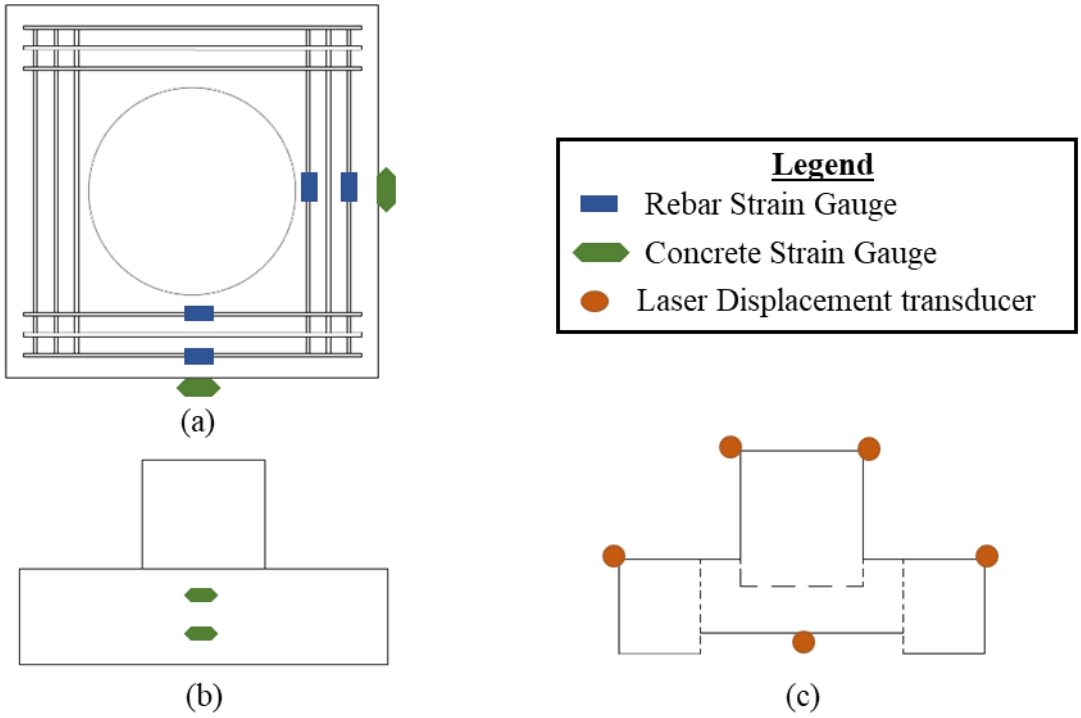

Figure 3-74: Instrumentation scheme for socket connection: (a) pile cap bottom view, (b) cap elevation, and (c) specimen elevation through centerline.

3.3.4. Experimental Results of Large-Scale Testing

The results from the large-scale tests are further analyzed in this section. Results are normalized to facilitate comparisons between specimen types. Normalization of results was performed like the small-scale test results in Task 2d.

Two different normalizations can be used to analyze the data (based on available specifications):

3. Based on AASHTO LRFD Bridge Design Specification 8th Edition (American Association of State Highway and Transportation Officials (AASHTO), 2017b):

$$V_{ni} = cA_{cv} + \mu(A_{vf}f_y + P_c)$$ Equation 3-4 AASHTO (5.7.4.3-3)

$$c = \frac{V_{ni,ex}}{A_{cv}}$$ Normalization based on cohesion (when $A_{vf} = P_c = 0$)

4. Based on AASHTO LRFD Guide Specification for ABC 1st Edition (American Association of State Highway and Transportation Officials (AASHTO), 2018):

$$V_n = 0.13\sqrt{f'_{cp}}\,A_{cv}$$ Equation 3-5 (3.6.6.6-1)

$$k = \frac{V_{ni,ex}}{\sqrt{f'_{cp}}A_{cv}}$$ *k* normalization

The interface area in both equations is:

$$A_{cv} = \pi d_v h_v$$ Equation 3-6

The *k* normalization will be used in the comparisons of the analysis of the results as it also includes concrete strength in its normalization. The measured compressive strengths, cracking loads, ultimate loads, and normalized ultimate loads are summarized in Table 3-14 for large scale specimens. The currently recommended value for *k* in the AASHTO LRFD Guide Specification for ABC is 0.13; all measured k values were above this currently recommended *k* value.

Table 3-14: Measured concrete strength and estimated versus measured ultimate strength and displacement for large-scale specimens

Spec.	**Compressive Strength on Test Day (ksi)**		**Cracking Load (kips)**	**Ultimate Load (kips)**	$\boldsymbol{c = \frac{V_{ni,ex}}{A_{cv}}}$	$\boldsymbol{k = \frac{V_{ni,ex}}{\sqrt{f'_{cp}}A_{cv}}}$
	Cap	*Plug*				
LP-1	*8.56*	*7.27*	*77*	*545.6*	*0.877*	*0.325*
LP-2	*8.58*	*7.41*	*70*	*> 1000*	*>1.61*	*>0.59*
LP-3	*8.58*	*7.41*	*83*	*> 1000*	*>1.61*	*>0.59*
LP-4	*8.58*	*7.41*	*82*	*> 1000*	*>1.61*	*>0.59*
MP-1*	*8.37*	*7.49*	*150*	*600.8*	*1.771*	*0.647*
MP-2*	*8.37*	*7.49*	*130*	*626.4*	*1.846*	*0.675*
SC-1	*8.56*	*7.27*	*79*	*511.0*	*0.739*	*0.274*
SC-2	*8.56*	*7.27*	*74*	*601.4*	*0.870*	*0.323*

*cracking and ultimate load are based on the load applied to the west plug.

3.3.4.1. Analysis of Results

This section compares similar variables between series of large-scale specimens. More details on the behavior of each specimen are found on previous sections.

Effect of Interface Roughness (1/4-inch versus 1/16-inch)

Like the small-scale specimens the interface surface condition was also evaluated in large scale specimens. The interface surface condition directly influences the cohesion component of the shear friction capacity. The conditions that were evaluated for this variable were: sandblasted (1/16-inch roughness), corrugated pipe left in place (metal finish), and exposed aggregate finish (1/4-inch roughness). The 1/4-inch and 1/16-inch roughness interfaces without corrugations are compared in this section.

The exposed aggregate finish (1/4-inch roughness) led to higher measured strength than the sandblasted finish (1/16-inch roughness), as shown in Figure 3-75. The normalized load versus deflection response for both specimens without corrugation was linear up to the failure load or maximum load of the test setup. The specimen with the exposed aggregate finish had a slightly softer response than the specimen with sandblasted finish with approximate slope of 10.1/in. for LP-1 and 5.7/in. for LP-2.

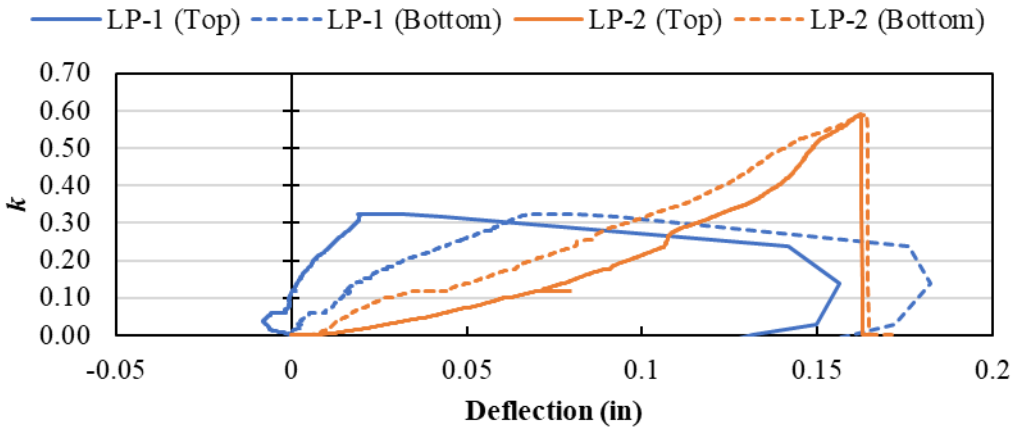

Figure 3-75: Normalized load (k) versus top and bottom deflection for (a) LP-1 (1/16-inch roughness) and (b) LP-2 (1/4-inch roughness) without corrugations

Additional cracking was observed in the specimen with exposed aggregate finish (LP-2) compared to the specimen with the sandblasted 1/16-inch roughness finish (LP-1), as shown in Figure 3-76.

Figure 3-76: Crack patterns at failure for (a) LP-1 (1/16-inch roughness) and (b) LP-2 (1/4-inch roughness) without corrugations

The increased roughness also led to increased engagement of the confinement reinforcement around the pocket, see Figure 3-77. The confinement reinforcement in LP-2 (exposed aggregate finish) reached a yield strain at approximately 230 kips, see RSG-PCN6 in Figure 3-77 (b), while the confinement reinforcement LP-1 remained less that yield even when the plug suddenly slid through the cap.

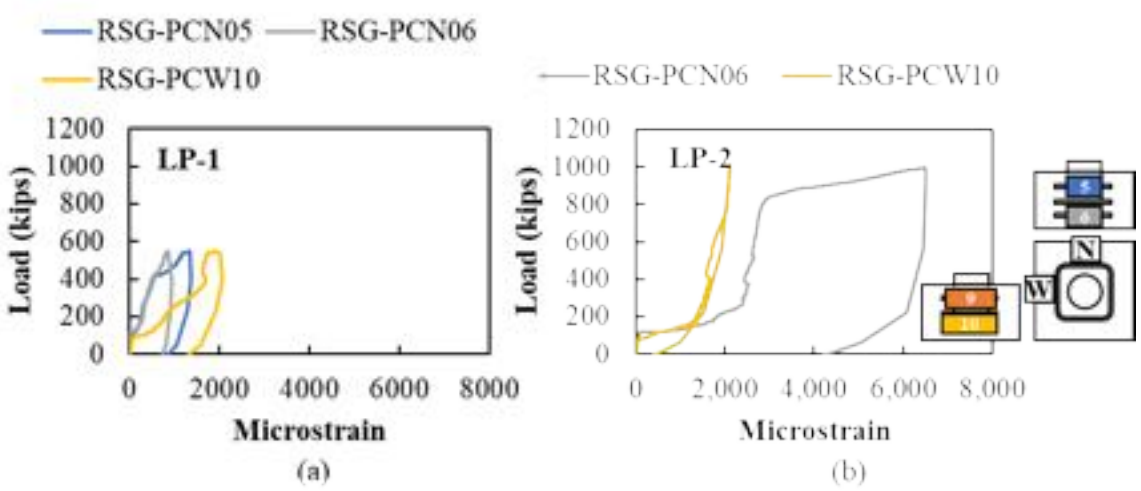

Figure 3-77: Rebar strain in confinement reinforcement around the pocket of (a) LP-1 (1/16-inch roughness) and (b) LP-2 (1/4-inch roughness) without corrugations

LP-1 and LP-2 cracked at similar loads, 77 and 70 kips, respectively. There was generally similar engagement of the longitudinal reinforcement between the LP-1 and LP-2 with the reinforcement reaching higher strains at higher loads, see Figure 3-78.

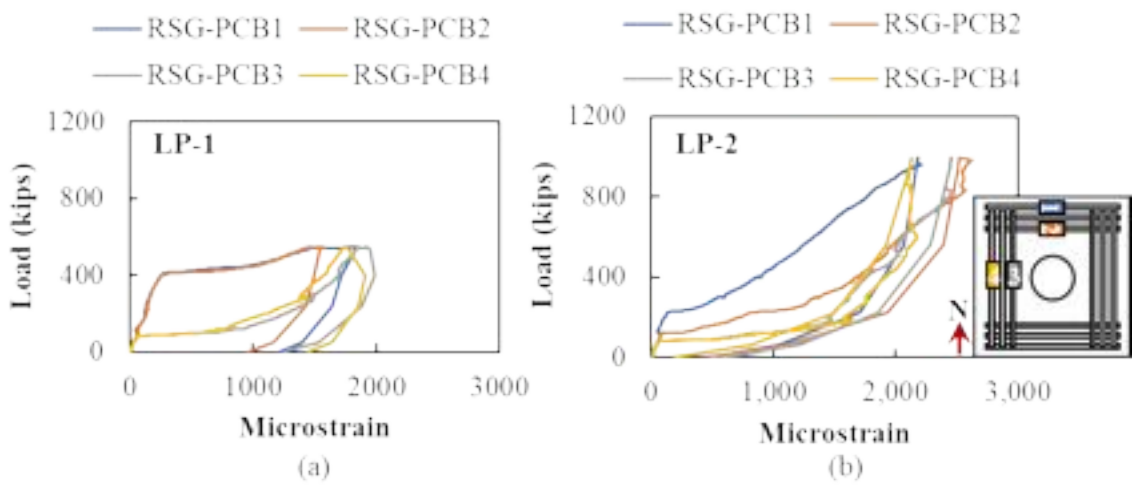

Figure 3-78: Rebar strain in longitudinal bars on bottom of (a) LP-1 (1/16-inch roughness) and (b) LP-2 (1/4-inch roughness) without corrugations

In general, the exposed aggregate finish with 1/4-inch surface roughness increased capacity and led to expansion and radial stresses around the plug when compared to the 1/16-inch average surface roughness from the sandblasted finish.

Effect of Presence of Metal Duct

There were three different sets of specimens in the large-scale test program that compared the behavior of corrugated interfaces with 1/16-inch surface roughness finish to the metal finish (duct left in place) and confinement benefits of leaving the metal duct in place. These include:

- LP-3 (sandblasted, 1/16-inch roughness) and LP-4 (metal)
- MP-2 (sandblasted, 1/16-inch roughness) and MP-1 (metal)
- SC-1 (sandblasted, 1/16-inch roughness) and SC-2 (metal)

There was generally a similar crack pattern at failure for the specimens with corrugation and sandblasted (1/16-inch roughness) finish and the metal pipe left in place. Crack patterns after failure for SC-1 (sandblasted finish) and SC-2 (metal pipe left in place) are shown in Figure 3-79 as an example. Crack patterns were similar for LP and MP specimens.

Figure 3-79: Cracking at failure for (a) SC-1 (sandblasted, 1/16-inch finish) and (b) SC-2 (metal pipe left in place

The normalized load versus top deflection plots for the large-plug, multi-plug and socket connection specimens are shown in Figure 3-80. The plots compare the response of the 1/16-inch concrete finish (duct removed) with the metal finish (duct left in place). The metal finish with the duct left in place generally had a softer response than the specimens with the duct removed the 1/16-inch roughness concrete finish, which would be consistent with a lower cohesion value. The ultimate capacity of the metal finish corrugated interface was slightly lower for the multi-plug specimens and slightly higher for the socket connection specimens. The large-plug specimens (LP-3 and LP-4) were both loaded to the 1000-kip capacity of the test frame.

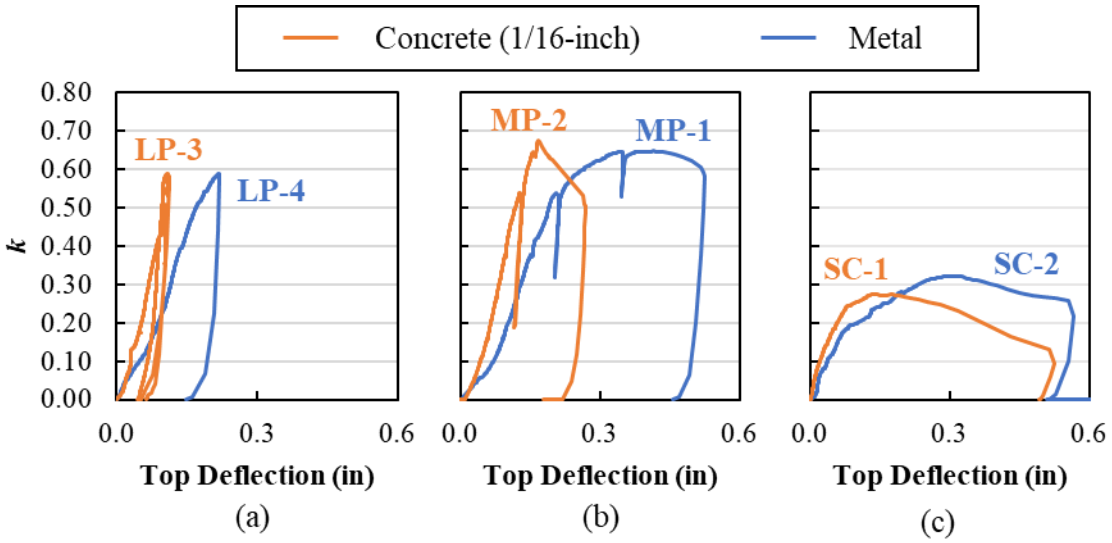

Figure 3-80: Normalized load versus top deflection plots for specimens with corrugation, (a) large-plug specimens, (b) multi-plug specimens, and (c) socket connection specimens

The cracking load was not affected by the type of finish between the concrete (1/16-inch roughness) and metal corrugated interfaces and whether the duct was left in place; for 1/16-

inch roughness concrete versus steel: 83 kips versus 82 kips, 130 kips versus 150 kips, and 79 kips versus 74 kips for LP, MP, and SC specimens, respectively. A sample comparison for the load versus strain in the longitudinal reinforcement is shown in Figure 3-81 for SC-1 and SC-2. Both specimens had longitudinal reinforcement yielding at the time of failure. The maximum measured strains were higher for SC-2 (with the metal finish).

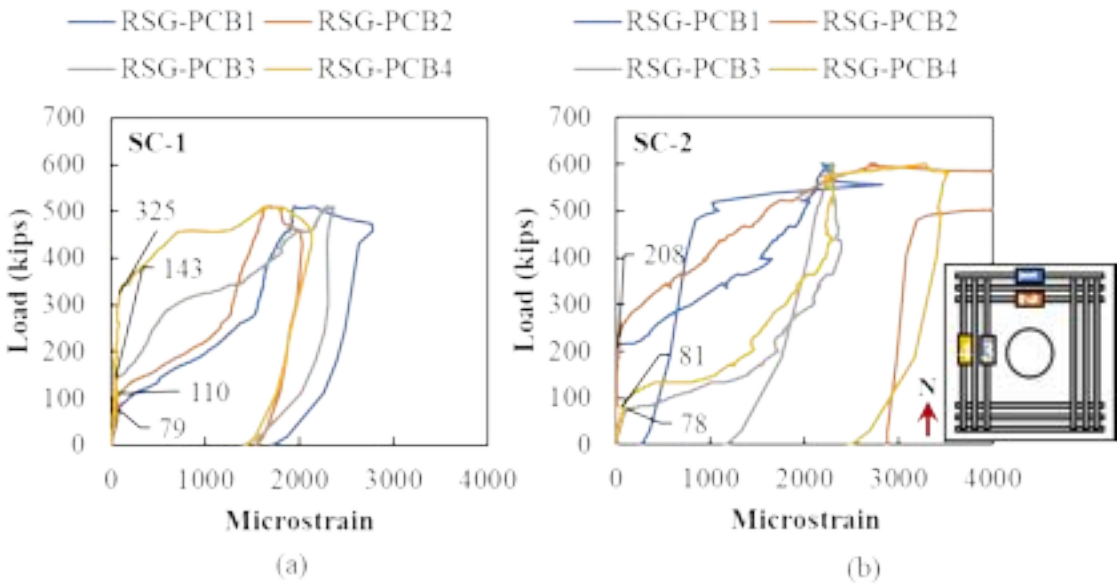

Figure 3-81: Load versus strain in longitudinal reinforcement for (a) SC-1 and (b) SC-2

Confinement reinforcement was provided in the cap around the plug for LP specimens, but not for MP and SC specimens. The load versus measured strain responses in the confinement reinforcement in the cap around the plug are shown in Figure 3-82. The presence of the metal duct did not have a clear benefit in terms of confinement of the plug concrete. Both specimens had similar engagement of the confinement reinforcement around the plug at the maximum applied load of 1,000 kips.

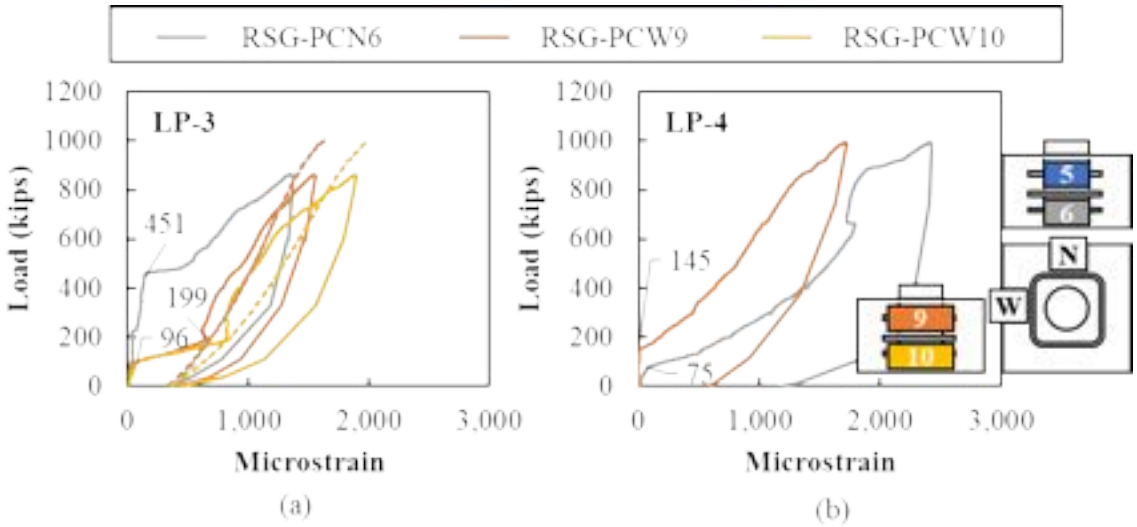

Figure 3-82: Load versus strain in confinement reinforcement around plug for (a) LP-3 and (b) LP-4

Reinforcement was provided in the socket beneath the embedded pile in the SC specimens. The load versus measured strain responses in the socket reinforcement running in the east-west direction below the tip of the embedded pile are shown in Figure 3-83. The socket reinforcement in the specimens without the metal duct generally engaged at a higher load and had smaller maximum strains at failure.

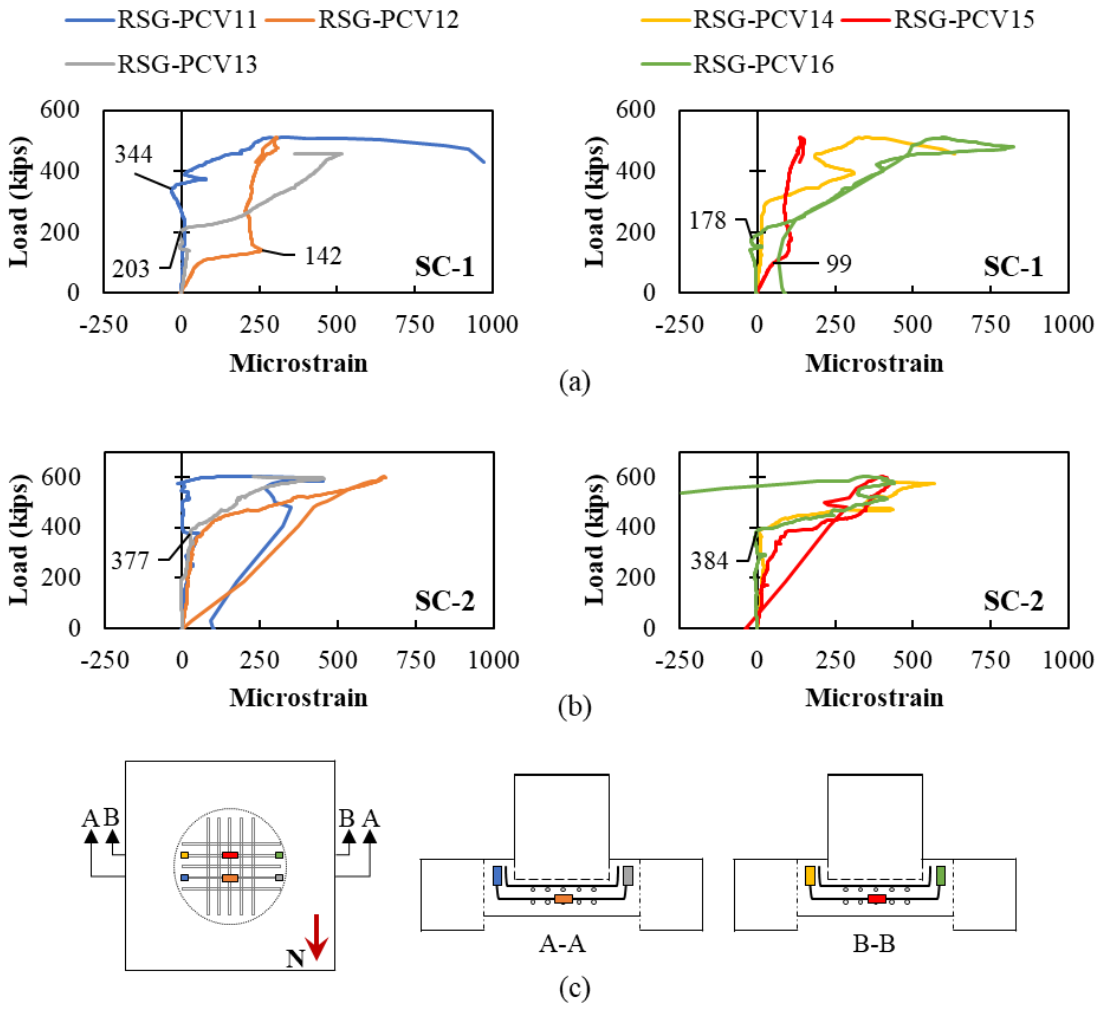

Figure 3-83: Load versus strain in socket reinforcement below pile in E-W direction for (a) SC-1 and (b) SC-2 and (c) location of RSGs

Overall, the presence of the metal duct did not impact the strength of the specimens, led to softer response (likely a result of less cohesion between the plug concrete and metal pipe), and did not noticeably help to confine the plug concrete.

Effect of Corrugation Spacing and Depth

The effect of the presence of the corrugation can be seen by comparing the response of LP-1 (smooth with 1/16-inch surface roughness) and LP-3 (corrugated with 1/16-inch roughness). The presence of corrugation led to a higher measured strength compared to the smooth interface specimen, as shown in Figure 3-84. The normalized load versus deflection response for LP-1 was linear up to failure. The response was linear up to approximately k

of 0.55 for LP-3; the two different slopes are present because of different load rates used for tests 1 and 2 for LP-3. Comparing the bottom deflections, the initial slopes were similar between LP-1 and LP-3 (initial loading rate for LP-3 was same as LP-1).

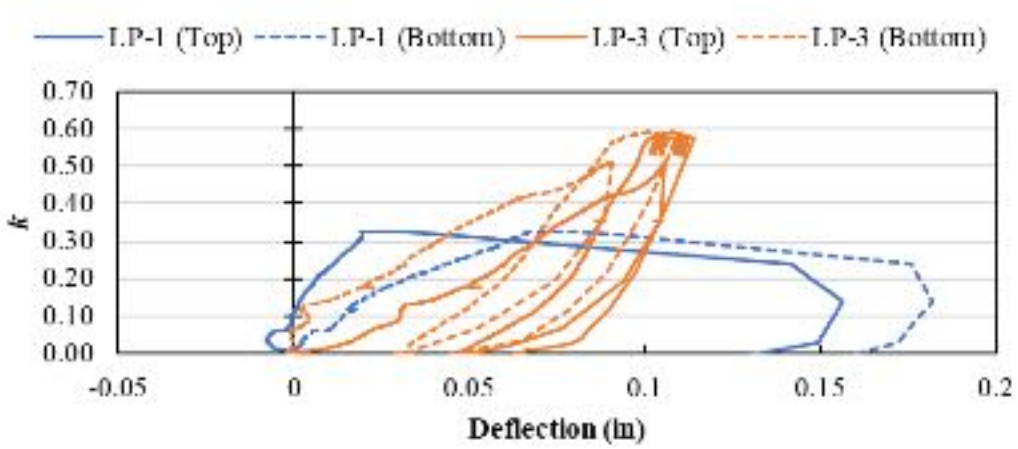

Figure 3-84: Normalized load (k) versus top and bottom deflection for (a) LP-1 (smooth with 1/16-inch roughness) and (b) LP-3 (corrugated with 1/16-inch roughness)

Similar crack patterns were observed between LP-1 and LP-3, see Figure 3-85.

Figure 3-85: Crack patterns at failure for (a) LP-1 (smooth with 1/16-inch roughness) and (b) LP-3 (corrugated with 1/16-inch roughness)

The load versus measured strain responses for the confinement reinforcement in the cap around the pocket for LP-1 and LP-3 are shown in Figure 3-86. The maximum measured strains were similar between LP-1 and LP-3 at the maximum applied loads.

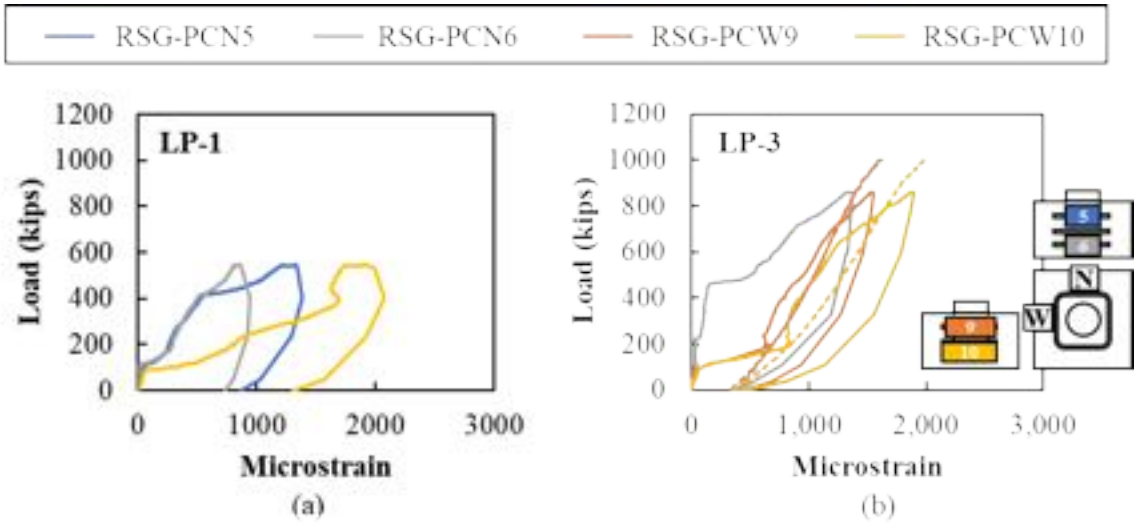

Figure 3-86: Rebar strain in confinement reinforcement around the pocket of (a) LP-1 (smooth with 1/16-inch roughness) and (b) LP-3 (corrugated with 1/16-inch roughness)

The load versus measured strain responses for the longitudinal bars on the bottom of the specimens for LP-1 and LP-3 are shown in Figure 3-87. Like the confinement reinforcement, the maximum measured strains were similar between LP-1 and LP-3 at the maximum applied loads.

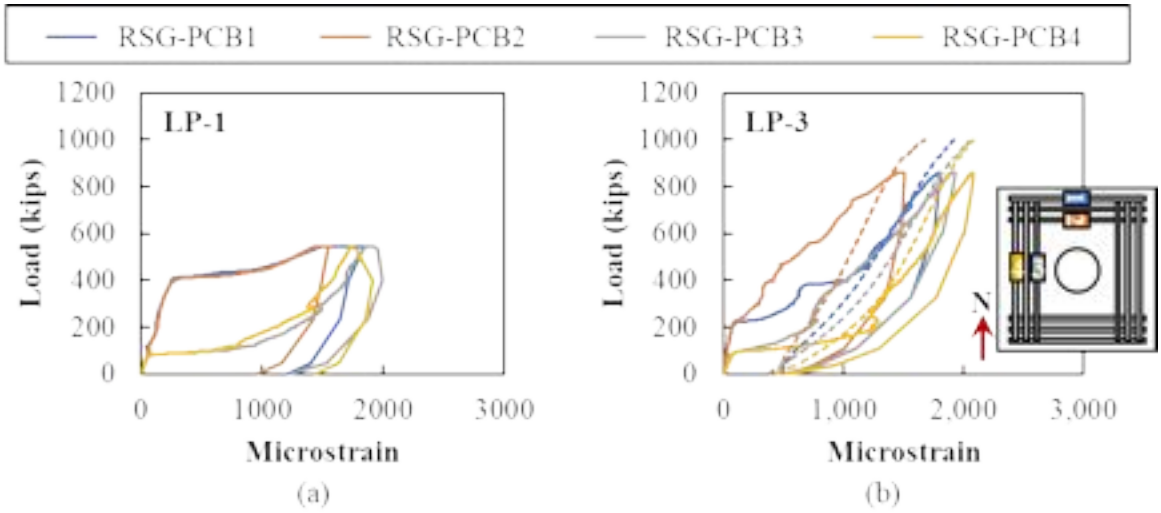

Figure 3-87: Rebar strain in longitudinal bars on bottom of (a) LP-1 (smooth with 1/16-inch roughness) and (b) LP-3 (corrugated with 1/16-inch roughness)

In general, the presence of corrugations led to much higher capacity and less engagement of the reinforcement at lower loads. The presence of the corrugations also seemingly added some ductility to the system. LP-1 (without corrugations) saw a sudden failure and sliding

of the plug, while LP-3 was beginning to show a non-linear response when the maximum load was applied.

Comparison between Pocket and Socket Behavior

There were six large-scale specimens with corrugated interfaces and 1/16-inch roughness concrete finish or metal duct finish. Four of these specimens had a pocket connection and two had a socket connection. The normalized load versus deflection curves for these specimens organized to better compare the behavior of the pocket and socket connections are shown in Figure 3-88. All specimens had a similar response to a normalized failure load of about 0.2. At this point, the response of the socket connections softened until a normalized failure load between 0.274 and 0.323. The pocket connections continued to gain strength until the failure of the specimen or the capacity of the load frame was reached.

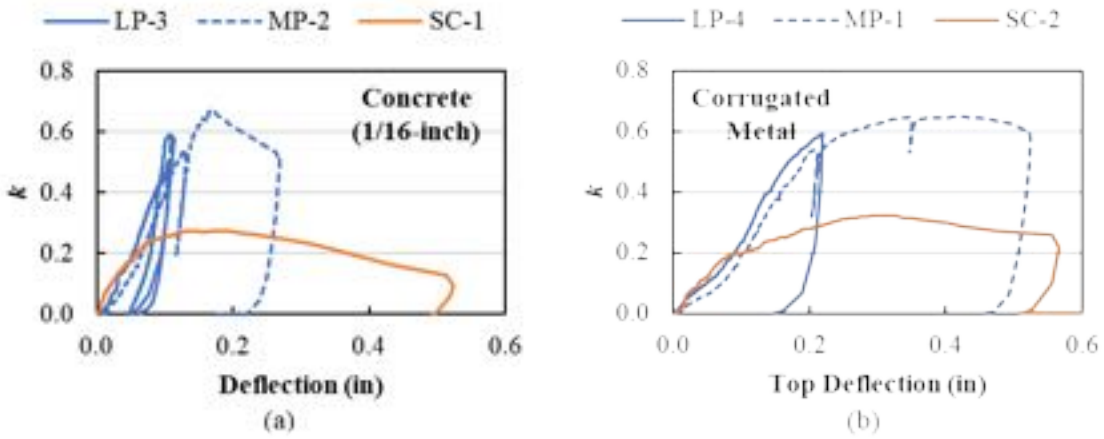

Figure 3-88: Normalized load (k) versus top and bottom deflection for LP, MP, and SC specimens with corrugated interface with (a) 1/16-inch concrete and (b) corrugated metal finish

The load on the pocket connection specimens is applied directly to the plug, as shown in Figure 3-89 (a), compared to the socket specimen where the load is applied to the pile, which has a much smaller area than the socket, as shown in Figure 3-89 (b). The interface length is clear for the pocket specimens, being the entire height of the pocket, and the pocket concrete would be passively confined along its entire length. The interface length for the socket specimen is not as clear. The interface length can be assumed to be the distance from the bottom of the embedded pile to the bottom of the socket, but the concrete may not be as effectively confined. The load is normalized using the distance from the

bottom of the pile to the bottom of the socket for SC-1 and SC-2 in Figure 3-88. This will be investigated further in Task 4.

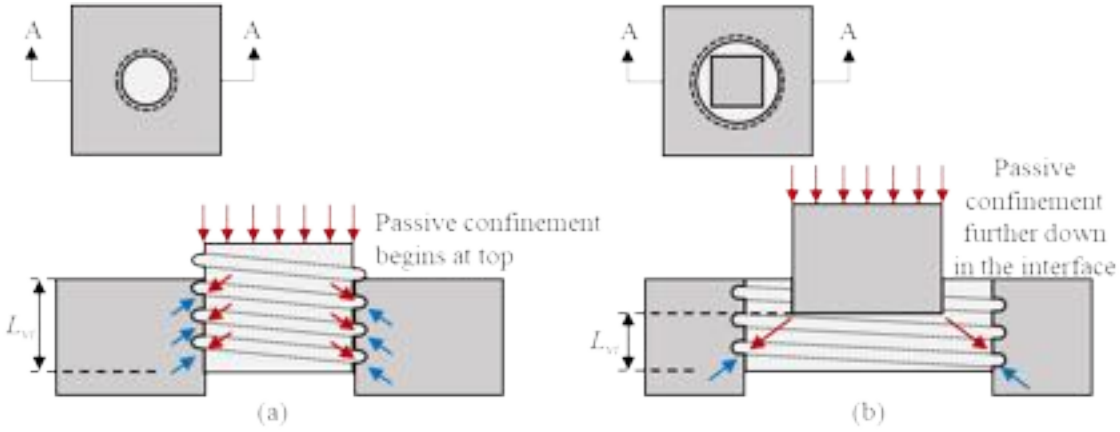

Figure 3-89: Cross section A-A of (a) LP and (b) SC specimens with sketch of confining stresses in pocket and socket from applied loads

The crack patterns between the socket and pocket type connections were generally similar to one another, as shown in Figure 3-90 as an example.

Figure 3-90: Crack patterns at failure for LP and SC specimens with corrugated interface (a) LP-3 and (b) SC-1

The longitudinal reinforcement strains were generally similar between the pocket and socket specimens, see results in previous sections. Other types of reinforcement were different between the two types of specimens.

Chapter 4: **Finite Element Modeling (ATENA)**

4.1. Introduction

This investigation was supported with numerical analyses using a finite element analysis (FEA) software called ATENA specifically designed for analyzing reinforced concrete structures. This chapter presents the validation models, material and modeling assumptions used for evaluating the shear friction capacity in pocket connections.

The main challenge to model the pocket connection was developing and calibrating the interface between the pile cap and pile. Along the research, many calibrations had been done to better estimate the capacity of the specimens and understating how each variable playing a role in the interface influences the response. In the following sub-sections, there is a summary of the assumptions made to estimate the specimens' capacity.

4.2. Material Modeling

Four main materials were defined and used when modeling any of the specimens: concrete, reinforcement, interface material, and steel plates.

The concrete material was defined using a prototype material called CC3DNonLinCementitious2. This material is a fracture-plastic model that combines tensile and compressive behaviors; fracture and plastic respectively (Cervenka et al., 2016). Thus, this model combination can be used to represent concrete cracking, crushing under high confinement, and crack closure due to crushing in other material directions. The stress-strain curve assumed for concrete compression is shown in Figure 4-1 (a).

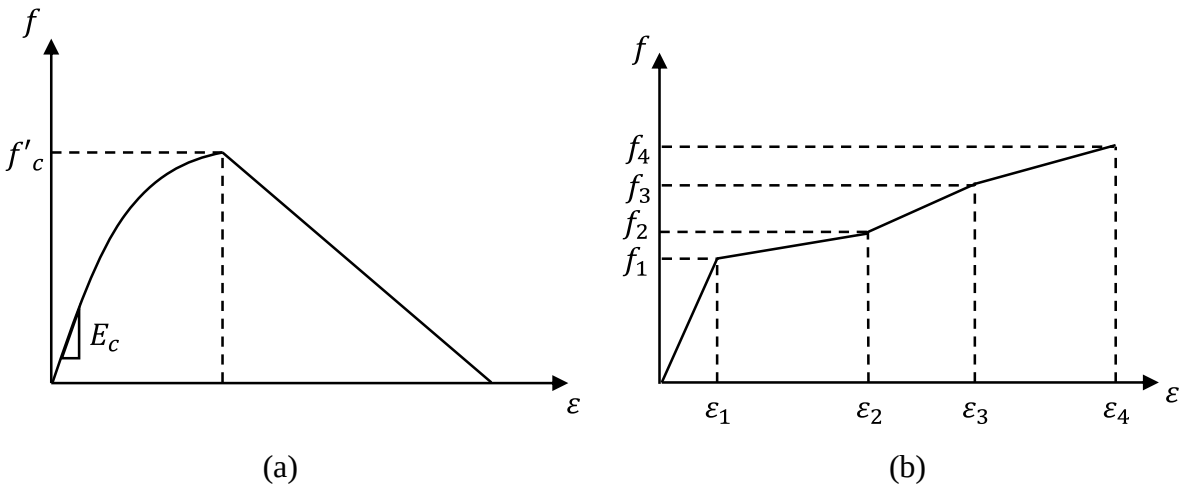

Figure 4-1: Stress-strain relationship: (a) concrete curve, (b) steel curve.

There are three different types of reinforcement that need to be considered when looking at shear friction and specimens used to test shear friction capacity: longitudinal steel, confining steel, and interface steel (just used for the validation models). A line element and steel material Reinforcement EC2 can be used for all three types of reinforcement; note though that this element and material only consider axial stresses and strains. The parameters that can be defined for Reinforcement EC2 are shown in Figure 4-1 (b).

Concrete strength was equally assigned to the cap and plug as 6.5 ksi for estimation purposes. Then, after the experimental testing, calibration was done with the measured concrete strengths. The reinforcement was assigned as Grade 60.

Steel plates are used for the loading point and supports. These plates were defined as a SOLID Elastic material, which is a material able to deform but not to crack. The load level will not be high enough to cause any plastic deformation in the plates (Prochazkova et al., 2016). Steel plates were used for loading purposes in all specimens on top of the plug as shown in Figure 4-2. A 2-inch circular steel plate was used in pocket connection specimen (diameter of the plate varied accordingly for each specimen) and for the socket connection a 2-inch square plate was used to equally distribute the load in the surface of the plug.

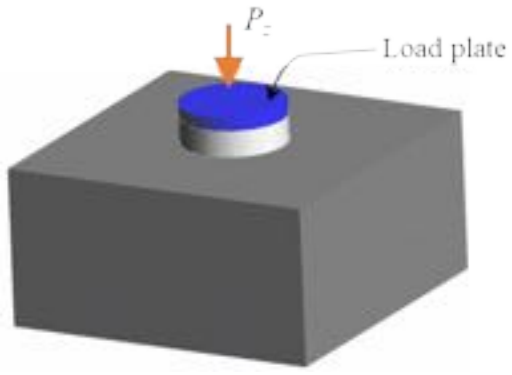

Figure 4-2: Steel plate used for load application.

4.2.1. Interface Material

Shear friction behavior is dependent on the assumptions made for the shearing plane. No interface material was defined for specimens where there was no cold joint, as shown in Figure 4-3 (a). The behavior of the shearing plane in this model was dependent on the concrete model used (CC3DNonLinCementitious2). An interface plane was defined for surfaces where a cold joint was present, as shown in Figure 4-3. The interface is modeled as another volume element and connected to the other volumes through a contact volume function in the finite element program. The properties of the interface material can be modified to impact the behavior of the shearing plane.

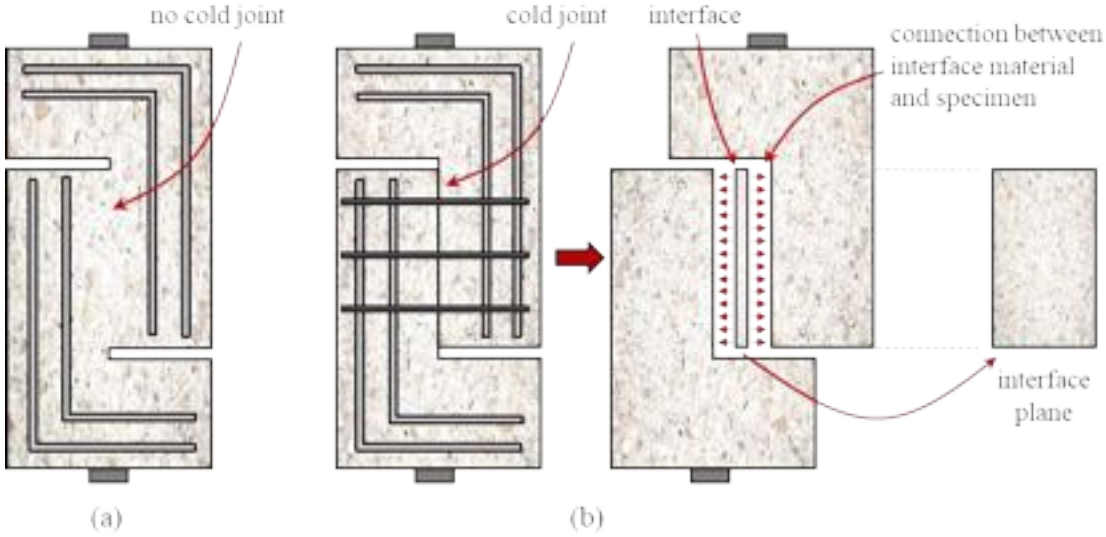

Figure 4-3: Modeling of specimens tested by Hofbeck et al. (Hofbeck et al., 1969a): (a) without reinforcement crossing the interface, (b) with reinforcement and cold joint

The behavior of the interface material is based on the Mohr-Coulomb criterion with failure occurring when the shear stresses violate this condition (Cervenka et al., 2016). The graph representing the interface failure condition is presented on Figure 4-4.

$$|\tau| \leq c - \sigma\phi, \quad \sigma \leq 0 \qquad \text{Equation 4-1}$$

Where:

c = cohesion coefficient

φ = angle of internal friction or slope of the failure envelope (negative)

σ = normal stress on interface plane (compression is negative as shown)

$$\tau = \tau_0 \sqrt{1 - \frac{(\sigma - \sigma_c)^2}{(f_t - \sigma_c)^2}} \qquad \text{Equation 4-2}$$

$$\tau_0 = \frac{c}{\sqrt{1 - \frac{{\sigma_c}^2}{(f_t - \sigma_c)^2}}} \qquad \text{Equation 4-3}$$

$$\sigma_c = -\frac{{f_t}^2 \phi}{c - 2 f_t \phi} \qquad \text{Equation 4-4}$$

f_t = tensile strength of the interface material

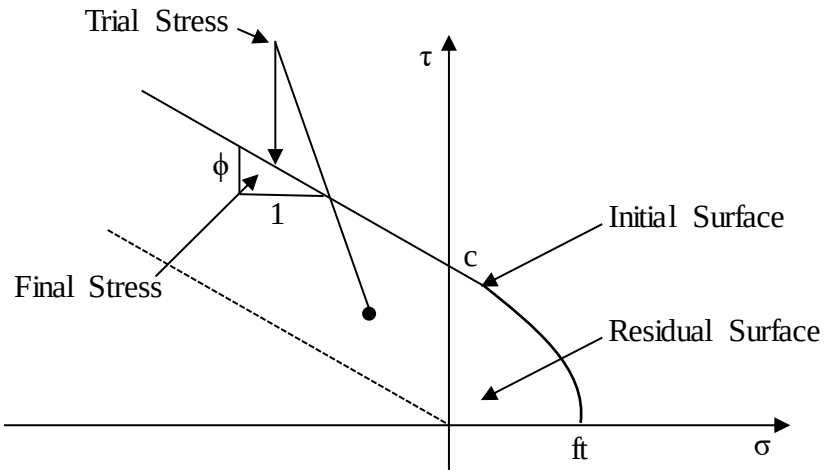

Figure 4-4: Failure surface for interface elements (modified from (Cervenka et al., 2016))

Typical interface material models for shear and tension are shown in Figure 4-5. The shear stress (τ) versus sliding displacement (Δv) is plotted in Figure 4-5 (a) with the initial elastic shear stiffness (K_{tt}). The tensile stress (σ) versus opening displacement (Δu) is plotted in Figure 4-5 (b) with the initial elastic normal stiffness (K_{nn}). These stiffnesses are recommended to be found using Equation 4-5 and Equation 4-6, where t is the width of the interface zone. It is also recommended that the stiffness of the interface material be approximately 10 times the stiffness of adjacent finite elements.

$$K_{nn} = \frac{E}{t} \qquad \text{Equation 4-5}$$

$$K_{tt} = \frac{G}{t} \qquad \text{Equation 4-6}$$

After shear or tension failure occurs additional stiffness values (K_{tt}^{min} and K_{nn}^{min}) are specified in order for the analysis to continue. These values are recommended to be around 0.001 times the initial stiffness values (Cervenka et al., 2016), which represents open contact after the failure of the interface (Cervenka et al., 2017).

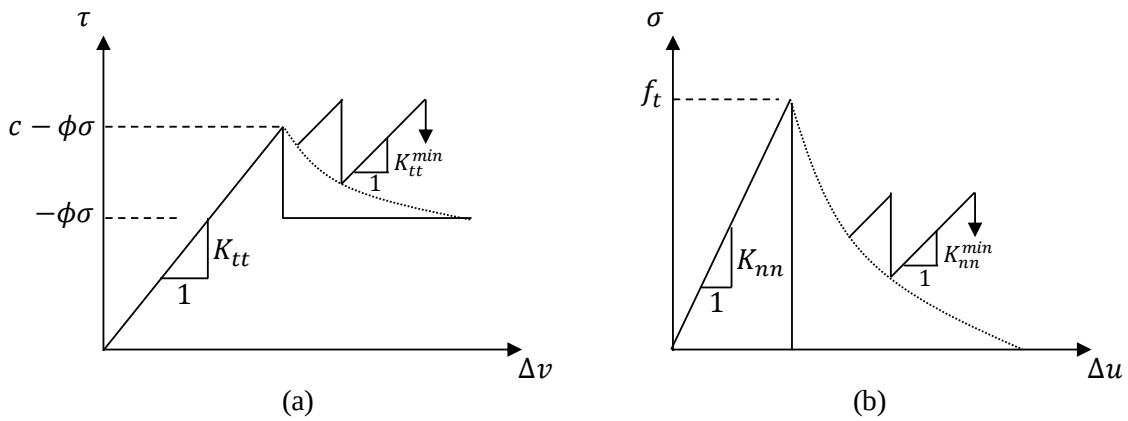

Figure 4-5: Typical interface model behavior in (a) shear and (b) tension (modified from (Cervenka et al., 2016))

As seen through the above discussion on the theory of the interface material, the main parameters involved in the definition of the interface material are: cohesion (c), friction (μ, which impacts φ), and tensile strength (f_t). The interface tension strength (f_t) depends on the tension strength of the weaker concrete next to the interface; if there is no information about the interface material it is recommended to use ½ - ¼ of the tensile strength of the weaker concrete. It is recommended to use a cohesion (c) 1-2 times the tensile strength of the interface material. Finally, it is recommended to use a coefficient of friction of 0.3 to 0.5 if no other information is given for the interface (Pryl & Cervenka, 2017). These values are all summarized in Table 4-1.

Table 4-1: Variables defining interface material

Factor		**Typical Ranges Recommended in ATENA**	**Typical Ranges from AASHTO LRFD**
Coefficient of Friction	μ	0.3 – 0.5	0.6 - 1.4
Tensile Strength of Interface	f_{ti}	¼ - ½ f_t	n/a
Cohesion	c	1-2 f_{ti}	0.025 – 0.40

Typical ranges for the coefficient of friction and cohesion factors for shear friction estimation provided by AASHTO LRFD (American Association of State Highway and Transportation Officials (AASHTO), 2017a) are also provided in Table 4-1.

4.3. Validation of Numerical Models

4.3.1. Monolithic Shear Friction (based on Hofbeck et al. (Hofbeck et al., 1969a))

The first model used to validate the interface capacity of our finite element program (ATENA) was a push-off specimen tested by Hofbeck et al. (Hofbeck et al., 1969a). In their study, they evaluated the shear transfer capacity of concrete with and without cracks in the interface plane. Hofbeck et al. (Hofbeck et al., 1969a) cast around 38 specimens, all with different properties related to number of stirrups crossing the interface, stirrup bar sizes, and concrete strength. All the evaluated specimens in the study were monolithically cast and had the same geometry. One of the specimens in their experimental program did not have any reinforcement crossing the interface plane. This specimen was modeled in ATENA for comparison to the experimental results. The details for this specimen are shown in Figure 4-6.

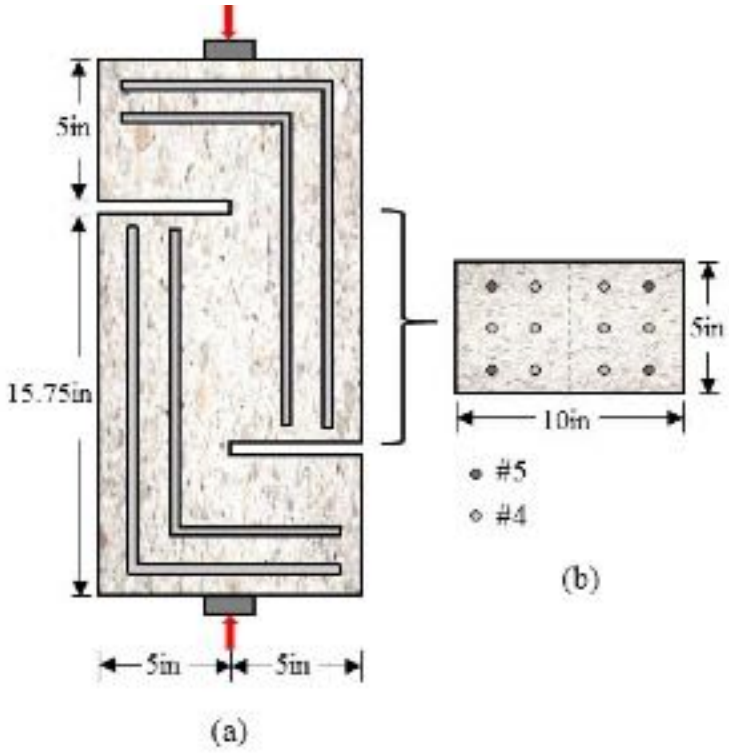

Figure 4-6: Push-off specimen created by Hofbeck et al. (Hofbeck et al., 1969a) (a) Geometry details, and (b) interface elevation and reinforcement details with no reinforcement crossing the interface

The materials used for this specimen were concrete and longitudinal steel reinforcement. There was no steel crossing the interface plane. Also, there was no cold joint, so no interface material was defined for this specimen; the connection between the two L-shaped sides was a fixed connection in the model. The main characteristics of all the materials defined in the software are shown in Table 4-2.

Table 4-2: Material Characteristics used in ATENA

Variable	Input
Concrete	
Young's Modulus (ksi)	3622.98
Poisson's Ratio	0.2
Tension Strength (ksi)	0.290
Compression Strength (ksi)	4.04
Reinforcement	
Young's Modulus (ksi)	29000
Yield Strength (ksi)	60

The results obtained from the numerical analysis are shown in Table 4-3 and Figure 4-7. The crack pattern obtained from ATENA shows a shear friction failure. The results from the numerical analysis were reasonably close to the experimental results.

Table 4-3: Results of specimen created by Hofbeck et al.(Hofbeck et al., 1969a)

Experimental Result V_u ***(kips)***	**ATENA Result** V_u ***(kips)***
24	31.60

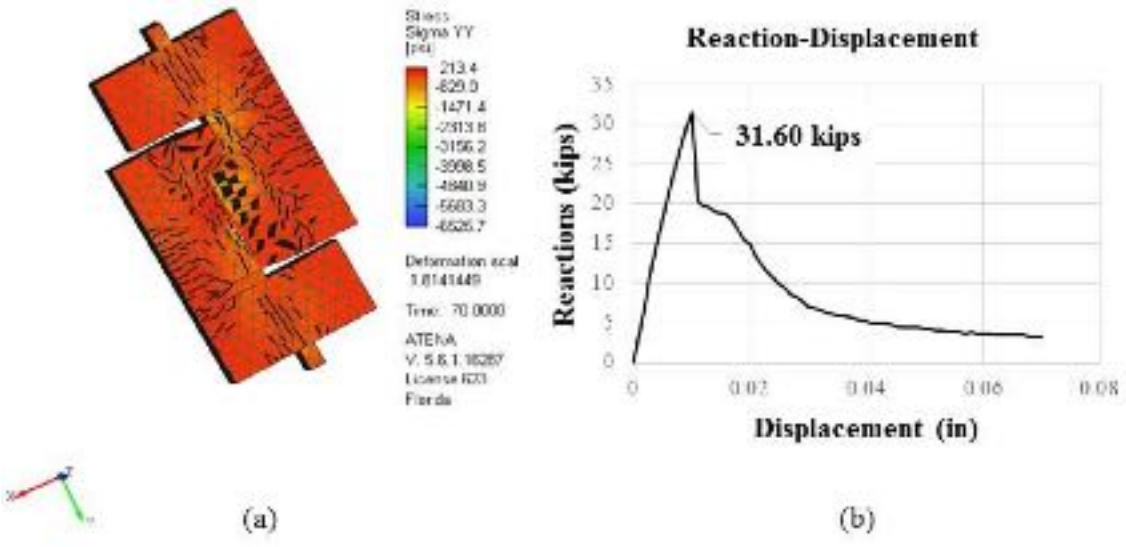

Figure 4-7: Summary of results for Hofbeck et al. (Hofbeck et al., 1969a) model (a) crack pattern at failure and (b) reaction-displacement curve.

1.1.1. Shear Friction of Cold Joint with Reinforcement (based on Kahn and Mitchell (L. F. Kahn & Mitchell, 2002))

The second model used to validate the interface capacity was one push-off specimen develop by Kahn and Mitchell (L. F. Kahn & Mitchell, 2002). The purpose of their study was to continue the evaluation of the shear friction capacity using concrete strength greater than 7,000 psi, and to check if the current ACI provisions were applicable to high strength concrete. Kahn and Mitchell (L. F. Kahn & Mitchell, 2002) cast 50 push-off specimens, all with different properties related to concrete strength, stirrups crossing the interface, and casting procedure. Kahn and Mitchell (L. F. Kahn & Mitchell, 2002) used the same test configuration and similar specimen sizes to Hofbeck et al. (Hofbeck et al., 1969a), so the results are comparable. One of the specimens with a cold joint between the sections (Figure 4-8) was selected to be modeled using ATENA.

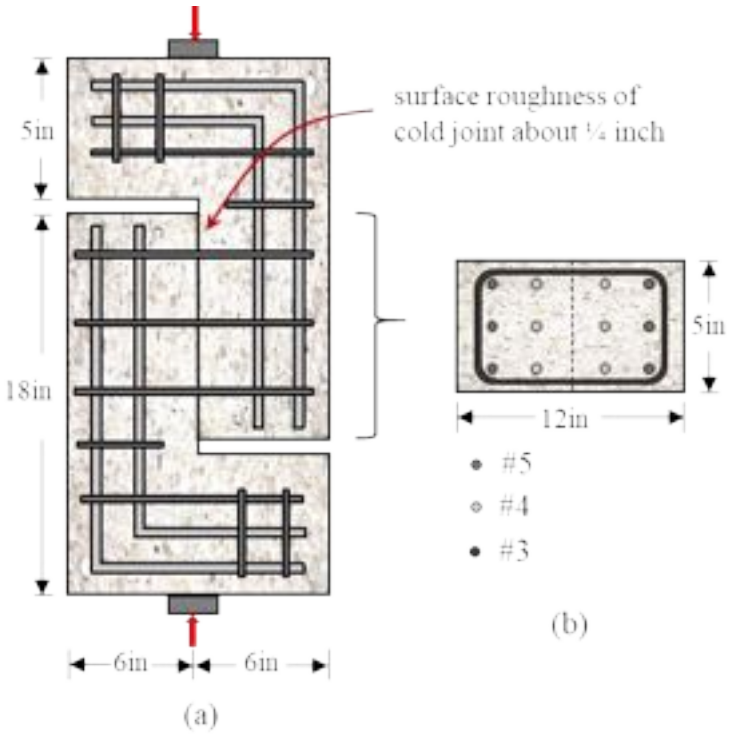

Figure 4-8: Push-off specimen created by Kahn and Mitchell. (a) Geometry details, and (b) Interface elevation and reinforcement details.

The specimen used for this validation had a cold joint in the shear plane, and three #3 stirrups crossing the interface. Because the specimen had a cold joint and steel crossing the interface, an interface volume element with interface material properties and diagonal line elements were used to better represent the interface condition. The characteristics of all the materials used are define in Table 4-4.

Table 4-4: Material Characteristics used in ATENA

Variable	Input
Concrete	
Young's Modulus (ksi)	6365.40
Poisson's Ratio	0.2
Tension Strength (ksi)	0.8376
Compression Strength (ksi)	12.47
Reinforcement	
Young's Modulus (ksi)	29000

Variable	Input
Yield Strength (ksi)	60
Interface Material	
Coefficient of Friction	1.4
Tensile Strength (ksi)	0.6282
Cohesion (ksi)	1.2563
Min. Stiffness (kip/in^3)	63.6540
Max. Stiffness (kip/in^3)	63653.97

The coefficient of friction was selected based on values recommended by the researchers (L. F. Kahn & Mitchell, 2002). Note that these values are higher than those recommended by ACI 318 and AASHTO LRFD, which both recommend a coefficient of friction of 1.0 for concrete placed against a surface with a ¼-inch surface roughness. The minimum and maximum stiffness, tensile strength, and cohesion were selected inside the range of ATENA's recommendations.

Reinforcement crossing the friction plane was modeled with three-line elements, as shown in Figure 4-9. Diagonal line elements were used to model the dowel action that resists shear friction. Line elements perpendicular to the friction plane were used to model the clamping force that occurring during shear friction failure. These elements were only used for reinforcement crossing the friction plane.

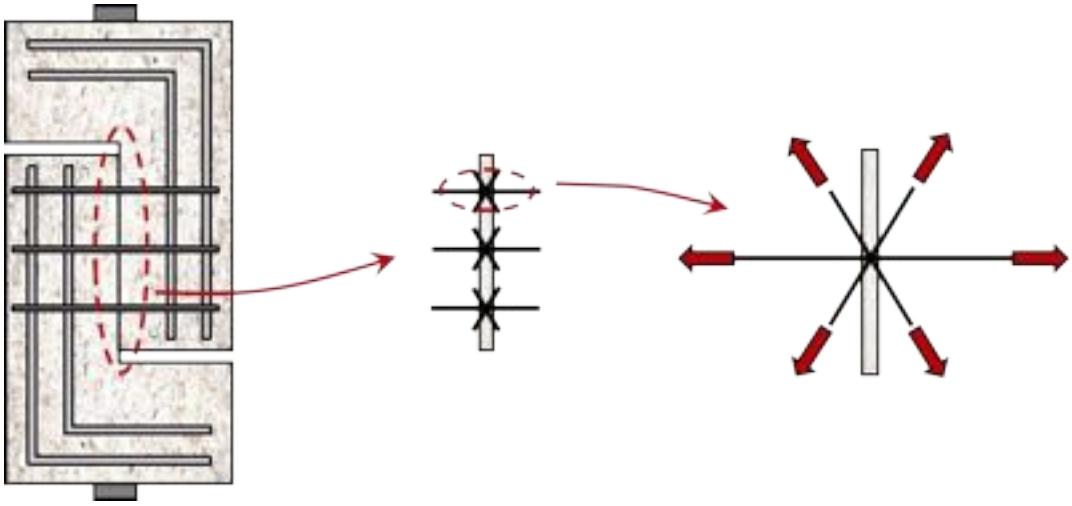

Figure 4-9: Dowell action of reinforcement crossing friction plane modeled as diagonal line elements

The results from this analysis are presented in Table 4-5 and Figure 4-10. A shear friction failure was observed in the specimen with a failure load similar to that obtained by the experimental results.

Table 4-5: Results of specimen created by Kahn and Mitchell (L. F. Kahn & Mitchell, 2002)

Experimental Result V_u ***(kips)***	**ATENA Result** ***Vu (kips)***
110.30	93.50

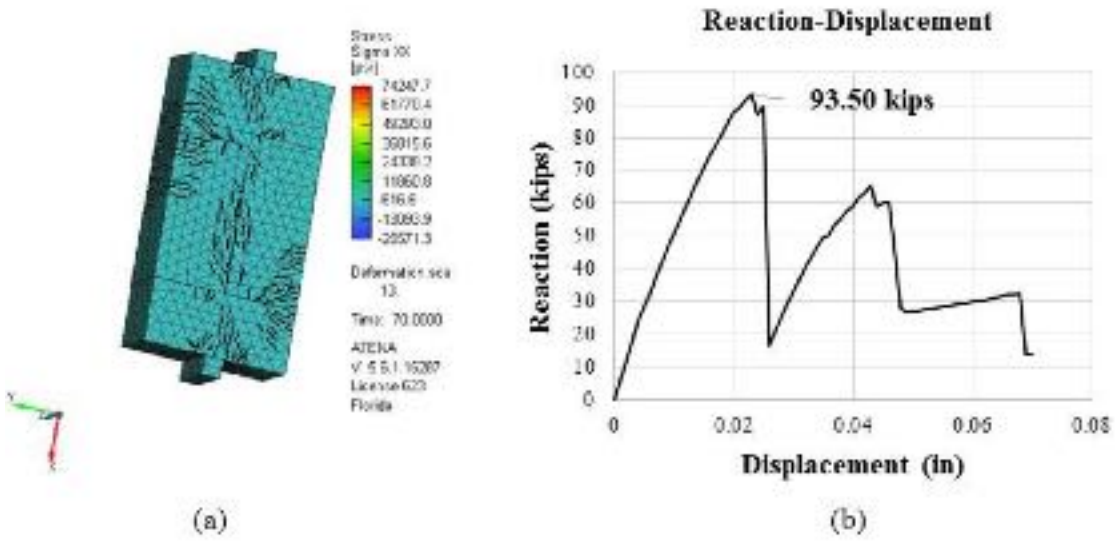

Figure 4-10: Summary of results for Kahn and Mitchell model (a) crack pattern at failure and (b) reaction-displacement curve.

4.4. Assumptions for Final Model

4.4.1. General Modeling Assumptions

For the volume elements (concrete, interface material, and steel plates) an unstructured automatically generated mesh with 1.2-inch elements size was used. For the line element (reinforcement) a structured mesh with 1-inch element size was used because the program automatically divides the bars into elements with the surrounding volume elements. Other structured and semi-structured meshes were explored for all specimens but were found to not satisfactorily model the behavior of the cylindrical interface surface.

The same boundary conditions were applied to all small- and large-scale models, shown in Figure 4-11:

- Z displacement was restrained across the surface of the bottom surface of the specimen (other than the location of the plug).
- X and Y displacement were restrained in three corner points.
- An incremental Z compression displacement of 0.01 inches was applied in the midpoint of the midline in the top plate.

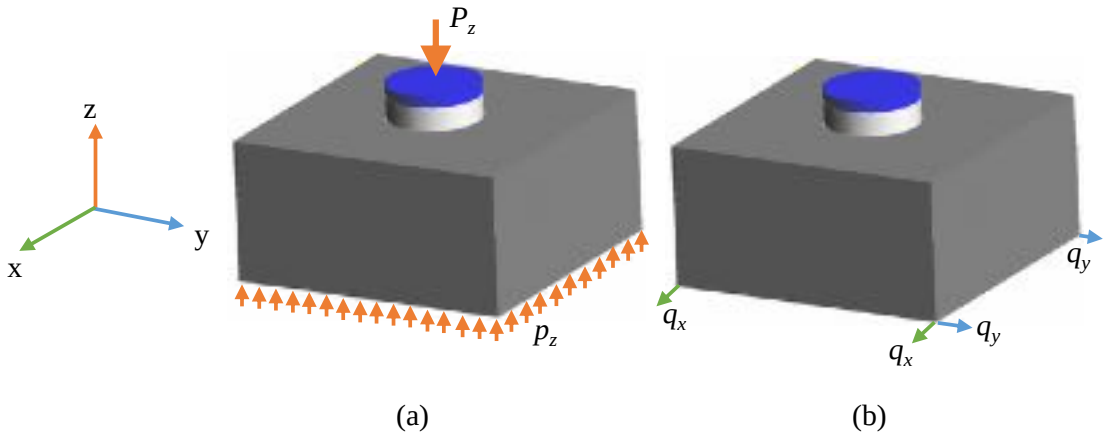

Figure 4-11: Assumed boundary conditions for ATENA modeling of second series of precast specimens along (a) z axis and (b) x and y axis.

The displacement was applied gradually in 70 steps until reaching the failure displacement of the interface.

4.4.2. Material Modeling Assumptions

A summary of the material properties used in the estimated modeling before each testing is shown in Table 4-6. The same material properties were used for all the small- and large-scale specimens. The specimens were later reanalyzed using the actual concrete strengths observed during experimental testing.

Table 4-6: Material Characteristics used in ATENA for preliminary results in precast series.

Variable	Input
Concrete	
Young's Modulus (ksi)	4596
Poisson's Ratio	0.2
Tension Strength (ksi)	0.392
Compression Strength (ksi)	6.5
Reinforcement	

Young's Modulus (ksi)	29000
Yield Strength (ksi)	60

4.4.2.1. Interface Material Modeling

Iterations were done with the lower and upper bound values recommended by ATENA (Table 4-1) however, none of them were found to best estimate the experimental results. In addition, other iterations were done changing just one variable in the interface material to evaluate how each of them influenced the results or how much the capacity of the specimen varied based on them. It was found that varying the friction coefficient at a lower range had more impact on the interface capacity than the cohesion coefficient. Since the tensile strength and maximum and minimum stiffness depend on the weaker concrete next to the interface, no iterations were done with these variables and were based on ATENA's recommendations. Based on this, three assumptions were made when defining the interface material:

1. For the specimens with 1/16-inch surface roughness, the interface condition was defined using the cohesion and friction values found on AASHTO LRFD for "concrete placed against a clean concrete surface, free of laitance, but not intentionally roughened" ($c = 0.075$, $\mu = 0.6$)
2. For the specimens with 1/4-inch surface roughness, full corrugated surface (both with pipe left in place and without it), and half corrugation, the interface condition was defined using the cohesion and friction values found on AASHTO LRFD for "normal weight concrete placed monolithically" ($c = 0.40$, $\mu = 1.4$)
3. For the monolithic cast specimen, a master-slave connection was assigned to ensure the monolithic behavior of the specimen. No interface material was used in this case.

The properties used for the upper and lower bound in the interface material are presented in Table 4-7.

Table 4-7: Interface Material Characteristics used in ATENA for precast specimens.

Interface Material – Lower Bound	
Coefficient of Friction	0.6
Tensile Strength (ksi)	0.1958
Cohesion (ksi)	0.075
Min. Stiffness (kip/in^3)	38.30
Max. Stiffness (kip/in^3)	38296
Interface Material – Upper Bound	
Coefficient of Friction	1.4
Tensile Strength (ksi)	0.1958
Cohesion (ksi)	0.4
Min. Stiffness (kip/in^3)	38.30
Max. Stiffness (kip/in^3)	38296

Chapter 5: **Estimation Performance**

5.1. Introduction

This chapter presents a modification of AASHTO LRFD BDS for corrugated interfaces, performance of current code expressions, comparison of the experimental results with the current code expressions for small and large scale specimens, and an evaluation of the current friction and cohesion coefficients when having corrugated interface.

5.2. AASHTO LRFD BDS Modified for Corrugated Interfaces

The shear friction mechanism for interfaces with corrugation and normal force caused by Poisson's effect and confinement, like those tested in this research, was refined based on the test results. These modifications are discussed in this section.

5.2.1. Failure of Ribs of Corrugation

The shear friction resistance provided by these specimens depends on the failure mechanism. Two different possible shear friction mechanisms were envisioned, one where the failure occurs from sliding between in-tact ribs as the cap expands, shown in Figure 5-1 (a), and the other where failure occurs with shearing off the corrugation ribs, shown in Figure 5-1 (b). All the specimens in this project had sufficient corrugation and confinement reinforcement to prevent the separation and sliding mechanism.

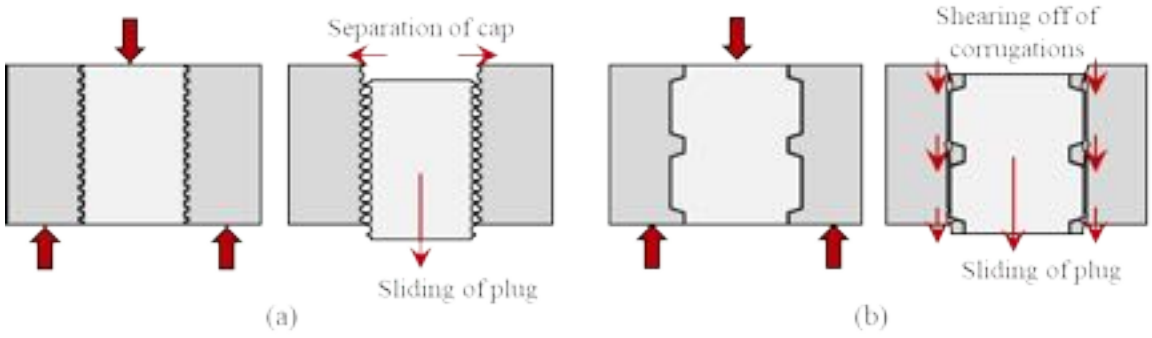

Figure 5-1: Possible failure mechanisms (a) sliding of plug with separation of cap and (b) sliding of plug with shearing off corrugations.

Failure of the specimens with corrugation in this project all occurred without significant expansion in the cap around the pocket, which shows that failure occurred due to shearing

off the corrugations. This observed failure mechanism was considered when developing the cohesion component.

5.2.2. Cohesion Component

The cohesion component of the shear friction capacity is likely dependent on whether the shear plane is through the corrugation (monolithic) or along the interface between cap and plug (non-monolithic). A sketch of two different shear friction failure cracks with these two different corrugation spacings is shown in Figure 5-2. The failure crack extends through the corrugation in the left portion for the closer spaced corrugation, Figure 5-2 (a), and through the right portion for further spaced corrugation, Figure 5-2 (b). The exact location of the failure crack would depend on the concrete strength of each portion in addition to the characteristics of the corrugation (spacing and depth).

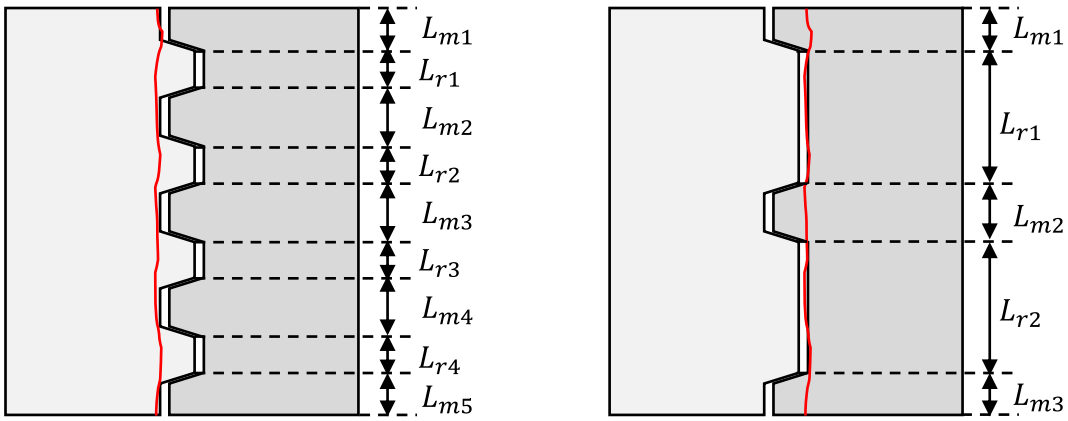

Figure 5-2: Area to consider for cohesion component of shear friction capacity for (a) closer and (b) wider spaced corrugations

The cohesion term of the shear friction capacity can then be found based on the area of the interface that is monolithic and non-monolithic along the predicted failure plane, shown in Equation 5-1.

$$V_{ni,c} = c_m A_{cv,m} + c_r A_{cv,r} \qquad \text{Equation 5-1}$$

where:

$L_{m,i}$ = length of monolithic component of the interface

$L_{r,I}$ = length of non-monolithic component of the interface

c_m = cohesion coefficient for monolithic concrete (0.4 in AASHTO LRFD 8th Edition)

c_r = cohesion coefficient for non-monolithic concrete (0.28 for roughened surfaces in AASHTO LRFD 8th Edition)

$A_{cv,m}$ = concrete interface area for monolithic component

$$A_{cv,m} = \pi d_{plug} \sum L_{m,i} \qquad \text{Equation 5-2}$$

d_{plug} = diameter of plug (to location of shear friction plane)

$A_{cv,r}$ = concrete interface area for non-monolithic component

$$A_{cv,r} = \pi d_{plug} \sum L_{r,i} \qquad \text{Equation 5-3}$$

$$A_{cv,r} = A_{cv} - A_{cv,m} \qquad \text{Equation 5-4}$$

5.2.3. Friction Component

The capacity of the initial tested components would suggest that there is a substantial friction component to the actual capacity. The friction component of the current AASHTO LRFD Bridge Design Specification is shown in Equation 5-5. The equation is made up of the coefficient of friction (μ) and the normal force ($A_{cv}f_y + P_c$).

$$V_{ni,f} = \mu(A_{vf}f_y + P_c) \qquad \text{Equation 5-5 friction component from AASHTO (5.7.4.3-3)}$$

When the vertical stress is applied on a plug with a corrugated interface, the corrugation will help to resist vertical stresses in the concrete, which will cause a horizontal displacement and horizontal stresses, shown in Figure 5-3.

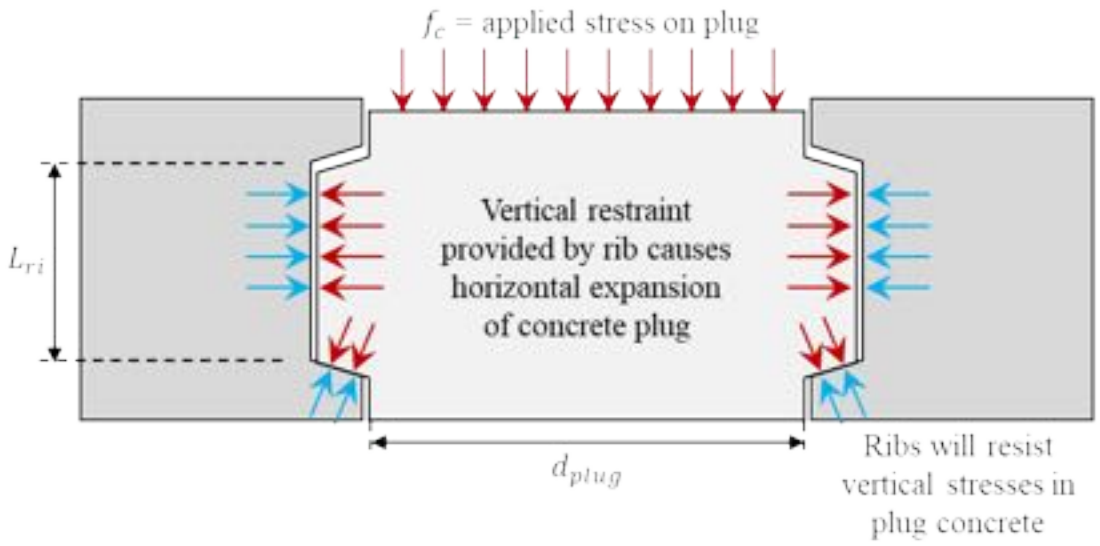

Figure 5-3: Ribs restrain vertical movement resulting in expansion of the plug

The vertical stress can be related to the horizontal stress through Poisson's ratio. This relationship can be used to relate vertical stress to horizontal stress, shown in Equation 5-6 and Equation 5-7.

$$P_c = (\upsilon_c \varepsilon_v) E_c A_r \qquad \text{Equation 5-6}$$

$$P_c = \upsilon_c \left(\frac{f_c}{E_c}\right) E_c A_r = \upsilon_c f_c (\pi d_{plug}) L_{ri} \qquad \text{Equation 5-7}$$

The actual behavior will be more complicated for several reasons. First, the above relationship assumes that all the vertical displacement is restrained at the location of the bottom rib. The vertical restraint of the plug is likely spread across multiple ribs. A possible solution to this would be to determine an effective or average depth over which to find the average strain to use in Equation 5-6. The effective or average depth could be used as the L_r component of Equation 5-7. This value can be assumed as the distance from the top of the interface to the mid-height of the corrugated interface.

Another complication to the equation is that the Poisson's ratio for concrete does not remain constant and is dependent on the material properties. The Poisson's ratio for concrete generally remains close to 0.20 but will dramatically increase as the concrete approaches its ultimate strength, shown in Figure 5-4.

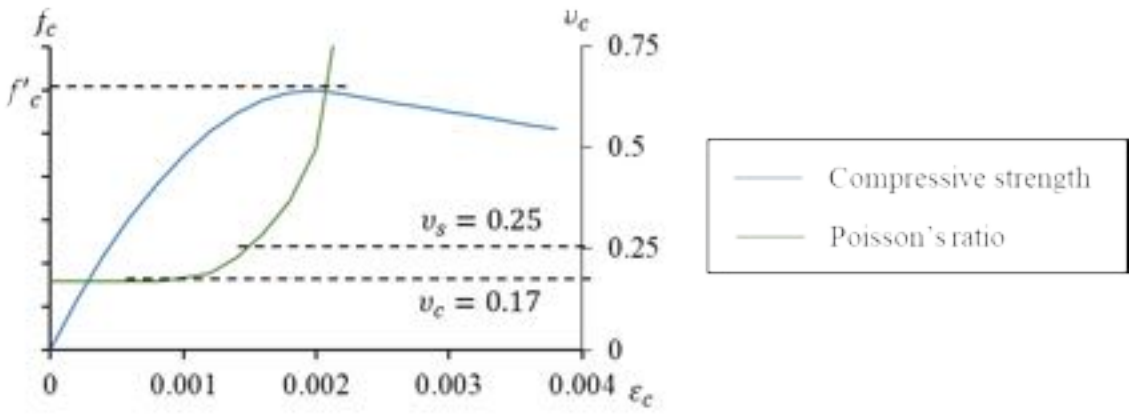

Figure 5-4: Relationship between concrete stress, concrete strain, and Poisson's ratio, similar to (Harries & Kharel, 2003)

Additionally, the applied stress will increase during the test, which means that the normal force component will increase during the test. The maximum stress that the plug will see is the compressive strength (f'_c). The compressive strength of the concrete can be assumed initially but note that the Poisson's ratio will increase as the compressive stress approaches the ultimate strength.

The additional friction component could be found as shown in Equation 5-8 and Equation 5-9.

$$V_{ni,f} = \mu(A_{vf} f_y + P_c) \qquad \text{Equation 5-8}$$

$$P_c = \upsilon_c f_c (\pi d_{plug}) L_{ri} \qquad \text{Equation 5-9}$$

Combining the cohesion component and the friction component would give an estimate capacity as shown in Equation 5-10.

$$V_{ni} = V_{ni,c} + V_{ni,f} \qquad \text{Equation 5-10}$$

5.3. Performance and comparison between codes

As described above, seven different methods were used to estimate the ultimate loads for the specimens described in this report:

1. AASHTO LRFD Bridge Design Specification 8th Edition (American Association of State Highway and Transportation Officials (AASHTO), 2017b)
2. AASHTO LRFD Guide Specifications for Accelerated Bridge Construction 1st Edition (Culmo et al., 2018)
3. ACI 318-19 (American Concrete Institute (ACI) Committee 318, 2019)
4. FIP (1999) (Federation Internationale de la Precontrainte, 1999)
5. fib Model Code (2010) (International Federation for Structural Concrete (fib), 2010)
6. CSA (2010) (Canadian Standards Association, 2010)
7. Proposed modified theory based on AASHTO LRFD BDS

Two of the design procedures, ACI 318-19 and CSA (2010), only consider shear friction capacity when there is reinforcement crossing the interface or an applied normal force across the interface. The estimated capacity for the specimens tested during this project would be zero, so these procedures are not included in the comparisons of Table 5-4 and Table 5-6.

5.4. Cohesion and Friction Factors used in Estimations

Different cohesion and friction factors were used based on the interface condition and corrugation spacing and depth of the specimen. The different codes and specifications have recommended values for cohesion and friction factors based on the interface conditions and roughness. The interface surfaces were classified by smooth with sandblasted surface preparation (1/16-inch roughness), smooth with exposed aggregate finish (1/4-inch roughness), corrugated with sandblasted surface preparation (1/16-inch roughness), corrugated with pipe left in place (metal finish), and monolithically cast specimen, as shown in Table 5-1.

The values used to calculate the shear friction capacity of each specimen are shown in Table 5-1. For AASHTO, FIP, and fib the same coefficients were used when having a 1/16-inch surface roughness even if the void was created using a corrugated pipe. The values were based on a smooth (sandblasted) interface when one or two corrugations were at the base of the interface. The values were based on corrugated (sandblasted) when half

corrugation was used. The coefficient values for these specifications were taken as the lower bound possible result.

Table 5-1: Friction and cohesion factors used to calculate the shear friction capacity per interface surface configuration

	AASHTO LRFD*		**Modified AASHTO BDS**			**FIP**		**fib**	
	c	μ	c_m	c_r	μ	β	μ	c	μ
Smooth (Sandblasted)	0.075	0.6	0.4	0.1575	0.8	0.2	0.60	0.35	0.6
Smooth (Exposed aggregate)	0.24	1.0	0.4	0.24	1.0	0.4	0.90	0.45	0.7
Corrugated (Sandblasted)	0.075	0.6	0.4	0.1575	1.1	0.2	0.60	0.35	0.6
Corrugated (Metal)	0.025	0.7	0.4	0.025	1.05	0.1	0.60	0.025	0.5
Monolithic	0.40	1.4	0.4	0.40	1.4	0.4	0.90	0.50	0.9

*These values are considered lower bound approach

For the modified AASHTO LRFD BDS approach, an average value was used for c_r and μ when having 1/16-inch surface roughness (smooth sandblasted). The average was between values found for "normal weight concrete placed against a clean, concrete surface, free of laitance, with surface intentionally roughened to an amplitude of 0.25 in." ($c = 0.24$, $\mu = 1.0$) and "concrete placed against a clean concrete surface, free of laitance, but not intentionally roughened" ($c = 0.075$, $\mu = 0.6$). Test results showed that even after the cohesion is broken, the corrugations engage the interface acting as a surface roughness. Thus, an average between the lower-bound value for smooth interface and the monolithic finish was used for the coefficient of friction. For example, the corrugated (sandblasted) has a 1.1 friction coefficient because of the average between smooth (sandblasted) and monolithic specimen.

5.5. Sample Calculations for Specimen S2-1

A sample calculation for each of the procedures for Specimen S2-1 is provided in the following sections. The shear friction capacity estimated using ACI 318-19 and CSA (2010) were zero, so they are not included in this section. A summary of the results for all the specimens is provided in Table 5-4 and Table 5-6.

Specimen S2-1 was 18 inches deep with the void created using a 12-inch Sonotube. There was a smooth surface between the cap and plug with sandblasted surface preparation (1/16-inch roughness).

5.5.1. AASHTO LRFD Bridge Design Specification

There was no reinforcement crossing the interface and no applied clamping force for Specimen S2-1, so:

Known: $A_{vf} = 0 \text{ in}^2$ $P_c = 0 \text{ kips}$

The finish of this surface was sandblasted finish (1/16-inch of roughness). As discussed above, the interface condition was assumed to be "For concrete placed against a clean concrete surface, free of laitance, but not intentionally roughened". This finish has the following interface shear factors:

For intentionally roughened interface: $c = 0.075 \text{ ksi}$ $\mu = 0.6$

$K_1 = 0.20$ $K_2 = 0.8 \text{ ksi}$

The total area of the interface is the circumference of the plug times the height of the interface. For Specimen S2-1:

$$A_{cv} = 2\pi\left(\frac{12 \text{ in}}{2}\right)(15 \text{ in}) = 565 \text{ in}^2$$

This area can be used with all the above factors to calculate the estimated shear friction capacity. For Specimen S2-1:

Equation 2-18 AASHTO (5.7.4.3-3):
$$V_{ni} = cA_{cv} + \mu\left(A_{vf}f_y + P_c\right) = (0.075\text{ ksi})(565\text{ in}^2) = 42.4\text{ kips}$$

Equation 2-19 AASHTO (5.7.4.3-4):
$$V_{ni} = K_1 f'_c A_{cv} = (0.20)(6.26\text{ ksi})(565\text{ in}^2) = 708\text{ kips}$$

Equation 2-20 AASHTO (5.7.4.3-5):
$$V_{ni} = K_2 A_{cv} = (0.8\text{ ksi})(565\text{ in}^2) = 452\text{ kips}$$

The smallest of these controls, so the predicted capacity is:

Estimated capacity: $V_{ni} = 42.4\text{ kips}$

The estimated capacity for all specimens were calculated following a similar procedure.

5.5.2. AASHTO LRFD Guide Specification for Accelerated Bridge Construction

The AASHTO LRFD Guide Specification for ABC differentiates between pocket and socket connections. An example is provided for Specimen S2-1 for the pocket connection and for Specimen SC-1 for the socket connection.

5.5.2.1. Pocket Connection Example

For Specimen S2-1 the total area of the interface is shown below:

Known: $d_v = 12\text{ in}$ $h_v = 15\text{ in}$

$$A_{cv} = \pi(12\ in)(15\ in) = 565\text{ in}^2$$

The estimated shear transfer resistance for specimen S2-1 is:

$$V_n = 0.13\sqrt{6.9\text{ ksi}}(565\text{ in}^2) = 193.7\text{ kips}$$

The estimated capacity for all specimens with pocket connections were calculated following a similar procedure.

The equation specifies using the compressive strength of the pocket concrete. This is likely because the connection specified in the AASHTO LRFD Guide Specifications for Accelerated Bridge Construction (American Association of State Highway and Transportation Officials (AASHTO), 2018) is for leaving the corrugated metal pipe in place. The assumption is that the shear friction failure will occur in the plug concrete adjacent to the steel pipe. This may not be a valid assumption in cases when the corrugated steel pipe is removed. It is recommended that the concrete strength used in Equation 2-22 be defined like the AASHTO LRFD BDS (American Association of State Highway and Transportation Officials (AASHTO), 2017b) Equation 2-19, where f'_c is defined as the "design concrete compressive strength of the weaker concrete on either side of the interface."

5.5.2.2. Socket Connection Example

As mentioned before, the AASHTO LRFD Guide Specification for ABC specifies that socket connections should be designed per shear friction requirements found in AASHTO LRFD BDS. Specimen SC-1 was used for this example; a similar procedure was used for Specimen SC-2.

Specimen SC-1 had a 14-inch high, 30-inch diameter socket which was created using a corrugated metal pipe. The interface was sandblasted (1/16-inch roughness). There was no reinforcement crossing the interface and no applied clamping force, so:

Known: $A_{vf} = 0 \text{ in}^2$ $P_c = 0 \text{ kips}$

The finish of this surface was sandblasted (1/16-inch roughness) however, the AASHTO LRFD Guide Specification for ABC specifies that for socket connections the cohesion factor (c), the friction factor (μ), and the K_1 and K_2 factors shall be taken as for "normal weight concrete placed against a clean concrete surface, free of laitance, with surface intentionally roughened to an amplitude of 0.25-in." This finish has the following interface shear factors:

For intentionally roughened interface:	$c = 0.24$ ksi	$\mu = 1.0$
	$K_1 = 0.25$	$K_2 = 1.5$ ksi

The total area of the interface is the circumference of the plug times the height of the interface. The interface height used in these calculations was from the bottom of the pile to the bottom of the socket. For SC-1 the interface height was 5.38-inch. The interface between the embedded pile and the plug concrete was ignored. For Specimen SC-1:

$$A_{cv} = 2\pi\left(\frac{30\ in}{2}\right)(5.62\ in) = 530\ \text{in}^2$$

This area can be used with all the above factors to calculate the estimated shear friction capacity. For Specimen SC-1:

Equation 2-18 AASHTO (5.7.4.3-3):	$V_{ni} = cA_{cv} + \mu\left(A_{vf}f_y + P_c\right) = (0.24\ \text{ksi})(530\ \text{in}^2) = 127.1\ kips$
Equation 2-19 AASHTO (5.7.4.3-4):	$V_{ni} = K_1 f'_c A_{cv} = (0.25)(7.27\ \text{ksi})(530\ \text{in}^2) = 963.28\ kips$
Equation 2-20 AASHTO (5.7.4.3-5):	$V_{ni} = K_2 A_{cv} = (1.5\ \text{ksi})(530\ \text{in}^2) = 795\ kips$

The smallest of these controls, so the predicted capacity is:

Estimated capacity:	$V_{ni} = 127.1\ kips$

5.5.3. FIP (1999)

According to the interface condition for Specimen S2-1, the β and μ were found from Table 2-8 and are shown below.

Known: $\beta = 0.2$ $f_{ctd} = 3.7$ MPa

$\mu = 0.6$ $\sigma_{fd} = 0$

As mentioned before, the interface area for Specimen S2-1 is 565 in^2 and can be used with all the above factors to calculate the estimated shear friction capacity.

$$\tau_{fd} = (0.2)(3.7 \text{ MPa}) + (0.6)(0) = 0.74 \text{ MPa} = 0.11 \text{ ksi}$$

$$\tau_{fd} = (0.11 \text{ ksi})(565 \text{ in}^2) = 60.6 \text{ kips}$$

5.5.4. Fib Model Code (2010)

According to the interface condition for Specimen S2-1, the c and μ were found on Table 2-9 and are shown below. Since there was no steel crossing the interface and no normal force applied the values of σ_n, ρ, and α are zero.

Known: $c = 0.35$ $f_{ctd} = 3.7$ MPa

$\mu = 0.6$ $f_{yd} = 0$

For Specimen S2-1:

$$v_{Rdi} = (0.35)(3.7 \text{ MPa}) = 1.3 \text{ MPa} = 0.19 \text{ ksi}$$

$$\tau_{fd} = (0.19 \text{ ksi})(565 \text{ in}^2) = 106.0 \text{ kips}$$

5.5.5. AASHTO LRFD BDS Modified for Corrugated Interfaces

For Specimen S2-1, the cohesion component would be found as shown below. The interface for Specimen S2-1 is smooth, so the entire interface area is assumed to have a cohesion factor associated with the sandblasted (1/16-inch roughness) finish).

$$V_{ni,c} = c_m A_{cv,m} + c_r A_{cv,r}$$

$$A_{cv,r} = \pi(12\ in)\left(\frac{15\ in}{2}\right) = 565 \text{ in}^2$$

$$V_{ni,c} = (0.4 \text{ ksi})(0.0 \text{ in}^2) + (0.1575 \text{ ksi})(565 \text{ in}^2) = 89.1 \text{ kips}$$

The monolithic area ($A_{cv,m}$) and non-monolithic area ($A_{cv,r}$) were based on the approximate areas of the ribs in the corrugations. The typical areas used for the specimens with corrugated interfaces are shown in Table 5-2.

Table 5-2: Typical interface areas for specimens with corrugated interfaces when using AASHTO LRFD BDS modified for corrugated interfaces

Cap Depth (in)	$A_{cv,m}$ (in^2)	$A_{cv,r}$ (in^2)	Specimen Example
14	126	288	S2-7
18	172	393	S2-10

For Specimen SC-1, the additional friction component could be found as shown below.

$$V_{ni,f} = \mu(A_{vf}f_y + P_c)$$

$$P_c = v_c f_c(\pi d_{plug})L_{ri}$$

$$P_c = (0.22)(6.95\text{ ksi})\pi(12\ in)\left(\frac{15\ in}{2}\right) = 432.0\text{ kips}$$

Assume $\mu = 0.8$
(referred to Table 5-1)

$$V_{ni,f} = (0.8)(432.0\text{ kips}) = 345.6\text{ kips}$$

Combining the cohesion component and the friction component would give an estimate capacity as shown below.

$$V_{ni} = V_{ni,c} + V_{ni,f} = 89.1\text{ kips} + 345.6\text{ kips} = 434.7\text{ kips}$$

5.6. Small-Scale Testing (Task 2)

The measured ultimate loads, estimated failure loads, and ultimate loads normalized by the estimated loads using the five different estimation procedures for the small-scale specimens are shown in Table 5-4 for all the specimens tested in Task 2. A normalized ultimate load greater than or equal to 1.0 is conservative and less than 1.0 is unconservative. The values presented in Table 5-4 for AASHTO LRFD BDS are using the lower bound cohesion and friction coefficients.

The average, standard deviation, and coefficient of variation (CoV) for the ultimate load normalized by the estimated failure load are shown in Table 5-3.

Table 5-3: Statistics for estimated failure loads in small-scale testing

Method	***AASHTO***	***ABC***	***FIP***	***fib***	***Mod.***
n =	37	37	37	37	37
Average =	16.56	3.11	11.14	17.82	1.22
St. Dev =	11.60	0.76	4.86	28.10	0.28
CoV =	0.700	0.244	0.436	1.577	0.231
< 1.0 (total) =	0	1	0	0	8
0.9 to 1.0 =	0	1	0	0	2
0.8 to 0.9 =	0	0	0	0	1
0.7 to 0.8 =	0	0	0	0	4
0.6 to 0.7 =	0	0	0	0	0
< 0.6 =	0	0	0	0	1

All four available estimation procedures provided conservative estimates of the 37 specimens tested in Task 2, with averages above 1.0. The equation provided in the AASHTO LRFD Guide Specification for ABC was the most accurate and precise of the four available estimation procedures, with average closest to 1.0 and smallest coefficient of variation.

The modified AASHTO LRFD BDS approach provided improved accuracy and precision, with an average of 1.22 and coefficient of variation of 0.231. However, there were eight specimens (21.6%) that had the failure load unconservatively estimated using the modified approach.

Table 5-4: Measured and estimated failure loads and ultimate loads normalized by estimated loads for small-scale testing.

Spec.	Ultimate Load (kips)						Normalized Ultimate Load				
	Measured[1]	*AASHTO*	*ABC*	*FIP*	*fib*	*Mod.*	*AASHTO*	*ABC*	*FIP*	*fib*	*Mod.*
S1-1	> 750.0	93.3	471.5	151.2	261.3	1532.0	8.04	1.59	4.96	2.87	0.49
S1-2	> 750.0	42.4	218.1	69.9	121.1	715.0	17.68	3.44	10.72	6.19	1.05
S1-3 [2]	243.8	21.2	105.3	34.5	59.7	343.8	11.50	2.32	7.06	4.09	0.71
S1-4	429.7	93.3	457.4	153.9	266.4	557.9	4.61	0.94	2.79	1.61	0.77
S2-1	339.0	42.4	193.7	60.6	106.0	434.7	7.99	1.75	5.60	3.20	0.78
S2-2	> 750.0	135.7	194.2	122.0	137.3	530.4	5.53	3.86	6.15	5.46	1.41
S2-3	320.2	42.4	193.7	60.2	105.3	413.7	7.55	1.65	5.32	3.04	0.77
S2-4	615.4	99.5	142.4	89.5	100.7	389.0	6.18	4.32	6.88	6.11	1.58
S2-5	356.0	31.1	141.7	43.3	75.7	305.0	11.45	2.51	8.23	4.70	1.17
S2-6	418.6	31.1	141.7	45.1	78.9	327.0	13.46	2.95	9.28	5.30	1.28
S2-7	719.5	42.4	193.2	60.8	106.4	560.6	16.96	3.72	11.83	6.76	1.28
S2-8	553.5	42.4	198.5	64.3	112.5	586.1	13.05	2.79	8.61	4.92	0.94
S2-9	662.2	14.1	198.5	30.7	7.7	489.9	46.84	3.34	21.57	86.29	1.35
S2-10	575.4	31.1	143.7	46.6	81.5	420.2	18.50	4.00	12.36	7.06	1.37
S2-11	399.8	31.1	143.7	46.0	80.4	405.0	12.86	2.78	8.70	4.97	0.99
S2-12	521.6	10.4	143.7	23.0	5.7	367.3	50.31	3.63	22.70	90.81	1.42
S2-13	605.6	42.4	200.2	53.8	94.2	335.2	14.28	3.02	11.25	6.43	1.81
S2-14	441.3	31.1	146.7	40.8	71.5	310.8	14.19	3.01	10.81	6.18	1.42
S2-15	631.2	99.5	146.7	81.7	91.9	406.4	6.34	4.30	7.73	6.87	1.55
S2-16	750.0	42.4	204.8	55.8	97.7	484.8	17.68	3.66	13.44	7.68	1.55
S2-17	533.3	14.1	200.0	27.8	7.0	400.9	37.72	2.67	19.16	76.62	1.33
S2-18	569.2	31.1	152.2	41.0	71.7	459.5	18.30	3.74	13.89	7.94	1.24

Spec.	Ultimate Load (kips)						Normalized Ultimate Load				
	Measured[1]	*AASHTO*	*ABC*	*FIP*	*fib*	*Mod.*	*AASHTO*	*ABC*	*FIP*	*fib*	*Mod.*
S2-19	482.6	10.4	152.2	20.5	5.1	404.7	46.55	3.17	23.55	94.21	1.19
S2-20	666.0	42.4	196.0	57.3	100.4	455.1	15.70	3.40	11.61	6.64	1.46
S3-1	364.1	31.1	115.5	36.1	63.1	305.3	11.71	3.15	10.10	5.77	1.19
S3-2	444.6	31.1	115.5	36.1	63.1	305.3	14.30	3.85	12.33	7.05	1.46
S3-3	440.9	31.1	115.5	36.1	63.1	305.3	14.18	3.82	12.23	6.99	1.44
S3-4	493.8	31.1	116.6	36.5	63.8	309.4	15.88	4.23	13.54	7.74	1.60
S3-5	340.7	10.4	116.6	18.2	4.6	261.5	32.86	2.92	18.68	74.73	1.30
S3-6	283.8	10.4	116.6	18.2	4.6	261.5	27.37	2.43	15.56	62.25	1.09
S3-7	413.6	31.1	116.3	36.6	64.1	308.0	13.30	3.56	11.29	6.45	1.34
S3-8	379.3	31.1	116.6	36.5	63.8	309.4	12.20	3.25	10.40	5.94	1.23
S3-9	364.6	31.1	116.3	36.6	64.1	308.0	11.72	3.14	9.95	5.69	1.18
S3-10	330.7	31.1	116.3	36.6	64.1	308.0	10.63	2.84	9.03	5.16	1.07
S3-11	352.4	31.1	116.6	36.5	63.9	309.4	11.33	3.02	9.65	5.51	1.14
S3-12	363.2	31.1	116.3	36.6	64.1	308.0	11.68	3.12	9.92	5.67	1.18
S3-13	387.5	165.9	116.6	73.0	91.3	437.6	2.34	3.32	5.30	4.24	0.89

[1] a measured load of 750 kips signifies that the capacity of the load cell was reached before failure of the specimen occurred

[2] S1-3 failed due to crushing of concrete on top of plug

5.7. Large-Scale Testing (Task 3)

The measured ultimate loads, estimated failure loads, and ultimate loads normalized by the estimated loads using the five different estimation procedures for the large-scale specimens are shown in Table 5-6. A normalized ultimate load greater than or equal to 1.0 is conservative and less than 1.0 is unconservative. The values presented in Table 5-6 for AASHTO LRFD BDS are using the lower bound cohesion and friction coefficients.

The average, standard deviation, and coefficient of variation (CoV) for the ultimate load normalized by the estimated failure load are shown in Table 5-5.

Table 5-5: Statistics for estimated failure loads in large-scale testing

Method	***AASHTO***	***ABC***	***FIP***	***fib***	***Mod.***
n =	8	8	8	8	8
Average =	34.03	4.58	15.71	42.57	1.55
St. Dev =	24.55	0.97	8.25	47.46	0.29
CoV =	0.721	0.212	0.525	1.115	0.189
< 1.0 (total) =	0	0	0	0	1
0.9 to 1.0 =	0	0	0	0	1
0.8 to 0.9 =	0	0	0	0	0
0.7 to 0.8 =	0	0	0	0	0
0.6 to 0.7 =	0	0	0	0	0
< 0.6 =	0	0	0	0	0

Like the small-scale testing, the four available estimation procedures provided conservative estimates for the eight specimens testing in Task 3. Again, the equation provided in the AASHTO LRFD Guide Specification for ABC was the most accurate and precise of the four available estimation procedures, with average closest to 1.0 and smallest coefficient of variation.

The modified AASHTO LRFD BDS approach again provided improved accuracy and precision, with an average of 1.55 and coefficient of variation of 0.189. One of the eight specimens (12.5%) had the failure load unconservatively estimated using the modified approach.

Table 5-6: Measured and estimated failure loads and ultimate loads normalized by estimated loads for large-scale testing.

Spec.	Ultimate Load (kips)						Normalized Ultimate Load				
	Measured[1]	*AASHTO*	*ABC*	*FIP*	*fib*	*Mod.*	*AASHTO*	*ABC*	*FIP*	*fib*	*Mod.*
LP-1	545.6	46.7	218.0	78.7	136.7	459.7	11.7	2.5	6.9	4.0	1.2
LP-2	> 1000.0	149.3	220.1	157.5	175.9	610.2	6.7	4.5	6.3	5.7	1.6
LP-3	> 1000.0	46.7	220.1	78.7	136.8	649.7	21.4	4.5	12.7	7.3	1.5
LP-4	> 1000.0	15.6	220.1	39.4	9.8	568.7	64.3	4.5	25.4	102.4	1.8
MP-1	600.8	8.5	120.7	21.3	5.3	314.0	70.8	5.0	28.2	113.8	1.9
MP-2	626.4	25.4	120.7	42.6	73.9	358.0	24.6	5.2	14.7	8.5	1.7
SC-1	511.0	38.0	121.7	64.1	111.4	521.0	13.4	4.2	8.0	4.6	1.0
SC-2	601.4	10.2	97.5	25.7	6.4	364.4	59.2	6.2	23.4	94.3	1.7

[1] a measured load of 1000 kips signifies that the capacity of the load frame was reached before failure of the specimen occurred

5.8. Evaluation of AASHTO LRFD BDS

Lower-bound assumptions were used in the previous section to determine the estimated shear friction capacity using the AASHTO LRFD Bridge Design Specifications (BDS). These lower-bound assumptions included using the smaller cohesion factor and coefficient of friction if an interface condition fell between two options and ignoring any normal force developed from Poisson's effect as the plug was being loaded. The effect of using different cohesion factors and coefficients of friction and including a normal force from the plug expansion will be investigated further in this section.

5.8.1. Effect of Cohesion and Friction Factors

There were a few lower-bound assumptions made when determining the cohesion and friction factors to be used in the AASHTO LRFD BDS shear friction equations, summarized in Table 5-7. The upper-bound and average values are also included in Table 5-7.

The smooth interface with exposed aggregate finish (1/4-inch roughness) is clearly specified in AASHTO LRFD BDS (c = 0.24, μ = 1.0), so lower and upper bounds are the same. Additionally, the monolithic cast specimen is explicitly specified (c = 0.4, μ = 1.4).

The interface constructed with Sonotube (smooth, no corrugations) with sandblasted (1/16-inch roughness) finish falls between the lower bound when the interface is not intentionally roughened (c = 0.075, μ = 0.6) and upper bound when having an intentionally roughened interface to an amplitude of 1/4 inch (c = 0.24, μ = 1.0).

The corrugated interfaces increase the roughness and the coefficient of friction. The upper bound for the coefficient of friction for the corrugated interfaces is the monolithic case (μ = 1.4). However, the corrugations do not influence the cohesion, so these upper bounds are the 1/4-inch roughened case (c = 0.24) for the sandblasted finish and the concrete placed against clean steel case (c = 0.025) for when the metal duct was left in place.

Table 5-7: Range of cohesion factors and coefficients of friction for AASHTO LRFD BDS

Interface Condition	$n_{specimens}$	**Lower-Bound**		**Average**		**Upper-Bound**	
		c	μ	c	μ	c	μ
Smooth (sandblasted)	8	0.075	0.6	0.1575	0.8	0.24	1.0
Smooth (Exposed aggregate)	4	0.24	1.0	0.24	1.0	0.24	1.0
Corrugated (sandblasted)	23	0.075	0.6	0.1575	1.0	0.24	1.4
Corrugated (Metal)	9	0.025	0.7	0.025	1.1	0.025	1.4
Monolithic	1	0.40	1.4	0.40	1.4	0.40	1.4

The range of K_1 and K_2 factors for AASHTO LRFD BDS are summarized in Table 5-8 with similar reasoning as the cohesion factor and coefficient of friction ranges.

Table 5-8: Range of K_1 and K_2 factors for AASHTO LRFD BDS

Interface Condition	$n_{specimens}$	**Lower-Bound**		**Average**		**Upper-Bound**	
		K_1	K_2 (ksi)	K_1	K_2 (ksi)	K_1	K_2 (ksi)
Smooth (sandblasted)	8	0.2	0.8	0.225	1.15	0.25	1.5
Smooth (Exposed aggregate)	4	0.25	1.5	0.25	1.5	0.25	1.5
Corrugated (sandblasted)	23	0.2	0.8	0.225	1.15	0.25	1.5
Corrugated (Metal)	9	0.2	0.8	0.2	1.15	0.2	1.5
Monolithic	1	0.25	1.5	0.25	1.5	0.25	1.5

The effect of modifying the cohesion factor and coefficient of friction on the overall statistics is shown in Table 5-9. Moving to the upper-bound values decreases the average but increases the variation. One reason for this is that the modification of the coefficient of friction does not have any effect on the estimated capacity if there is no normal force reinforcement crossing the shear friction plane.

Table 5-9: Statistics for estimated failure loads using AASHTO LRFD BDS with different values for cohesion factor and coefficient of friction (without normal force)

Assumptions =	***Lower-Bound***	***Average***	***Upper-Bound***
n =	45	45	45
Average =	19.19	14.28	12.75
St. Dev =	15.33	17.09	17.77
CoV =	0.799	1.197	1.394
< 1.0 (total) =	0	0	0
0.9 to 1.0 =	0	0	0
0.8 to 0.9 =	0	0	0
0.7 to 0.8 =	0	0	0
0.6 to 0.7 =	0	0	0
< 0.6 =	0	0	0

The effect of the normal force component will be investigated in the next section.

5.8.2. Effect of Normal Force Component

From the experimental results, expansion of the plug was observed while loading the specimens. This behavior was experimentally observed with the confinement reinforcement placed around the pocket which was engaged during testing. This measured engagement of the confinement reinforcement was different between specimens, with the difference related to the interface condition including the corrugation spacing and depth and the surface preparation. For simplicity, it will be assumed that all plugs had equal expansion.

The expansion of concrete in general is dependent on Poisson's ratio. The Poisson's ratio for concrete generally remains close to 0.20 but will increase as the concrete approaches its ultimate strength. The Poisson's ratio was measured using ASTM C469 for twelve specimens in Series 2 with measured values between 0.19 and 0.22. The Poisson's ratio can be used to determine the normal force applied to the interface using Equation 5-11, which was discussed in §5.2.3.

$$P_c = \upsilon_c f_c (\pi d_{plug}) L_{ri} \qquad \text{Equation 5-11}$$

See the discussion in §5.2.3. For simplicity, L_{ri} is taken as half the interface height ($0.5L_{interface}$), the concrete stress (f_c) is taken as the compressive strength, and the Poisson's ratio (ν_c) is equal to 0.20.

The effect of including a normal force on the statistics for the test specimens can be seen in Table 5-10. Adding the normal force improved the accuracy and precision of the estimates, with averages closer to 1.0 and smaller coefficients of variation when compared with the values in Table 5-9. Using the upper bound assumptions for the cohesion and coefficient of friction led to 19 of 45 specimens (42.4%) having unconservative estimates for shear friction capacity.

Table 5-10: Statistics for estimated failure loads using AASHTO LRFD BDS with different values for cohesion factor and coefficient of friction (with normal force)

Assumptions =	***Lower-Bound***	***Average***	***Upper-Bound***
n =	45	45	45
Average =	2.22	1.41	1.07
St. Dev =	0.66	0.34	0.29
CoV =	0.299	0.244	0.270
< 1.0 (total) =	1	6	19
0.9 to 1.0 =	0	0	9
0.8 to 0.9 =	1	2	2
0.7 to 0.8 =	0	3	3
0.6 to 0.7 =	0	0	2
< 0.6 =	0	1	3

5.8.3. Comparison of Estimation Procedures

A comparison of three of the best performing estimation procedures is shown in Table 5-11. Using the estimated failure load from AASHTO LRFD BDS with the average values for the cohesion and coefficient of friction and normal force from Equation 5-11 will result in similar precision and slightly more conservative estimates as compared to the AASHTO LRFD BDS procedure modified for corrugated interfaces. Using the AASHTO LRFD Guide Specification for ABC will lead to more conservative results and increased precision compared to the other two procedures.

Table 5-11: Statistics for estimated failure loads using AASHTO LRFD BDS with average values for cohesion factor and coefficient of friction (with normal force) compared to modified procedure for corrugated interfaces and AASHTO LRFD Guide Spec. for ABC

Method =	***BDS Avg. w/P_c***	***BDS Mod.***	***Guide for ABC***
n =	45	45	45
Average =	1.41	1.26	3.32
St. Dev =	0.34	0.31	0.89
CoV =	0.244	0.244	0.267
< 1.0 (total) =	6	9	1
0.9 to 1.0 =	0	3	1
0.8 to 0.9 =	2	1	0
0.7 to 0.8 =	3	4	0
0.6 to 0.7 =	0	0	0
< 0.6 =	1	1	0

The procedures for estimating the shear friction capacity of pocket and socket connections in the AASHTO LRFD Guide Specification for ABC perform well compared to other currently available procedures. Modifications can be made to the current AASHTO LRFD BDS estimation procedures to improve the accuracy and precision of the estimations, but with an increased number of unconservative estimates.

In general, it is recommended to use the AASHTO LRFD Guide Specification for ABC equations for estimation of the shear friction capacity of the interface in pocket and socket connections.

Chapter 6: **Design Recommendations**

6.1. Introduction

This section summarizes the design details and recommendations for this connection based on the shear friction testing. The complete design of this connection can be performed using the appropriate specifications and manuals, e.g., AASHTO LRFD Guide Specification for ABC (American Association of State Highway and Transportation Officials (AASHTO), 2018), AASHTO LRFD BDS (American Association of State Highway and Transportation Officials (AASHTO), 2017b), FDOT SDG (Florida Department of Transportation (FDOT), 2021), and FDOT Structures Detailing Manual (Florida Department of Transportation (FDOT), 2020)

6.2. Construction Recommendations

The Florida Department of Transportation has different construction recommendations when using prefabricated bridge elements and systems. Some of the recommendations for precast footings and pile caps found in the Structures Design Manual are listed below:

- Use a removable corrugated pipe to transfer shear without need of reinforcement in the plug-cap interface.
- The surface shall be presoaking and prepared to obtain “saturated surface dry” (SSD) condition. The void needs to be filled with water for 4 to 5 hours and removed prior pouring the concrete.
- In addition to the SSD condition, an exposed aggregate finish surface should be provided for all interfacing surfaces. This finish is specified as a 1/16-inch roughness finish that can be obtained by sandblasting.
- Specify in-fill concrete to include shrinkage reducing admixture and provide a seven-day moist cure.

These recommendations were generally confirmed from the test results in this project. Some of the relevant observations and conclusions from the testing program are listed below.

- Removing of the steel corrugated duct and intentionally roughening through sandblasting or chiseling led to strength equal or greater than those when the duct was left in place, which is the current recommendation for the AASHTO LRFD Guide Specification for ABC.
- Using an exposed aggregate finish (1/4-inch roughness) without corrugations led to equal or greater strength than specimens with corrugations and 1/16-inch roughness.
- Minimal cohesion was observed when the corrugated metal pipe was left in place.

Some of these surface preparations were new to the precasters in this project. Mockups and clear specifications should be used to ensure that the precaster is able to properly construct the pockets and achieve the desired interface conditions.

6.3. Pocket Connection Design and Construction Details

The minimum edge distance between the edge of the pile and edge of the pile cap is specified as 9 inches in AASHTO LRFD BDS §10.7.1.2, independent of the pile size. In common practice, the edge distance varies with pile size; it is typical practice to use a minimum edge distance of $0.5d_{pile}$, which is equal to 9 inches for 18-inch piles. FDOT Structures Design Guidelines (§3.5.4) specifies that center-to-center pile spacing should not be less than $3.0d_{pile}$.

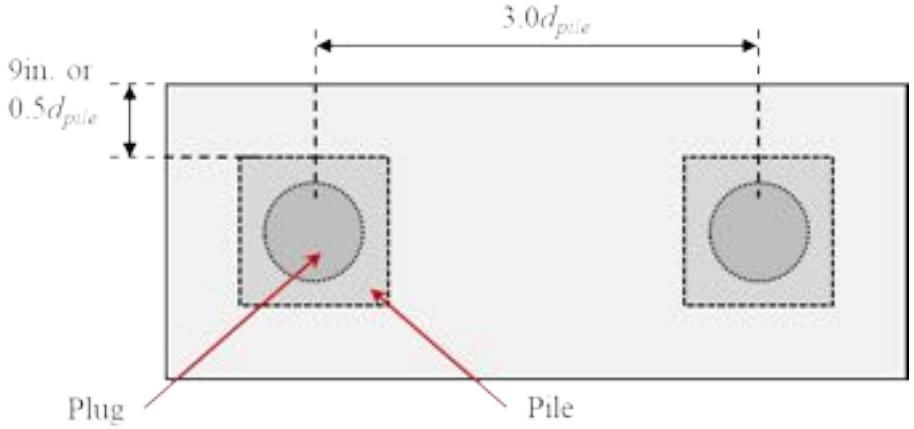

Figure 6-1: Current edge distance and spacing requirements for piles and pile caps in AASHTO LRFD BDS and FDOT SDG

These requirements translate to the distance between the edge of the pocket or plug to the edge of the cap as shown in Figure 6-2. The distance between edge of pocket and edge of cap will be greater than the pocket or plug diameter as long as the typical practice of a $0.5d_{pile}$ edge distance between edge of pile and edge of cap be provided, as shown in Figure 6-2 (a). If only the minimum AASHTO LRFD BDS allowed edge distance of 9 inches is provided for 30-inch piles with 18-inch pockets, then the edge distance would be less than the diameter of the plug, as shown in Figure 6-2 (b).

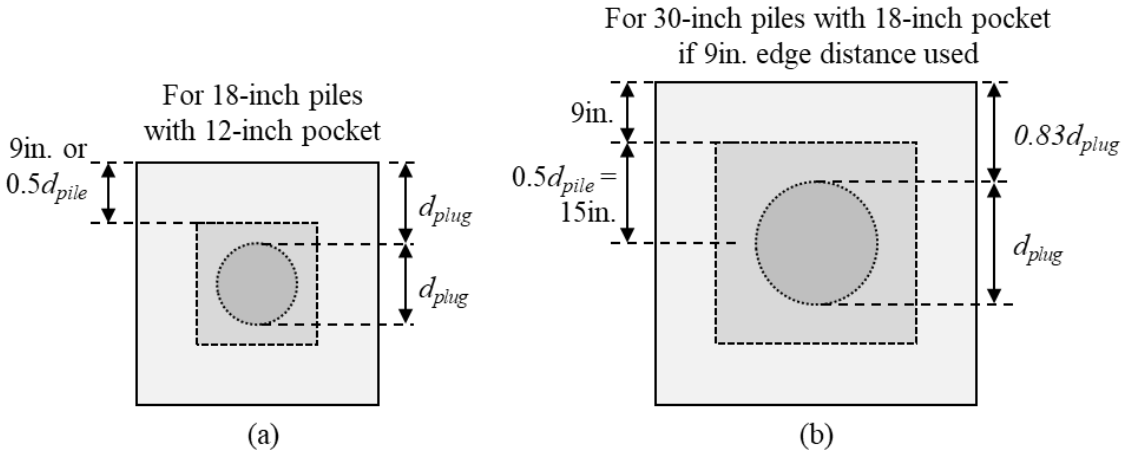

Figure 6-2: Distance between the edge of the pocket or plug and the edge of the cap for (a) 18-inch piles with 12-inch pockets and (b) 30-inch piles with 18-inch pockets when only 9-inch edge distance is provided

Several specimens were tested with decreasing edge distances in Series II, see Task 2d. Some of the conclusions from these tests are summarized below:

1. Edge had a noticeable effect on the normalized strength only when the edge distance was decreased in two directions. Large failure cracks typically extended diagonally out of the plug toward the corner of the cap. Decreasing the edge distance in one direction did not have as significant an effect on this diagonal distance as decreasing the edge distance in two directions.
2. The normalized strength for specimens with $0.5d_{plug}$ were still above the estimated strength using all estimation procedures.

The minimum spacing between piles, as specified in FDOT SDG, is three times the pile size, as shown in Figure 6-3 (a). A narrower spacing was tested for the multi-plug

specimens, as shown in Figure 6-3 (b). The specimens with multiple plugs had similar or better performance to the similar specimens with a single plug, so there was no negative multi-plug effect observed.

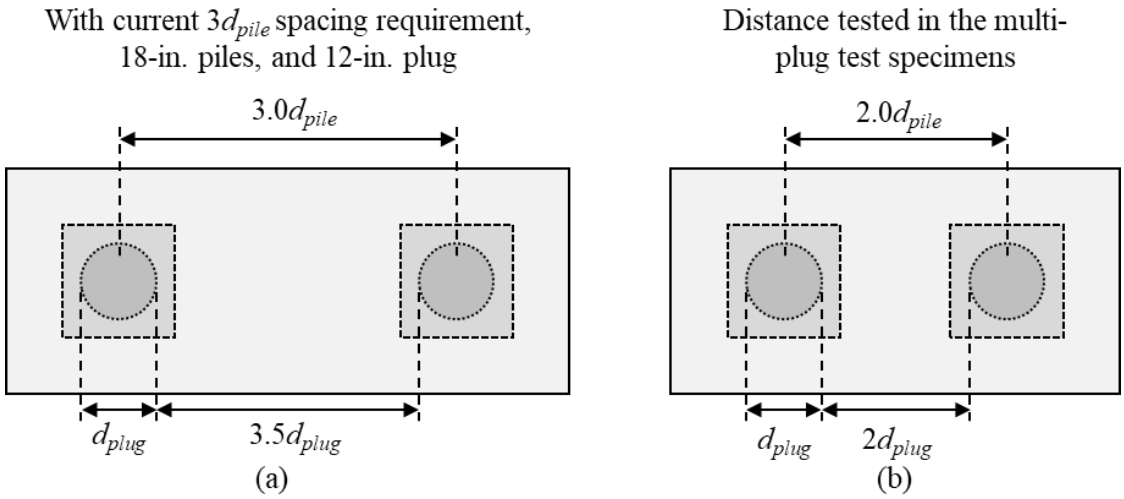

Figure 6-3: Spacing between piles and plugs (a) as specified in FDOT SDG and (b) minimum tested

A cap reinforcement detail like that provided in the FDOT Structure Detailing Manual, shown in Figure 6-4, was used in the test specimens. Confinement reinforcement around the pocket was provided in most specimens but was also omitted in several specimens.

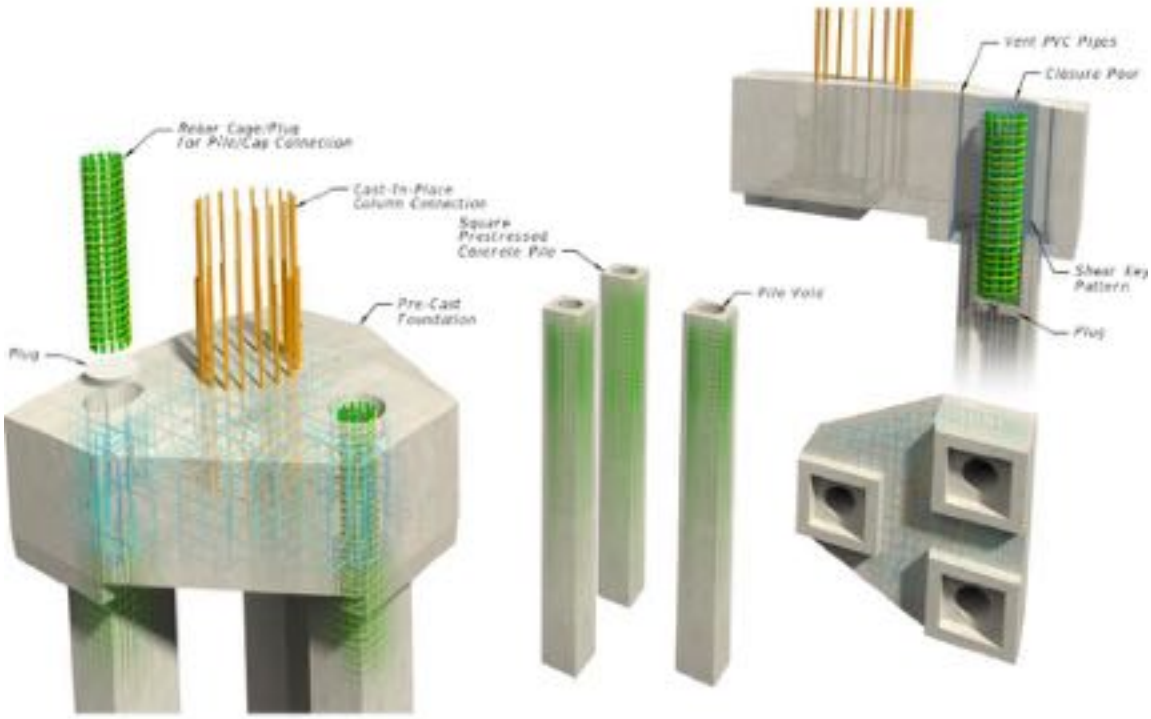

Figure 6-4: Sample detail for precast footings provided in FDOT Structures Detailing Manual

There were several conclusions related to the reinforcement in the cap:

1. The confinement reinforcement saw higher strains in specimens with smaller edge distances in two directions. This shows that as there is less concrete area to resist the splitting cracks, the confinement reinforcement becomes more important.
2. Decreasing the longitudinal reinforcement in the cap decreased the normalized strength of the specimens. Changing the confinement reinforcement did not have a significant effect on the strength of the specimens with $1d_{plug}$ edge distance. However, it is assumed that the confinement reinforcement would influence the strength for smaller edge distances.
3. The normalized strength for specimens with all variety of reinforcement (even those without any confinement reinforcement and those without any longitudinal reinforcement) were still above the estimated strength using all estimation procedures.

To summarize:

1. It is suggested to use a minimum edge distance of $0.5d_{pile}$ between the edge of the pile and edge of the cap. This will provide sufficient distance between the edge of the plug and edge of the cap.
2. The currently required center-to-center pile spacing of $3d_{pile}$ does not negatively affect the shear friction capacity of the cap-to-plug interface.
3. No confinement reinforcement is required around the pocket for shear friction purposes if the minimum edge distance of $0.5d_{pile}$ is provided between the edge of the pile and edge of the cap. Using a reinforcement detail like that proposed in the FDOT Structures Detailing Manual is sufficient for providing confinement around the pocket for shear friction capacity.

6.4. Socket Connection Design and Construction Details

The socket connection specimens in this project were designed primarily based on the capacity of the load frame, standard pile size, and the available corrugated metal pipe sizes by local vendors. Socket design should generally follow the specifications provided by the AASHTO LRFD Guide Specification for ABC (American Association of State Highway and Transportation Officials (AASHTO), 2017b). Several different observations from the design, detailing, construction and testing of the socket connection specimens are summarized in this section.

6.4.1. Tolerances for Socket Connection

The tolerances for socket connections are specified in the Proposed Guidelines for Prefabricated Bridge Elements and Systems Tolerances (NCHRP Project 12-98) (Culmo, n.d.). The specified diameter of the void for the socket connection (S_w) can be found using Equation 6-1. The void is sized based on the minimum tolerable clearance between the edge of the void and edge of embedded element (t_{min_el}), outer diameter of the embedded element ($O.D.$), and pile width tolerance (T_w).

$$S_w = 2t_{min\ \_el} + O.D. + 2T_w \text{ (in.)}$$

Equation 6-1
NCHRP (Culmo, n.d.)
(4.6.4.1)

For the socket connection investigated in this project, the specified void diameter in the cap needed to be greater than or equal to the value found in Equation 6-2. The values assumed for this project were as follows:

- t_{min_el} = 0 in. (no clear distance between edge of pile and edge of void)
- *O.D.* found based on the diagonal distance between opposite corners of the 18-in. square pile, as shown in Equation 6-2.

$$O.D. = \sqrt{(18\text{ in})^2 + (18\text{ in})^2} = 25.5\text{ in} \qquad \text{Equation 6-2}$$

- T_w = 3.25 in. (based on a maximum pile lateral installation tolerance of 3 in., from Table 4.6.4.1-1 in NCHRP Project 12-98 (Culmo, n.d.))

Substituting these values into Equation 6-1 gave the following specified void diameter:

$$S_w = 2(0\text{ in}) + 25.5\text{ in} + 2(3.25\text{ in}) = 32\text{ in}$$

A plug diameter of 30 in. was still used to ensure the specimen capacity remained under the 1,000-kip capacity of the available test frame. In a field application, the next size up corrugated metal pipe should be used. The plug diameter in a field application would need to be much larger if the maximum pile lateral installation tolerance was 6 in., which would require using T_w of 6.125 in.

6.4.2. Punching Shear Capacity of Plug and Socket Reinforcement

A combined punching shear and shear friction failure may occur in the plug or socket under the pile. A punching shear failure will prevent the entire plug from pushing through together. Additional reinforcement was provided in the test specimens to help resist the punching shear failure. This recommendation was made by a design engineer who helped to create the current specifications for socket connection. Two layers of #4 bars with five bars in each direction in each layer are proposed to help resist the punching shear failure in the plug, as shown in Figure 6-5.

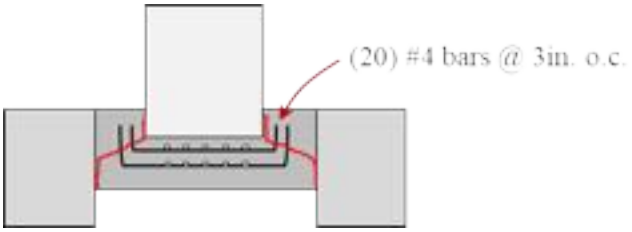

Figure 6-5: Reinforcement layout in the pocket of the specimen

6.4.2.1. Estimated Punching Shear Capacity

The punching shear capacity was found below based on ACI 318-19 (American Concrete Institute (ACI) Committee 318, 2019) including the additional bars in the plug. The nominal shear strength for two-way members with shear reinforcement is calculated by:

$$v_n = v_c + v_s$$

Equation 6-3
ACI 318-19 (22.6.1.3)

The stress corresponding to the nominal two-way shear strength provided by concrete is as follows:

$$v_c = 2\lambda_s\lambda\sqrt{f'_c}$$

Equation 6-4
ACI 318-19 (22.6.6.1)

where:

λ_s = size effect factor

λ = modification factor

f'_c = concrete strength (psi)

The size effect factor is determined by:

$$\lambda_s = \sqrt{\frac{2}{1+\frac{d}{10}}} \leq 1$$

Equation 6-5
ACI 318-19 (22.5.5.1.3)

The d in this equation is the depth of the steel. This was assumed to be the distance from the top of the plug to the bottom layer of steel shown in Figure 6-5.

$$\lambda_s = \sqrt{\frac{2}{1 + \frac{12.25 \text{ in.}}{10}}} \leq 1$$

$$\lambda_s = 0.95 \leq 1$$

Assuming a concrete strength of 6.5 ksi for the plug, the shear strength provided by concrete was:

$$v_c = 2 \times (0.95)(1.0)\sqrt{6{,}500 \text{ psi}}$$

$$v_c = 153.2 \text{ psi}$$

The stress corresponding to the nominal two-way shear strength provided by the reinforcement is shown in Equation 6-6.

$$v_s = \frac{A_v f_{yt}}{b_o s}$$ Equation 6-6
ACI 318-19 (22.6.7.2)

where:

A_v = area of shear reinforcement contained by a peripheral line around pile (in^2)

f_{yt} = yield strength of transverse reinforcement (psi)

b_o = perimeter of critical section for two-way shear (in)

s = center-to-center spacing of shear reinforcement (in)

The area of shear reinforcement was assumed to include all 10 bars in a layer and 2 legs per bar, so the total area can be found as shown below:

$$A_v = 2(10)(0.2 \text{ in}^2) = 4 \text{ in}^2$$

The spacing between shear reinforcement (s) was assumed to be equal to the spacing between the vertical legs of the reinforcement in each of the layers (1.5 in.). The perimeter of the critical section was assumed to be the perimeter of the void region (πd_{plug})

$$v_s = \frac{(4 \text{ in}^2)(60 \text{ ksi})}{(\pi)(30 \text{ in.})(1.5 \text{ in.})} = 1697.7 \text{ psi}$$

Thus, the nominal shear strength is:

$$v_n = 153.2 \text{ psi} + 1697.65 \text{ psi} = 1{,}851 \text{ psi} = 1.8 \text{ ksi}$$

This nominal shear strength corresponds to an applied load as shown below in Equation 6-7.

Equation 6-7
Based on ACI 318-19 §22.6.1.4

$$V_n = v_n d b_o$$

No v_s:

$$V_n = (0.153 \text{ ksi})(12.25 \text{ in.})(\pi)(30 \text{ in.}) = 176 \text{ kips}$$

With v_s:

$$V_n = (1.8 \text{ ksi})(12.25 \text{ in.})(\pi)(30 \text{ in.}) = 2{,}078 \text{ kips}$$

The addition of the reinforcement increased the punching shear capacity to attempt to engage more of the plug in the shear friction failure.

6.4.2.2. Observed Response of Socket Reinforcement

The reinforcement provided beneath the embedded pile was engaged during testing in both the horizontal portion beneath the pile and the vertical leg extending beside the pile; an example of this engagement is shown in Figure 6-6 for SC-1.

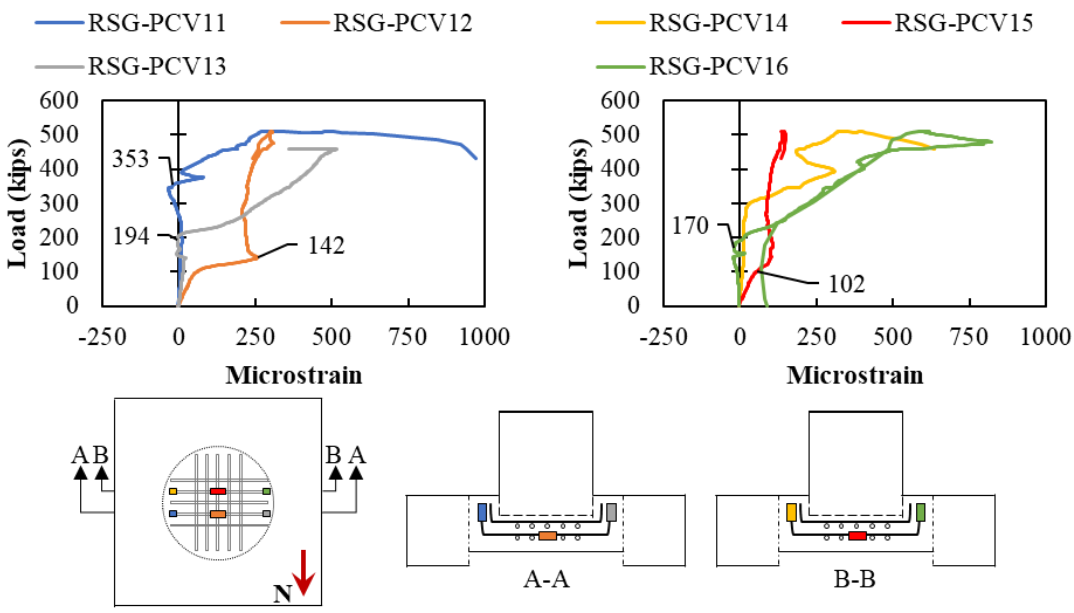

Figure 6-6: Sample load versus microstrain plots for socket reinforcement in SC-1

While the reinforcement was engaged, the cracking after failure on top and bottom of the plug, shown in Figure 6-7, still suggested that the entire plug-to-cap interface was not engaged.

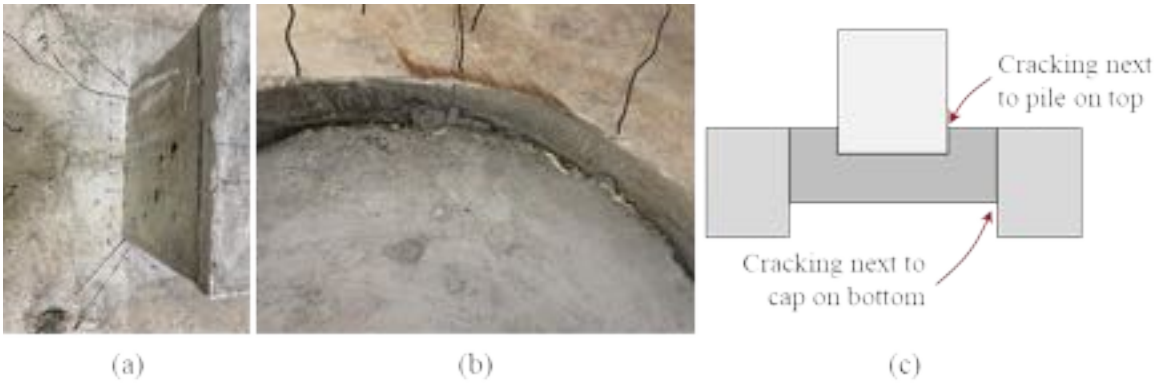

Figure 6-7: Location of cracking in socket specimens, SC-1 shown, (a) on top next to the pile, (b) on bottom next to the cap, and (c) schematic highlighting location of cracking

The reinforcement beneath the pocket was engaged during testing, so it does appear to help distribute stresses in the plug concrete, but it does now allow the entire plug-to-cap interface to engage during the testing.

6.4.3. Assumed Interface Area for Socket Connections

As mentioned before, the AASHTO LRFD Guide Specification for ABC (American Association of State Highway and Transportation Officials (AASHTO), 2018) specifies that socket connections should be designed per shear friction requirements found in AASHTO LRFD BDS (American Association of State Highway and Transportation Officials (AASHTO), 2017b). The guide does not clarify what interface should be checked and what interface area should be used in the calculations. There are two different interfaces, between the plug and cap and between the pile and plug, which may control, and several different possible interface heights, shown in Figure 6-8 (a). As discussed above and shown in Figure 6-7, a crack after failure was observed next to the pile on top of the specimens and next to the cap on the bottom of the specimen, suggesting a combined failure along the pile-to-plug and plug-to-cap interfaces, as shown in Figure 6-8 (b).

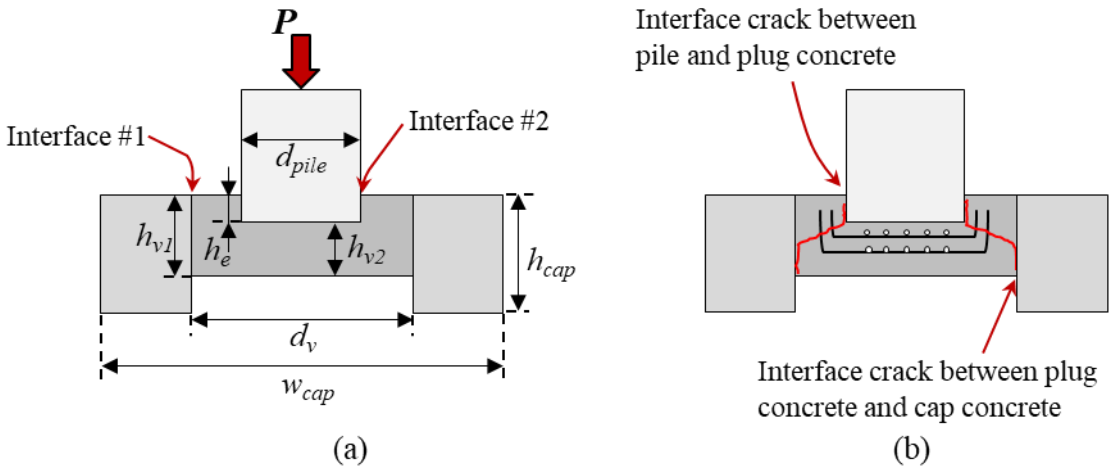

Figure 6-8: Socket Specimen: (a) interface detail and (b) failure characteristics

The embedded pile was not intentionally roughened, so there would be only minor cohesion and friction as compared to the corrugated interface between the plug and cap. For this reason, only the interface between the plug and cap is suggested to be used when calculating the shear friction capacity. The height that is recommended to be used to calculate the capacity of the interface is the distance between the bottom of the pile and bottom of the plug, h_{v2} as shown in Figure 6-8 (a).

For the specimens in this project, the precaster experienced some difficulties trying to place and hold the embedded pile in the void while casting the concrete. The actual pile embedment length and squareness varied slightly from the construction plans for both specimens (SC-1 and SC-2). According to measurements taken after casting of the specimens, the average embedment length for Specimen SC-1 was 5.38 inches and for Specimen SC-2 was 4.31 inches. The details of the measurements were discussed on Task 3d. The interface length for these specimens was assumed to be equal to the height of the socket (11 inches) minus the average measured embedment lengths, which led to 5.62 inches for SC-1 and 6.69 inches for SC-2. These assumptions led to ultimate loads normalized by the estimated load using the AASHTO LRFD Guide Specification for ABC of 4.2 for SC-1 and 6.2 for SC-2.

Chapter 7: **Summary, Conclusions, and Recommendations**

The shear friction capacity between precast pile caps and precast piles was investigated using pocket and socket connections. A modified push-trough specimen was envisioned for this project; thus, a preliminary experimental testing was done to four small-scale specimens to evaluate the proposed test setup and test protocol. Based on this, thirty-three small-scale specimens were design, constructed and experimentally tested to evaluate all possible combination in the test matrix. Later eight large-scale specimens with different experimental variables, specimen geometry, and specimen dimensions were experimentally tested to further investigate the connection. Some of the principal variables tested in the small-scale and large-scale specimens were corrugation spacing and depth, surface preparation, interface height, edge distance, and reinforcement layout. The performance of current code expressions for shear friction, behavior of the overall connection using corrugated pipes and surface preparation, the currently used cohesion and friction values, and the design and construction details were evaluated to better understand current recommendations and behavior of the connection.

This section summarizes the conclusions from the small-scale testing, large-scale testing, and the construction and design details of the investigated connection.

7.1. Small-scale Testing

1. All specimens with the 12-inch diameter plug failed due to a shear friction failure at the interface between the plug and cap. Even the monolithically cast specimen failed due to a shear friction failure at the interface. Most of the shear friction failures were preceded by radial cracking extending out of the plug toward the exterior surfaces of the cap.
2. Normalizing by interface area and the square root of concrete strength was found to be a reasonable approach for normalizing the results (i.e., similar results were observed between specimens where only interface area and concrete strength varied).
3. Specimens with an exposed aggregate finish with 1/4-inch surface roughness had the highest normalized strength among all specimens tested (higher than corrugated

interface with 1/16-inch surface roughness). This is based on testing of 12-inch diameter plugs and should be verified with larger diameter plugs.

4. Specimens with a smooth interface and 1/16-inch surface roughness are sensitive to the casting procedure (e.g., time between casts, surface preparation, specific concrete properties). Normalized strengths varied from *k* of 0.122 (for a specimen cast at FDOT SRC) to 0.393 (for a specimen cast at Coreslab Structures (Miami), Inc.). Specimens with a corrugated interface had less variability in normalized strength between those cast at FDOT SRC and Coreslab Structures (Miami), Inc.
5. Specimens with a rougher interface (e.g., exposed aggregate, corrugated) experience more expansion than specimens with smooth interface, demonstrated by more cracking and rebar engagement.
6. The corrugated metal pipe provides only minor cohesion between the plug concrete and metal pipe and failed at lower loads than specimens with the corrugated interface with 1/16-inch surface roughness concrete finish. The plug rotated during testing when a continuous pipe was provided. Cutting the pipe at mid-height helped to restrict the rotation but led to lower capacities.
7. The corrugation size and spacing affects the strength of the interface. Providing single or double ribs at the base of the pocket increased the normalized strength of specimens compared to those with a smooth interface (comparing only specimens cast at FDOT SRC). Half spacing of the corrugations still had a lower normalized strength than the full corrugations.
8. Edge had a noticeable effect on the normalized strength only when the edge distance was decreased in two directions. Large failure cracks typically extended diagonally out of the plug toward the corner of the cap. Decreasing the edge distance in one direction did not have as significant an effect on this diagonal distance as decreasing the edge distance in two directions.
9. The confinement reinforcement saw higher strains in specimens with smaller edge distances in two directions. This shows that as there is less concrete area to resist the splitting cracks, the confinement reinforcement becomes more important.
10. Decreasing the longitudinal reinforcement in the cap decreased the normalized strength of the specimens. Changing the confinement reinforcement did not have a

significant effect on the strength of the specimens with $1d_{plug}$ edge distance. However, it is assumed that the confinement reinforcement would influence the strength for smaller edge distances.

11. The currently procedures available to estimate the strength of this interface (AASHTO LRFD Bridge Design Specification and AASHTO LRFD Guide Specification for ABC) were found to conservative estimate the ultimate capacity of the interface for the specimens tested. Finite element modeling or the proposed revised theory can be used to estimate the strength of the specimens more accurately.

7.2. Large-scale Testing

1. All large-scale specimens (other than LP-2, LP-3, and LP-4) failed due to a shear friction failure at the interface between the plug and cap. The socket connection specimens failed due to a combined shear friction failure at the interface between the pile and plug and plug and cap. Most of the shear friction failures were preceded by radial cracking extending out of the plug toward the exterior surfaces of the cap.
2. The current procedures available to estimate the strength of this interface (AASHTO LRFD Bridge Design Specification and AASHTO LRFD Guide Specification for ABC) were found to conservative estimate the ultimate capacity of the interface for the specimens tested. Finite element modeling or the proposed revised theory can be used to estimate the strength of the specimens more accurately. This will be discussed in more detail in Task 4.
3. Specimens with a rougher interface (e.g., exposed aggregate, corrugated) had higher capacity and experience more expansion than specimens with smooth interface, demonstrated by rebar engagement.
4. The presence of the metal duct did not impact the strength of the specimens, led to softer response (likely a result of less cohesion between the plug concrete and metal pipe), and did not noticeably help to confine the plug concrete. Specimens where the corrugated metal pipe was left in place experienced a more sudden failure (when cohesion was overcome at higher load).

5. Socket connections specimens had lower normalized shear friction capacity than larger plug specimens simulating pocket connections.

7.3. Design and Construction Recommendations

Based on the small and large scale specimens and their experimental evaluation:

1. It is recommended to use the AASHTO LRFD Guide Specification for ABC equations for estimation of the shear friction capacity of the interface in pocket and socket connections. These equations may be used for interfaces where the corrugated metal pipe is removed in pocket and socket connections.
2. The AASHTO LRFD BDS shear friction procedure can be used with a normal force to account for plug expansion and the proposed average cohesion factors and coefficients of friction for more accurate and precise estimates when needed.

Design details for pocket and socket connections were also evaluated based on the results of the shear friction testing. These recommendations were not evaluated based on flexural performance of pocket and socket connections.

Related to the interface condition:

1. Removing of the corrugated steel pipe and intentionally roughening through sandblasting or chiseling led to strength equal or greater than those when the duct was left in place, which is the current recommendation for the AASHTO LRFD Guide Specification for ABC. If the corrugated steel pipe is removed, then the minimum of the cap and plug concrete should be used to find the shear friction capacity.
2. Using an exposed aggregate finish (1/4-inch roughness) without corrugations led to equal or greater strength than specimens with corrugations and 1/16-inch roughness.
3. Minimal cohesion was observed when the corrugated metal pipe was left in place.

Related to cap sizing and reinforcement for pocket connections:

1. It is suggested to use a minimum edge distance of $0.5d_{pile}$ between the edge of the pile and edge of the cap. This will provide sufficient distance between the edge of the plug and edge of the cap.
2. The currently required center-to-center pile spacing of $3d_{pile}$ does not negatively affect the shear friction capacity of the cap-to-plug interface.
3. No confinement reinforcement is required around the pocket for shear friction purposes if the minimum edge distance of $0.5d_{pile}$ is provided between the edge of the pile and edge of the cap. Using a reinforcement detail like that proposed in the FDOT Structures Detailing Manual is sufficient for providing confinement around the pocket for shear friction capacity.

Related to socket connections:

1. The size of the socket should be sufficient to account for tolerances, including pile lateral installation tolerances.
2. Two layers of reinforcement should be placed beyond the tip of the embedded pile with legs extending beside the embedded pile, as used in this project. This reinforcement helps to engage more of the socket concrete in the shear friction resistance and prevents a punching shear failure from occurring in the socket.
3. The shear friction capacity of the socket connection can be found using AASHTO LRFD Guide Specification for ABC recommendations. The interface area to be considered should be the interface between the socket and cap with a height equal to the vertical distance between the end of the pile and end of the socket.

7.4. Recommended Future Research

The following future research needs were identified during this research project:

- Connection performance under flexure: The focus of this project was on the shear friction capacity of the pocket and socket connection between precast piles and precast pile caps. These connections were only tested under pure compression in this research project. Additional research is needed to evaluate the performance of the connection under flexural loads and a combination of flexure and axial load.

This work would expand on the work in this project and that done by other researchers [55].

- Additional interface conditions: Changes were made to the FDOT Structures Design Guidelines [54] after the experimental portion of the project was completed. The revised SDG requires a 1/4-inch roughness surface for interface surfaces. The 1/4-inch roughness was tested in this research for smooth interfaces, but not for corrugated interfaces. The 1/4-inch roughness may not be needed for interfaces with corrugations, but further research is needed.
- Additional depths and details for socket connections: Only two socket connection specimens were tested in this research. The socket connection interface only partially engaged. Additional research is needed to investigate the effect of different embedment lengths and different depth sockets on the interface strength.

LIST OF REFERENCES

Ali, M., & White, R. (1999). Enhanced Contact Model for Shear Friction of Normal and High-Strength Concrete. *ACI Structural Journal*, *96*(3), 348.

American Association of State Highway and Transportation Officials. (2016). *LRFD Bridge Design Specifications*.

American Association of State Highway and Transportation Officials (AASHTO). (2017a). *AASHTO LRFD Bridge Design Specification, Customary U.S. Units, 8th Edition*.

American Association of State Highway and Transportation Officials (AASHTO). (2017b). *AASHTO LRFD Bridge Design Specification, Customary U.S. Units, 8th Edition*.

American Association of State Highway and Transportation Officials (AASHTO). (2018). *LRFD Guide Specifications for Accelerated Bridge Construction (1st Edition)*.

American Concrete Institute (ACI) Committee 318. (2019). *Building Code Requirements for Structural Concrete (ACI 318-19) and Commentary*.

Anderson, A. (1960). Composite Designs in Precast and ast-in-Place Concrete. *Progressive Architecture*, *41*(9), 174.

ASTM International. (2013). *Standard Test Method for Bond Strength of Epoxy-Resin Systems Used with Concrete by Slant Shear*.

ASTM International. (2015). *Standard Test Method for Measuring Pavement Macrotexture Depth Using a Volumetric Technique*.

Bass, R., Carrasquillo, R., & Jirsa, J. (1989). Shear Transfer Across New and Existing Concrete Interfaces. *ACI Journal*, *86*(4), 383.

Birkeland, P., & Birkeland, H. (1966). Connections in Precast Concrete Construction. *Journal of the American Concrete Institute*, *63*(3), 345.

Canadian Standards Association. (2010). *Design of concrete structures*.

Cervenka, V., Cervenka, J., & Cervenka, J. (2016). *ATENA Program Documentation Part 1—Theory* (p. 330). Cervenka Consulting s.r.o.

Cervenka, V., Cervenka, J., Janda, Z., & Pryl, D. (2017). *ATENA Program Documentation—User's Manual for ATENA-GiD Interface* (p. 127).

Culmo, M. (n.d.). *Proposed Guidelines for Prefabricated Bridge Elements and Systems Tolerances (NCHRP Project 12-98)* (p. 80).

Culmo, M., Marsh, L., Stanton, J., & Mertz, D. (2018). *Recommended AASHTO Guide Specifications for ABC Design and Construction* (No. 242; p. 219).

Department of Transportation Federal Highway Administration. (2004). *Parker River-Precast Abutment Reinforcement -Drawings*. http://utcdb.fiu.edu/bridgeitem?id=211

Federation Internationale de la Precontrainte. (1999). *FIP Practical design of structural concrete*.

Figueira, D., Sousa, C., Calcada, R., & NEves, A. (2016). Push-Off Tests in the Study of Cyclic Behavior of Interfaces Between Concrete Cast at Different Times. *Journal of Structural Engineering*, *142*(1).

Florida Department of Transportation. (2015). *Prefabricated Bridge Elements and Systems (PBES) Conceptual Drawings*.

Florida Department of Transportation. (2017). *FDOT Structures Detailing Manual* (No. 2).

Florida Department of Transportation (FDOT). (2020). *Structures Detailing Manual (FDOT Structures Manual—Volume 2)* (p. 332).

Florida Department of Transportation (FDOT). (2021). *Stuctures Design Guidelines—FDOT Structures Manual—Volume 1* (p. 402).

Frenay, J. (1985). *Shear Transfer Across a Single Crack In Reinforced Concrete Under Sustained Loading—Part I. Experiments*.

Garber, D. (2016). *Compilation of Accelerated Bridge Construction (ABC) Bridges*. Florida International University (FIU).

Hanson, N. (1960). Precast-Prestressed Concrete Bridges 2. Horizontal Shear Connections. *PCA*, *2*(2), 38.

Harries, K. A., & Kharel, G. (2003). Experimental Investigation of the Behavior of Variably Confined Concrete. *Cement and Concrete Research*, *33*, 873–880.

Hawash, A. (2018, April 19). *Difference Between Pocket and Socket Connections* [Personal communication].

Hofbeck, J., Ibrahim, I., & Mattock, A. H. (1969a). *Shear transfer in reinforced concrete*. *66*, 119–128.

Hofbeck, J., Ibrahim, O., & Mattock, A. (1969b). Shear Transfer in Reinforced Concrete. *ACI*, *66*(2), 119.

Hovell, C., Avendano, A., Moore, A., Dunkman, D., Bayrak, O., & Jirsa, J. (2013). *Structural Performance of Texas U-Beams at Prestress Transfer and Under Shear-Critical Loads* (p. 355). The University of Texas at Austin.

International Federation for Structural Concrete (fib). (2010). *Fib Model Code 2010 Final draft, Volume 1*.

Julio, E., Branco, F., & Silva, V. (2004). Concrete to Concrete Bond Strength. Infleunce of the Roughness of the Substrate Surface. *Construction and Building Materials*, *18*(9), 675.

Julio, E., & Santos, P. (2008). Development of a Laser Roughness Analyser to Predict in Situ the Bond Strength of Concrete To Concrete Interfaces. *Magazine of Concrete Research*, *60*(5), 329.

Kahn, L. F., & Mitchell, A. D. (2002). Shear friction tests with high-strength concrete. *Structural Journal*, *99*(1), 98–103.

Kahn, L., & Mitchell, A. (2002). Shear Friction Tests with High-Strength Concrete. *ACI Structural Journal*, *99*(1), 98.

Kono, S., Tanaka, H., & Watanabe, F. (2003). Interface Shear Transfer for High Strength Concrete and High Strength Shear Friction Reinforcement. *High Performance Materials In Bridges*, 319.

Long, A., & Murray, A. (1984). The "Pull-Off" Partially Destructive Test for Concrete. *ACI*, 327.

Loov, R. (1978). *Design of Precast Connections. Paper Presented at a Seminar Organized by Compa International*.

Loov, R., & Patnaik, A. (1994). Horizontal Shear Strength of Composite Concrete Beams With a Rough Interface. *PCI JOURNAL*, 48.

Marsh, L., & Stanton, J. (2011). *Application of Accelerated Bridge Construction Connections in Moderate-to-High Seismic Regions* (No. 698).

Mast, R. (1962). *Shear Tests of Barrel Shell Joints (Unpublished Work)*.

Mattock, A. (1994). Reader Comments- Horizontal Shear Strength of Composite Concrete Beams With a Rough Interface. *PCI Journal*, *39*(1), 48.

Mattock, A., & Hawkins, N. (1972). Shear Transfer in Reinforced Concrete—Recent Research. *PCI Journal*, *17*(2), 55.

Mattock, A., & Kaar, P. (1961). Precast-Prestressed Concrete Bridges 4. Shear Test of Continuous Girders. *PCA*, *3*(1), 19.

Mattock, A., Li, W., & Wang, T. (1976). Shear transfer in lightweight reinforced concrete. *PCI Journal*, *21*(1), 20.

Mohamad, M., Ibrahim, I., Abdullah, R., Rahman, A., Kueh, A., & Usman, J. (2015). Friction and Cohesion Coefficients of Composite Concrete to Concrete Bond. *Cement & Concrete Composites*, *56*, 1.

Momayez, A., Ehsani, M., Ramezanianpour, A., & Rajaie, H. (2005). Comparison of Methods for Evaluating Bond Strength Between Concrete Substrate and Repair Materials. *Cement and Concrete Research*, *35*, 748.

Myers, J., Sells, E., & Volz, J. (2013). *Aggregate Interlock Push-Off Test Results of Self-Consolodating Concrete (Scc) For Use in Infrastructure Elements*. New Developments in Structural Engineering and Construction.

North Carolina Department of Transportation. (1999). *Beaufort and Morehead Railroad Trestle Bridge-Substructure Piers -Drawings*. http://utcdb.fiu.edu/Carteret%20Number110%20Contract%20Plans.pdf

Prochazkova, Z., Cervenka, J., Janda, Z., Pryl, D., & Mikolaskova, J. (2016). *ATENA Program Documentation—ATENA Science—GiD Tutorial* (p. 147).

Pruijssers, A., & Lung, G. (1985). *Shear Transfer Across a Crack in Concrete Subjected to Repeated Loading*.

Pryl, D., & Cervenka, J. (2017). *ATENA Program Documentation Part 11—Troubleshooting Manual* (p. 63).

Rahal, K. (2010). Shear-Transfer Strength of Reinforced Concrete. *ACI Structural Journal*, *107*(4), 419.

Randl, N. (1997). *Investigations on Transfer of Forces between Old and New Concrete at Different Joint Roughness*. University of Innsbruck.

Randl, N. (2013). Design Recommendations for Interface Shear Transfer in fib Model Code 2010. *Structural Concrete*, *14*(3), 230.

Restrepo, J., Tobolski, M., & Matsumoto, E. (2011). *Development of a Precast Bent Cap System for Seismic Regions* (NCHRP Report 681; p. 115). National Cooperative Highway Research Program (NCHRP).

Rudie, C., Poulson, J., Ryzhikov, V., Molas, T., & PB, A. (2008). *Innovative Solutions For Rapid Construction*. http://utcdb.fiu.edu/Summer%202008%20ASPIRE.pdf

Santos, P., & Julio, E. (2010). *Recommended Improvements to Current Shear-Friction Provisions of Model Code*. 2.

Santos, P., & Julio, E. (2011). Factors Affecting Bond between New and Old Concrete. *ACI Structural Journal*, *108*(4), 449.

Santos, P., Julio, E., & Silva, V. (2007). Correlation Between Concrete to Concrete Bond Strength and the Roughness of the Substrate Surface. *Construction and Building Materials*, *21*(8), 1688.

Walraven, J., Frenay, J., & Pruijssers, A. (1987). Influence of Concrete Strength and Load History on Shear Friction Capacity of Concrete Members. *PCI Journal*, *32*(1), 66.

Walraven, J., & ReinHardt, H. (1981). Theory and Experiments on the Mechanical Behaviour of Cracks in Plain and Reinforced Concrete Subjected to Shear Loading. *Heron*, *26*.

Walraven, J., & Stroband, J. (1994). Shear Friction in High-Strength Concrete. *Special Publication*, *149*, 311.

Williams, C., Massey, J., Bayrak, O., & Jirsa, J. (n.d.). *Investigation of Interface Shear Transfer Using Push-Through Tests*.

Xu, J., Wu, C., Li, Z.-X., & Ng, C.-T. (2015). Numerical Analysis of Shear Transfer Across an Initially Uncrack Reinforced Concrete Member. *Engineering Structures*, *102*, 296.

APPENDIX A. SMALL-SCALE RESULTS

Series I Results

The results from the initial experimental testing of the first four specimens are summarized in this section. These specimens were constructed and tested to evaluate the proposed test procedure used to test the shear friction interface of these specimens. Some of the details for specimens in Series I are shown in Figure A - 1. A corrugated plastic pipe was used to construct the pockets in three of the specimens (S1-1, S1-2, and S1-3) and a sonovoid was used to create a smooth interface finish in one specimen (S1-4). The pipe or form was removed in all specimens and the interface surface was intentionally roughened to a 1/16-inch surface roughness. Three different sizes were investigated.

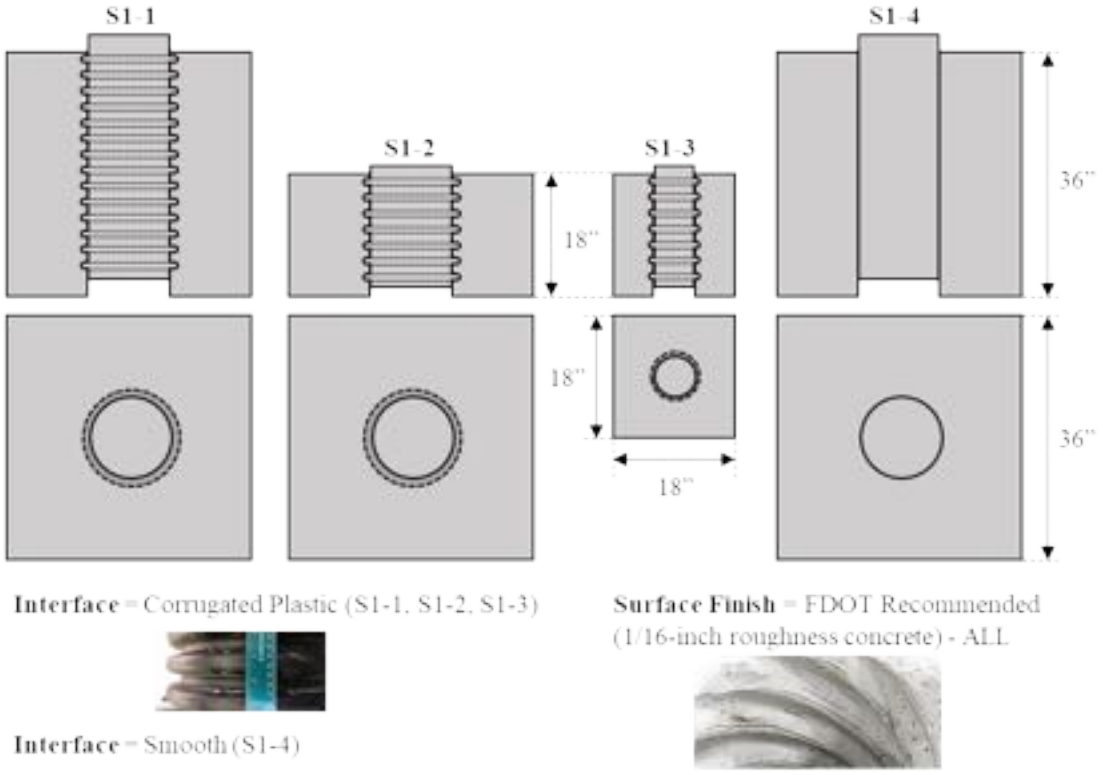

Figure A - 1: Select details on Series I specimens

The estimated and measured ultimate strengths of these specimens are summarized in Table A - 1. The concrete compressive strengths measured on the day of testing for the cap and plug are also shown in Table A - 1. The measured compressive strengths were significantly higher than the specified strengths.

Table A - 1: Measured concrete strength and estimated versus measured ultimate strength and displacement for preliminary test specimens

Specimen	Compressive Strength on Test Day (ksi)		Ultimate Strength (kips)				
	Cap	*Plug*	*AASHTO*	*ABC*	*ATENA*	*Proposed*	*Measured*
S1-1	7.57	8.45	271.43	412.3	388.03	1893.1	> 750 kips
S1-2	7.96	8.79	108.57	187.4	182.34	884.2	> 750 kips
S1-3	7.69	8.20	54.29	93.7	175.37	421.7	243.8*
S1-4	8.05	7.98	271.43	412.3	388.03	557.9	429.7

*failed due to crushing of concrete on top of plug

Specimen S1-1 Results

Specimen 1 had a corrugated interface between the plug and cap. The specimen was loaded to the capacity of the test setup (750 kips) but did not fail. Only minor displacement (0.06 inches at 750 kips) was observed. The strain in the longitudinal reinforcement on the bottom of the specimen had only minor strains, shown in Figure A - 2, suggesting there was no significant expansion of the plug or splitting stresses at the bottom of the specimen.

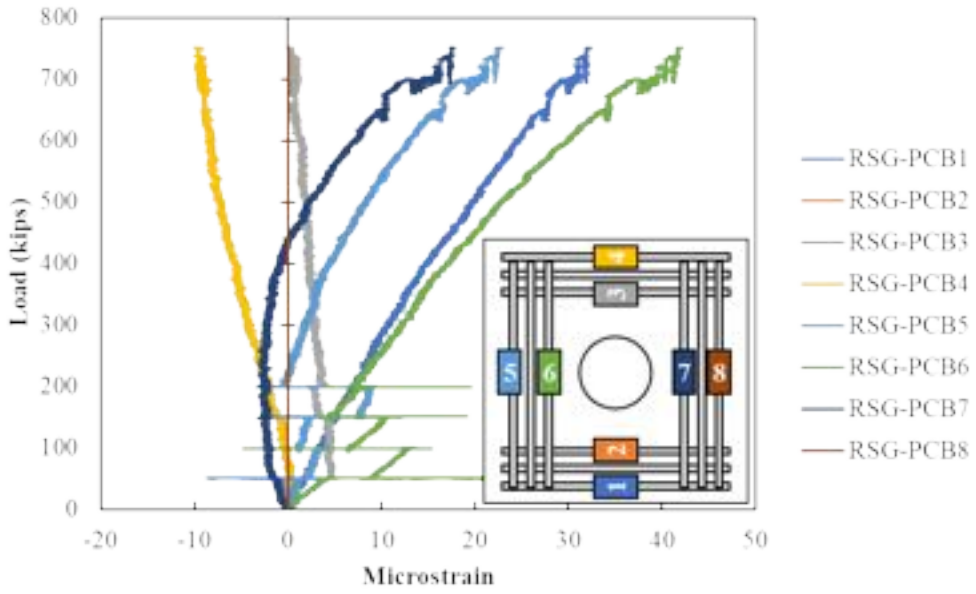

Figure A - 2: Rebar strain in longitudinal bars on bottom of Specimen S1-1

Only minor stresses were measured in the confinement reinforcement in the cap around the plug, shown in Figure A - 3 for the confinement reinforcement located at mid-height of the

plug. There were slightly larger stresses in the confinement reinforcement at the top and mid-height than at the bottom of the cap.

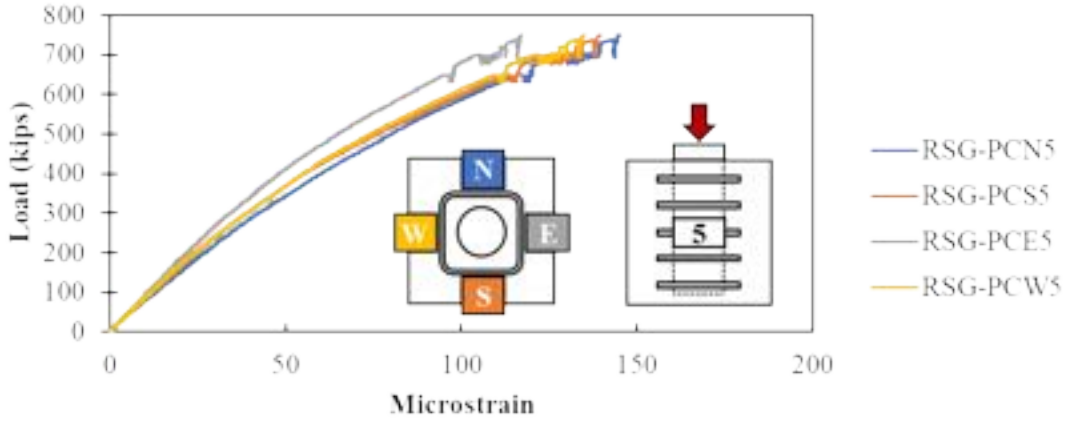

Figure A - 3: Rebar strain gauges on confining reinforcement at mid-height of the plug of Specimen S1-1

The measured strains in the vertical reinforcement in the cap and plug are shown in Figure A - 4. The vertical strains in the plug decrease toward the bottom of the plug, showing the transfer of stress from plug to cap. The vertical strains in the cap are similar at the three different heights, and the top two levels had similar vertical strains between the cap and plug. These results suggest the ribs in the corrugation are effective in transferring stresses between cap and plug.

Concrete strain gauge readings are shown in Figure A - 5. Strains were relatively similar along the height of the specimen. Strain gauge CSG-PCW2 appears to start to behave non-linearly suggesting that cracking may have been starting in this location. CSG-PCE2 and CSG-PCE3 both began to show decreasing tensile stress, suggesting a crack developing next to these gauges.

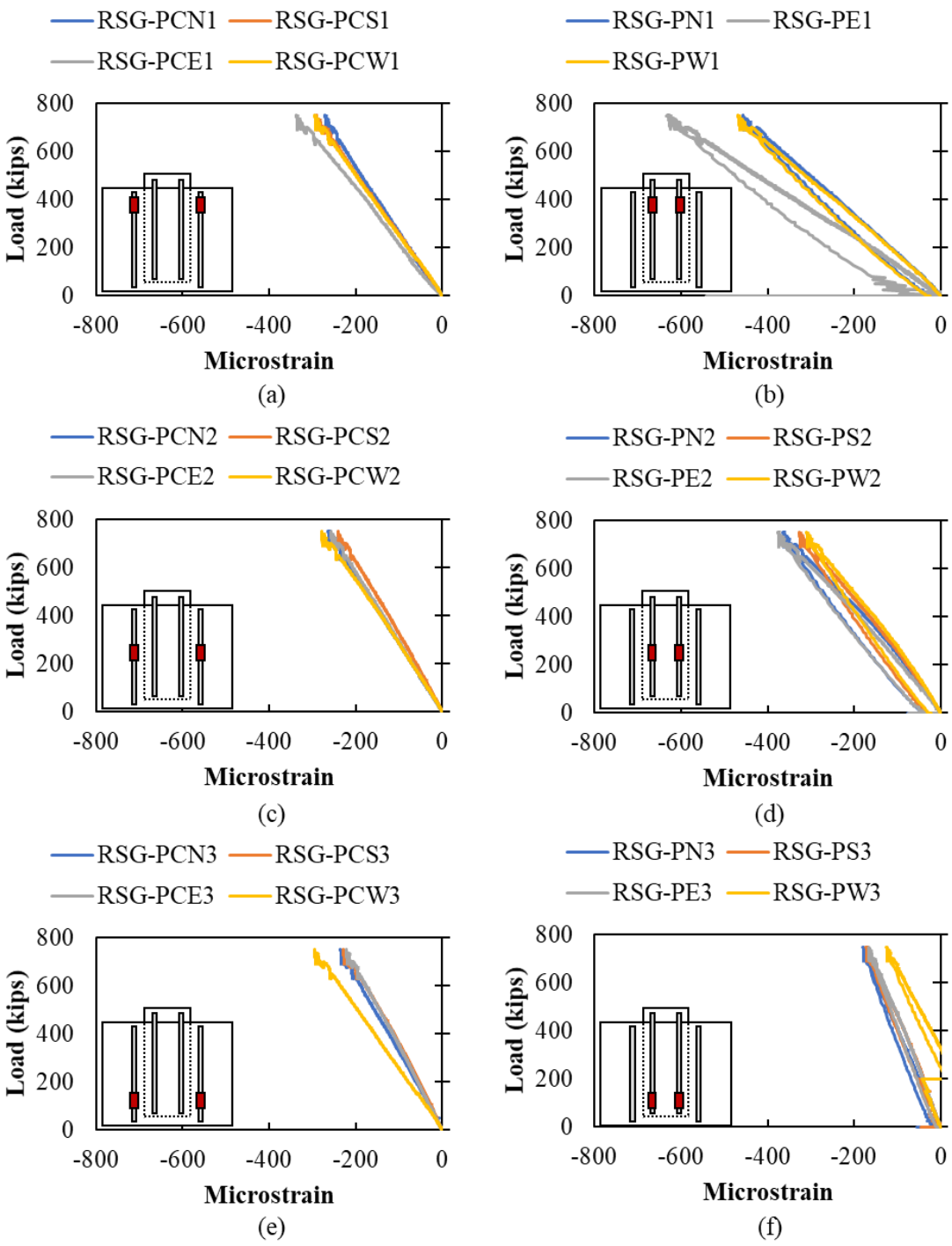

Figure A - 4: Rebar strain gauges in vertical reinforcement in plug and cap of Specimen S1-1

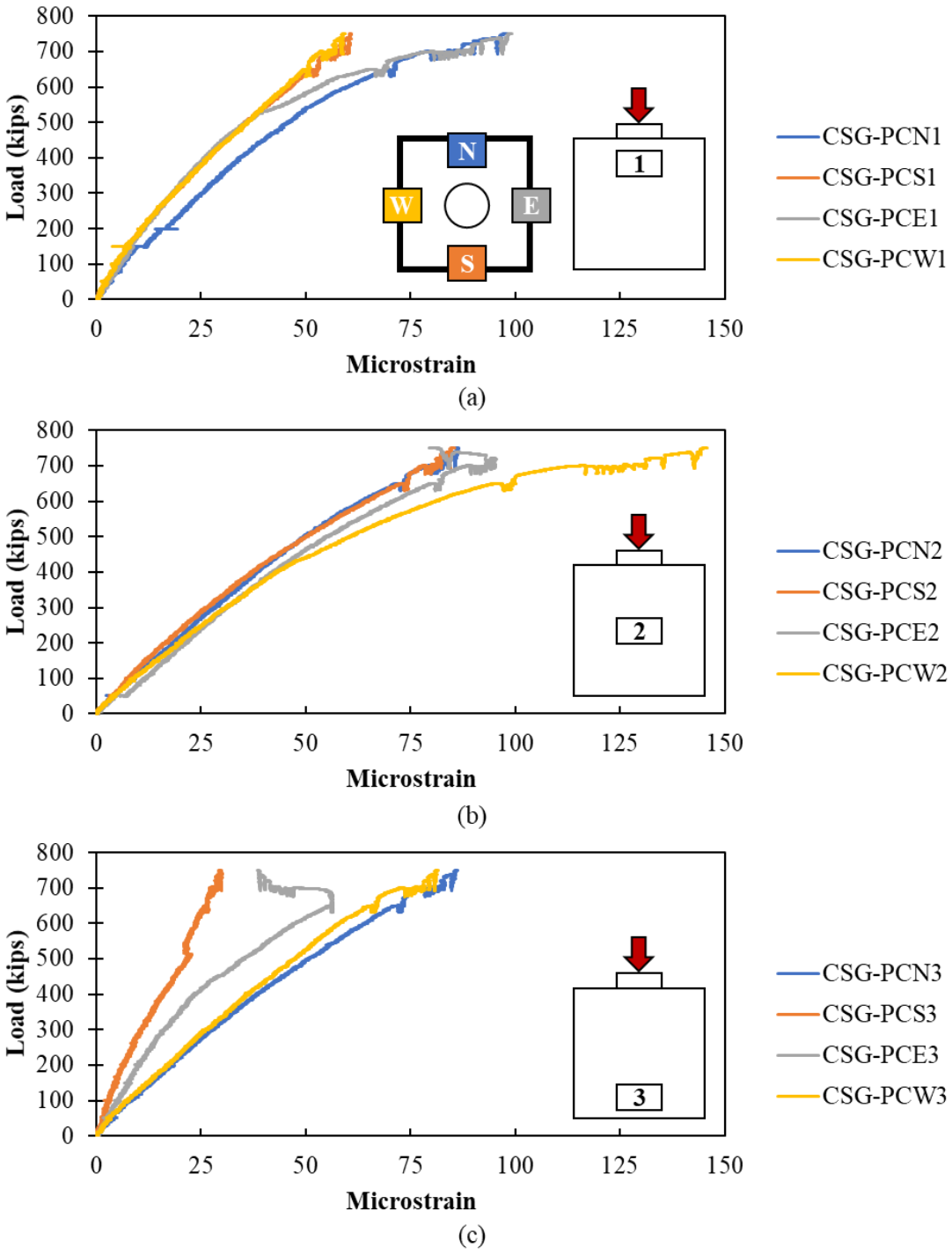

Figure A - 5: Concrete surface gauges on the sides of cap at (a) top, (b) mid-height and (c) bottom of Specimen S1-1

Specimen S1-2 Results

Specimen 2 had the same corrugation between the plug and cap as Specimen 1 but had half the overall height. This specimen was loaded to the capacity of the test setup (750 kips) but did not fail.

Cracking was detected between 350 and 400 kips through the instrumentation. The rebar strain gauges in the longitudinal steel on the bottom of the section on the north and south sides of the specimens began to be engaged at a load of around 390 kips, shown in Figure A - 6. The gauges on the east and west faces were not engaged, so it appears that a crack developed across the section in the north-south direction.

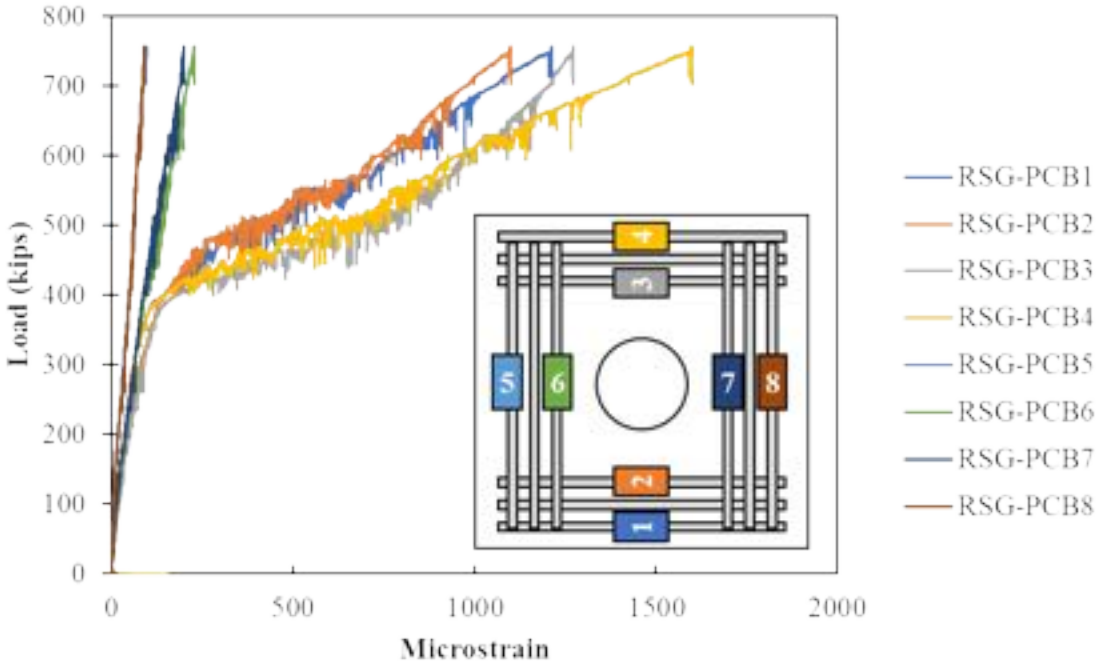

Figure A - 6: Rebar strain in longitudinal bars on bottom of Specimen S1-2

The longitudinal reinforcement reached between 1,100 and 1,600 microstrain. Using the slope of the high strain, it would have likely taken approximately an additional 118 kips to reach yield in the longitudinal reinforcement.

Estimated slope of RSG-PCB4:

$$slope_{RSG-PCB4} = \frac{1{,}547\ k - 1{,}326\ k}{739\ \mu\varepsilon - 684\ \mu\varepsilon} = 4.0\ {}^{k}/_{\mu\varepsilon}$$

$$\varepsilon_y = \frac{60\ ksi}{29{,}000\ ksi} = 2{,}070\ \mu\varepsilon$$

Additional force required to cause yield: $\Delta F_{y,RSG-PCB4} = (2{,}070\ \mu\varepsilon - 1600\ \mu\varepsilon)\left(4.0\ {}^{k}/_{\mu\varepsilon}\right) = 118\ kips$

The concrete surface gauges toward the bottom of the north and south faces of the specimens also indicated cracking at around 340 kips on the north face and 390 kips on the south face, shown in Figure A - 7. This would suggest that the crack first started on the north side of the specimen at the bottom and then extended across the full width of the specimen in the north-south direction.

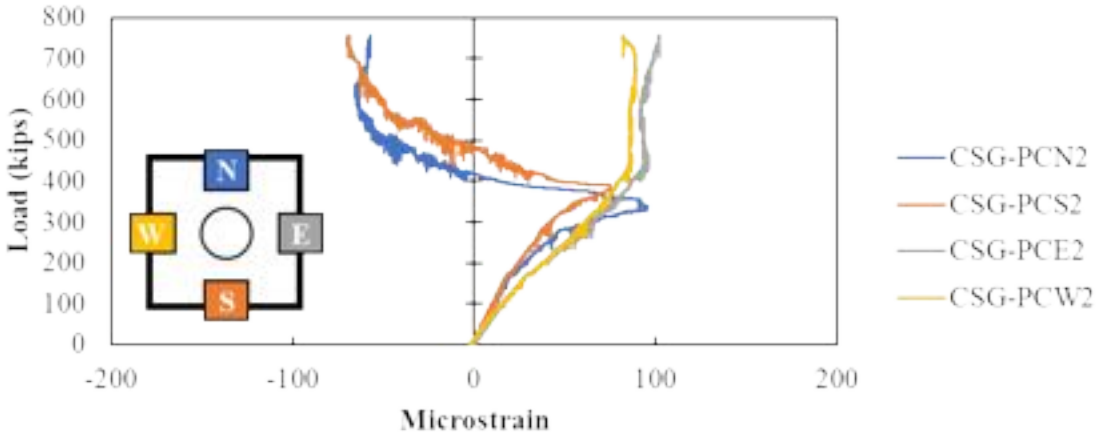

Figure A - 7: Concrete surface gauges on the sides of cap closest to bottom of Specimen S1-2

The confining reinforcement around the pocket engaged more at the bottom of the section compared to the top of the section, shown in Figure A - 8. This reinforcement seems to also be resisting the opening of the crack that appears to be running across the entire cap in the north-south direction. The confinement reinforcement toward the bottom of the specimen began to be more engaged at around 390 kips, see Figure A - 8(b), while the confinement reinforcement higher in the section did not engage until between 450 and 500 kips, see Figure A - 8(a). These measurements from the confinement reinforcement also show that the crack started at the bottom of the section and was progressing up the cap.

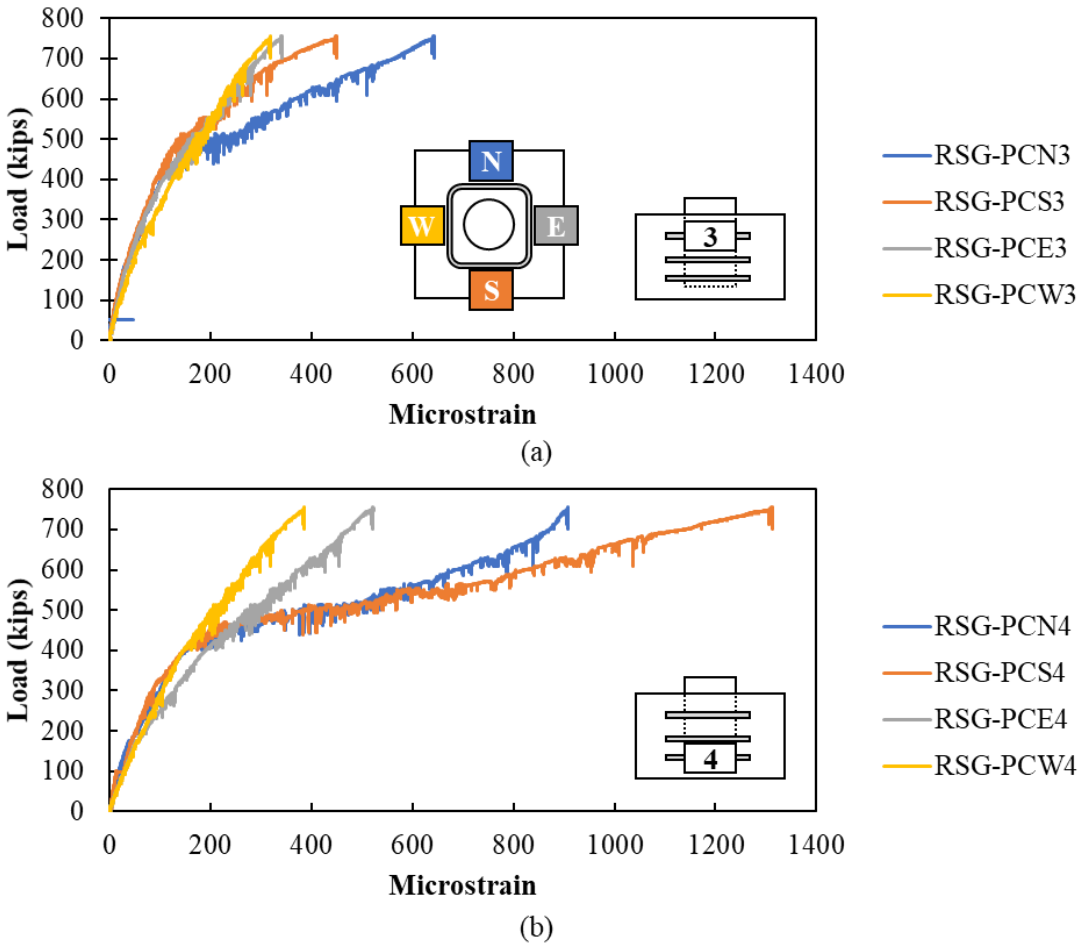

Figure A - 8: Rebar strain gauges on confining reinforcement at (a) top and (b) bottom of the plug of Specimen S1-2

The strains in the bottom confinement reinforcement reached around 900 microstrain on the north and around 1,300 microstrain on the south side of the cap. Using the slope of the high strain, it would have likely taken approximately an additional 220 kips to reach yield in the confinement reinforcement.

Estimated slope of RSG-PCS4:

$$slope_{RSG-PCS4} = \frac{1{,}258\ k - 1{,}107\ k}{737\ \mu\varepsilon - 694\ \mu\varepsilon} = 3.5\ {}^{k}/_{\mu\varepsilon}$$

Additional force required to cause yield:

$$\Delta F_{y,RSG-PCS4} = (2{,}070\ \mu\varepsilon - 1{,}300\ \mu\varepsilon)\left(3.5\ {}^{k}/_{\mu\varepsilon}\right) = 220\ kips$$

The yielding of the longitudinal reinforcement would have likely impacted the slope though as the confinement reinforcement would have picked up more of the load after yielding of the longitudinal bars.

The strains in the vertical reinforcement in the cap and plug are shown in Figure A - 9. Strains in the plug are higher than the cap at the top of the specimen and then higher in the cap than the plug in the bottom of the specimen. This shows how the stresses are transferring from the plug to the cap through the specimen.

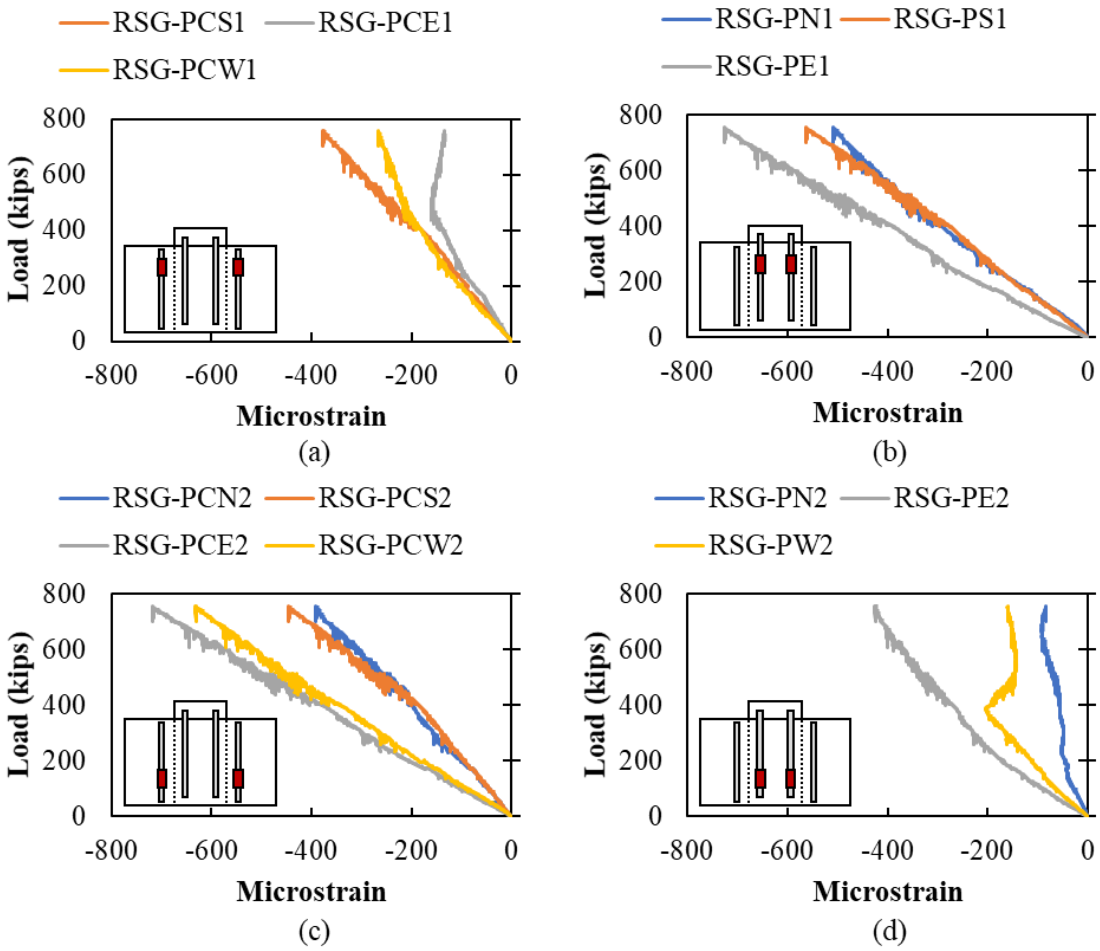

Figure A - 9: Rebar strain gauges in vertical reinforcement in plug and cap (a) top of cap, (b) top of plug, (c) bottom of cap, and (d) bottom of plug of Specimen S1-2

Specimen S1-3 Results

Specimen 3 was half the scale of Specimen 1 with a similar corrugated interface between the cap and plug. The observed failure of this specimen was crushing of the concrete in the top of the plug at a load of 243.8 kips. The stress in the plug at time of failure is approximately equal to the compressive strength of the concrete.

Stress in plug concrete at failure:

$$f_{c,fail} = \frac{243.8\ k}{\pi\left(\frac{6"}{2}\right)^2} = 8.6\ ksi$$

Only minor strains were measured in the longitudinal reinforcement on the bottom of the specimens, shown in Figure A - 10.

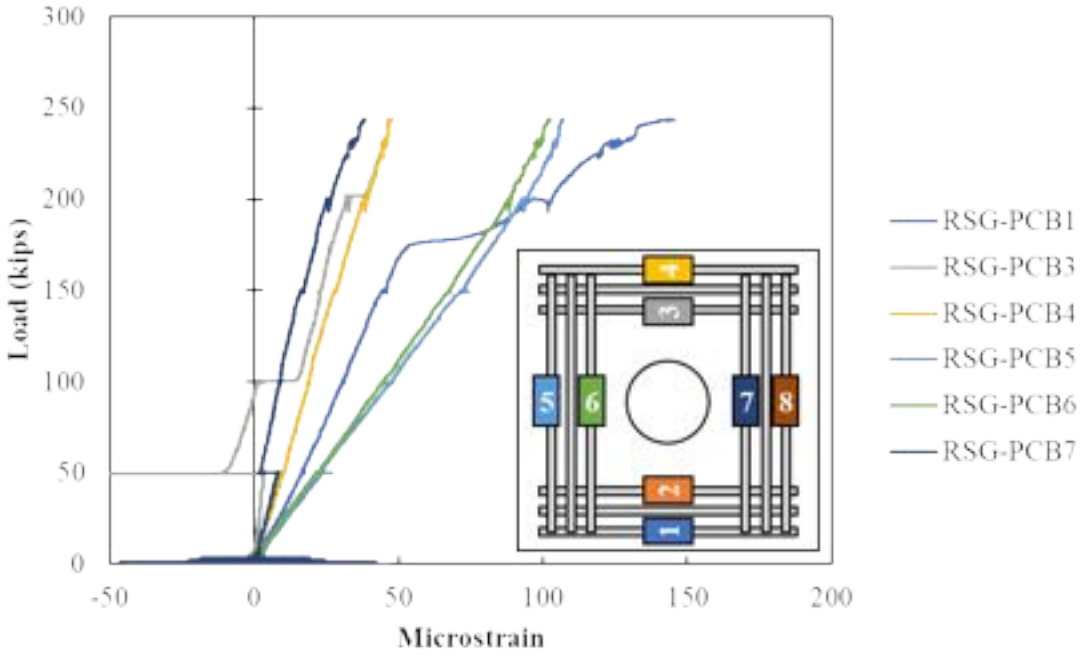

Figure A - 10: Rebar strain in longitudinal bars on bottom of Specimen S1-3

Measured strain in the vertical reinforcement in the cap and plug are shown in Figure A - 11. Similar strains were observed in the top and bottom of the cap and bottom of the plug. Larger strains were measured in the top of the plug. These results suggest a relatively short distance was required for the stress to be transferred from plug to cap.

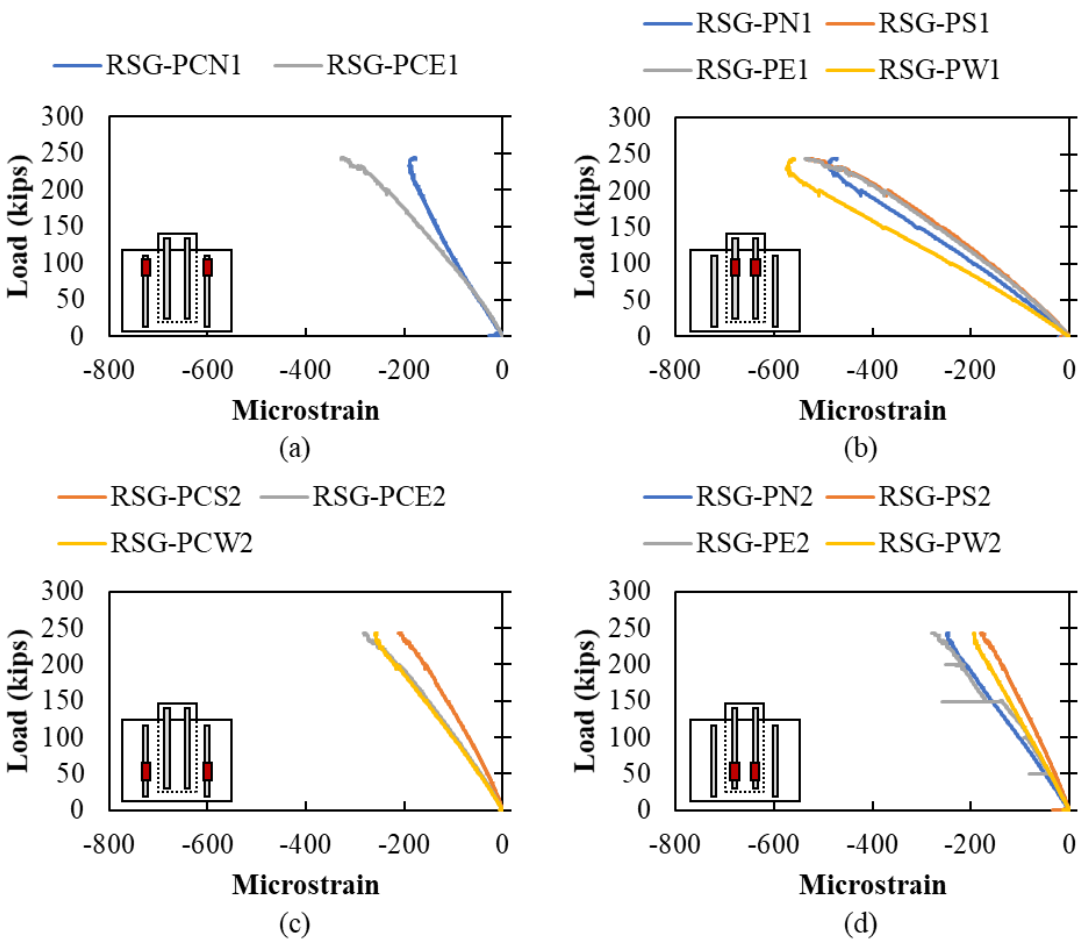

Figure A - 11: Rebar strain gauges in vertical reinforcement in plug and cap (a) top of cap, (b) top of plug, (c) bottom of cap, and (d) bottom of plug of Specimen S1-3

The measured strain in the confinement reinforcement in the cap around the plug are shown in Figure A - 12. Only minor strains were observed with slightly higher strains in the confinement reinforcement toward the top of the specimen.

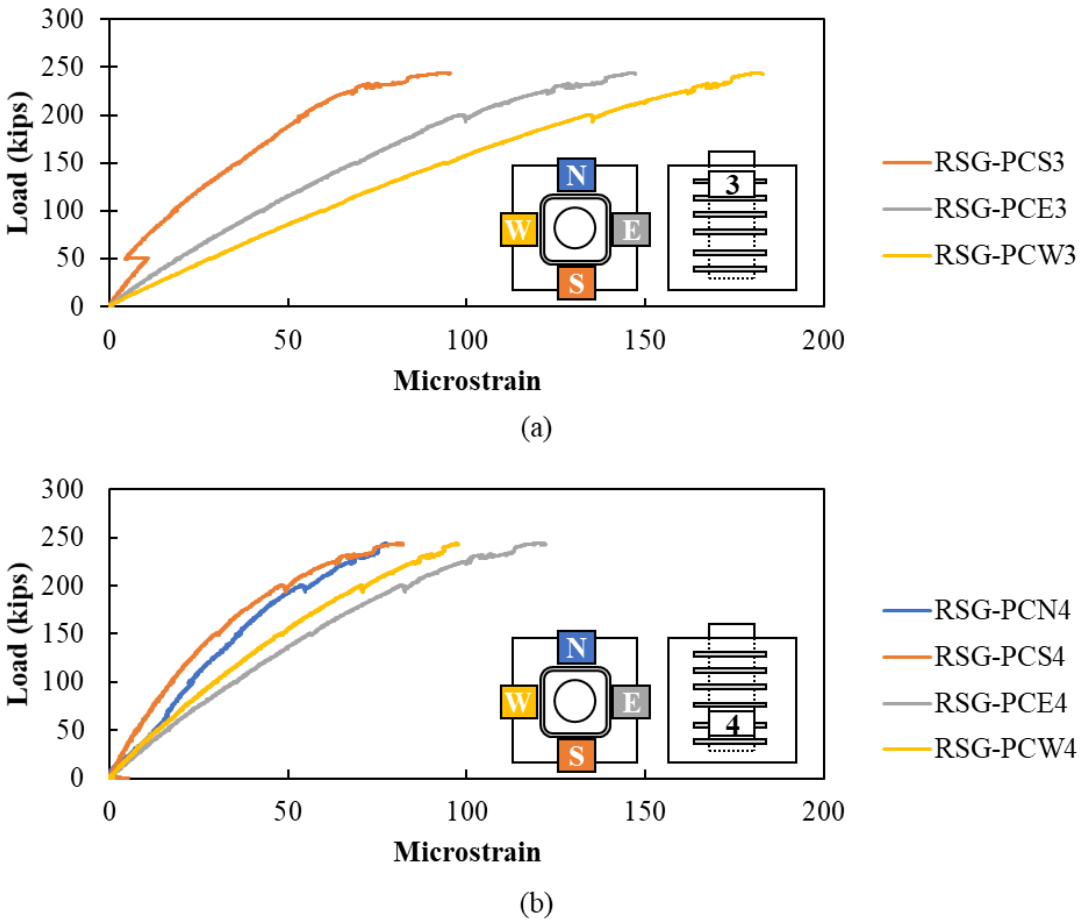

Figure A - 12: Rebar strain gauges on confining reinforcement at (a) top and (b) bottom of the plug of Specimen S1-3

The measured strain in the concrete strain gauges on the four outside faces of the cap are shown in Figure A - 13. Only minor strains were observed with minimal difference between the gauges toward the top and bottom of the specimen.

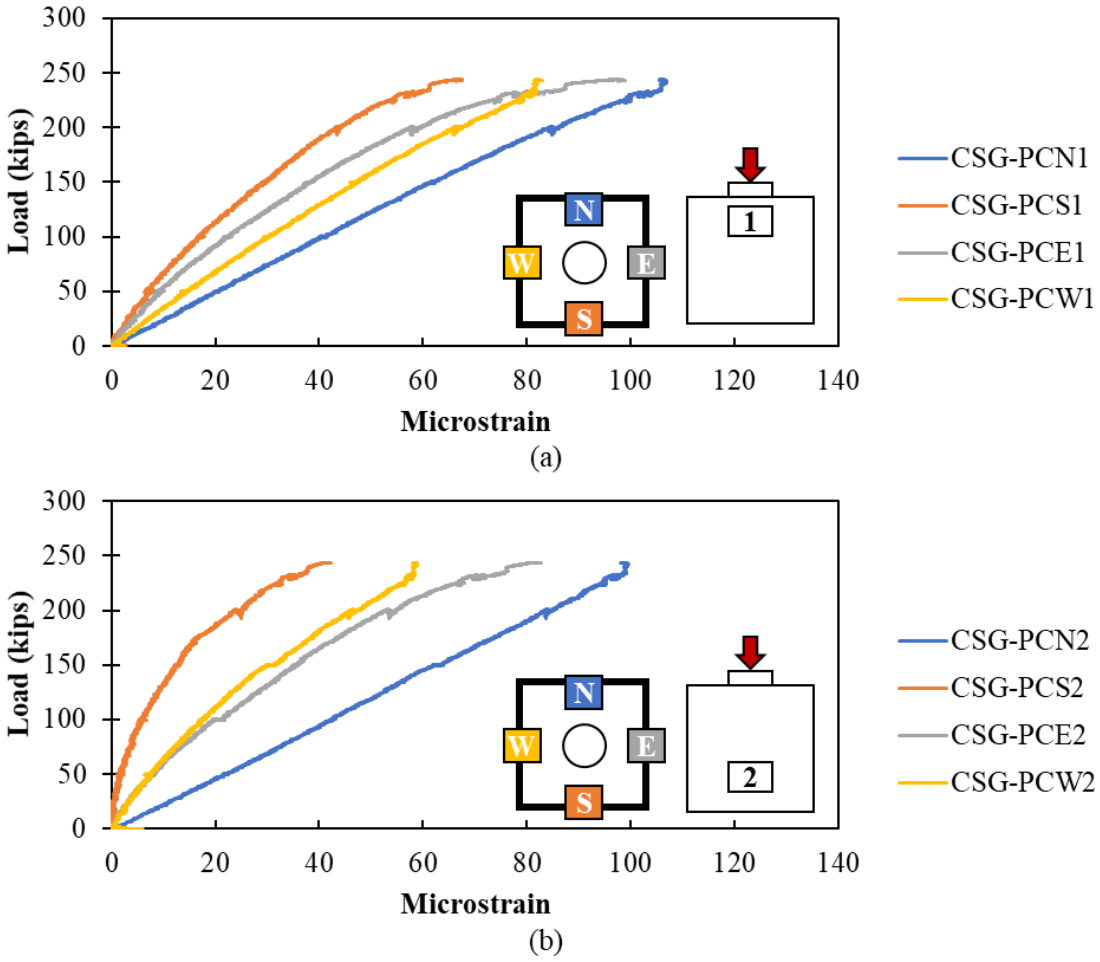

Figure A - 13: Concrete surface gauges on the sides of cap closest to (a) top and (b) bottom of Specimen S1-3

Specimen S1-4 Results

Specimen S1-4 had a smooth interface between the plug and cap and was the same size as Specimen S1-1. The observed failure for this specimen was a shear friction failure along the interface between the cap and plug. A fairly linear response was observed until sliding of the plug began at a load of 429.7 kips, as shown in the load versus deflection response in Figure A - 14. After sliding began, the plug still held a load of around 370 kips. Load was applied until the plug had slid 0.5 inch.

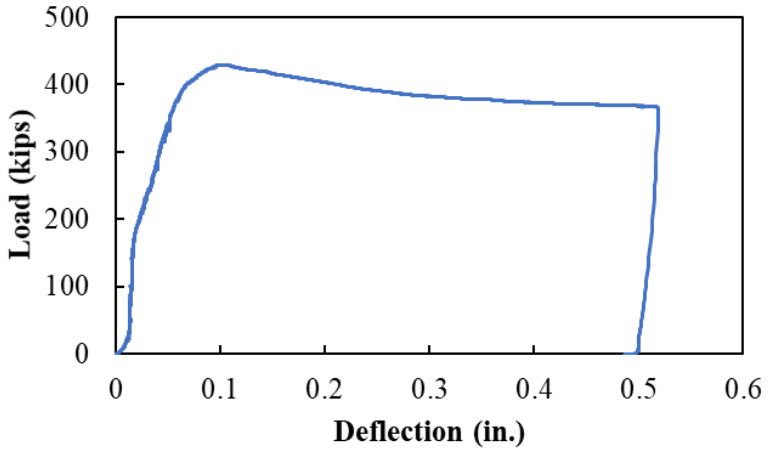

Figure A - 14: Load versus deflection curve for Specimen S1-4

A crack opened on the bottom of the specimen at a load of around 300 kips; signaled by a sharp increase in strain gauges RSG-PCB5, RSG-PCB6, and RSG-PCB7 as shown in Figure A - 15. Note that strain gauges RSG-PCB2 and RSG-PCB8 were not working during the testing.

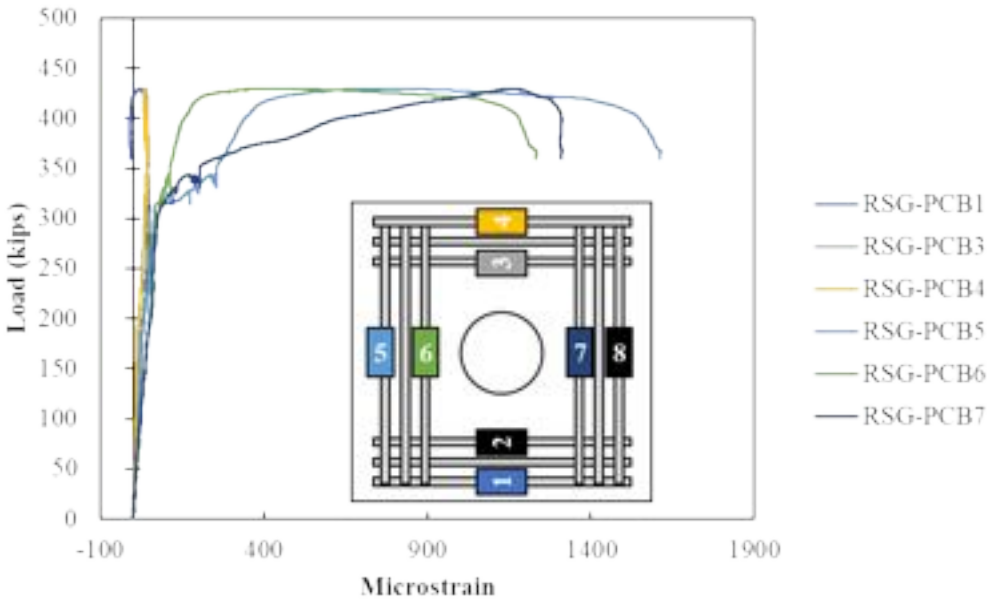

Figure A - 15: Rebar strain in longitudinal bars on bottom of Specimen S1-4

The cracking was also observed in the concrete surface gauges, signaled by a reversal from tension to compressive stresses in CSG-PCE3 and CSG-PCW3 in Figure A - 16.

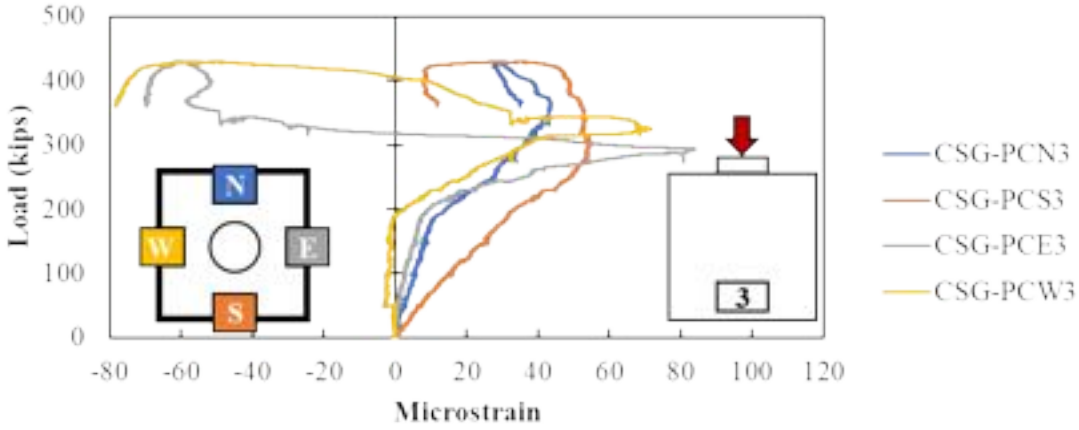

Figure A - 16: Concrete surface gauges on the sides of cap closest to bottom of Specimen S1-4

Cracking was also observed visually after the test was complete, as shown in Figure A - 17. Cracking was observed to extend onto the top of the cap toward the plug on the west side.

(a) (b) (c)

Figure A - 17: Cracking on the (a) east, (b) top, and (c) west faces of Specimen S1-4 after failure

This cracking in the specimen occurred before the plug began to slide but suggests that the plug caused expansion of the cap prior to it pushing through. The confining steel in the cap also appears to have engaged during the sliding of the plug, shown in Figure A - 18. The confining reinforcement was engaged along the same plane as the cracking, shown by RSB-PCE5 and RSB-PCW5 both showing large increases in strain.

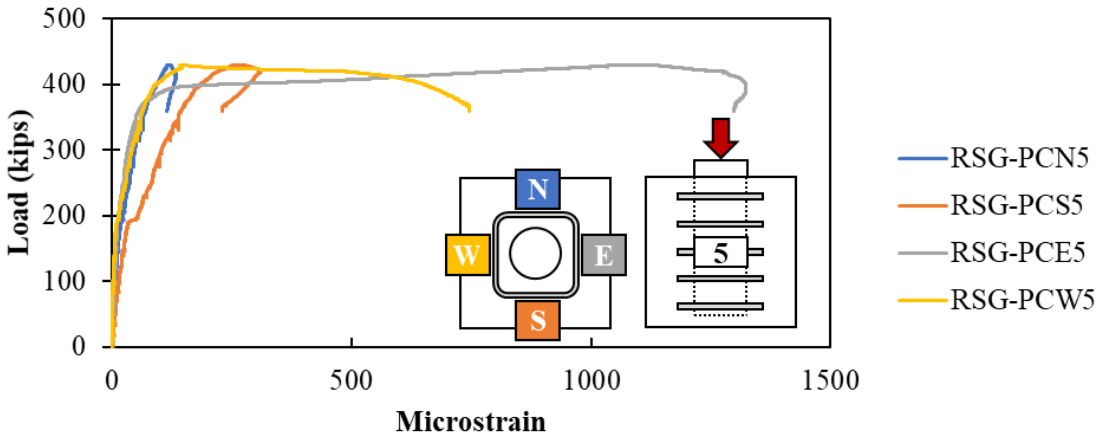

Figure A - 18: Rebar strain gauges on confining reinforcement at mid-depth of the plug of Specimen S1-4

Specimen S1-4 had a smooth interface between the plug and cap, so it was initially assumed that only the cohesion component of the shear friction capacity should be considered. It appears that there were some stresses perpendicular to the friction plane though, evident from the cracking stresses, so there would have also likely also been a friction component to the shear friction resistance.

The measured strains in the vertical reinforcement in the cap and plug are shown in Figure A - 19. The vertical strain remains about the same in the top, mid-height, and bottom of the cap, while it is highest at the top of the plug. The vertical strain at the bottom of the plug is about equal to the vertical strain at all levels of the cap. The results in Figure A - 19 can be compared to the results from the specimen with the same dimensions with a corrugated interface shown in Figure A - 4. The strains in the cap with corrugated interface are comparable to the mid-height vertical strain gauges, showing there is a decrease in the length required to transfer stresses from plug to cap.

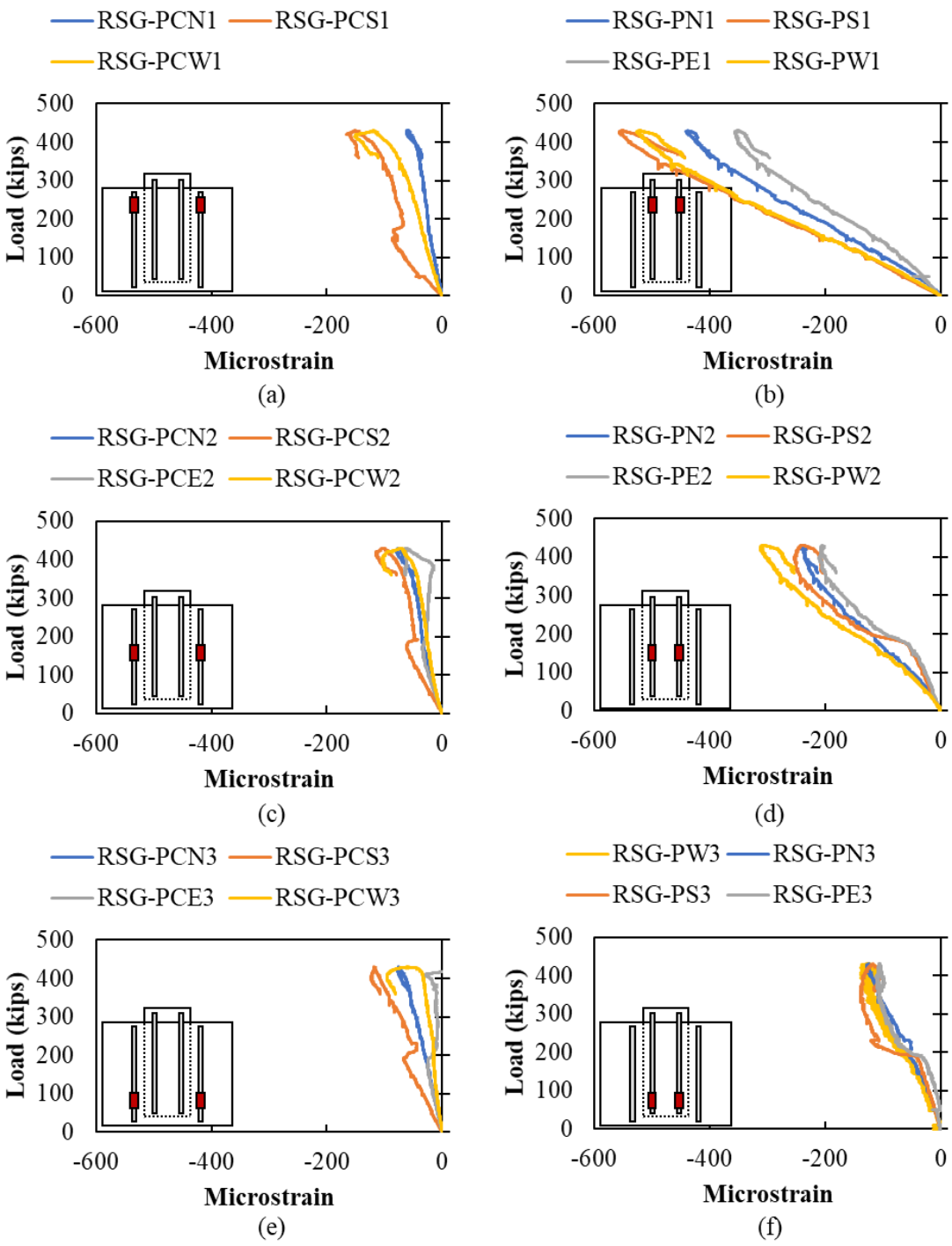

Figure A - 19: Rebar strain gauges in vertical reinforcement in plug and cap of Specimen S1-4

Series II Results

The goal of Series II was to investigate the effect of (1) interface surface condition and (2) corrugation spacing and depth. Two different specimen heights were tested (14 and 18

inches) with variations of interface surface conditions and corrugation spacings and depths. All specimens had a 12-inch plug with 12-inch edge distance (distance from edge of plug to edge of cap) on all faces.

The results and observations for specimens in Series II are summarized in this section. The experimental results, and the concrete strengths of the day of testing for both the cap and the plug are summarized on Table A - 2. The concrete strengths measured were higher than the specified.

Table A - 2: Measured concrete strength and estimated versus measured ultimate strength for second set of specimens

Specimen	**Compressive Strength on Test Day (ksi)**		**Ultimate Strength (kips)**				
	Cap	*Plug*	*AASHTO*	*ABC*	*ATENA*	*Proposed*	*Measured*
S2-1	6.26	6.95	135.7	187.4	153.0	403.2	339.0
S2-2	6.33	6.98	135.7	187.4	265.1	688.3	>750
S2-3	6.20	6.95	135.7	187.4	238.4	413.7	320.2
S2-4	6.33	6.98	99.5	137.4	253.8	504.8	615.4
S2-5	6.02	6.91	99.5	137.4	222.7	305.0	356.0
S2-6	6.41	6.91	99.5	137.4	337.2	315.5	418.6
S2-7	6.30	6.91	135.7	187.4	972.6	677.8	719.5
S2-8	6.85	7.29	135.7	187.4	972.6	522.2	553.5
S2-9	6.39	7.29	135.7	187.4	972.6	655.8	662.2
S2-10	6.72	7.11	99.5	137.4	808.8	508.7	575.4
S2-11	6.59	7.11	99.5	137.4	808.8	375.5	399.8
S2-12	6.59	7.11	99.5	137.4	808.8	470.5	521.6
S2-13	5.25	7.42	135.7	187.4	292.5	335.2	605.6
S2-14	5.52	7.40	99.5	137.4	229.2	310.8	441.3
S2-15	5.52	7.40	99.5	137.4	508.2	529.1	631.2
S2-16	5.54	7.76	135.7	187.4	630.1	581.3	>750
S2-17	5.52	7.40	135.7	187.4	630.1	508.3	533.3
S2-18	5.55	7.97	99.5	137.4	508.2	558.6	569.2
S2-19	5.55	7.97	99.5	137.4	508.2	520.4	482.6
S2-20	5.77	7.11	135.7	187.4	630.1	543.6	666.0

Specimen S2-1 Results

Specimen S2-1 was 18-inch deep, had a smooth surface between the cap and plug with sandblasted (1/16'' of roughness) surface preparation.

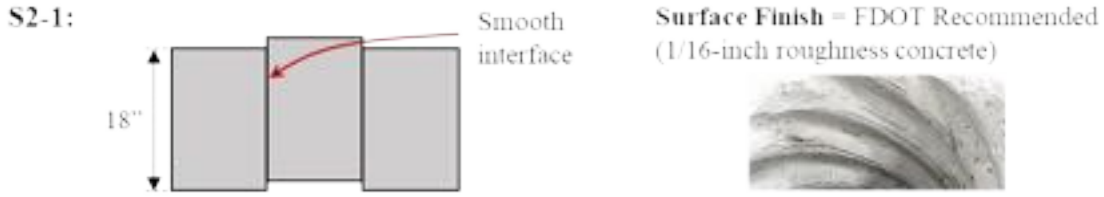

The load versus deflection plot for S2-1 is shown in Figure A - 20. The specimen held a load of 270 kips when the plug started to move, and then the specimen continued to take additional load until its maximum load of 337.4 kips. The specimen was loaded until 0.45 inches of plug movement. A slight difference was noticed between the displacement of the top and bottom of the plug.

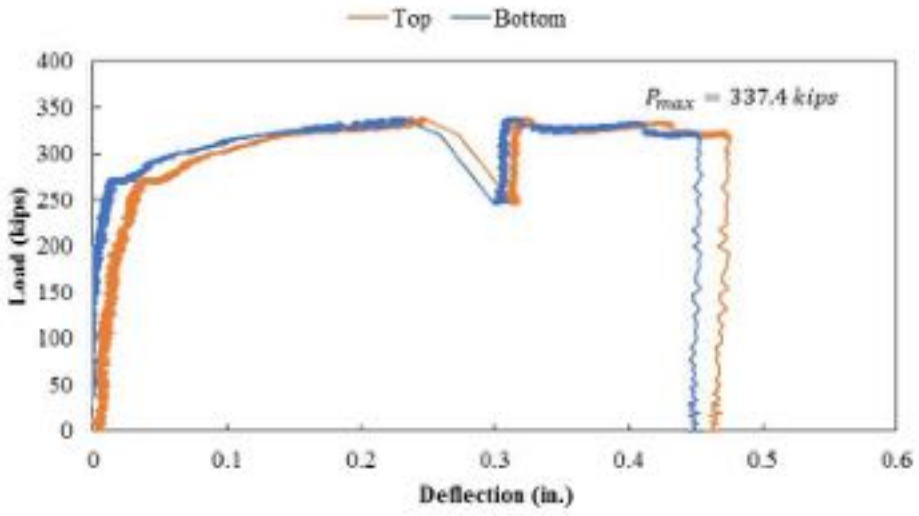

Figure A - 20: Load-Displacement curve for Specimen S2-1

The strain on the bottom in the longitudinal reinforcement were more engaged in the east side of the specimen than in the north side, shown in Figure A - 21, suggesting that there was expansion of the plug or splitting stresses at the bottom of the specimen. A crack opened on the bottom of the specimen at a load of around 260 kips as can be observed in the gauges RSG-PB3 and RSG-PCB4 (Figure A - 21).

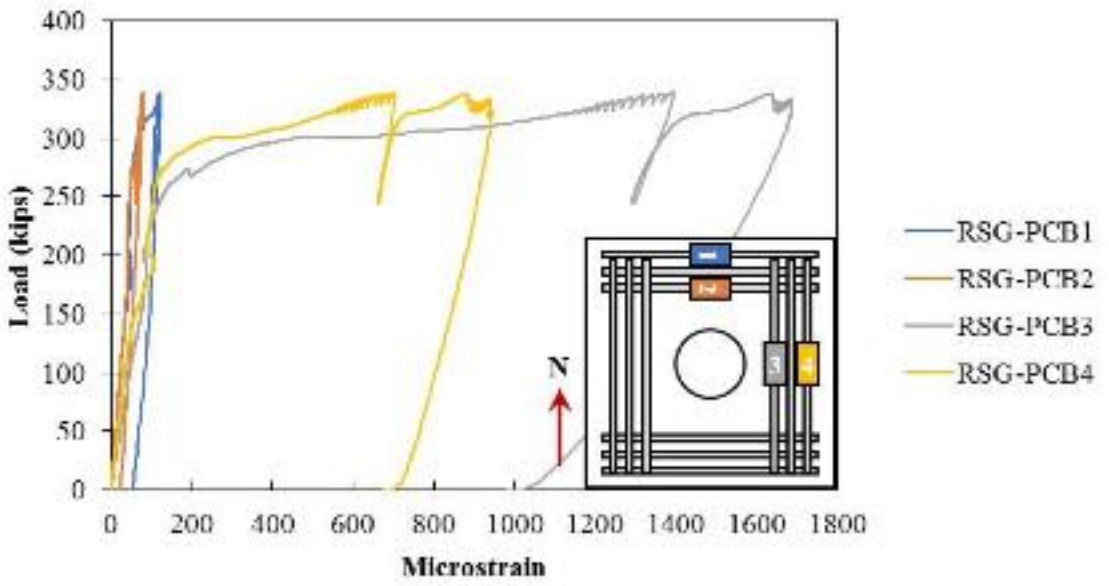

Figure A - 21: Rebar strain in the longitudinal bars on bottom of the Specimen S2-1

Cracking was also observed in the concrete strain gauges and visually after the test was completed as shown in Figure A - 22 and Figure A - 23. Cracks were observed to extend from the bottom of the cap onto the top toward the plug in the east and west side.

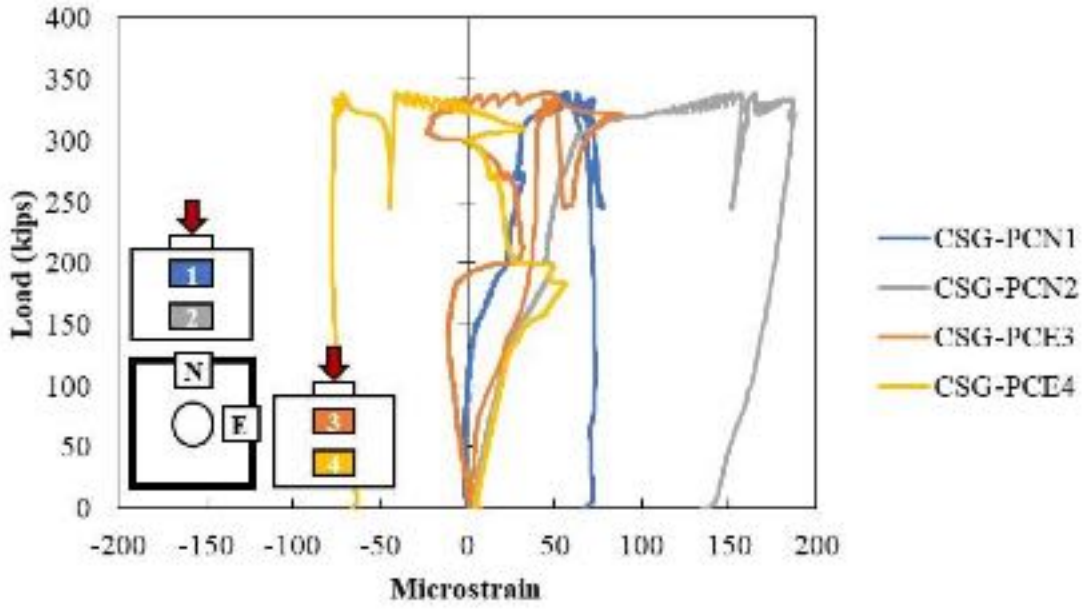

Figure A - 22: Concrete strain gauge on the concrete surface of Specimen S2-1

Figure A - 23: Cracking on the (a) east side and (b) bottom of specimen S2-1

In the same way as the longitudinal reinforcement, the confining reinforcement around the pocket were more engaged in the east side of the plug. The gauge that was placed in the bottom (RSG-PCE12) experienced larger stresses than the one above (RSG-PCE11) as shown in Figure A - 24, meaning that there was more expansion in the plug at the bottom than the top.

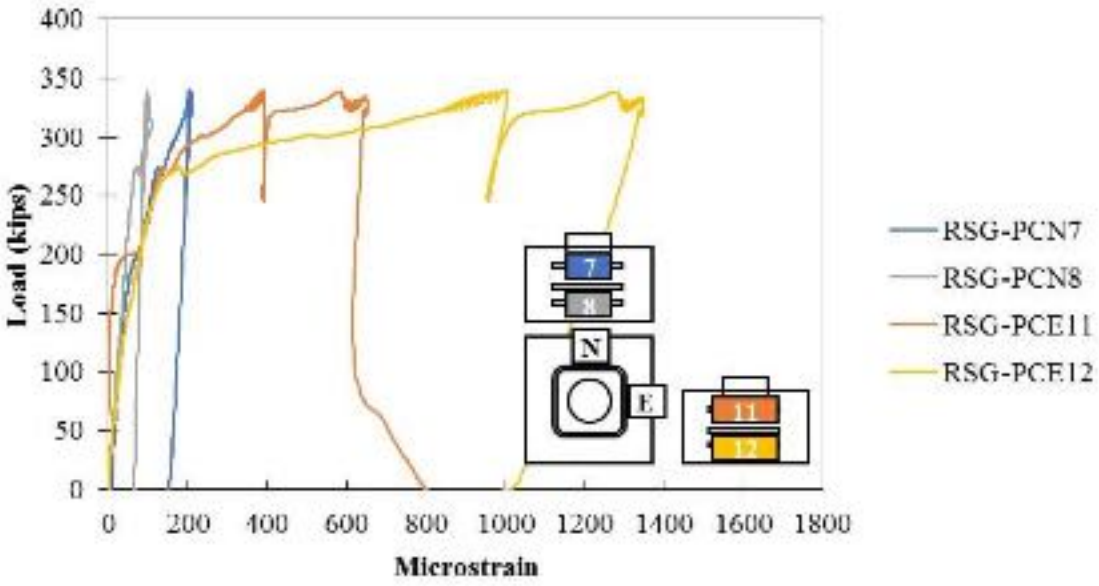

Figure A - 24: Confining reinforcement around the pocket of the Specimen S2-1.

The measured strains in the vertical reinforcement in the plug and cap are shown in Figure A - 25. The vertical strains in the cap were similar in the north and east side. In addition,

the stresses in the plug decrease toward the bottom of the plug (From RSG-PE15 to RSG-PE16), showing the transfer of stress from plug to cap.

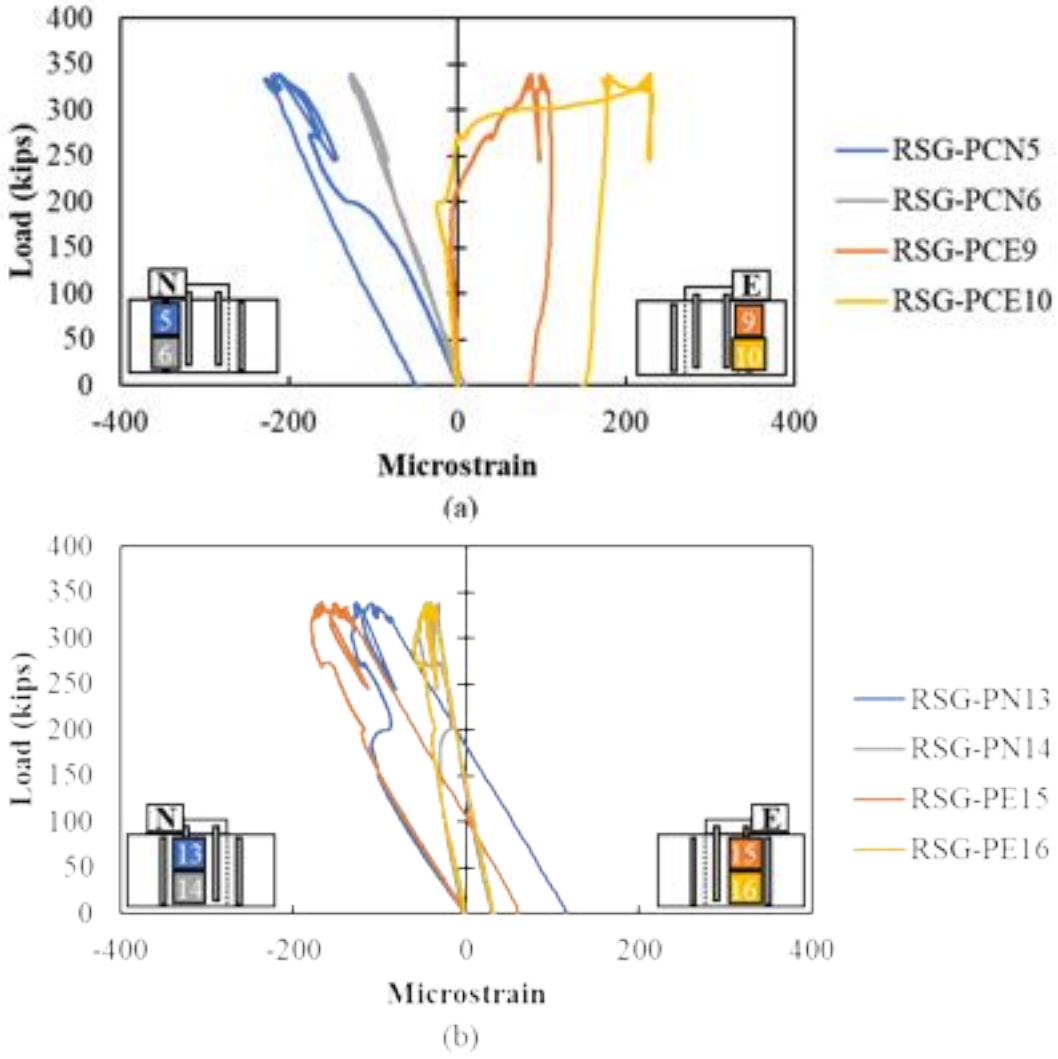

Figure A - 25: Rebar strain gauges in vertical reinforcement in plug and cap for Specimen S2-1

Specimen S2-2 Results

Specimen S2-2 was 18-inch deep, had a smooth surface between the cap and plug with exposed aggregate surface finish.

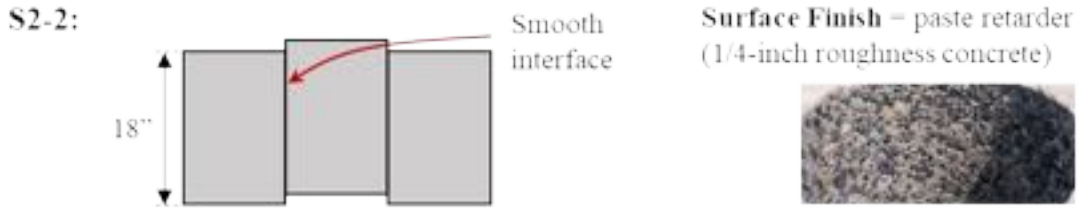

The actuator got until its maximum load of 750 kips and the specimen did not fail, suggesting that having an exposed aggregate finish provide a good adhesive bonding between the two concrete elements. The load-deflection graph is shown Figure A - 26. A noticeable difference was observed between the displacement of the top and bottom of the plug. This suggests that there was some sliding of the plug followed by reengagement of the aggregate interlock.

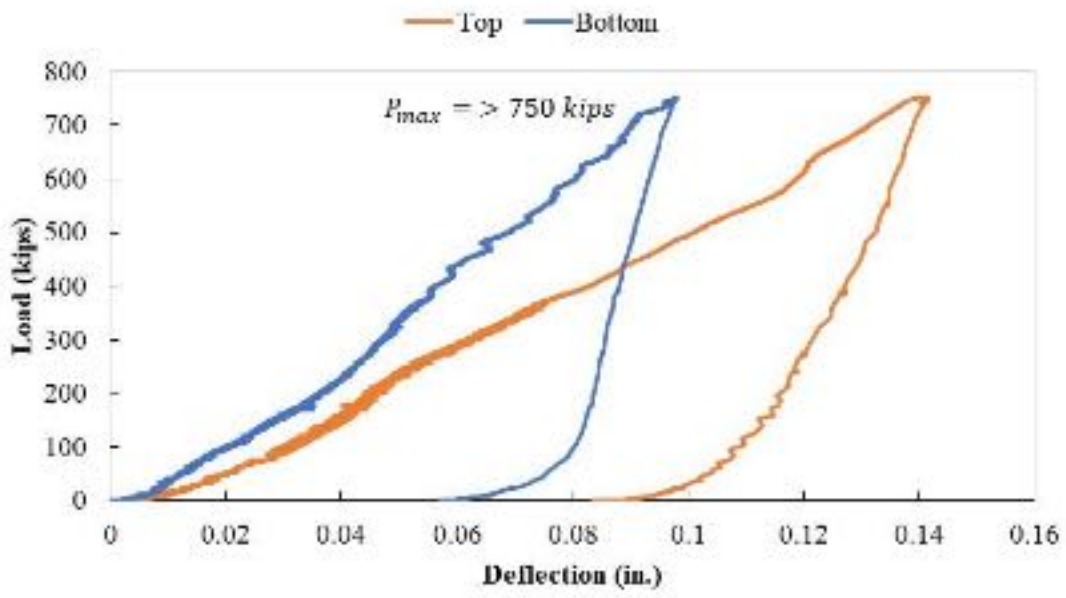

Figure A - 26: Load versus deflection curve for Specimen S2-2

The strain on the bottom in the longitudinal reinforcement were more engaged in the east side of the specimen than in the north side as well as Specimen S2-1, shown in Figure A - 27, suggesting that were splitting stresses at the bottom of the specimen. Cracking was

observed in three different ways, meaning that the specimen was near to failure. A crack opened on the bottom of the specimen at a load of around 250 kips as can be observed in the gauges RSG-PB3 and RSG-PCB4 (Figure A - 27).

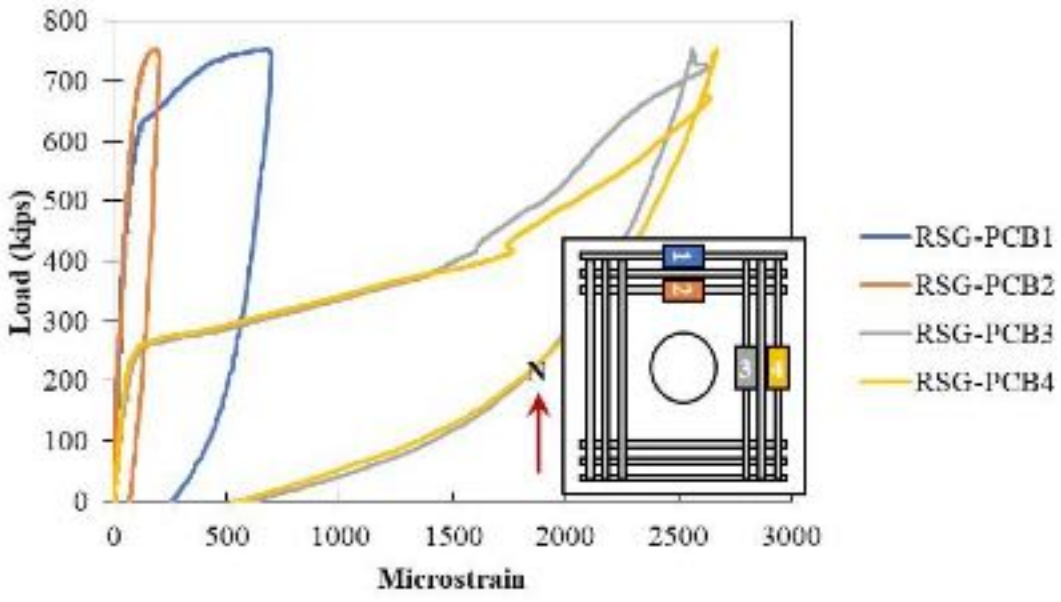

Figure A - 27: Rebar strain in longitudinal bars on bottom of Specimen S2-2

Cracking was also observed in the concrete strain gauges at a load of approximately 250 kips specifically on the bottom gauge on the east side of the specimen (CSG-PCE4) as shown in Figure A - 28.

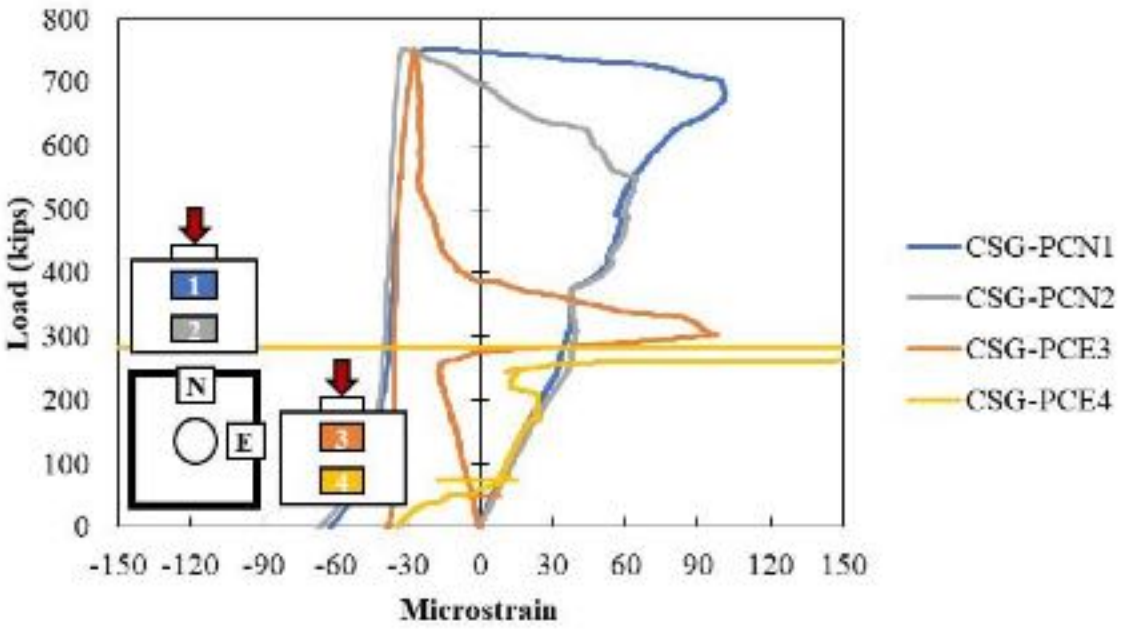

Figure A - 28: Concrete surface gauges on the cap of Specimen S2-2

Cracking was visually observed after the test was completed as shown in Figure A - 29. The cracking was observed to extend from the bottom of the cap onto the top toward the plug in the east and west side as the Specimen S2-1.

Figure A - 29: Cracking on the (a) surface of the cap and (b) bottom of the specimen S2-2

In the same way as the longitudinal reinforcement, the confining reinforcement around the pocket were more engaged in the east side of the plug than the north side. The gauge that was placed in the bottom (RSG-PCE12) was slightly more engaged than the gauge placed

above (RSG-PCE11) as shown in Figure A - 30, meaning that there the plug expansion was not symmetric through the height of the interface.

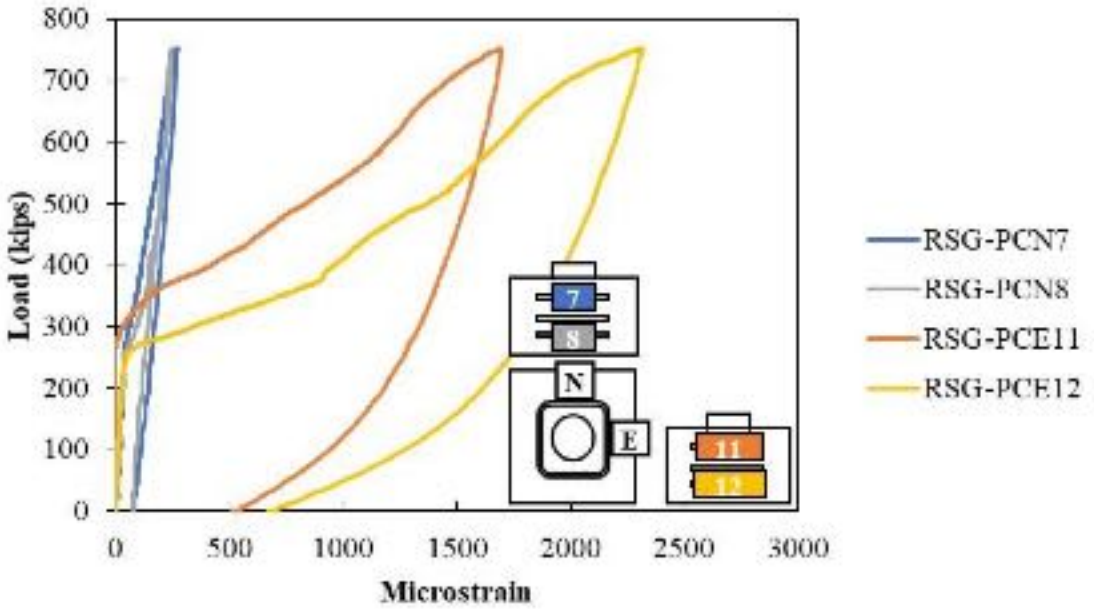

Figure A - 30: Rebar strain gauges on confining reinforcement around the pocket of Specimen S2-2

The strains in the vertical reinforcement in the plug and cap are shown in Figure A - 31. The vertical strains in the cap were slightly higher than the vertical strains in the plug. These results suggest that a relatively short distance was required for the stress to be transferred from plug to cap.

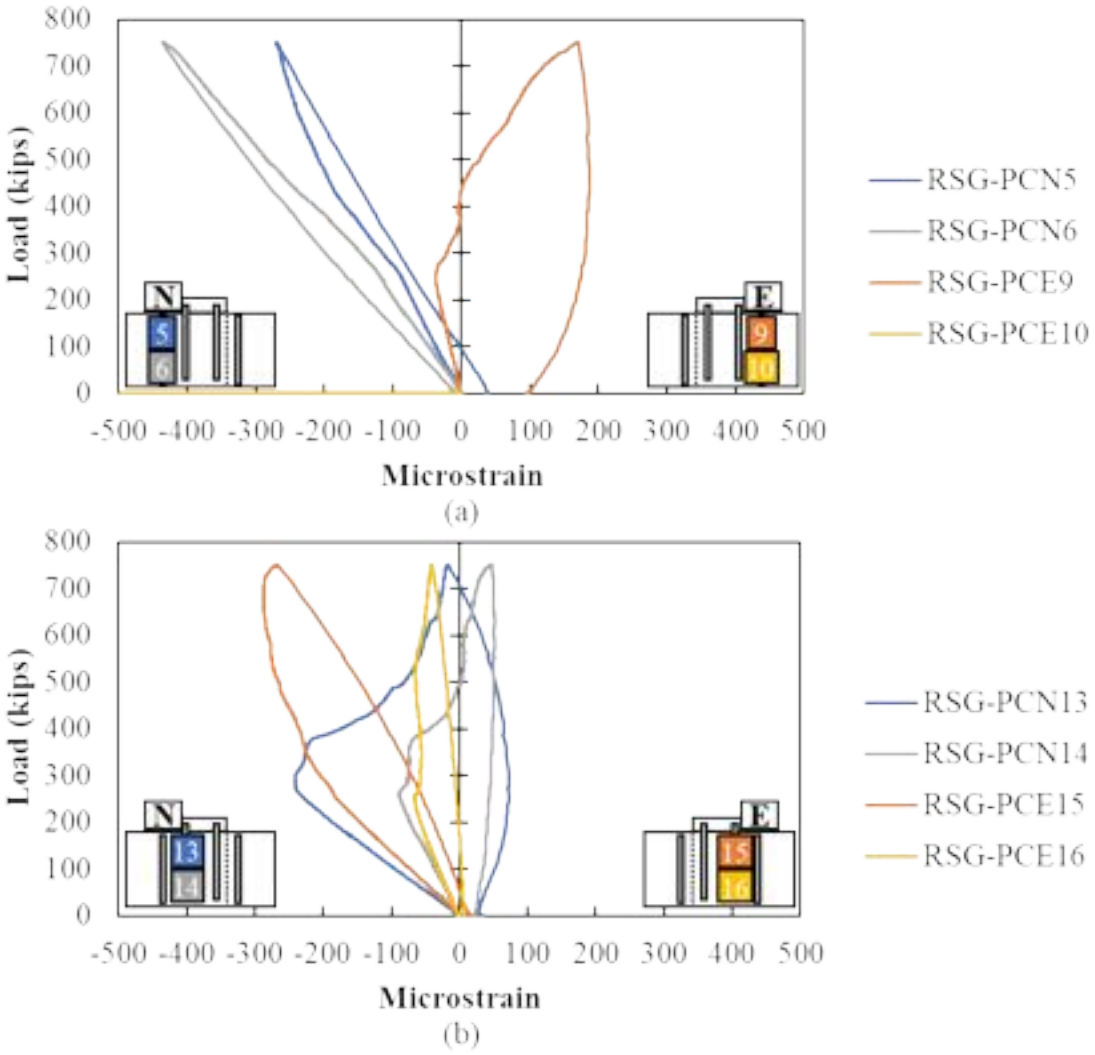

Figure A - 31: Rebar Strain gauges in vertical reinforcement in (a) cap and (b) plug of Specimen S2-2.

Specimen S2-3 Results

Specimen S2-3 was 18-inch deep, had a smooth surface between the cap and plug with sandblasted (1/16'' of roughness) surface preparation. In addition, the void was created using a sonotube with one single rib in the bottom of the interface.

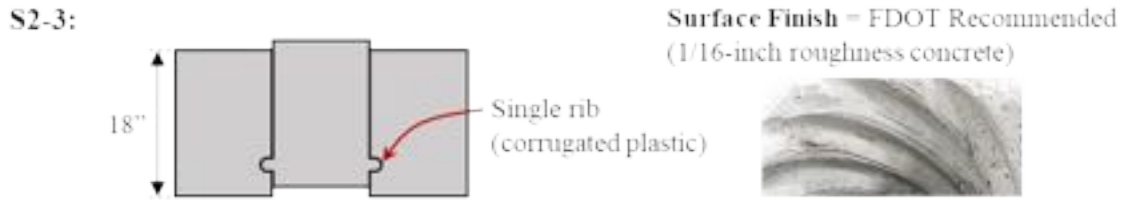

The plug started to slide around 250 kips. The maximum load was 320.1 kips, and after failure the specimen still held a load of 240 kips. The specimen was loaded until 0.5-inch displacement of the plug. The load displacement curve is shown in Figure A - 32, the results of the LDT placed in the bottom was not included because the LDT was not reading correctly since the bottom of the plug was not smooth as observed in Figure A - 35 (b).

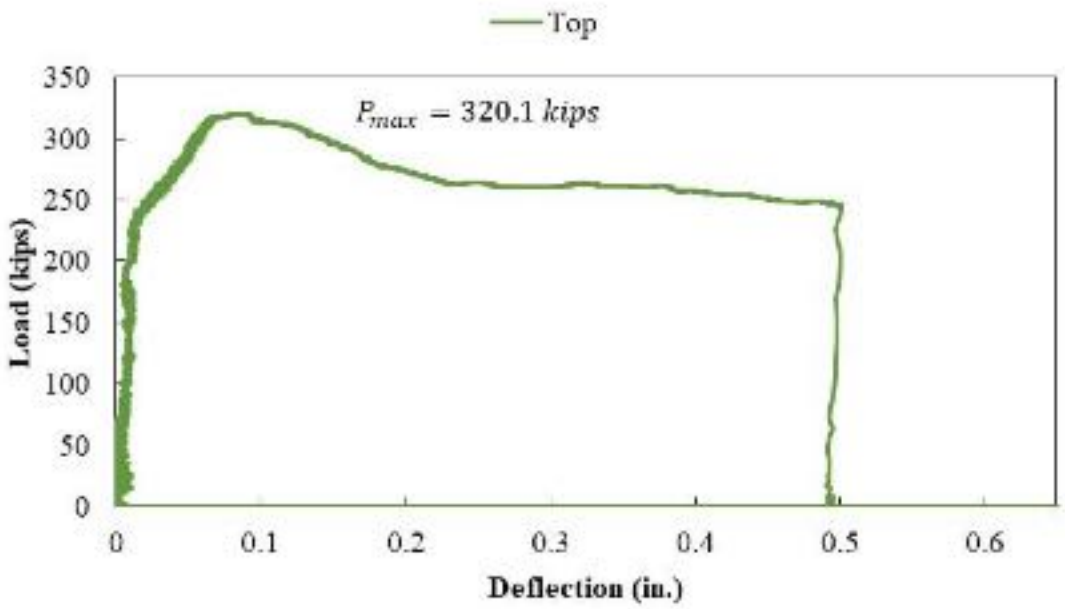

Figure A - 32: Load versus deflection curve for Specimen S2-3.

As well as the first two specimens, the strain on the bottom in the longitudinal reinforcement were more engaged in the east and west side of the specimen, shown in Figure A - 33. A crack opened on the bottom of the specimen at a load of around 175 kips

as can be observed in the gauges RSG-PB3 and RSG-PCB4 (Figure A - 33). Comparing this response with the other two specimens, plug expansion and splitting stresses at the bottom of the specimens was observed in all three specimens.

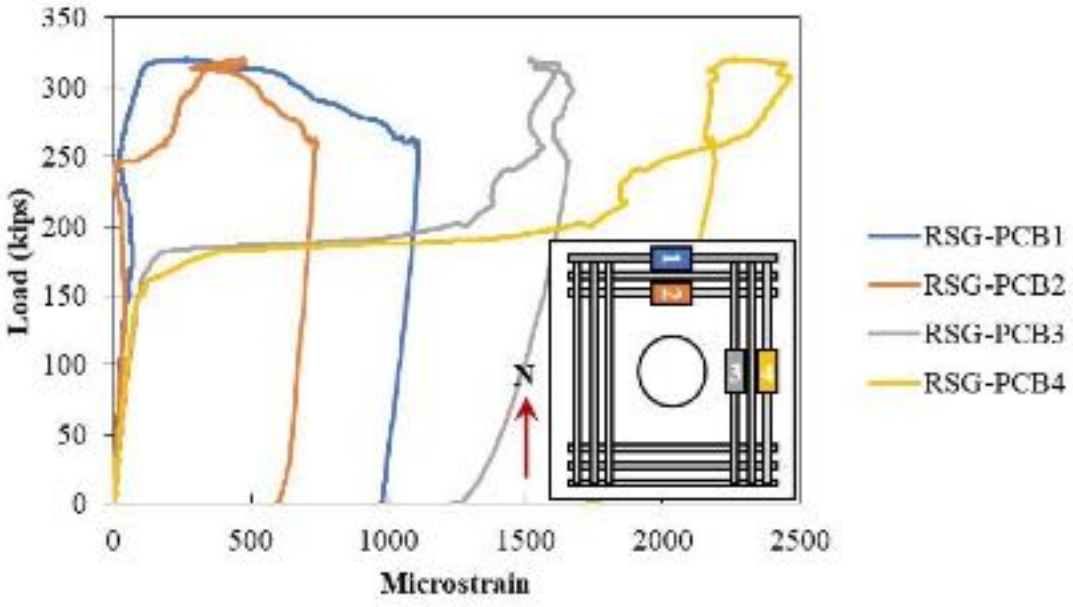

Figure A - 33: Rebar strain gauges in the longitudinal reinforcement on the bottom of Specimen S2-3

Cracking was also observed in the surface concrete at a load of around 150 kips specifically on the bottom gauge on the east side of the specimen (CSG-PCE4) as shown in Figure A - 34. The cracks appeared before the plug started to move, meaning that the plug might cause expansion of the cap before movement.

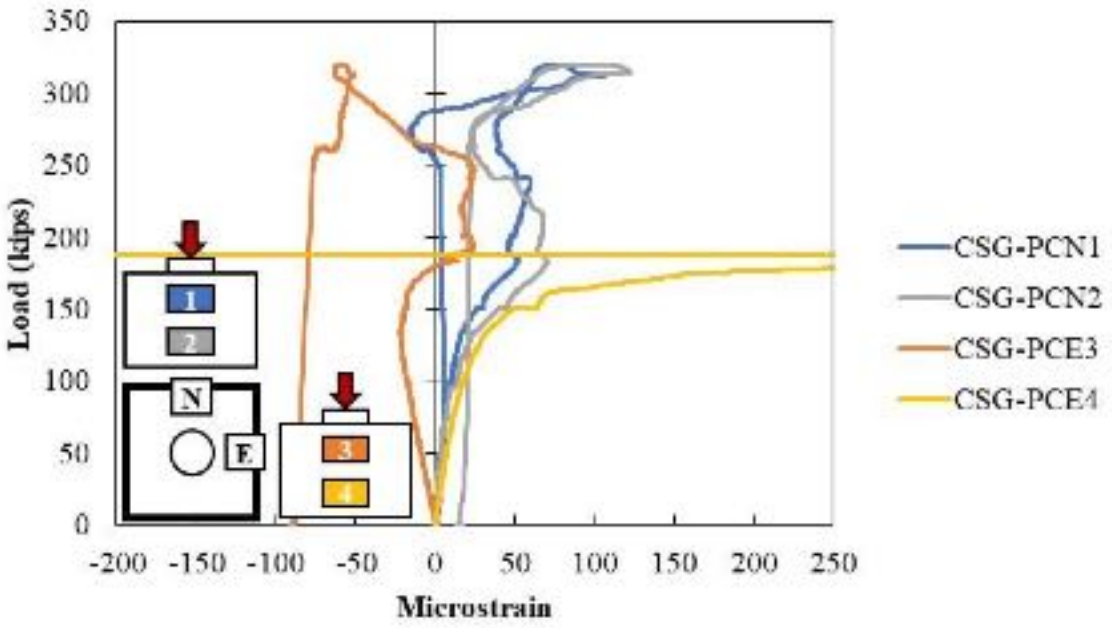

Figure A - 34: Concrete strain gauges in the surface of the cap of Specimen S2-3

Cracking was visually observed as shown in Figure A - 35. The cracking was observed to extend from the bottom of the cap onto the top toward the plug in the east and west side. More splitting stresses were observed on the bottom cap when having a single rib on the interface.

Figure A - 35: Cracking on (a) cap and (b) bottom of the Specimen S2-3

The confining reinforcement around the pocket were more engaged in the east side of the plug than the north side. However, engagement was observed in the bottom gauge (RSG-PCN8) on the north side as shown in Figure A - 36. As mentioned before, this distribution

of the stresses show that more expansion was transfer to the cap before pushing through of the plug.

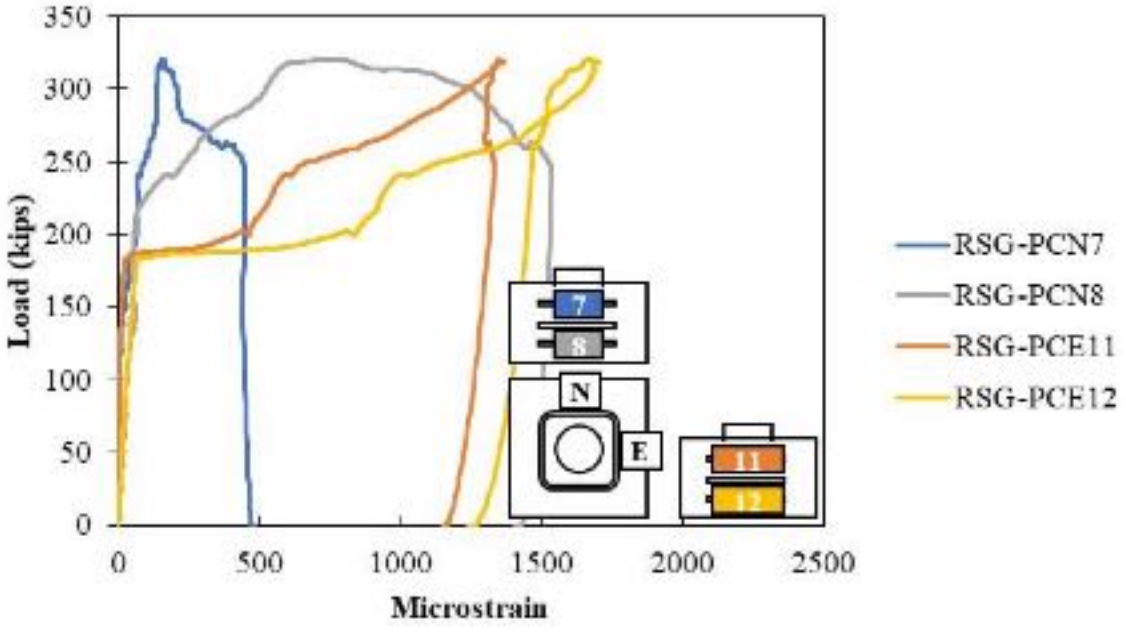

Figure A - 36: Confining reinforcement around the pocket of Specimen S2-3.

The measured strains in the vertical reinforcement in the plug and cap are shown in Figure A - 37.

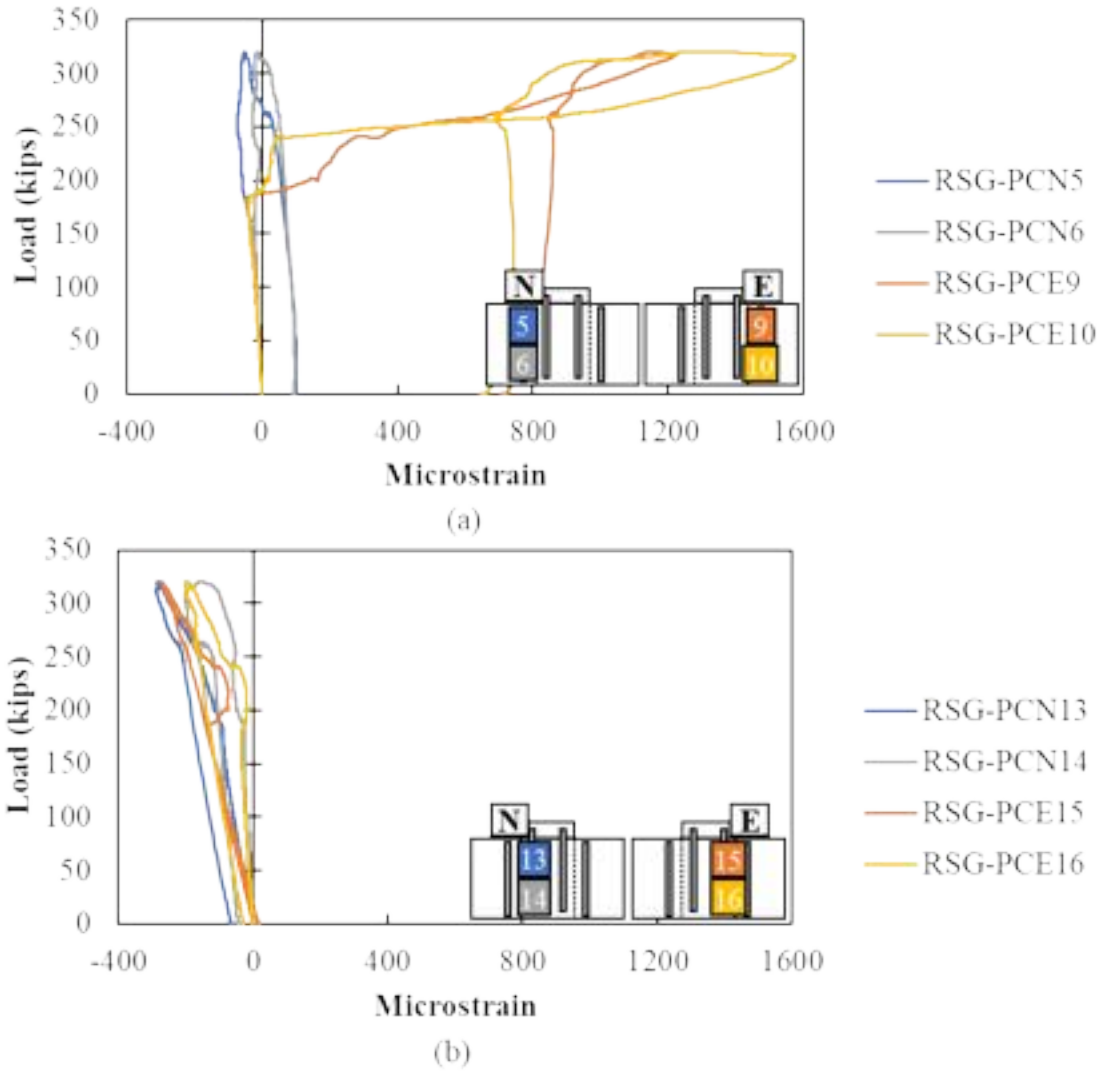

Figure A - 37: Rebar strain gauges in vertical reinforcement on (a) the cap and (b) plug of Specimen S2-3.

Specimen S2-4 Results

Specimen S2-4 was 14-inch deep, had a smooth surface between the cap and plug with exposed aggregate surface finish.

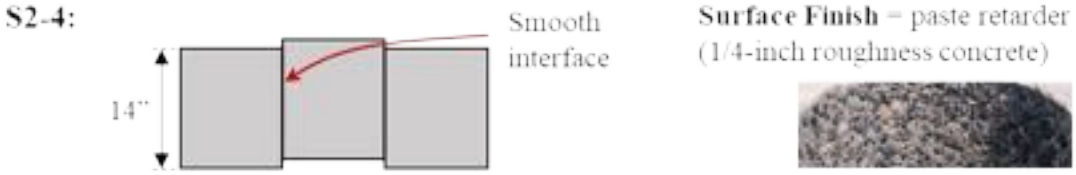

The maximum load was 615.40 kips where the plug started to move. After failure, the specimen still held a load of around 400 kips. The specimen was loaded until 0.5-inch displacement of the plug. The load displacement curve is shown in Figure A - 38. A slightly difference was noticed between the displacement of the top and bottom of the plug.

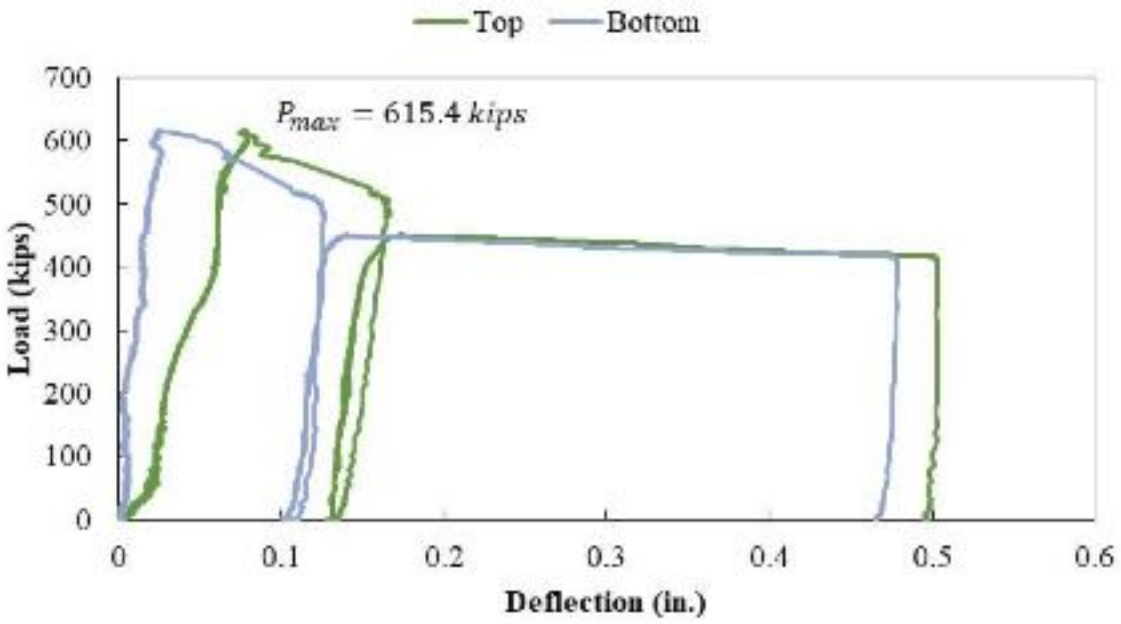

Figure A - 38: Load versus deflection curve for Specimen S2-4

The strain on the bottom in the longitudinal reinforcement were more engaged in the east side of the specimen, shown in Figure A - 39. A crack started on the bottom of the specimen at a load of around 170 kips as can be observed in the gauges RSG-PB3 and RSG-PCB4 (Figure A - 39).

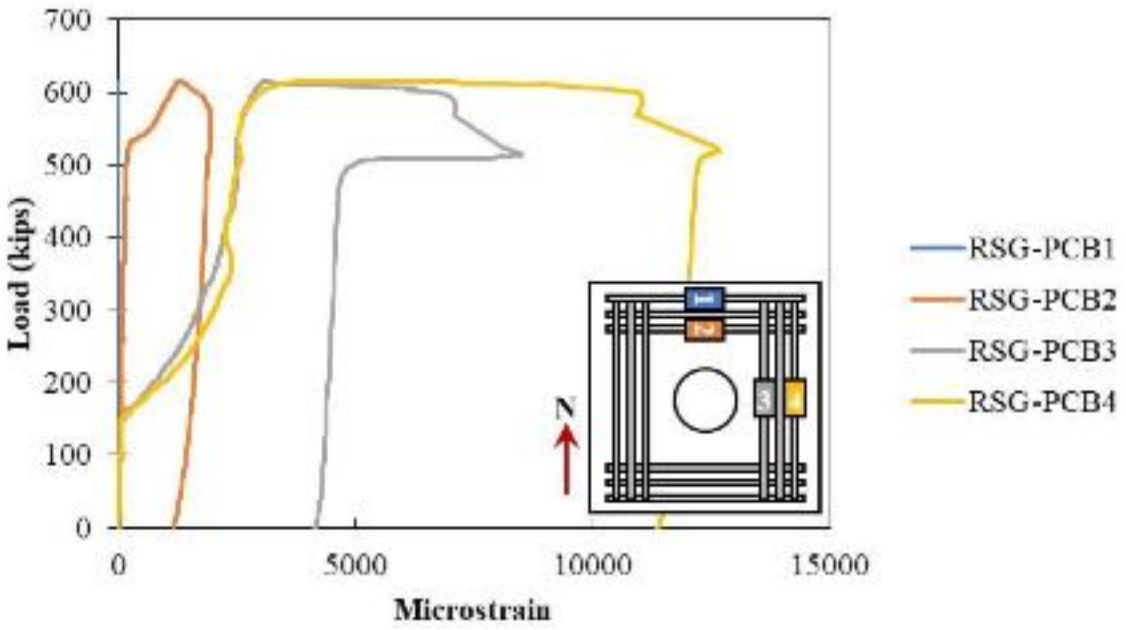

Figure A - 39: Rebar strain gauges in longitudinal reinforcement in the bottom of Specimen S2-4

Cracking was also observed in the surface concrete at a load of around 170 kips on the bottom gauges in the east side of the specimen (CSG-PCE4 and CSG-PCE3) as shown in Figure A - 40. In this specimen, cracking was later observed in the north side on a load of around 500 kips. Crack propagation was initiated from the bottom to the top of the cap before plug movement.

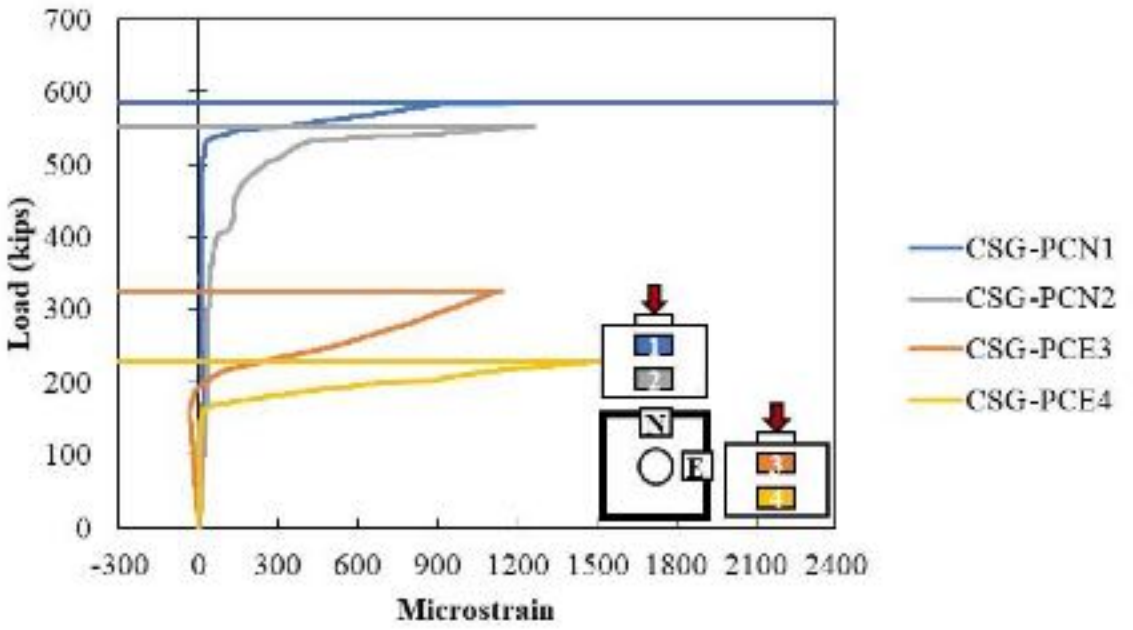

Figure A - 40: Concrete strain gauges in the surface of the cap of Specimen S2-4.

Cracking was visually observed when the testing was finished as shown in Figure A - 41. The cracks were observed to extend in the east and west side.

Figure A - 41: Specimen S2-4 (a) elevation before testing and (b) bottom cracking after testing

The confining reinforcement around the pocket were more engaged in the east side of the specimen than the north side. The east-bottom gauge was engaged on a load of 170 kips as shown in Figure A - 42. As mentioned before, the distribution of the stresses suggests that expansion of the plug starts at the bottom and it is not evenly distributed throughout the height.

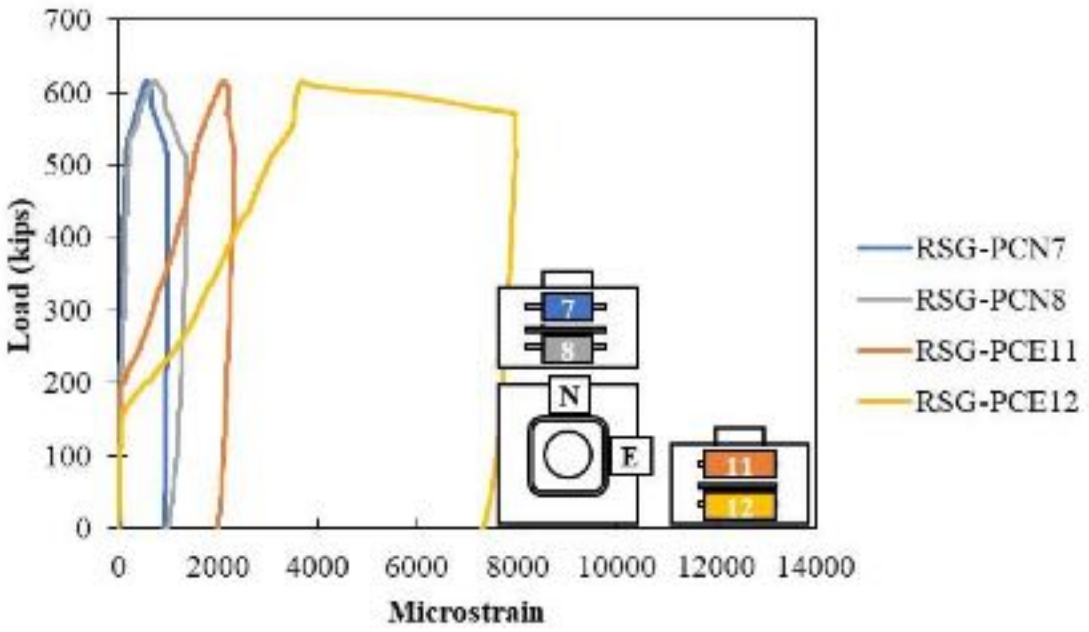

Figure A - 42: Confining reinforcement around the pocket of Specimen S2-4

The stresses in the vertical reinforcement were also measured. As well as the confining reinforcement, the east side was more engaged than the north side of the specimen as shown in Figure A - 43. Tension developed in the vertical reinforcement in the cap, suggesting that an internal horizontal crack around the plug may have developed toward failure.

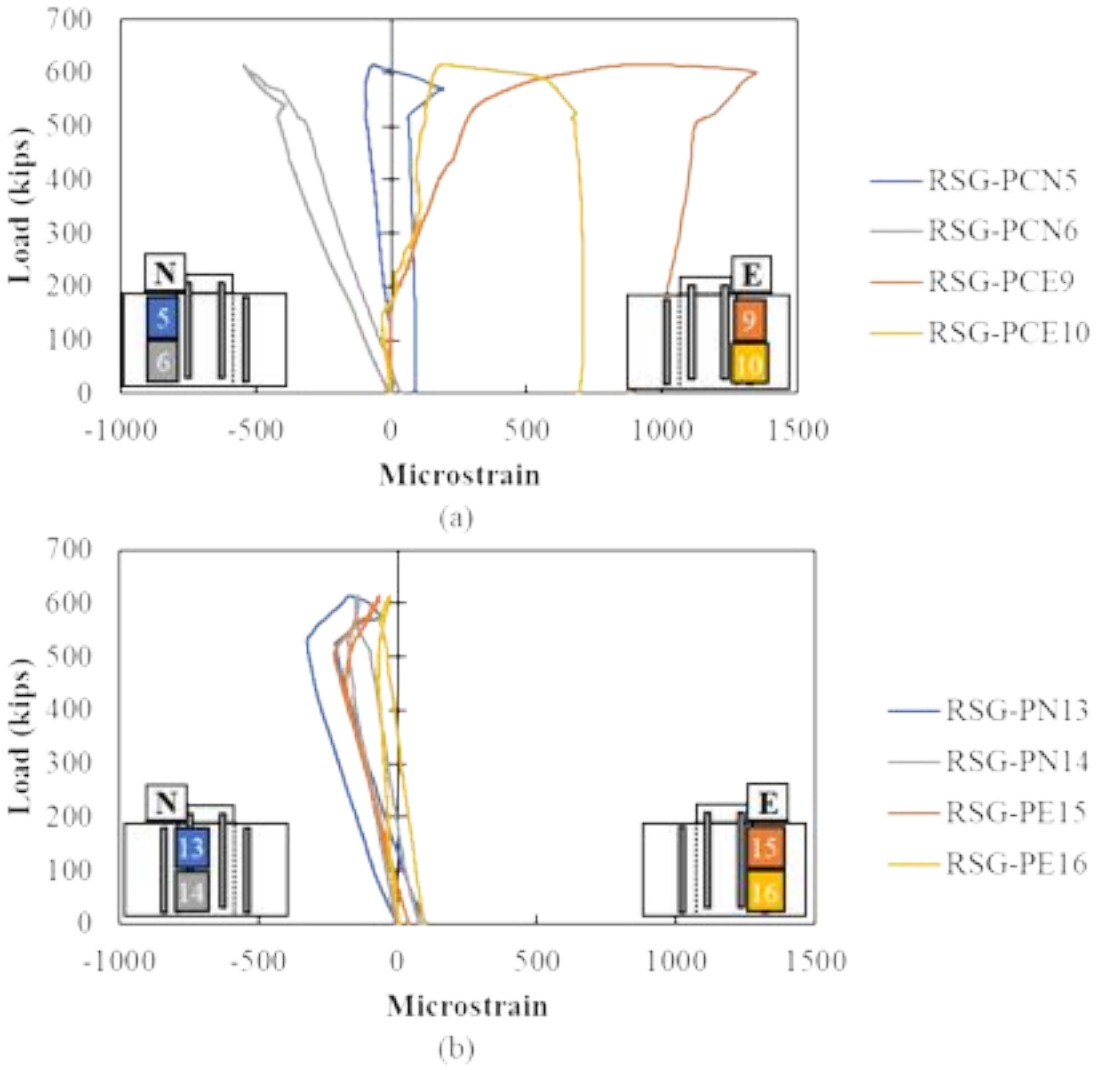

Figure A - 43: Rebar strain gauges in vertical reinforcement on (a) the cap and (b) plug of Specimen S2-4

Specimen S2-5 Results

Specimen S2-5 was 14-inch deep, had a smooth surface between the cap and plug with sandblasted (1/16'' roughness) surface preparation. As well as specimen S2-3, the void was created using a sonotube with one single rib in the bottom of the interface.

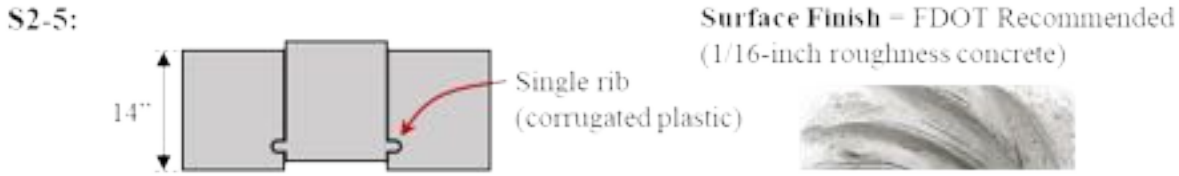

The plug started to move with a load of around 300 kips, and the failure load was 356 kips. After failure, the specimen still held a load of 270 kips. The specimen was loaded until 0.5-inch displacement of the plug. The load displacement curve is shown in Figure A - 44.

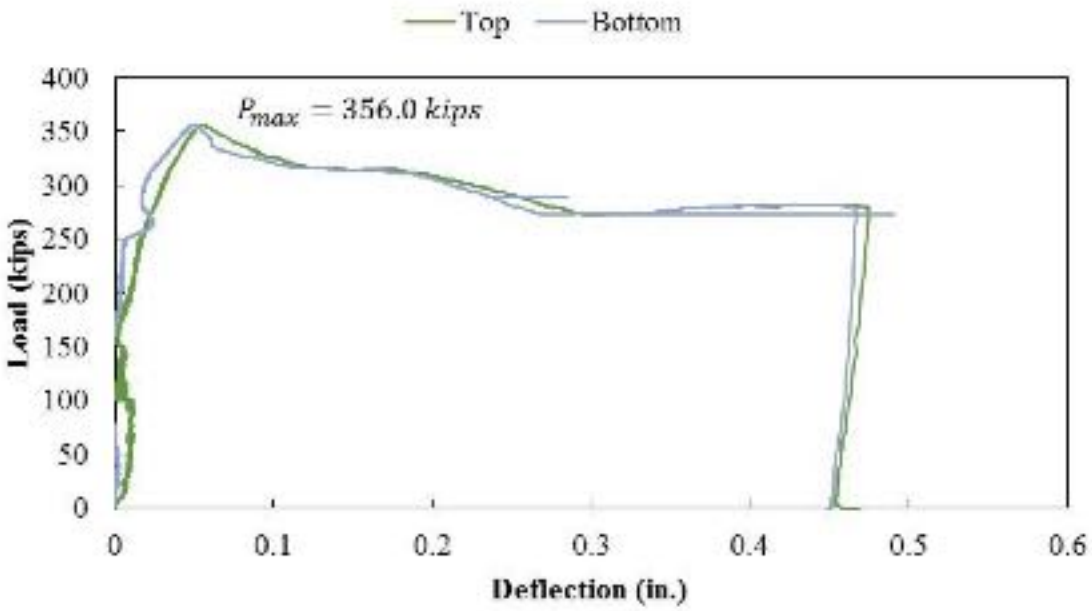

Figure A - 44: Load versus deflection curve for Specimen S2-5

The stresses in the longitudinal rebar on the bottom of the specimen are shown in Figure A - 45. A crack opened on the bottom of the cap on the east side with a load of around 120 kips as measured in gauges RSG-PCB3 and RSG-PCB4. Later when the load was around 350 kips, another crack opened in the north side of the specimen as can be observed in the gauges RSG-PCB1 and RSG-PCB2.

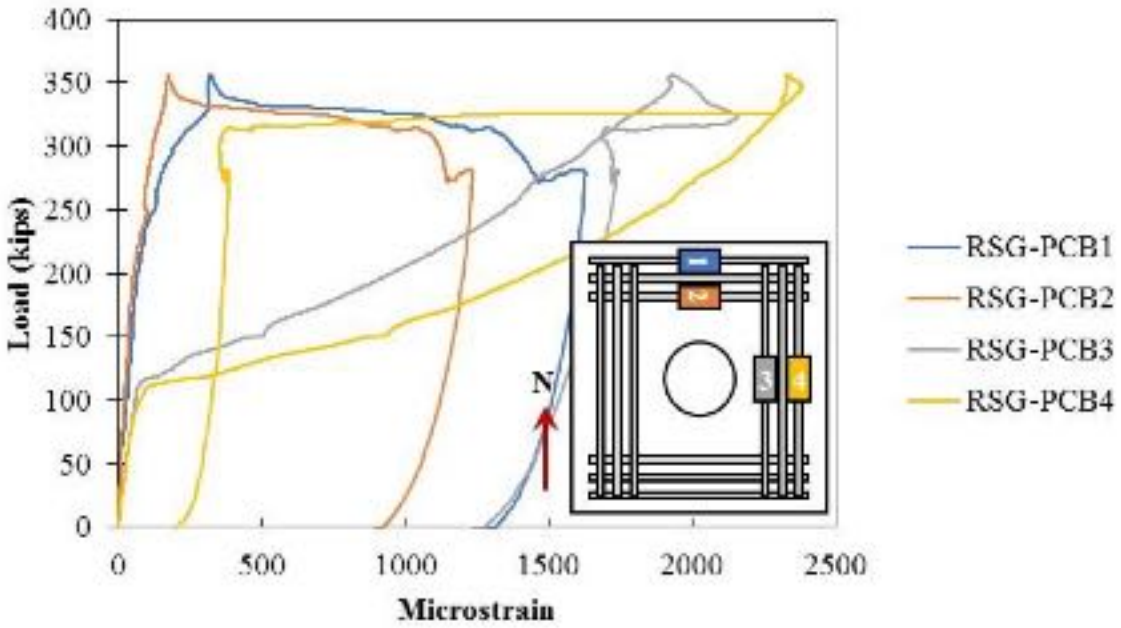

Figure A - 45: Rebar strain gauges in the longitudinal reinforcement on bottom of Specimen S2-5

Cracking was observed on the east face at around 132 kips, as shown in Figure A - 46. Cracking extended through the gauges on the north side and opened up at the ultimate capacity.

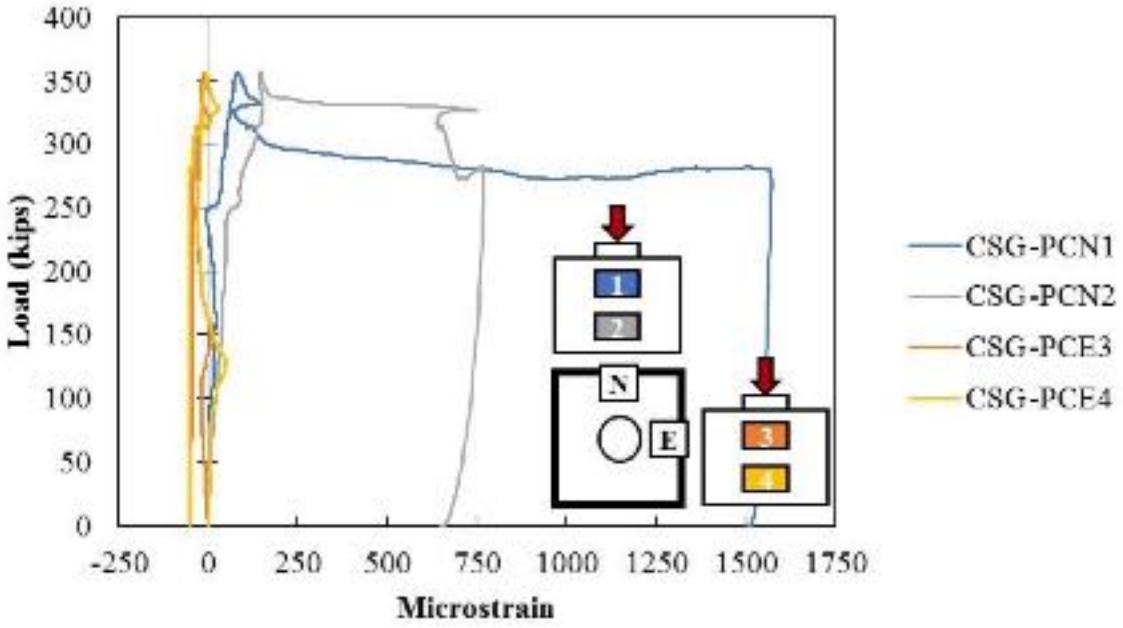

Figure A - 46: Concrete strain gauges in the surface of Specimen S2-5

Cracking was visually observed as shown in Figure A - 47. The cracks extended from the bottom of the cap to the top toward the plug in the north and south sides. More splitting stresses were observed on the bottom cap when having a single rib on the interface.

Figure A - 47: Cracking on a (a) cap and (b) bottom of the Specimen S2-5

The confining reinforcement around the pocket started to engage in the east side of the plug of a load around 130 kips according to gauges RSG-PCE11 and RSG-PCE12. In the same way, engagement was observed in the north side of the specimen at a load of 250 kips as

shown in Figure A - 48. The distribution of the stresses shows that there was expansion of the plug before sliding.

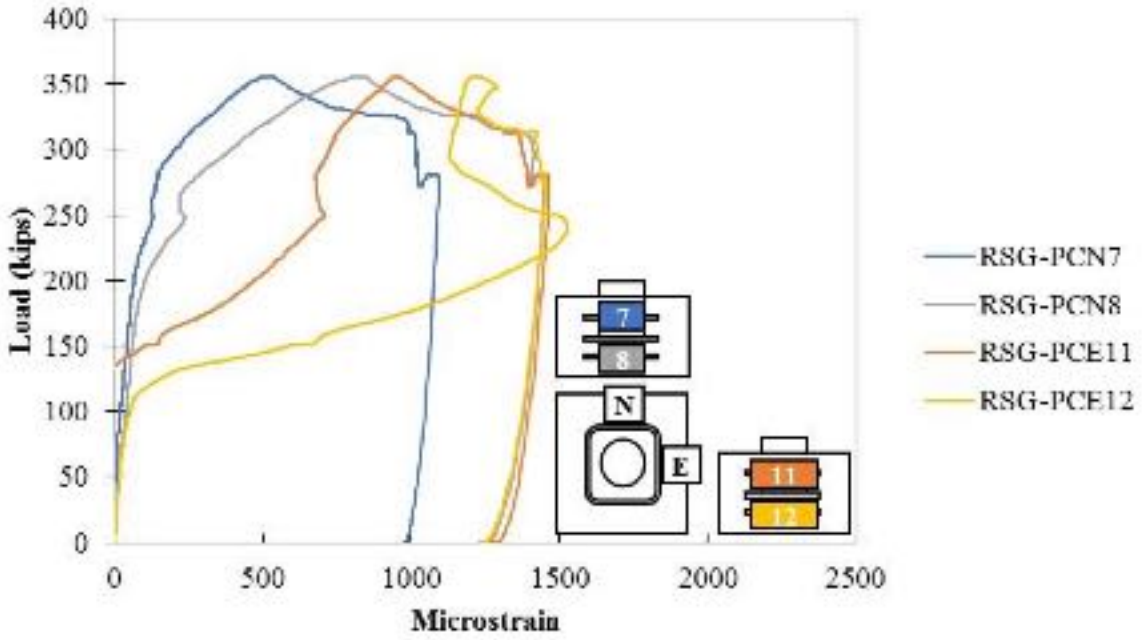

Figure A - 48: Confining reinforcement around the pocket of Specimen S2-5.

More stresses were observed in the vertical reinforcement of the plug than the vertical reinforcement of the cap as shown in Figure A - 49. Suggesting that a largest distance was required to transfer the stresses from the plug to cap.

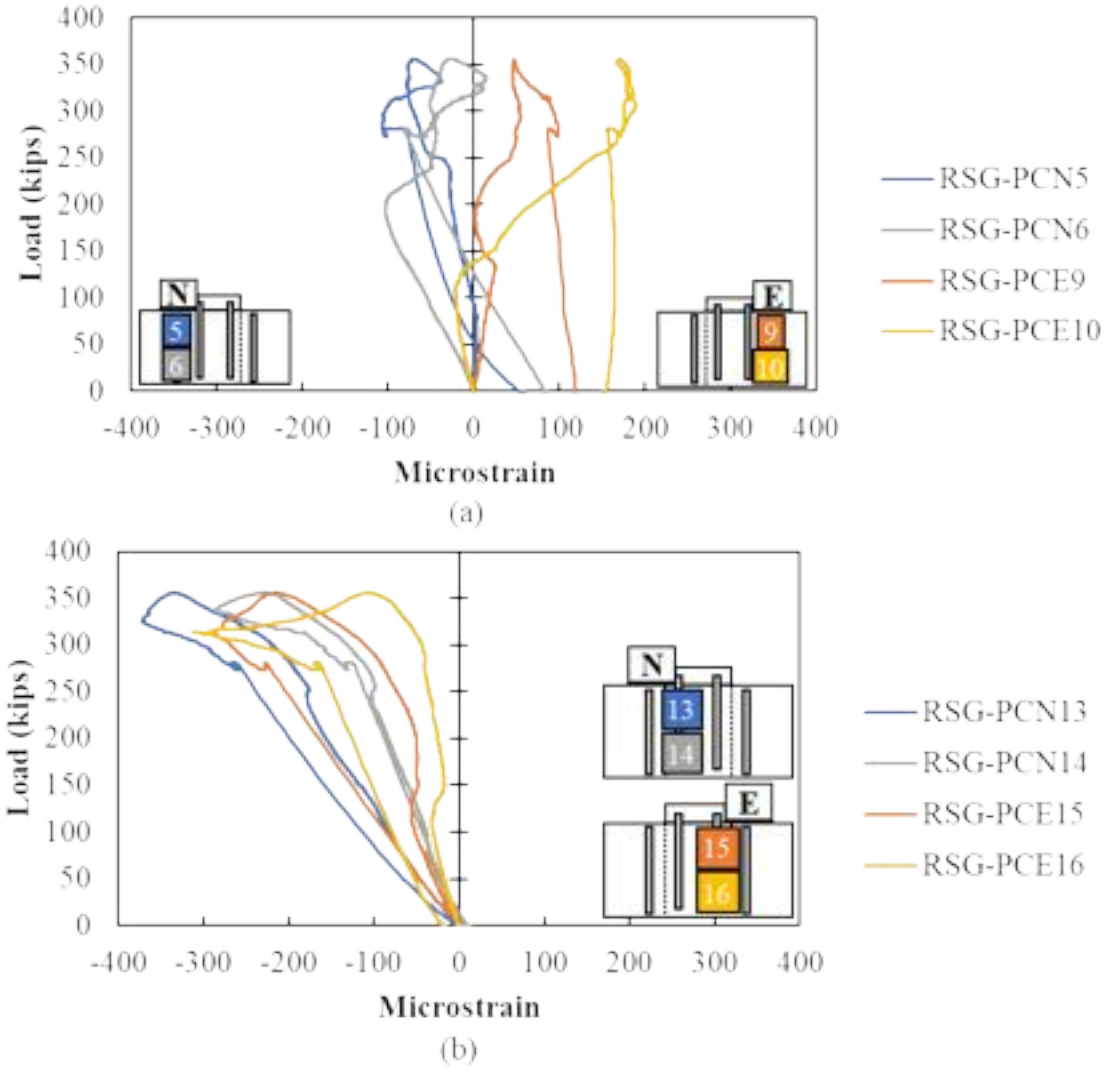

Figure A - 49: Rebar strain gauges in vertical reinforcement on (a) cap and (b) plug of Specimen S2-5

Specimen S2-6 Results

Specimen S2-6 was 14-inch deep, had a smooth surface between the cap and plug with sandblasted (1/16'' roughness) surface preparation. In this case, the void was created using a sonotube with two ribs in the bottom of the interface.

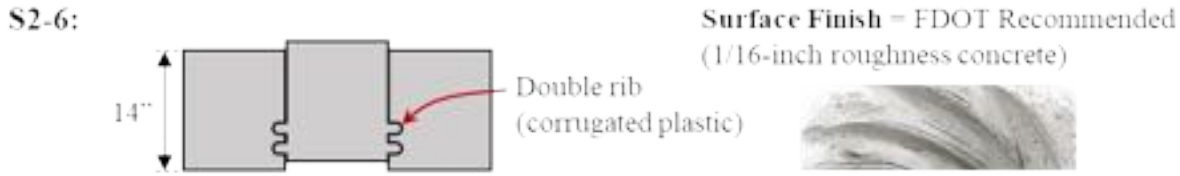

The failure load was 418.6 kips, and after failure the specimen still held a load of 200 kips. The plug started to slide around 200 kips and the total displacement of it was 0.5-inch as shown in Figure A - 50. A slight difference was noticed between the displacement of the top and bottom of the plug.

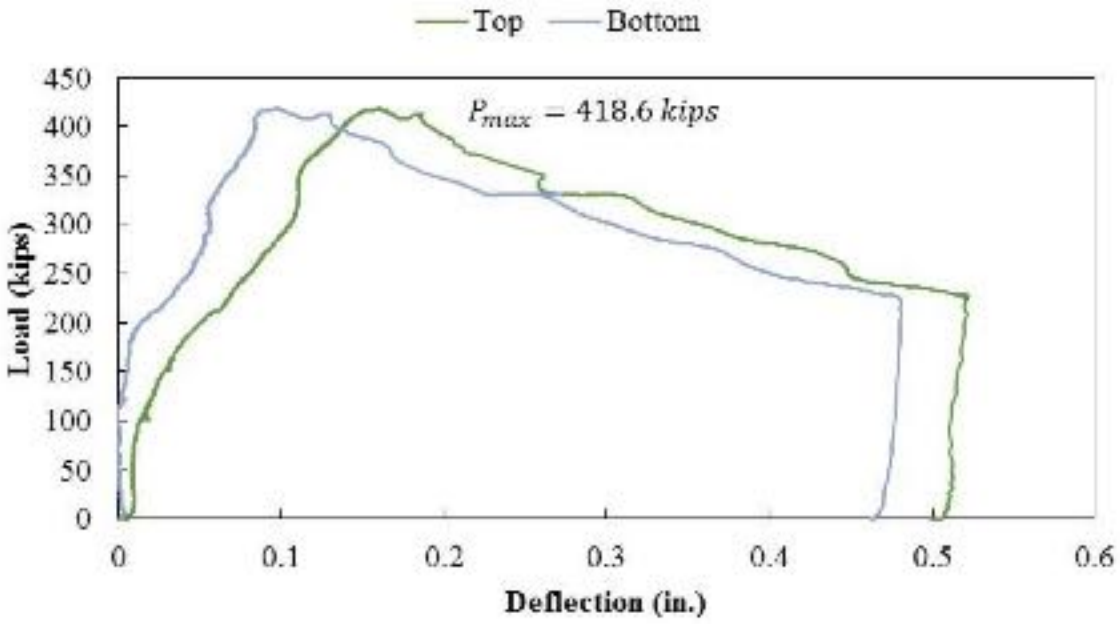

Figure A - 50: Load versus deflection curve for Specimen S2-6

The stresses in the longitudinal rebar on the bottom of the specimen were measured. According to RSG-PCB3 and RSG-PCB4 the reinforcement on the east side started to engage at a load around 110 kips. In the same way, the gauges RSG-PCB1 and RSG-PCB2

placed on the north side of the specimen showed engagement around 200 kips (Figure A - 51).

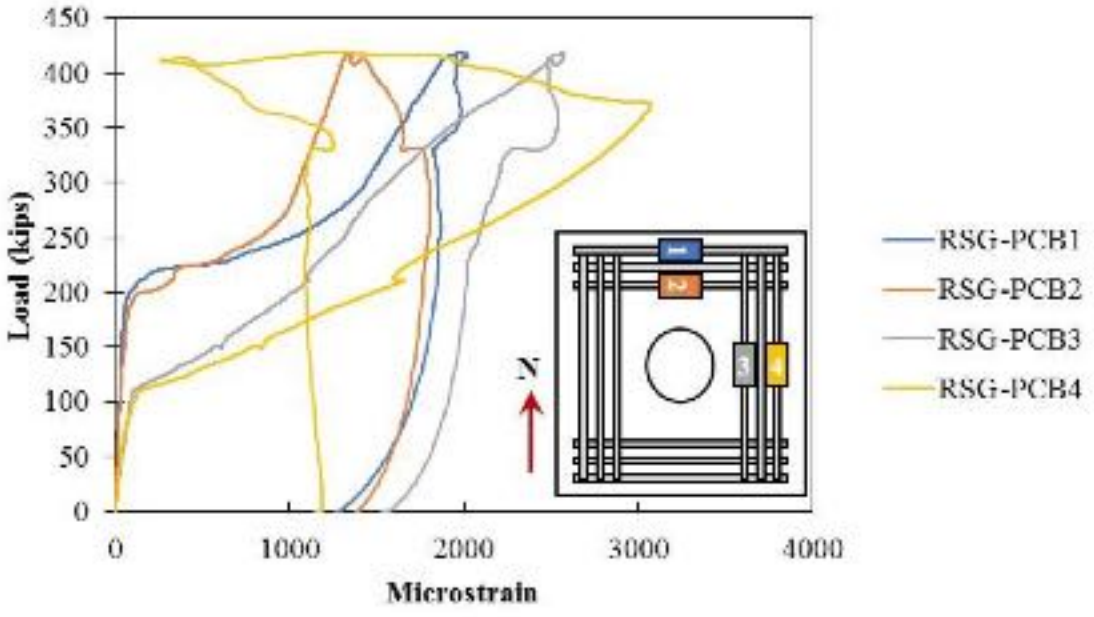

Figure A - 51: Rebar strain gauges in the longitudinal reinforcement on bottom of Specimen S2-6

Concrete strain gauges were place on the surface of the cap to measure cracks as shown in Figure A - 52. Cracking was determined using the CSGs on the east face at approximately 110 kips and on the north face of the specimen at approximately 230 kips.

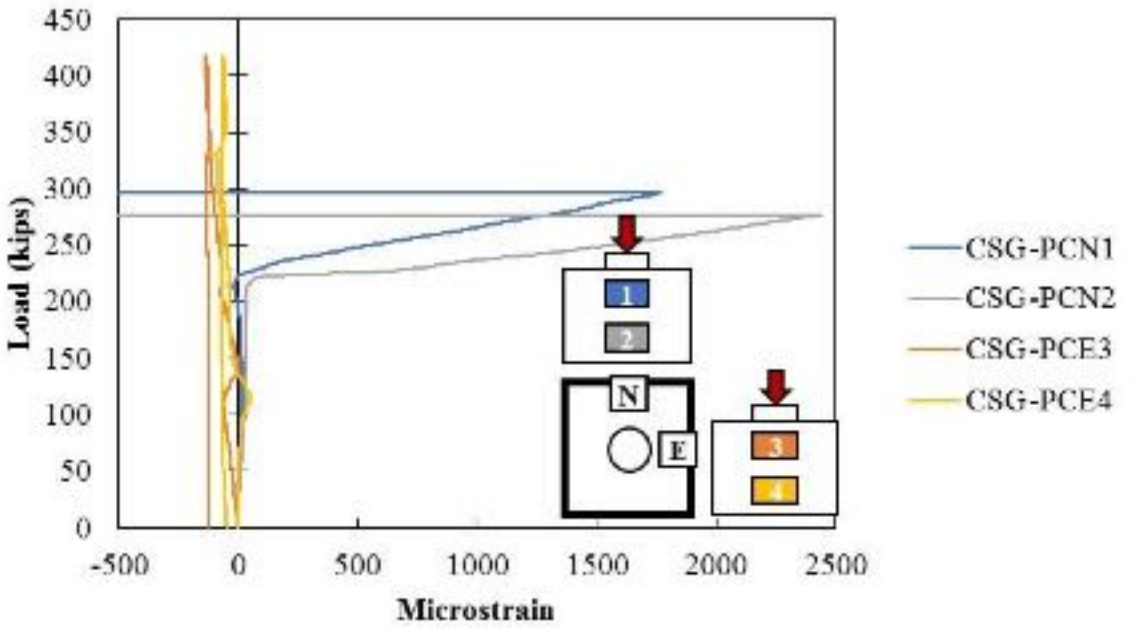

Figure A - 52: Concrete strain gauges in the surface of Specimen S2-6

Cracking was visually observed when the testing was finished as shown in Figure A - 53. As mentioned before, the crack extended from the bottom of the specimen towards the top. This specimen had small cracks before testing in the north side as shown in Figure A - 53(a).

Figure A - 53: Cracking on (a) cap and (b) bottom of the Specimen S2-6

The stresses in the confining reinforcement around the pocket were measured as shown in Figure A - 54. The engagement of the reinforcement was almost simultaneously starting

with RSG-PCE12 with a load of around 100 kips to RSG-PCN7 with a load of around 240 kips.

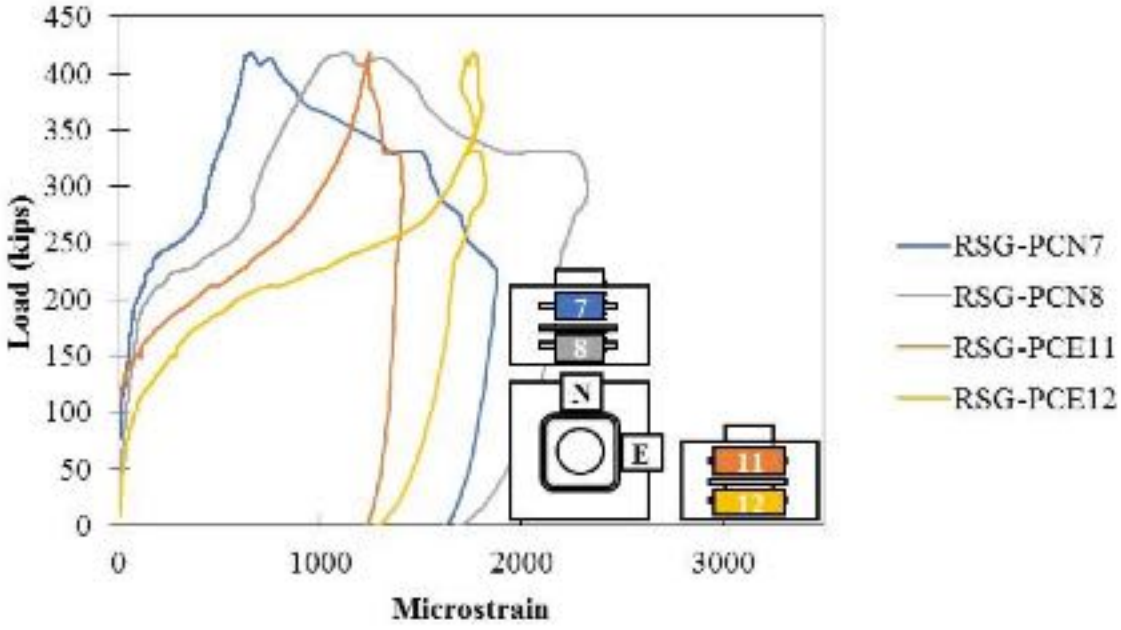

Figure A - 54: Confining reinforcement around the pocket of Specimen S2-6

The stresses in the vertical reinforcement were also measured as shown in Figure A - 55. On the east side of the specimen, higher stresses were found in the cap than in the plug. However, on the north side the stresses were higher in the cap than in the plug. This shows how the stresses are transferring from the plug to the cap through the specimen.

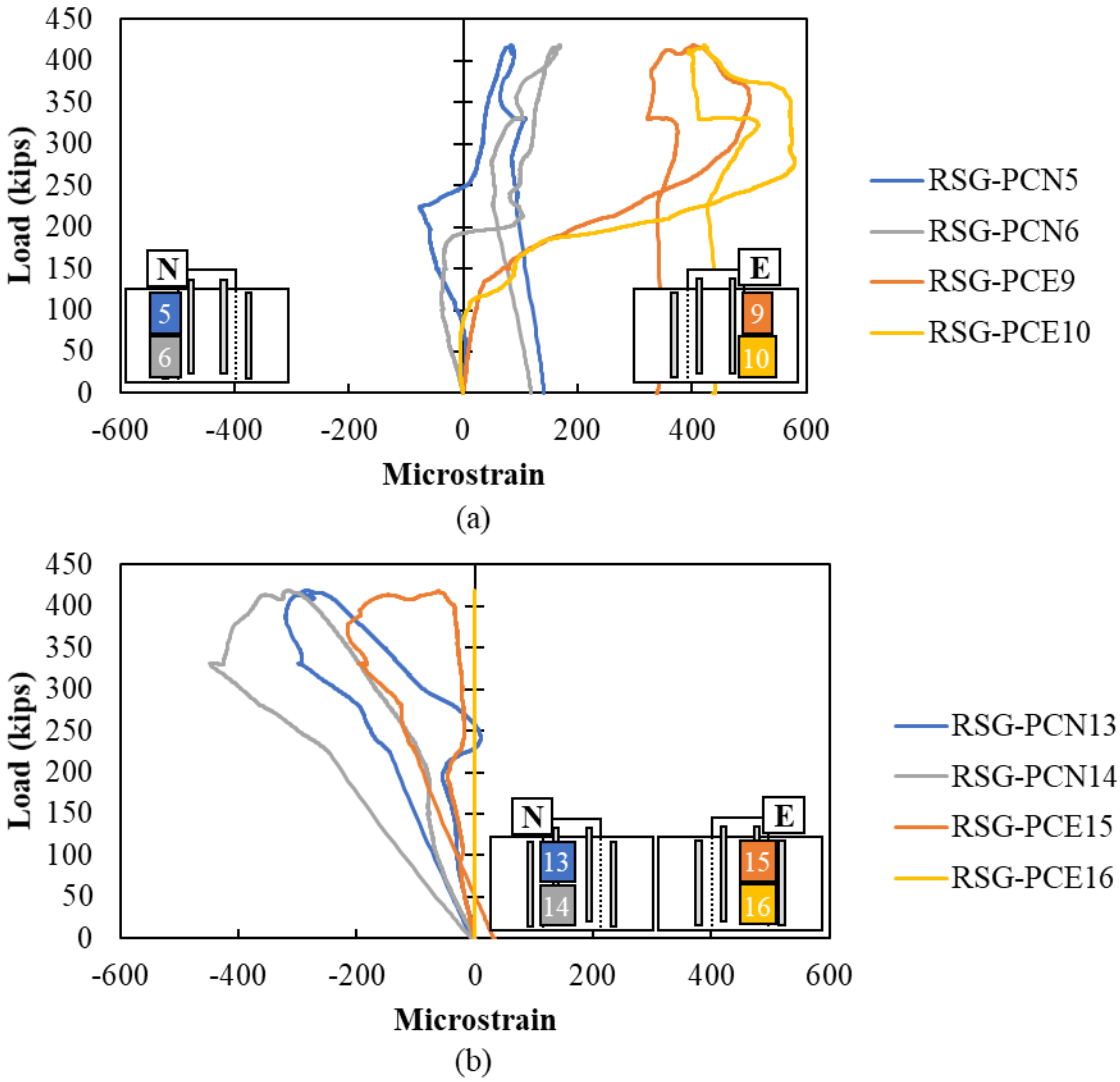

Figure A - 55: Rebar strain gauges in vertical reinforcement on (a) cap and (b) plug of Specimen S2-6

Specimen S2-7 Results

Specimen S2-7 was 18-inch deep, had a corrugated surface between the cap and plug with sandblasted (1/16'' of roughness) surface preparation. The void was created using a corrugated metal pipe.

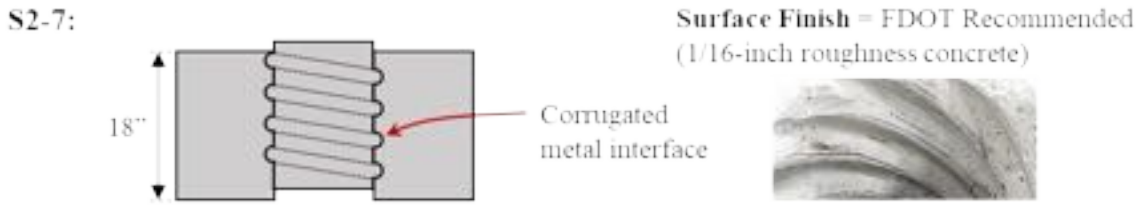

The failure load for this specimen was 719.5 kips. After failure, the specimen still held a load of around 400 kips. The specimen was loaded until 0.5-inch displacement of the plug. The load displacement curve is shown in Figure A - 56.

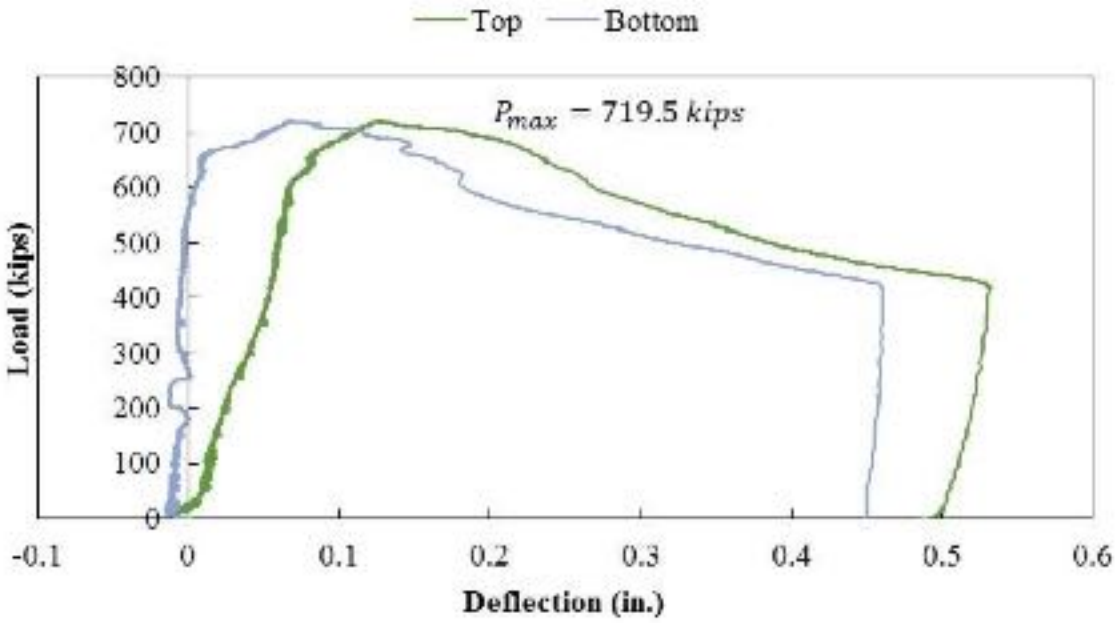

Figure A - 56: Load versus deflection curve for Specimen S2-7

The bottom reinforcement placed on the east side of the specimen started to engage between 200 kips and 300 kips according to the RSG-PCB3 and RSG-PCB4 gauges. Later when the load was around 400 kips the longitudinal reinforcement on the north side of the specimen was also engaged. Potentially, cracks were forming on the bottom of the

specimen on both directions. The reading of the longitudinal reinforcement in the bottom is shown in Figure A - 57.

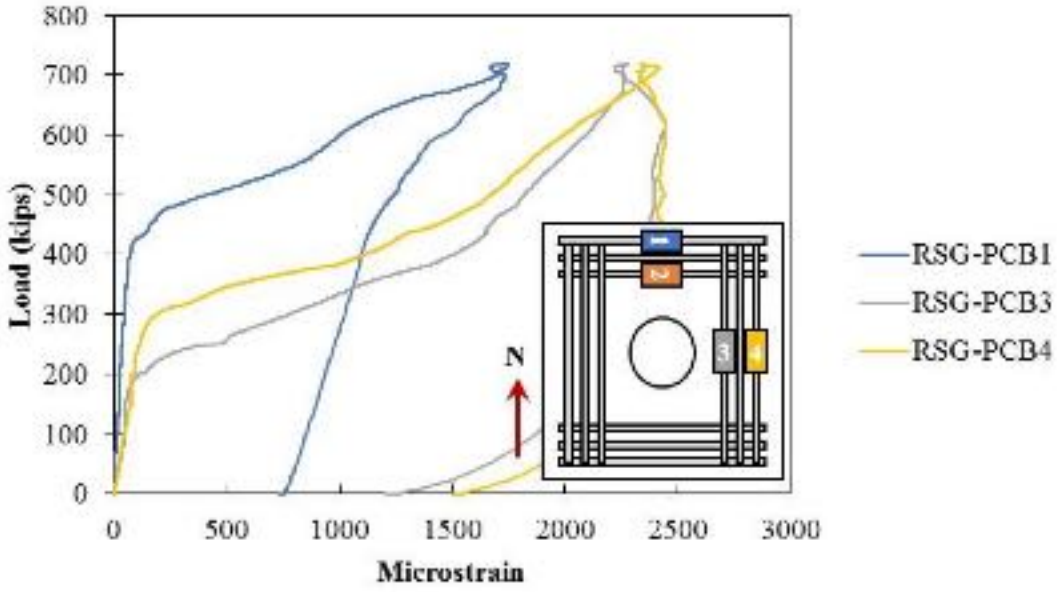

Figure A - 57: Rebar strain gauges in the longitudinal reinforcement on bottom of Specimen S2-7

In the same way a crack was measured around 300 kips on the east side with the concrete surface gauges. The reading of the concrete surface gauges is shown in Figure A - 58.

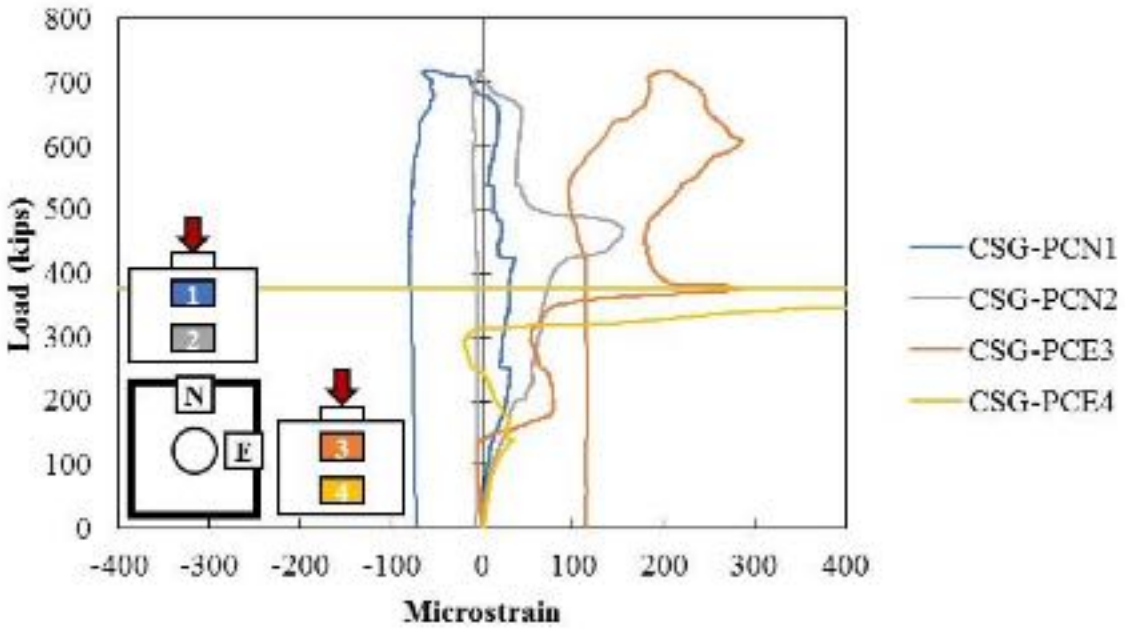

Figure A - 58: Concrete strain gauges in the surface of Specimen S2-7

When the testing was finished, cracks were also observed as shown in Figure A - 59. Cracks extended from the bottom, going up to the cap toward the plug as the reading of the gauges suggested. Bigger cracks were observed on the east-west side than the north-south side of the specimen.

Figure A - 59: Cracking on (a) cap and (b) bottom of Specimen S2-7

The confining reinforcement around the pocket started to engage in the east side of the plug of a load around 230 kips according to gauge RSG-PCE12. The other three gauges started

to engage around 300 kips. The distribution of the stresses shows that there was expansion of the plug before it started to slide.

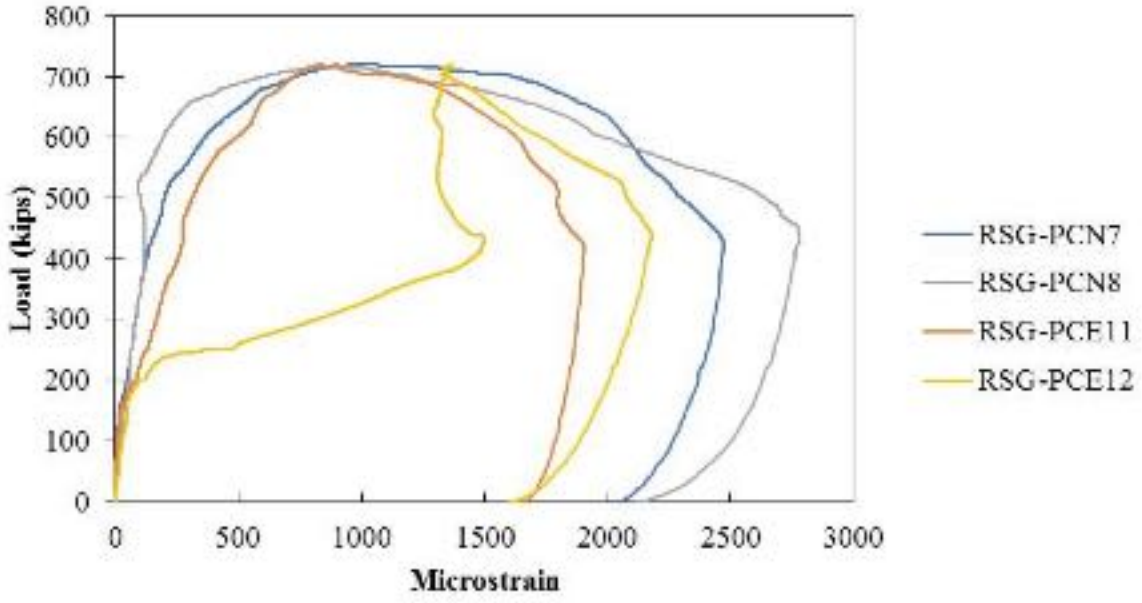

Figure A - 60: Confining reinforcement around the pocket of Specimen S2-7

The measured strains in the vertical reinforcement in the cap and plug are shown in Figure A - 61. The vertical strains in the plug decrease toward the bottom of the plug, showing transfer of stress from plug to cap. The stresses in the cap were similar in each side of the specimen, and through the height of the specimen. These results suggest the ribs in the corrugation are effective in transferring stresses between the elements.

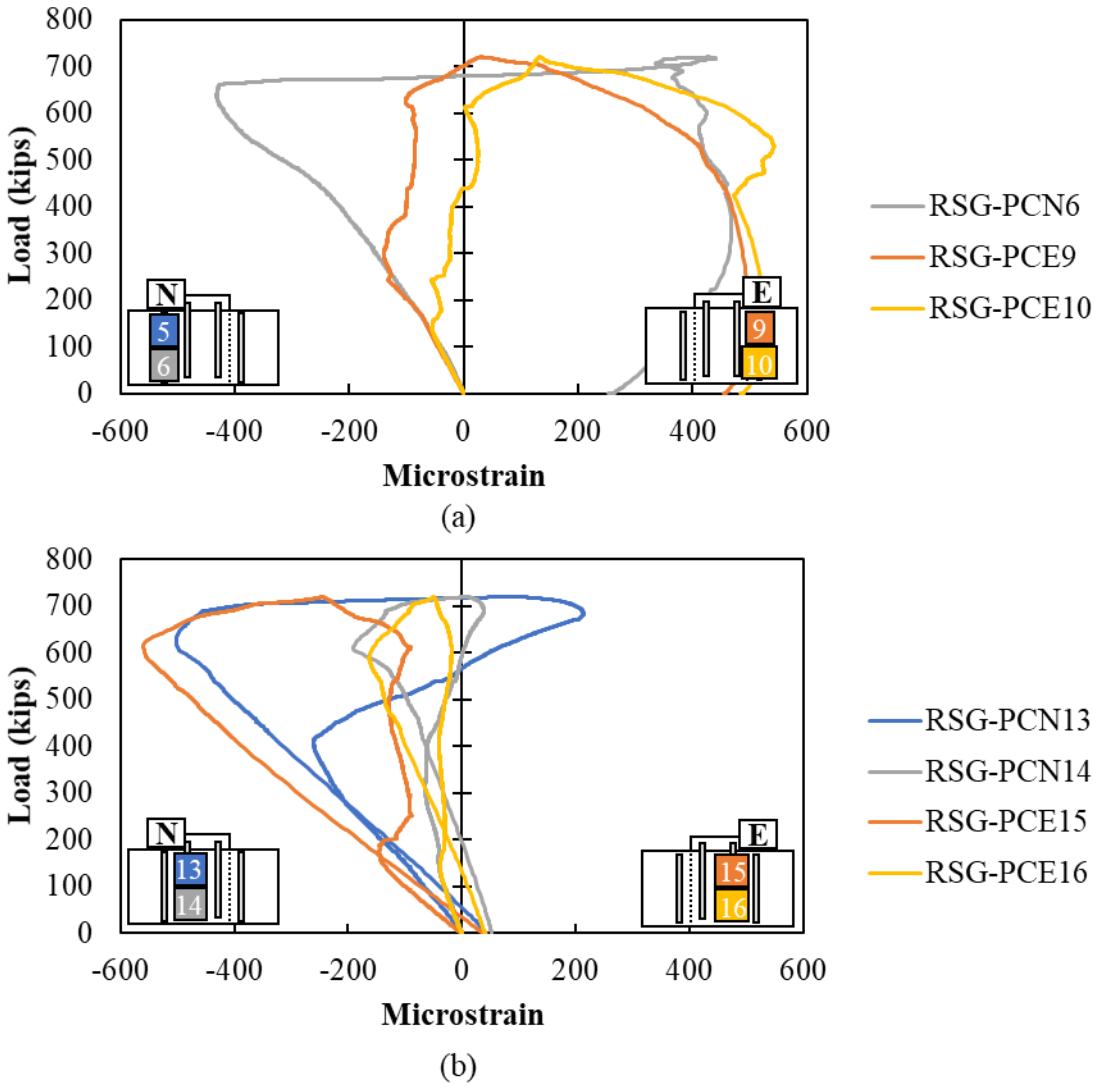

Figure A - 61: Rebar strain gauges in vertical reinforcement on (a) cap and (b) plug of Specimen S2-7.

Specimen S2-8 Results

Specimen S2-8 was 18-inch deep and had a corrugated surface between the cap and plug with sandblasted (1/16'' of roughness) surface preparation. The corrugated interface was created with half spacing for the corrugations (compared to S2-7) by filling in every other corrugation in the interface.

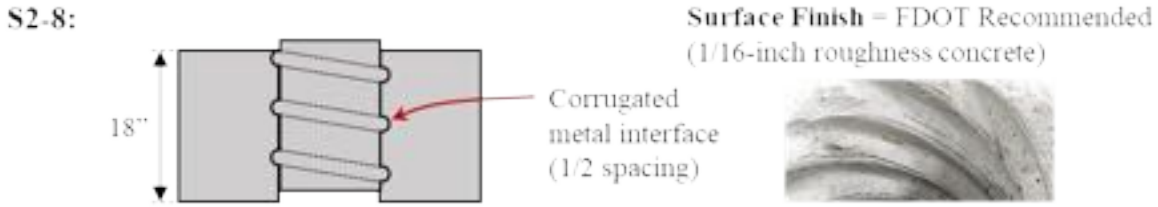

The plug started to slide around 300 kips. The maximum load was 553.5 kips, and after failure the specimen still held a load of 370 kips. The specimen was loaded until 0.45-inch displacement of the plug. The load displacement curve is shown in Figure A - 62.

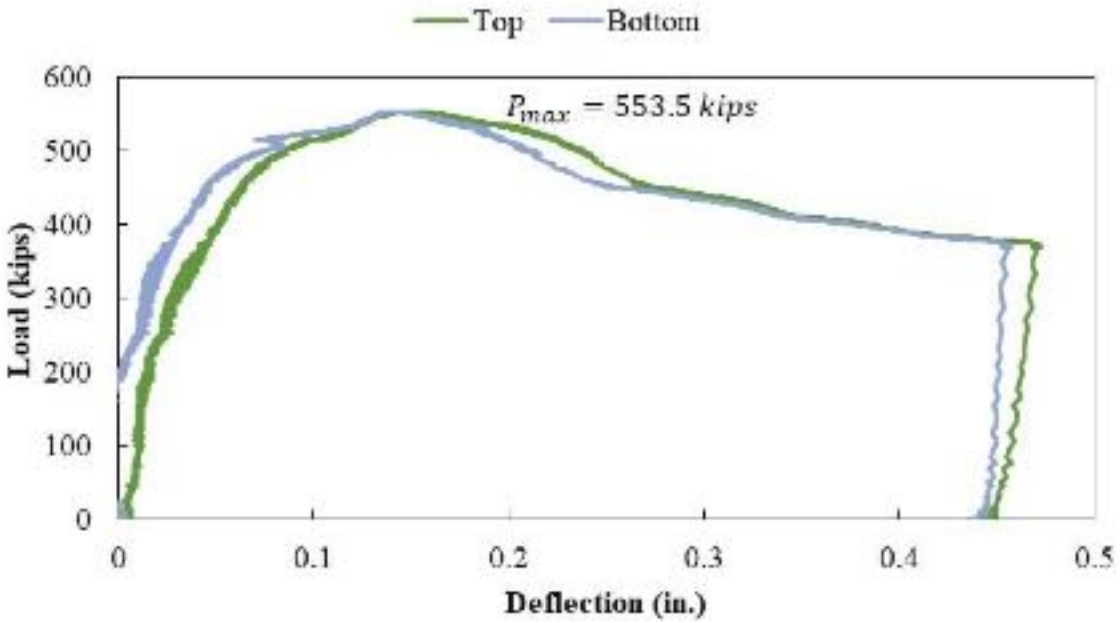

Figure A - 62: Load versus deflection curve for Specimen S2-8

The readings of the stain gauges in the longitudinal reinforcement in the bottom of the specimen are shown in Figure A - 63. The bottom reinforcement started to engage in a load of around 200 kips. A crack opened on the bottom of the specimen at a load 180 kips in the east side of the specimen as can be observed in the gauges RSG-PB3 and RSG-PCB.

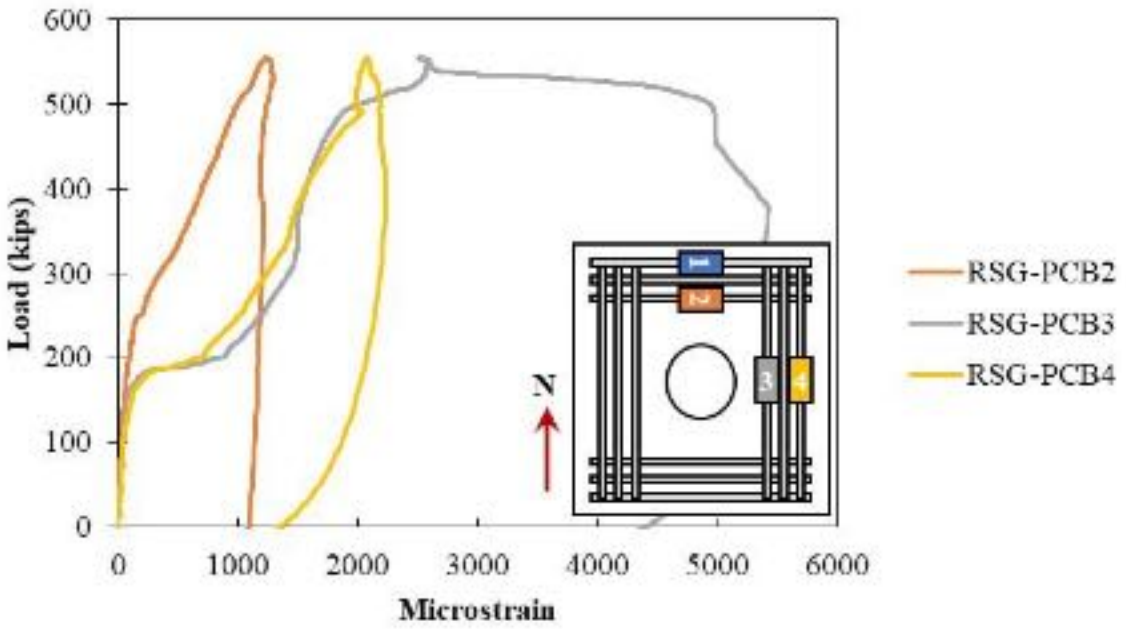

Figure A - 63: Rebar strain gauges in the longitudinal reinforcement on the bottom of Specimen S2-8

Cracking was also observed in the surface concrete at a load of around 130 kips on the bottom gauge on the east side of the specimen (CSG-PCE4). Another crack was read on the north side of the specimen of a load around 160 kips according to CGS-PCN2. As shown in Figure A - 64, the propagation of the cracks started in the bottom of the specimen going towards the top of the cap.

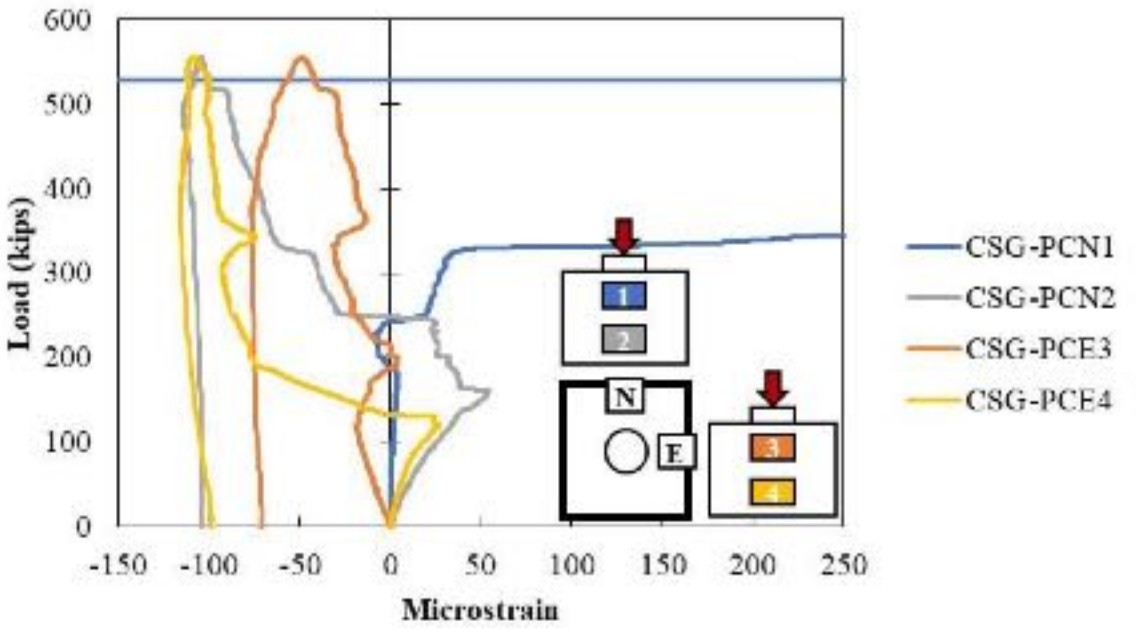

Figure A - 64: Concrete strain gauges in the surface of the cap of Specimen S2-8

Cracking was visually observed as shown in Figure A - 65. As shown in all the results, the plug started to move after formation of the cracks.

Figure A - 65: Cracking on (a) cap and (b) bottom of Specimen S2-8

The confining reinforcement around the pocket were more engaged in the north side of the plug than the east side. However, engagement was observed in the top gauge (RSG-PCE11) on the east side as shown in Figure A - 66. As mentioned before, this distribution of the stresses show that more expansion was transfer to the cap before pushing through of the plug.

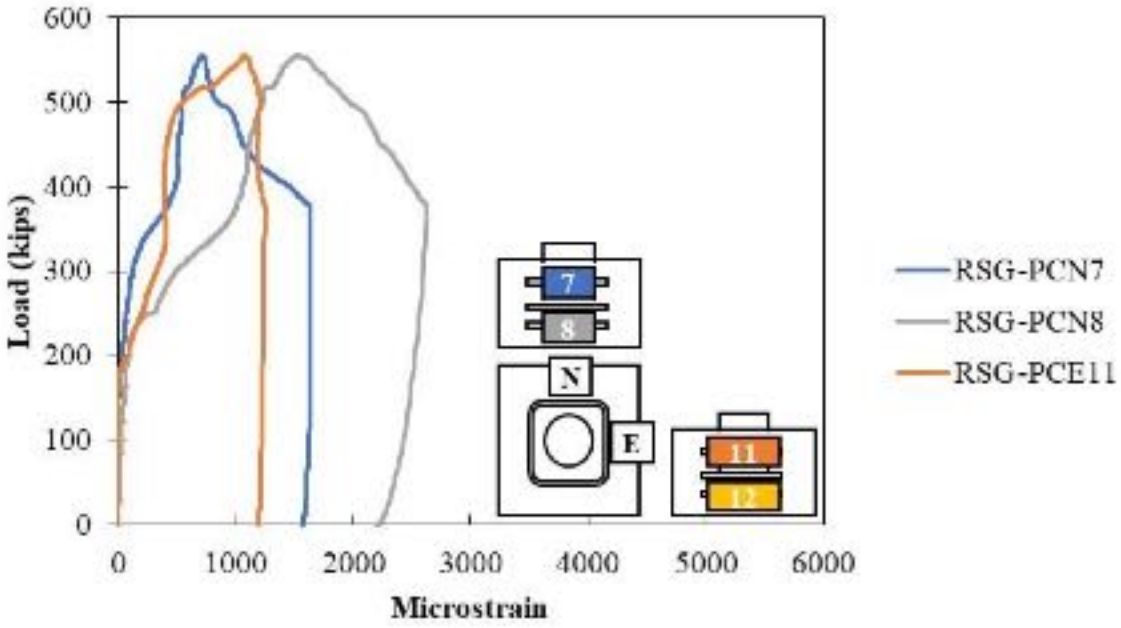

Figure A - 66: Confining reinforcement around the pocket of Specimen S2-8

The measured strains in the vertical reinforcement in the plug and cap are shown in Figure A - 67. As Specimen S2-7 (full corrugated), the stresses in the vertical reinforcement on top of the plug were higher than in the bottom, suggesting transfer of stresses from plug to cap. The measured strains in the cap were similar in all sides and through the height of the interface.

As expected, specimen S2-8 (1/2 corrugated) had less capacity than the specimen S2-7 (full corrugated). Also, similar stresses distributions and cracks propagation was seen during the testing. These results suggest the ribs in the corrugation are effective in transferring stresses between the interfaces.

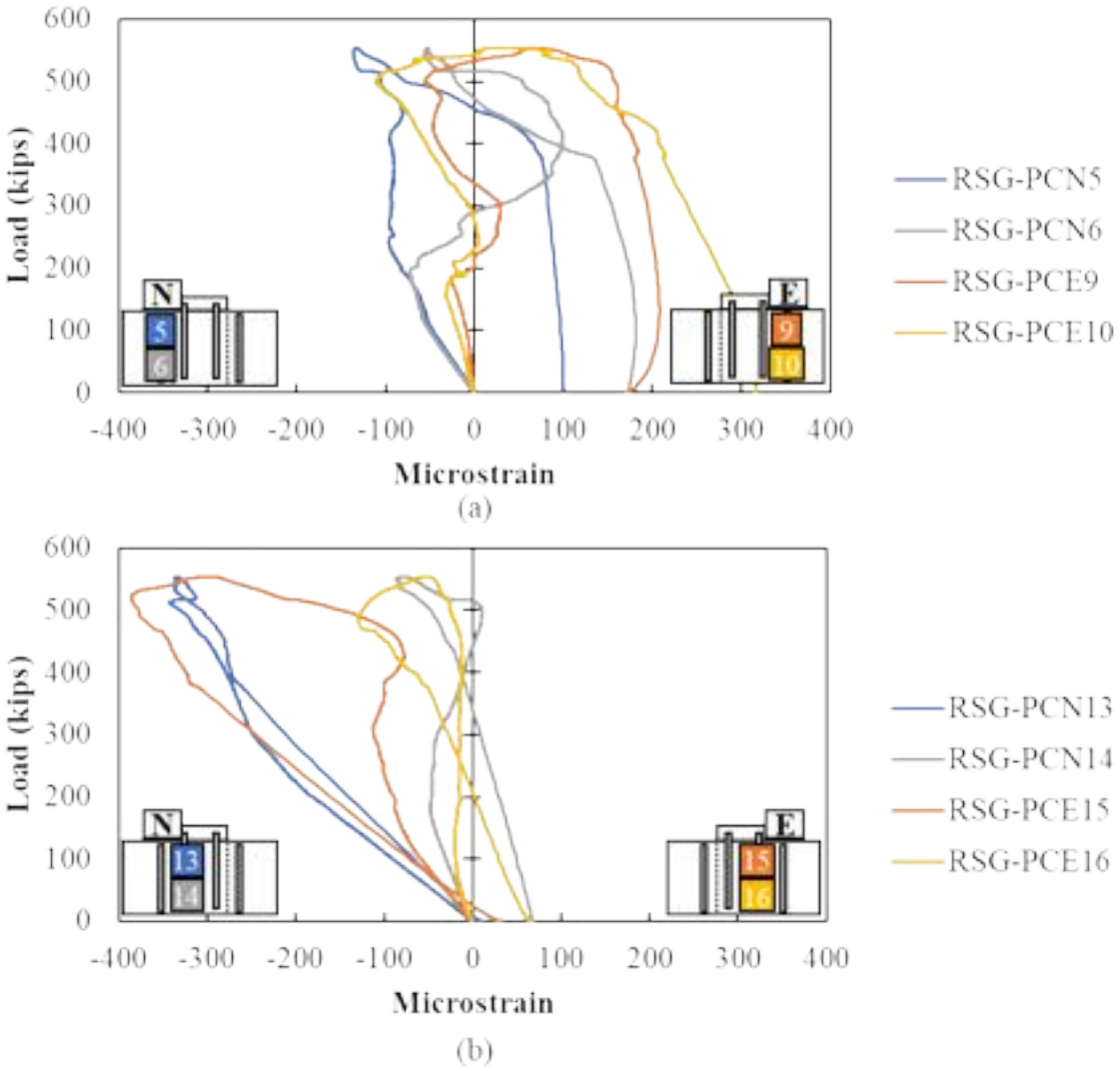

Figure A - 67: Rebar strain gauges in vertical reinforcement on (a) the cap and (b) plug of Specimen S2-8

Specimen S2-9 Results

Specimen S2-9 was 18-inch deep, had a corrugated surface between the cap and plug. The void was created using a corrugated metal pipe, and the pipe was left in place.

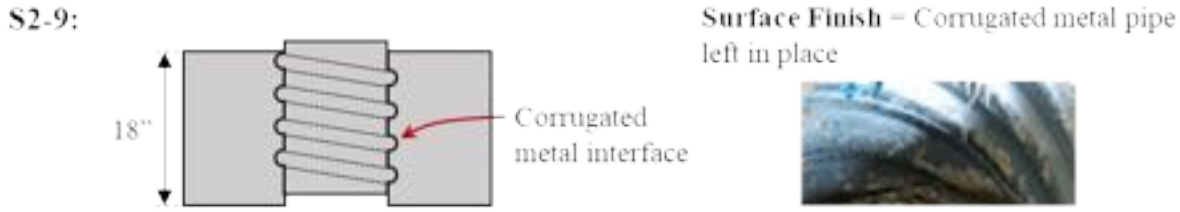

The failure load for this specimen was 662.2 kips. An issue happened with the hydraulic ram at approximately 600 kips, the testing was stopped. The specimen was unloaded and then loaded to failure. The specimen was loaded until 0.6-inch displacement of the plug. The load displacement curve is shown in Figure A - 68.

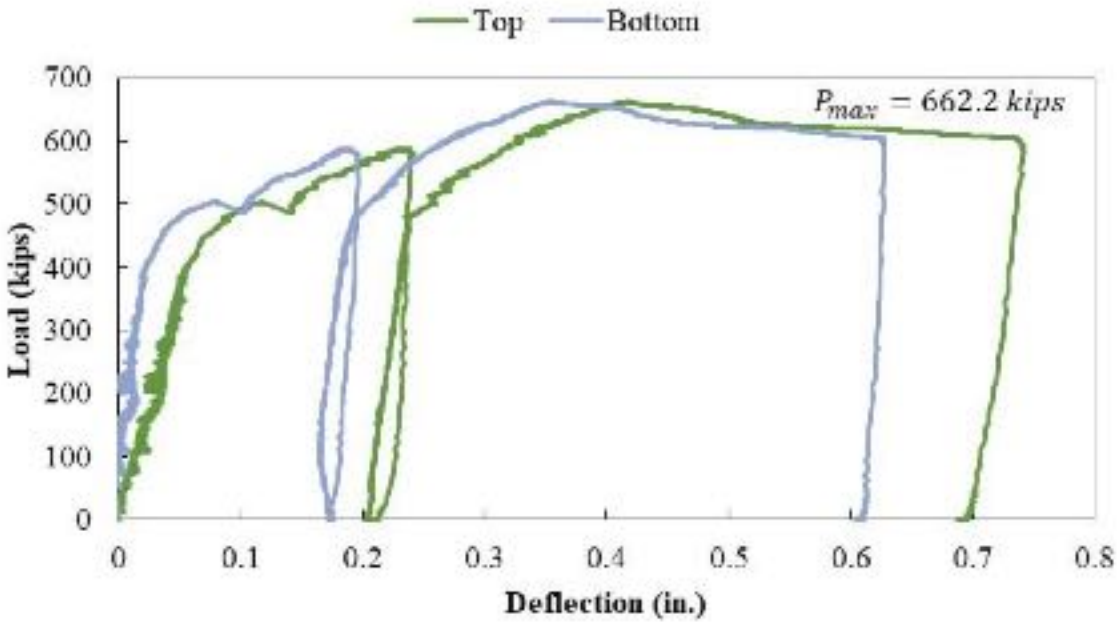

Figure A - 68: Load versus deflection curve for Specimen S2-9

The strain gauges placed in the longitudinal reinforcement in the bottom of the specimen are shown in Figure A - 69. All gauges read engagement of the rebars between 110 kips and 190 kips. Potentially, cracks were forming on the bottom of the specimen on both directions in around the same load.

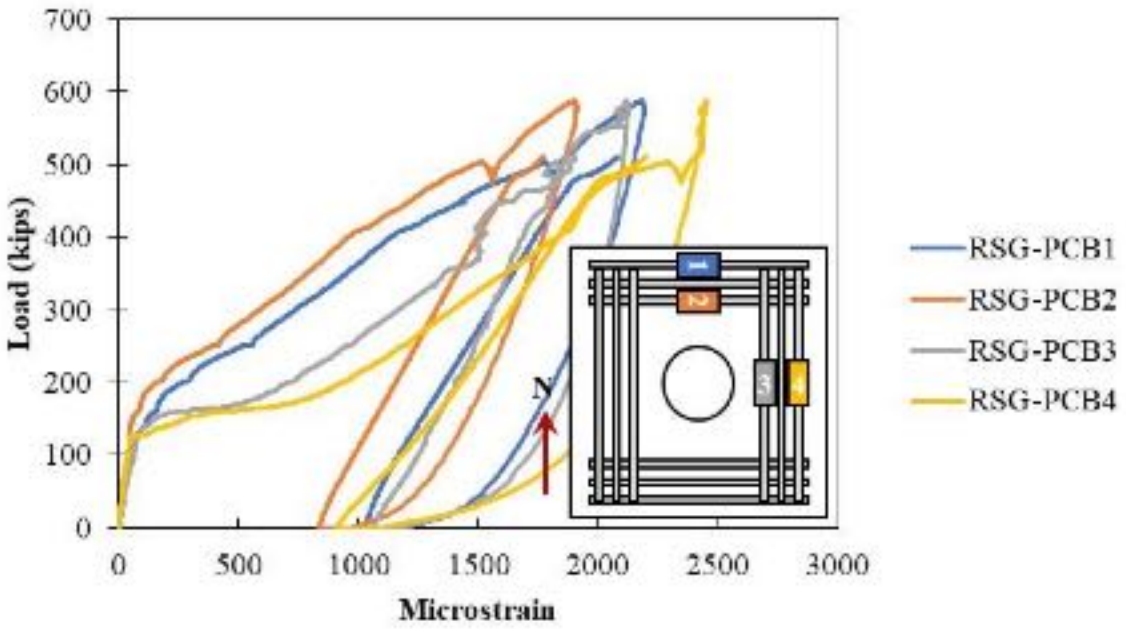

Figure A - 69: Rebar strain gauges in the longitudinal reinforcement on bottom of Specimen S2-9

Cracks were measured in the bottom of the surface concrete in both sides of the specimen around 130 kips. Later, cracks were opened on top of the specimen in both sides too in a load of 420 kips. The reading of the concrete surface gauges is shown in Figure A - 70.

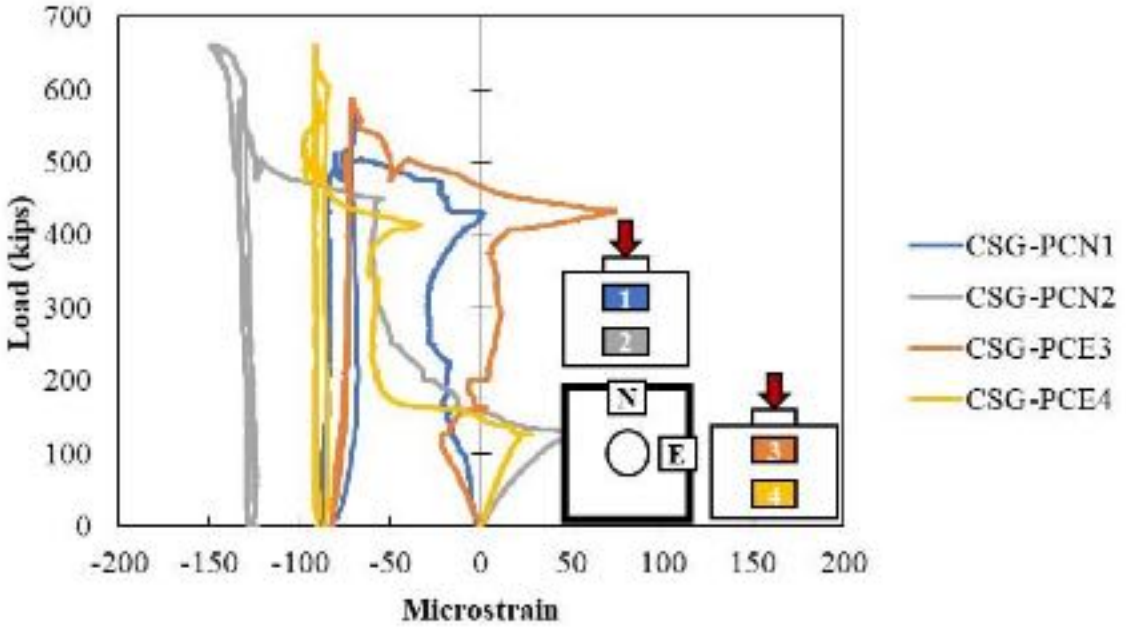

Figure A - 70: Concrete strain gauges in the surface of Specimen S2-9

When the testing was finished, cracks were also observed as shown in Figure A - 71. Cracks extended from the bottom, going up to the cap toward the plug as the reading of the gauges. Bigger cracks were observed on the east-west side than the north-south side of the specimen.

Figure A - 71: Cracking on (a) cap and (b) bottom of Specimen S2-9

The confining reinforcement around the pocket started to engage in both sides of the plug between a load of 150 kips – 200 kips according to the reading of gauges shown in Figure A - 72. Since movement of the plug started of around 400 kips, it seems than there was some expansion of the plug before sliding began.

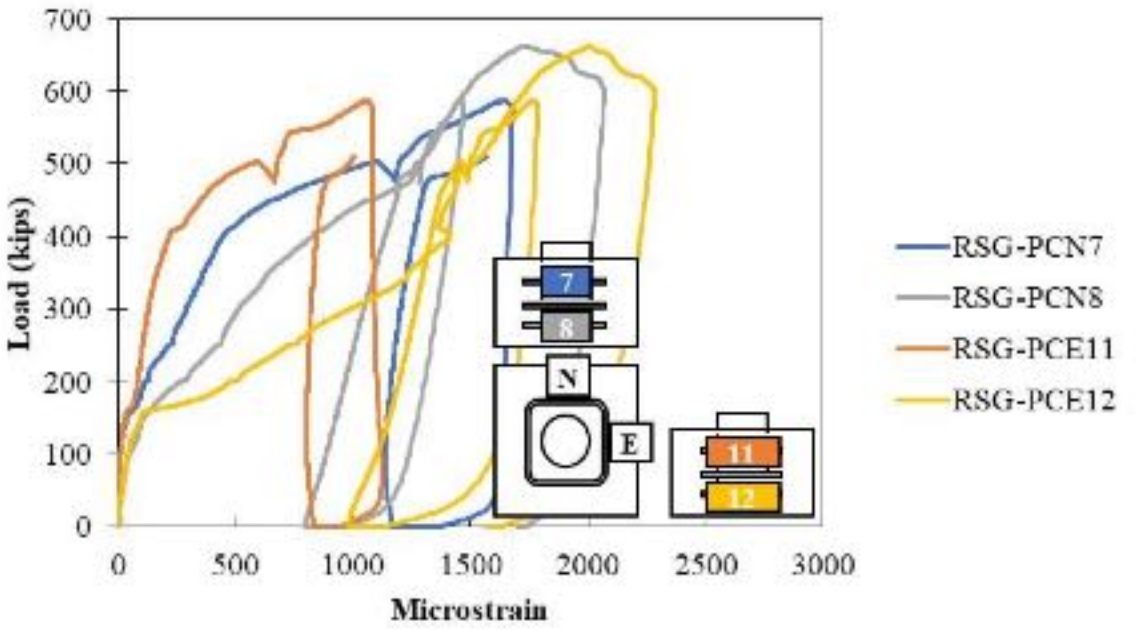

Figure A - 72: Confining reinforcement around the pocket of Specimen S2-9

In this specimen rotation was noticed in the interface. It seems that after the bonding was broken, the plug started to rotate following the corrugation path. This rotation can be observed in Figure A - 73. In Figure A - 73 (b), we can see how the reference lines that were drawn in the plug and cap before the testing does not match after testing.

Figure A - 73: Details of plug rotation in (a) separation of the interface is observed and in (b) reference lines does not mach.

The measured strains in the vertical reinforcement in the cap and plug are shown in Figure A - 74. The vertical strains in the plug decrease toward the bottom of the plug, showing

transfer of stress from plug to cap. The stresses in the cap were similar in each side of the specimen.

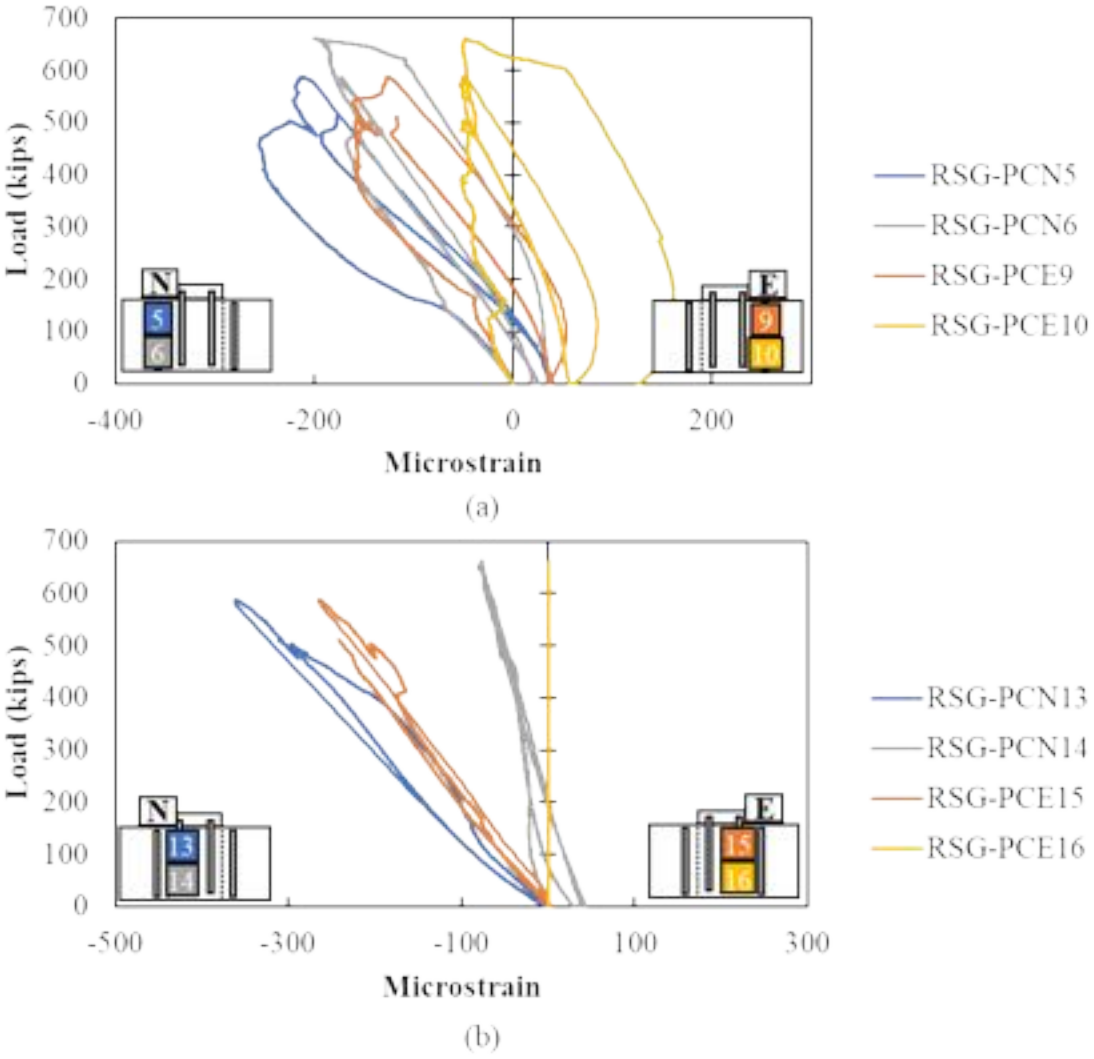

Figure A - 74: Rebar strain gauges in vertical reinforcement on (a) cap and (b) plug of Specimen S2-9

Specimen S2-10 Results

Specimen S2-10 was 14-inch deep, had a corrugated surface between the cap and plug with sandblasted (1/16'' of roughness) surface preparation. The void was created using a corrugated metal pipe.

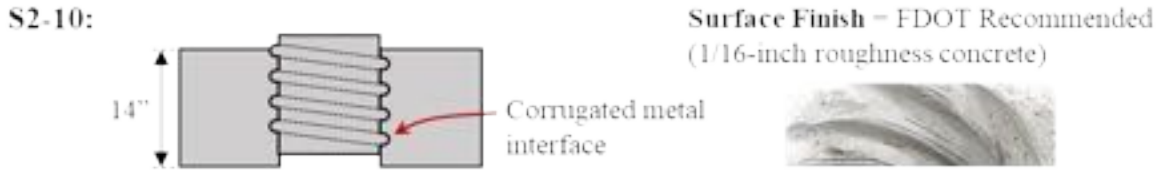

The failure load for this specimen was 575.4 kips. After failure, the specimen still held a load of around 330 kips. The specimen was loaded until 0.5-inch displacement of the plug. The load displacement curve is shown in Figure A - 75.

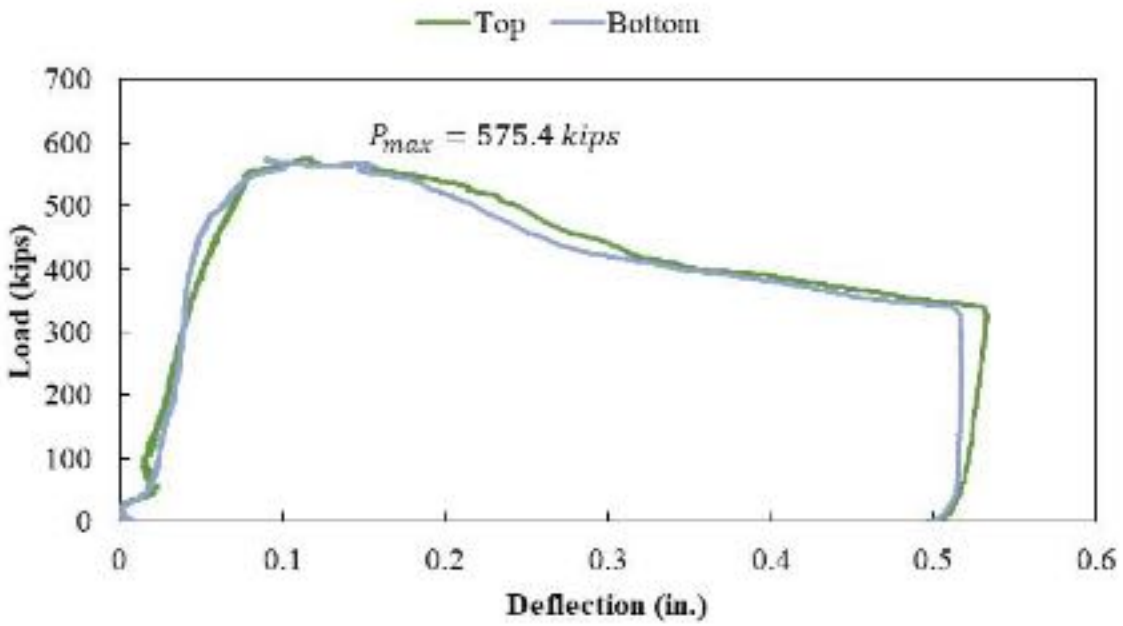

Figure A - 75: Load versus deflection curve for Specimen S2-10

The bottom reinforcement placed on the north side of the specimen started to engage on a load around 150 kips according to the RSG-PCB1 and RSG-PCB2 gauges. Later when the load was around 300 kips the longitudinal reinforcement on the east side of the specimen was also engaged. Potentially, cracks were forming on the bottom of the specimen on both

directions. The reading of the longitudinal reinforcement in the bottom is shown in Figure A - 76.

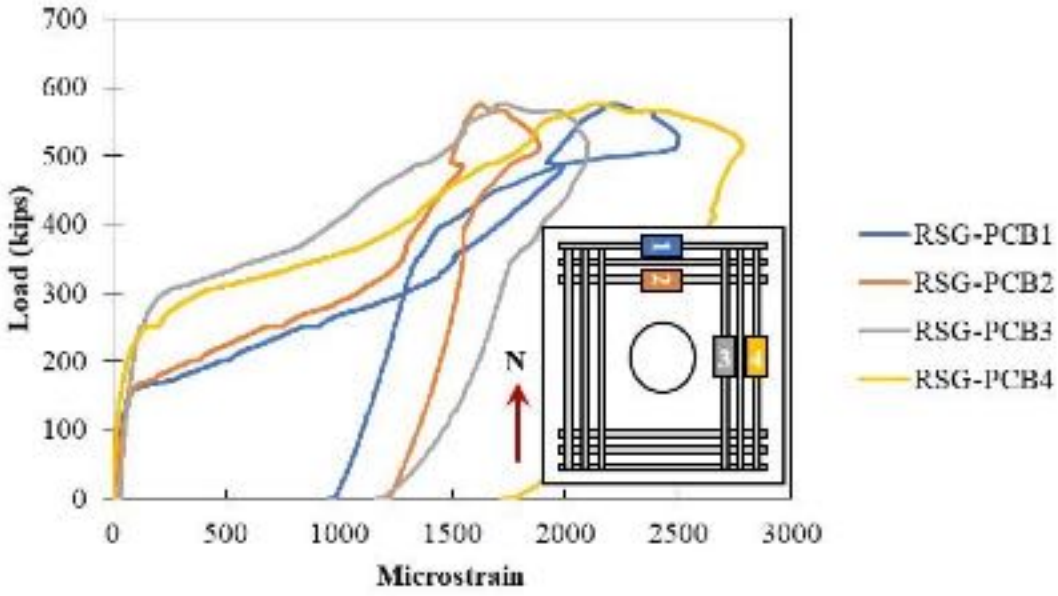

Figure A - 76: Rebar strain gauges in the longitudinal reinforcement on bottom of Specimen S2-10

A crack was measured around 170 kips on the north side of the specimen in the bottom part with the concrete surface gauges. Later, when the load was around 230 kips another crack was measured in the east side of the specimen according to CSG-PCE4. Crack propagation seemed to start at the bottom part of the specimen towards the top. The reading of the concrete surface gauges is shown in Figure A - 77.

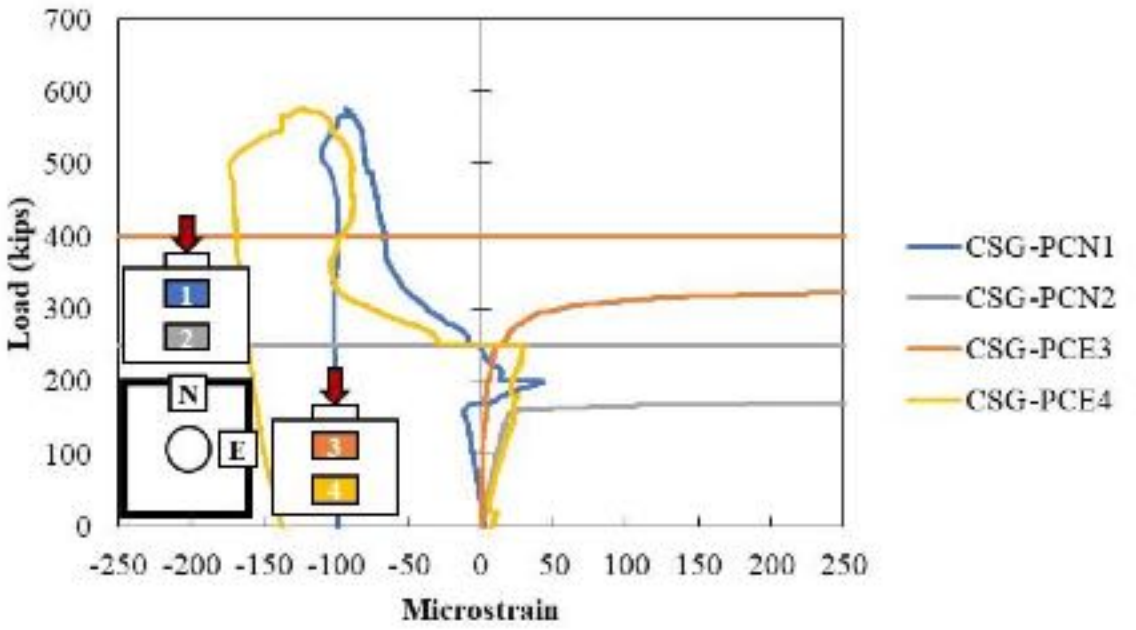

Figure A - 77: Concrete strain gauges in the surface of Specimen S2-10

When the testing was finished, cracks were also observed as shown in Figure A - 78. Even though cracking started on the north side of the specimen, bigger cracks were observed on the east-west side than the north-south side of the specimen.

Figure A - 78: Cracking on (a) cap and (b) bottom of Specimen S2-10

The confining reinforcement around the pocket started to engage in the north side of the plug of a load around 180 kips according to gauge RSG-PCN8. The other side of the specimen started to engage around 300 kips according to RSG-PCE11 and RSG-PCE12. The measured strains in the confining reinforcement are shown in Figure A - 79.

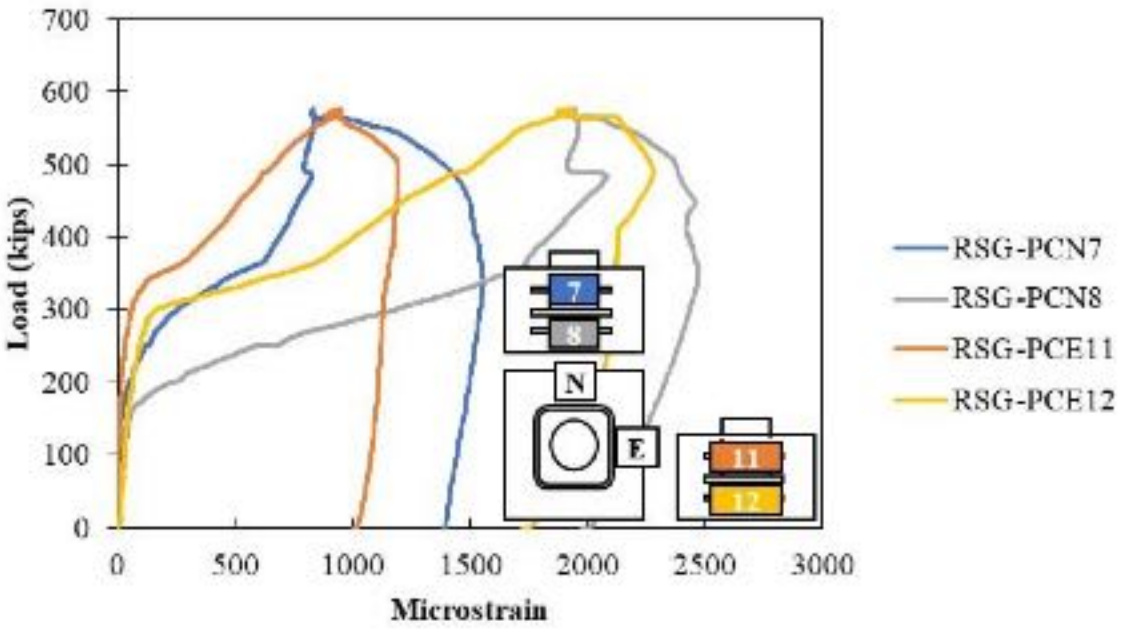

Figure A - 79: Confining reinforcement around the pocket of Specimen S2-10

The measured strains in the vertical reinforcement in the cap and plug are shown in Figure A - 80. The vertical strains in the plug decrease toward the bottom of the plug, showing transfer of stress from plug to cap. The stresses in the cap were similar in each side of the specimen, and through the height of the specimen. The use of corrugations to create an interface showed a good transfer of stresses in the interface.

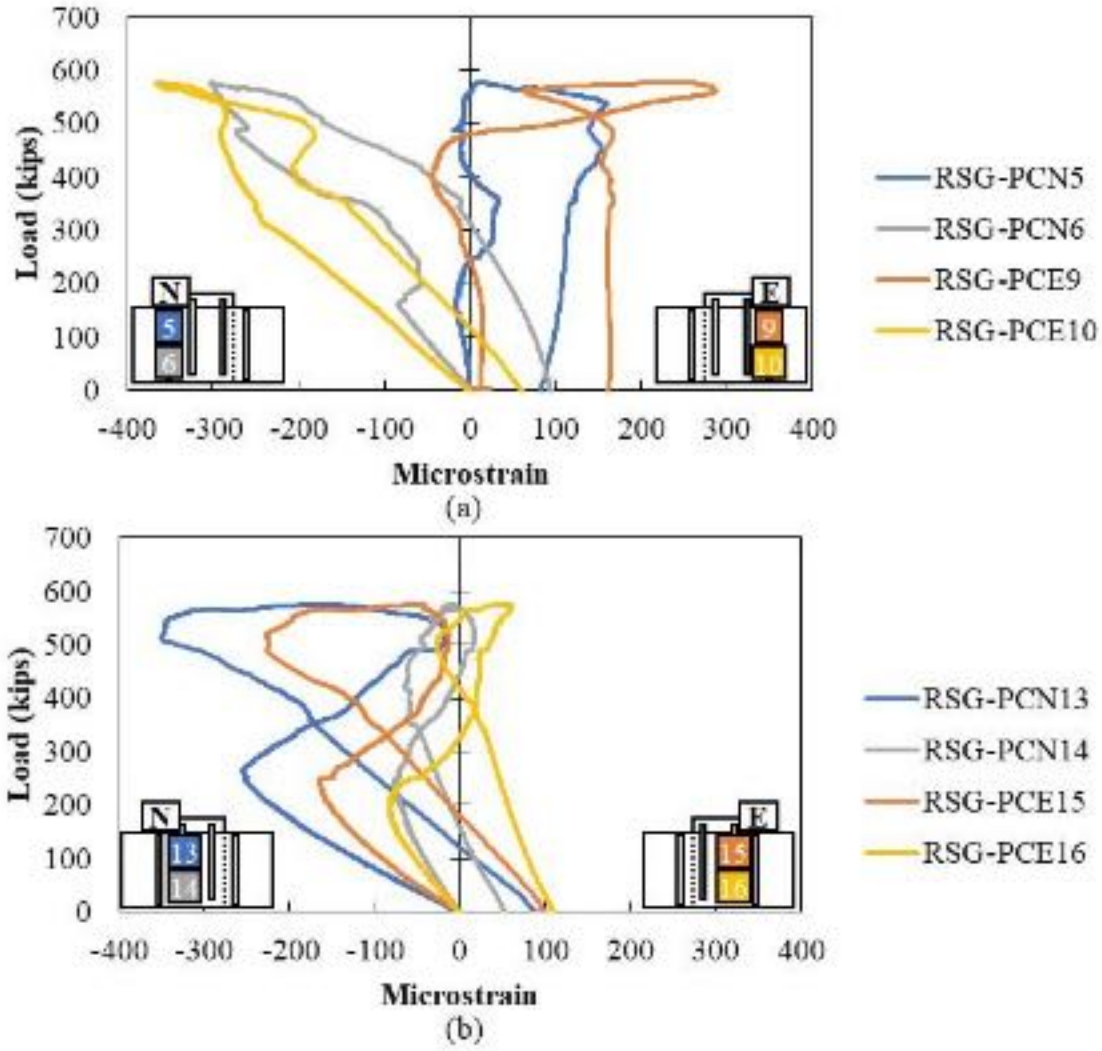

Figure A - 80: Rebar strain gauges in vertical reinforcement on (a) cap and (b) plug of Specimen S2-10

Specimen S2-11 Results

Specimen S2-11 was 14-inch deep, had a corrugated surface between the cap and plug with sandblasted (1/16'' of roughness) surface preparation. Like S2-8, every other corrugation in the plug was filled in during cap construction to create a half-spacing corrugation.

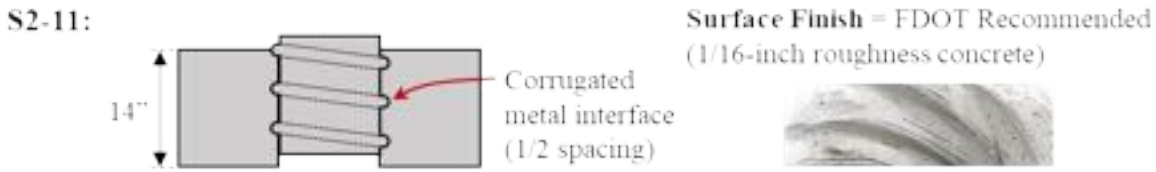

The plug started to slide around 300 kips; more sliding was observed after failure of the specimen. The maximum load was 399.8 kips, and after failure the specimen still held a load of 270 kips. The specimen was loaded until almost 0.50-inch displacement of the plug. The load displacement curve is shown in Figure A - 81.

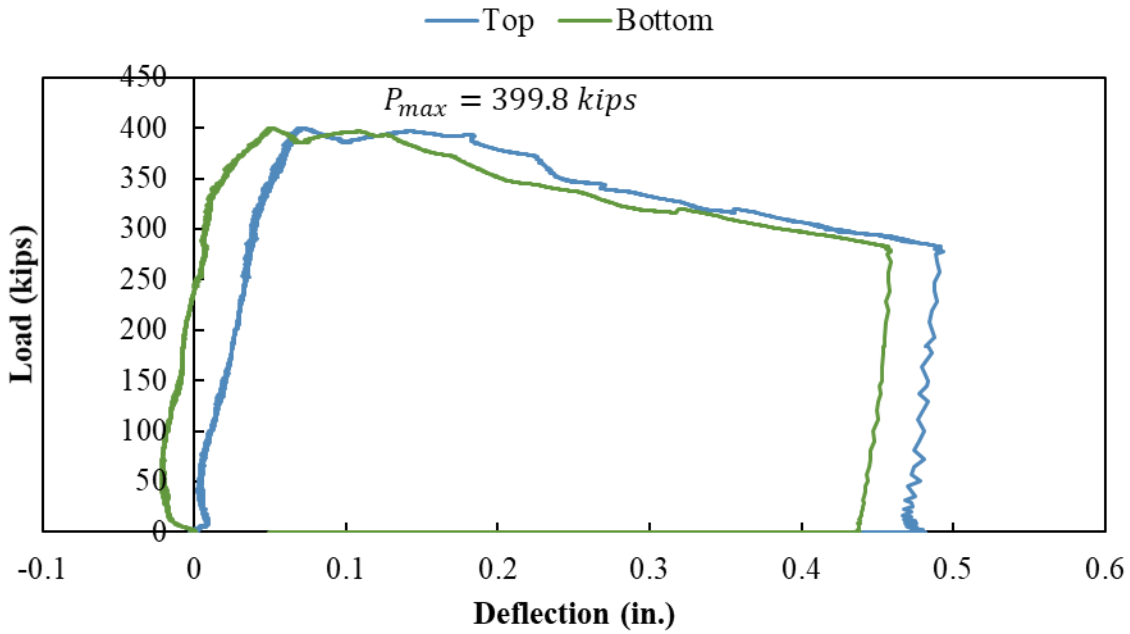

Figure A - 81: Load versus deflection curve for Specimen S2-11

The readings of the stain gauges in the longitudinal reinforcement in the bottom of the specimen are shown in Figure A - 82. The bottom reinforcement started to engage in the east side at a load of around 100 kips. Later, when the load was 150 kips the reinforcement

placed on the north side started to get engaged too. Potentially, cracks started to form in the bottom of the specimen.

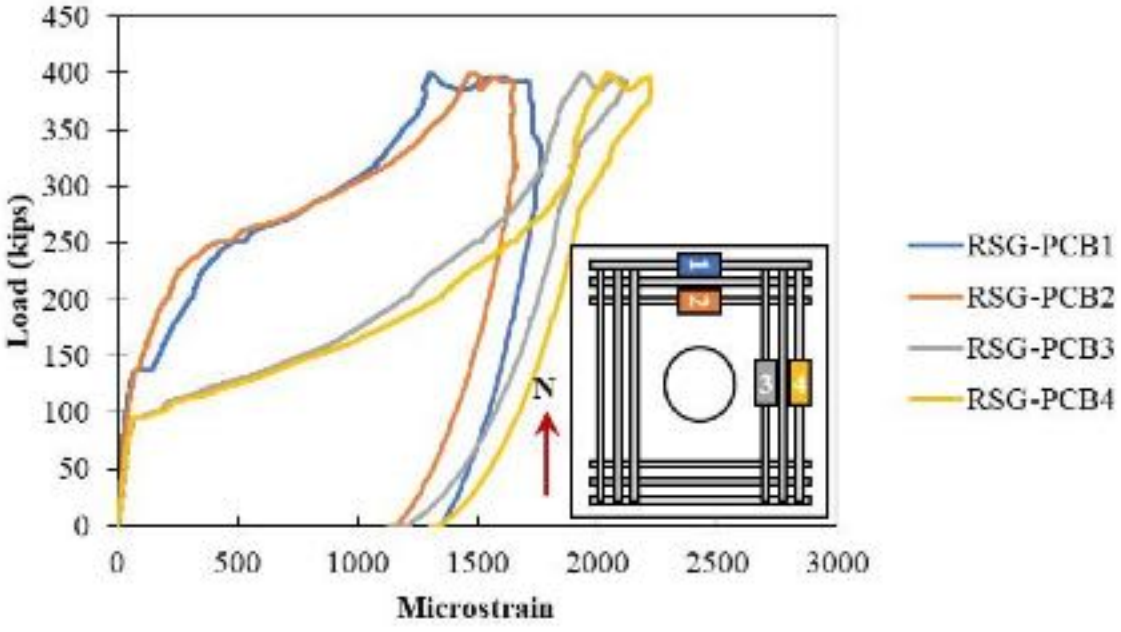

Figure A - 82: Rebar strain gauges in the longitudinal reinforcement on the bottom of Specimen S2-11

Cracking was also observed in the surface concrete at a load of around 100 kips on the east side of the specimen according to CSG-PCE3 and CSG-PCE4. As shown in Figure A - 83, the propagation of the cracks started in the bottom of the specimen going towards the top of the cap.

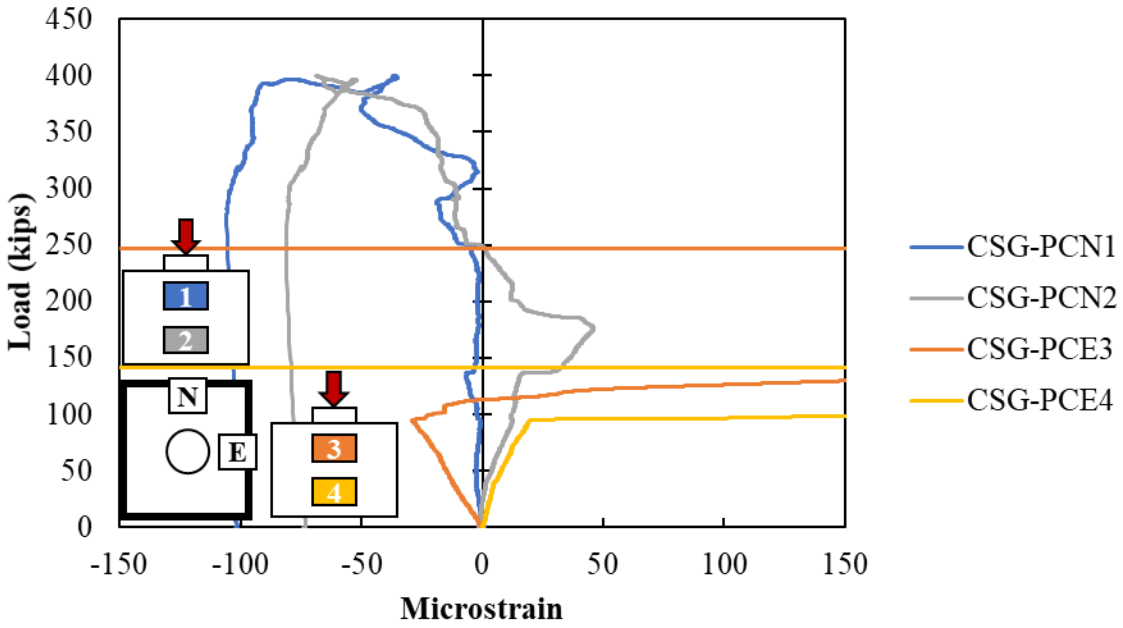

Figure A - 83: Concrete strain gauges in the surface of the cap of Specimen S2-11

Cracking was visually observed as shown in Figure A - 84. As shown in all the results, the plug started to move after propagation of the cracks. Meaning that expansion of the plug happened before sliding.

Figure A - 84: Cracking on (a) cap and (b) bottom of Specimen S2-11

The confining reinforcement around the pocket were first engaged in the east side of the plug on a load of around 100 kips. When the load was around 250 kips, the reinforcement in the north side of the specimen started to engage too. The reading of the gauges placed in the confining reinforcement are shown in Figure A - 85.

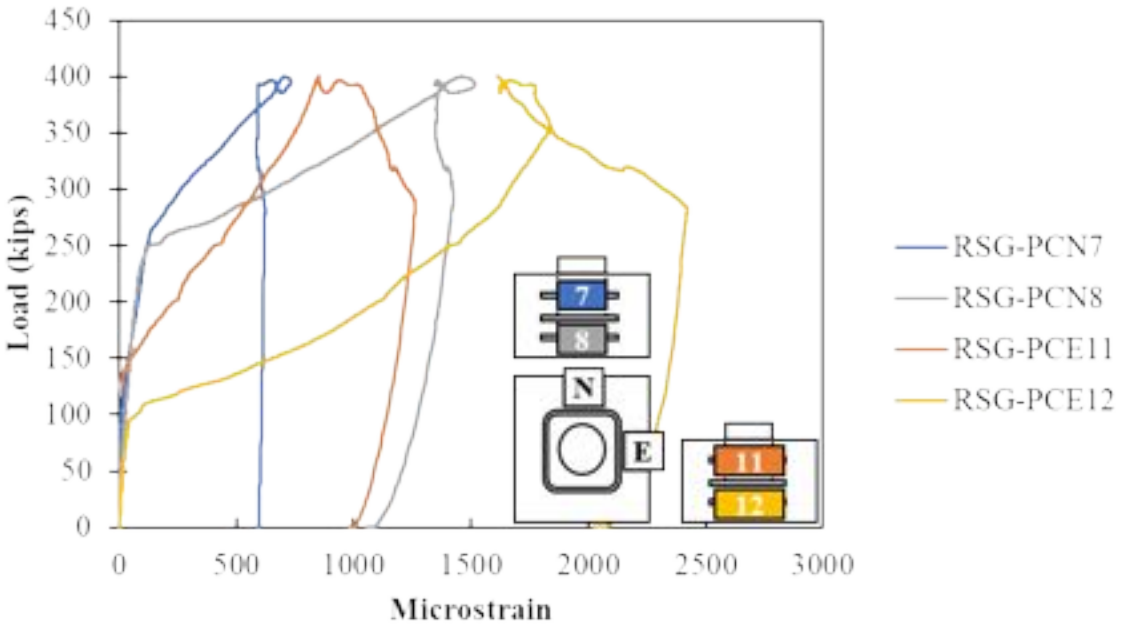

Figure A - 85: Confining reinforcement around the pocket of Specimen S2-11

The measured strains in the vertical reinforcement in the plug and cap are shown in Figure A - 86. The stresses in the vertical reinforcement in the top of the plug were higher than in the bottom, suggesting transfer of stresses from plug to cap. The measured strains in the cap were similar in all sides and through the height of the interface.

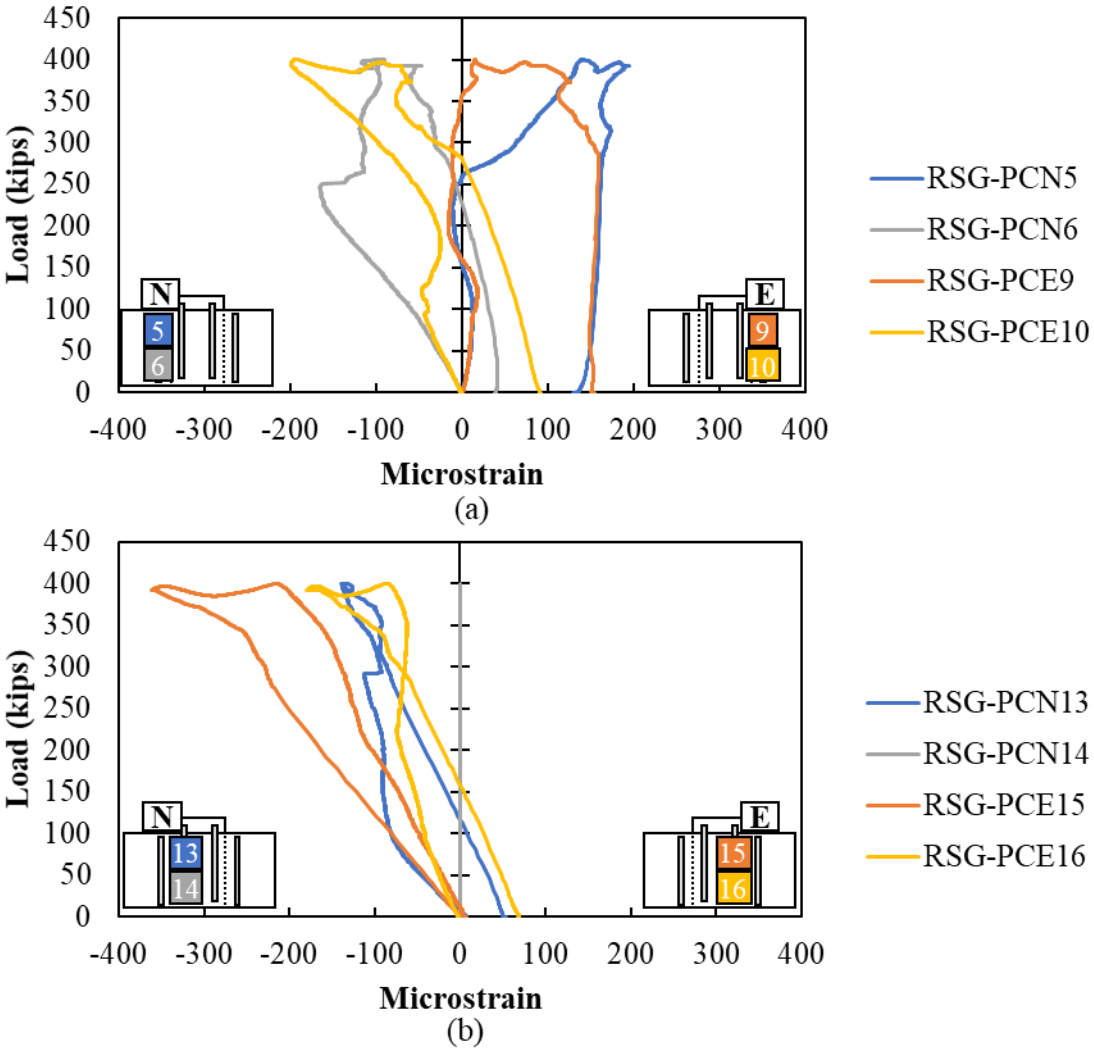

Figure A - 86: Rebar strain gauges in vertical reinforcement on (a) the cap and (b) plug of Specimen S2-11

Specimen S2-12 Results

Specimen S2-12 was 14-inch deep, had a corrugated surface between the cap and plug. The void was created using a corrugated metal pipe, and the pipe was left in place.

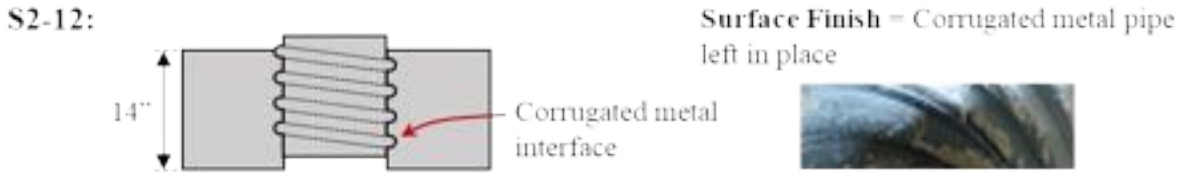

The plug started to slide at a load of around 300 kips. The failure load for this specimen was 521.6 kips. The specimen was loaded until 0.6-inch displacement of the plug. The load displacement curve is shown in Figure A - 87.

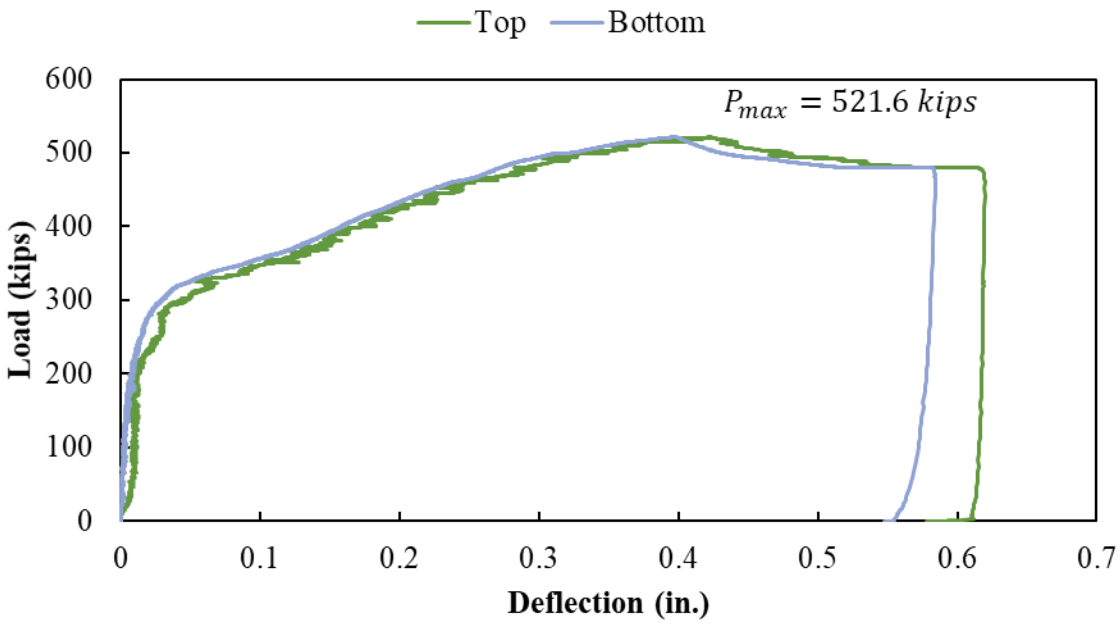

Figure A - 87: Load versus deflection curve for Specimen S2-12

The strain gauges placed in the longitudinal reinforcement in the bottom of the specimen are shown in Figure A - 88. All gauges read engagement of the rebars between 100 kips and 200 kips. Potentially, cracks were forming on the bottom of the specimen on both directions around the same load.

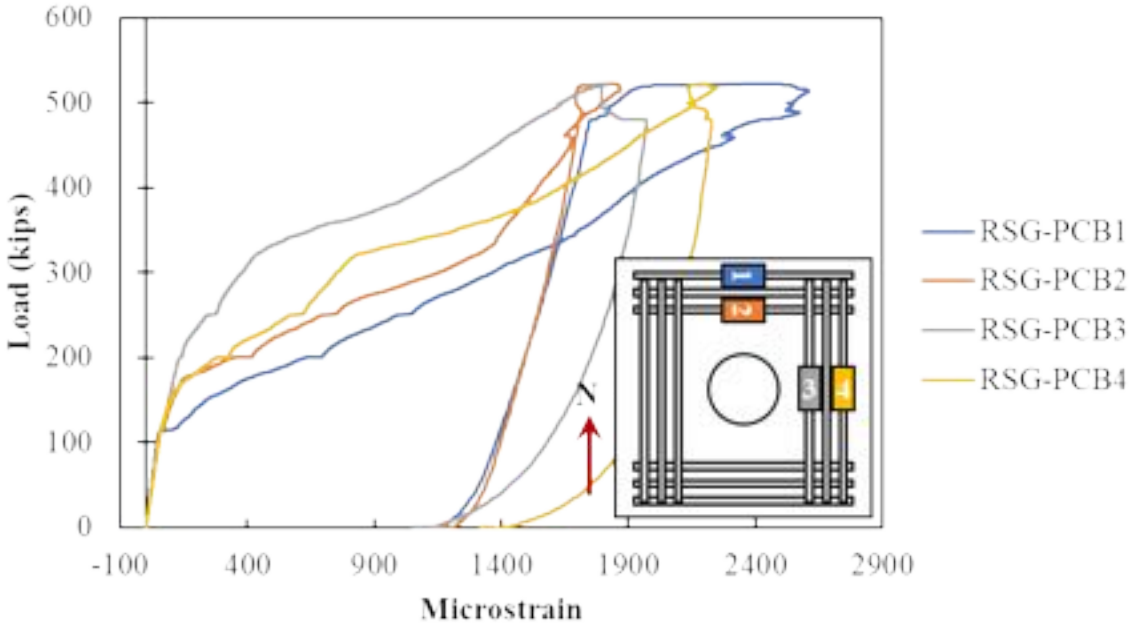

Figure A - 88: Rebar strain gauges in the longitudinal reinforcement on bottom of Specimen S2-12

Cracks were also measured in the surface concrete in both sides of the specimen around 100 kips. The reading of the concrete surface gauges is shown in Figure A - 89.

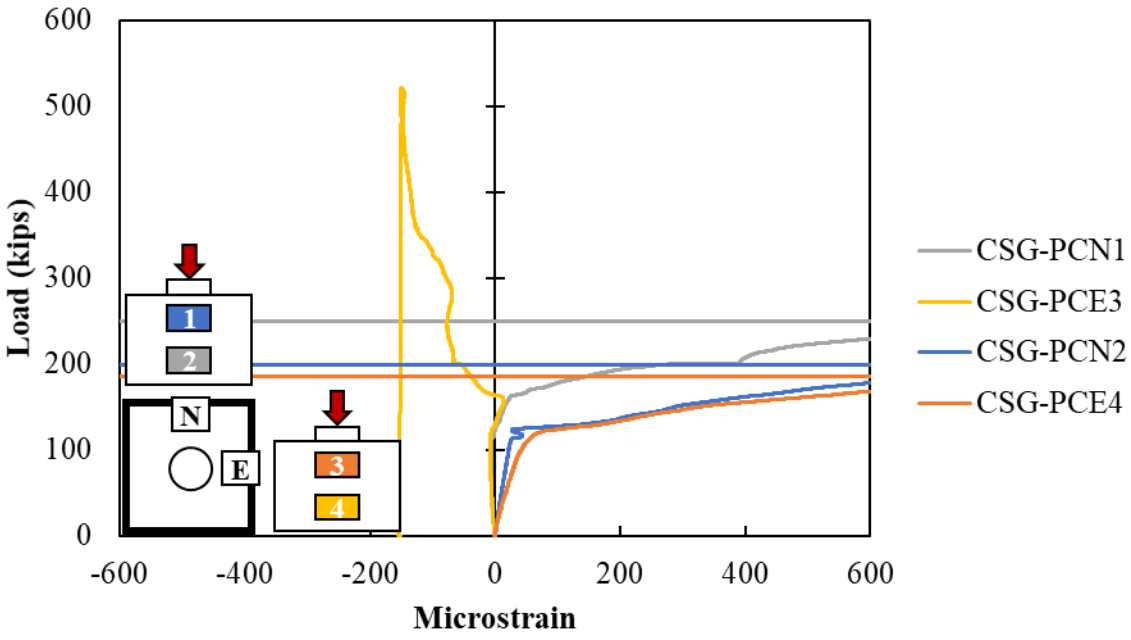

Figure A - 89: Concrete strain gauges in the surface of Specimen S2-9

When the testing was finished, cracks were also observed as shown in Figure A - 90. Cracks extended from the bottom, going up to the cap toward the plug as the reading of the gauges. Bigger cracks were observed on the north-south side than the east-west side of the specimen.

Figure A - 90: Cracking on (a) cap and (b) bottom of Specimen S2-12

The confining reinforcement around the pocket started to engage in both sides of the plug after 200 kips of loading according to the reading of gauges shown in Figure A - 91. Since movement of the plug started of around 300 kips, it seems than there was some expansion of the plug before sliding began.

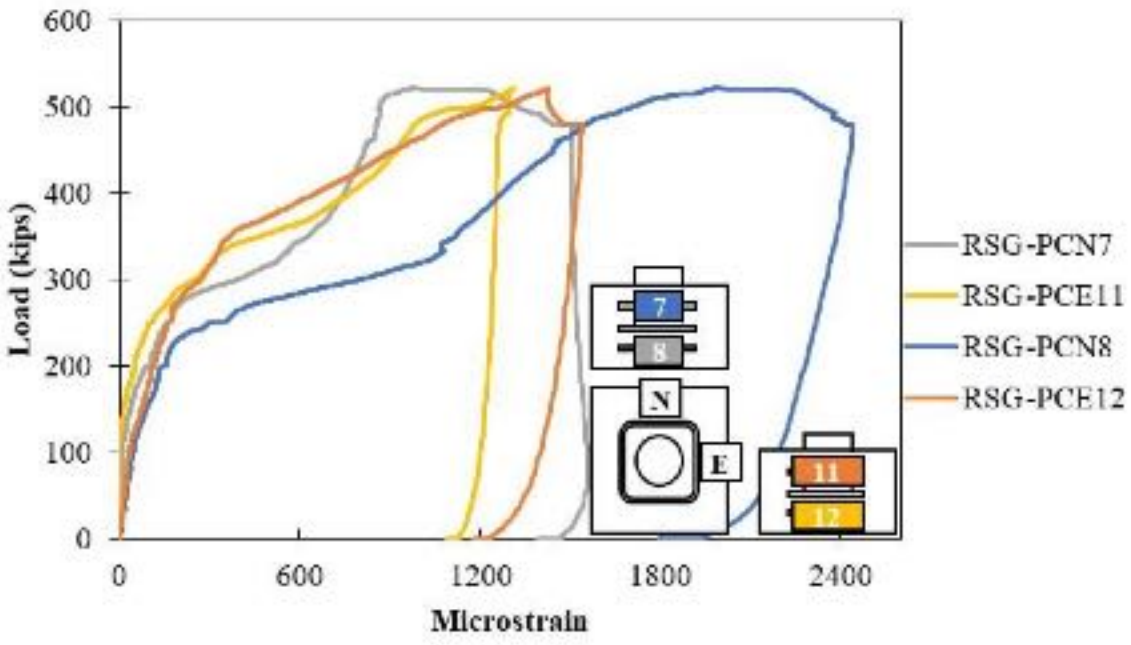

Figure A - 91: Confining reinforcement around the pocket of Specimen S2-12

As well as specimen S2-9, in this specimen rotation was noticed in the interface. This time, the rotation was measure using a string potentiometer as shown in Figure A - 93(a). The load versus rotation of the plug was plotted as shown in Figure A - 92. Besides this graph, the rotation was observed after testing was finished (Figure A - 93). In Figure A - 93(b), we can see how the reference lines that were drawn in the plug and cap before the testing does not match after testing.

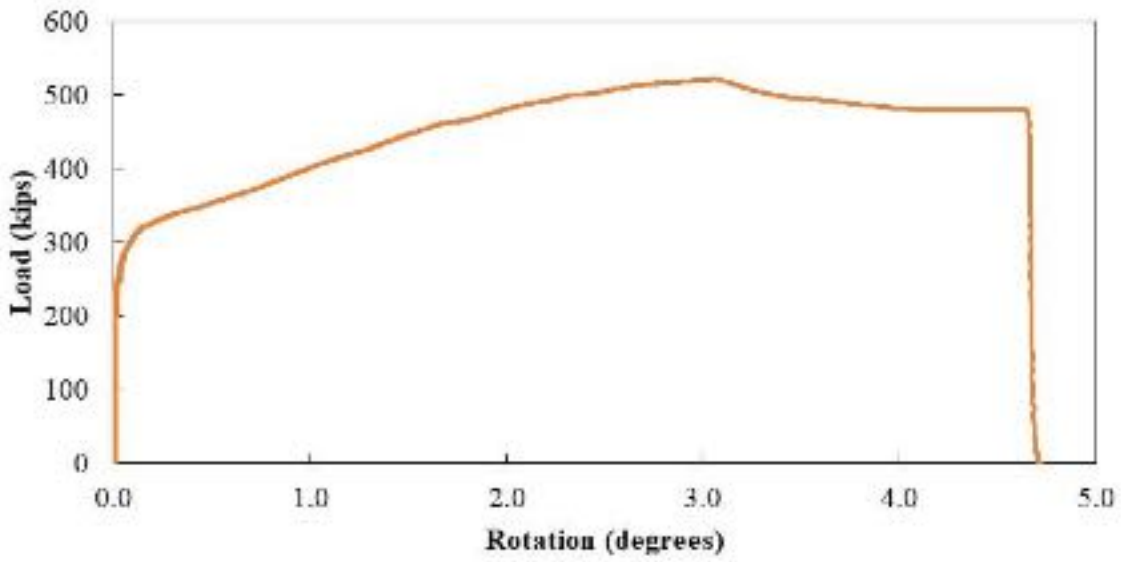

Figure A - 92: Load versus rotation (degrees) of the plug of Specimen S2-12

Figure A - 93: Details of plug rotation (a) before testing (b) after testing of specimen S2-12

The measured strains in the vertical reinforcement in the cap and plug are shown in Figure A - 94. The vertical strains in the cap decrease toward the bottom of the specimen, showing transfer of stress from cap to plug. The stresses in the plug were higher in the bottom and then decreased towards the top of the plug.

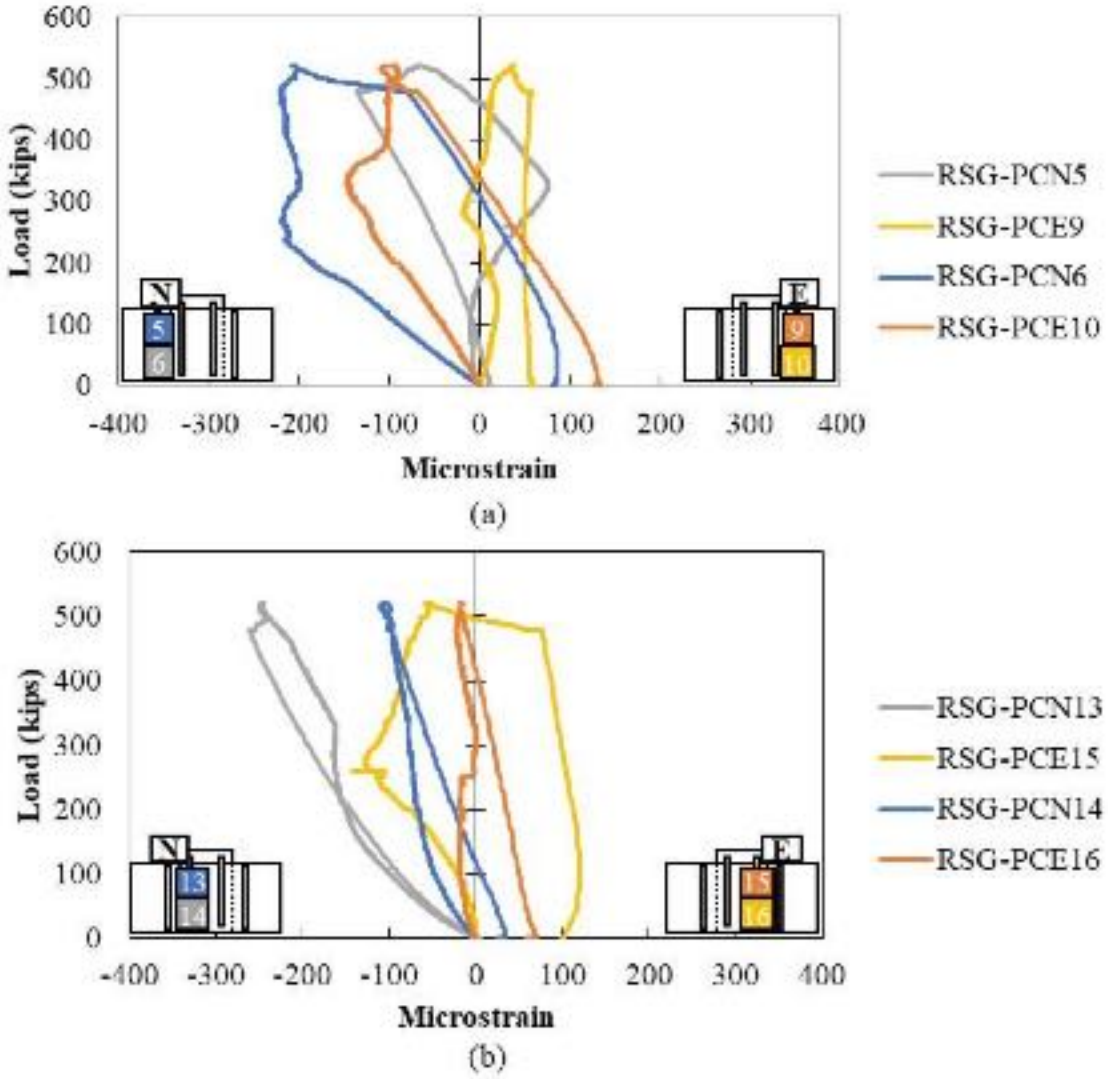

Figure A - 94: Rebar strain gauges in vertical reinforcement on (a) cap and (b) plug of Specimen S2-12

Specimen S2-13 Results

Specimen S2-13 was 18-inch deep, had a smooth surface between the cap and plug with sandblasted (1/16'' of roughness) surface preparation. The equivalent specimen is S2-1.

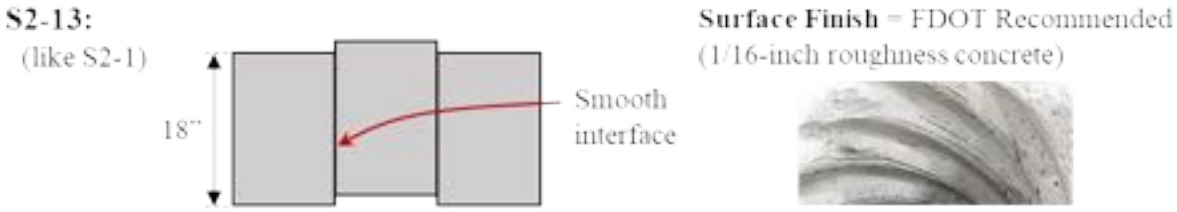

The load versus deflection plot for S2-13 is shown in Figure A - 95. The specimen held a load of around 420 kips when the plug started to move, and then the specimen continued to take additional load until its maximum load of 605.60 kips. The specimen was loaded until 0.45 inches of plug movement. The difference in the capacity between S2-1 and S2-13 is thought to be related to the sensitivity of the smooth interface to surface finish and casting procedure for the plug.

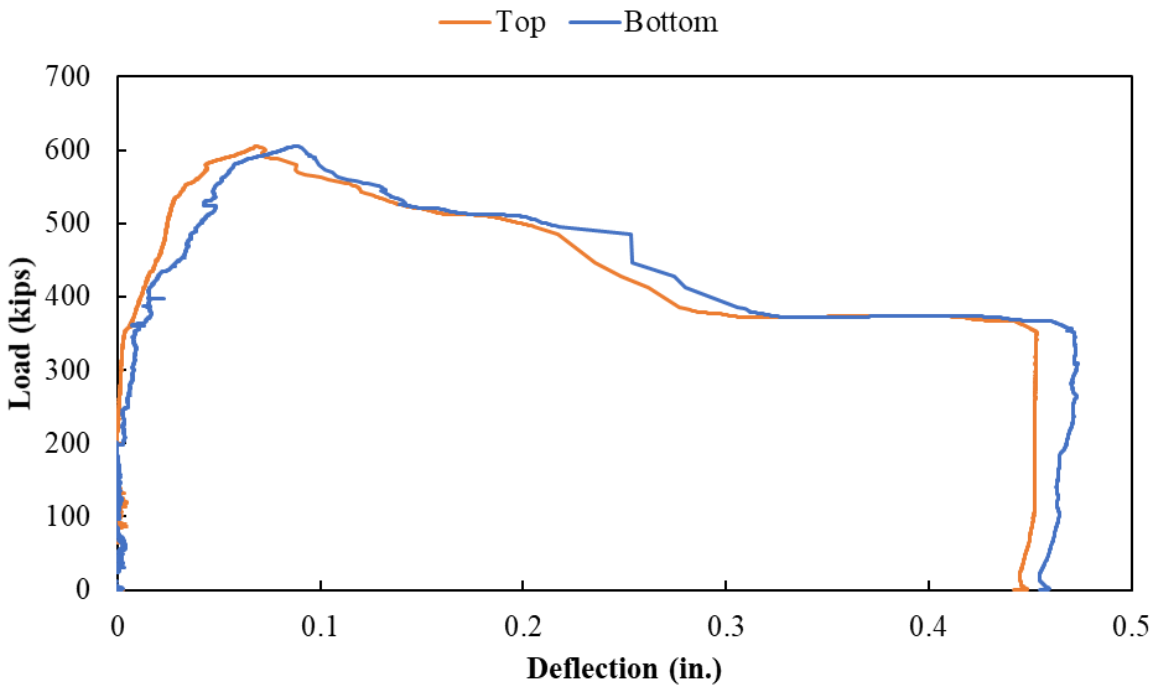

Figure A - 95: Load-Displacement curve for Specimen S2-13.

Cracking was observed in the concrete strain gauges and visually after the test was completed as shown in Figure A - 96 and Figure A - 97. Cracks were observed to extend from the bottom of the cap onto the top toward the plug in the north and south side around 360 kips.

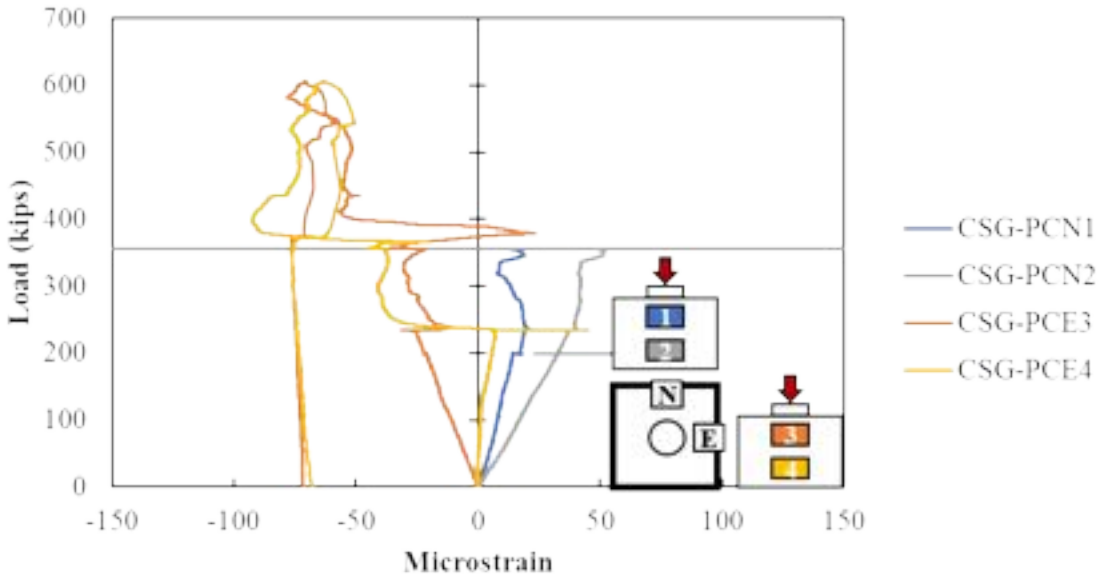

Figure A - 96: Concrete strain gauge on the concrete surface of Specimen S2-13

Figure A - 97: Cracking on the (a) east side and (b) bottom of specimen S2-13

Specimen S2-14 Results

Specimen S2-14 was 14-inch deep, had a smooth surface between the cap and plug with sandblasted surface finish.

The maximum capacity was 441.3 kips. The laser displacement placed on top of the plug indicated sliding around 250 kips however faster movement was observed in the bottom part of the plug as shown in Figure A - 98.

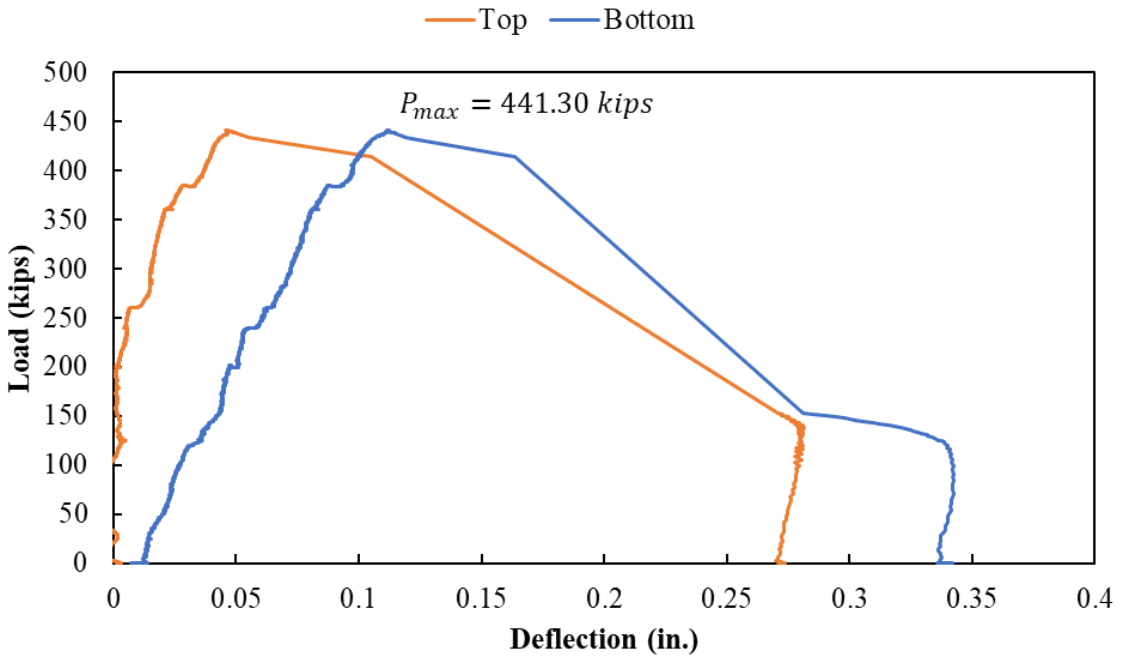

Figure A - 98: Load displacement curve for Specimen S2-14

Cracking was observed in the surface concrete at a load of around 130 kips in the north side of the specimen as shown in Figure A - 99. In this specimen, cracking was later observed in the east side on a load of around 250 kips. Crack propagation was initiated from the bottom to the top of the cap. The crack pattern after testing is shown in Figure A - 100.

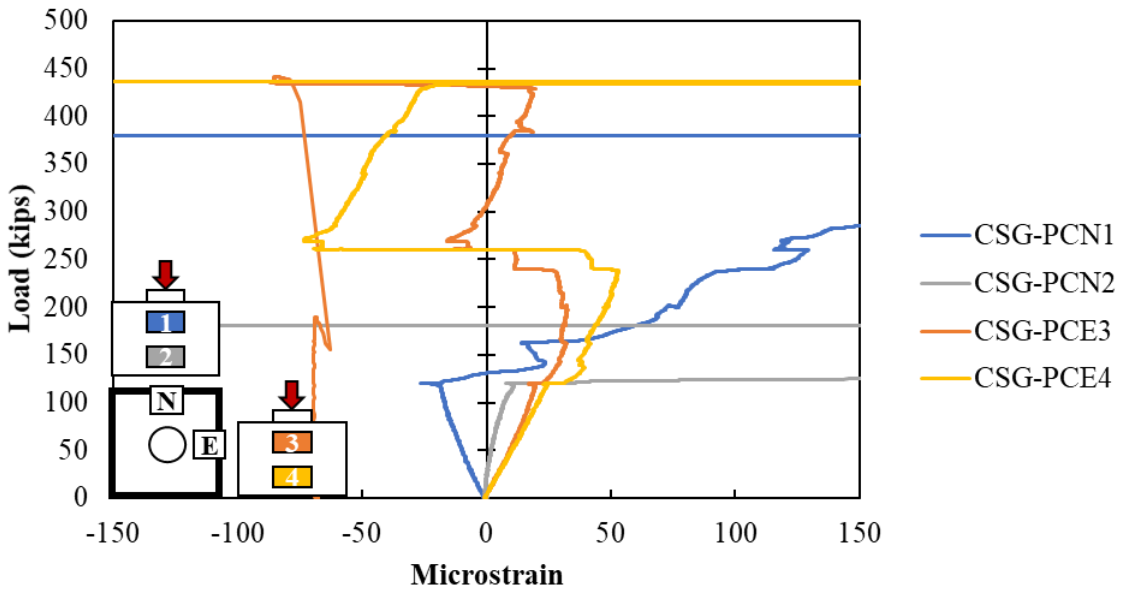

Figure A - 99: Concrete strain gauge on the concrete surface of Specimen S2-14

Figure A - 100: Cracking on the (a) south side and (b) east side on specimen S2-14

Specimen S2-15 Results

Specimen S2-15 was 14-inch deep, had a smooth surface between the cap and plug with a paste retarder finish.

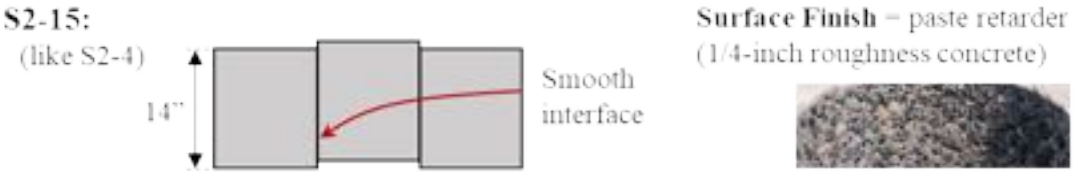

The plug started to move with a load of around 300 kips, and the failure load was 631.2 kips. After failure, the specimen still held a load of 400 kips and the specimen was loaded until 0.45-inch displacement of the plug. The load displacement curve is shown in Figure A - 101.

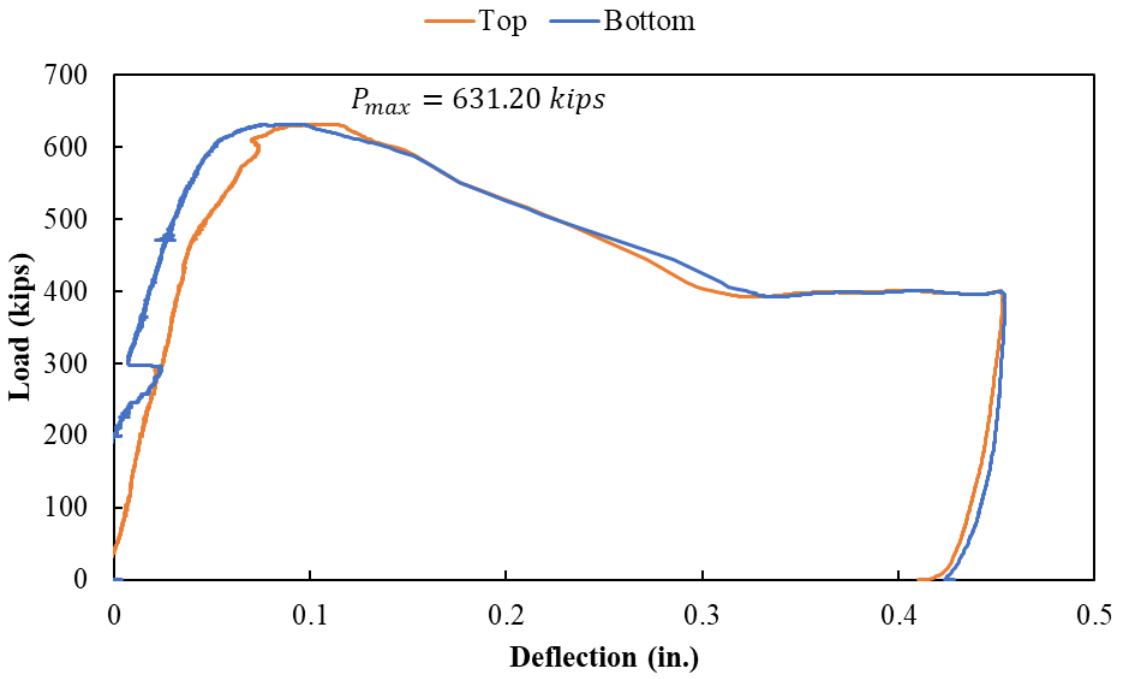

Figure A - 101: Load displacement curve for specimen S2-15

Cracking was also measured with the surface concrete gauges at a load of around 100 kips in the east side of the specimen as shown in Figure A - 102. Cracks were also observed later in the north side in a load around 300 kips. Cracking was visually observed as shown

in Figure A - 103. The cracks extended from the bottom of the cap to the top toward the plug.

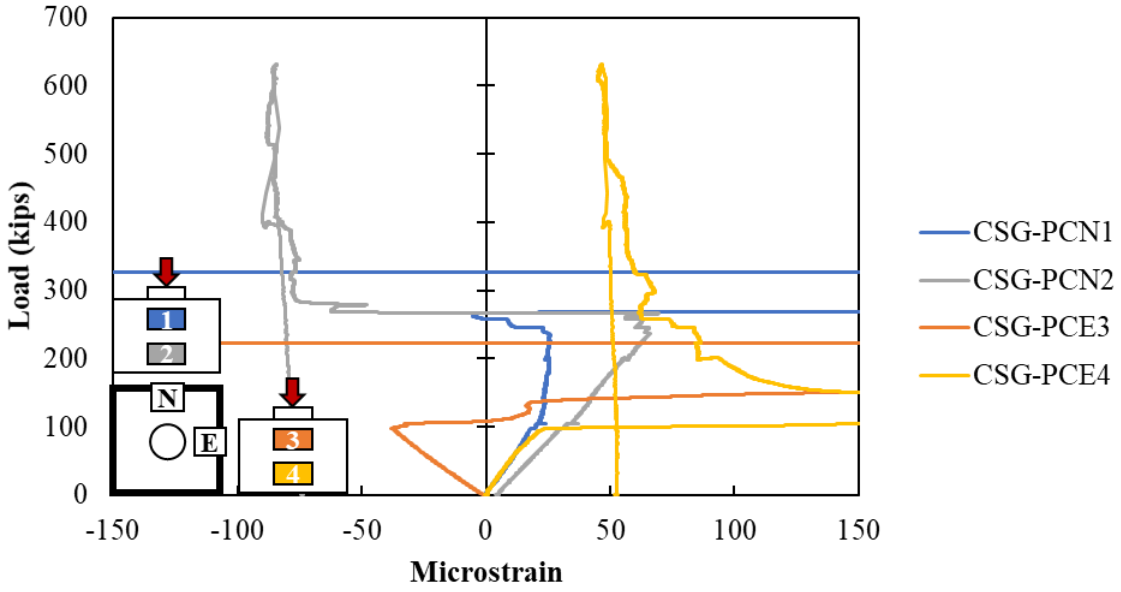

Figure A - 102: Concrete surface gauges on the cap on specimen S2-15

Figure A - 103: Cracking on the (a) north side and (b) top of the cap

Specimen S2-16 Results

Specimen S2-16 was 18-inch deep, had a corrugated surface between the cap and plug with sandblasted (1/16'' of roughness) surface preparation. The void was created using a corrugated metal pipe.

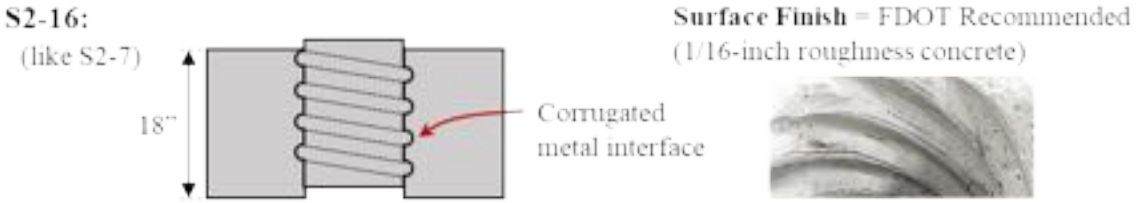

The load was applied to this specimen in two different cycles. The load was initially increased to 300 kips during the first cycle. There was an issue with the hydraulic ram at 300 kips that required the specimen to be unloaded and reloaded. The load was increased to 750 kips (the maximum capacity of the test setup) during the second cycle, but the specimen did not reach its ultimate capacity. The load displacement curve for the second load cycle for this specimen is shown in Figure A - 104.

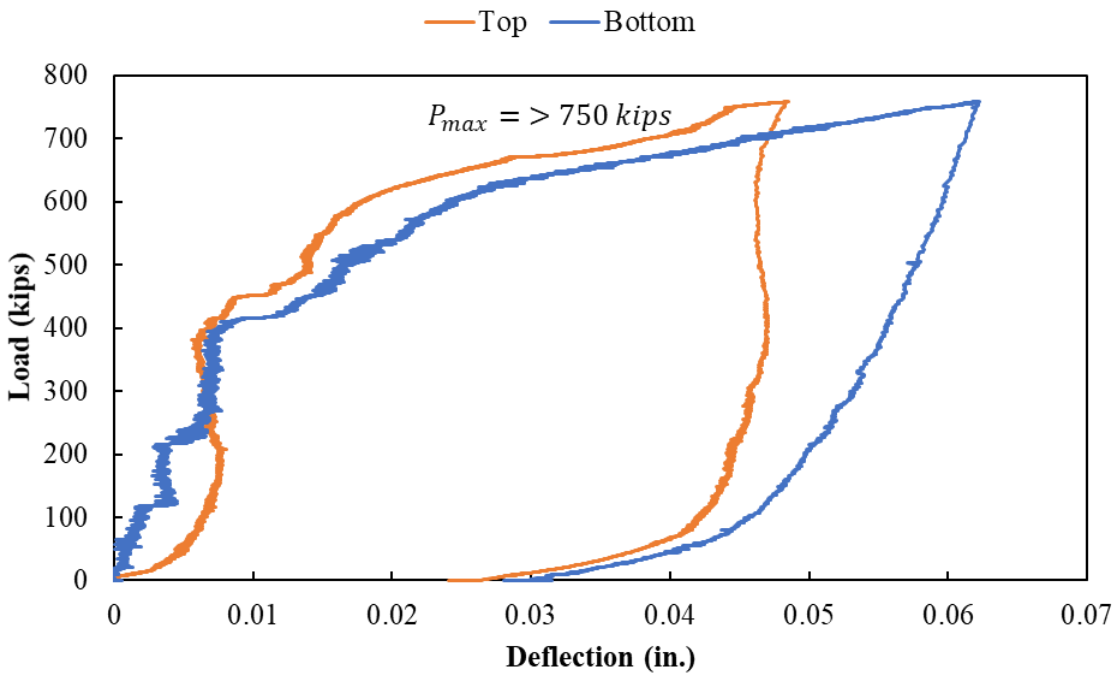

Figure A - 104: Load displacement curve for specimen S2-16

Cracks were measured with the surface concrete gages around 400 kips and 450 kips on the east and north side, respectively. However visual cracks were observed around 200 kips. The reading of the concrete surface gauges is shown in Figure A - 105. When the testing was finished, cracks were also observed as shown in Figure A - 106.

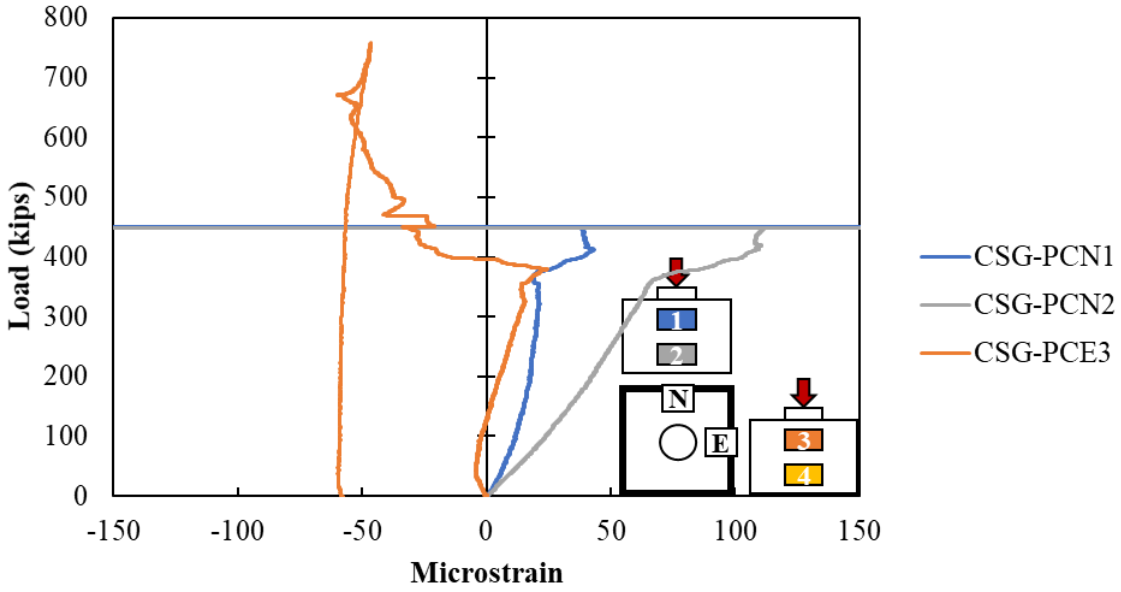

Figure A - 105: concrete strain gauges on the surface of specimen S2-16

Figure A - 106: cracking on the (a) east side and (b) bottom of specimen S2-16

Specimen S2-17 Results

Specimen S2-17 was 18-inch deep, had a corrugated surface between the cap and plug. The void was created using a corrugated metal pipe, and the pipe was left in place. The equivalent specimen was S2-9.

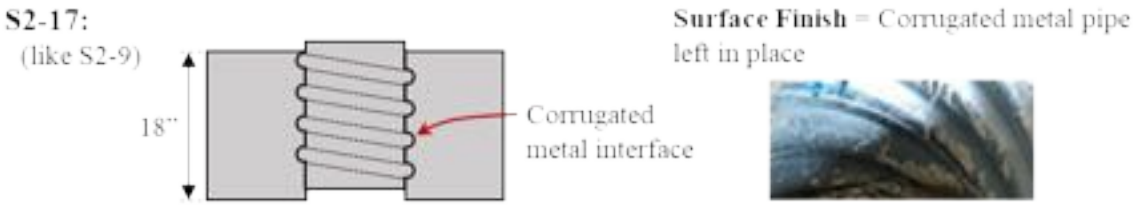

The difference between these specimens is that in S2-17 to create the void the corrugated pipe was first cut in half and put it back together without the corrugations lining up. The idea was trying to avoid the rotation seen in S2-9. The failure load for this specimen was 533.3 kips. The specimen was loaded until 0.45-inch displacement of the plug. The load displacement curve is shown in Figure A - 107.

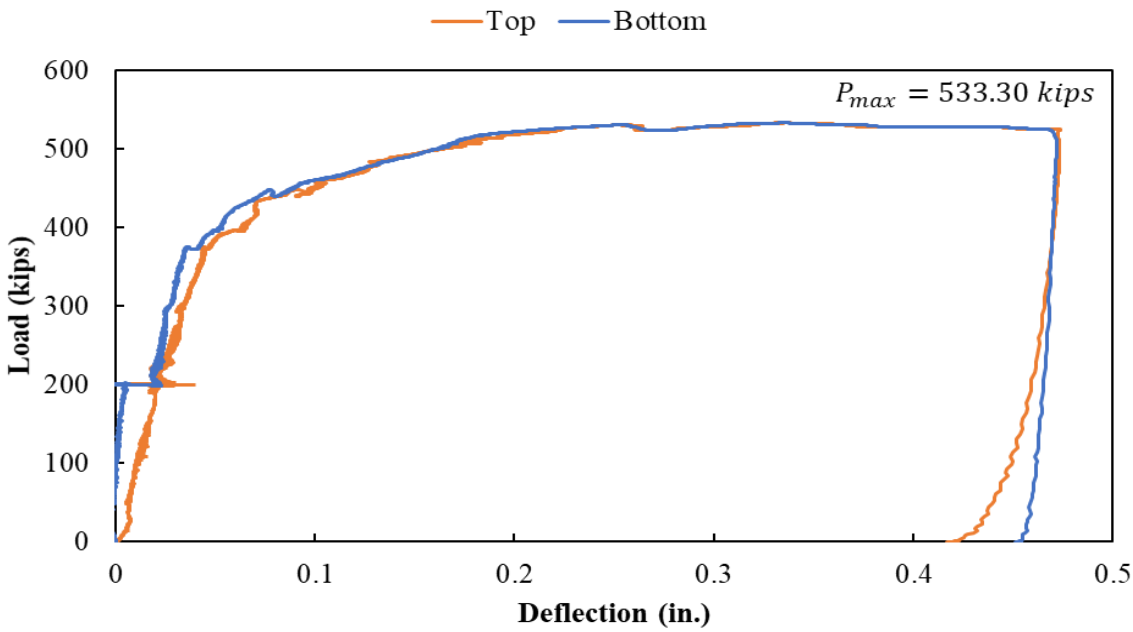

Figure A - 107: Load displacement curve for specimen S2-17

Cracks were measured in the surface concrete in both sides of the specimen around 160 kips as shown in Figure A - 108. When the testing was finished, cracks were also observed

as shown in Figure A - 109. Cracks extended from the bottom, going up to the cap toward the plug.

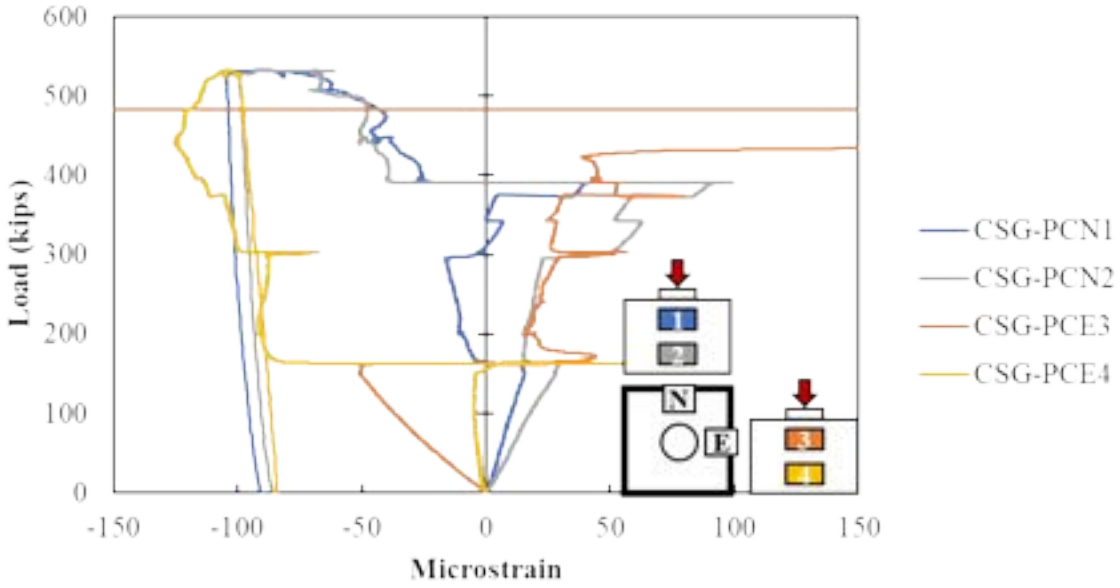

Figure A - 108: Concrete strain gauges on the concrete surface of Specimen S2-17

Figure A - 109: Cracking on the (a) east side and (b) top of the specimen S2-17

Specimen S2-18 Results

Specimen S2-18 was 14-inch deep, had a corrugated surface between the cap and plug with sandblasted (1/16'' of roughness) surface preparation. The void was created using a corrugated metal pipe.

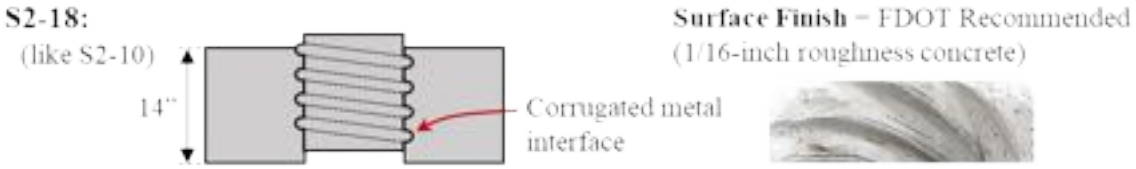

The failure load for this specimen was 569.20 kips. After failure, the specimen still held a load of around 330 kips. The specimen was loaded until 0.45-inch displacement of the plug. The load displacement curve is shown in Figure A - 110.

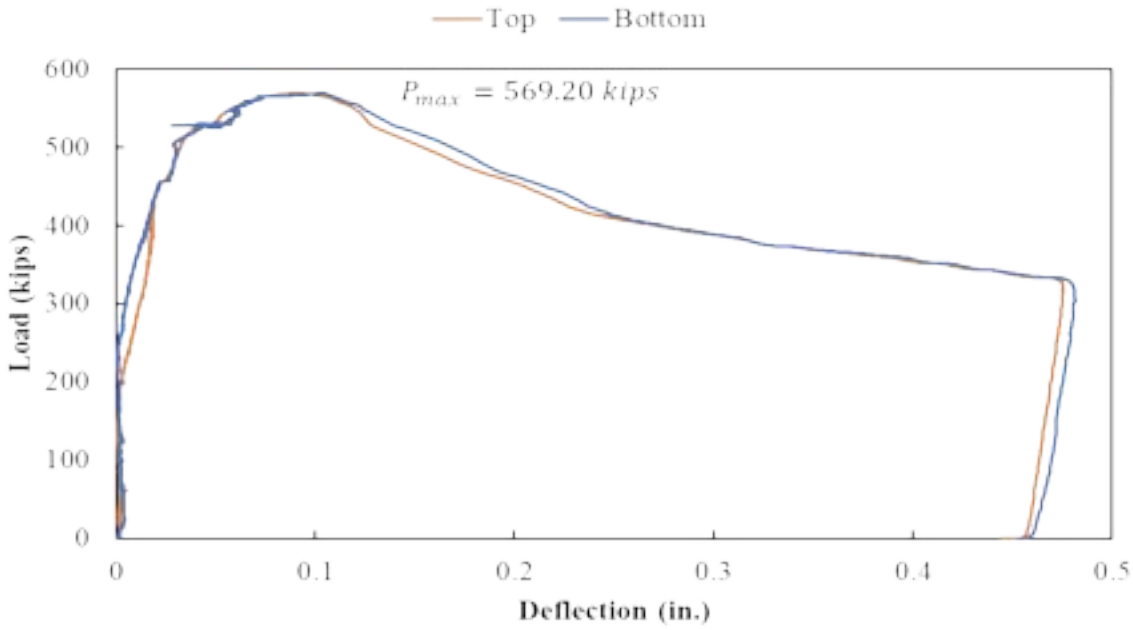

Figure A - 110: Load displacement curve for Specimen S2-18

A crack was measured around 180 kips on the east side of the specimen in the bottom part with the concrete surface gauges. This crack was also visually observed in a stop made at 200 kips of loading. Later, when the load was around 450 kips cracks were measured in the north side of the specimen. Crack propagation seemed to start at the bottom part of the specimen towards the top. The reading of the concrete surface gauges is shown in Figure

A - 111. When the testing was finished, cracks were also observed as shown in Figure A - 112.

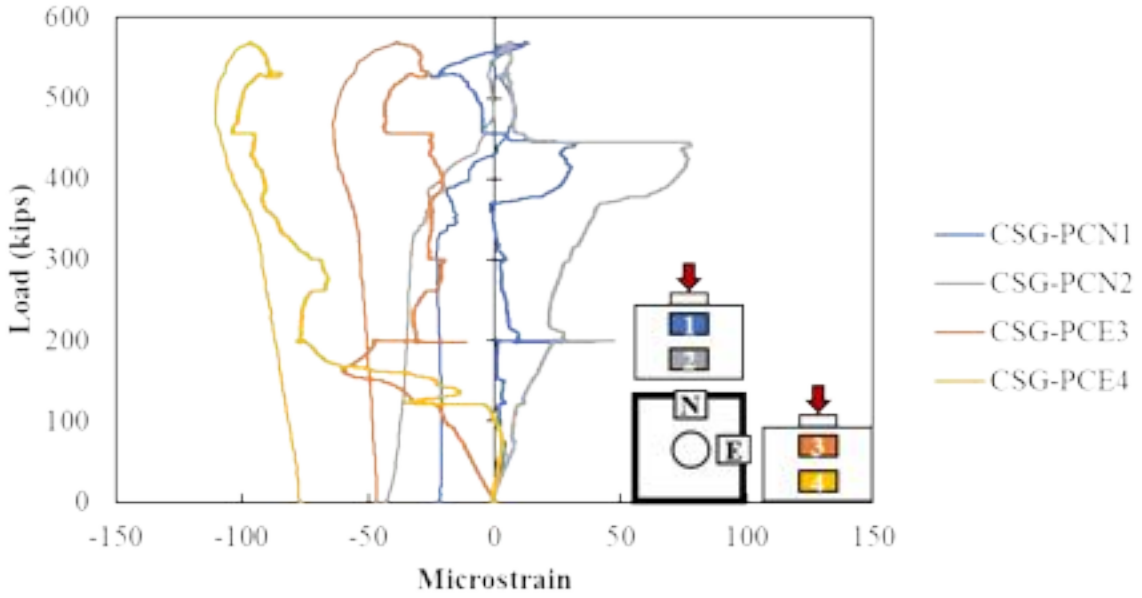

Figure A - 111: Concrete strain gauges on the concrete surface of Specimen S2-18

Figure A - 112: Cracking on the (a) east side and (b) top of the specimen S2-18

Specimen S2-19 Results

Specimen S2-19 was 14-inch deep, had a corrugated surface between the cap and plug. The void was created using a corrugated metal pipe, and the pipe was left in place as well as specimen S2-17.

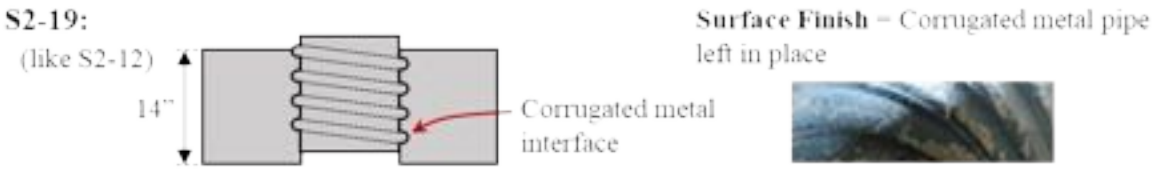

The plug started to slide at a load of around 300 kips. The failure load for this specimen was 482.6 kips. The specimen was loaded until around 0.5-inch displacement of the plug. The load displacement curve is shown in Figure A - 113.

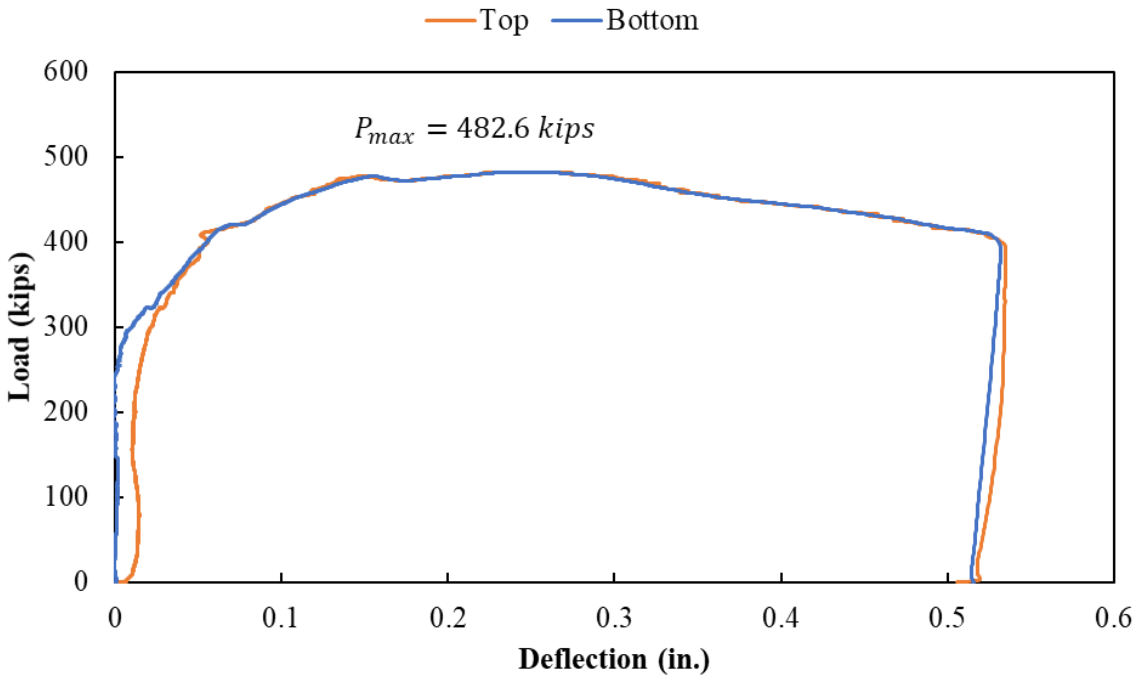

Figure A - 113: Load deflection curve for specimen S2-19

Cracks were measured in the surface concrete in the east side of the specimen around 150 kips. Later, around 250 kips cracks were measured in the north side. The reading of the concrete surface gauges is shown in Figure A - 114. When the testing was finished, cracks were also observed as shown in Figure A - 115.

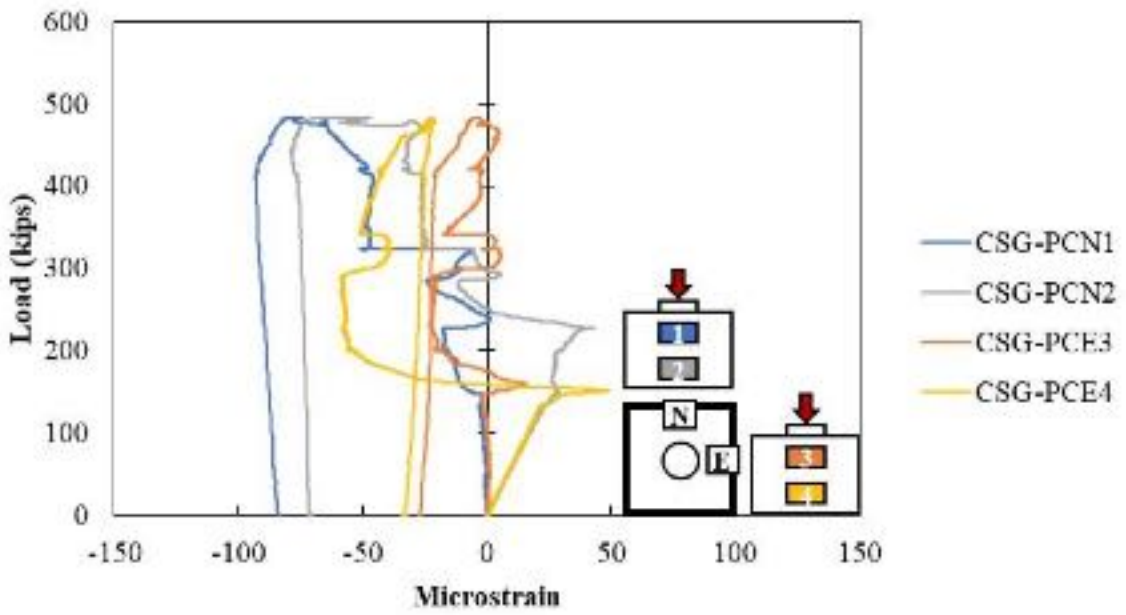

Figure A - 114: Concrete strain gauges on the concrete surface of Specimen S2-19

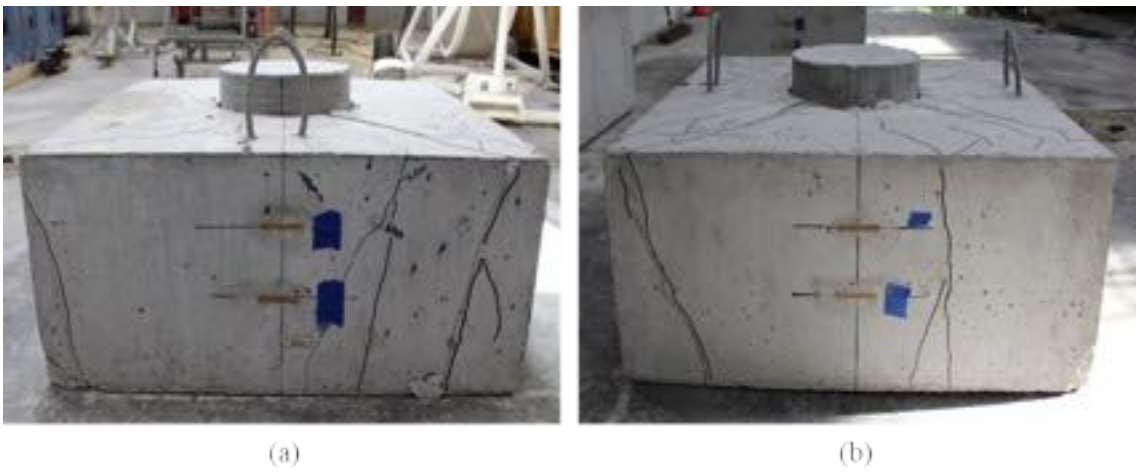

Figure A - 115: Cracking on the (a) east side and (b) north side of specimen S2-19

Specimen S2-20 Results

Specimen S2-20 was 18-inch deep, had a corrugated surface between the cap and plug. The void was created using a corrugated metal pipe, the pipe was removed, and the plug was poured 156 days after the cap. This specimen is like S2-9 and S2-17.

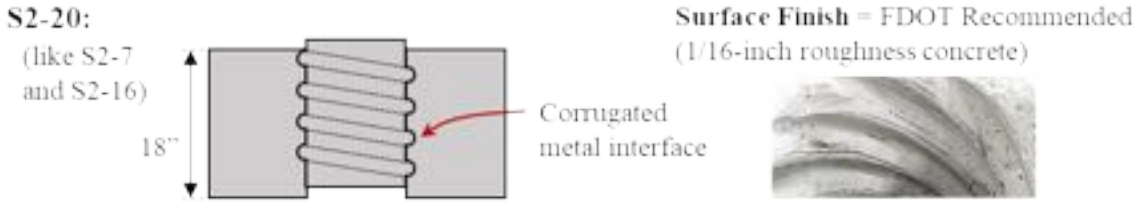

The failure load for this specimen was 666.0 kips. The specimen was loaded until 0.45-inch displacement of the plug. The load displacement curve is shown in Figure A - 116.

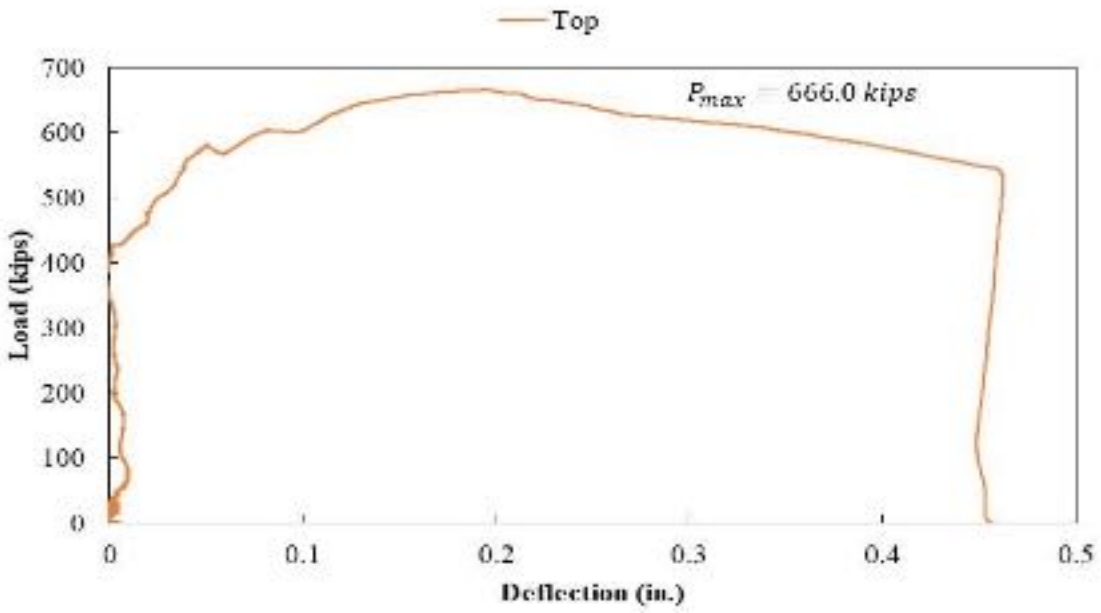

Figure A - 116: Load displacement curve for specimen S2-20

Cracks started to develop on both sides of the specimen around 200 kips. The reading of the concrete surface gauges is shown in Figure A - 117. When the testing was finished, cracks were also observed as shown in Figure A - 118. Cracks extended from the bottom, going up to the cap toward the plug.

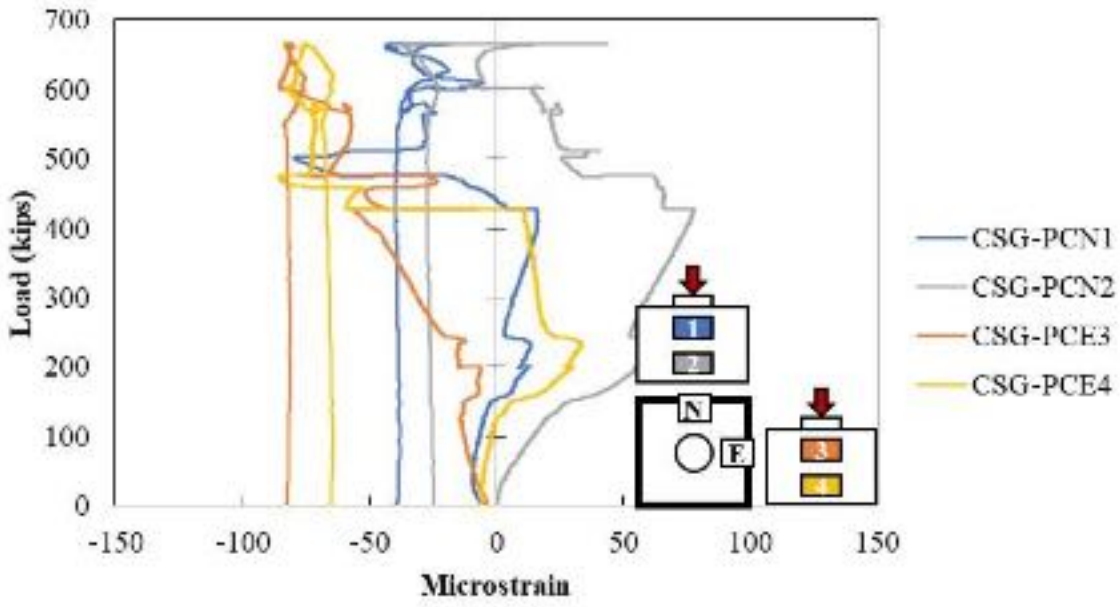

Figure A - 117: Concrete strain gauges on the concrete surface of specimen S2-20

Figure A - 118: Cracking on the (a) south side and (b) bottom of the specimen

Series III Results

The results and observations for the third set of specimens are summarized in this section. The goal of Series II was to investigate the effect of (1) edge distance and (2) longitudinal and confinement reinforcement in the cap. All specimens were 14-inch deep and had a corrugated interface with either sandblasted finish (1/16-inch surface roughness) or corrugated metal pipe left in place.

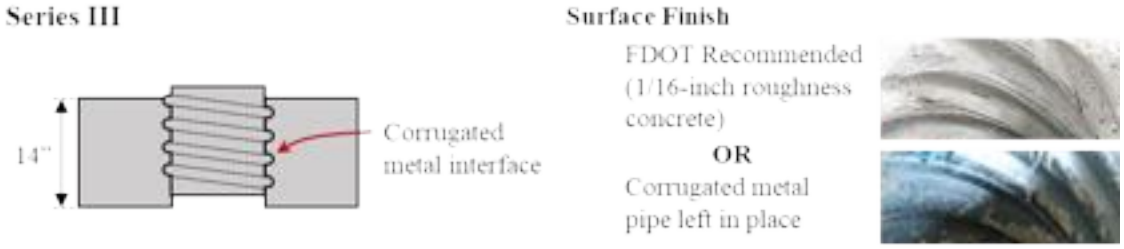

The experimental results and the concrete strengths on the day of testing for both the cap and the plug are summarized in Table A - 3. The concrete strengths measured were lower than the specified.

Table A - 3: Measured concrete strength and ultimate strength for third series of specimens

Specimen	**Compressive Strength on Test Day (ksi)**		**Ultimate Strength (kips)**				
	Cap	*Plug*	*AASHTO*	*ABC*	*ATENA*	*Proposed*	*Measured*
S3-1	4.58	4.59	99.5	137.4	486.9	365.5	364.1
S3-2	4.58	4.59	99.5	137.4	501.6	365.5	444.6
S3-3	4.58	4.59	99.5	137.4	500.8	365.5	440.9
S3-4	4.66	4.68	99.5	137.4	507.7	365.5	493.8
S3-5	4.66	4.68	99.5	137.4	501.6	327.2	340.7
S3-6	4.66	4.68	99.5	137.4	507.7	327.2	283.8
S3-7	4.69	4.65	99.5	137.4	509.1	365.5	377.9
S3-8	4.66	4.68	99.5	137.4	508.1	365.5	379.3
S3-9	4.69	4.65	99.5	137.4	366.7	365.5	364.6
S3-10	4.69	4.65	99.5	137.4	290.4	365.5	330.7
S3-11	4.67	4.68	99.5	137.4	445.5	365.5	352.4
S3-12	4.69	4.68	99.5	137.4	339.6	365.5	363.2
S3-13	4.67	4.68	165.9	137.4	800.3	543.2	387.5

Specimen S3-1 Results

Specimen S3-1 had no longitudinal reinforcement and typical reinforcement around pocket. The interface finish was sandblasted (1/16-inch roughness).

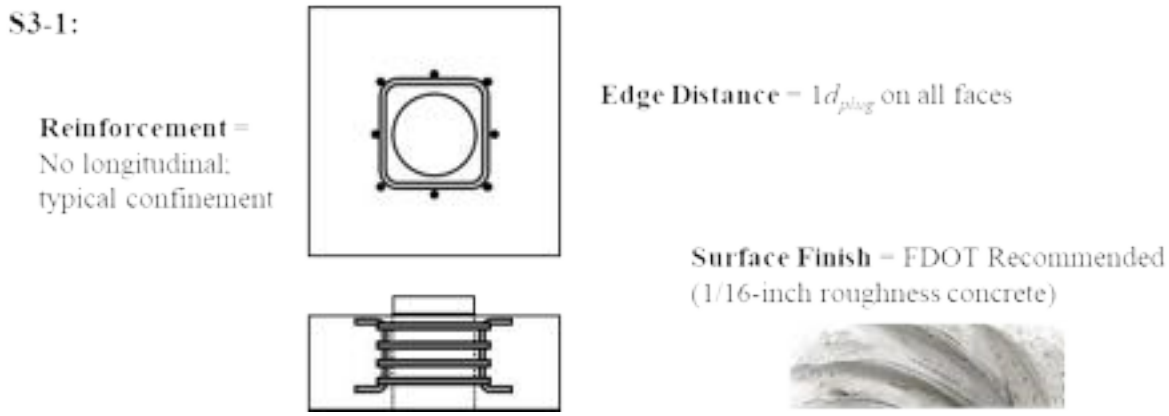

The maximum load was 364.1 kips when a sudden failure occurred and the plug suddenly slid ¼ inch. The load displacement curve is shown in Figure A - 119. The top and bottom of the plug moved almost simultaneously.

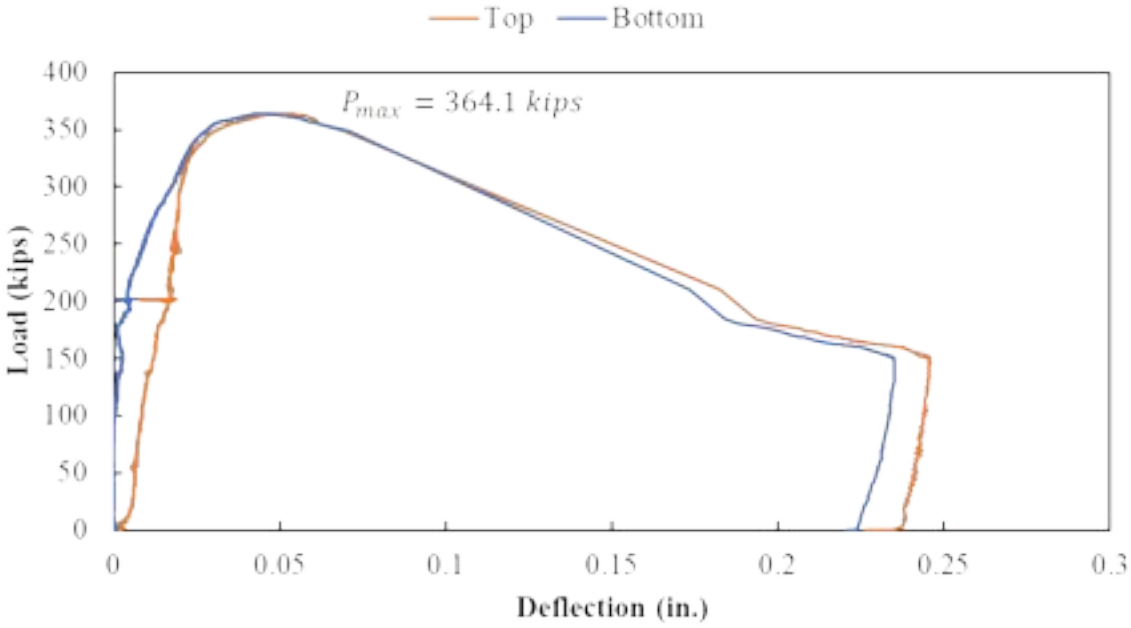

Figure A - 119: Load-deflection curve for specimen S3-1

The confining reinforcement around the pocket started to engage on the north side at around 140 kips and on the west side at around 180 kips. Even though the top and bottom gauges in the west side were engaged almost simultaneously, the bottom gauge (RSG-PCW8) experienced a larger strain at the end of testing, as shown in Figure A - 120. The bottom of the plug started to move (i.e. the plug started to slide) at the same time the confinement reinforcement on the west side of the plug was engaged (200 kips).

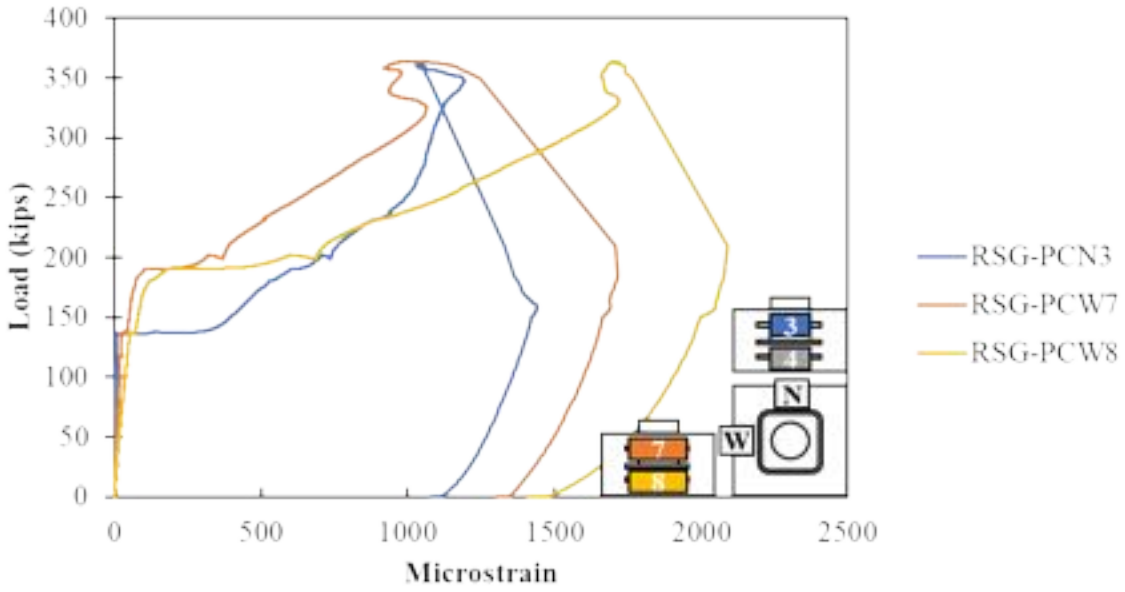

Figure A - 120: Confinement reinforcement around pocket for Specimen S3-1

Cracking was observed in the surface concrete at a load of around 130 kips in both north and east sides of the specimen, as shown in Figure A - 121. Crack propagation was initiated before plug movement.

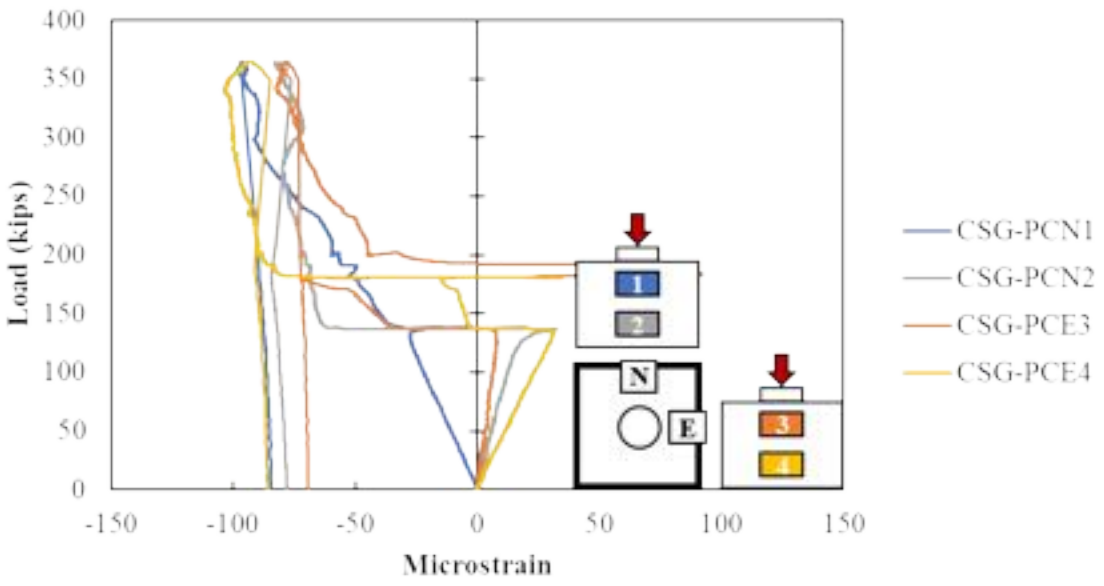

Figure A - 121: Concrete strain gauges in the surface of the cap of Specimen S3-1

Cracking was visually observed when the testing was finished, as shown in Figure A - 122. A circular-shaped crack developed around the plug at failure in addition to the several radial cracks extending from the plug to the sides of the specimen.

Figure A - 122: Specimen S3-1 (a) elevation during testing and (b) bottom cracking after testing.

The stresses in the vertical reinforcement were also measured. As well as the confining reinforcement, the west side was more engaged than the north side of the specimen as shown in Figure A - 123. In addition, similar stresses were found in the cap and the plug

and the stresses in the plug decrease toward the bottom of the plug (From RSG-PW10 to RSG-PW12), showing the transfer of stress from plug to cap.

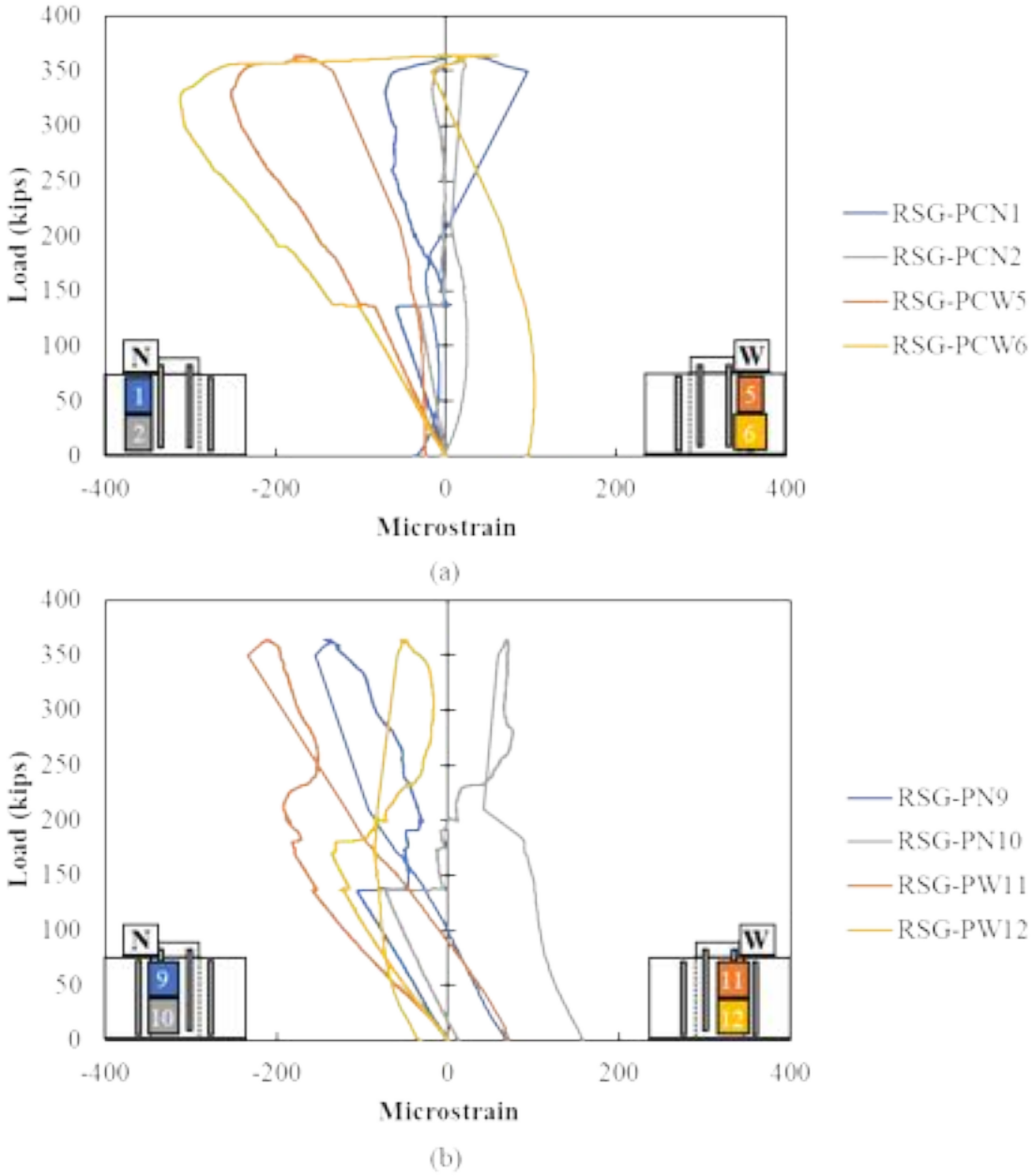

Figure A - 123: Rebar strain gauges in vertical reinforcement on (a) cap and (b) plug of Specimen S3-1.

Specimen S3-2 Results

Specimen S3-2 had no reinforcement around pocket and typical longitudinal reinforcement. The interface finish was sandblasted (1/16-inch roughness concrete).

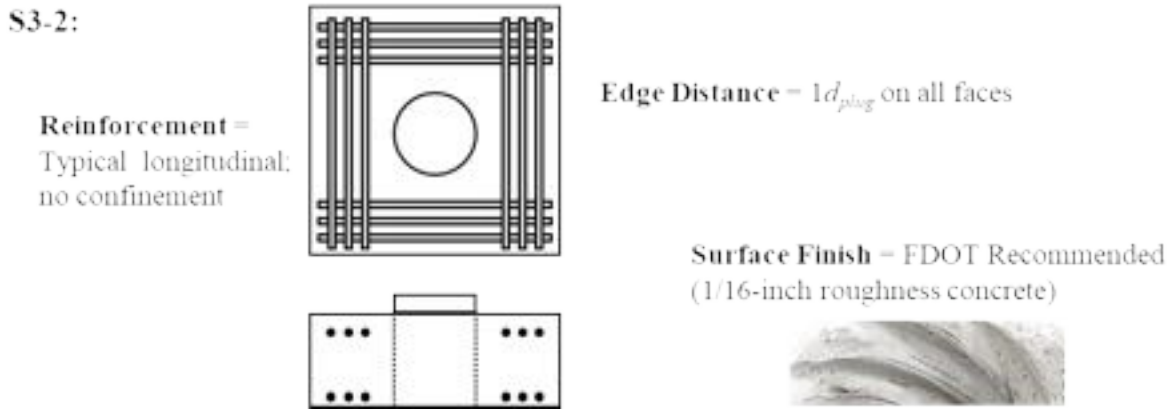

The failure load for this specimen was 444.6 kips. After failure, the specimen still held a load of around 270 kips. The specimen was loaded until 0.5-inch displacement of the plug. Comparing this result with S3-1 shows that having longitudinal reinforcement increases the interface capacity and provide a ductile behavior because cracking is controlled in the cracking plane of the specimen. The load displacement curve is shown in Figure A - 124.

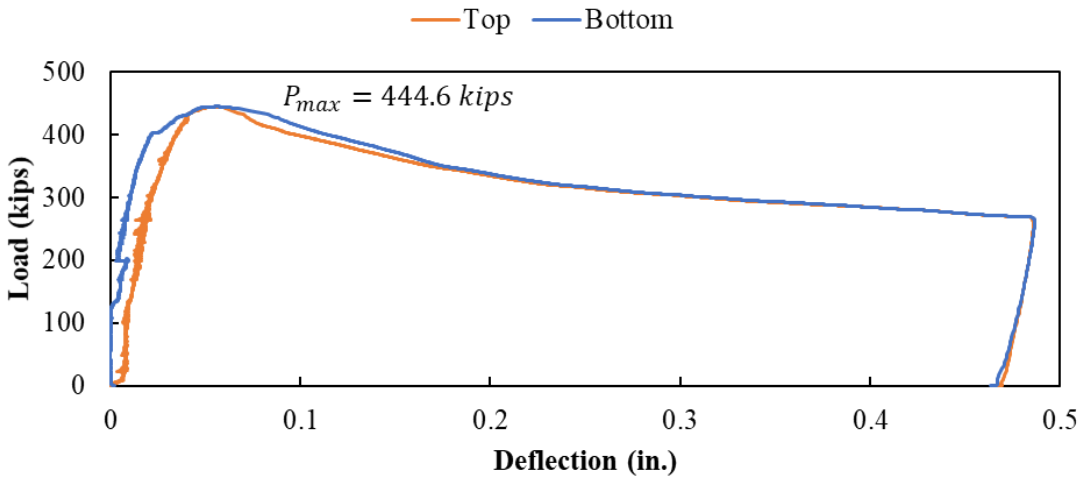

Figure A - 124: Load versus deflection curve for Specimen S3-2

The bottom reinforcement started to engage almost simultaneously in both faces (north and west) of the specimen according to readings. Potentially, cracks were forming on the

bottom of the specimen in both directions. The strain in the longitudinal reinforcement in the bottom is shown in Figure A - 125.

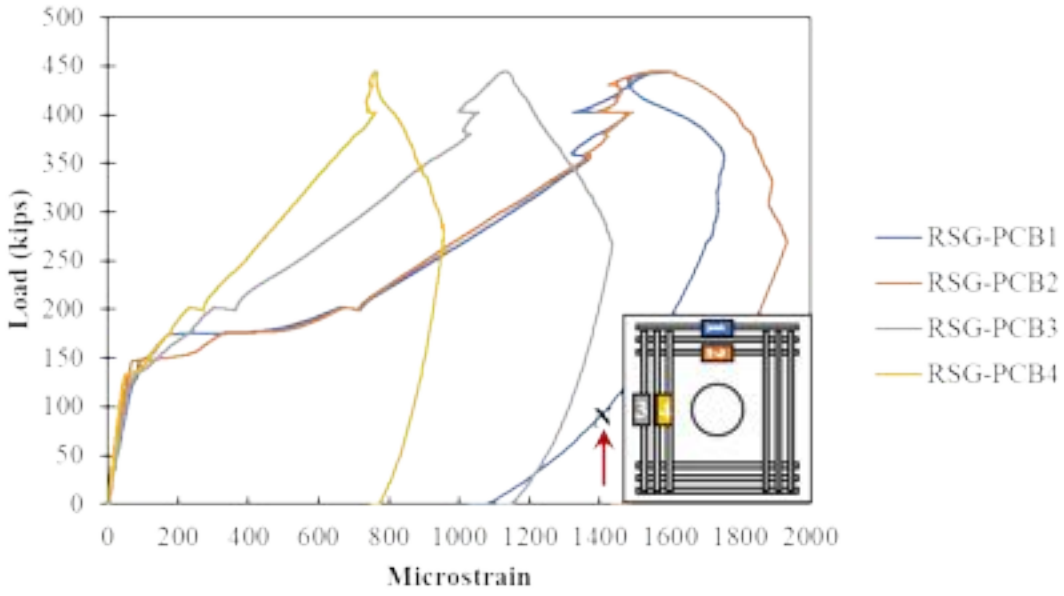

Figure A - 125: Rebar strain gauges in the longitudinal reinforcement on bottom of Specimen S3-2

A crack was measured around 150 kips on the north and east side of the specimen indicated by the bottom gauges placed on both sides (CSG-PCN2 and CSG-PCN4), shown in Figure A - 126. Crack propagation seemed to start at the bottom part of the specimen towards the top.

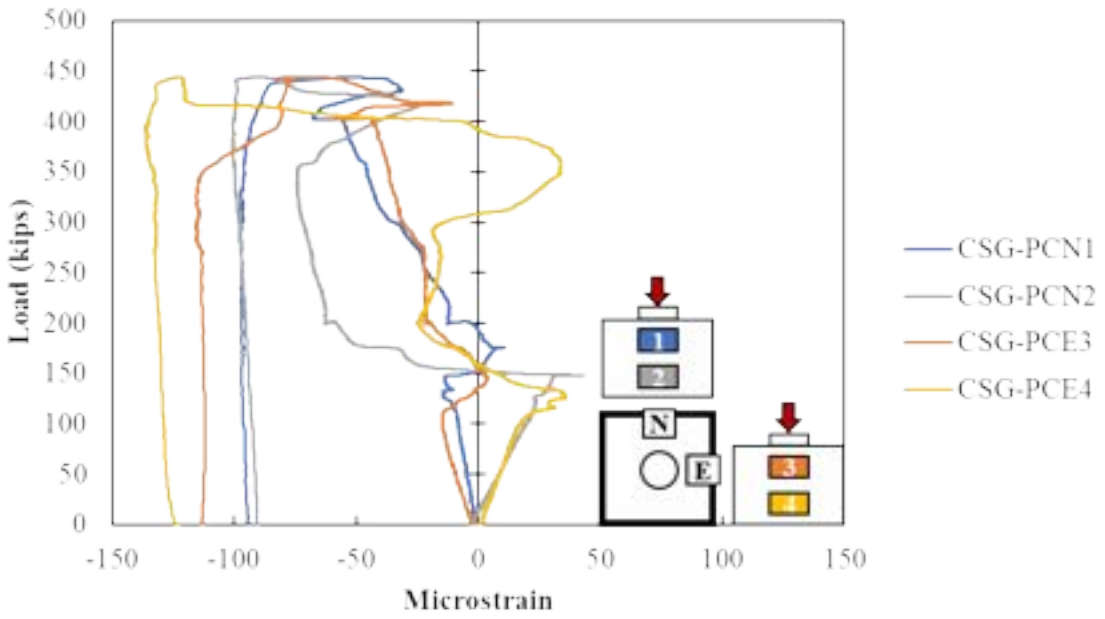

Figure A - 126: Concrete strain gauges in the surface of Specimen S3-2

When the testing was finished, cracks were also observed as shown in Figure A - 127. The cracks were observed to extend radially from the plug to all sides of the specimen.

Figure A - 127: Cracking after testing on (a) east side of cap and (b) bottom of Specimen S3-2.

The measured strains in the vertical reinforcement in the plug are shown in Figure A - 128. The stresses in the vertical reinforcement on top of the plug in the north side were higher than in the bottom, suggesting transfer of stresses from plug to cap. No vertical

reinforcement was provided in the cap around the pocket because there was no confinement reinforcement present.

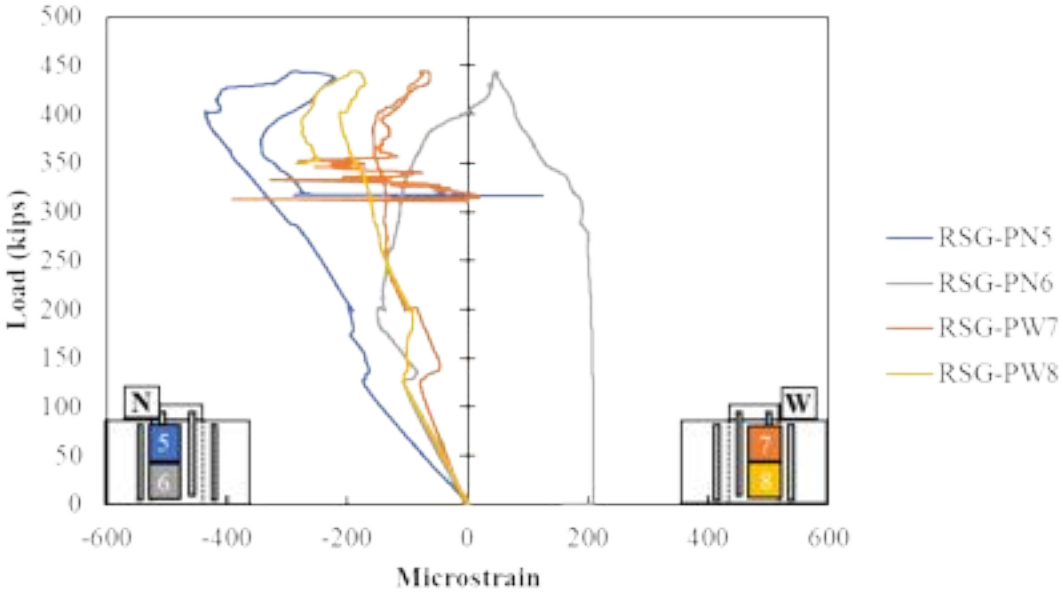

Figure A - 128: Rebar strain gauges in vertical reinforcement on plug of Specimen S3-2

Specimen S3-3 Results

Specimen S3-3 had typical reinforcement around pocket and 2 #4 bars in all faces as longitudinal reinforcement. The interface finished was sandblasted (1/16'' of roughness).

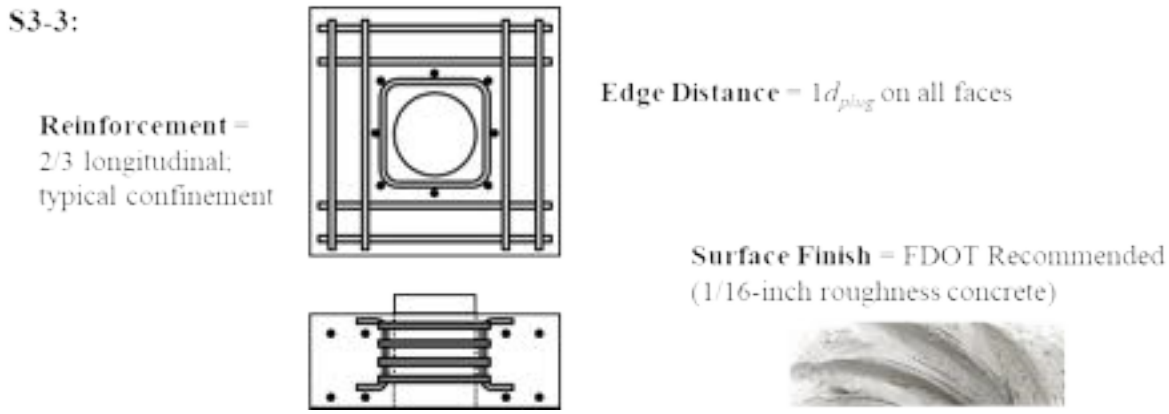

The failure load for this specimen was 440.9 kips. The specimen was loaded until 0.5-inch displacement of the plug. Adding 2 #4 bars in all faces as longitudinal reinforcement increased the capacity 80 kips more than specimen S3-1, which had no longitudinal reinforcement. More importantly, after failure of the interface there was ductile behavior with the specimen holding approximately 300 kips during the sliding of the plug. The load displacement curve is shown in Figure A - 129.

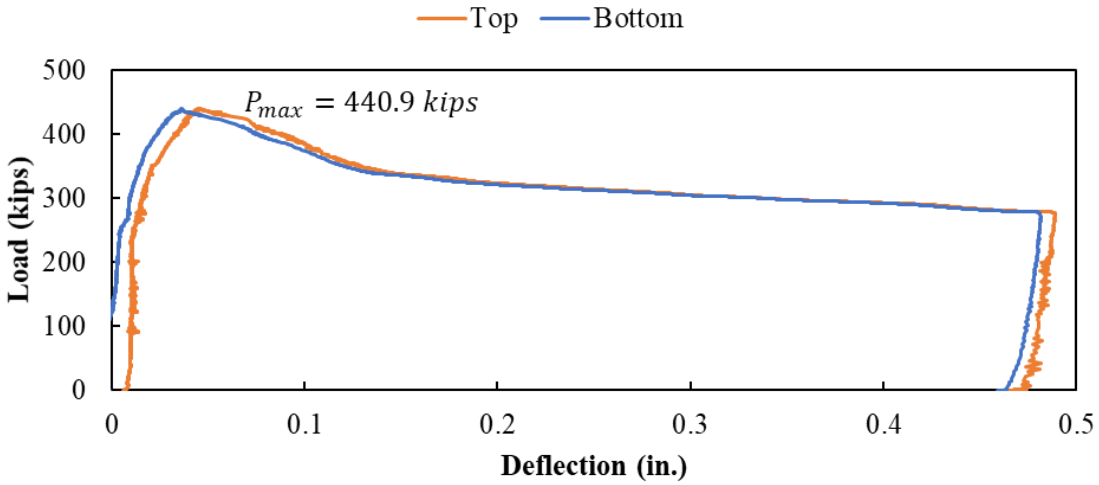

Figure A - 129: Load versus deflection curve for Specimen S3-3

The bottom reinforcement placed on the north side of the specimen started to engage at a load around 100 kips according to the RSG-PCB1 and RSG-PCB2 gauges, as shown in

Figure A - 130. Later when the load was around 250 kips the longitudinal reinforcement on the west side of the specimen was also engaged. At this point, the plug started to move. Potentially, cracks were forming on the bottom of the specimen in both directions.

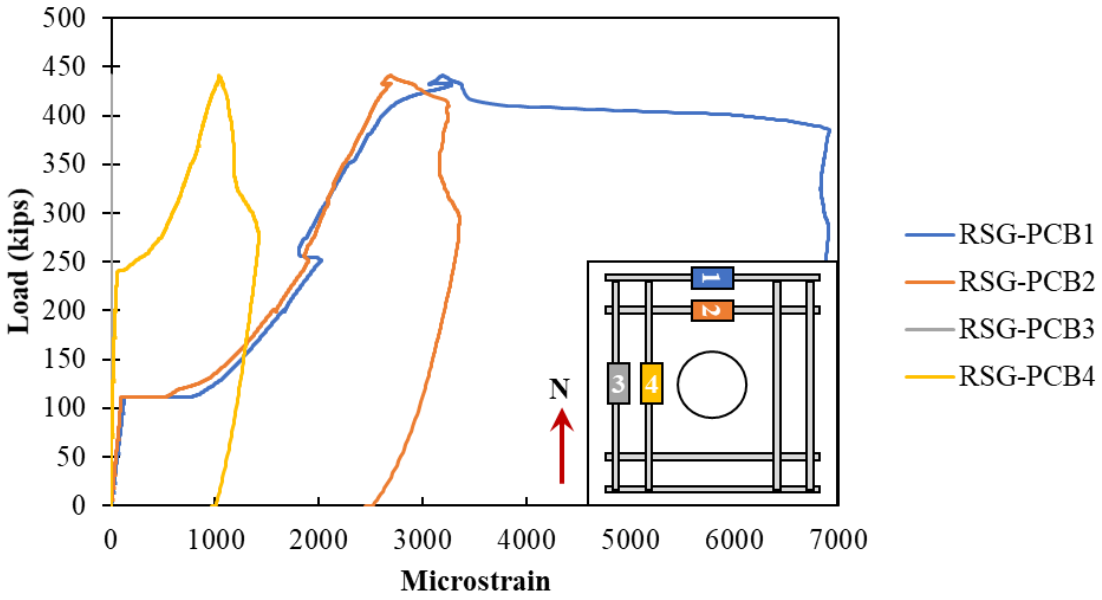

Figure A - 130: Rebar strain gauges in the longitudinal reinforcement on bottom of Specimen S3-3

Cracking was measured around 100 kips on the north side of the specimen with the concrete surface gauges, as shown in Figure A - 131. There may have also been minor cracking adjacent to gauge CSG-PCE3 at around 100 kips, as the strain stopped increasing at this point. A clear crack was observed on the bottom of the east side of the specimen going through gauge CSG-PCE4 at a load of approximately 250 kips.

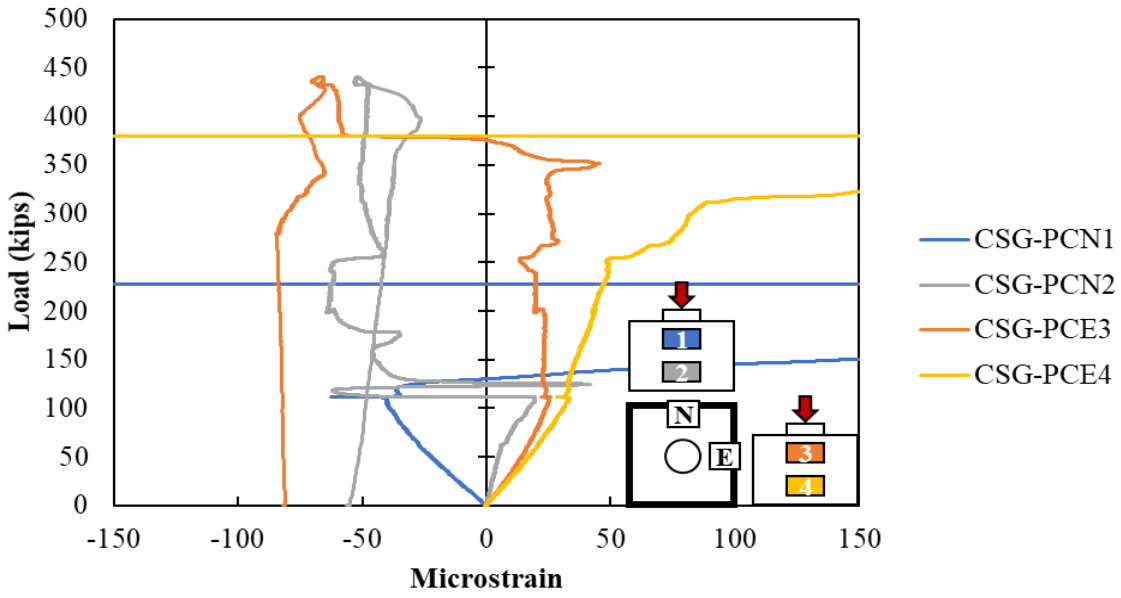

Figure A - 131: Concrete strain gauges in the surface of Specimen S3-3

The crack pattern at failure for S3-3 is shown in Figure A - 132. Larger cracks were observed on the north-south side than the east-west side of the specimen. Some of the largest cracks extended radially out of the plug to the corners of the specimen.

Figure A - 132: Cracking after testing on (a) bottom of the cap and (b) top of the cap of Specimen S3-3

The confining reinforcement around the pocket started to engage in the north side of the plug of a load around 110 kips according to gauge RSG-PCN8, as shown in Figure A - 133.

The west side of the specimen started to engage around 250 kips according to RSG-PCE12. More engagement was observed in the bottom stirrups around the plug.

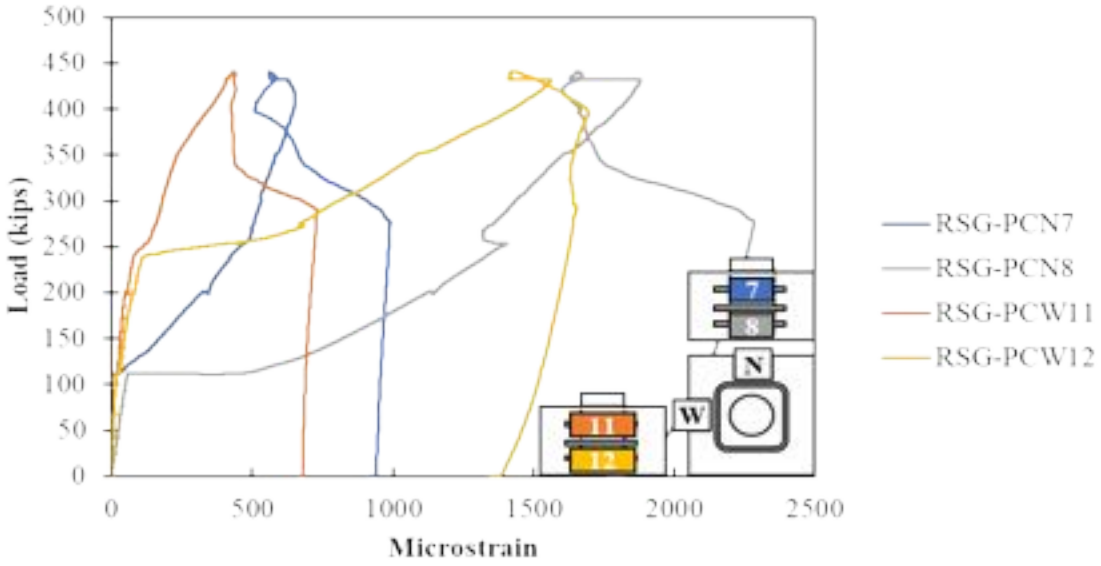

Figure A - 133: Confining reinforcement around pocket of Specimen S3-3

The measured strains in the vertical reinforcement in the cap and plug are shown in Figure A - 134. The vertical strains in the plug decrease toward the bottom of the plug and increase in the bottom of the cap, showing transfer of stress from plug to cap.

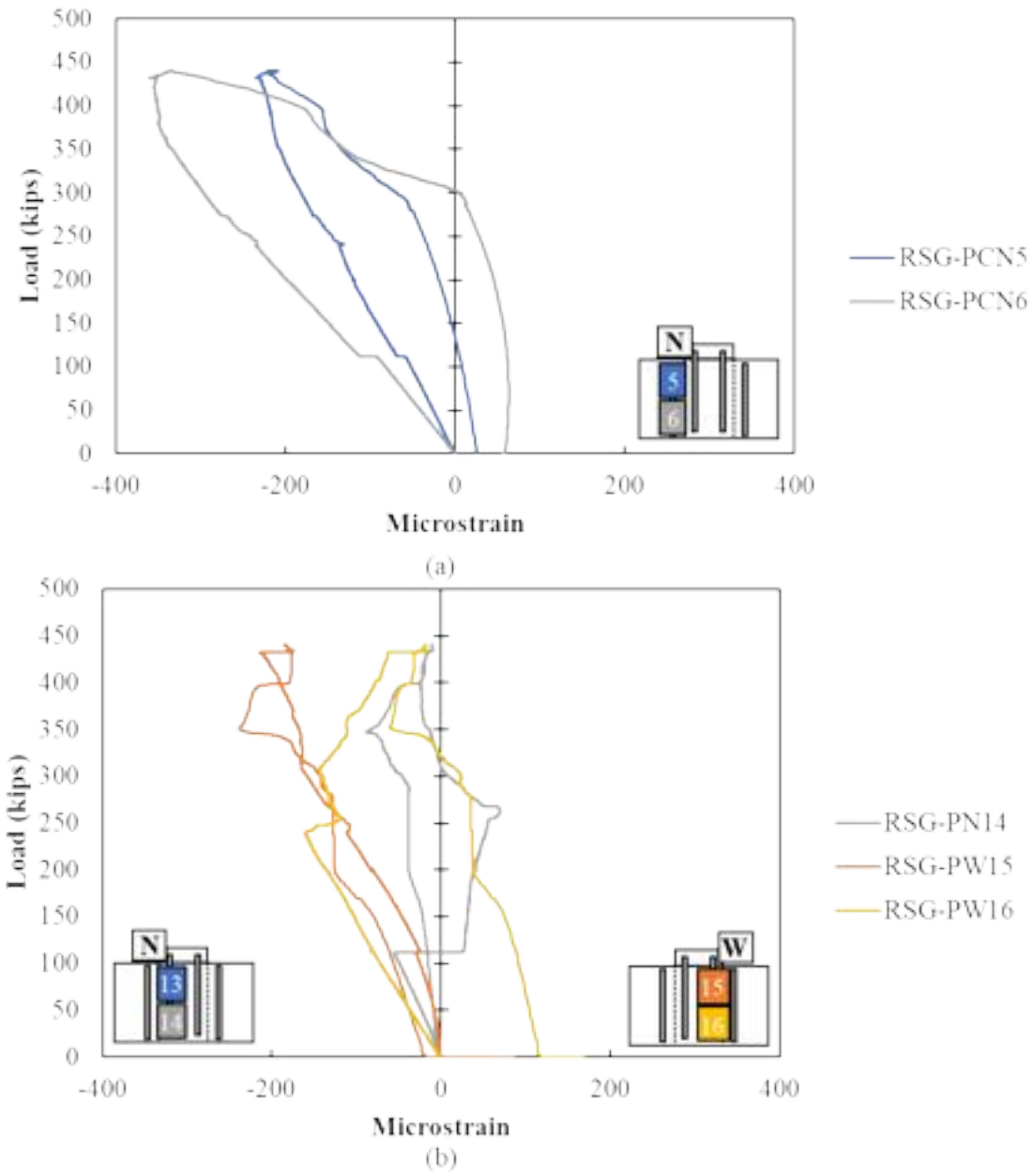

Figure A - 134: Rebar strain gauges in vertical reinforcement on (a) cap and (b) plug of Specimen S3-3

Specimen S3-4 Results

Specimen S3-4 had typical longitudinal reinforcement and 2#3 stirrups and 8#8 vertical bars around pocket. The interface finished was sandblasted (1/16'' of roughness).

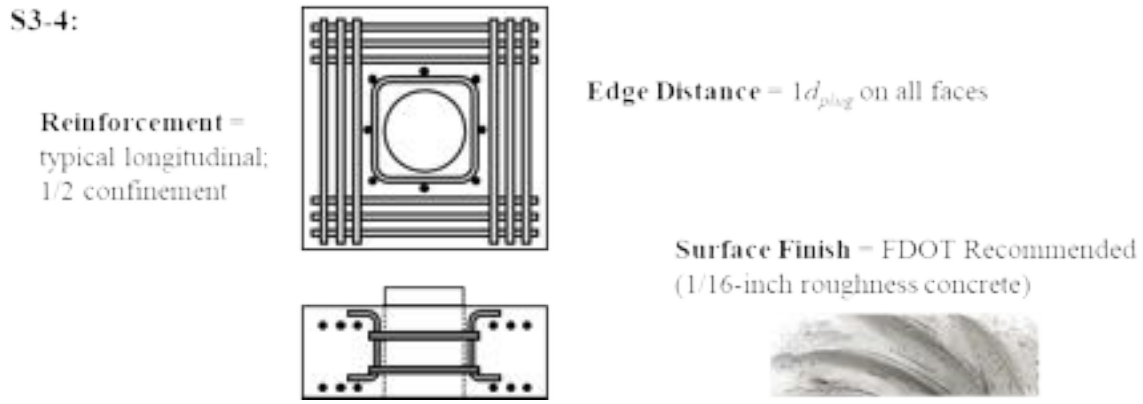

The interface capacity was 493.8 kips, and after failure the specimen still held a load of 300 kips. The specimen was loaded until 0.5-inch of displacement of the plug and the top and bottom moved simultaneously. Adding two stirrups to the confinement reinforcement around the pocket did not affect the overall response/behavior of the specimen when compare to specimen S3-2 which failed at 444.6 kips. The load displacement curve is shown in Figure A - 135.

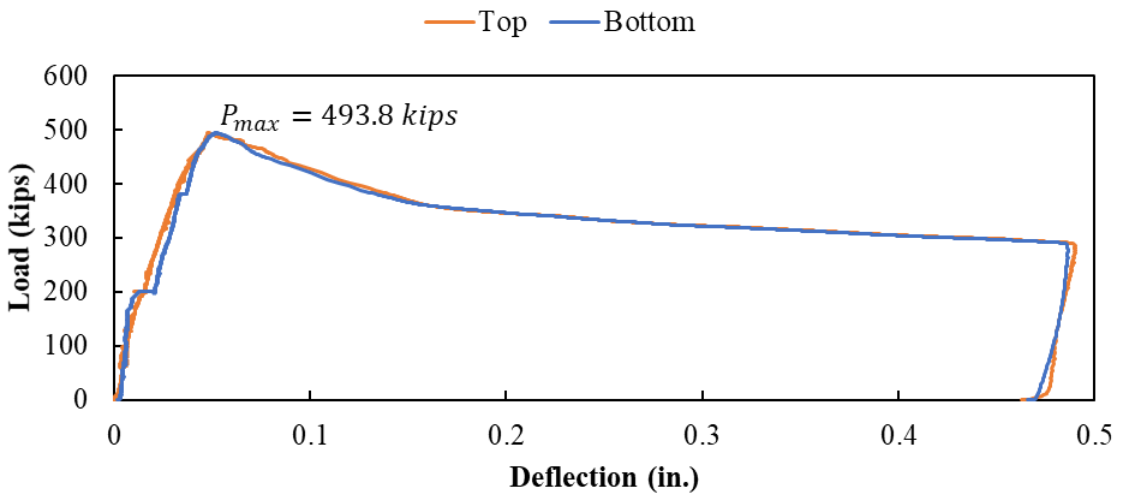

Figure A - 135: Load versus deflection curve for Specimen S3-4

The readings of the stain gauges in the longitudinal reinforcement in the bottom of the specimen are shown in Figure A - 136. The bottom reinforcement started to engage in the

north side at a load of around 200 kips. Later, when the load was around 275 kips the reinforcement placed on the west side started to get engaged. The cracking of the cap and engagement of the longitudinal reinforcement at 200 kips occurred at the same time as the first slip of the bottom of the plug (see Figure A - 135). This was also when the load on the plug was held constant for 5 to 10 minutes as cracks were being marked on the specimen.

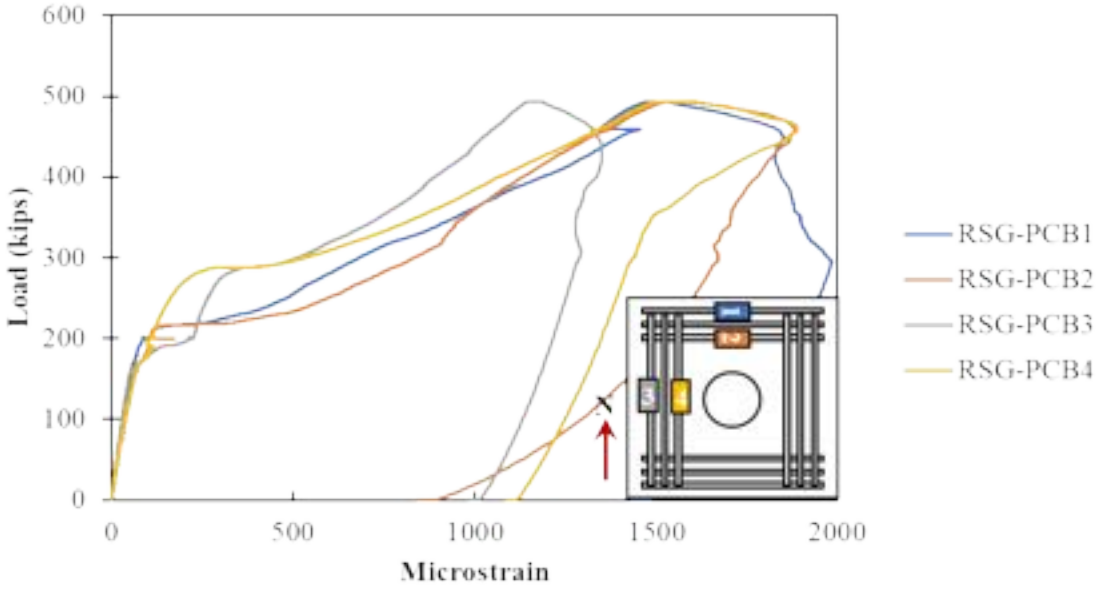

Figure A - 136: Rebar strain gauges in the longitudinal reinforcement on the bottom of Specimen S3-4

Cracking was also observed in the surface concrete at a load of around 200 kips on the north and east side of the specimen according to CSG-PCN2 and CSG-PCE4, as shown in Figure A - 137.

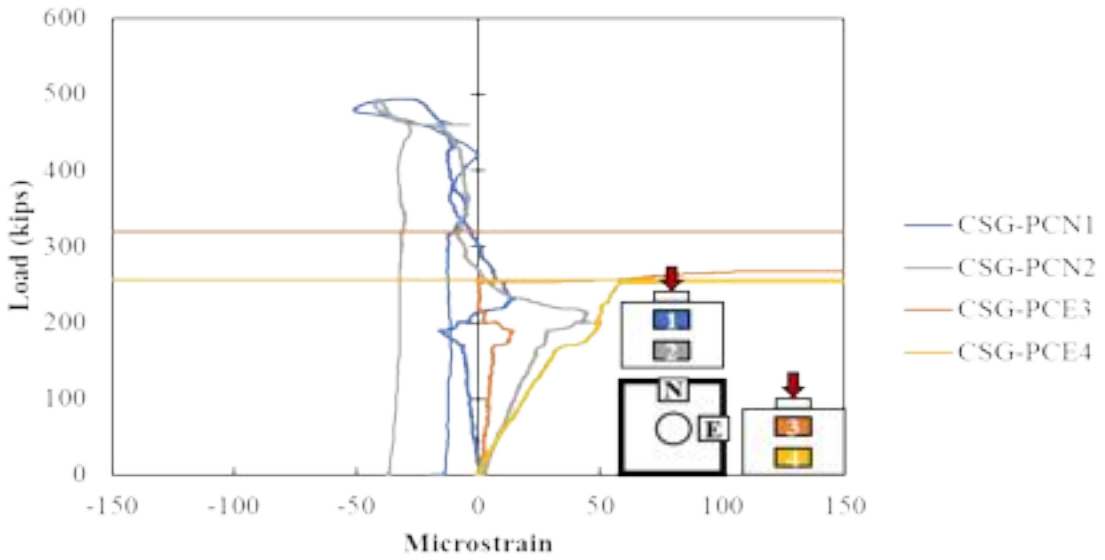

Figure A - 137: Concrete strain gauges in the surface of the cap of Specimen S3-4

The crack pattern at failure for S3-4 is shown in Figure A - 138. The cracks were observed to extend in all sides of the specimen in the top and bottom. A large radial crack extended from the side of the plug to the south-west corner of the specimen.

Figure A - 138: Cracking on (a) cap and (b) bottom of Specimen S3-4

The confining reinforcement around the pocket were first engaged in the north side of the plug at a load of around 200 kips, as shown in Figure A - 139. When the load was around 290 kips, the reinforcement in the west side of the specimen started to engage. More engagement was observed in the bottom reinforcement around pocket.

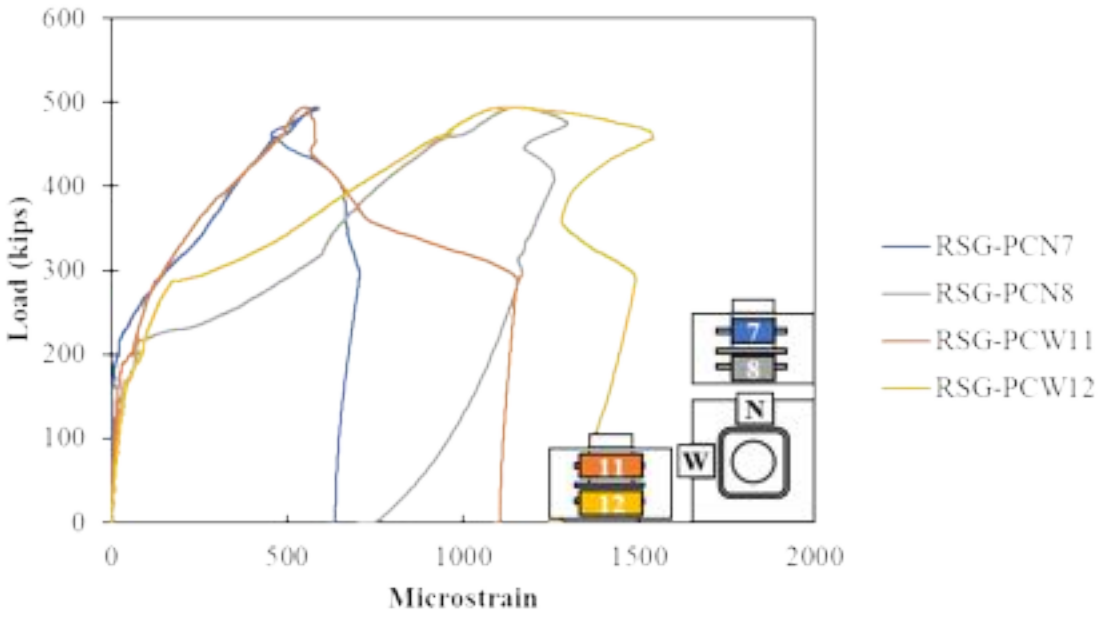

Figure A - 139: Confining reinforcement around pocket of Specimen S3-4

The measured strains in the vertical reinforcement in the plug and cap are shown in Figure A - 140. The stresses in the vertical reinforcement in the top of the plug were higher than in the bottom, suggesting transfer of stresses from plug to cap. The measured strains in the cap were similar in all sides and through the height of the interface.

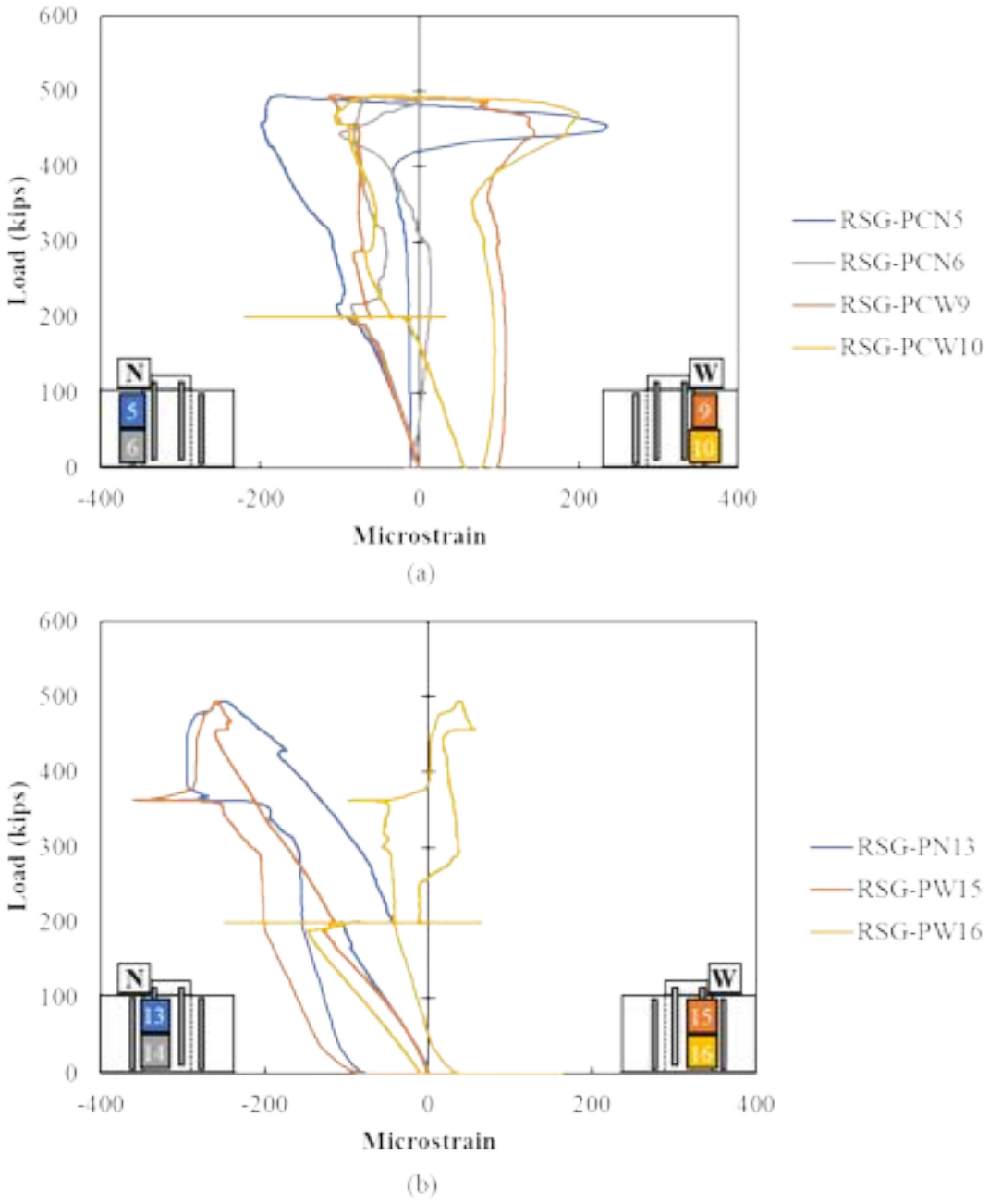

Figure A - 140: Rebar strain gauges in vertical reinforcement on (a) cap and (b) plug of specimen S3-4

Specimen S3-5 Results

Specimen S3-5 had no reinforcement around pocket and typical longitudinal reinforcement as specimen S3-2. The difference is that the corrugated pipe was left in place.

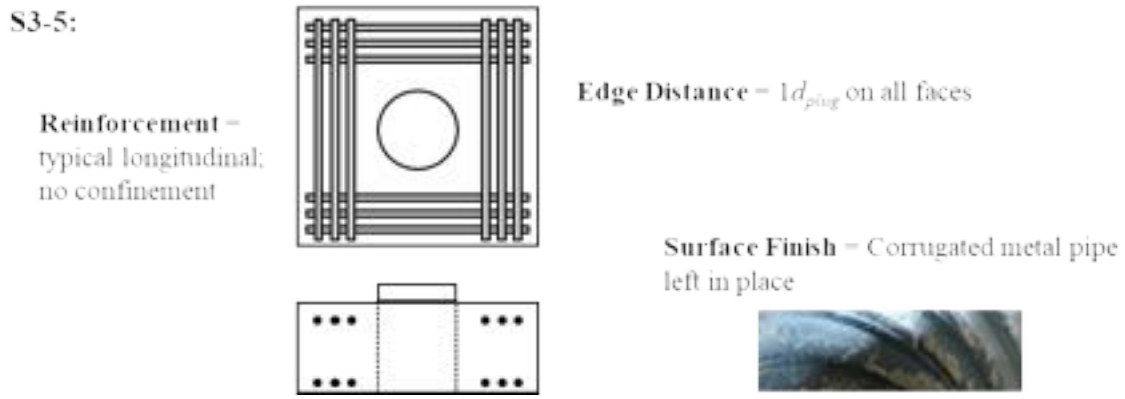

The failure load for this specimen was 340.7 kips. The specimen was loaded until 0.5-inch displacement of the plug. Having a metal finish decreased the capacity 100 kips, compared to the similar specimen with a 1/16-inch surface finish. In addition, little rotation of the plug was seen. The load displacement curve is shown in Figure A - 141.

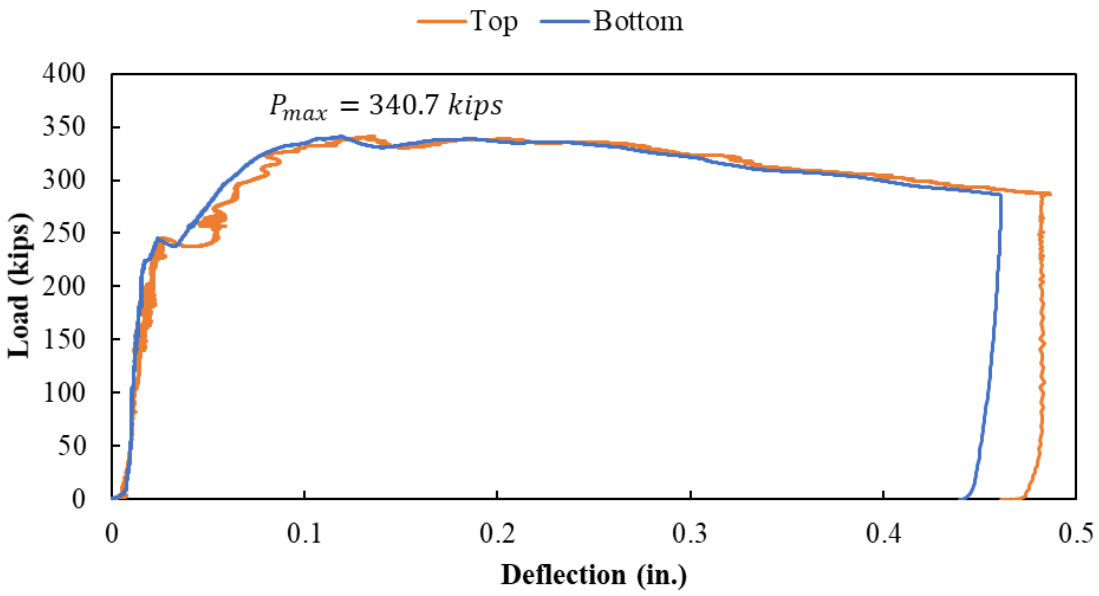

Figure A - 141: Load versus deflection curve for Specimen S3-5

The strain gauges placed in the longitudinal reinforcement in the bottom of the specimen are shown in Figure A - 142. The bottom reinforcement placed on the north side of the

specimen started to engage at a load around 100 kips according to the RSG-PCB1 and RSG-PCB2 gauges. Later when the load was around 250 kips the longitudinal reinforcement on the west side of the specimen was also engaged.

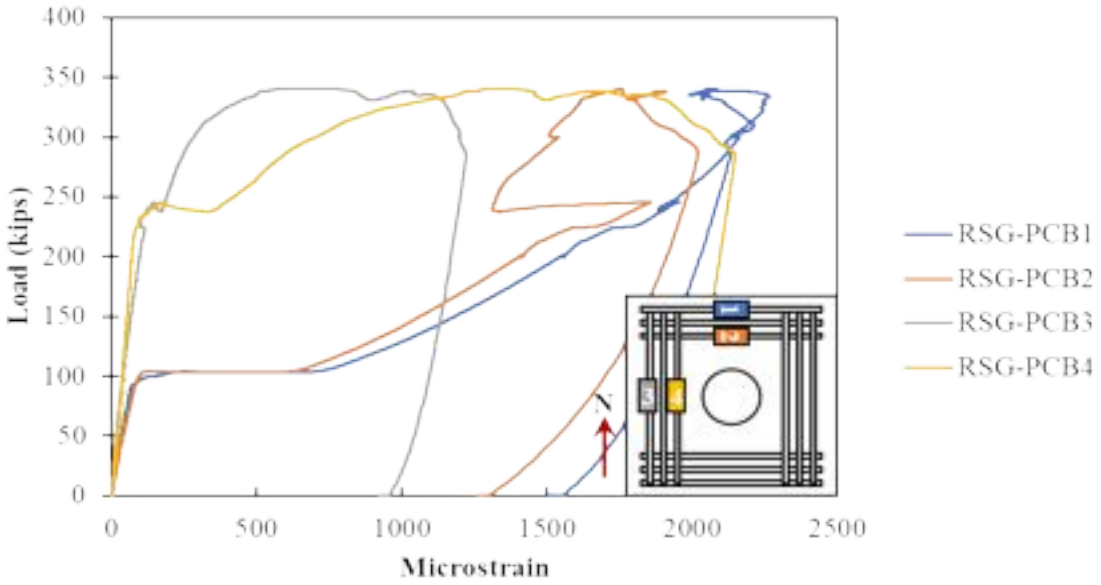

Figure A - 142: Rebar strain gauges in the longitudinal reinforcement on bottom of Specimen S3-5

Cracks were also observed using the surface concrete gauges in both sides of the specimen around 100 and 220 kips, as shown in Figure A - 143.

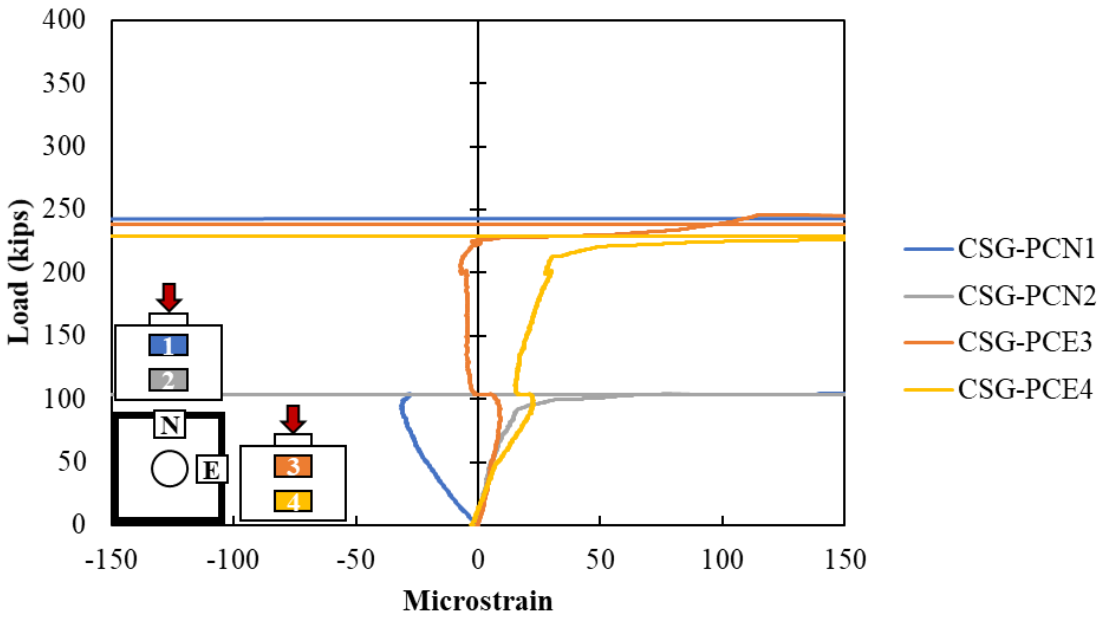

Figure A - 143: Concrete strain gauges in the surface of Specimen S3-5

The crack pattern at failure for S3-5 is shown in Figure A - 144. The cracks were observed to extend radially from the plug toward all the corners of the specimen.

Figure A - 144: Cracking on (a) cap and (b) bottom of Specimen S3-5

The measured strains in the vertical reinforcement in the plug are shown in Figure A - 145. The stresses in the vertical reinforcement on top of the plug in both sides were higher than in the bottom, suggesting transfer of stresses from plug to cap.

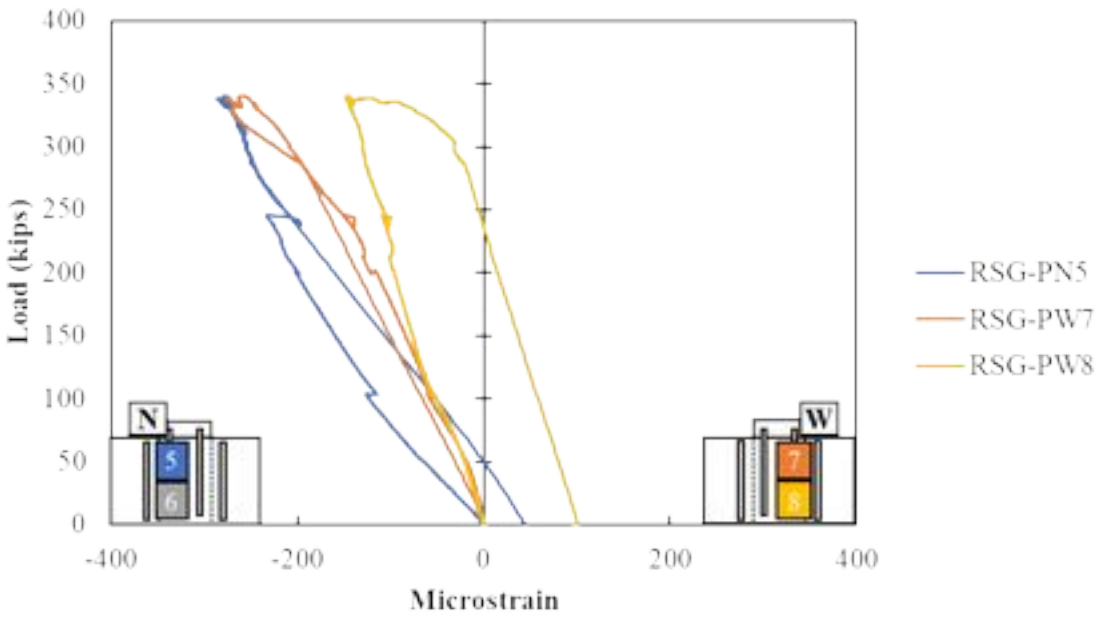

Figure A - 145: Rebar strain gauges in vertical reinforcement on plug of Specimen S3-5

Specimen S3-6 Results

Specimen S3-6 had typical longitudinal reinforcement and 2#3 stirrups and 8#8 vertical bars around pocket as well as S3-4. The interface finished was with the corrugated pipe left in place.

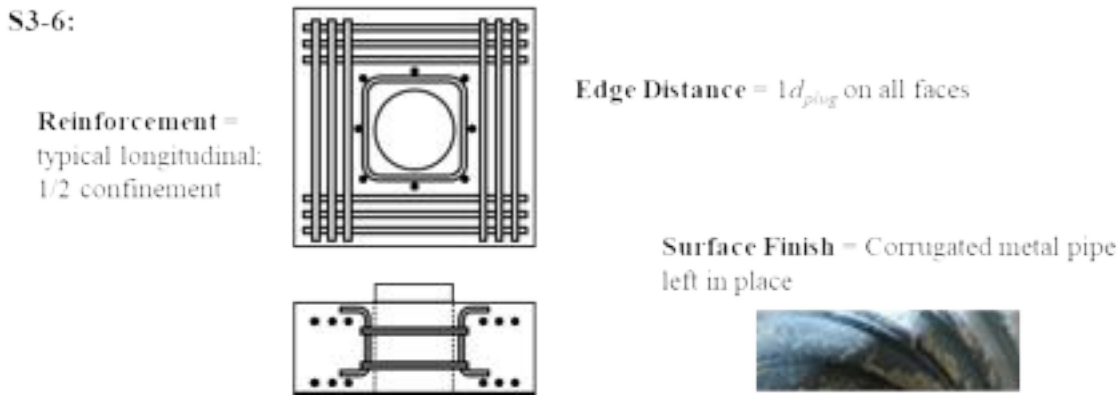

The maximum load was 283.8 kips. The specimen was loaded until 0.5 inch of displacement. Having a metal finish in this specimen decreased the capacity 200 kips when compared with specimen S3-4 which failed at 493.8 kips. The load versus displacement curve is shown in Figure A - 146.

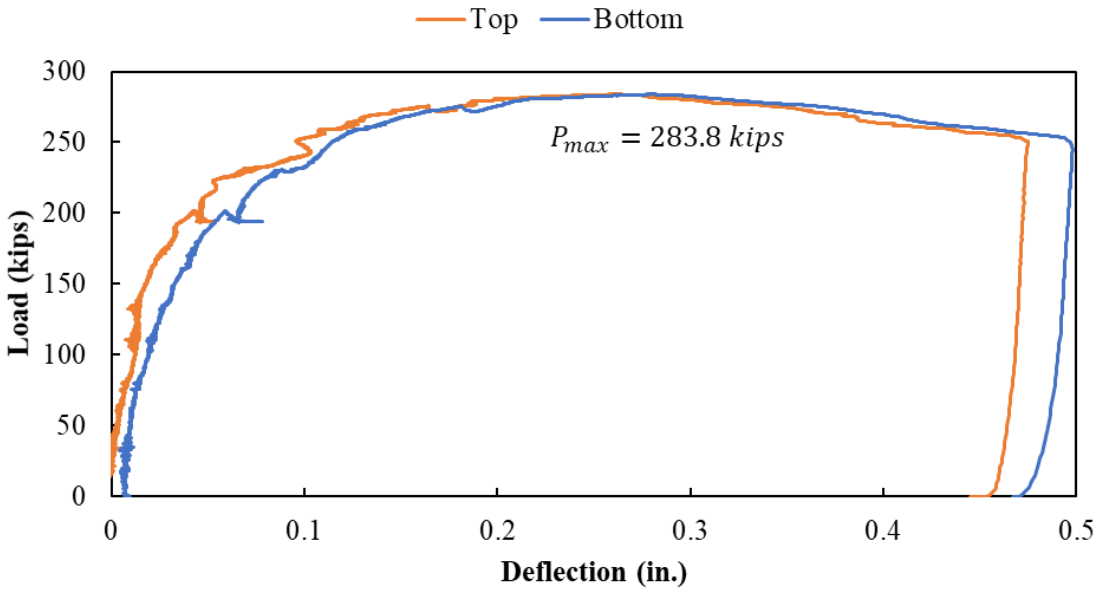

Figure A - 146: Load versus deflection curve for Specimen S3-6

The readings of the stain gauges in the longitudinal reinforcement in the bottom of the specimen are shown in Figure D.29. The bottom reinforcement started to engage in the north side (RSG-PCB1 and RSG-PCB2) at a load of around 80 kips. Later, when the load was around 140 kips the reinforcement placed on the west side started to get engaged. The reinforcement in this specimen started to engage earlier than the longitudinal reinforcement placed in specimen S3-4.

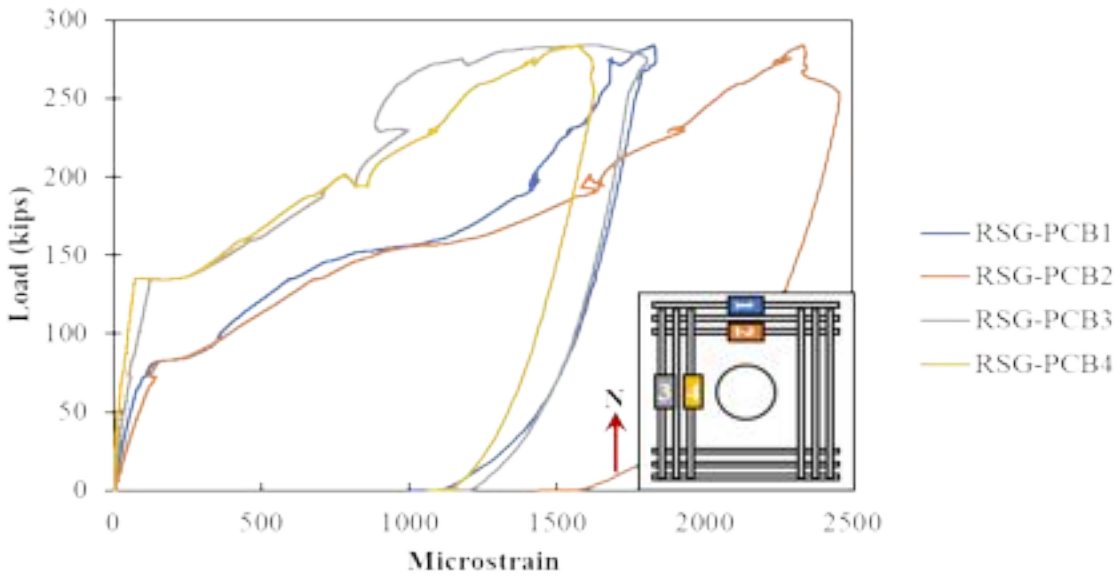

Figure A - 147: Rebar strain gauges in the longitudinal reinforcement on the bottom of Specimen S3-6

Cracking was also observed in the surface concrete at a load of around 80 kips on the north side of the specimen according to CSG-PCN1 and CSG-PCN2, as shown in Figure A - 148.

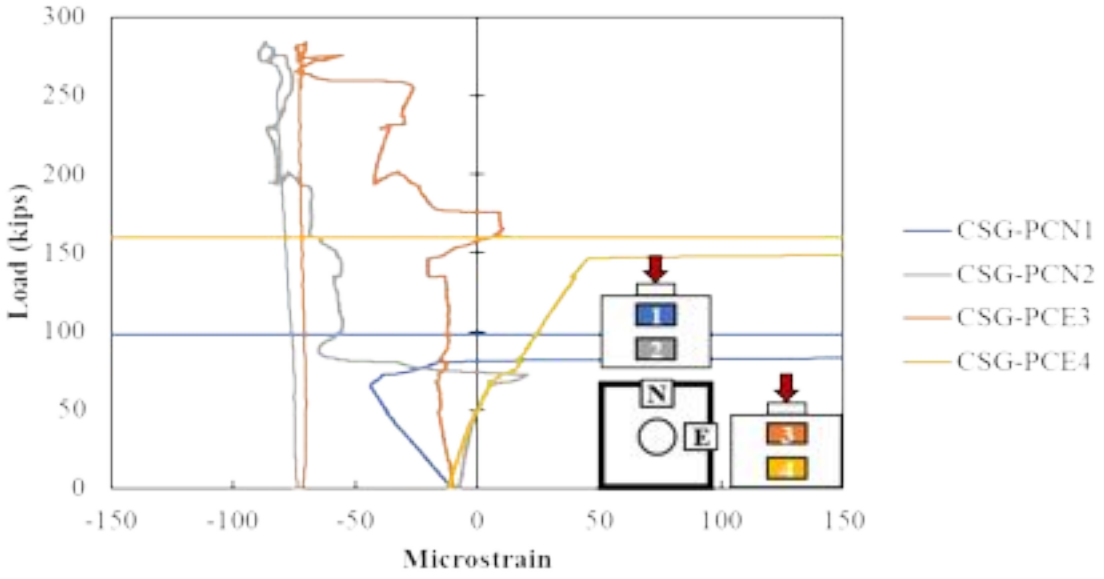

Figure A - 148: Concrete strain gauges in the surface of the cap of Specimen S3-6

The crack pattern at failure for S3-6 is shown in Figure A - 149. The cracks were observed to extend radially from the plug to all sides of the specimen in the top and bottom. The

largest cracks were observed extending radially from the plug to the corners of the specimen.

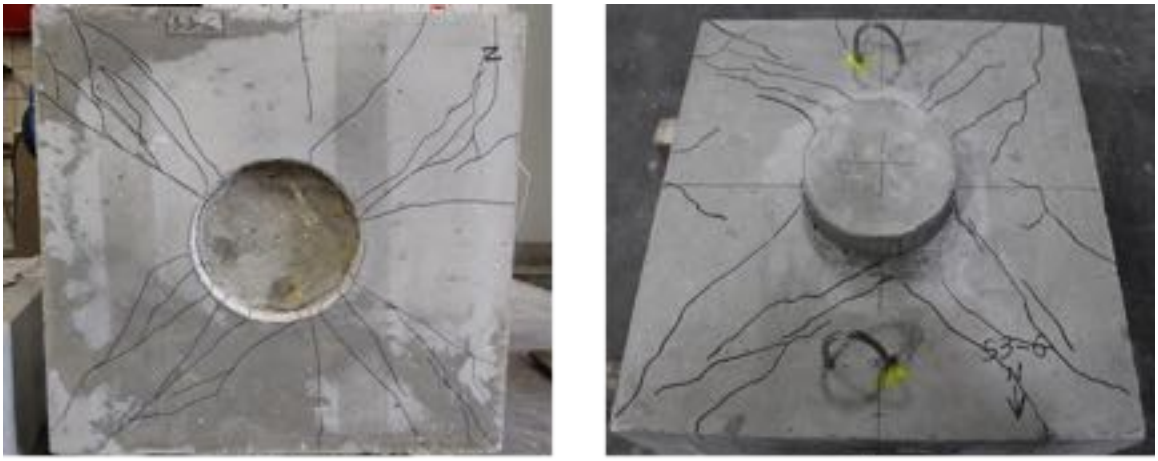

Figure A - 149: Cracking after testing on (a) bottom and (b) top of Specimen S3-6

The confining reinforcement around the pocket were first engaged in the north side of the plug on a load of around 80 kips, as shown in Figure A - 150. When the load was around 140 kips, the reinforcement in the west side of the specimen started to engage. More engagement was observed in the bottom reinforcement around pocket.

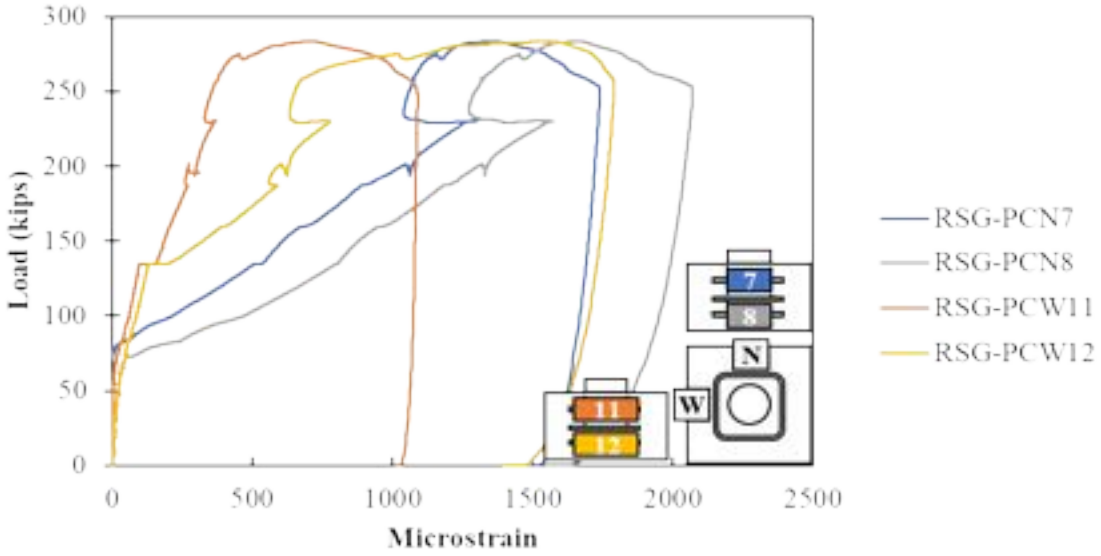

Figure A - 150: Confining reinforcement around pocket of Specimen S3-6

The measured strains in the vertical reinforcement in the plug and cap are shown in Figure A - 151. The stresses in the vertical reinforcement in the top of the plug were higher than in the bottom, suggesting transfer of stresses from plug to cap.

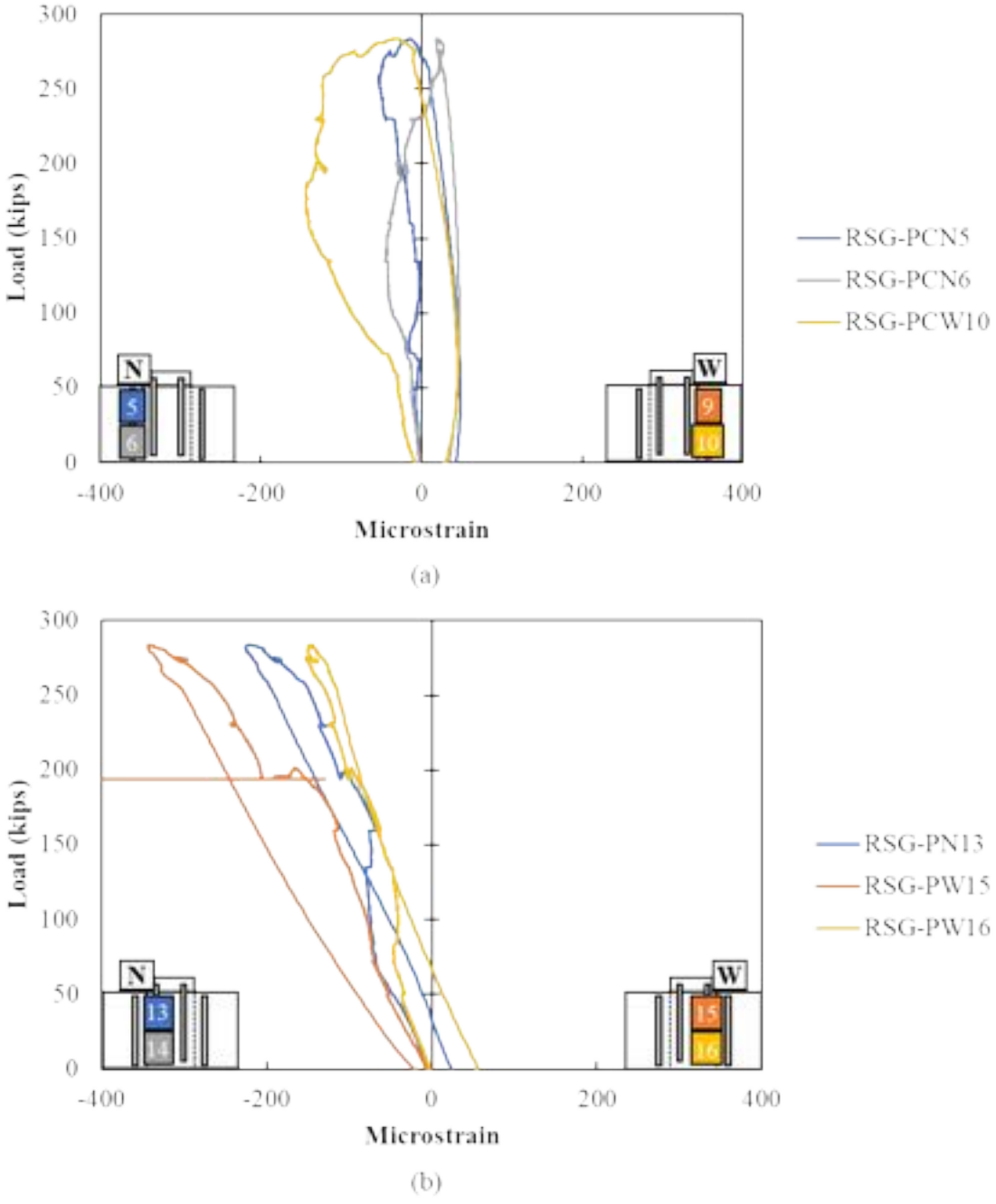

Figure A - 151: Rebar strain gauges in vertical reinforcement on (a) cap and (b) plug of Specimen S3-6

Specimen S3-7 Results

Specimen S3-7 had 3 #4 bars in two faces and 1 #7 bar in the other two faces as longitudinal reinforcement and typical reinforcement around pocket. The interface finish was sandblasted (1/16-inch roughness concrete finish).

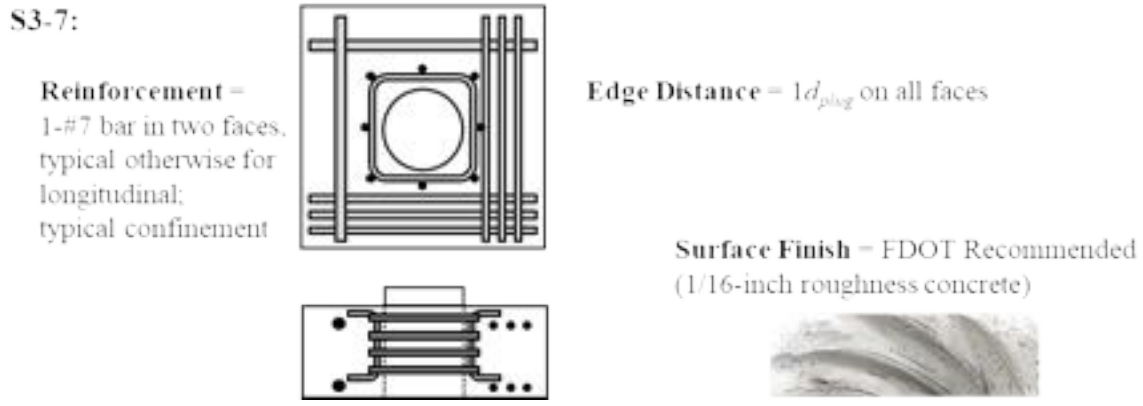

The capacity of the interface was 377.9 kips and after failure the specimen held a load of around 280 kips. The load displacement curve is shown in Figure A - 152.

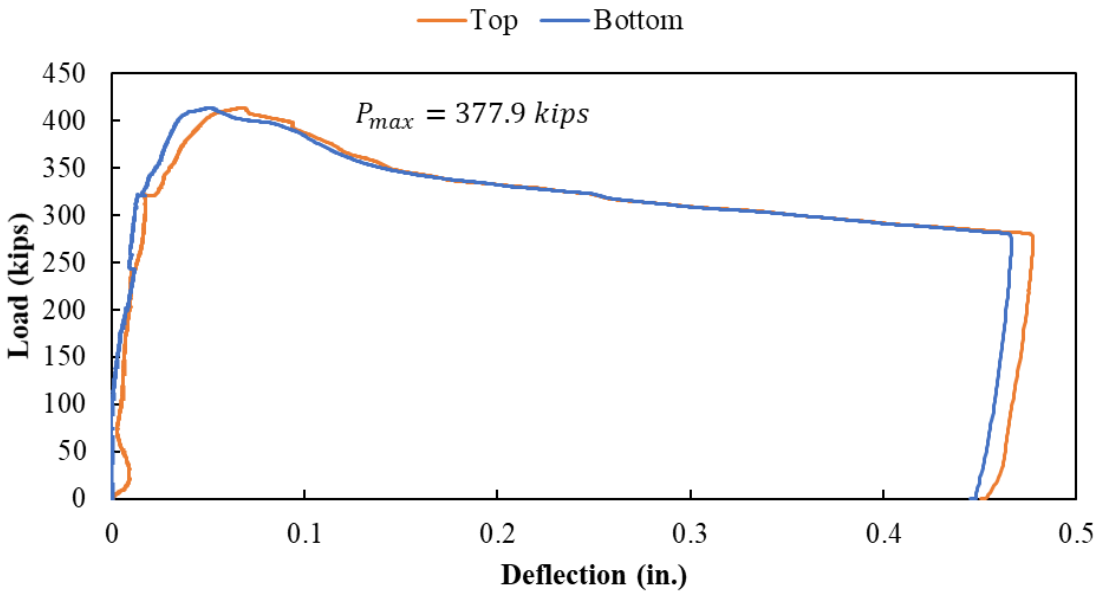

Figure A - 152: Load versus deflection curve for Specimen S3-7

This specimen can be compared with two specimens: Specimen S3-1 (no longitudinal reinforcement) and specimen S3-3 (2 #4 bars in each face). According to the results, having

this reinforcement layout does not increase the capacity of the specimen when compared to specimen S3-1, which had no confinement or longitudinal reinforcement. Specimen S3-3 had a higher failure load than Specimen S3-7 although it had less area of reinforcement crossing the failure plane.

The readings of the stain gauges in the longitudinal reinforcement in the bottom of the specimen are shown in Figure A - 153. The bottom reinforcement started to engage in the north side at a load of around 110 kips. Later, when the load was 250 kips the reinforcement placed on the west side started to engage.

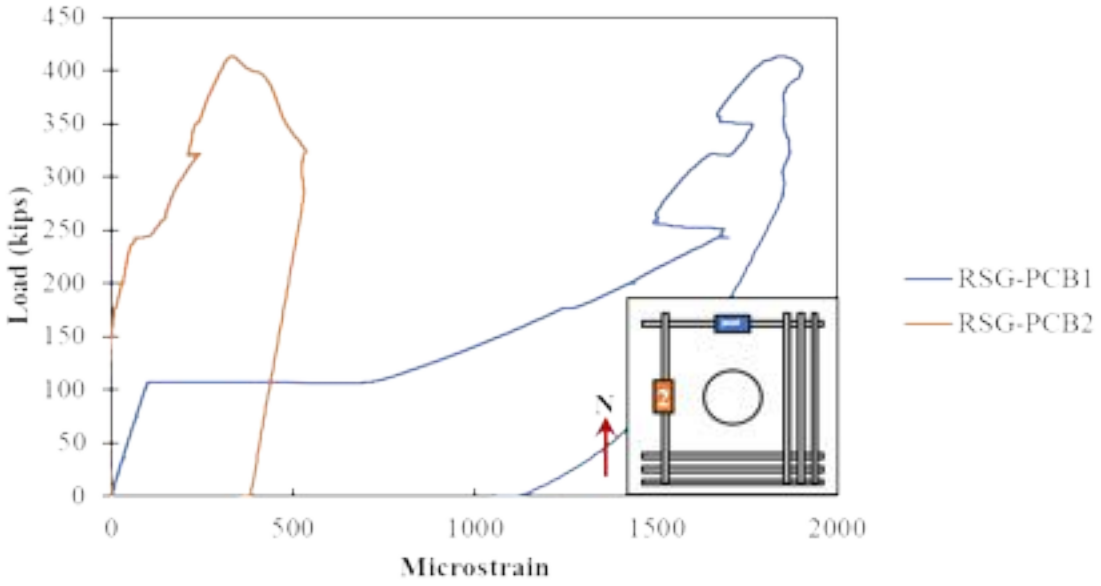

Figure A - 153: Rebar strain gauges in the longitudinal reinforcement on the bottom of Specimen S3-7

Cracking was also observed in the surface concrete at a load of around 100 kips on the north side of the specimen according to CSG-PCN1 and CSG-PCN2, as shown in Figure A - 154. Then when the load was around 170 kips cracks started to form on the east side.

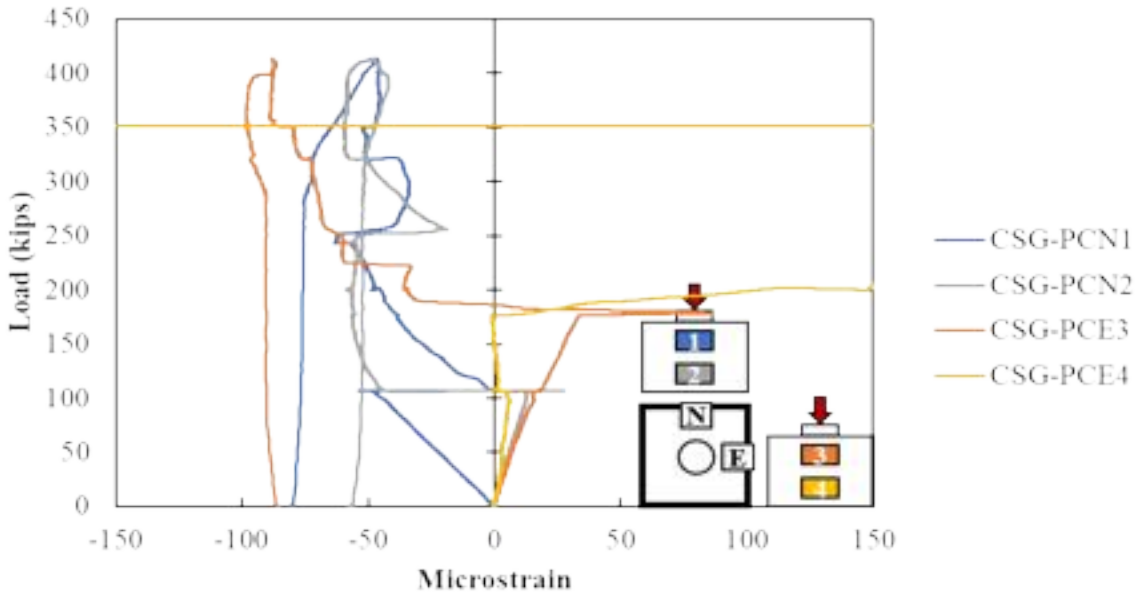

Figure A - 154: Concrete strain gauges in the surface of the cap of Specimen S3-7

The crack pattern at failure for S3-7 is shown in Figure A - 155. The cracks were observed to extend radially from the edge of the plug toward all sides of the specimen in the top and bottom.

Figure A - 155: Cracking on(a) cap and (b) bottom of Specimen S3-7

The confining reinforcement around the pocket were first engaged in the north side of the plug on a load of around 100 kips, as shown in Figure A - 156. When the load was around 250 kips, the reinforcement in the west side of the specimen started to engage.

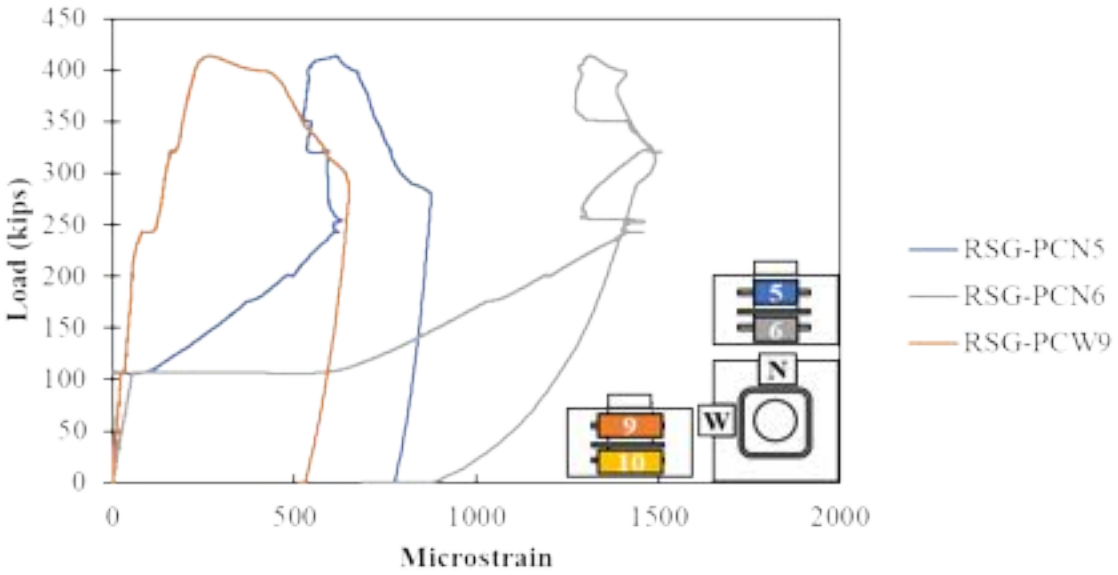

Figure A - 156: Confining reinforcement around the pocket of Specimen S3-7

The measured strains in the vertical reinforcement in the plug and cap are shown in Figure A - 157. Slightly more stresses were observed in the vertical reinforcement of the plug than the vertical reinforcement of the cap. Suggesting that a larger distance was required to transfer the stresses from the plug to cap.

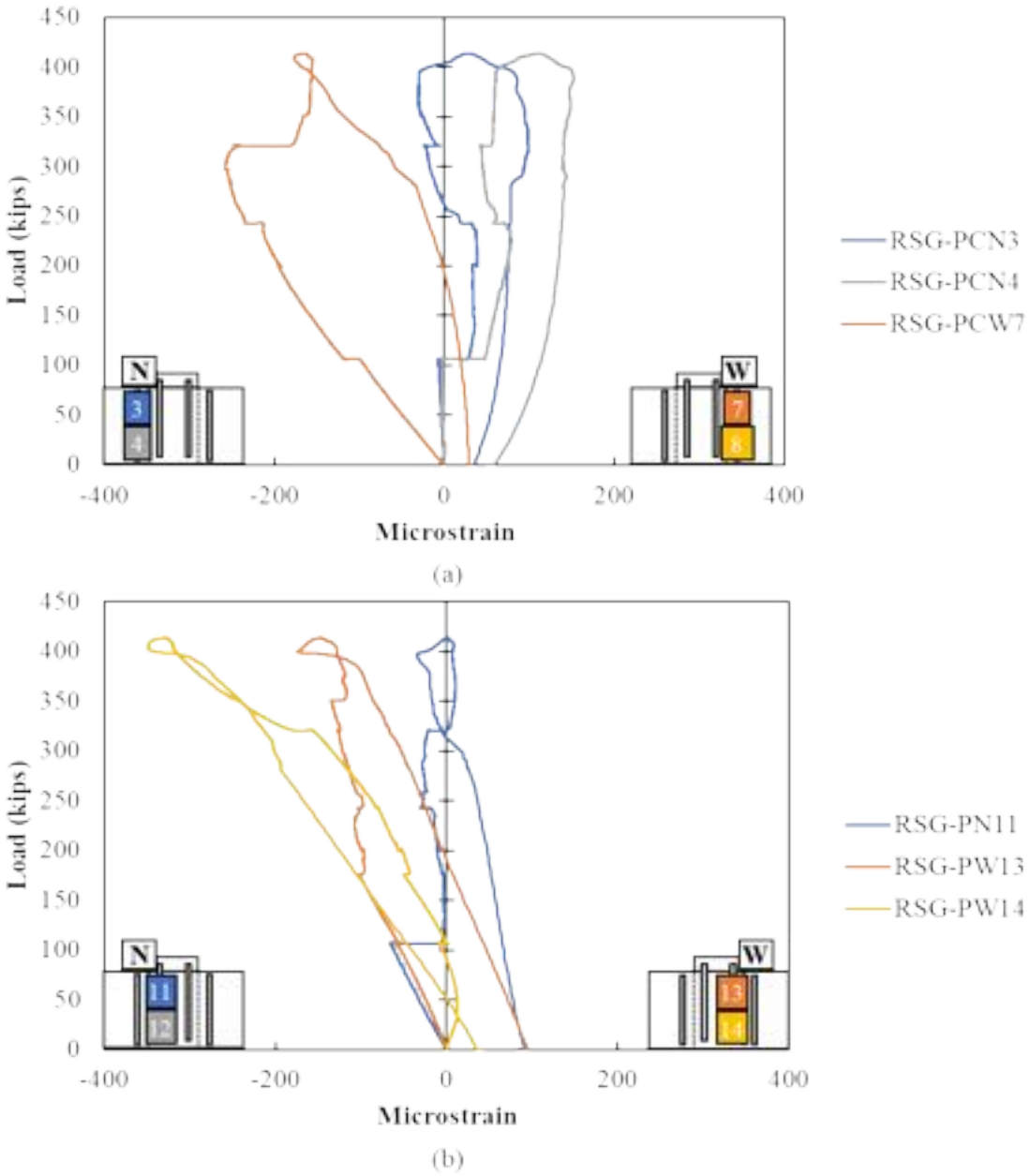

Figure A - 157: Rebar strain gauge in vertical reinforcement on (a) the cap and (b) plug of Specimen S3-7

Specimen S3-8 Results

Specimen S3-8 had 3 #4 bars and 1 #7 bar as longitudinal reinforcement and typical reinforcement around pocket. The interface finished was sandblasted (1/16'' of roughness).

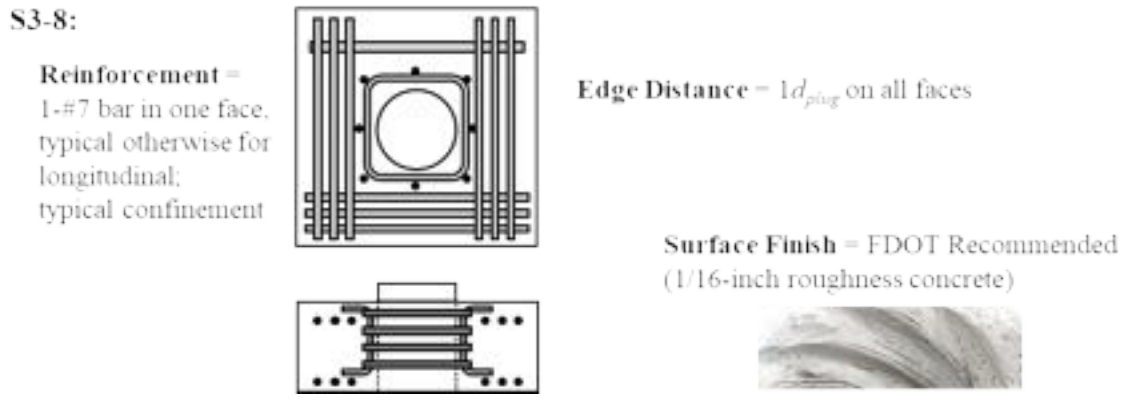

The interface capacity was 379.3 kips, and after failure the specimen still held a load of around 300 kips. This specimen had a similar behavior of the previous specimen. The load displacement curve is shown in Figure A - 158.

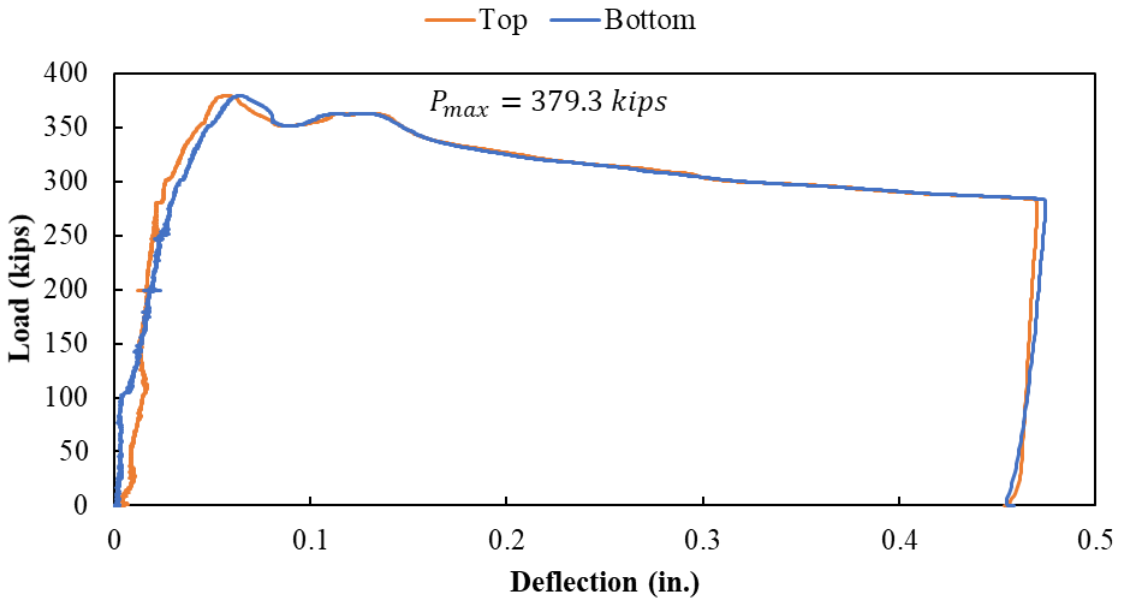

Figure A - 158: Load versus deflection curve for Specimen S3-8

The readings of the stain gauges in the longitudinal reinforcement in the bottom of the specimen are shown in Figure A - 159. The bottom reinforcement started to engage in the

north side at a load of around 100 kips. Then, when the load was around 120 kips the reinforcement placed on the west side started to get engaged.

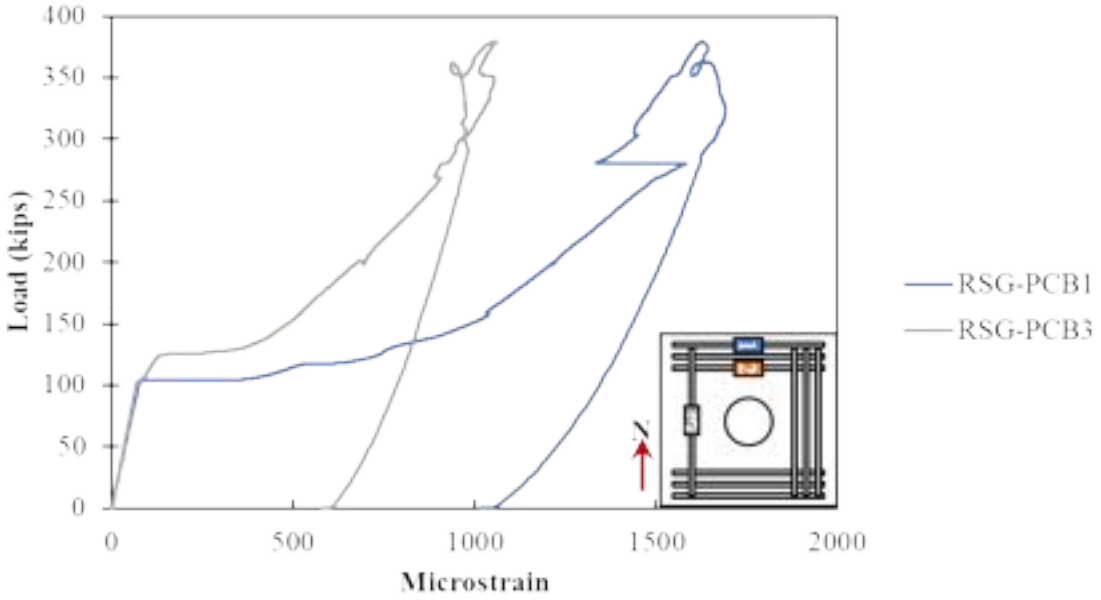

Figure A - 159: Rebar strain gauges in the longitudinal reinforcement on the bottom of Specimen S3-8

Cracking was also observed in the surface concrete at a load of around 100 kips in both faces, as shown in Figure A - 160.

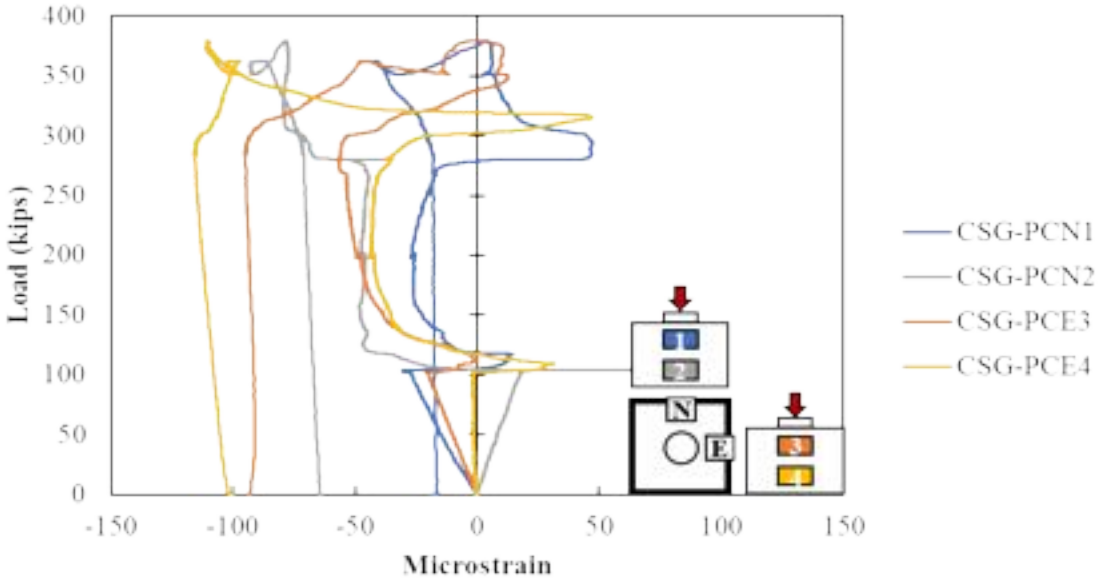

Figure A - 160: Concrete strain gauges in the surface of Specimen S3-8

The crack pattern at failure for S3-8 is shown in Figure A - 161. The cracks were observed to extend radially from the side of the plug toward all sides of the specimen in the top and bottom.

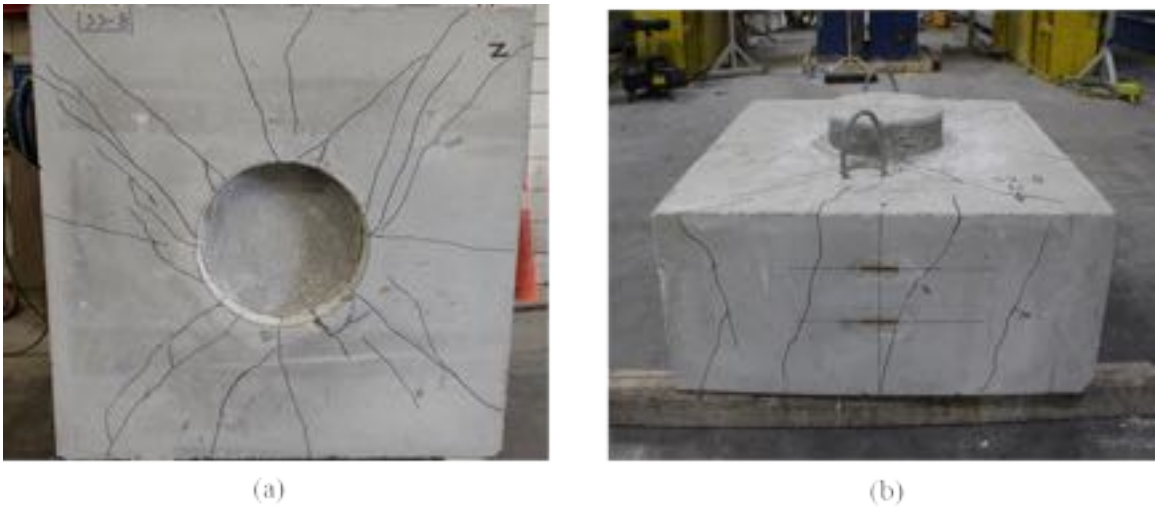

Figure A - 161: Cracking on (a) bottom and (b) cap of Specimen S3-8

The confining reinforcement around the pocket were engaged on both sides (north and west) around 110 kips, as shown in Figure A - 162. More engagement was observed in the bottom reinforcement around pocket than in the top reinforcement.

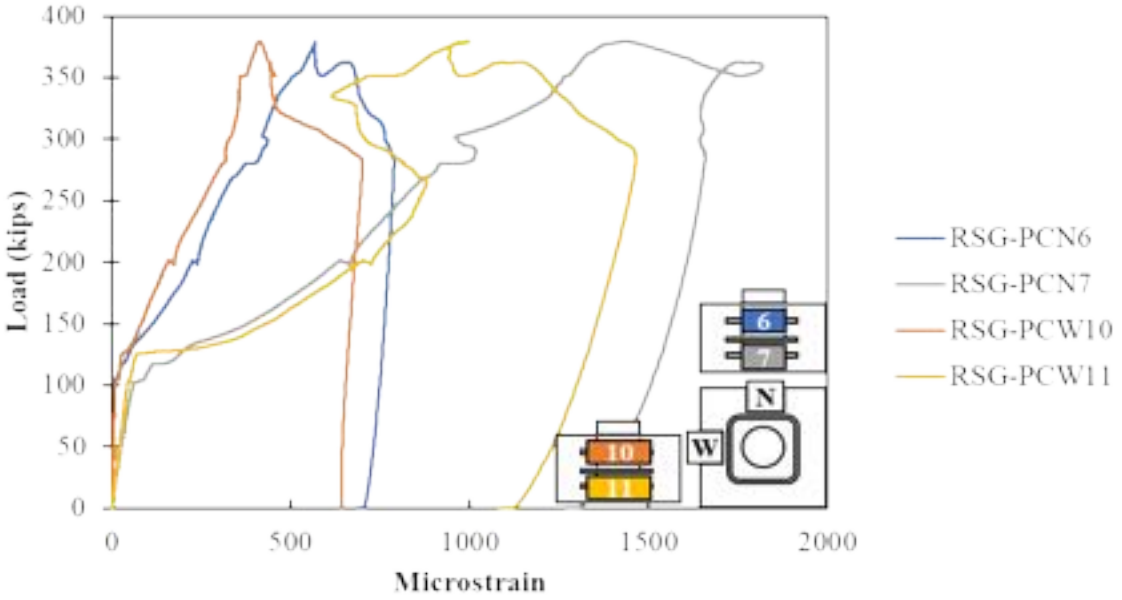

Figure A - 162: Confining reinforcement around pocket of Specimen S3-8

The measured strains in the vertical reinforcement in the plug and cap are shown in Figure A - 163. Higher stress was observed in the vertical reinforcement of the plug than the vertical reinforcement of the cap. Suggesting that a larger distance was required to transfer the stresses from the plug to cap.

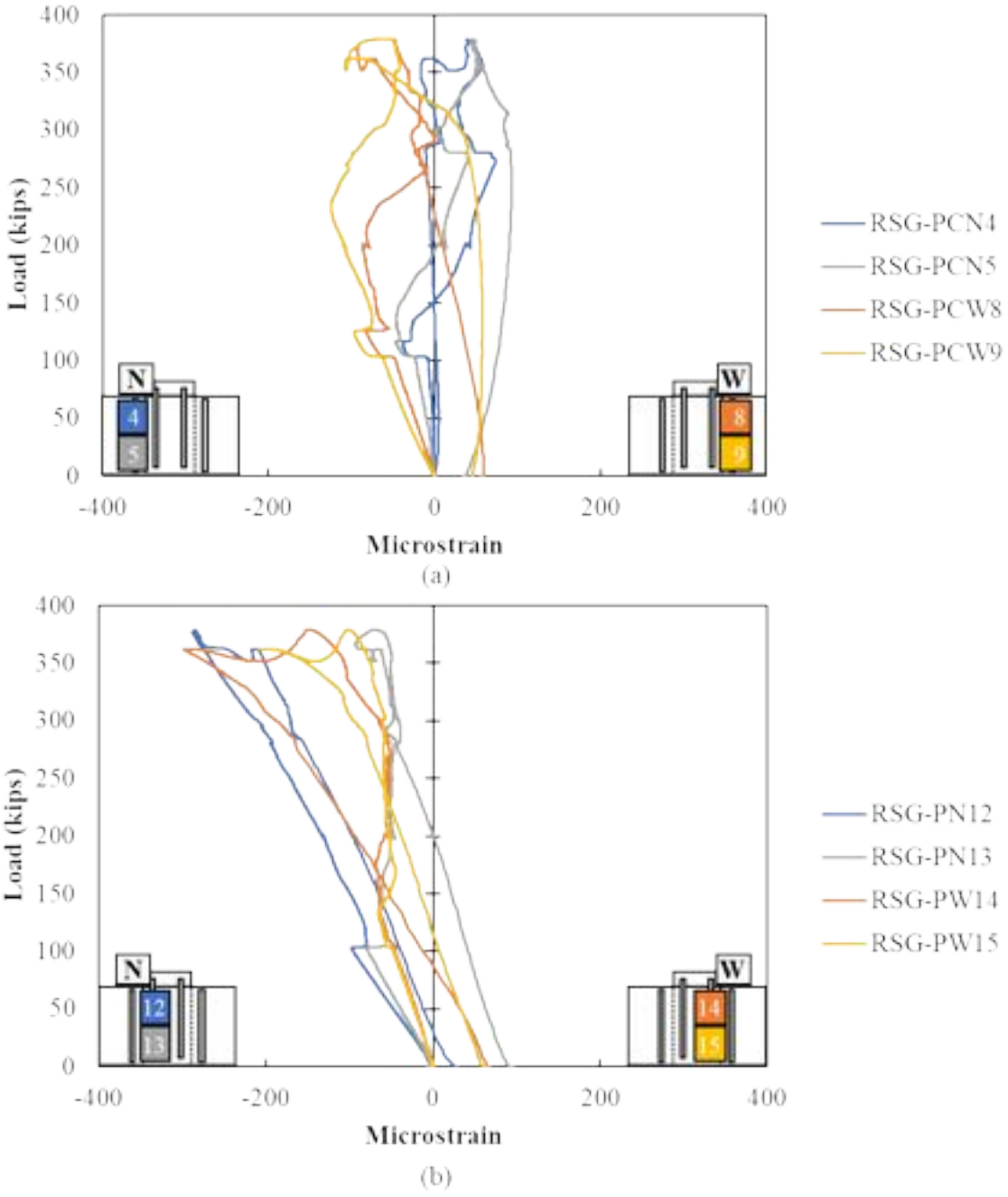

Figure A - 163: Rebar strain gauges in vertical reinforcement on (a) cap and (b) plug of Specimen S3-8

Specimen S3-9 Results

Specimen S3-9 had typical reinforcement around pocket and 3 #4 bars and 1 #7 bar as longitudinal reinforcement. The west face of the specimen had $0.5d_{plug}$ as edge distance. The interface finished was sandblasted (1/16'' of roughness)

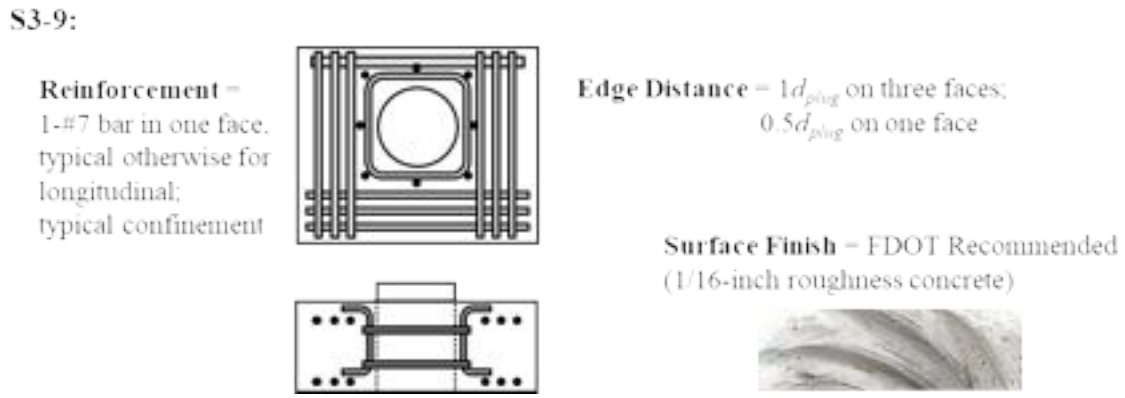

The maximum load was 364.6 kips, and after failure the specimen still held a load of 230 kips. The specimen was loaded until 0.5-inch displacement of plug. The load displacement curve is shown in Figure A - 164.

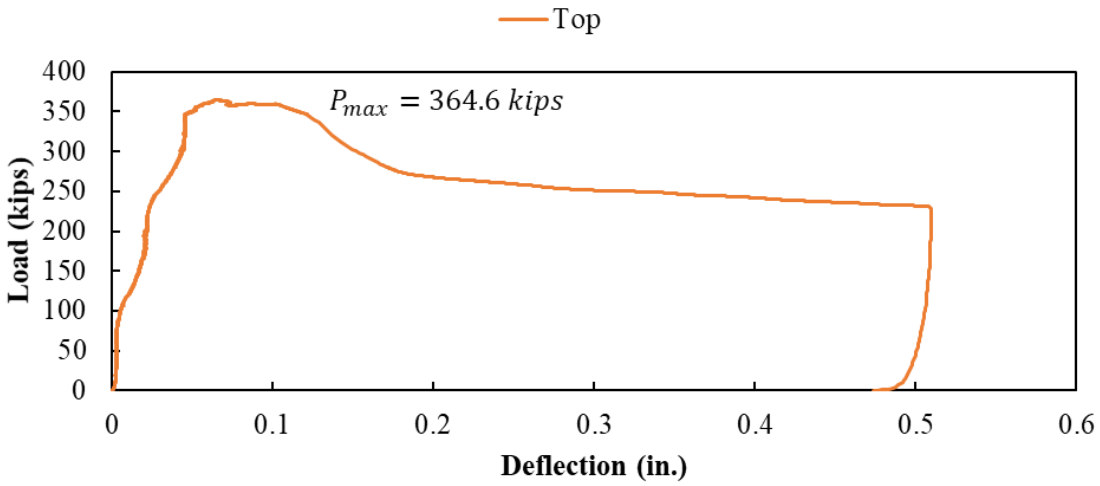

Figure A - 164: Load versus deflection curve for Specimen S3-9

This specimen had the same reinforcement scheme as S3-8. Although, as mention before, one face of the specimen had less area of concrete, the capacity of both specimens was similar.

The readings of the stain gauges in the longitudinal reinforcement in the bottom of the specimen are shown in Figure A - 165. Gauges RSG-PCB1 and RSG-PCB2 were damaged. The bottom reinforcement started to engage in the west side at a load of around 100 kips.

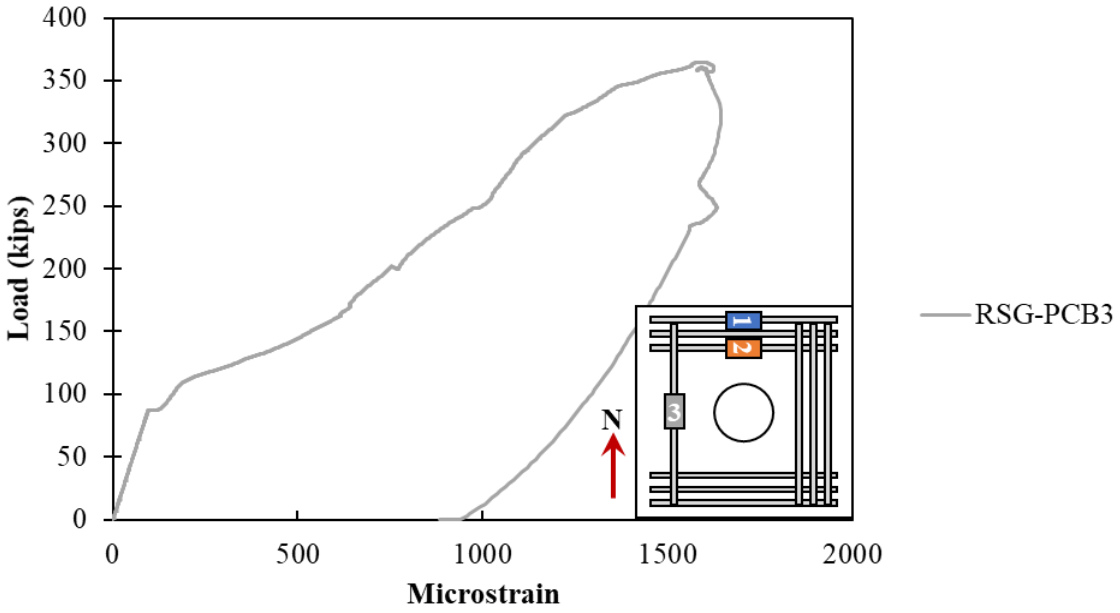

Figure A - 165: Rebar strain gauges in the longitudinal reinforcement on the bottom of Specimen S3-9

Cracking was also observed in the surface concrete at a load between 100 and 150 kips on the north and east side of the specimen according to CSG-PCN2 and CSG-PCE4, as shown in Figure A - 166. The propagation of the cracks started in the bottom of the specimen going towards the top of the cap.

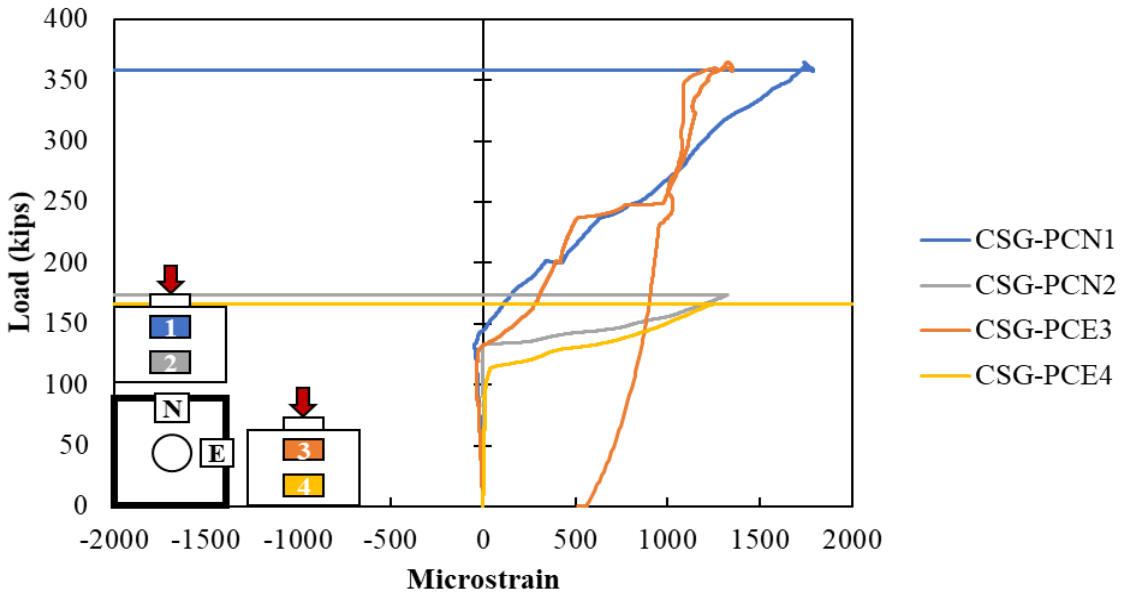

Figure A - 166: Concrete strain gauges in the surface of the cap of Specimen S3-9

The crack pattern at failure for S3-9 is shown in Figure A - 167. The cracks were observed to extend radially from the pocket with more cracking concentrated on the side with the shorter edge distance. Some cracking parallel to the edge was also observed on the side with the shorter edge distance, shown in Figure A - 167(b).

Figure A - 167: Cracking on (a) cap and (b) bottom of Specimen S3-9

The confining reinforcement around the pocket were engaged in all sides of the plug on a load between 120 and 150 kips, as shown in Figure A - 168.

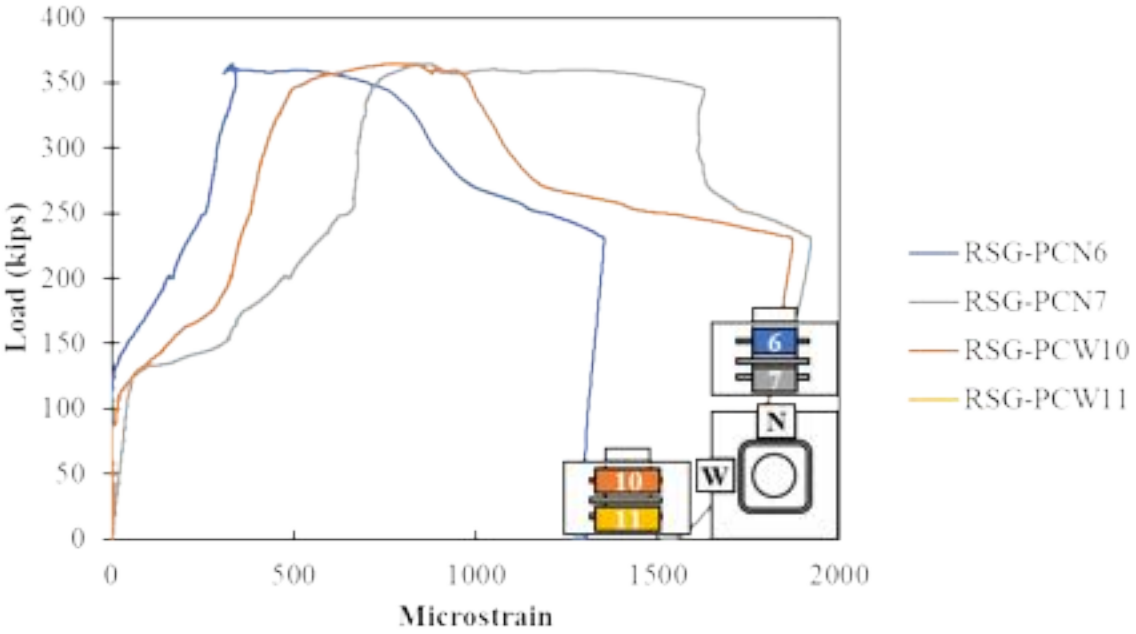

Figure A - 168: Confining reinforcement around pocket of Specimen S3-9

The measured strains in the vertical reinforcement in the plug and cap are shown in Figure A - 169. The stresses in the vertical reinforcement in the top of the plug were higher than in the bottom, suggesting transfer of stresses from plug to cap. Slightly more stresses were observed in the vertical reinforcement of the plug suggesting that a largest distance was required to transfer the stresses from the plug to cap.

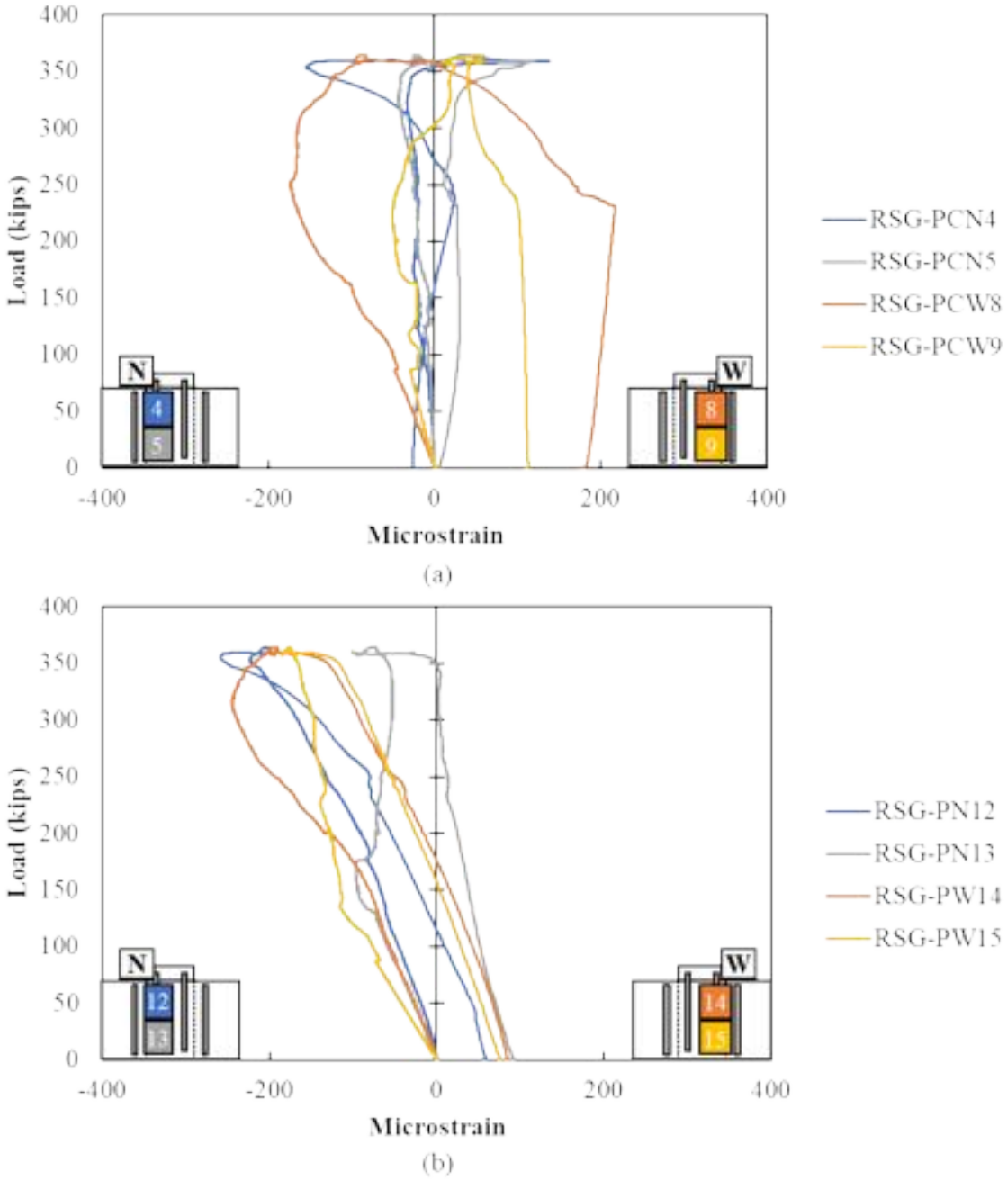

Figure A - 169: Rebar strain gauges in vertical reinforcement (a) cap and (b) plug of Specimen S3-9

Specimen S3-10 Results

Specimen S3-10 had typical reinforcement around pocket and 3 #4 bars and 1 #7 bar as longitudinal reinforcement. The north and west faces of the specimen had $0.5d_{plug}$ as edge distance. The #7 bars were located on those faces.

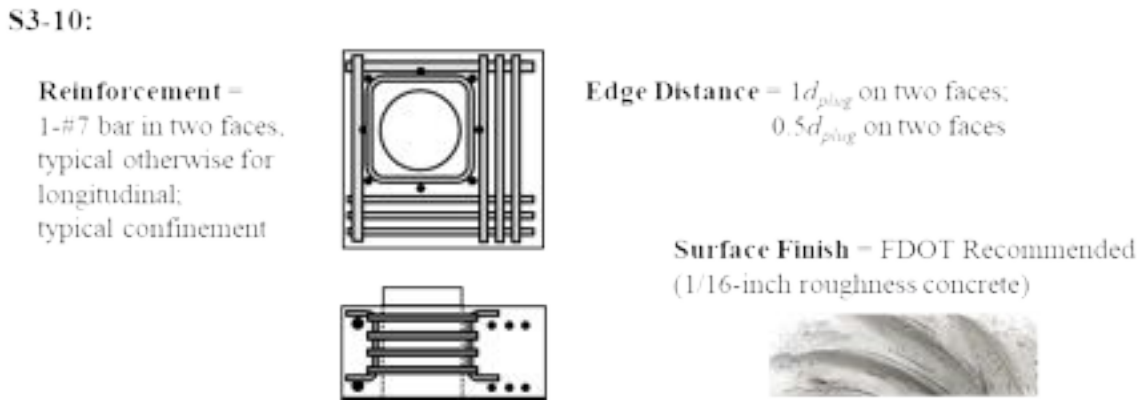

The interface finish was sandblasted (1/16-inch roughness concrete finish). The interface capacity was 330.7 kips. This specimen had 50 kips less capacity than specimen S3-7, which had the same reinforcement layout. The load displacement curve is shown in Figure A - 170.

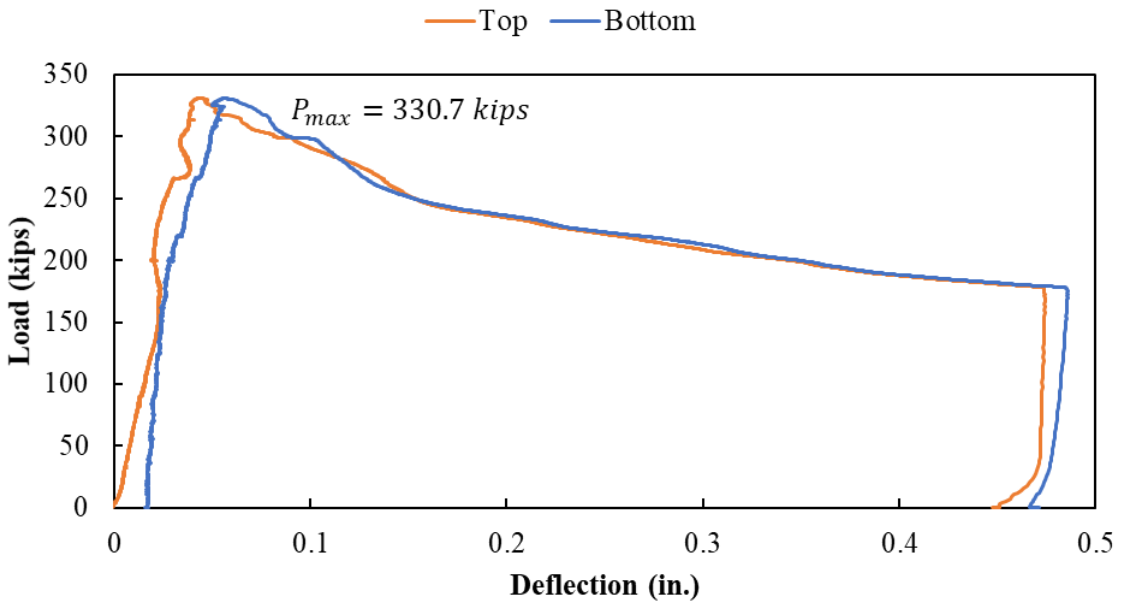

Figure A - 170: Load versus deflection curve for Specimen S3-10

The readings of the stain gauges in the longitudinal reinforcement in the bottom of the specimen are shown in Figure A - 171. The bottom reinforcement started to engage in the west side before 100 kips. Then, when the load was around 120 kips the reinforcement placed on the north side started to engage.

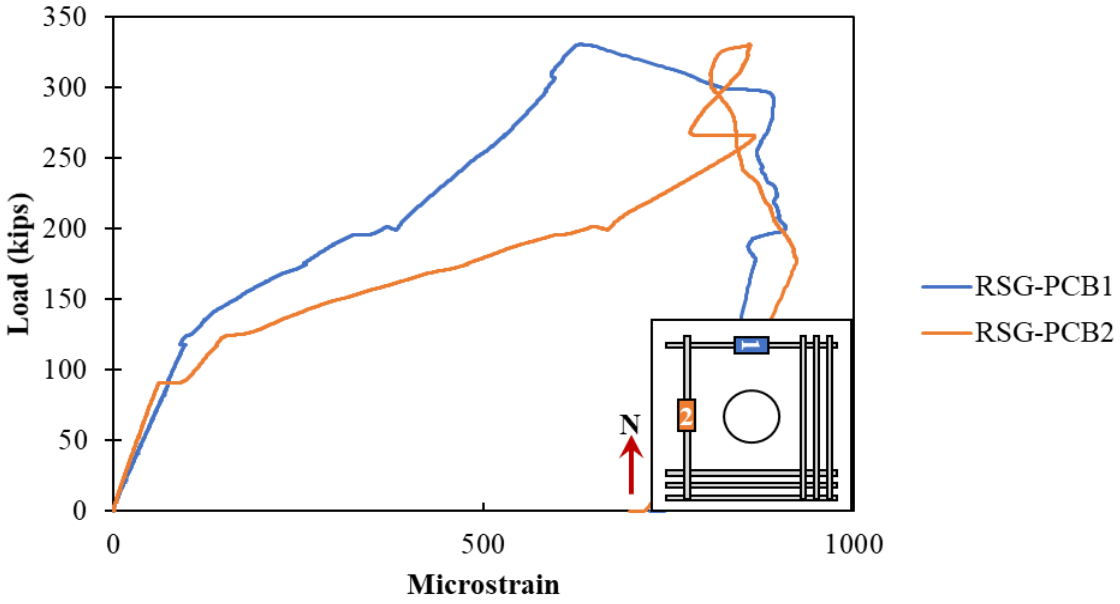

Figure A - 171: Rebar strain gauges in the longitudinal reinforcement on the bottom of Specimen S3-10

Cracking was also observed in the surface concrete at a load of around 90 kips in the east side of the specimen, as shown in Figure A - 172. A crack opened on the north side of the specimen at a load around 125 kips.

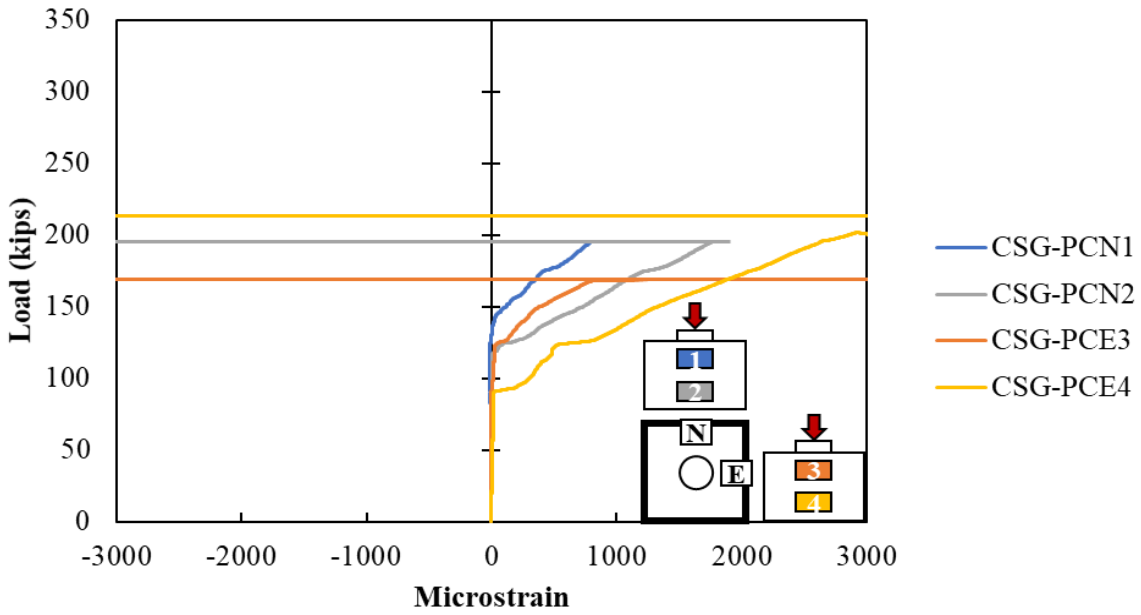

Figure A - 172: Concrete strain gauges in the surface of Specimen S3-10

The crack pattern at failure for S3-10 is shown in Figure A - 173. The cracks were observed to extend radially from the plug toward all sides, but there was a concentration of cracking and larger cracks observed toward the corner between the two short edges.

Figure A - 173: Cracking after testing on (a) bottom and (b) cap of Specimen S3-10

The confining reinforcement around the pocket were engaged on both sides (north and west) between 80 and 120 kips, as shown in Figure A - 174. More engagement was observed in the bottom reinforcement around pocket located in the north side than in the west side.

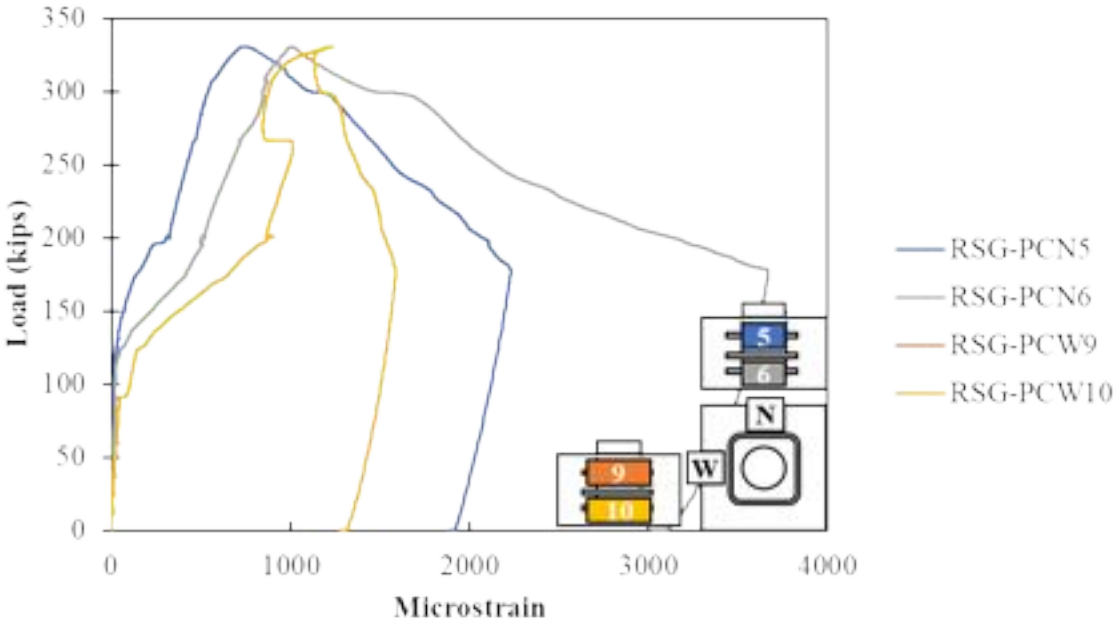

Figure A - 174: Confining reinforcement around pocket of Specimen S3-10

The measured strains in the vertical reinforcement in the plug and cap are shown in Figure A - 175. More stresses were observed in the vertical reinforcement of the cap than the vertical reinforcement of the plug. Suggesting that a short distance was required to transfer the stresses from the plug to cap. The measured strains in the plug were similar in all sides and through the height of the interface.

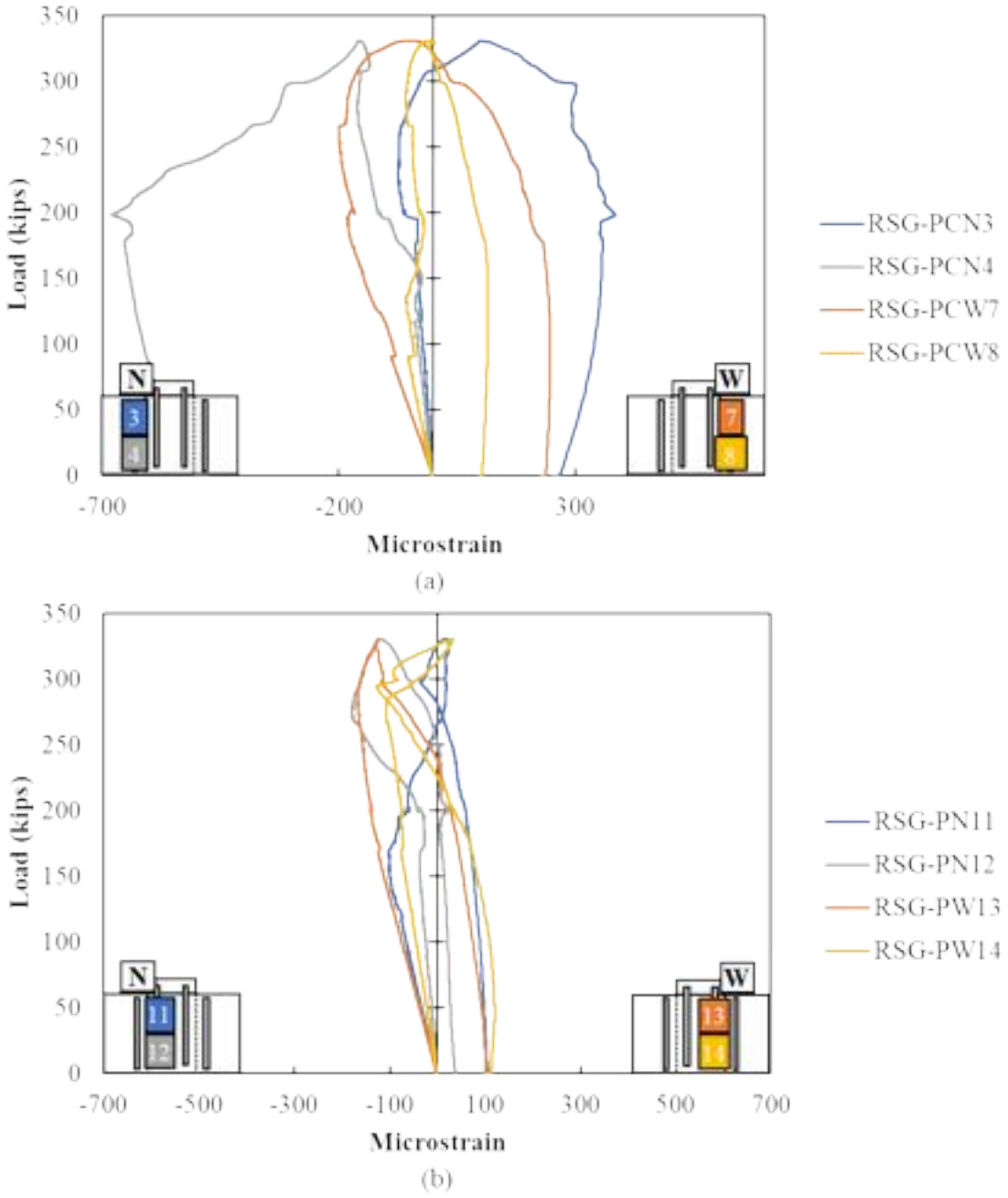

Figure A - 175: Rebar strain gauges in vertical reinforcement on (a) cap and (b) plug of Specimen S-10

Specimen S3-11 Results

Specimen S3-11 had typical reinforcement around pocket and 3 #4 bars and 1 #7 bar as longitudinal reinforcement. The west face of the specimen had $0.75d_{plug}$ as edge distance. The interface finished was sandblasted (1/16-inch roughness concrete finish).

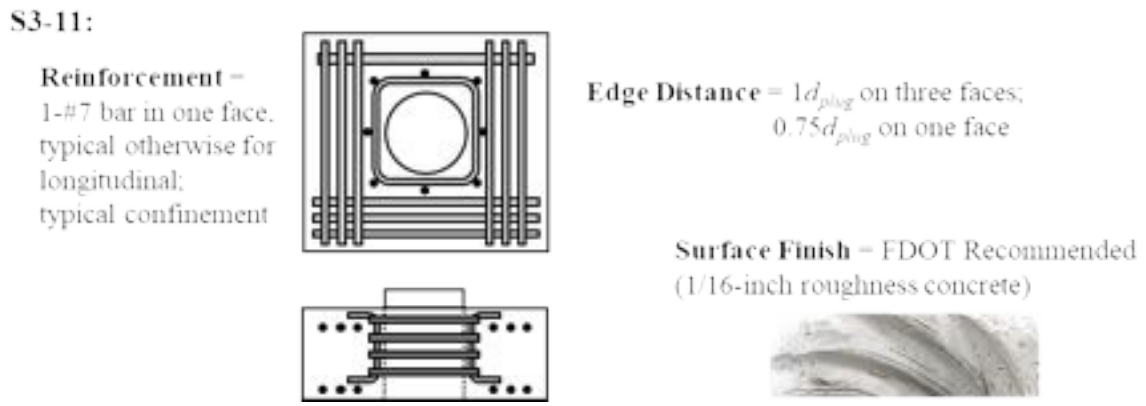

The interface capacity was 352.4 kips, and after failure the specimen still held a load of 220 kips. Similar behavior was seen between this specimen and S3-9. The load displacement curve is shown in Figure A - 176.

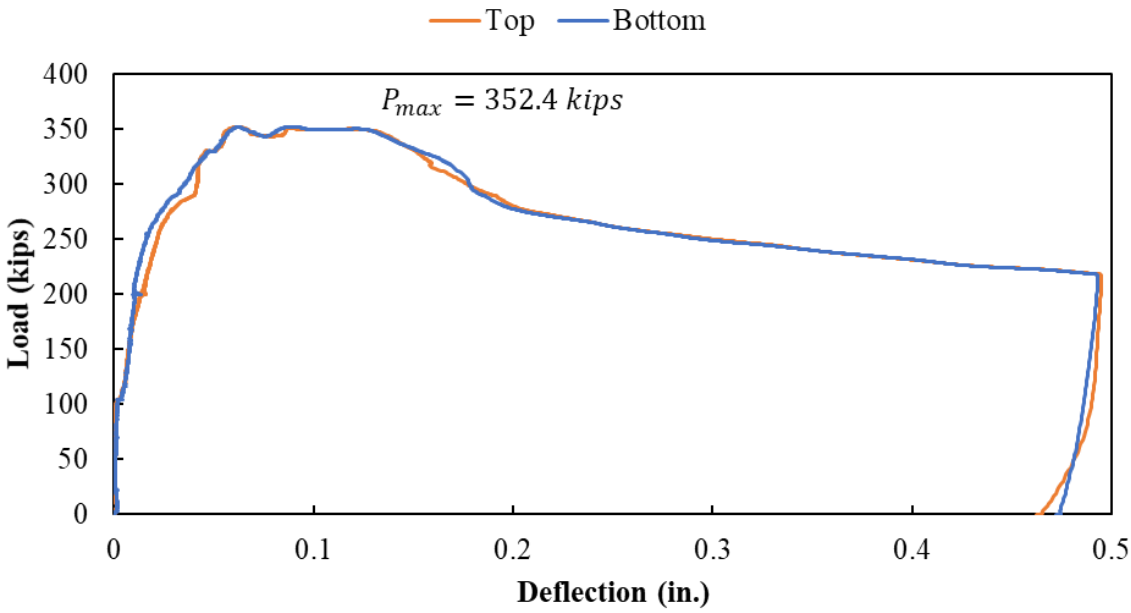

Figure A - 176: Load versus deflection curve for Specimen S3-11

The readings of the stain gauges in the longitudinal reinforcement in the bottom of the specimen are shown in Figure A - 177. The bottom reinforcement started to engage in both sides around 100 kips.

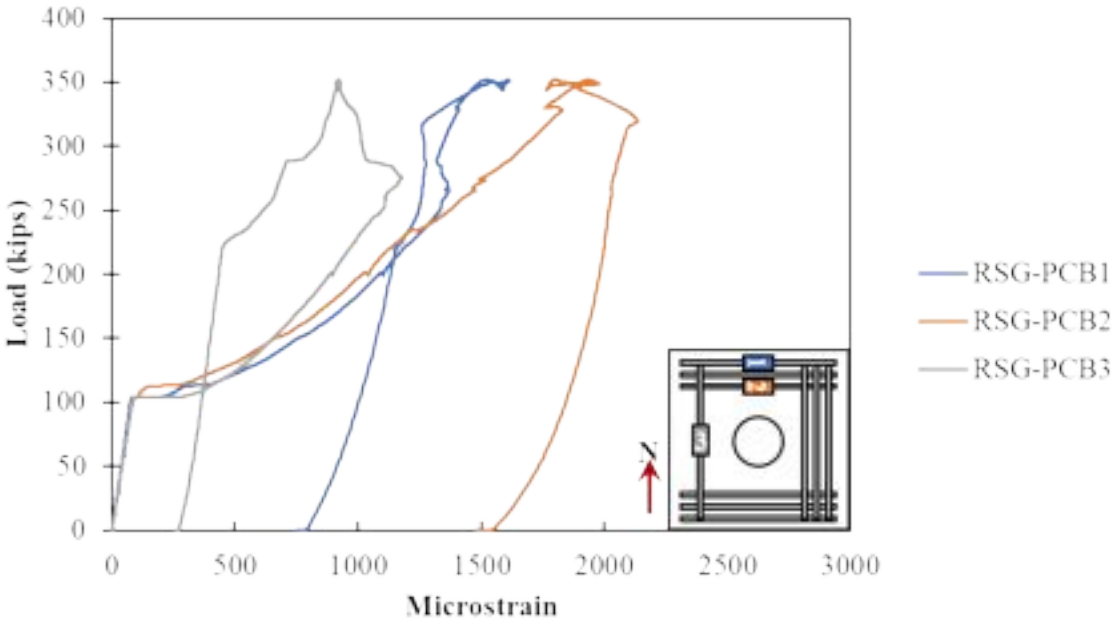

Figure A - 177: Rebar strain gauges in the longitudinal reinforcement on the bottom of Specimen S3-11

Cracking was also observed in the surface concrete at a load of 100 kips on the north and east side of the specimen according to CSG-PCN2 and CSG-PCE4, as shown in Figure A - 178.

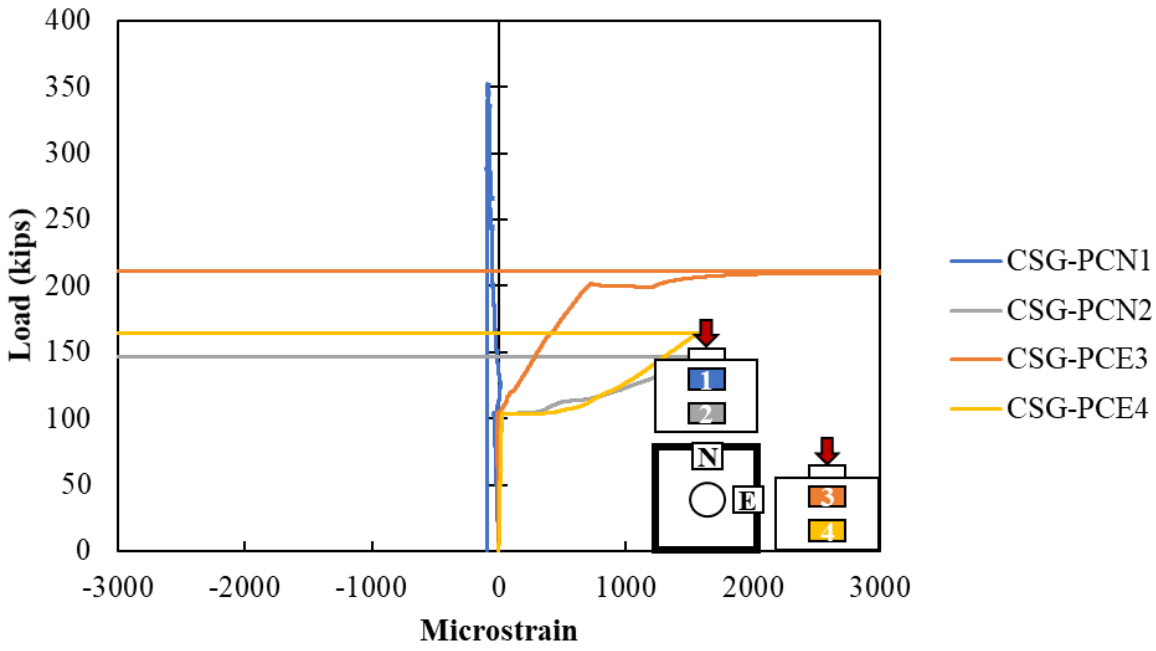

Figure A - 178: Concrete strain gauges in the surface of the cap of Specimen S3-11

The crack pattern at failure for S3-11 is shown in Figure A - 179. The cracks were observed to extend radially from the plug in all directions with most cracking going to the corners of the face with the reduced edge distance.

Figure A - 179: Cracking on (a) bottom after testing and (b) cap during testing of Specimen S3-11

The confining reinforcement around the pocket were engaged in all sides of the plug at a load of 100 kips as shown in Figure A - 180. Higher strains were observed in the confinement reinforcement toward the bottom of the plug.

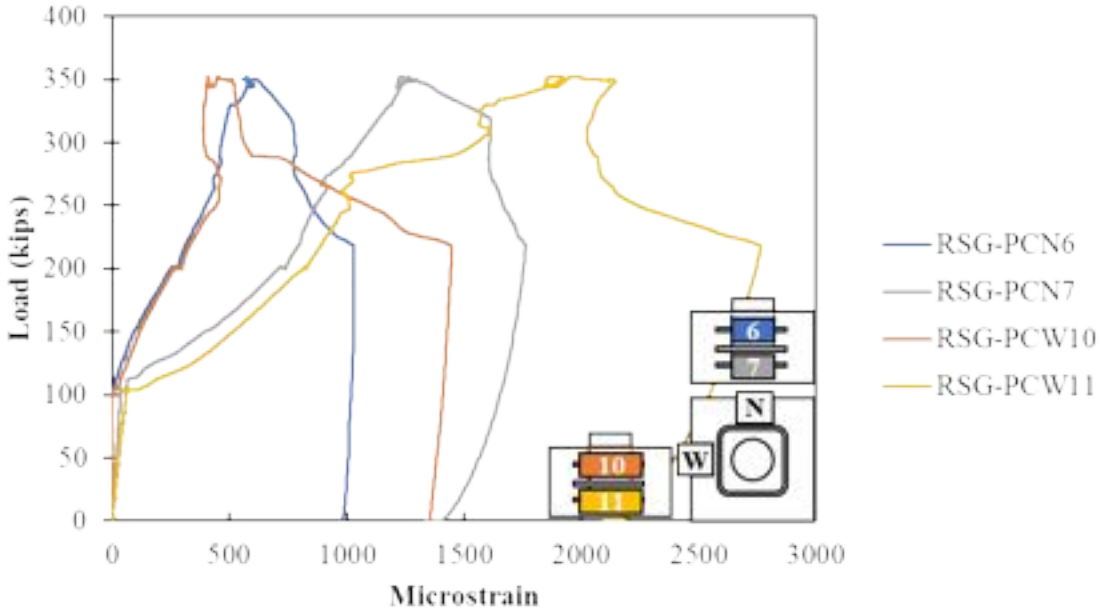

Figure A - 180: Confining reinforcement around pocket of Specimen S3-11

The measured strains in the vertical reinforcement in the plug and cap are shown in Figure A - 181. Slightly higher stresses were observed in the vertical reinforcement of the plug compared to the cap suggesting that a larger distance was required to transfer the stresses from the plug to cap. The stresses in the plug were higher in the bottom and then decreased towards the top of the plug.

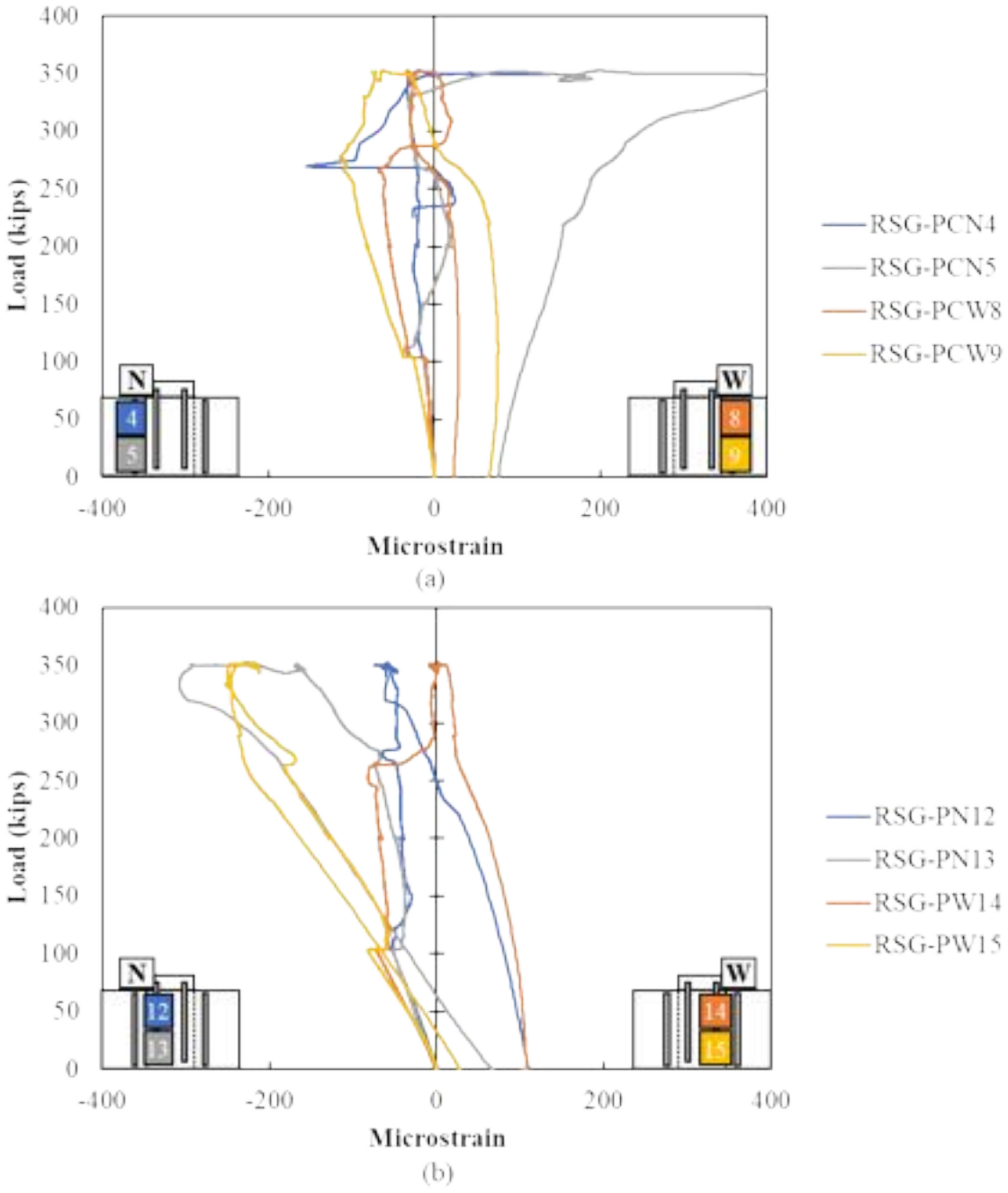

Figure A - 181: Rebar strain gauges in vertical reinforcement (a) cap and (b) plug of Specimen S3-11

Specimen S3-12 Results

Specimen S3-12 had typical reinforcement around pocket and 3 #4 bars and 1 #7 bar as longitudinal reinforcement. The north and west faces of the specimen had $0.75d_{plug}$ as edge

distance; the #7 bars were located on those faces. The interface finish was sandblasted (1/16-inch roughness concrete finish).

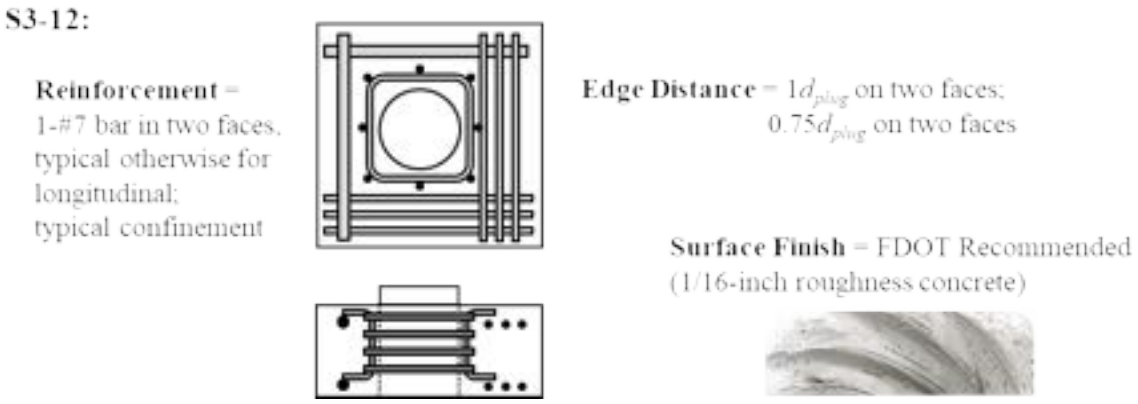

The interface capacity was 363.2 kips. After failure, the specimen still held a load of 200 to 250 kips and was loaded until 0.5-inch of displacement of the plug. This specimen was like S3-10 and had 30 kips more capacity. The load displacement curve is shown in Figure A - 182.

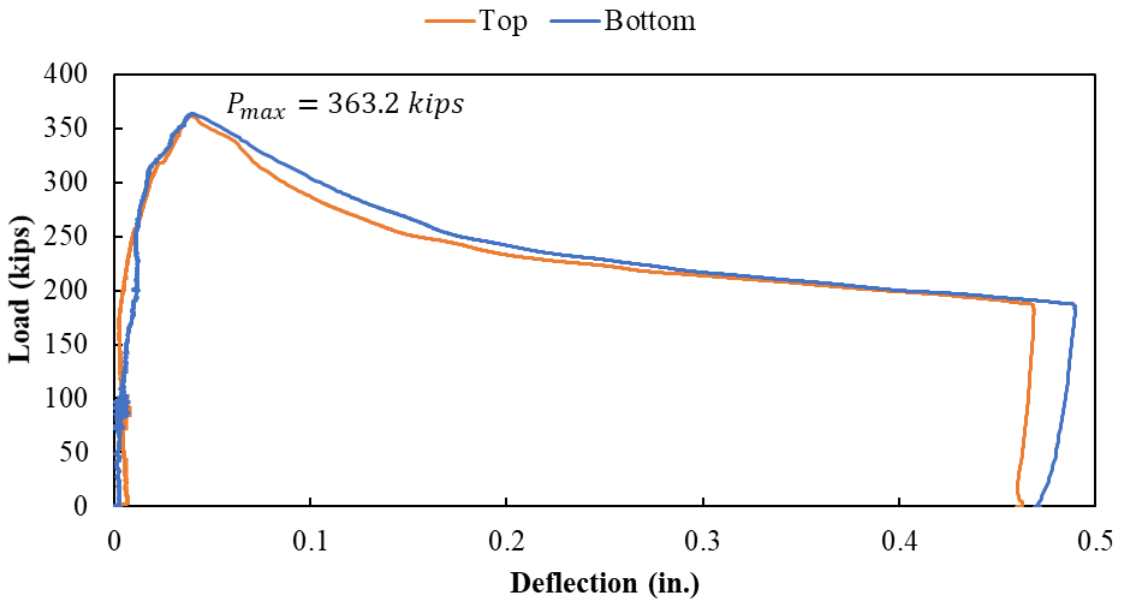

Figure A - 182: Load versus deflection curve for Specimen S3-12

The readings of the stain gauges in the longitudinal reinforcement in the bottom of the specimen are shown in Figure A - 183. The bottom reinforcement started to engage in both sides at a load around 120 kips. Similar engagement was seen after testing in both faces.

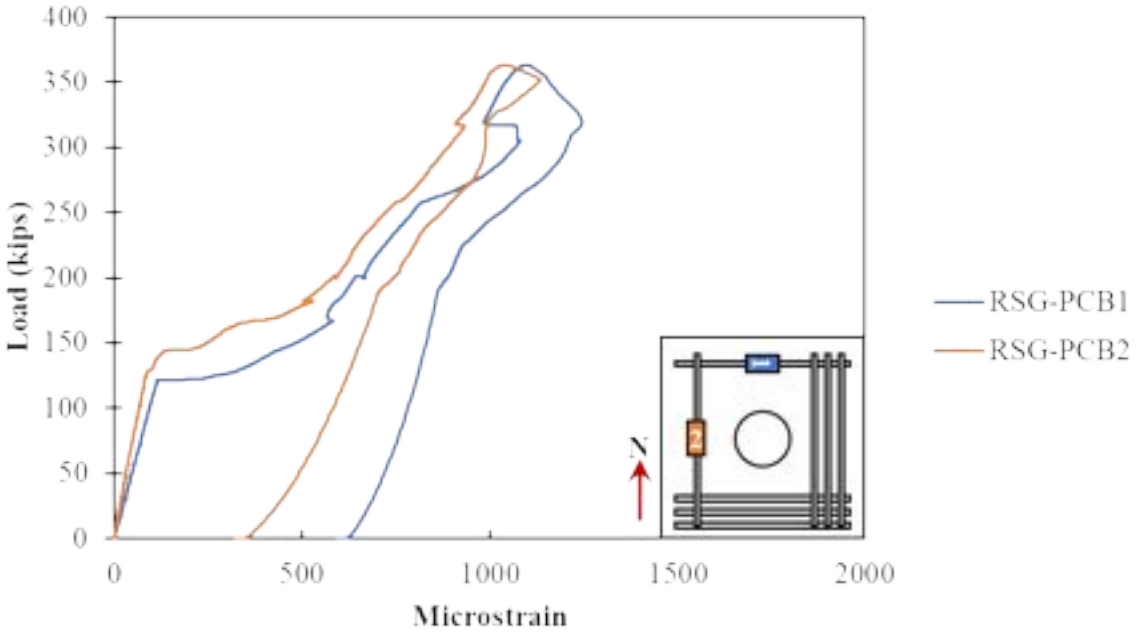

Figure A - 183: Rebar strain gauges in the longitudinal reinforcement on the bottom of Specimen S3-12

Cracking was also observed in the surface concrete at a load of around 120 kips in the north side of the specimen, as shown in Figure A - 184.

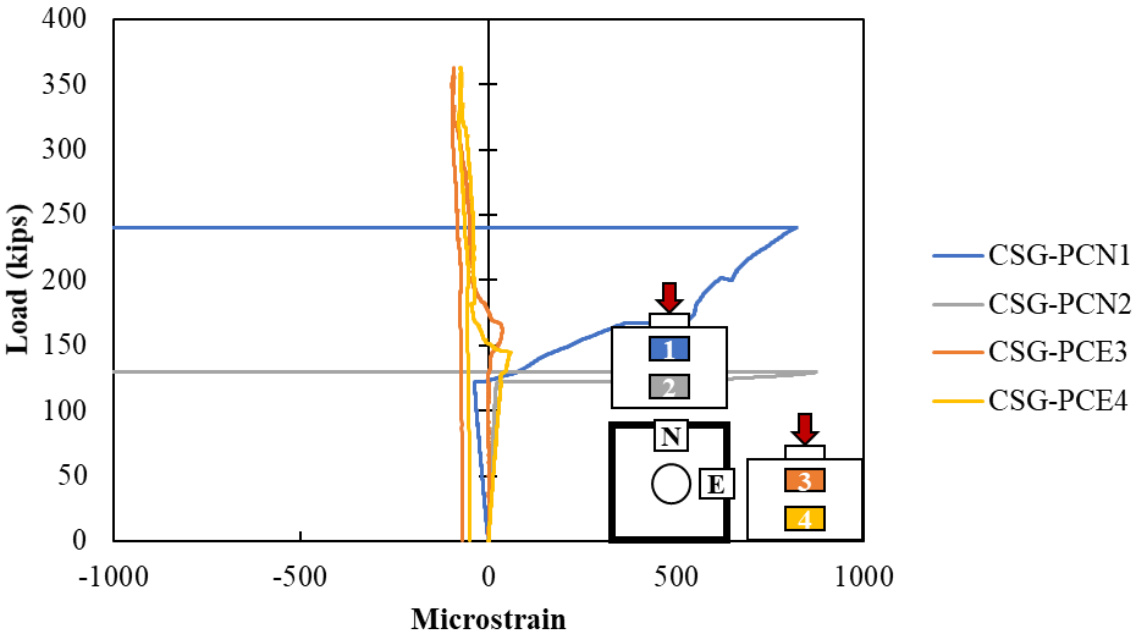

Figure A - 184: Concrete strain gauges in the surface of Specimen S3-12

The crack pattern at failure for S3-12 is shown in Figure A - 185. The cracks were observed to extend radially from the plug toward all faces with more cracking extending toward the faces with shorter edge distances. Some cracking parallel to the exterior faces was also observed on the bottom of the specimen on the shorter edges.

Figure A - 185: Cracking after testing on (a) bottom and (b) cap of Specimen S3-12

The confining reinforcement around the pocket were engaged on both sides (north and west) between 120 and 150 kips, as shown in Figure A - 186. More engagement was observed in the bottom reinforcement around pocket than the one in the top

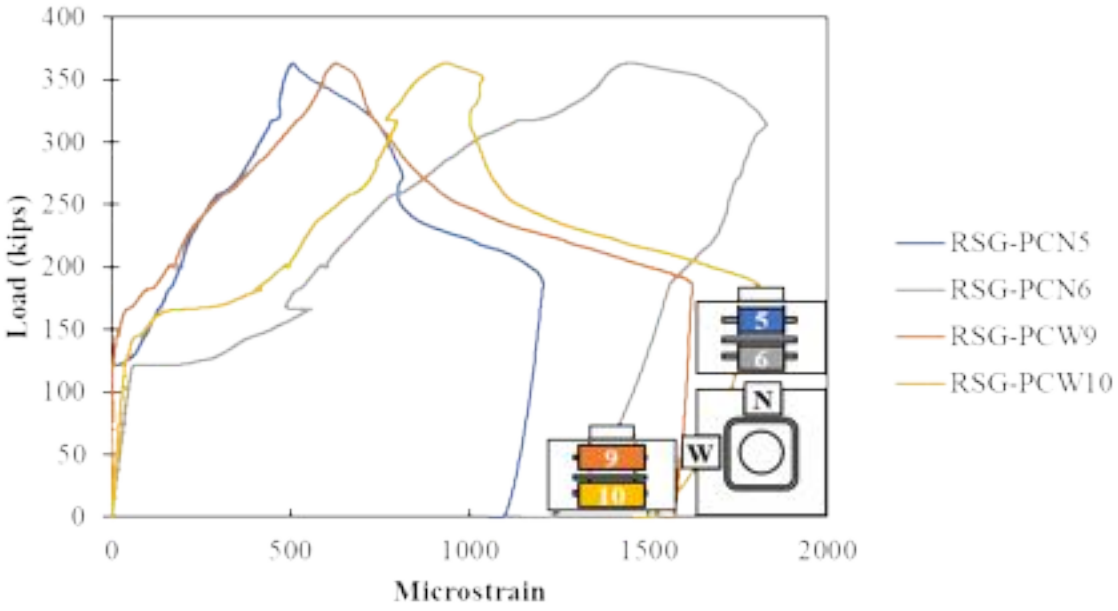

Figure A - 186: Confining reinforcement around pocket of Specimen S3-12

The measured strains in the vertical reinforcement in the plug and cap are shown in Figure A - 187. Slightly higher stresses were observed in the vertical reinforcement of the plug suggesting that a larger distance was required to transfer the stresses from the plug to cap.

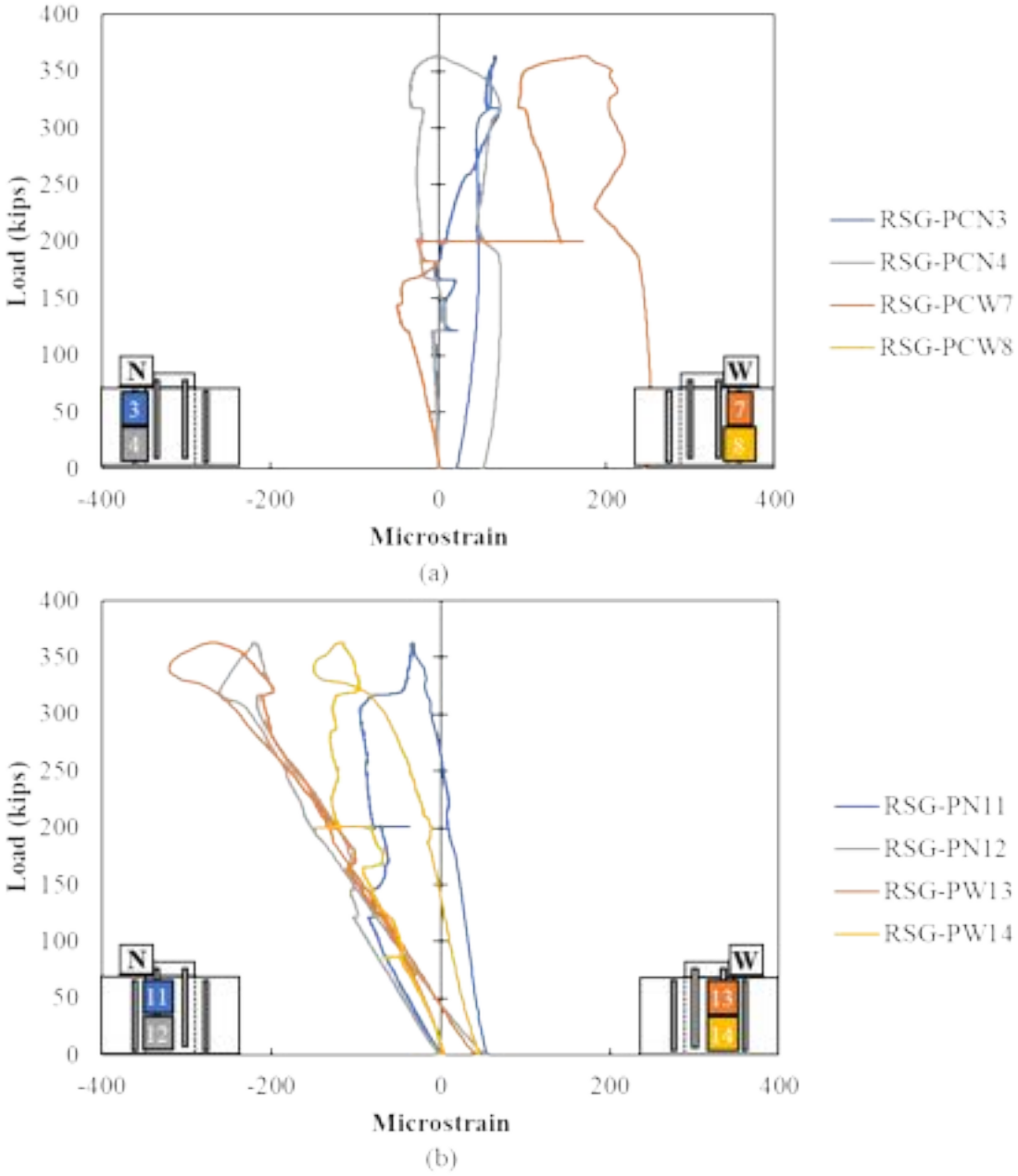

Figure A - 187: Rebar strain gauges in vertical reinforcement on (a) cap and (b) plug of Specimen S-12

Specimen S3-13 Results

Specimen S2-13 was 14-inch height and had a plug that was monolithically cast with the cap. The maximum load was 387.5 kips, and after failure the specimen still held a load of 245 kips. The specimen was loaded until 0.5-inch displacement of the plug. The load displacement curve is shown in Figure A - 188.

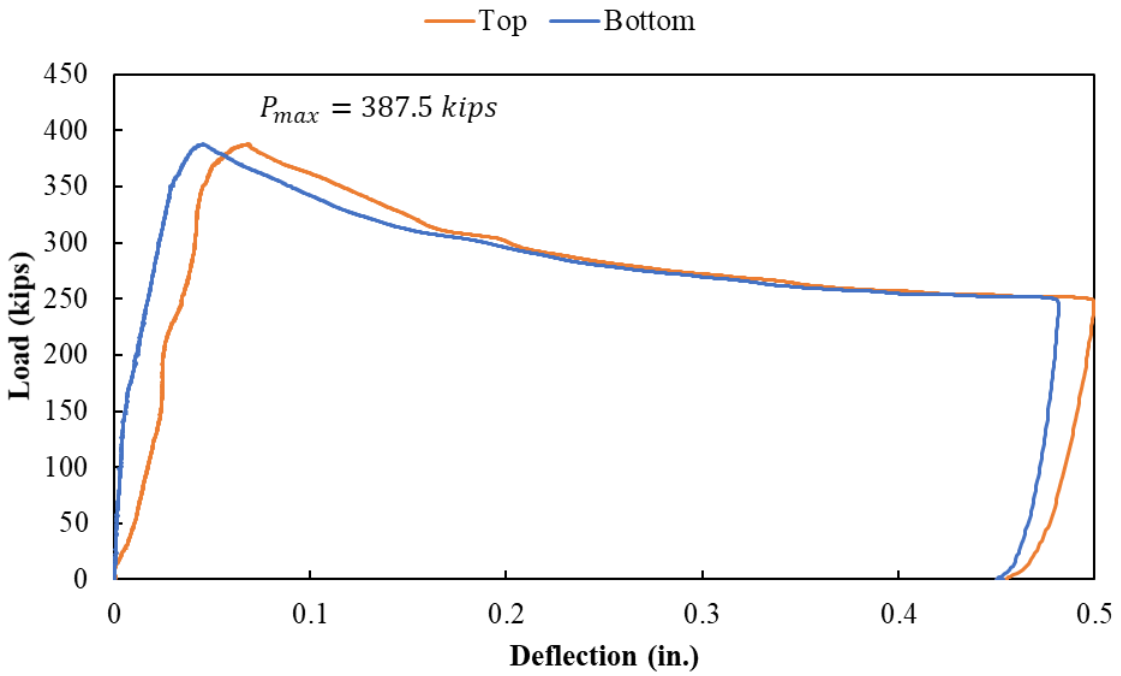

Figure A - 188: Load versus deflection curve for Specimen S3-13

The readings of the stain gauges in the longitudinal reinforcement in the bottom of the specimen are shown in Figure A - 189. The bottom reinforcement started to engage in the west side at a load of around 130 kips. Then, when the load was around 250 kips the reinforcement placed on the north side started get engage.

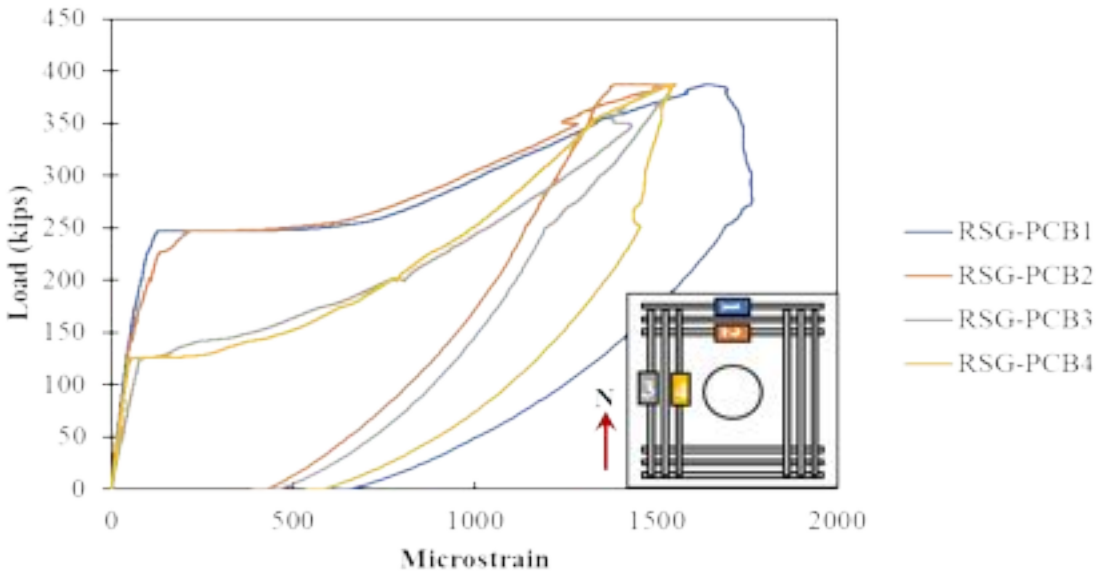

Figure A - 189: Rebar strain gauges in the longitudinal reinforcement on the bottom of Specimen S3-13

Cracking was also observed in the surface concrete at a load of around 130 kips on the east side of the specimen (CSG-PCE3 and CSG-PCE4), as shown in Figure A - 190. Cracking was seen in the north side of the specimen at a load around 250 kips.

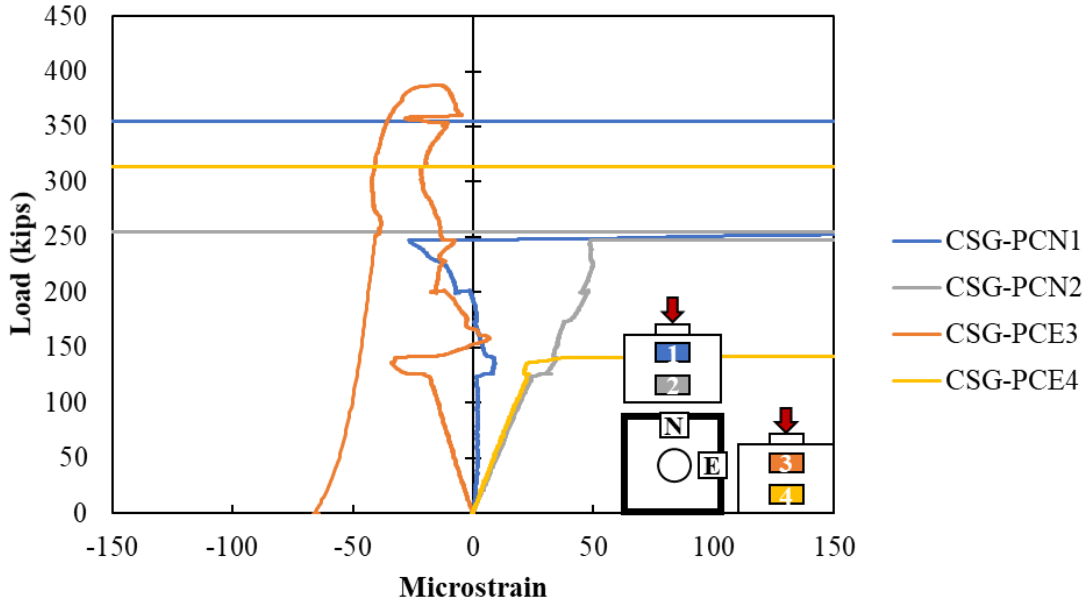

Figure A - 190: Concrete strain gauges in the surface of the cap of Specimen S3-13

The crack pattern at failure for S3-12 is shown in Figure A - 191. Small cracks were seen on all faces of the specimen. Splitting of cover of the plug was progressively seen during testing as shown in Figure A - 191 (c) and (d).

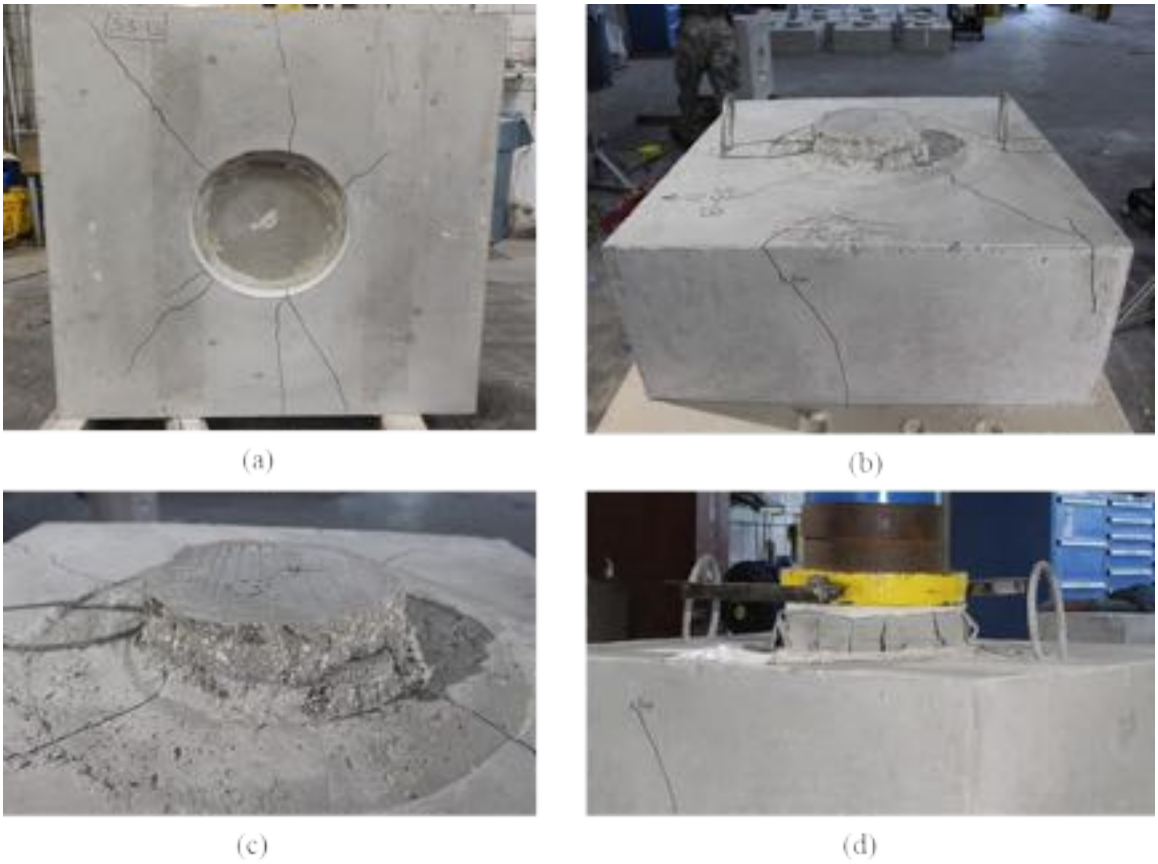

Figure A - 191: Failure details on (a) bottom, (b) cap, (c) top of plug and (d) plug detail during testing of the Specimen S3-13

As in the longitudinal reinforcement, the confining reinforcement around the pocket were first engaged specifically in the bottom gauge on the west side at 125 kips, as shown in Figure A - 192. The north side of the confinement reinforcement began to be more heavily engaged at a load of around 250 kips.

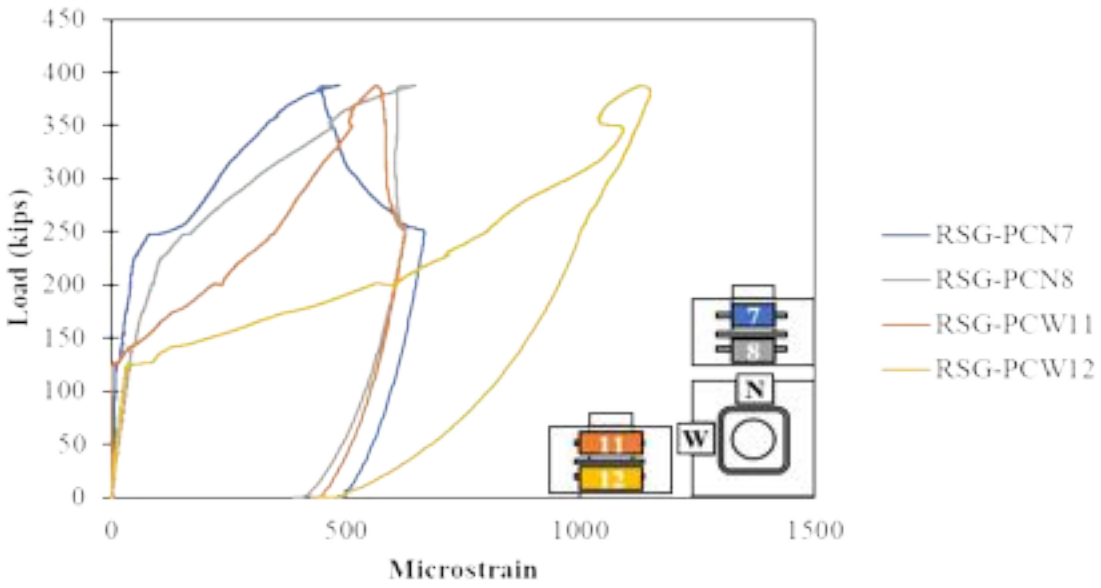

Figure A - 192: Confining reinforcement around the pocket of Specimen S3-13

The measured strains in the vertical reinforcement in the plug and cap are shown in Figure A - 193. Slightly higher stresses were observed in the vertical reinforcement of the plug suggesting that a largest distance was required to transfer the stresses from the plug to cap.

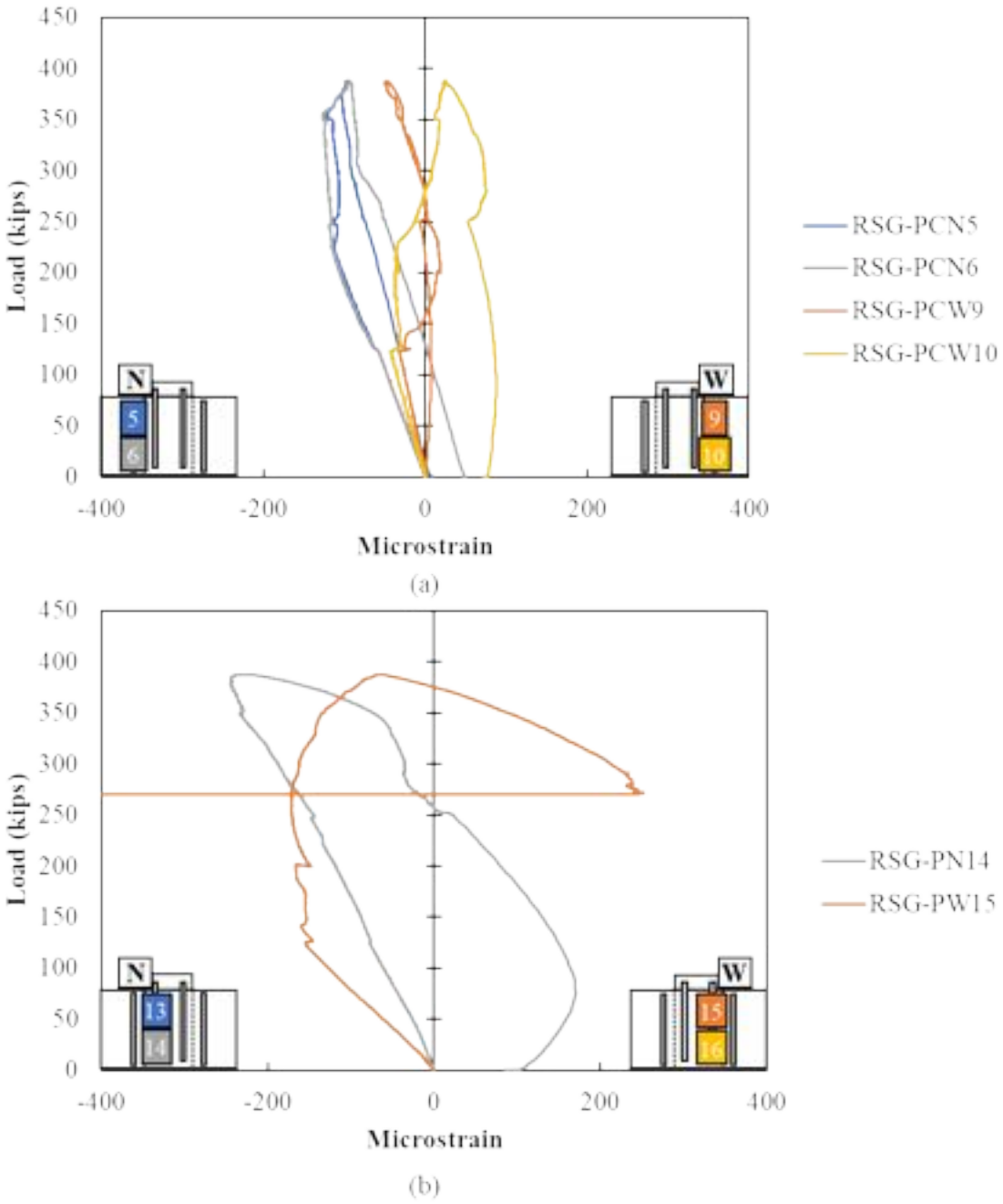

Figure A - 193: Rebar strain gauges in vertical reinforcement on (a) the cap and (b) plug of Specimen S3-13

APPENDIX B. LARGER-SCALE RESULTS

Larger Plug Specimens

The results and observations for the larger plug specimens are summarized in this section. The measured compressive strengths (higher than specified), cracking loads, and ultimate loads are summarized in Table B - 1 for larger plug specimens.

Cracking was for all specimens occurred between 75 and 130 kips based on CSG and RSG measurements. Failure of LP-1 occurred at 545.6 kips. The other three specimens reached 1000 kips without failing immediately. LP-2 appeared to still have more strength. LP-3 and LP-4 appeared to be close to or at their failure loads.

Table B - 1: Measured concrete strength, cracking load, and estimated versus ultimate strength for larger plug testing

Spec.	**Compressive Strength on Test Day (ksi)**		**Cracking Load (kips)**	**Ultimate Load (kips)**				
	Cap	*Plug*		*Measured*	*AASHTO*	*ABC*	*ATENA*	*Theory*
LP-1	8.56	7.27	77	*545.6*	*149.3*	*218.0*	*366.2*	*459.7*
LP-2	8.58	7.41	70	*> 1000*	*149.3*	*220.1*	*704.5*	*794.6*
LP-3	8.58	7.41	83	*> 1000**	*149.3*	*220.1*	*704.5*	*788.0*
LP-4	8.58	7.41	82	*> 1000***	*149.3*	*220.1*	*704.5*	*730.0*

*sliding of the plug occurred as the load was maintained at 1000 kips for LP-3

** load versus deflection plot appeared to be leveling out at 1000 kips for LP-4

More details on each test are provided in the following sections.

Specimen LP-1 Results

Specimen LP-1 had a smooth interface surface between the cap and plug (i.e., no corrugation) with sandblasted (1/16'' of roughness) surface preparation.

The load versus deflection plot for LP-1 is shown in Figure B - 1. The maximum capacity was 545.6 kips. The specimen experienced a sudden failure at this load; the top and bottom of the plug both slid instantly as the load dropped to around 400 kips. This result would suggest that the specimen failed as soon as the cohesion between the pile cap and plug concrete failed. The friction between the pile cap and plug concrete still allowed for the load to remain at 400 kips at the plug deflection of around 0.17 inches.

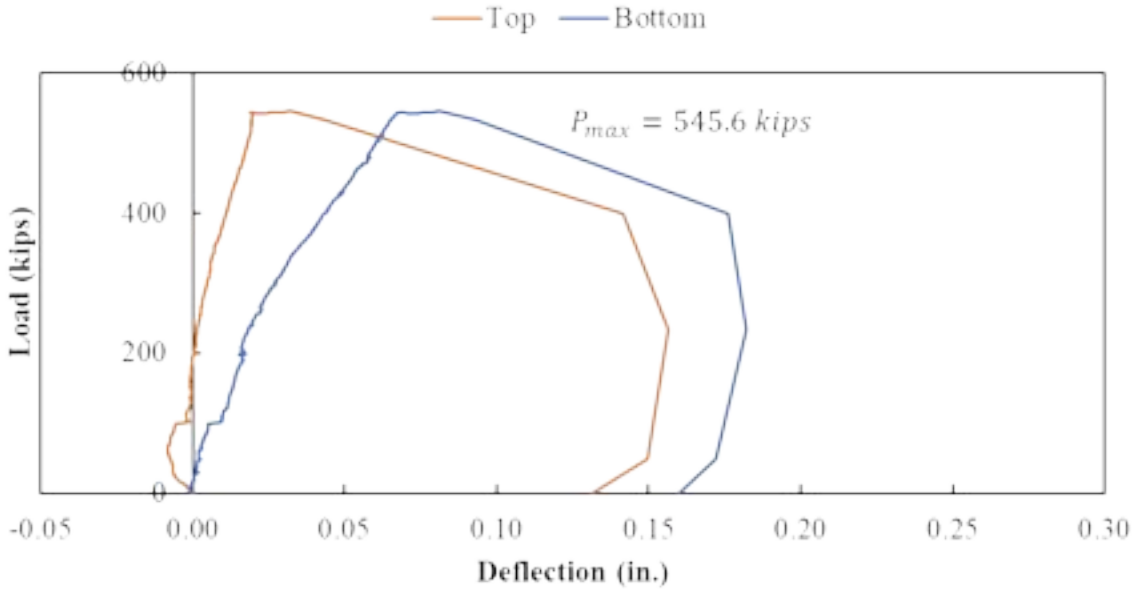

Figure B - 1: Load displacement curve for Specimen LP-1

The load versus measured rebar strain in the longitudinal bars for LP-1 is shown in Figure B - 1. The response in all RSGs was linear up to 77 kips, when RSG-PCB3 and RSG-PCB4 both increased in strain without increase in load, highlighted with a red circle in Figure B - 2. This would indicate first cracking at the bottom of the west face at 77 kips. Cracking was observed visually during the first stop of testing at 100 kips on the east and west sides of the specimen, as shown in Figure B - 3 (a). The response in RSG-PCB1 and RSG-PCB2 continued to be linear elastic to 411 kips when the strain began to increase without increasing load, highlighted with a green circle in Figure B - 2. First cracking was observed visually on the north and south side of LP-1 at 200 kips, but cracking was not in the middle of the specimen, which is why it was not captured by RSG-PCB1 and RSG-PCB2, as shown in Figure B - 3(b). The maximum observed strains in the rebar were around 2,000 με at failure (close to the yield strain).

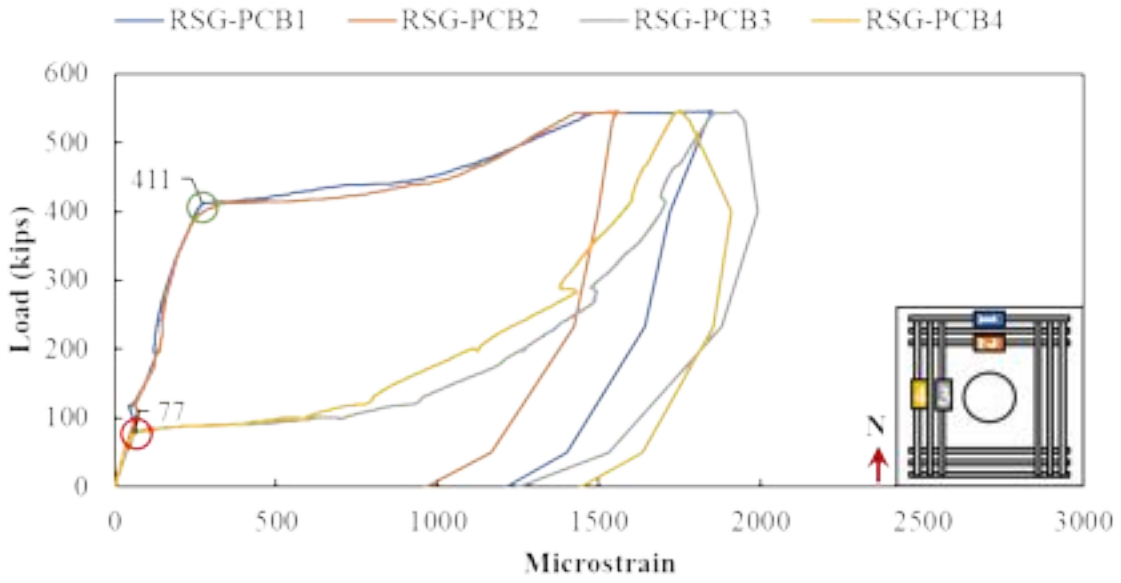

Figure B - 2:Rebar strain in the longitudinal bars on bottom of the Specimen LP-1

Figure B - 3: Crack progression during testing at (a) 100 kips and (b) 200 kips

The load versus measured strains using the horizontal CSGs on the outside of LP-1 are shown in Figure B - 4. Cracking was observed between 71 and 78 kips on the west side of the specimen based on the CSG readings. As stated above, this coincided with the first visually observed crack on the east and west side at 100 kips. The visually observed cracking on the north and south side was not through or immediately adjacent to the CSG, which is why it was not clearly detectable in Figure B - 4. The measured tensile strain in CSG-PSN2 had an increase slope around 72 kips and began to have decreasing tension at approximately 100 kips, highlighted in Figure B - 4, which can both indicate cracking.

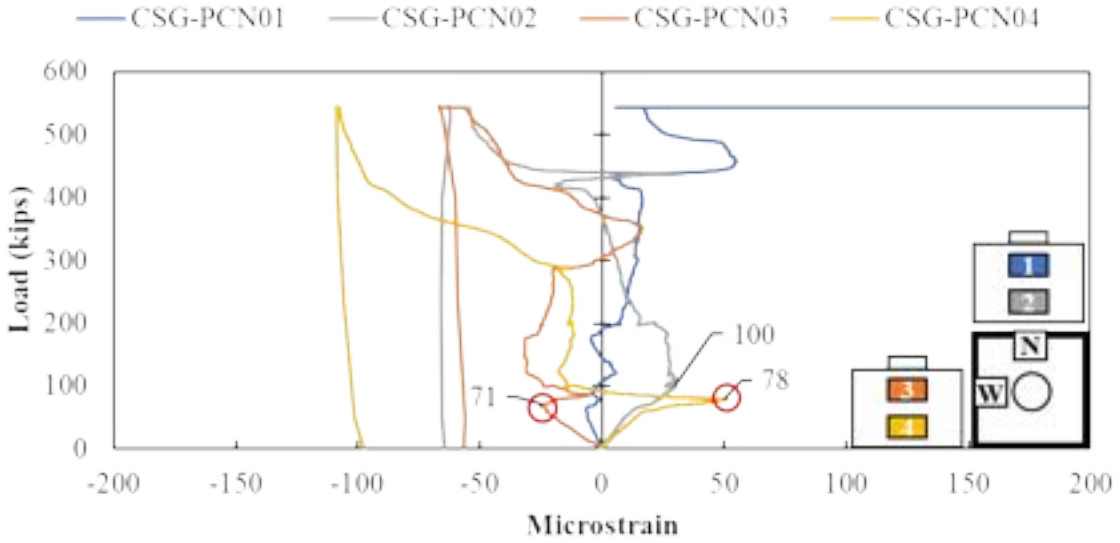

Figure B - 4: Concrete strain on the concrete surface of Specimen LP-1

The load versus strains in the confining reinforcement around the pocket in LP-1 were measured as shown in Figure B - 5. The engagement of the reinforcement began at a load of 86 kips on the west side and 116 kips on the north side, which roughly coincides with the observed cracking loads. The strains in the confining reinforcement reach around 2,000 με at failure, which is close to the yield strain and similar to the maximum strain in the bottom longitudinal reinforcement.

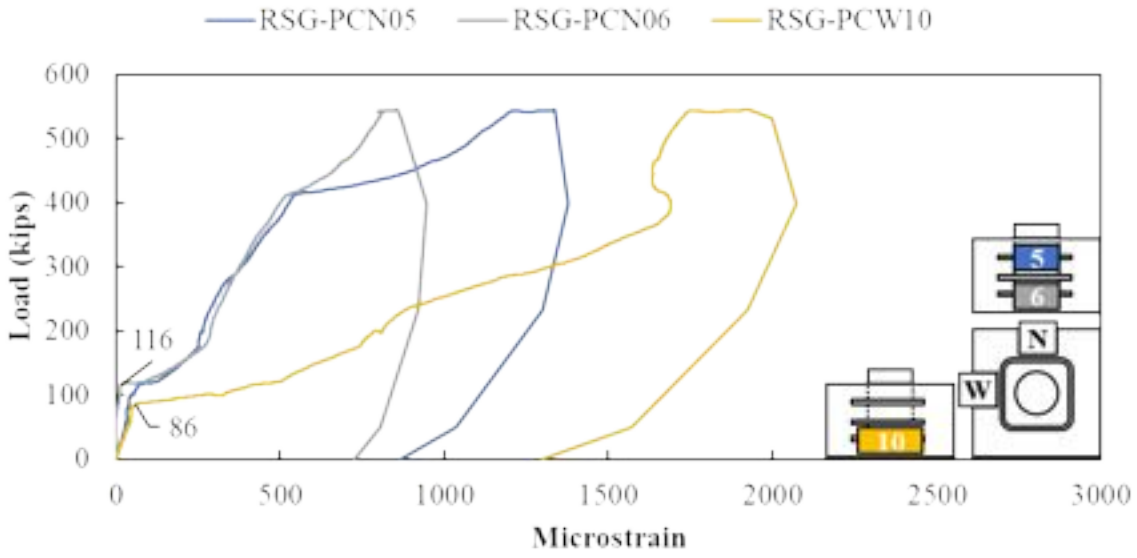

Figure B - 5: Confining reinforcement around the pocket of Specimen LP-1

Measured strain in the vertical reinforcement in the cap and plug for LP-1 are shown in Figure B - 6. Strain in the vertical reinforcement in the cap around the pocket began in compression, see Figure B - 6(a). Strain in RSG-PCW11 and RSG-PCW12 had an abrupt slope change at 86 kips, which is approximately the time of first cracking noted above. Strain in RSG-PCN7 on the north face continued approximately linear in compression 410 kips, which was the cracking load noted in Figure B - 2.

The vertical compression strain in the plug began in compression with slightly higher strains than the adjacent RSGs in the pile cap, see Figure B - 6(b). These compression strains began to decrease after 189 kips with tension beginning to develop between 350 and 450 kips. Tension was measured strains in RSG-PCW11 throughout testing.

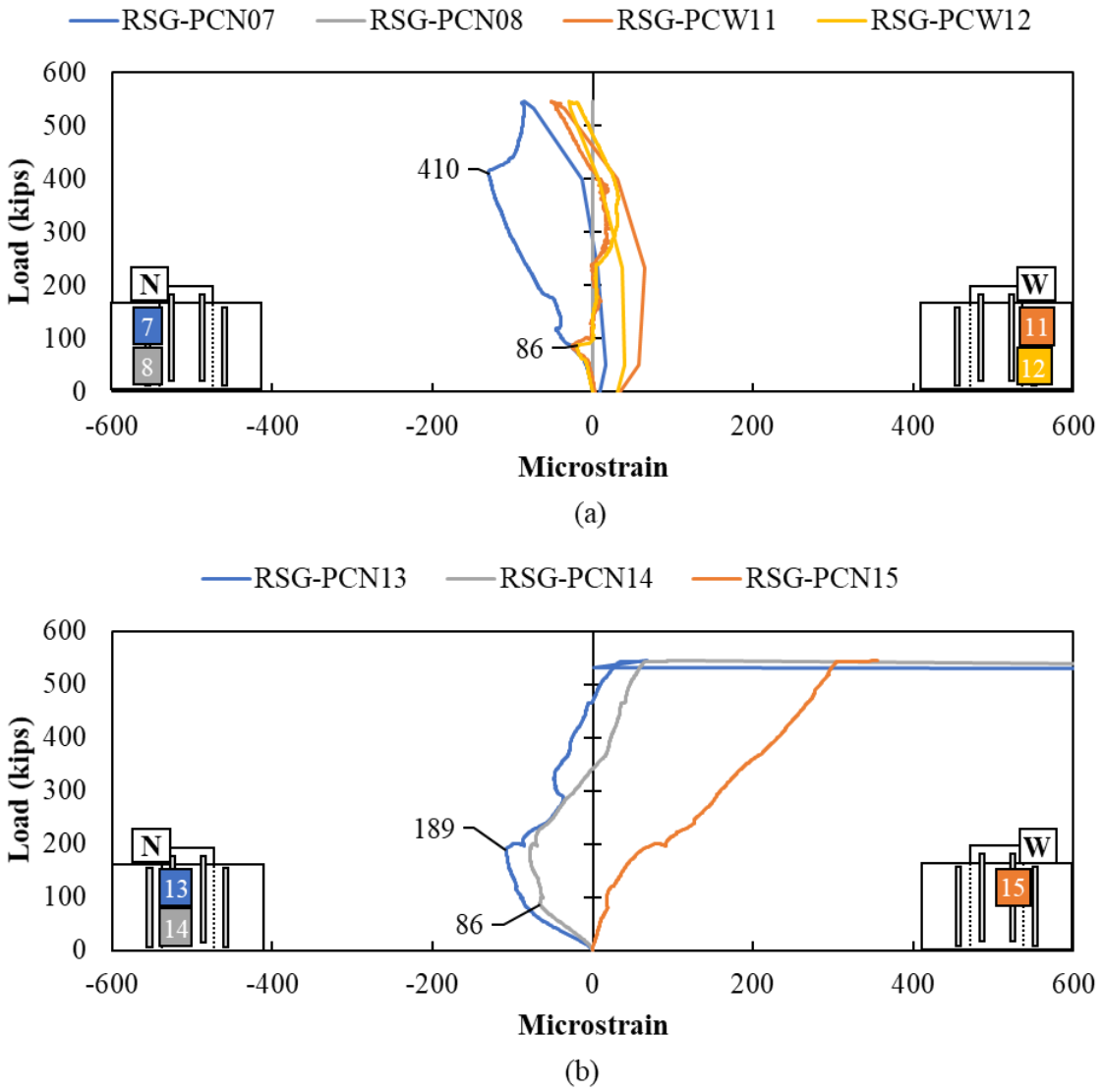

Figure B - 6: Rebar strain gages in vertical reinforcement in (a) cap and (b) plug of Specimen LP-1

Photographs of the specimen after failure are shown in Figure B - 7. Spalling around the sides of the extended plug occurred at the failure load when the plug suddenly slid 0.1 inches down, shown in Figure B - 7(a). The cracking extended radially from the bottom of the plug and up the sides of the specimen, as shown in Figure B - 7(b) and (c).

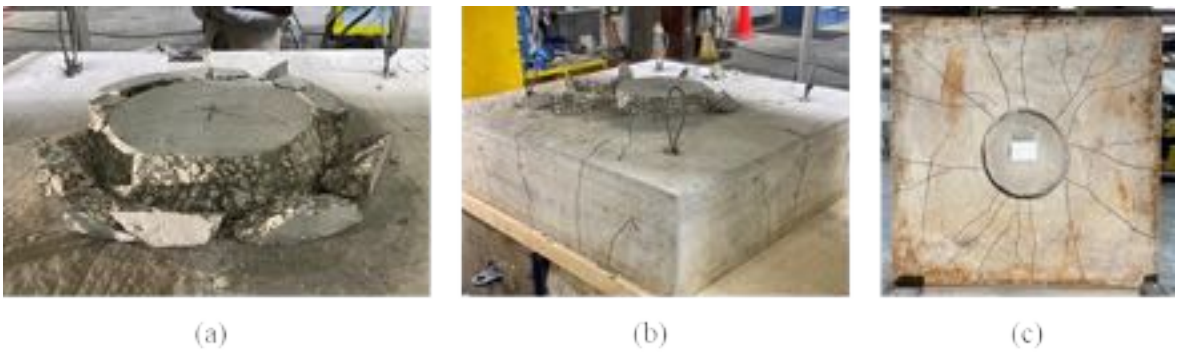

Figure B - 7: Failure and cracking pattern of Specimen LP-1 (a) plug detail, (b) south-east view and (c) bottom view.

Specimen LP-2 Results

Specimen LP-2 had a smooth surface between the cap and plug (i.e., no corrugation) with exposed aggregate surface finish.

The load versus deflection plot for LP-2 is shown Figure B - 8. The applied load reached the capacity of the test setup (1000 kips) before the failure of the specimen occurred. Like the small-scale specimens, this result suggests that having an exposed aggregate finish provide a good adhesive bonding between the plug and pile cap.

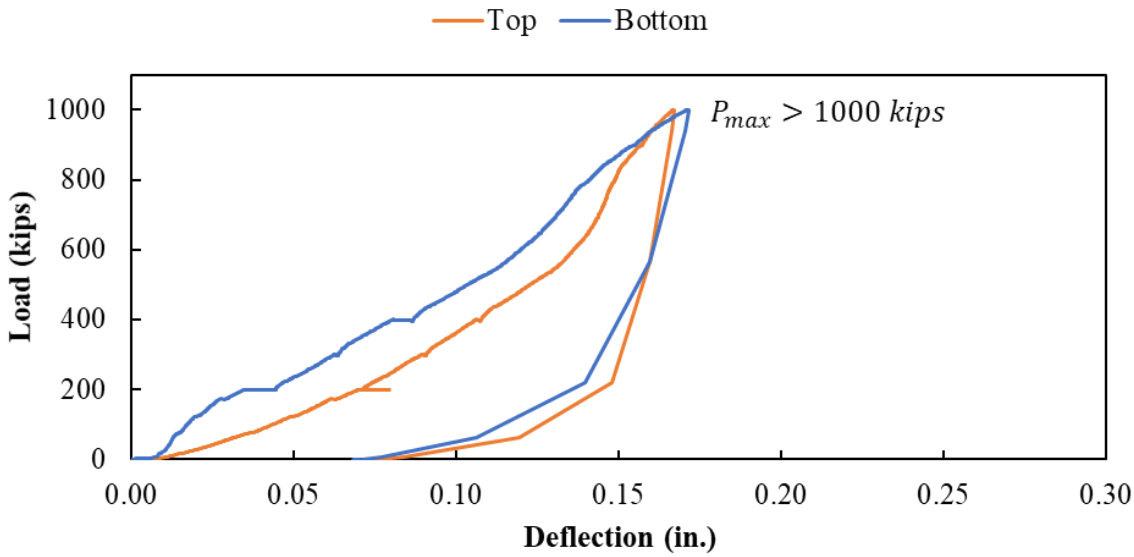

Figure B - 8: Load versus deflection curve for Specimen LP-2

The load versus measured rebar strain in the longitudinal bars for LP-2 is shown in Figure B - 9. The response in all RSGs was linear up to 79 kips, when RSG-PCB4 increased in

strain without increase in load, highlighted in Figure B - 9. RSG-PCB2 began to engage at 122 kips and RSG-PCB1 at 220 kips. The strains continued to increase after first cracking to maximum strains between 2,000 and 2,600 με at failure.

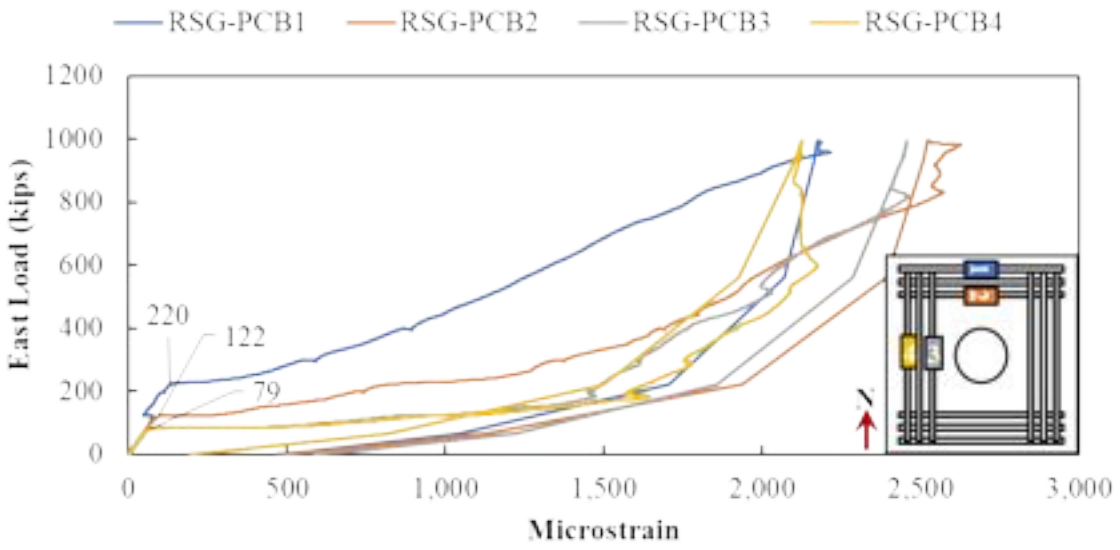

Figure B - 9: Rebar strain in longitudinal bars on bottom of Specimen LP-2

Cracking was visually observed during testing on all four faces of LP-2 at 200 kips, as shown in Figure B - 10, which corresponds to the cracking loads determined from the RSGs in the longitudinal reinforcement.

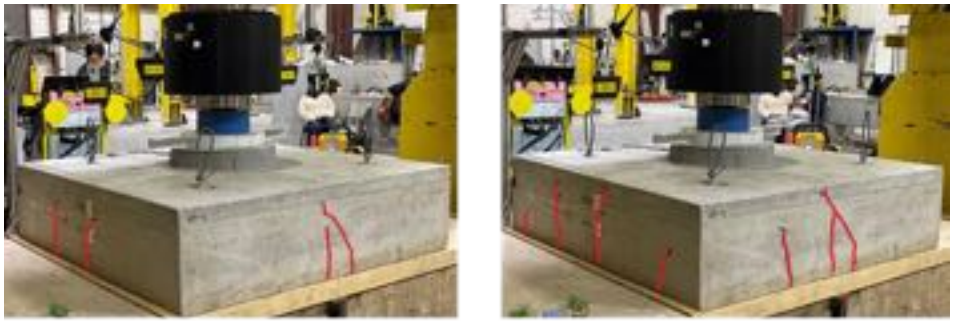

Figure B - 10: Crack progression during testing at (a) 200 kips and (b) 300 kips.

The load versus measured strains using the horizontal CSGs on the outside of LP-2 are shown in Figure B - 11. Cracking was observed between 62 and 82 kips on the west side and 62 and 122 kips on the north side of the specimen based on the CSG readings. These

cracking loads are similar to those determined from longitudinal RSGs and visual inspection as described above.

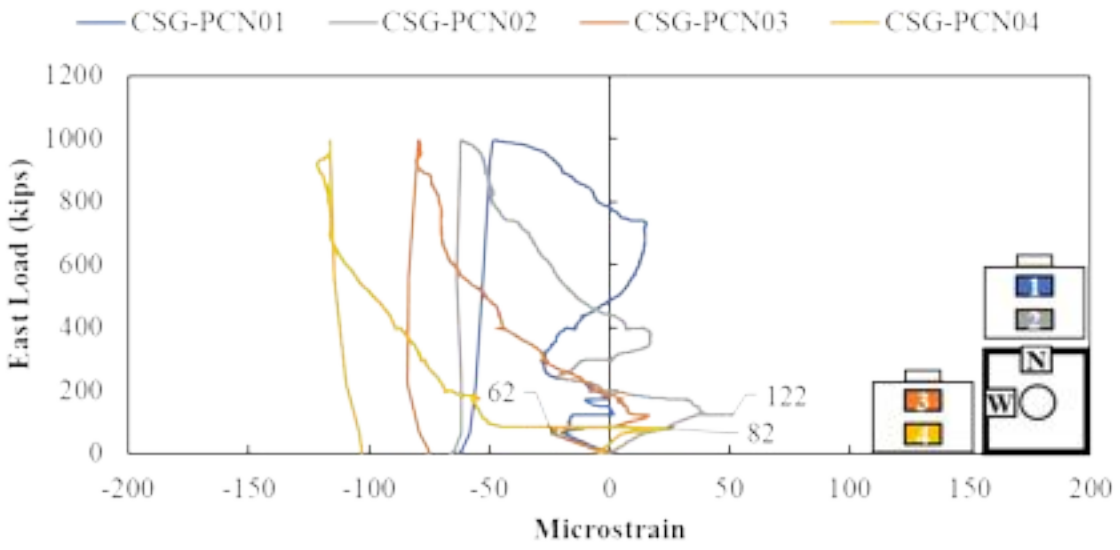

Figure B - 11: Concrete surface gages on the cap of Specimen LP-2.

The load versus strains in the confining reinforcement around the pocket in LP-2 were measured as shown in Figure B - 12. The engagement of the reinforcement began at a load of 75 kips on the west side and 120 kips on the north side, which in the range of the observed cracking loads. The strains in the confining reinforcement reach around 6,500 με at failure, which is much larger than the measured strains in the longitudinal reinforcement and shows there is more expansion around the pocket for LP-2 than LP-1.

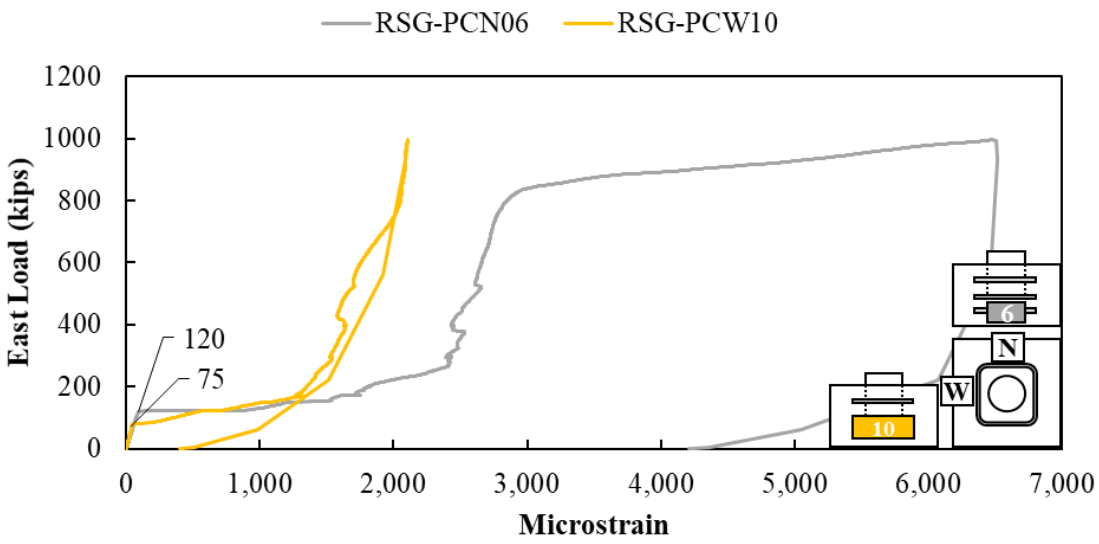

Figure B - 12: Confining reinforcement around the pocket of Specimen LP-2

Measured strain in the vertical reinforcement in the cap and plug for LP-2 are shown in Figure B - 13. Strain in the vertical reinforcement in the cap around the pocket began in compression and all had a sudden drop in compression strains starting at around 79 kips, see Figure B - 13(a). Strains continued in compression with maximum strains between -200 and -300 με at failure.

The vertical compression strain in the plug (other than RSG-PCN13), began in compression with similar strains to the adjacent RSGs in the pile cap, see Figure B - 13(b). These compression strains began to decrease after around 80 kips with tension beginning to develop around 200 kips in RSG-PCN15 and RSG-PCN16.

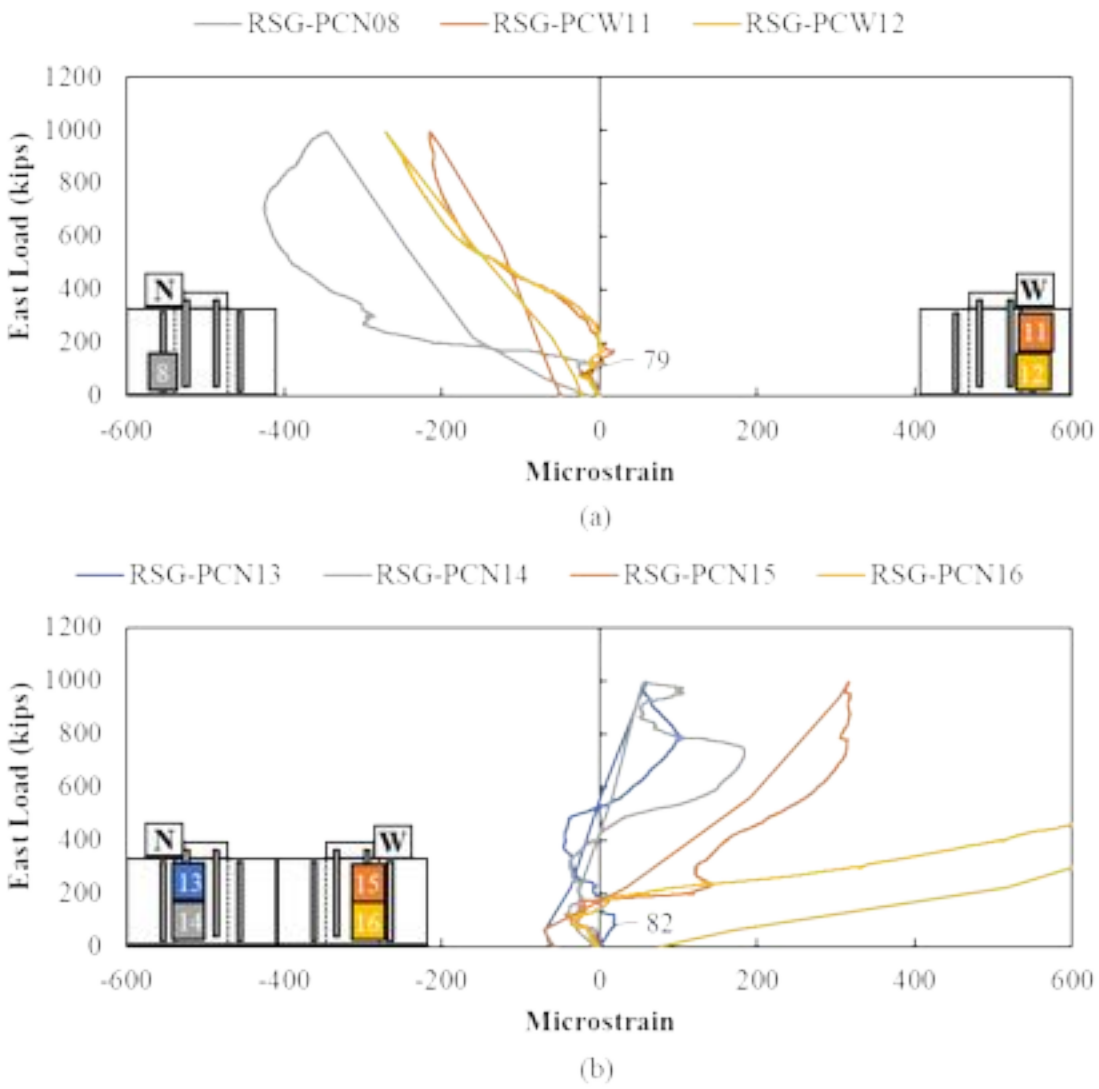

Figure B - 13: Rebar strain gage in vertical reinforcement on (a) cap and (b) plug of Specimen LP-2

Photographs of LP-2 after testing are shown in Figure B - 14. The cracking was observed to extend from the bottom of the cap onto the top toward the plug in all sides of the specimen as LP-2.

(a) (b)

Figure B - 14: Cracking after testing on (a) south-west side and (b) bottom of the Specimen LP-2.

Specimen LP-3 Results

Specimen LP-3 had a corrugated surface between the cap and plug with sandblasted (1/16'' of roughness) surface preparation. The void was created using a corrugated metal pipe.

The load versus displacement curve for LP-3 is shown in Figure B - 15. This specimen had two parts of testing. In the first part, the specimen was loaded until 860 kips at a load rate of 0.02 kips/sec when the actuator stopped receiving load; this is labeled "Test 1" in Figure B - 15. The specimen was then unloaded and reloaded using a different hydraulic pump, labeled "Test 2" in Figure B - 15. The second pump had a different set of controls, which only allowed for a load rate of 2 kips/sec.

The load versus deflection curves for top and bottom were beginning to flatten at 1000 kips, but load was still increasing slightly. There were some problems removing load from the specimen. The plug continued to push through as the load was maintained between 900 and 1000 kips. The failure load for this specimen was greater than 1000-kip load.

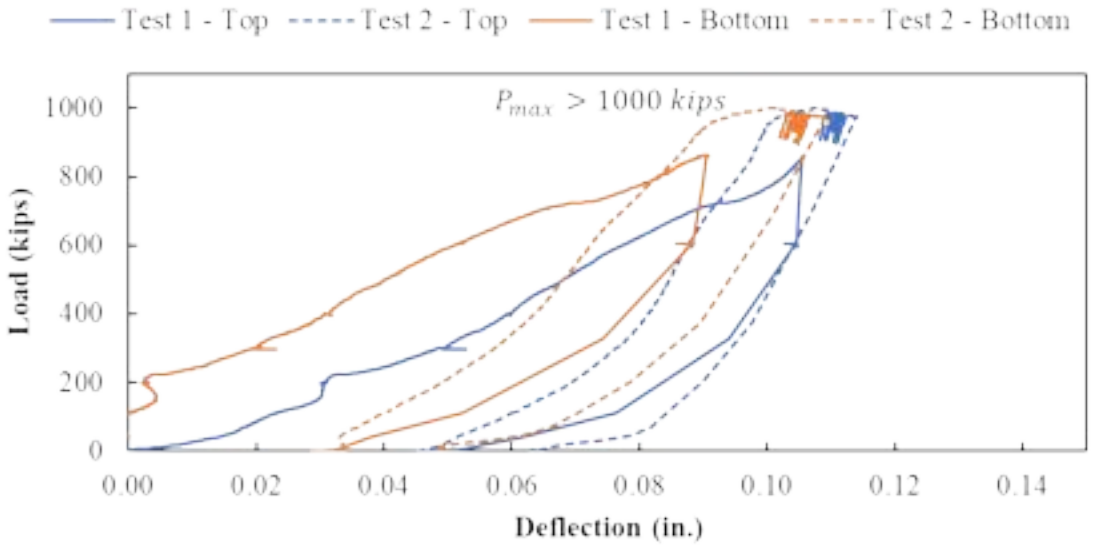

Figure B - 15: Load versus deflection curve for Specimen LP-3

The bottom reinforcement placed on the west side of the specimen started to engage at a load around 84 kips according to RSG-PCB3 and RSG-PCB4, as shown in Figure B - 16. The longitudinal reinforcement on the north side of the specimen began to engage at a load around 212 kips. The strains continued to increase after first cracking to maximum strains between approximately 1,700 and 2,100 με at failure during Test 2.

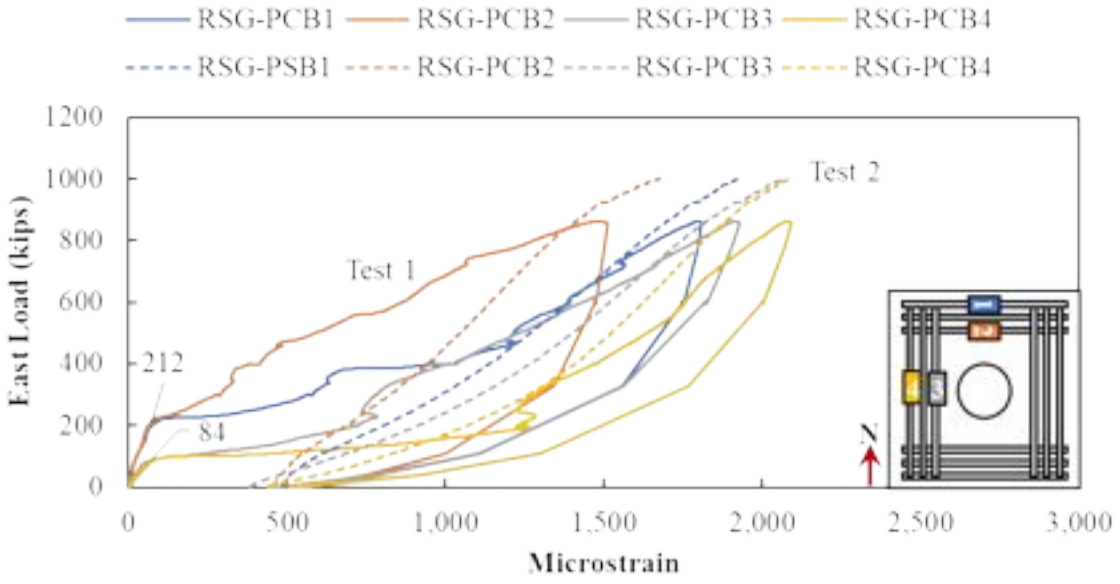

Figure B - 16: Rebar strain gages in the longitudinal reinforcement on bottom of the Specimen LP-3

Cracking was first visually observed on LP-3 at the first stop at 200 kips on the east and west sides of the specimen, as shown in Figure B - 17(a). Cracking was first observed on the north and south sides of the specimen at the second stop of 300 kips, as shown in Figure B - 17(b).

Figure B - 17: Crack progression for LP-3 during testing at (a) 200 kips and (b) 300 kips

Cracking was also observed with the surface concrete strain gages at a load around 84 kips on the west face and around 184 kips on the north face, as shown in Figure B - 18.

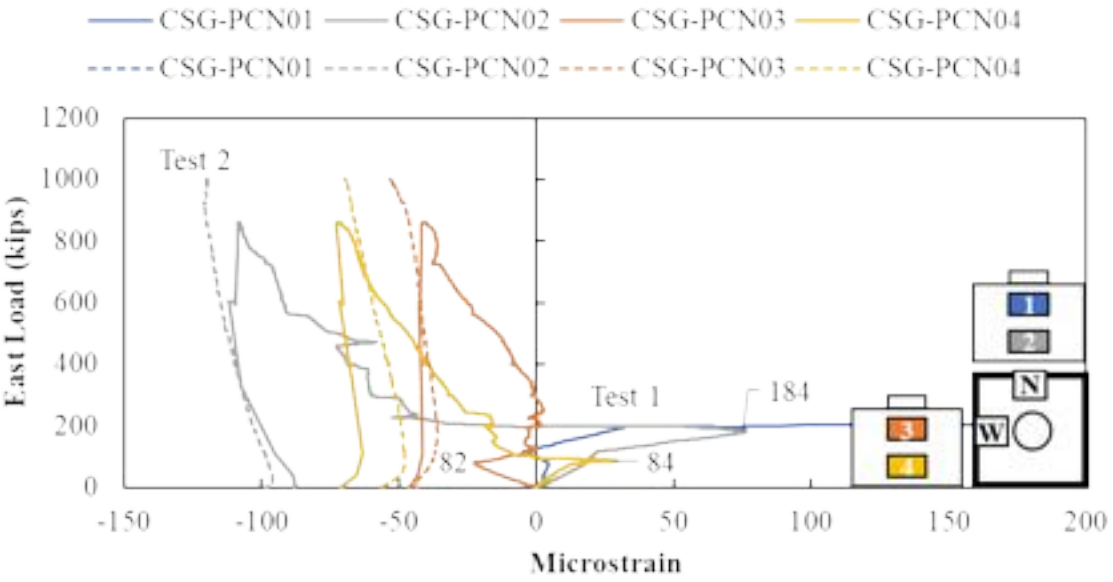

Figure B - 18: Concrete strain gages in the surface of Specimen LP-3

The confining reinforcement around the pocket started to engage in the west side of the plug of a load around 96 kips according to gages RSG-PCW9 and RSG-PCW10, as shown

in Figure B - 19. The other side of the specimen started to engage around 451 kips according to RSG-PCW06.

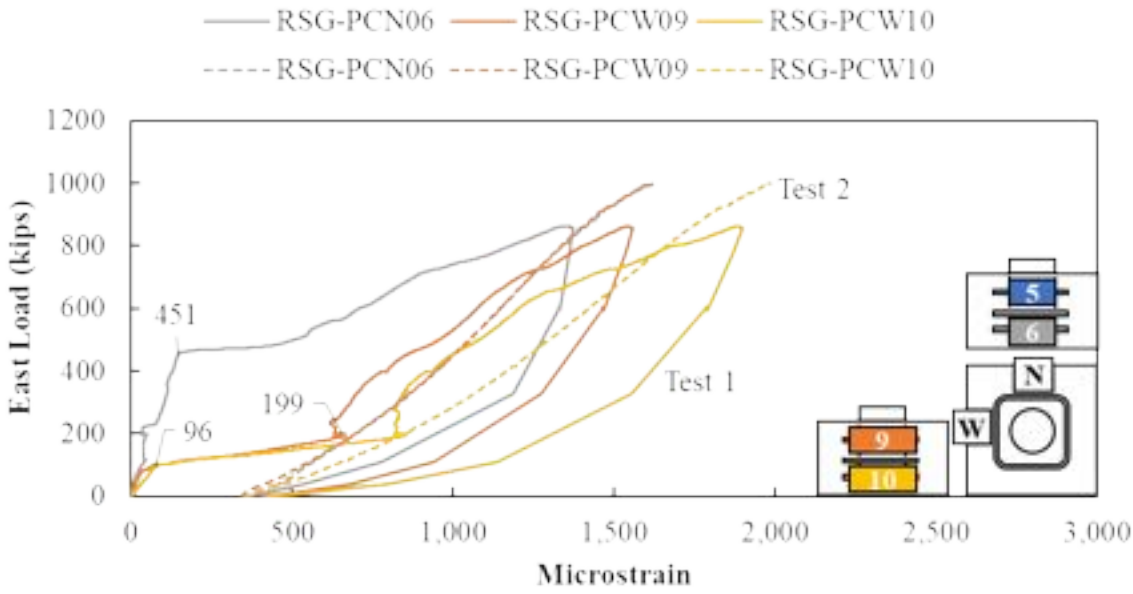

Figure B - 19: Confining reinforcement around pocket of Specimen LP-3.

Measured strain in the vertical reinforcement in the cap and plug for LP-3 are shown in Figure B - 20. Strain in the vertical reinforcement in the cap around the pocket began in compression and all had a sudden drop in compression strains starting at around 101 kips for RSG-PCN7 and around 451 kips for RSG-PCN8 and RSG-PCN12, see Figure B - 20(a). Strains generally remained between -70 and 50 με after this for RSG-PCN7 and RSG-PCN12. Tensile strains developed in RSG-PCN8 with a strain at 1000 kips of around 250 με.

The vertical compression strain in the plug, began in compression with similar strains to the adjacent RSGs in the pile cap, see Figure B - 20 (b). These compression strains began to decrease after between 99 and 121 kips with tension beginning to develop around 121 kips in RSG-PCN13 and RSG-PCN14. Tensile strains up to 400 με developed at the 1000 kips maximum applied load.

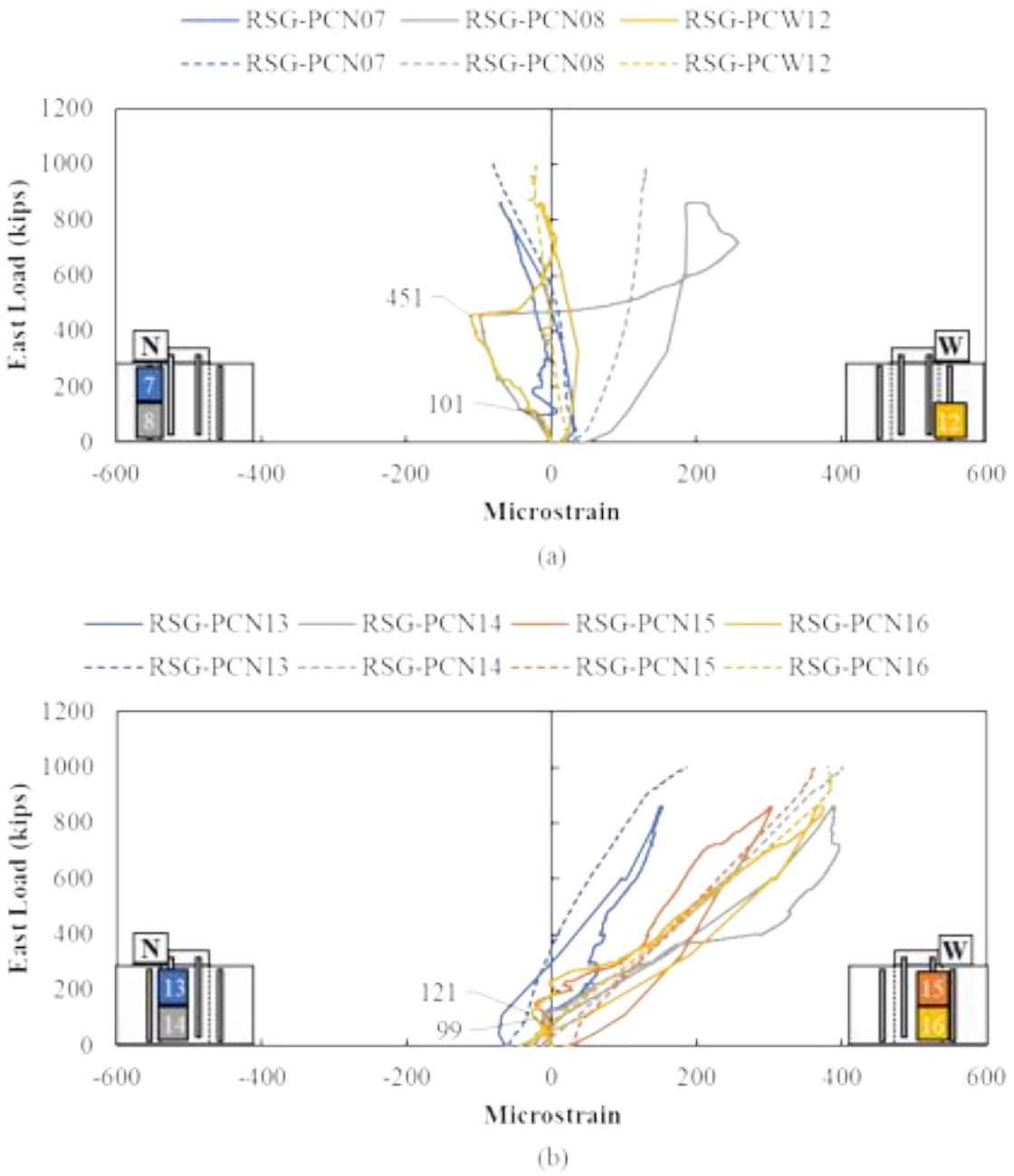

Figure B - 20: Rebar strain gages in vertical reinforcement on (a) cap and (b) plug of Specimen LP-3

The crack pattern after the conclusion of testing on the sides and bottom of the specimen is shown in Figure B - 21. Cracks extended radially from the bottom of the plug, Figure B - 21(b), and continued vertically up the sides of the specimen, Figure B - 21(a).

Figure B - 21: Cracking after testing on (a) south-west view and (b) bottom of specimen LP-3

Specimen LP-4 Results

Specimen LP-4 had a corrugated surface between the cap and plug. The void was created using a corrugated metal pipe, and the pipe was left in place.

The load versus displacement plot for LP-4 is shown in Figure B - 22. The actuator reached the maximum load of 1000 kips. The load displacement curve was starting to level out at this point, so the failure load will be assumed to be approximately 1000 kips.

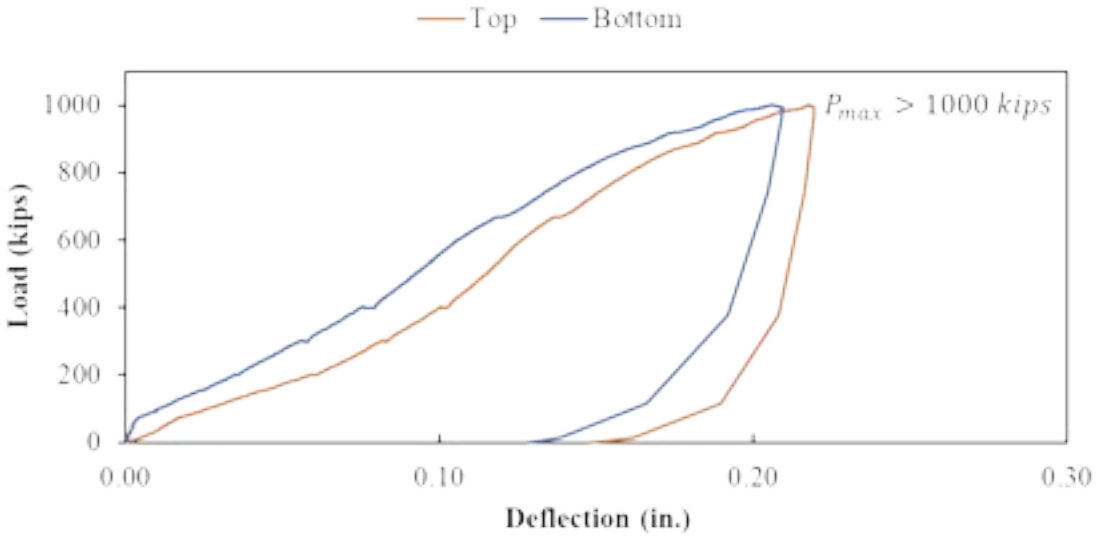

Figure B - 22: Load versus deflection curve for Specimen LP-4

The load versus measured strain responses for the longitudinal reinforcement in the bottom of the specimen are shown in Figure B - 23. All gauges showed engagement of the rebars between about 91 kips and 142 kips. RSGs on reinforcement toward the north face showed engagement slightly before gauges on reinforcement toward the west face of the specimens; this would suggest that cracking occurred first on the north and south faces and then on the east and west faces of the specimen.

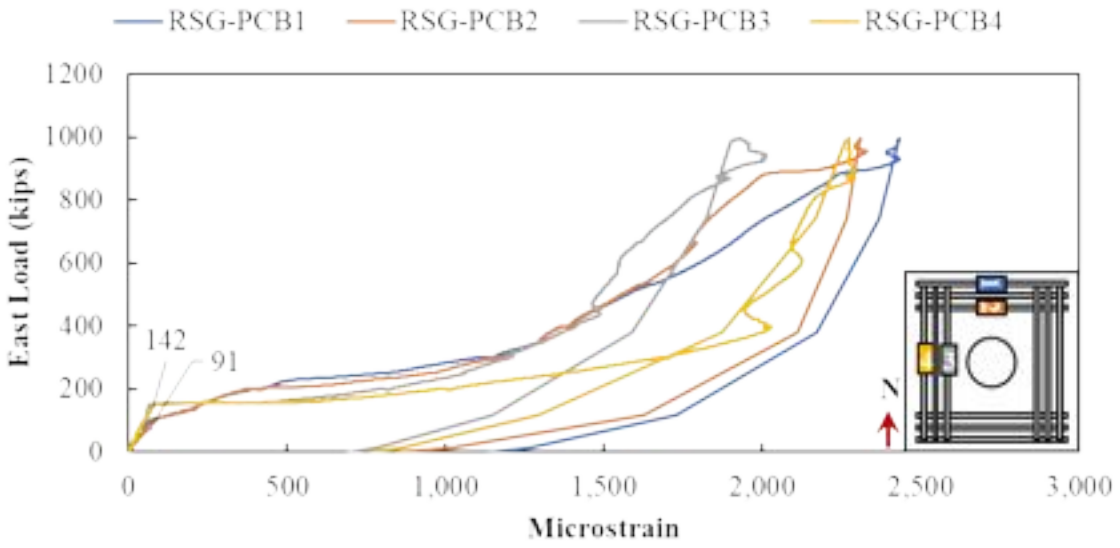

Figure B - 23: Rebar strain gages in the longitudinal reinforcement on bottom Specimen LP-4

As suggested by the longitudinal gage readings, cracks were visually seen at the first stop at 200 kips in both directions as shown in Figure B - 24(a). Existing cracks continued to grow and new cracks developed on all sides of the specimen as the load was increased, as shown in Figure B - 24(b).

Figure B - 24: Crack propagation during testing at (a) 200 kips and (b) 300 kips.

The readings of the concrete surface gauges are shown in Figure B - 25. Cracks were observed in the surface concrete in the north side of the specimen between 74 and 135 kips and at around 152 kips on the west side.

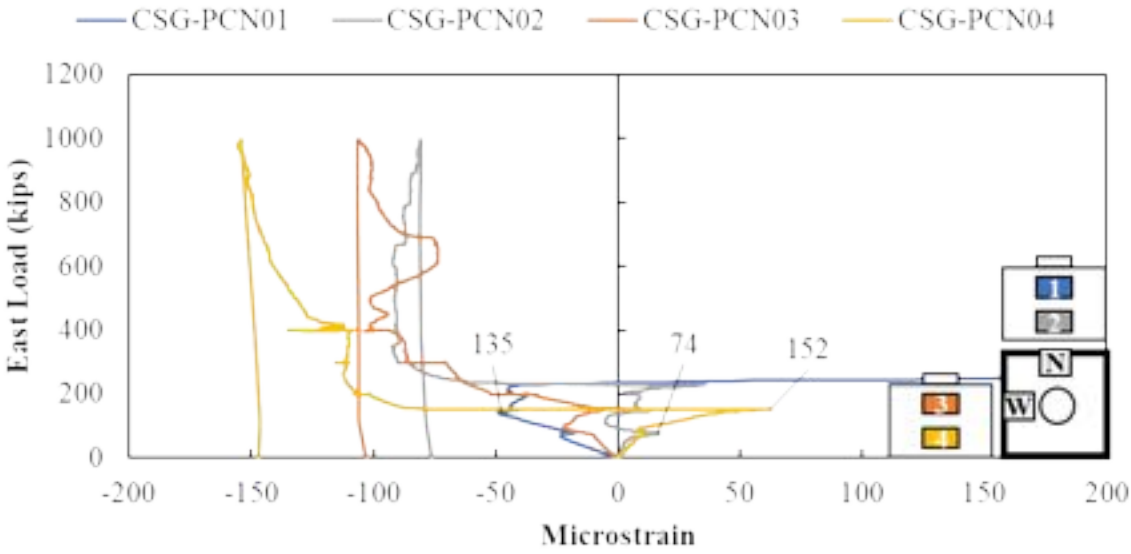

Figure B - 25: Concrete strain gages on the concrete surface of Specimen LP-4

The confining reinforcement around the pocket started to engage on both sides of the plug between 75 and 145 kips of loading according to the reading of RSGs shown in Figure B - 26.

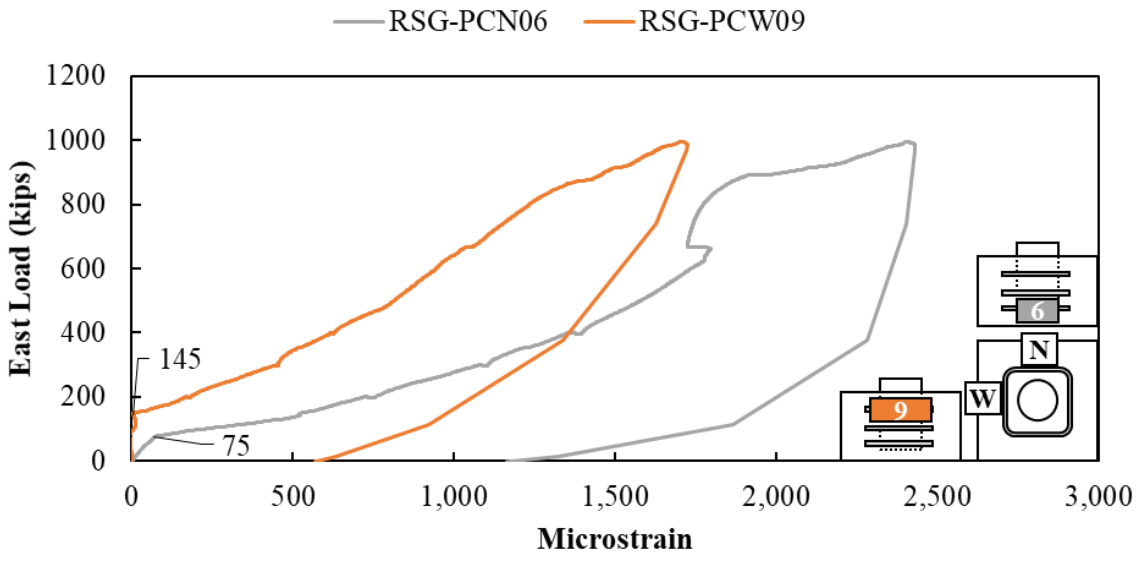

Figure B - 26: Confining reinforcement around the pocket of specimen LP-4

Measured strain in the vertical reinforcement in the cap and plug for LP-4 are shown in Figure B - 27. Strain in the vertical reinforcement in the cap around the pocket began in compression with approximately a linear slope until 80 kips for RSG-PCN8 toward the north face and 151 kips for RSG-PCN11 toward the west face, see Figure B - 27(a). Strains continued in compression for RSG-PCN8 with maximum strains between -75 με at 1000 kips. Strain was around 0 με at 1000 kips for RSG-PCN11.

The vertical compression strain in the plug for RSG-PCN13 and RSG-PCN14, began in compression with similar strains to the adjacent RSGs in the pile cap, see Figure B - 27(b). These compression strains began to decrease after around 88 kips with tension beginning to develop around 230 kips in RSG-PCN13. RSG-PCN15 experienced tensile strains through all of testing with maximum tensile strains at around 410 με.

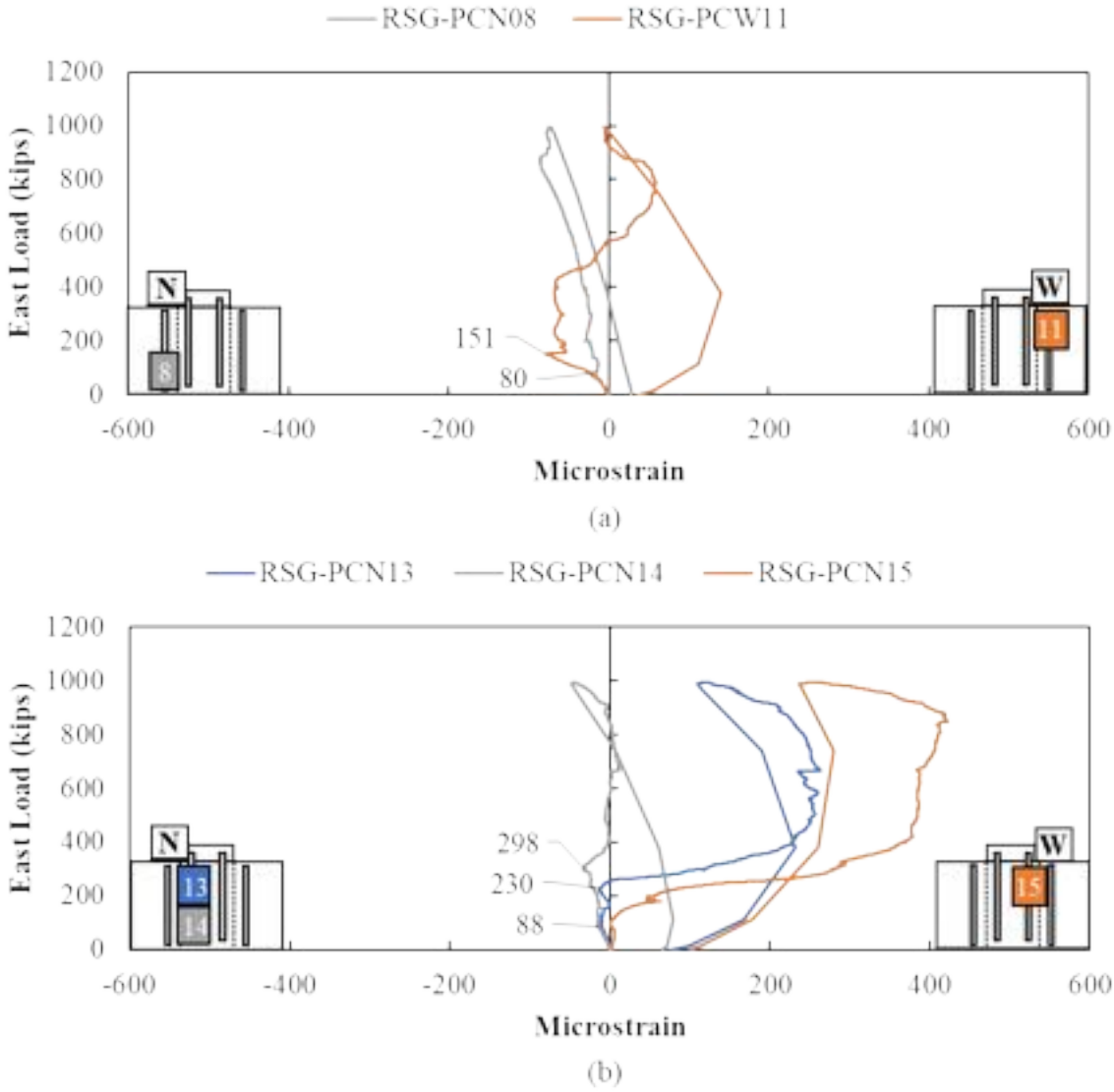

Figure B - 27: Rebar strain gages in vertical reinforcement on (a) the cap and (b) plug of Specimen LP-4

The crack pattern after the conclusion of testing is shown in Figure B - 28. Cracking again extended radially from the bottom of the plug and continued up the sides of the specimen. Spalling around the top of the plug was observed after the conclusion of testing.

Figure B - 28: Failure and cracking pattern of Specimen LP-4 (a) south-east view, (b) plug detail, and (c) bottom view.

Multi-plug Specimens

The results and observations for the multi plug specimens are summarized in this section. The measured compressive strengths (higher than specified), cracking loads, and ultimate loads are summarized in Table B - 2 for the multi plug specimens. The measured cracking load was 33 percent higher and measured failure load 4 percent higher for the specimen with sandblasted surface preparation (MP-2) than the specimen with the corrugated metal duct left in place (MP-1).

Table B - 2: Measured concrete strength, cracking load, and estimated versus ultimate strength for multi-plug specimens

Spec.	**Compressive Strength on Test Day (ksi)**		**Cracking Load (kips)**	**Ultimate Load (kips)**				
	Cap	*Plug*		*Measured*	*AASHTO*	*ABC*	*ATENA*	*Theory*
MP-1	8.37	7.49	150	*600.8**	*81.4*	*120.7*	*642.4*	*482.0*
MP-2	8.37	7.49	130	*626.4**	*81.4*	*120.7*	*642.4*	*513.3*

*failure load on west plug

The west plug load versus deflection plots for MP-1 and MP-2 are shown in Figure B - 29. Both specimens experienced a shear friction failure along the plug-to-cap interface. MP-2 (with sandblasted surface preparation) had a stiffer response and more rapid drop in load once the maximum load was reached compared to MP-1.

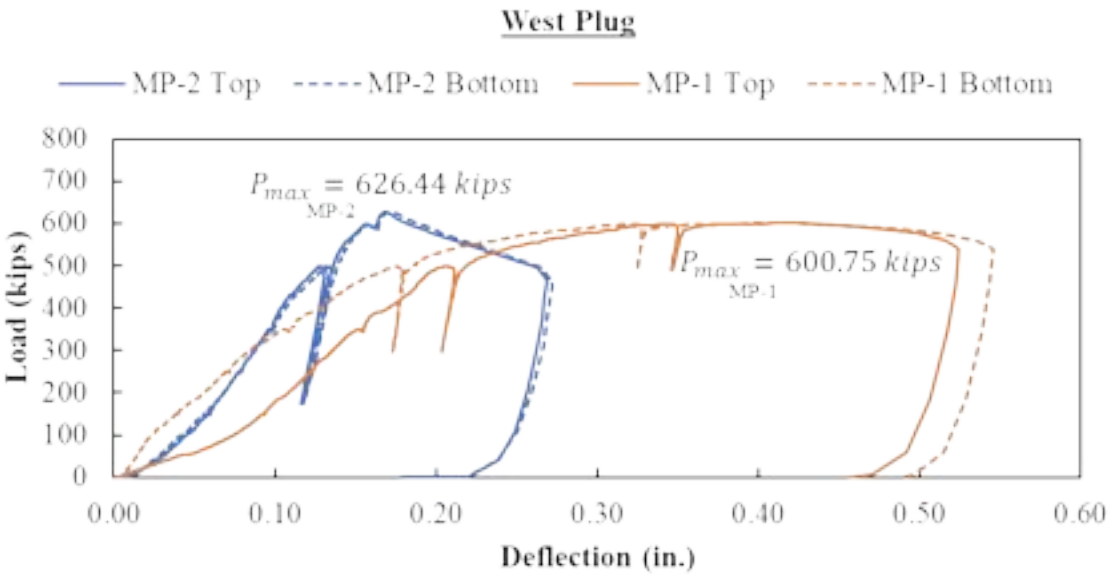

Figure B - 29: Load versus deflection plots for MP-1 and MP-2

More details on each test are provided in the following sections.

Specimen MP-1 Results

Specimen MP-1 had a corrugated surface between the cap and plug. The void was created using a corrugated metal pipe, and the pipe was left in place. The load versus deflection plot for both plugs in MP-1 is shown in Figure B - 30. The maximum capacity was 600.8 kips on the west plug while a load of 163.4 kips was being maintained on the east plug. A 6 percent difference was noticed between the displacement of the top (0.56 in.) and bottom (0.53 in.) of the west plug right before the load was removed.

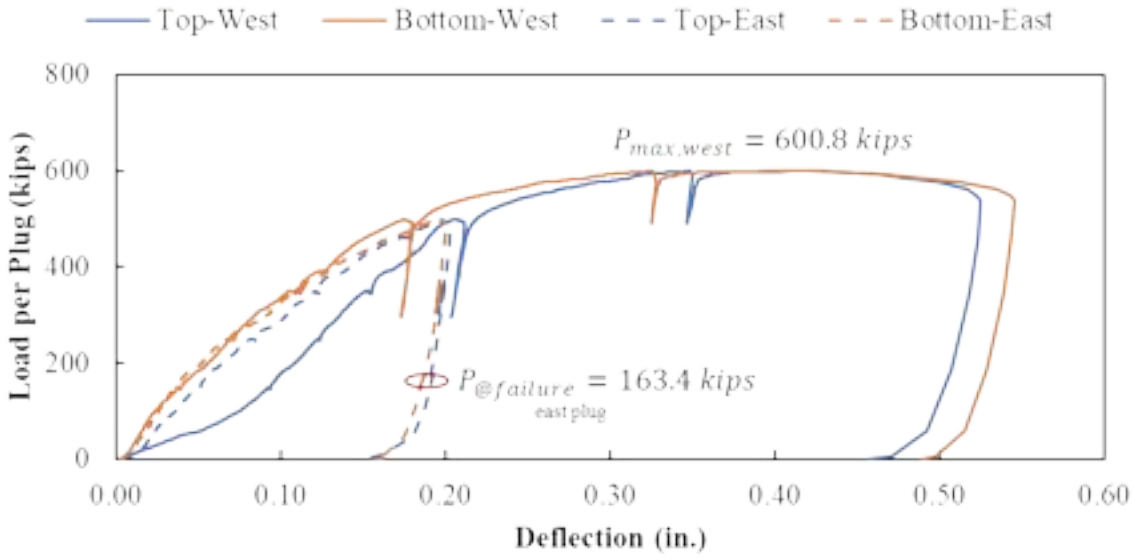

Figure B - 30: Load versus deflection curve for Specimen MP-1

The strains measured by the rebar strain gauges placed on the longitudinal reinforcement in the bottom of MP-1 are shown in Figure B - 31. Strains are plotted versus the east plug load for Figure B - 31(a) and versus the west plug load for Figure B - 31(b). The longitudinal RSGs were linear elastic until between 120 and 443 kips (on an individual plug). The longitudinal RSGs on near the plug toward the east and west faces of the specimen (RSG-PCB8 and RSG-PCB12) were the first to show signs of engagement at between 120 and 130 kips. The reinforcement between the plugs (RSG-PCB9 and RSG-PCB11) engaged later at 180 kips. The highest strains at failure were measured around the west plug, which was loaded to failure. Strains in the longitudinal reinforcement around the plug reached up to 11,500 με at failure, well above estimated yield strains of around 2,100 με. Several other RSGs in the longitudinal reinforcement around the pockets showed clear signs of yielding at failure: RSG-PCB3, RSG-PCB8, RSG-PCB11 and RSG-PCB12.

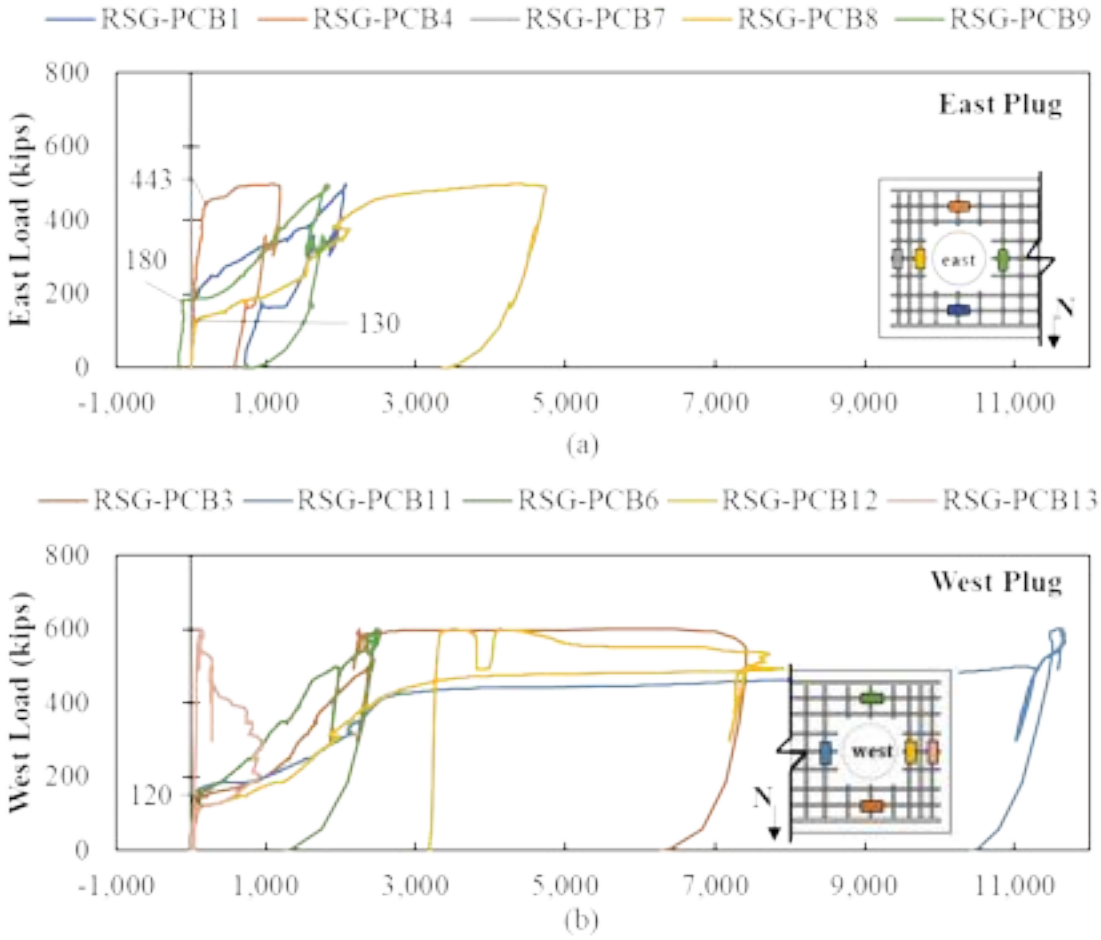

Figure B - 31: Rebar strain gages in the longitudinal reinforcement on bottom of Specimen MP-1

Cracking was first visually observed on MP-1 at the first stop at 150 kips on the west face and north and south faces toward the west plug, shown in Figure B - 32(a). These cracks continued to grow, and additional cracks began to develop around the east side of the specimen at the next stop at 250 kips, shown in Figure B - 32(b). The visually observed cracking generally corresponded to cracking noticed by RSG and CSG readings.

Figure B - 32: Crack propagation during testing at (a) 150 kips and (b) 250 kips on MP-1

Total load on the system (i.e., both plugs) plotted versus concrete strain for MP-1 are shown in Figure B - 33. Cracking was first observed with the CSGs around 180 kips to the north of the west plug, see CSG-PCN5 and CSG-PCN6. Generally, compression strains were measured on the north face between the plugs and toward the east side of the specimen.

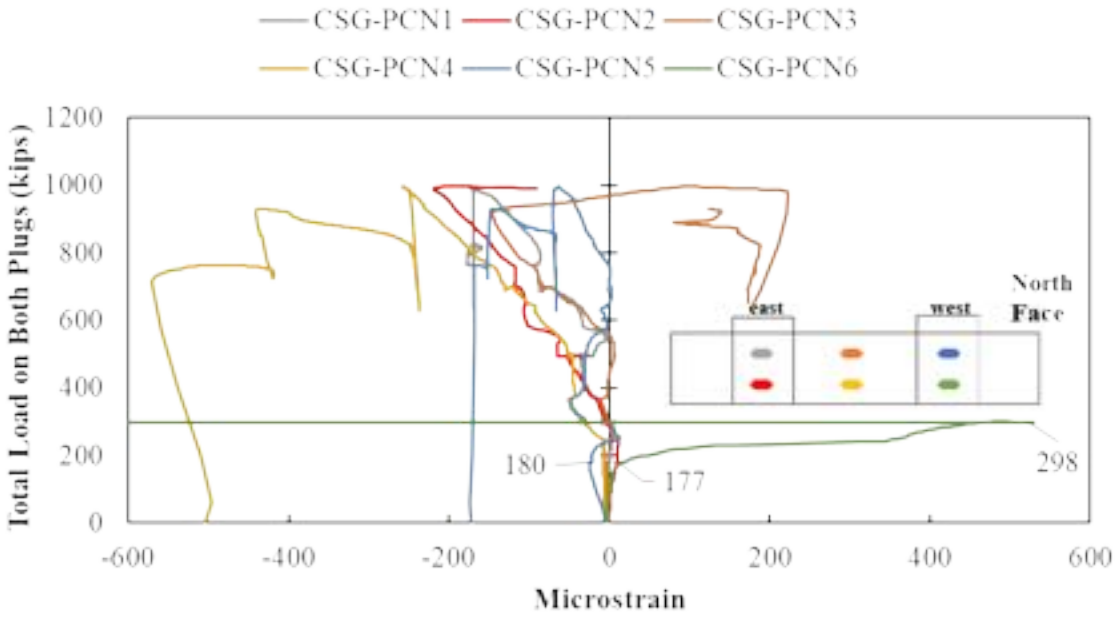

Figure B - 33: Concrete strain gages on the concrete surface of Specimen MP-1

The load in the closest plug plotted versus strain in the vertical rebar is shown in Figure B - 34. Measured vertical strains were generally in compression and similar between the cap and plug RSGs, which would suggest good stress transfer between the plug and cap.

Compression strains began to drop and tensile strains develop in some of the reinforcement as the load was increased, which would suggest horizontal cracking in the plug and cap.

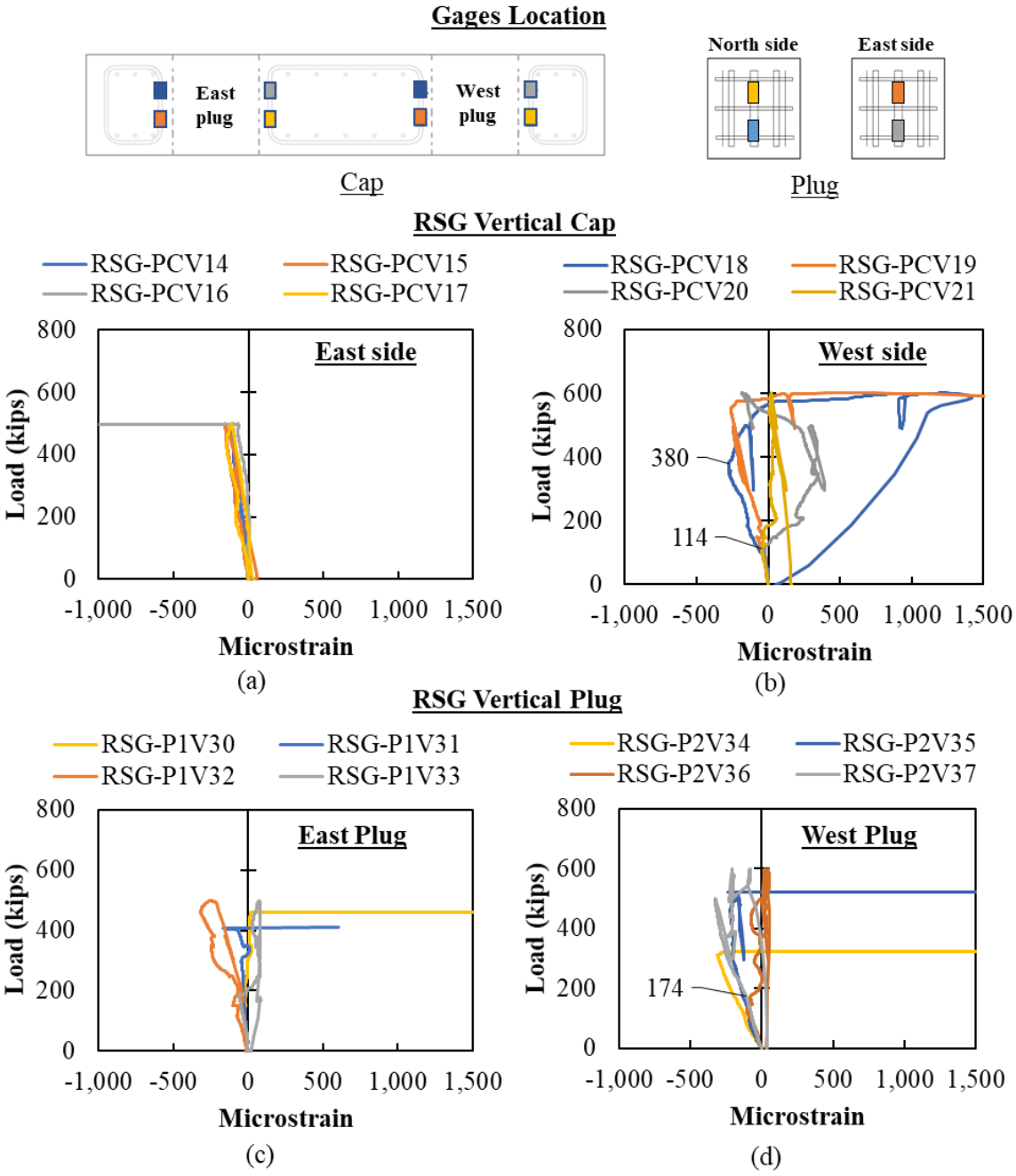

Figure B - 34: Rebar strain gages in vertical reinforcement on (a) cap around east plug, (b) cap around west plug, (c) east plug, and (d) west plug.

The crack pattern after failure of MP-1 is shown in Figure B - 35. Cracks extended radially from the bottom and top of the plugs and continued on the sides of the specimens. The

cracking was concentrated around the west plug, since this was the plug that was loaded until failure. Only minor cracking was observed between the plugs, which would be consistent with compression stresses generally developing between the plugs.

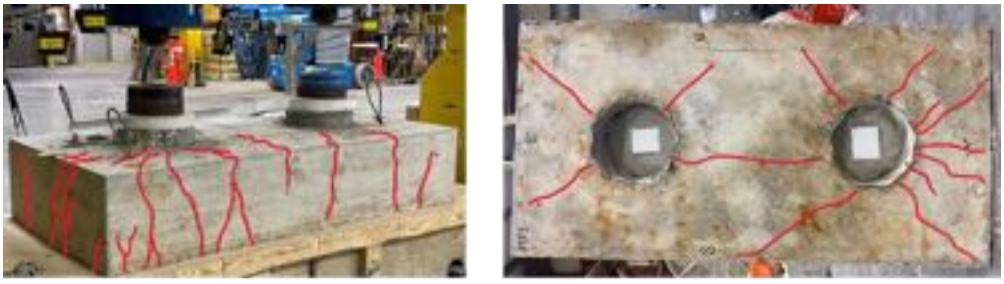

Figure B - 35: Cracking after testing on (a) south-west view and (b) bottom of specimen MP-1.

Specimen MP-2 Results

Specimen MP-2 had a corrugated surface between the cap and plug with sandblasted surface preparation. The void was created using a corrugated metal pipe. The load versus deflection plot for east and west plugs in MP-2 is shown in Figure B - 36. The maximum capacity was 626.4 kips on the west plug and the load at failure was 198.3 kips for the east plug. A sudden failure was observed after reaching the maximum load in the west plug of 626.4 kips; the displacement in the plug jumped from 0.17 inches to 0.27 inches suddenly. The load was then removed from the specimen.

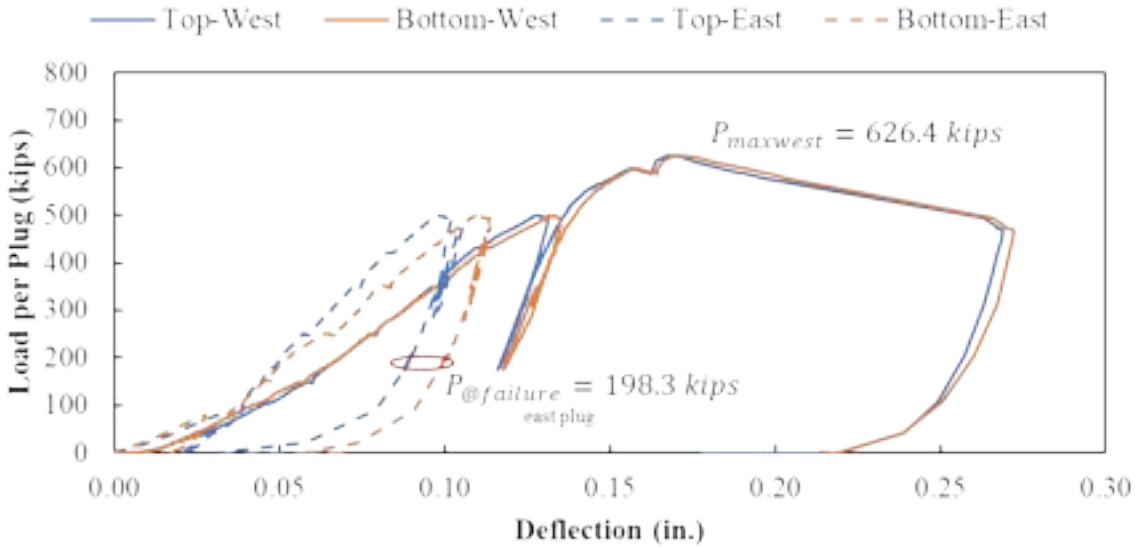

Figure B - 36: Load versus deflection curve for Specimen MP-2

Cracking was first visually observed on MP-1 at the first stop at 150 kips on the north and south faces toward the west plug, shown in Figure B - 37(a). These cracks continued to grow, and additional cracks began to develop on the west face and around the east side of the specimen at the next stop at 250 kips, shown in Figure B - 37(b). The visually observed cracking generally corresponded to cracking noticed by RSG and CSG readings.

Figure B - 37: Crack progression during testing at (a) 150 kips and (b) 250 kips

The strains measured by the rebar strain gauges placed on the longitudinal reinforcement in the bottom of MP-2 are shown in Figure B - 38. Strains are plotted versus the east plug load for Figure B - 38(a) and versus the west plug load for Figure B - 38(b) and (c). The longitudinal RSGs were linear elastic until between 105 and 243 kips (on an individual plug). The signs of first cracking were observed in RSG-PCB3 at 105 kips, on the north face near the west plug; this corresponded to the first cracks visually observed at 150 kips.

The reinforcement around the plugs toward the outside faces engaged before the reinforcement between the plugs. The reinforcement between the plugs (RSG-PCB10 and RSG-PCB11) engaged later at around 230 kips. The highest strains at failure were measured between the two plugs, around 11,150 με in RSG-PCB10, well above estimated yield strains of around 2,100 με. Several other RSGs in the longitudinal reinforcement around the pockets showed clear signs of yielding at failure: RSG-PCB10, RSG-PCB11, RSG-PCB12 and RSG-PCB13.

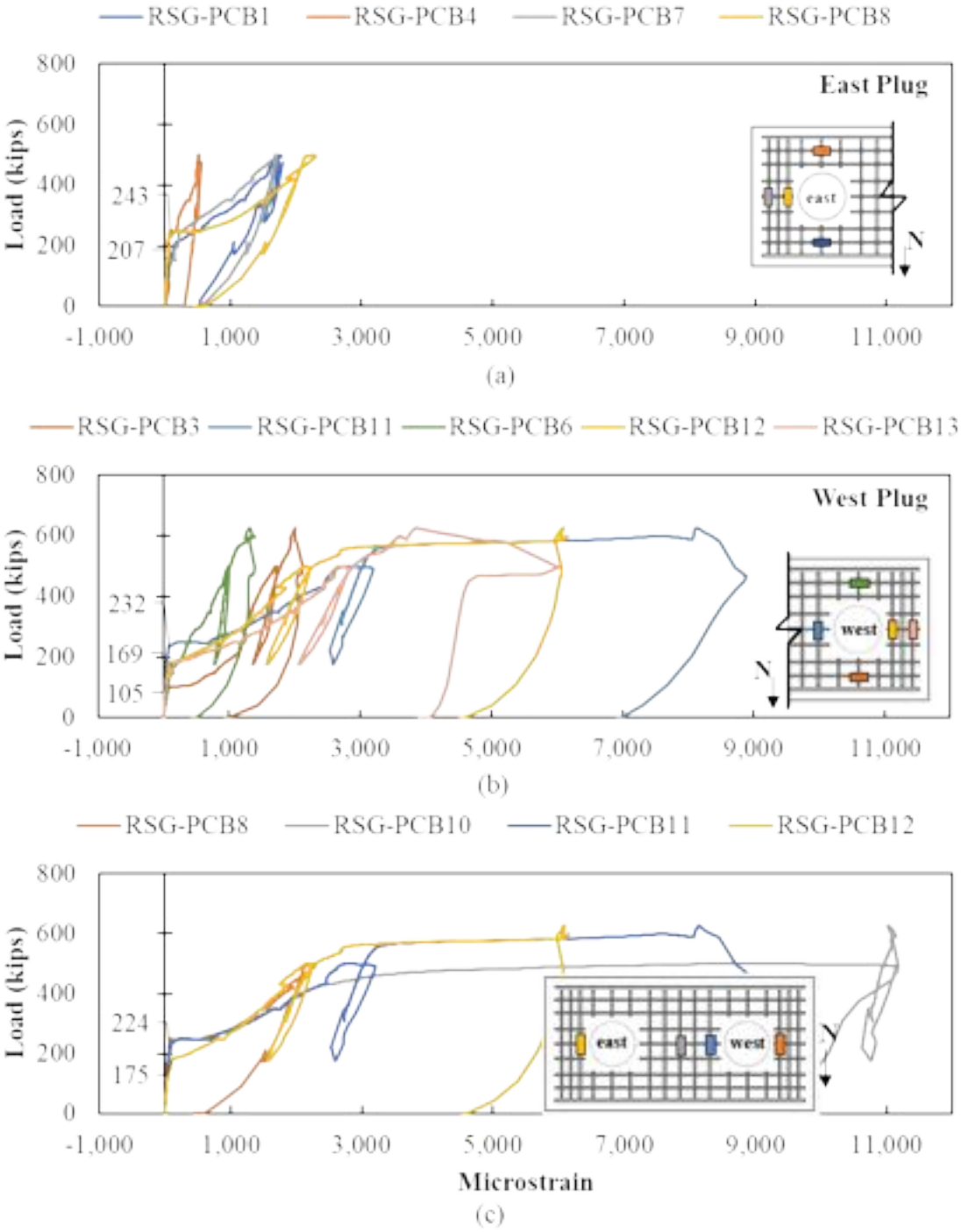

Figure B - 38: Rebar strain gages in the longitudinal reinforcement on bottom of Specimen MP-2

Total load on the system (i.e., both plugs) plotted versus concrete strain for MP-2 are shown in Figure B - 39. Cracking was first observed with the CSGs around 158 kips to the north of the west plug, see CSG-PCN5 and CSG-PCN6. Cracking was observed to the north of

the east plug between around 300 and 350 kips, see CSG-PCN1 and CSG-PCN2. Compression was measured between the plugs with maximum compression strains of around -430 με in CSG-PCN4 as the plug was sliding.

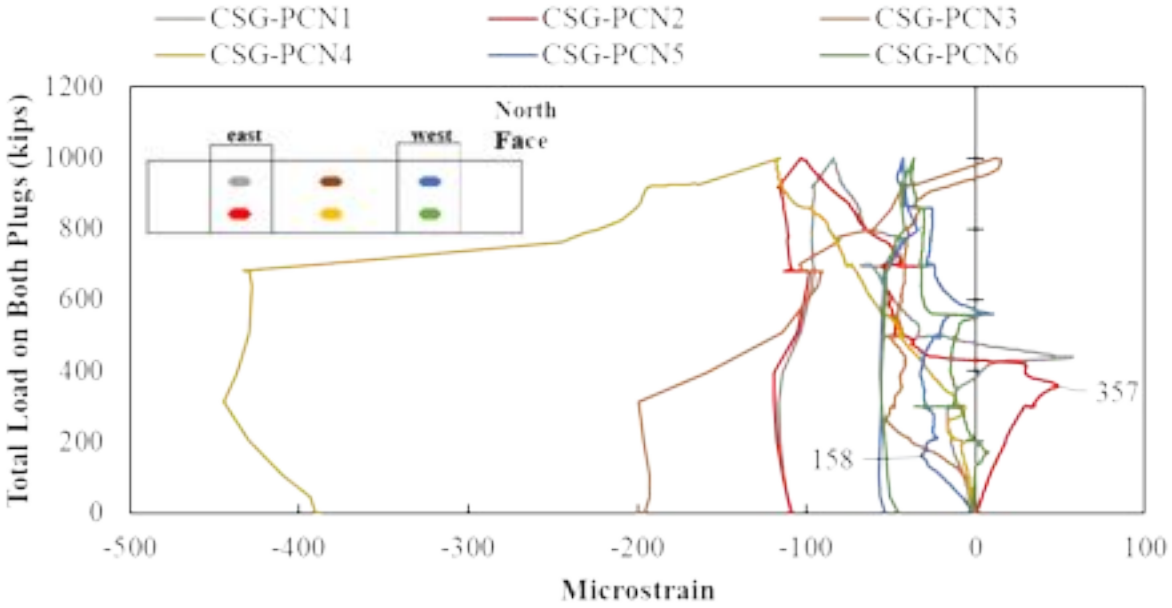

Figure B - 39: Concrete strain gages on the concrete surface of Specimen MP-2

The load in the closest plug plotted versus the strain in the vertical rebar is shown in Figure B - 40. Measured vertical strains were generally in compression at the start of testing and similar between the cap and plug RSGs, which would suggest good stress transfer between the plug and cap. Compression strains began to drop and tensile strains develop in some of the reinforcement as the load was increased, which would suggest horizontal cracking in the plug and cap. Tensile strains up to 1,000 με were measured in RSG-PCV18 after sliding of the plug at failure.

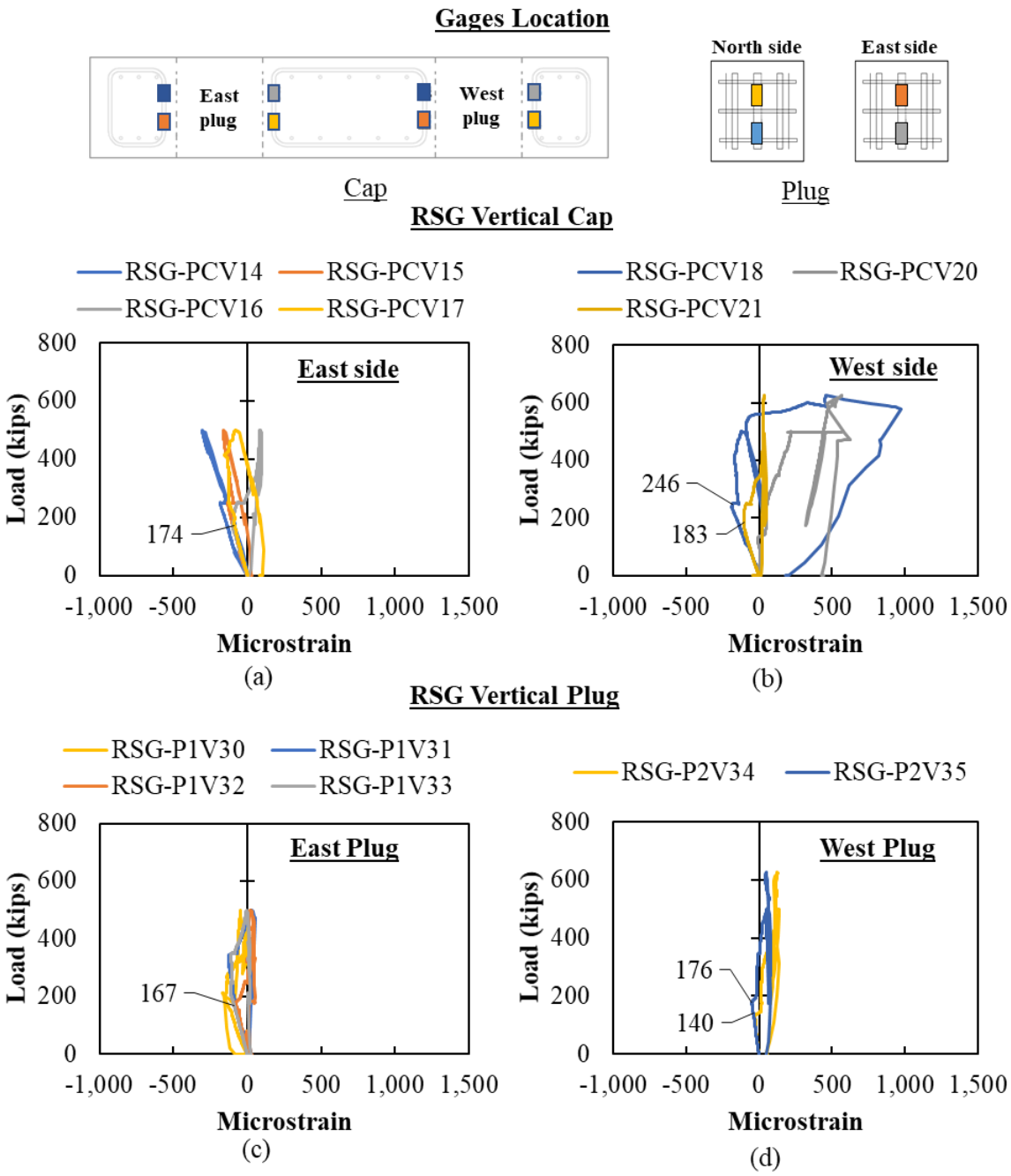

Figure B - 40: Rebar strain gages in vertical reinforcement on (a) cap around east plug, (b) cap around west plug, (c) east plug, and (d) west plug for Specimen MP-2

The crack pattern after failure of MP-2 is shown in Figure B - 41. Cracks extended radially from the bottom and top of the plugs and continued on the sides of the specimens. The cracking was concentrated around the west plug, since this was the plug that was loaded

until failure. Only minor cracking was observed between the plugs, which would be consistent with compression stresses generally developing between the plugs.

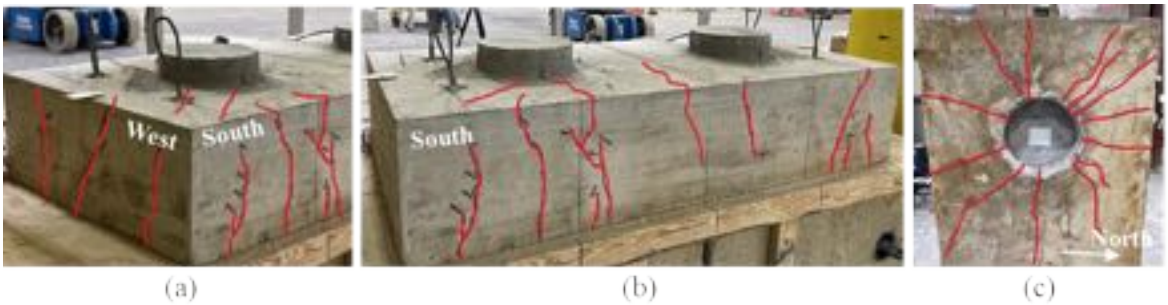

Figure B - 41: Failure and cracking pattern of Specimen MP-2 on (a) south-west view, (b) south view, and (c) bottom view

Socket Connection Specimens

The results and observations for socket connection specimens are summarized in this section. The measured compressive strengths (higher than specified), cracking loads, and ultimate loads are summarized in Table B - 3 for socket connection specimens.

Table B - 3: Measured concrete strength, cracking load, and estimated versus ultimate strength for socket connection specimens

Spec.	**Compressive Strength on Test Day (ksi)**		**Cracking Load (kips)**	**Ultimate Load (kips)**				
	Cap	*Plug*		*Measured*	*AASHTO*	*ABC**	*ATENA*	*Theory*
SC-1	8.56	7.27	79	*511.0*	*121.7*	*177.7*	*609.4*	*631.6*
SC-2	8.56	7.27	74	*601.4*	*97.5*	*142.4*	*609.4*	*467.8*

*found using AASHTO LRFD Guide Specification for ABC Equation (3.6.6.6-1)

AASHTO LRFD Guide Specifications for Accelerated Bridge Construction specifies socket connections should be designed based on the shear friction specifications found on AASHTO LRFD Bridge Design Specifications for normal-weight concrete placed against a clean concrete surface. The value in Table B - 3 is still provided using Equation (3.6.6.6-1).

The load versus displacement plots for SC-1 and SC-2 are shown in Figure B - 42. Both specimens had similar initial stiffnesses up to approximately 340 kips, at which point the

SC-2 response began to soften. SC-2 had a larger deflection at its ultimate load than SC-1, 0.32 inches versus 0.14 inches.

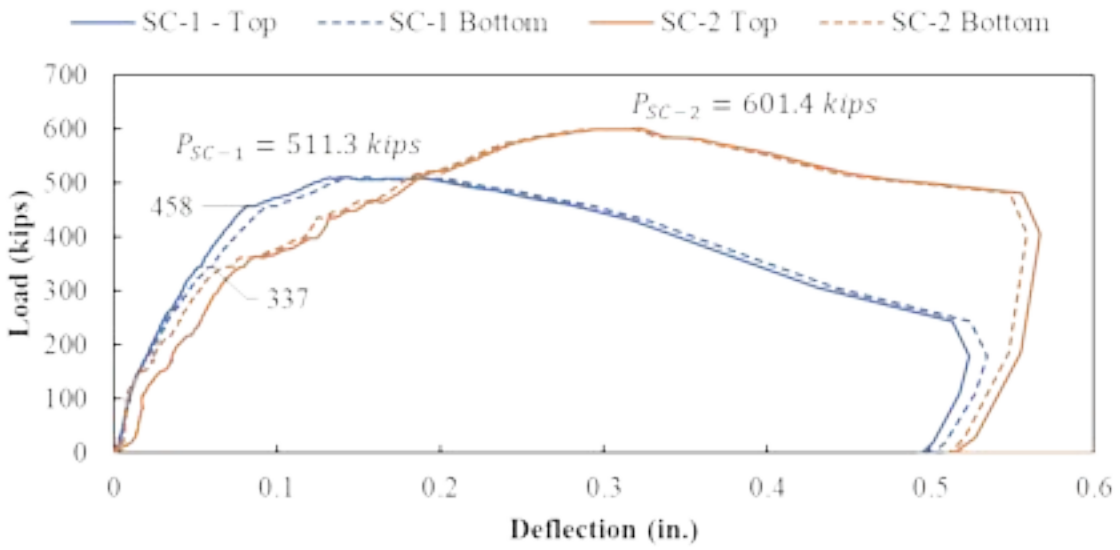

Figure B - 42: Load versus displacement curve for Specimens SC-1 and SC-2

More details on each test are provided in the following sections.

Specimen SC-1

Specimen SC-1 had a corrugated surface between the cap and plug with sandblasted surface preparation. The void was created using a corrugated metal pipe, but the metal pipe was removed before casting of the plug.

The load versus displacement plots for the top and bottom of the plug for SC-1 is shown in Figure B - 43. The top and bottom of the plug measured the same displacement with a linear elastic slope to 135 kips. The bottom of the plug then began to experience slightly larger deflection (about 2 percent) throughout testing. The plug began to push through at approximately 450 kips with a peak load of 511.3 kips at approximately 0.15 inches displacement. The specimen held approximately 250 kips at 0.5 inches deflection, when the load was completely removed.

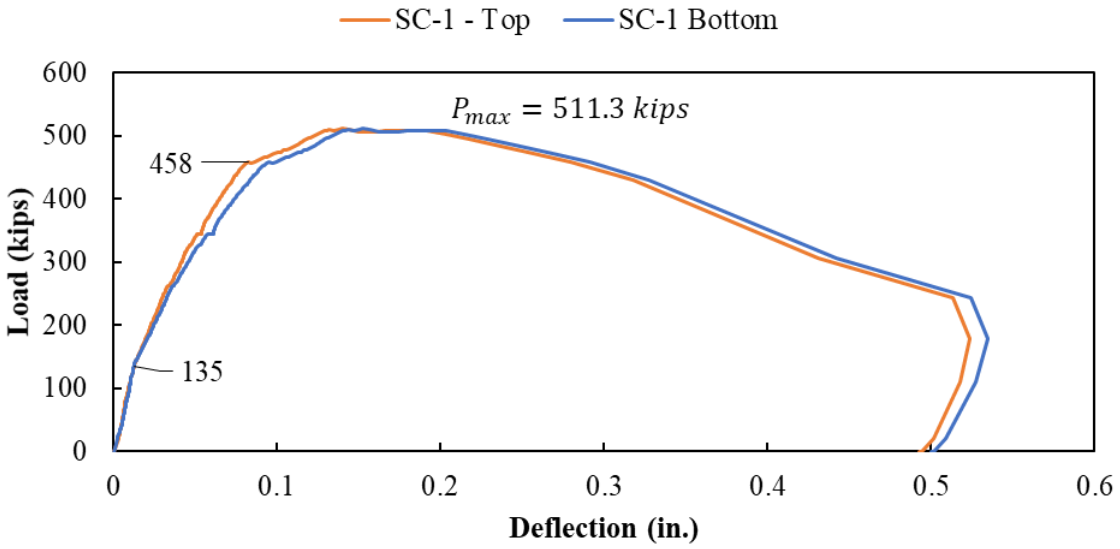

Figure B - 43: Load versus deflection curve for Specimen SC-1

The strain gauges placed on the longitudinal reinforcement in the bottom of SC-1 are shown in Figure B - 44. First cracking occurred on the north face of the specimens, with engagement of RSG-PCB1 and RSG-PCB2 occurring at 79 and 110 kips, respectively. Engagement of the reinforcement toward the west face occurred at higher loads (143 and 325 kips). The largest strain measured during the failure of SC-1 was about 2,780 με (RSG-PCB1), which is slightly higher than the estimated yield strain of approximately 2,100 με (assuming 60 ksi yield strength). The other reinforcement was near or slightly below the estimated yield strain for the rebar.

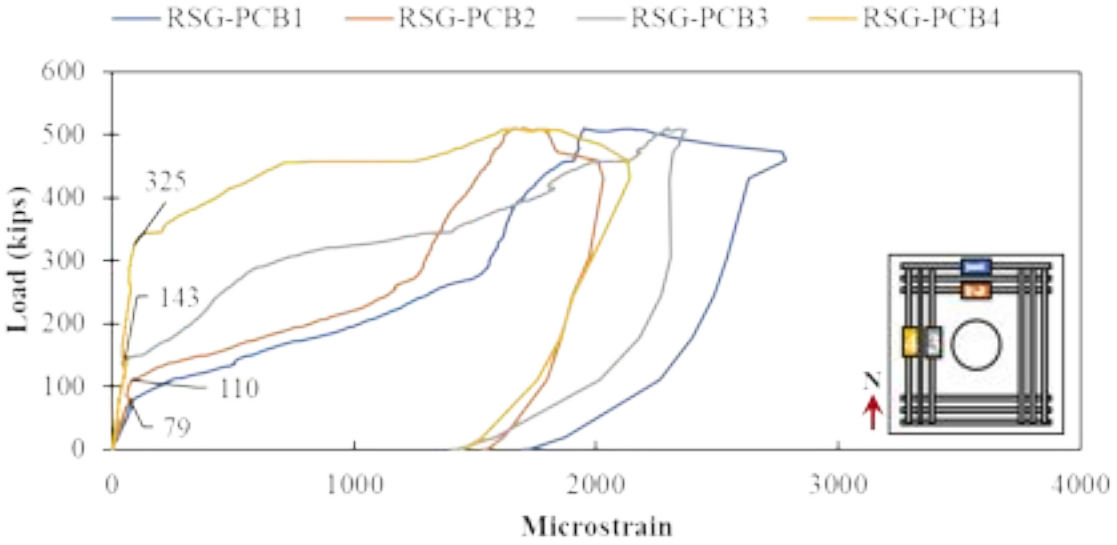

Figure B - 44: Rebar strain gages in the longitudinal reinforcement on bottom of Specimen SC-1

Cracking was first visually observed on all faces of SC-1 at the first stop at 350 kips, as shown in Figure B - 45. More cracking was observed on the north and south faces of the specimen, which corresponds to the additional engagement of the reinforcement toward the north face of the specimen.

Figure B - 45: Crack pattern at 350 kips for SC-1

Load versus concrete strain measured by the CSGs on the north and west face of SC-1 are shown in Figure B - 46. Cracking was first indicated by the CSGs at around 80 kips with first cracking occurring on the north face; the top CSGs were the first to indicate cracking. Cracking was observed by the bottom CSGs between 124 and 140 kips for the north and west faces, respectfully. The top gauges showing first sign of cracking is opposite what was observed visually.

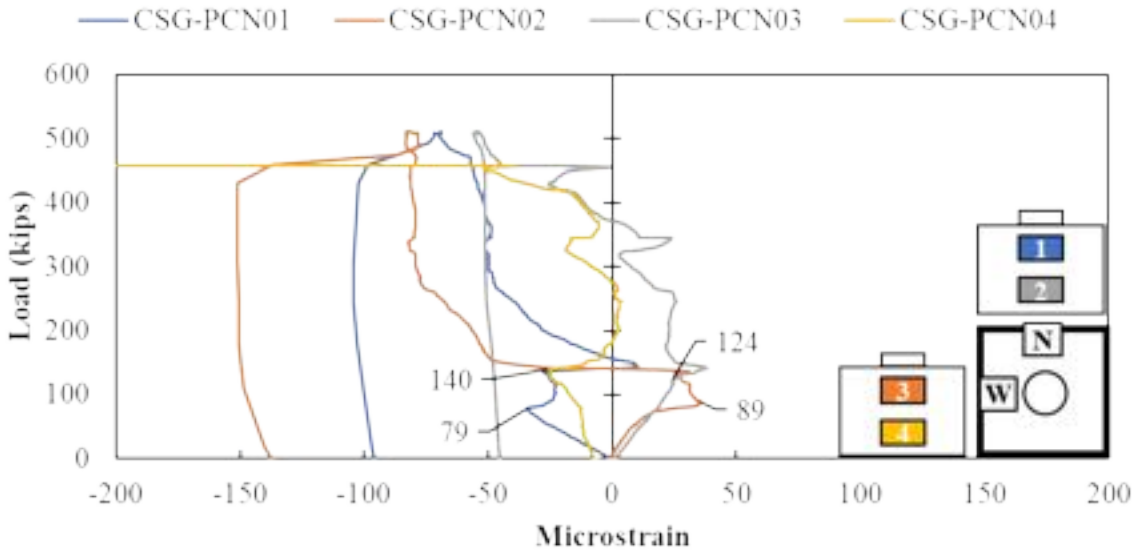

Figure B - 46: Concrete strain gages in the surface of Specimen SC-1

Measured strain for the horizontal rebar placed in the void is shown in Figure B - 47 and Figure B - 48. Two layers of reinforcement in each direction (east-west and north-south) were placed beneath the tip of the embedded pile. The east-west rebar was on top of the north-south rebar in each layer.

RSGs were placed horizontally at the middle of the plug rebar and vertically toward the ends of the vertical leg of the plug rebar. Generally, the horizontal RSG at the middle of the plug rebar below the tip of the embedded pile was the first to show signs of engagement, at loads around 100 kips. The vertical leg of the plug rebar would generally engage later, above 170 kips, and then increase in strains larger than those in the horizontal RSGs. The vertical leg of the plug rebar on the west side of the plug engaged at a lower load than the east side, see RSG-PCV7, RSG-PCV10, RSG-PCV13, and RSG-PCV16 in Figure B - 47; this behavior was likely a result of the pile leaning slightly toward the west. Maximum measured strains were around 1500 με at failure (RSG-PCV26); strains in all other RSGs remained under 800 με.

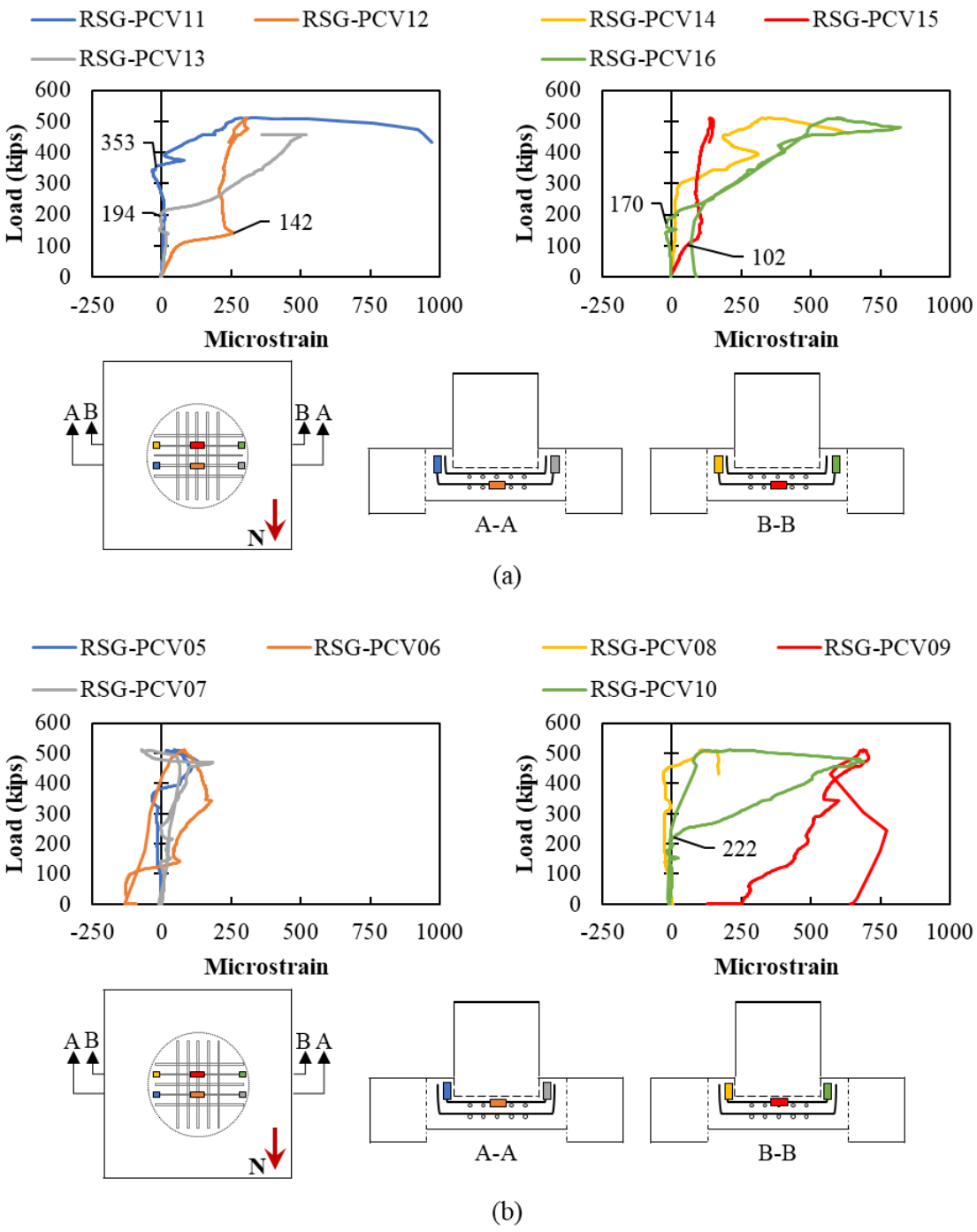

Figure B - 47: Load versus strain measured using RSG for (a) bottom layer and (b) top layer of void reinforcement in Specimen SC-1 in the east-west direction.

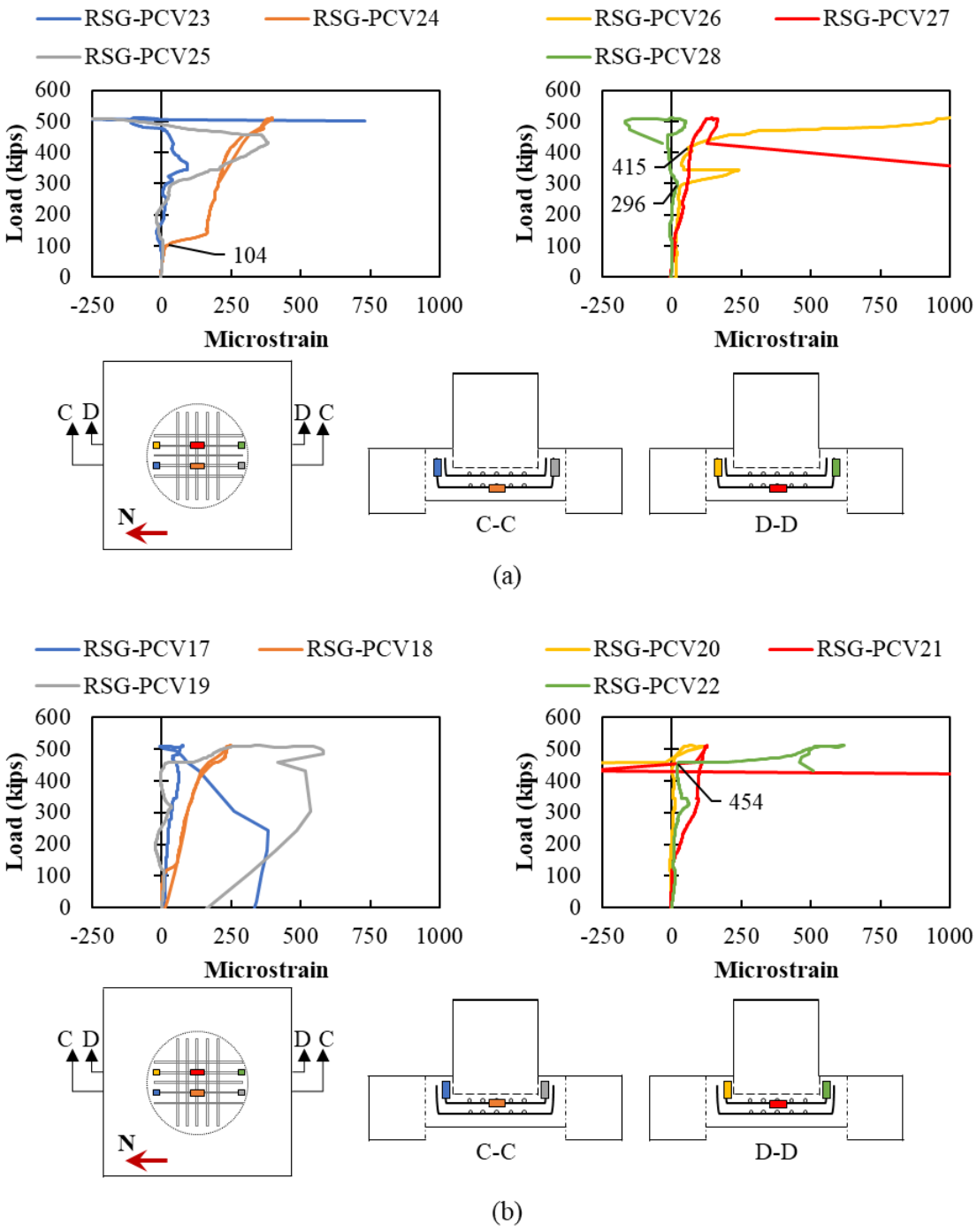

Figure B - 48: Load versus strain measured using RSG for (a) bottom layer and (b) top layer of void reinforcement in Specimen SC-1 in the north-south direction.

The crack pattern after failure for SC-1 is shown in Figure B - 49. Cracks extended radially from the bottom of the plug and continued up the sides of the cap. Some of these cracks continued onto the top of the cap and into the plug toward the embedded pile.

Figure B - 49: Cracking on (a) cap and (b) bottom of specimen SC-1

An interface crack was noticed between the pile and plug concrete on the top of the system and between the plug and cap on the bottom of the system, as shown in Figure B - 50. The end of the embedded pile was smooth, so little cohesion or friction would have been present between the pile and plug concrete.

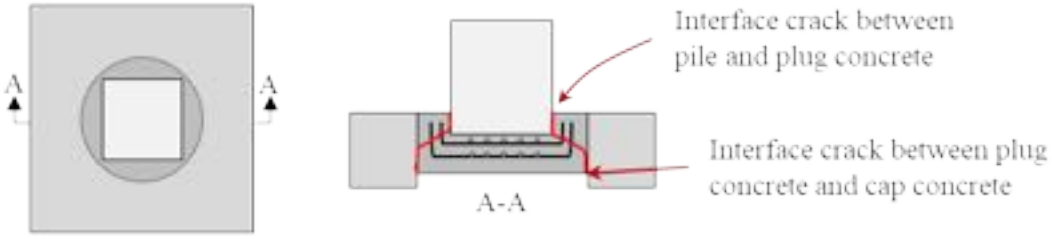

Figure B - 50: Observed interface cracks in SC-1

The depth of the interface crack between the pile and plug (on top) and plug and cap (on bottom) was measured using a 0.075-inch-thick metal crack gauge. Depths were measured at eight locations around the bottom of the plug, see Figure B - 51 (a), and at eight locations along the east and south faces of the pile, see Figure B - 51(b). The crack gauge would not fit in the interfaces on the north and west faces of the pile.

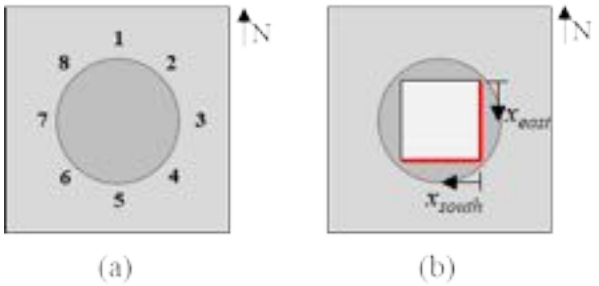

Figure B - 51:Location of cracking separation measurements on (a) bottom of the specimen and (b) top of the specimen SC-1

The depths of the interface cracks are summarized in Table B - 4 for the bottom of Specimen SC-1. The distance between the bottom of the cap and the bottom of the plug is also included in Table B - 4. The maximum measured depth was 2 ¼ inches on the west side of the plug, as shown in Table B - 4 indicated by the number three. The plug moved a ¼-inch more on the west side as indicated on the measurements of the bottom of plug to bottom of the cap (#1, #2, #3, and #4) (Table B - 4).

Table B - 4: Crack separation measurements for bottom of Specimen SC-1

Location (Figure B - 51 (a))	**Crack depth from bottom of plug at interface using 0.075-inch-thich crack gauge (inch)**	**Distance from bottom of cap to bottom of plug (inch)**
1	1 ¾	2 ½
2	1 ½	2 ½
3	2 ¼	2 ½
4	1	2 ½
5	1 1/8	2 ¾
6	1	2 ¾
7	1 ½	2 ¾
8	1 5/8	2 ¾

The depth of interface cracks was also measured at the top of the cap around the embedded pile using a 0.006-inch-thick metal crack gauge. Measurements were taken every 2 inches along the edge of the pile on the east and south sides of the pile, indicated by a red line on

Figure B - 51 (b) and listed in Table B - 5. The maximum depth of the interface crack was greater than 4 ½ -inch on the east side of the pile near the south-east corner.

Table B - 5: Crack separation measurements for top of Specimen SC-1

***x* (inch)** Figure B - 51 **(b)**	**Crack depth from top of cap at interface using 0.006-inch-thich crack gauge (inch)**	
	East Face	*South Face*
2	1 5/8	0
4	2 ¼	1 ½
6	0	1 ¼
8	1 ½	1 ¾
10	2 ½	1 ½
12	0	1 ½
14	1	¾
16	> 4 ½	1 ¾

Specimen SC-2

Specimen SC-2 had a corrugated surface between the cap and plug. The void was created using a corrugated metal pipe, and the pipe was left in place.

The load versus displacement plots for the top and bottom of the plug for SC-2 is shown in Figure B - 52. The top and bottom of the plug measured similar displacements throughout testing, with less than a 2 percent different. The curves were linear to about 100 kips; at this point there was a decreased stiffness with another linear range to around 344 kips. The load then continued to increase with a decreasing slope until its peak load of 601.4 kips at about 0.32 inches displacement. The specimen continued to hold load as the plug pushed through, with a load of 480 kips when the load was removed at 0.55 inches displacement.

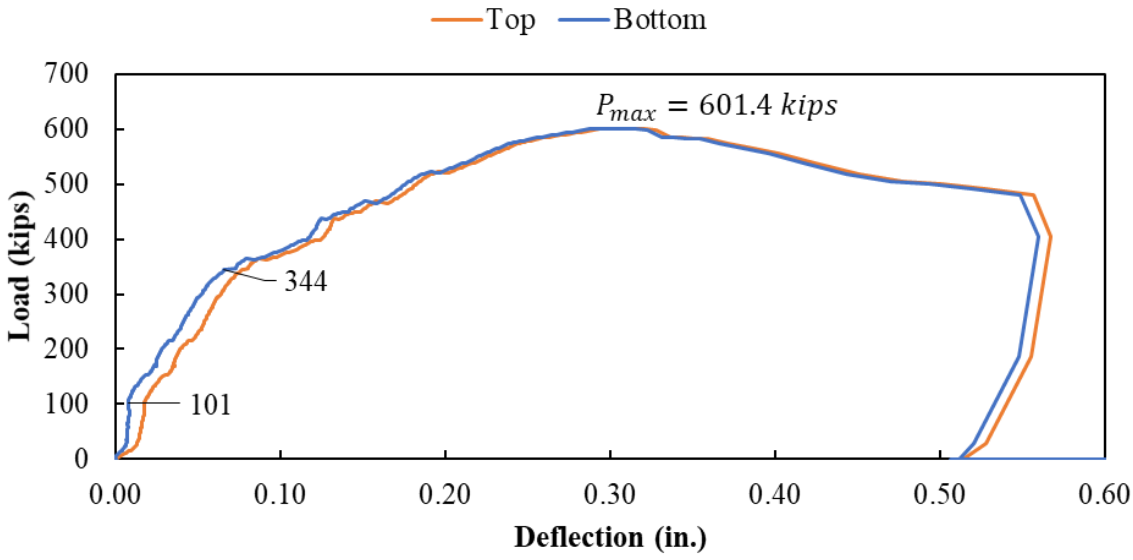

Figure B - 52: Load versus deflection curve for Specimen SC-2

The strain gauges placed in the longitudinal reinforcement in the bottom of SC-2 are shown in Figure B - 53. First cracking occurred on the west face of the specimens, with engagement of RSG-PCB3 and RSG-PCB3 occurring at 78 and 81 kips, respectively. Engagement of the reinforcement toward the north face occurred at higher loads (about 208 kips). The largest strain measured during the failure of SC-2 was more than 9,000 με (RSG-PCB2), which is much higher than the estimated yield strain of approximately 2,100 με (assuming 60 ksi yield strength). RSG-PCB4 read strains up to 3,500 με at failure and RSG-PCB1 and RSG-PCB3 around 2,200 με.

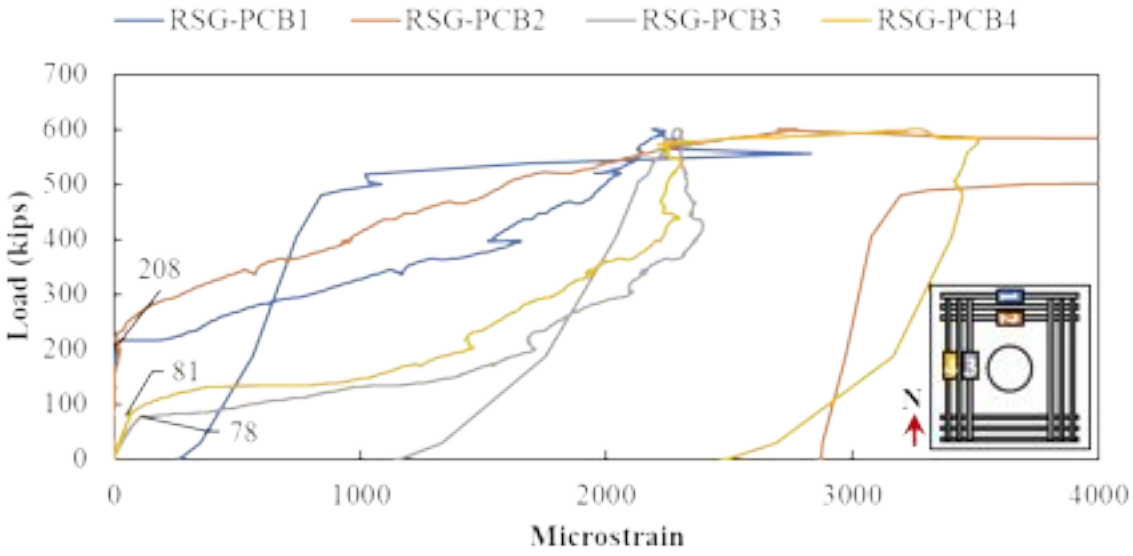

Figure B - 53: Rebar strain gages in the longitudinal reinforcement on bottom of Specimen SC-2

Cracking was first visually observed on all faces of SC-2 at the first stop at 175 kips, as shown in Figure B - 54 (a). A large crack formed from the bottom of the north face to the top face next to the plug. Existing cracks grew in size and length and additional cracks formed as the load was increased, see Figure B - 54 (b).

Figure B - 54: Crack pattern at (a) 175 kips and (b) 350 kips for SC-2

Load versus concrete strain measured by the CSGs on the north and west face of SC-2 are shown in Figure B - 55. Cracking was first indicated by the CSGs at around 76 kips with first cracking occurring on both faces; the bottom CSGs were the first to indicate cracking. Cracking was observed by the top CSGs between 191 and 208 kips for the west and north faces, respectfully.

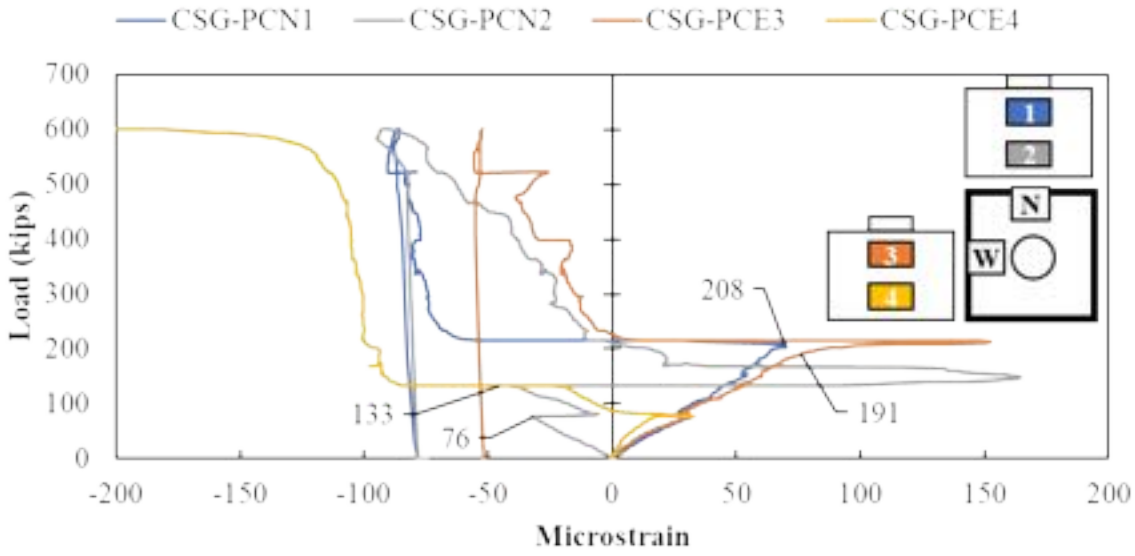

Figure B - 55: Concrete strain gages in the concrete surface of Specimen SC-2

Measured strain for the horizontal rebar placed in the void is shown in Figure B - 56 and Figure B - 57. Two layers of reinforcement in each direction (east-west and north-south) were placed beneath the tip of the embedded pile. The east-west rebar was on top of the north-south rebar in each layer.

RSGs were placed horizontally at the middle of the plug rebar and vertically toward the ends of the vertical leg of the plug rebar. The vertical leg of the north-south plug rebar toward the south side of SC-2 was the first to engage at loads between 140 and 150 kips, see RSG-PCV19, RSG-PCV22, RSG-PCV25, and RSG-PCV28 in Figure B - 57; this behavior might indicate that the pile was leaning towards the south during testing. The horizontal portion of the north-south plug rebar was next to become non-linear at loads between 190 and 250 kips. The east-west oriented plug rebar engaged at higher loads between 363 and 405 kips. Maximum measured strains in the vertical leg portion of the plug reinforcement were around 2,400 με (RSG-PCV17) with most strains less than 750 με. The maximum strains in the horizontal portion of the plug reinforcement were about 800 με in RSG-PCV24.

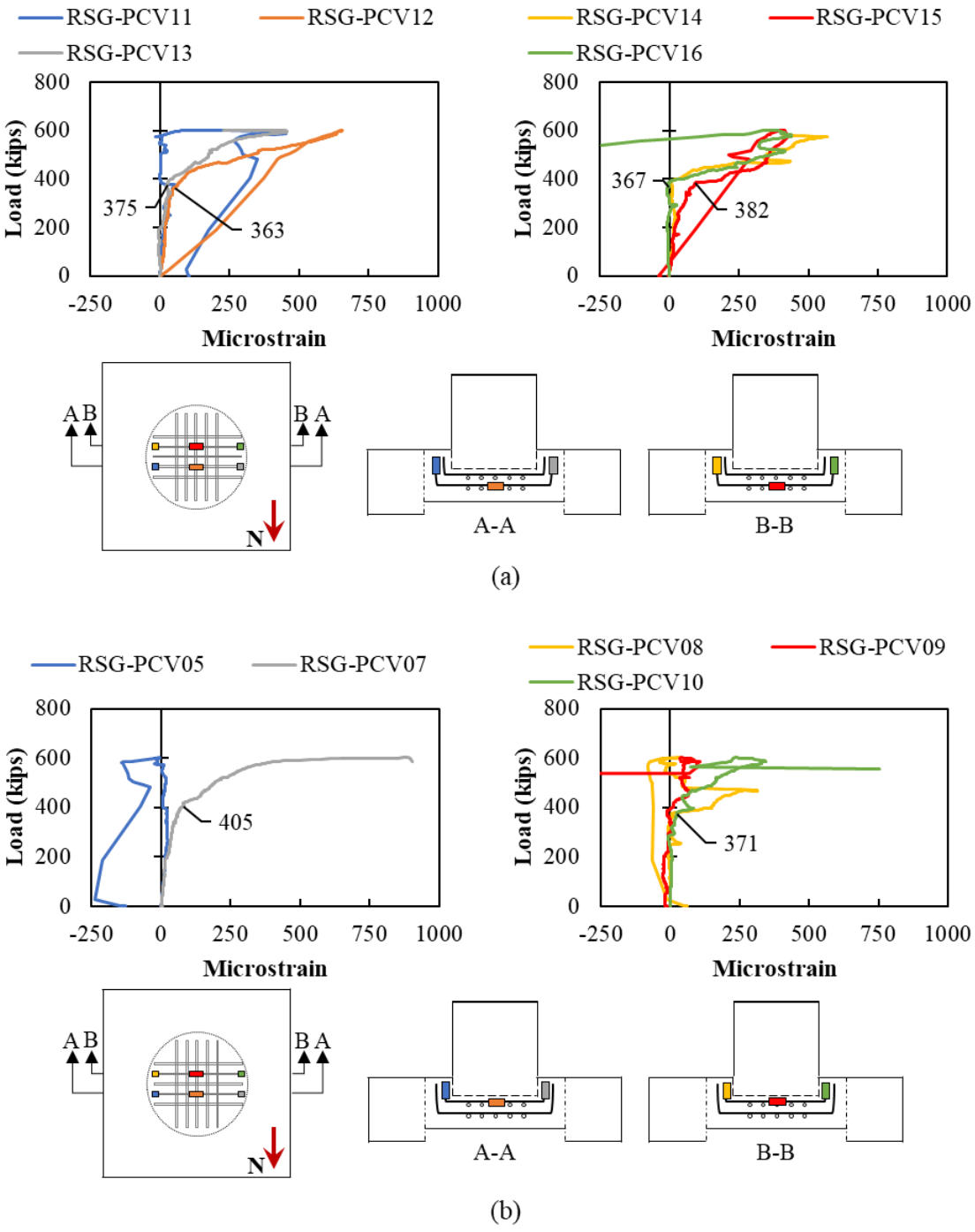

Figure B - 56: Load versus strain measured using RSG for (a) bottom layer and (b) top layer of void reinforcement in Specimen SC-2 in the east-west direction.

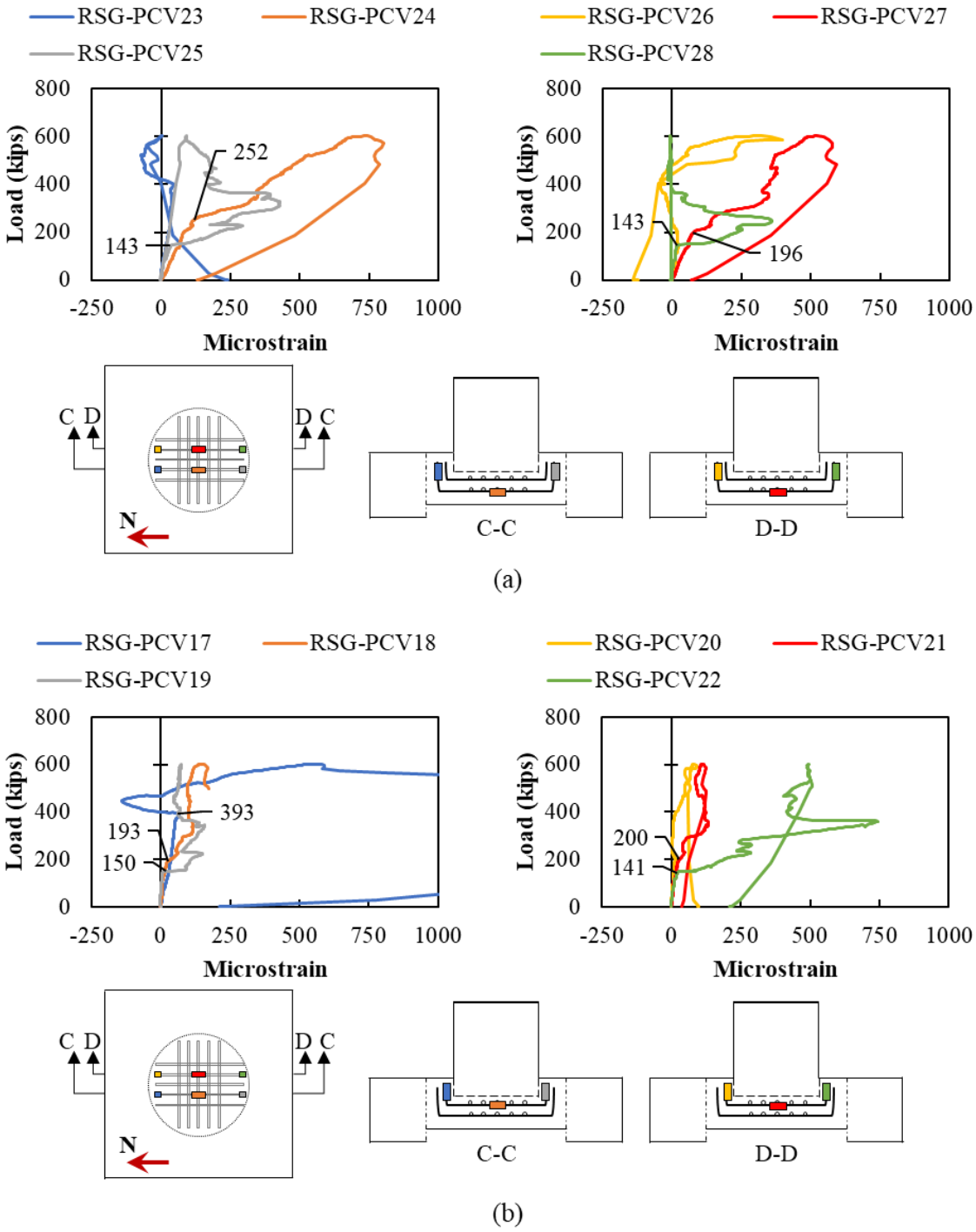

Figure B - 57: Load versus strain measured using RSG for (a) bottom layer and (b) top layer of void reinforcement in Specimen SC-2 in the north-south direction.

The crack pattern after failure for SC-2 is shown in Figure B - 58. Cracks extended radially from the bottom of the plug and continued up the sides of the cap. Some of these cracks continued onto the top of the cap and into the plug toward the embedded pile.

Figure B - 58: Cracking on (a) cap and (b) bottom of Specimen SC-2

Like SC-1, an interface crack was noticed between the pile and plug concrete on the top of the system and between the metal pipe and cap on the bottom of the system, as shown in Figure B - 59. The end of the embedded pile was smooth, so little cohesion or friction would have been present between the pile and plug concrete.

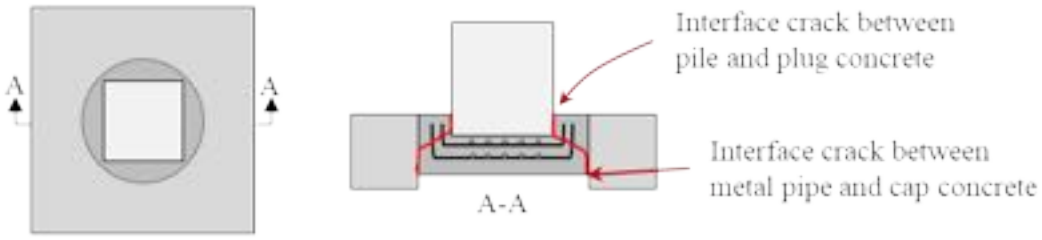

Figure B - 59: Observed interface cracks in SC-2

The depth of the interface crack between the pile and plug on top of Specimen SC-2 was measured using a 0.006-inch-thick metal crack gauge. Depths were measured at eight locations two inches apart along the north face of the pile, as shown in Figure B - 51. The crack gauge would not fit in the interface along any other face of the pile on top of the specimen. The crack gauge would also not fit in the interface between the plug and cap on either side of the metal pipe on the bottom of the specimen. The maximum interface crack depth was found to be greater than 4 inches on the north side of the pile near the west face.

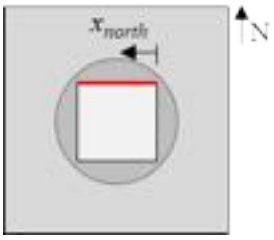

Figure B - 60: Location of cracking separation measurements of specimen SC-2

Table B - 6: Crack separation measurements for specimen SC-2

***x* from** Figure B - 60 **(inch)**	**Crack depth from top of cap at interface using 0.006-inch-thich crack gauge (inch)**
	North Face
2	2 ¼
4	2 ¾
6	2 ½
8	2 ½
10	2 ¾
12	2 ¼
14	2
16	>4

VITA

FATIMA VIEIRA

Born, Lecheria, Venezuela

2009-2014	B.S., Civil Engineering Santa Maria University Barcelona, Venezuela
2016-2018	M.S., Civil Engineering Florida International University Miami, Fl, USA
2018-2022	Doctoral Candidate Florida International University Miami, Fl, USA

PUBLICATIONS AND PRESENTATIONS

Poster Presentation – Graduate Student Appreciation Week (GSAW), *Preliminary Investigation of the Shear Friction Capacity of Interfaces without Steel Crossing the Interface*, Miami (Fl), April 2019.

Garber, Vasconcelos, and Vieira, ASCE Annual Conference, *Preliminary Investigation of Shear Friction Capacity in Pocket Connections*, Orlando (Fl), July 2019.

Garber, Vasconcelos, and Vieira, PCI Committee Days and Technical Conference, *Preliminary Investigation of the Shear Friction Capacity of Interfaces without Steel Crossing the Interface*, Rosemont (IL), September 2019.

Poster Presentation – ABC International Conference, *Preliminary Investigation of Pocket Connection between Pile and Pile Cap*, Miami (Fl), December 2019.

Garber, Vasconcelos, and Vieira, *Evaluation of Shear Friction Behavior of Cylindrical Pocket Connections*. Submitted to ACI on 10/26/2021